

**Strategies to Evade Resistance: Combining  
Biophysical and Biochemical Approaches to  
Discover Compounds Addressing New Bacterial  
Target Systems**

**DISSERTATION**

zur Erlangung des Grades  
des Doktors der Naturwissenschaften  
der Naturwissenschaftlich-Technischen Fakultät III  
Chemie, Pharmazie, Bio- und Werkstoffwissenschaften  
der Universität des Saarlandes

Von

**Christian Brengel**

Saarbrücken

2016

Tag des Kolloquiums: 22.09.2016

Dekan: Prof. Dr.-Ing. Dirk Bähre

Vorsitz: Prof. Dr. Andriy Luzhetskyy

Berichterstatter: Prof. Dr. Rolf W. Hartmann

Prof. Dr. Claus-Michael Lehr

Akad. Mitarbeiter: Dr. Stefan Boettcher

Die vorliegende Arbeit wurde von Januar 2012 bis Januar 2016 unter Anleitung von Herrn Univ.-Prof. Dr. Rolf W. Hartmann in der Fachrichtung 8.2 Pharmazeutische und Medizinische Chemie der Naturwissenschaftlich-Technischen Fakultät III der Universität des Saarlandes sowie am Helmholtz-Institut für Pharmazeutische Forschung Saarland (HIPS) angefertigt.





***„Man sollte alles so einfach wie möglich sehen - aber  
auch nicht einfacher“***

***Albert Einstein***

# SUMMARY

The rising number of resistant bacteria combined with the innovation gap in the antibiotic development has become a huge health problem. Such infections are insufficient to be treated with the approved antibiotic agents on the market resulting in an increasing number of deaths and a financial burden on the healthcare system. Thus, there is a need for antiinfectives with new modes of action.

*P. aeruginosa*, a Gram-negative pathogen often associated with antibiotic resistance, controls the production of major virulence factors and biofilm formation via a quorum sensing system. PqsD and PqsR are key player proteins in this system. The interruption of their function by small molecules should lower virulence of the bacterium without exerting a selection pressure on it. A biophysical method-guided binding mode characterization supports the optimization of these small molecules. Influence of the compounds on biofilm formation validates their pharmacological efficiency on this lifestyle characteristic for chronic infections.

*M. tuberculosis* that still kills millions of people worldwide is hard to be eradicated because of a dormant state and a huge number of resistances. The high content of CYP enzymes encoded in the genome provides a promising base for new drug targets. CYP121 is essential for growth *in vitro*; CYP125 plays an important role for survival *in vivo*. Biophysical and biochemical test systems are used for identification and characterization of the first hit molecules.

# ZUSAMMENFASSUNG

Das zunehmende Auftreten von resistenten Bakterien verbunden mit einer Innovationslücke in der Antibiotikaentwicklung führen zu einer ansteigenden Zahl an Todesopfern und einer finanziellen Belastung des Gesundheitssystems. Folglich besteht ein dringender Bedarf an Antiinfektiva mit neuen Wirkmechanismen.

*P. aeruginosa*, ein Gram-negativer Krankheitserreger, der oft im Zusammenhang mit Antibiotikaresistenzen steht, kontrolliert die Produktion von Virulenzfaktoren sowie die Biofilmbildung mittels eines „Quorum Sensing-Systems“. PqsD und PqsR sind Schlüsselproteine in diesem System. Das Stören ihrer Wirkungsweise mittels kleiner Moleküle sollte die Virulenz des Bakteriums herabsetzen, ohne einen Selektionsdruck auszuüben. Eine biophysikalische Methode zur Aufklärung des Bindungsmodus dieser kleinen Moleküle unterstützt hier auch deren Optimierung. Der Einfluss der Verbindungen auf die Biofilmbildung, die für chronische Infektionen essentiell ist, validiert deren pharmakologische Wirksamkeit.

*M. tuberculosis* tötet immer noch Million Menschen auf der ganzen Welt und ist wegen seiner Dormanz und einer großen Anzahl an Resistenzen schwer zu behandeln. Eine hohe Anzahl an CYP Enzymen im Genom dieser Bakterien bietet eine vielversprechende Grundlage für neue Wirkstofftargets. CYP121 ist essentiell für das *in vitro* Wachstum; CYP125 spielt eine wichtige Rolle für das *in vivo* Überleben. Biophysikalische und biochemische Methoden werden verwendet, um Hit-Verbindungen zu identifizieren und biologisch zu charakterisieren.

# PAPERS INCLUDED IN THIS THESIS

This thesis is divided into four publications and two manuscripts submitted for publication, which are referred to in the text by their letters.

**A Biophysical Screening of a Focused Library for the Discovery of Novel Antimycobacterials targeting CYP121**

Christian Brengel,\* Andreas Thomann,\* Alexander Schifrin, Giuseppe Allegretta, Ahmed Kamal, Jörg Hauptenthal, Sang Hyun Cho, Scott G. Franzblau, Jens Eberhard, and Rolf W. Hartmann

*Manuscript in preparation*

\*These authors contributed equally

**B Discovery and biophysical evaluation of first low nanomolar hits targeting CYP125 of *M. tuberculosis***

Christian Brengel,\* Andreas Thomann,\* Jens Eberhard, and Rolf W. Hartmann

*Manuscript in preparation*

\*These authors contributed equally

**C Biochemical and Biophysical Analysis of a Chiral PqsD Inhibitor Revealing Tight-Binding Behavior and Enantiomers with Contrary Thermodynamic Signatures**

Michael P. Storz,\* Christian Brengel,\* Elisabeth Weidel, Michael Hoffmann, Klaus Hollemeyer, Anke Steinbach, Rolf Müller, Martin Empting, and Rolf W. Hartmann

*ACS Chem. Biol.* **2013**, *8*, 2794-2801.

\*These authors contributed equally

**D Combining in Silico and Biophysical Methods for the Development of *Pseudomonas aeruginosa* Quorum Sensing Inhibitors: An Alternative Approach for Structure-Based Drug Design**

J. Henning Sahner,\* Christian Brengel,\* Michael P. Storz, Matthias Groh, Alberto Plaza, Rolf Müller, and Rolf W. Hartmann

*J. Med. Chem.* **2013**, *56*, 8656-8664.

\*These authors contributed equally

**E Structure Optimization of 2-Benzamidobenzoic Acids as PqsD Inhibitors for *Pseudomonas aeruginosa* Infections and Elucidation of Binding Mode by SPR, STD NMR, and Molecular Docking**

Elisabeth Weidel, Johannes C. de Jong, Christian Brengel, Michael P. Storz, Matthias Negri, Alberto Plaza, Anke Steinbach, Rolf Müller, and Rolf W. Hartmann  
*J. Med Chem.* **2013**, *56*, 6146-6155.

**F Application of dual inhibition concept within looped autoregulatory system toward antivirulence agents against *Pseudomonas aeruginosa* infections**

Andreas Thomann, Antonio G. Gomes de Mello Martins, Christian Brengel, Martin Empting and Rolf W. Hartmann  
*ACS Chem. Biol.* **2016**, *11*, 1279–1286

# CONTRIBUTION REPORT

The author wishes to clarify his contributions to the Publications/Manuscript **A–F** in the thesis.

- A** The author heterologously expressed CYP121 and designed the LC-MS/MS-based functional enzyme assay. He was involved in the synthesis of Mycocyclosin. Furthermore, he planned, executed, measured, and analysed the SPR and heme assay screening. Additionally, he developed the antimycobacterial growth assay and determined the MIC values on *M. bovis*. He planned the project, conceived and wrote the manuscript.
- B** The author heterologously expressed CYP121, CP125, and CYP142. Furthermore, he planned, executed, measured, and analysed the SPR and heme assay screening. He planned the project, conceived and wrote the manuscript.
- C** The author designed and generated the site-directed mutagenesis constructs. Furthermore, he heterologously expressed PqsD and the mutants of the enzyme. He planned, executed, measured, and analysed the ITC experiments. He was significantly involved in the interpretation of the results and contributed to writing of the manuscript.
- D** The author designed and generated the site-directed mutagenesis constructs. Furthermore, he heterologously expressed PqsD and the mutants of the enzyme. He planned, executed, measured, and analysed the SPR and ITC experiments. He was significantly involved in the interpretation of the results and contributed to writing of the manuscript.
- E** The author designed and generated the site-directed mutagenesis constructs. Furthermore, he heterologously expressed PqsD and the mutants of the enzyme. He planned, executed, measured, and analysed the ITC experiments. Furthermore, he contributed to the interpretation of the results.
- F** The author designed and performed the biofilm assay and the antibiotic susceptibility test. Furthermore, he contributed to the interpretation of the results.

# FURTHER PAPERS OF THE AUTHOR THAT ARE NOT PART OF THIS DISSERTATION

## **A Mechanistic details for anthraniloyl transfer in PqsD: the initial step in HHQ biosynthesis**

Michael C. Hutter, Christian Brengel, Matthias Negri, Claudia Henn, Christina Zimmer, Rolf W. Hartmann, Anke Steinbach, Rolf Müller, and Martin Empting  
*J. Mol. Model.* **2014**, 2:2255.

## **B Molecular basis of HHQ biosynthesis: molecular dynamic simulation, enzyme kinetic and surface plasmon resonance studies**

Anke Steinbach Christine K. Maurer, Elisabeth Weidel, Christian Brengel, Rolf W. Hartmann, and Matthias Negri  
*BMC Biophys.* **2013**, 6:10.

## **C Validation of PqsD as an Anti-biofilm Target in *Pseudomonas aeruginosa* by Development of Small-Molecule Inhibitors**

Michael P. Storz, Christine K. Maurer, Christina Zimmer, Nathalie Wagner, Christian Brengel, Johannes C. de Jong, Simon Lucas, Mathias Müsken, Susanne Häussler, Anke Steinbach, and Rolf W. Hartmann  
*J. Am. Chem. Soc.* **2012**, 134, 16143-16146

## **D QSAR-guided Optimization of 2-sulfonylpyrimidines to tackle biofilm formation and eDNA release of *Pseudomonas aeruginosa***

Andreas Thomann, Christian Brengel, Carsten Börger, Dagmar Kail, Anke Steinbach, Martin Empting, and Rolf W. Hartmann  
*Manuscript in preparation*

# Abbreviations

3D	Three dimensional
AQ	2-alkyl-4-quinolones
ACoA	Anthraniloyl coenzyme A
ATP	Adenosine triphosphate
BCG	<i>Mycobacterium bovis</i> BCG
CLSM	Confocal laser scanning microscopy
CoMFA	Comparative Field Molecular Analysis
CV	Crystal violet
CYP	Cytochrome P450 enzyme
DSF	Differential scanning fluorimetry
DMMB	1,9-dimethyl methylene blue
eDNA	Extracellular DNA
FRET	Fluorescence resonance energy transfer
HHQ	4-hydroxy-2-heptylquinoline
HPLC	High Pressure Liquid Chromatography
IC50	Concentration of a drug that is required for 50% inhibition <i>in vitro</i>
igr	Defect in intracellular growth
ITC	Isothermal titration calorimetry
IQS:	Integrated quorum sensing system
IUPAC	International Union of Pure and Applied Chemistry
KA	Association constant
K <sub>D</sub>	Dissociation constant
LC	Liquid Chromatography
MS	Mass spectrometry
MDR	Multi drug resistance
MIC	Minimum inhibitory concentration
Mtb	<i>Mycobacterium tuberculosis</i>
MTT	3-(4,5-dimethylthiazol-2-yl)-2,5-diphenyltetrazolium
NMR	Nuclear Magnetic Resonance Spectroscopy
OD <sub>600</sub>	Optical density at 600nm
PCR	Polymerase chain reaction
PQS	3,4-dihydroxy-2-heptylquinoline
pqs	<i>Pseudomonas</i> quinolone signal
PI	Propidium iodide
QSAR	Quantitative-Structure-Activity-Relationship
RNAP	DNA-dependent ribonucleic acid polymerase



SPR	Surface plasmon resonance spectroscopy
SPW	Surface plasmon wave
TB	Tuberculosis
TDR	Totally drug-resistant
XDR	Extensively drug-resistant

# Contents

<b>1</b>	<b>Introduction</b> .....	<b>1</b>
1.1	<i>Mycobacterium tuberculosis</i> .....	2
1.1.1	Mycobacterial CYP enzymes .....	3
1.2	<i>Pseudomonas aeruginosa</i> .....	5
1.2.1	Quorum sensing systems in <i>P. aeruginosa</i> .....	6
1.2.2	The “Pseudomonas Quinolone Signal” and its influence on virulence factors and biofilm .....	8
1.2.3	Biofilm and persistence .....	9
1.2.4	PqsD as a key enzyme in the synthesis of HHQ and PQS.....	10
1.3	Rational Drug Design.....	11
1.3.1	Ligand-based approaches .....	12
1.3.2	Structure-based approaches .....	12
1.3.3	Biochemical and molecular biological assay systems in rational drug design .....	13
1.3.4	Biophysical methods in rational drug design .....	20
<b>2</b>	<b>Aims of the thesis</b> .....	<b>27</b>
<b>3</b>	<b>Results</b> .....	<b>30</b>
A	Biophysical Screening of a Focused Library for the Discovery of Novel Antimycobacterials targeting CYP121 .....	30
B	Discovery and biophysical evaluation of first low nanomolar hits targeting CYP125 of <i>M. tuberculosis</i> .....	52
C	Biochemical and Biophysical Analysis of a Chiral PqsD Inhibitor Revealing Tight-Binding Behavior and Enantiomers with Contrary Thermodynamic Signatures.....	68
D	Combining in Silico and Biophysical Methods for the Development of Pseudomonas aeruginosa Quorum Sensing Inhibitors: An Alternative Approach for Structure-Based Drug Design.....	88
E	Structure Optimization of 2-Benzamidobenzoic Acids as PqsD Inhibitors for Pseudomonas aeruginosa Infections and Elucidation of Binding Mode by SPR, STD NMR, and Molecular Docking .....	110
F	Application of dual inhibition concept within looped autoregulatory system toward antivirulence agents against <i>Pseudomonas aeruginosa</i> infections.....	134

<b>4</b>	<b>Final Discussion .....</b>	<b>152</b>
4.1	Targeting bacterial of CYP enzymes.....	152
4.1.1	Targeting CYP121 as a new antimycobacterial strategy (Manuscript A) .....	152
4.1.2	Blockage of cholesterol metabolism induces <i>in vivo</i> intoxication (CYP125) (Manuscript B).....	155
4.2	Interrupting pqs system as anti-virulence and -biofilm strategy (Publications: C-E) .....	157
4.2.1	Biophysical methods in the prediction of binding modes .....	159
4.2.2	Targeting biofilm as a bacterial lifestyle in chronic infections (Publication: F) .....	164
4.3	New antimicrobial targets and anti-virulence strategy .....	166
4.4	Outlook.....	167
<b>5</b>	<b>References .....</b>	<b>169</b>
<b>6</b>	<b>Acknowledgements.....</b>	<b>177</b>
<b>7</b>	<b>Appendix .....</b>	<b>180</b>
7.1	Supporting Informations.....	180
7.2	Curriculum Vitae.....	393





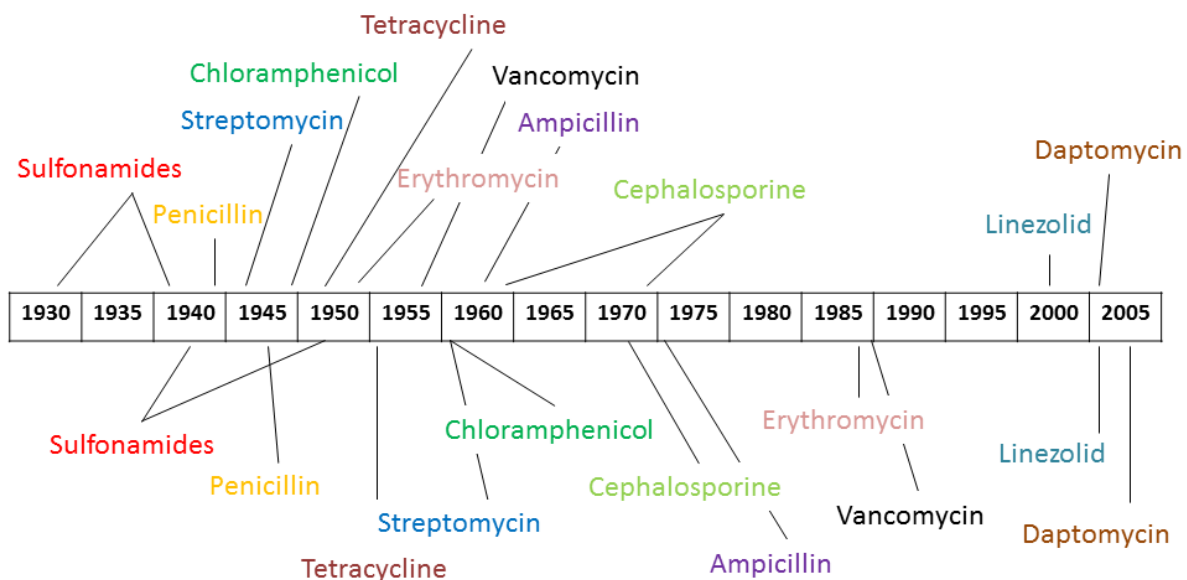
# 1 Introduction

In the so-called “pre-antibiotic era”, infectious diseases were among the major causes for human morbidity and mortality. <sup>[1]</sup> At the beginning of the 20<sup>th</sup> century, first progress in medical science yielded decisive breakthroughs, which were able to change this unsatisfactory situation. Especially, the research of Paul Ehrlich resulting in atoxyl, the first synthetic antimicrobial drug, and the discovery of the natural product penicillin by Alexander Fleming heralded a period designated as the “antibiotic era”. <sup>[2,3]</sup> These early success stories were followed by the “golden era of antibiotic discovery” from the 1950s to 1970s, which culminated in a hasty statement of the Surgeon General of the United States of America, William Stewart, in 1967: “The time has come to close the book on infectious diseases. We have basically wiped out infection in the United States.” <sup>[4,5]</sup> Indeed, introduction of antibiotics on the market significantly lowered the mortality rate of bacterial infections. <sup>[6]</sup> However, the occurrence of the first clinically observed resistances destroyed all hopes to close the books of infectious diseases. Interestingly, in the 1930s, first reports about a sulfonamide-resistant *Streptococcus pyogenes* in the military environment came out, where the antibiotic was used prophylactically. <sup>[7]</sup> The emergence of multi drug-resistant (MDR) bacteria is associated with severe clinical problems and increasing healthcare costs. <sup>[8]</sup> The World Health Organization (WHO) specifies different groups of patients in modern medicine that rely on appropriate antibiotic therapy like, for instance, immunocompromised, surgical, or critically ill patients. Now that the antibiotic sources have run out, these patients are threatened by an increasing number of resistant bacteria. <sup>[9]</sup> Such resistances can occur endogenously by gene mutations under selection pressure or exogenously through transmission of genetic material. These genetic changes encode for different mechanisms of resistance like mutations of the target, efflux pumps, reduced permeability etc. The responsible genes are summarized under the term “resistome”. <sup>[10]</sup> A closer look into the time line of antibiotics introduction to the market and the development of resistances against them efficiently demonstrates the challenge of this issue (**Figure 1**). <sup>[11]</sup> Moreover, the misuse or overuse of antibiotics in clinics and agriculture accelerated the appearance of resistant mutants. <sup>[12]</sup> Tempted by the early success story and the negligence concerning the increased inefficiency of available drugs between 1962 and 2000, no new antibiotic class was introduced to the market. <sup>[13]</sup> These facts demonstrate that there is an urgent need for new strategies to overcome aforementioned bacterial resistances. Unfortunately, identification of new potent candidates seems to be difficult to realize. The majority of approved antibiotics originate from natural sources like *Streptomyces* (Waksman platform), which, however, seem to be exploited. Furthermore, high throughput screenings and rational drug design campaigns of pharmaceutical companies completely failed. <sup>[14]</sup>

There is a need for novel ways of thinking, especially in case of rational design of new antibiotics. Our concepts of how to develop a drug against bacteria have to be reconsidered to overcome the problems that led to the failure of previous development campaigns. <sup>[15]</sup> Besides addressing special requirements directly linked to characteristics of a new bacterial target, there are additional parameters that have to

be taken into account. For example, it is necessary to keep in mind that physicochemical properties needed to enter bacterial cells follow different rules than those defined for eukaryotic cells. Furthermore, structural properties that could be recognized by efflux pumps have to be excluded from design concepts. Hence, an early proof of intracellular activity is important. Apart from the typical antibiotic concept, new approaches have to be followed to overcome the resistance crisis. An example is to avoid targets associated with direct killing of bacteria and, instead, focus on pathways that control their pathogenicity. This anti-virulence strategy could possibly prevent resistance development by supporting the patient's immune clearance. <sup>[10,14,16]</sup>

## Antibiotic deployment



## Antibiotic resistance observation

**Figure 1.** Link between antibiotic deployment and observation of resistant bacterial strains [adapted from Clatworthy, Pierson et. al <sup>[11]</sup>]

### 1.1 Mycobacterium tuberculosis

*M. tuberculosis* (Mtb) is the leading cause for the infectious disease ‘tuberculosis’ (TB). <sup>[17]</sup> The bacterium has a long history. Archaeological discoveries of skeletons with bone TB older than 4000 years gave evidence for the age of the disease. <sup>[18]</sup> In 1882, Robert Koch described the connection between the symptoms of TB and the bacterium Mtb for the first time, leading to a deeper

understanding of the disease.<sup>[17]</sup> Most common transmission route of the bacterium is a droplet infection. Mtb typically affects the alveolar macrophages of the lungs and survives inside of these cells. The result is an attraction of polymorphonuclear leukocytes to the infection site and an immunoreaction that ends in the development of granuloma. Furthermore, Mtb is able to enhance the survival rate in macrophages by blocking phagosome maturation.<sup>[19]</sup> In an advanced stage, the bacteria are able to adopt a dormant state, which is not easy to be treated with conventional antibiotics.<sup>[20]</sup>

The development of chemotherapeutics against Mtb started with the discovery of streptomycin in the early 19<sup>th</sup> century.<sup>[21]</sup> Initial success stories culminated in a broad range of first line (isoniazid, rifampicin, ethambutol, and pyrazinamide) and second line (kanamycin, amikacin, mifloxacin, ethionamid, etc.) antimycobacterial agents, which are deployed depending on susceptibility of the bacterium or physical condition of the patient.<sup>[22]</sup> Despite versatile options for the treatment, TB is still a major cause of death by a bacterial infection. The WHO registered 1.5 million deaths caused by TB and 9 million new infections in the year 2013.<sup>[23]</sup> One key problem making the treatment challenging is the insusceptible dormant state demanding the need for a long term therapy.<sup>[24]</sup> This fact hampers the eradication especially in economically weak countries.<sup>[25]</sup> Additionally, there is an increased global rate of multidrug-resistant and extensively drug-resistant TB (MDR-TB and XDR-TB).<sup>[21]</sup> The emergence of totally drug-resistant TB (TDR-TB) emphasises the urgent need for new anti-TB drugs.<sup>[26]</sup>

### 1.1.1 Mycobacterial CYP enzymes

The elucidation of the Mtb genome in 1998 created a base for the identification of new potential drug targets.<sup>[27]</sup> Surprisingly, the sequencing uncovered an unexpectedly high content of genes encoding for cytochrome P450 (CYP) enzymes. The occurrence of such CYP enzymes distinguishes Mtb from most other pathogenic bacteria. With respect to the differences in their size, the percentage of CYP enzymes (20 Mtb CYPs) in Mtb is higher than that in the human genome.<sup>[28]</sup> CYP enzymes typically catalyze an oxygenation with the help of the cofactor heme (iron protoporphyrin IX).<sup>[29]</sup> The name P450 originates from the spectroscopically observed absorbance maximum at 450 nm after the complexation of carbon monoxide in the reduced iron stage.<sup>[30]</sup> The addition of the oxygen to the substrate occurs in several steps depicted in **Figure 2. b**).<sup>[31]</sup> A large number of studies confirm a contribution of CYP enzymes to viability and virulence of Mtb.<sup>[29,32]</sup>

CYP121 came in the focus of drug development as it was shown to be essential for Mtb viability. A deletion of CYP121 gene resulted in an Mtb mutant that was not able to grow *in vitro*. Furthermore, the affinity of different azole antifungals to CYP121 correlated with their ability to inhibit mycobacterial growth.<sup>[33,34]</sup> The enzymatic function of CYP121 was elucidated by a detailed look at the adjacent gene clusters.<sup>[35]</sup> The enzyme is responsible for the conversion of cyclodityrosine (cYY) to mycocyclosin (**Figure 2. a**). However, the function of substrate or product in the biological context is still unknown.<sup>[35,36]</sup> The fact that CYP121 is essential for viability promoted the development of



selective inhibitors for this enzyme. However, no inhibitory effects on Mtb cells have been reported. [32] Although the CYP121-binding azole antifungals possess a promising *in vitro* and *in vivo* anti-TB activity, their clinical use for this indication is difficult due to their problematic selectivity and pharmacokinetic profile. Given by the fact that the azoles with the best antimycobacterial efficacy only have a low oral bioavailability, high dose are needed for a sufficient effect. This high dose combined with the long term treatment of Mtb infection increases the possibility of adverse effects. [37–44]

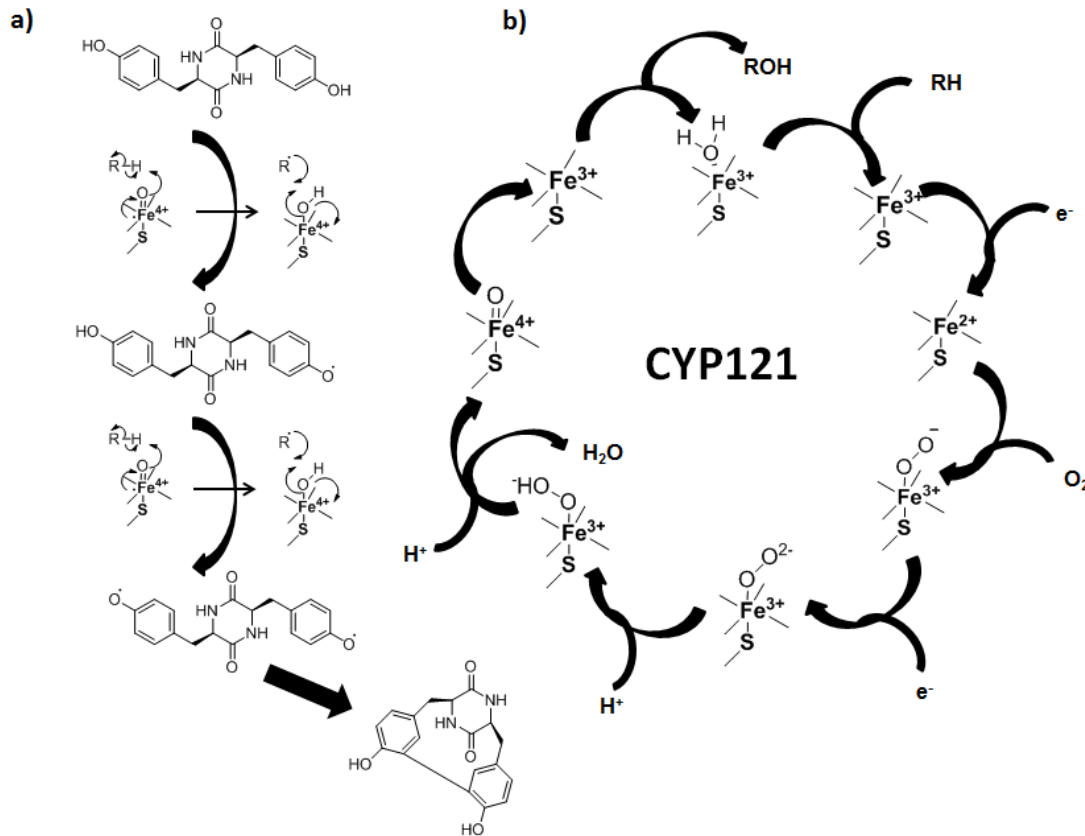


**Figure 2.** a) Proposal for the detailed mechanism of cYY conversion to mycocyclosin by CYP121 [adapted from Belin et al. [35]]. b) CYP121 as an example for the P450 catalytic cycle mechanism [adapted from Munro et al. [31]].

A second P450 enzyme, CYP125 was shown to be essential for Mtb survival in mice. [29] The discovery of CYP125 as a target enzyme started with identification of a region in the Mtb genome, which was required for survival in macrophages and mice. [45,46] The following studies renamed the region “*igr*” (defect in intracellular growth), which encodes for several proteins. [47] Further investigations identified the *igr* region as a major player in cholesterol metabolism. [48] Although the role of *igr* was clarified, there was still a missing link between cholesterol and intracellular growth. Two studies answered the question by producing knock-out mutants in *Mycobacterium bovis* (close

relative to Mtb) and two Mtb strains. CYP 125 seemed to be the key player in the *igr* operon. A knock-out leads to an intoxication of the bacteria under cholesterol pressure by the metabolite cholest-4-en-3-one (Figure 3).<sup>[49,50]</sup> Even though there is a bypass enzyme (CYP 142) in the Mtb lab strain, clinical isolates seem to lack such a surrogate.<sup>[49,51]</sup> Furthermore, cholesterol is a nutrition source and degradation products are used in the production of virulence factors.<sup>[52]</sup> Additionally, cholesterol seems to play a role in persistence.<sup>[53]</sup> These findings render CYP125 an attractive target for drug design.<sup>[52]</sup>

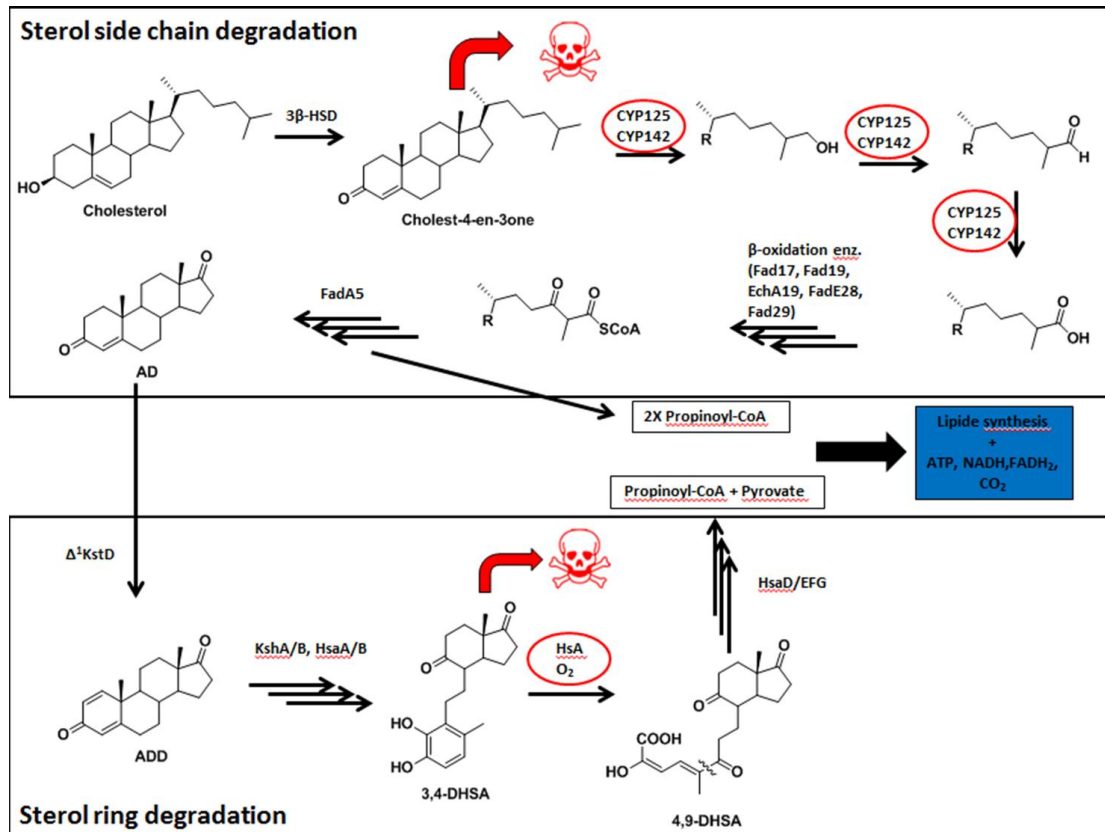


**Figure 3.** Cholesterol metabolism in Mtb with focus on the side chain degradation by CYP125 [adapted from Ouellet et al.<sup>[52]</sup>].

## 1.2 Pseudomonas aeruginosa

*Pseudomonas aeruginosa* is a common opportunistic pathogen that belongs to the group of Gram-negative bacteria.<sup>[54]</sup> The natural habitat includes soil and surfaces in aqueous environment. *P. aeruginosa* demonstrates a high degree of adaptability and resistance to antibiotic agents.<sup>[55]</sup> Therefore, it is not surprising that this pathogen is able to colonize a variety of human tissues. Frequent occurrence of infections in the bloodstream, ear, respiratory and urinary tract could be observed, especially as a secondary infection of immunocompromised patients. In this context, there is a high incidence of nosocomial infections in patients suffering from cystic fibrosis. Due to a high

intrinsic resistance to common antibiotic therapy and a strong tendency to form new resistance mechanism, such an infection is hard to be treated. <sup>[56]</sup> Examples for intrinsic and acquired resistances are efflux pumps (e.g., cephalosporins, carbapenems, aminoglycosides and quinolones), outer membrane impermeability (e.g., carbapenems, aminoglycosides, and quinolones),  $\beta$ -lactamases (e.g., penicillins), target mutations of gyrase (e.g., quinolones), and membrane changes of lipid A (e.g., aminoglycosides, polymyxins). <sup>[57]</sup> Accordingly, there is an urgent need for new therapeutic options. A problem with standard bacteriostatic or bactericidal approaches is the fact that these lead to a selection pressure, which again supports the formation of resistance. Therefore, a promising concept could be a so-called “anti-virulence strategy”. <sup>[58]</sup> Virulence factors are molecules produced by the pathogen to invade the host or escape from defence mechanisms. <sup>[59]</sup> That means, in theory, that blocking virulence factor production decreases pathogenicity and facilitates the clearance of pathogens by the immune system. An advantage of this strategy over conventional antimicrobial therapy concepts is the avoidance of selection pressure towards the bacteria and, consequently, of resistance development. <sup>[58]</sup> In *P. aeruginosa*, certain virulence factors and resistance mechanisms are controlled by special signal systems, which represent a more comprehensive target for interference with pathogenicity. <sup>[60]</sup>

### 1.2.1 Quorum sensing systems in *P. aeruginosa*

A first description of such a signal system was made in 1979 for the marine bacteria *Vibrio fischeri* and *Vibrio harveyi*, where it served as a control mechanism for group behaviour like bioluminescence. <sup>[61]</sup> Later, the concept of bacterial communication was defined as “quorum sensing (QS)”. <sup>[62]</sup> The principle came more and more into focus as similar signalling systems were described for other bacterial species, among those also human pathogens. Studies have shown that several pathogens control the expression of certain virulence factors via a QS system. <sup>[63]</sup> *P. aeruginosa* uses QS for the cell density-dependent control of virulence factors expression and biofilm formation. <sup>[64]</sup> This system offers an innovative point of attack for a comprehensive anti-virulence strategy to overcome resistance development.

The *P. aeruginosa* QS system consists of three major control cycles (*las*, *rhl*, *pqs*). <sup>[64]</sup> Every cycle is composed of three main parts: the signal molecules, their biosynthesis enzymes, and the receptors. Signal molecule concentration regulates the activity of the specific control cycles. At a crucial threshold, these signals trigger their own expression and thus, they are designated as “autoinducers”. The second key component is the receptor that regulates gene expression after QS signal binding. Those genes include clusters encoding for biosynthesis enzymes of the QS signal molecules and virulence factors. <sup>[64]</sup> As depicted in **Figure 4**, the *las* system consists of the QS signal molecule (*N*-(3-oxododecanoyl)homoserine lactone (3-oxo-C12-HSL)), the synthase of the QS signal (LasI), and the transcription regulation receptor (LasR). <sup>[65]</sup> The same basic structure can be transferred to the *rhl* system with *N*-butanoylhomoserine lactone (C4-HSL) as QS signal, RhlI as the signal synthase, and RhlR as receptor. <sup>[66]</sup> On top of that, *P. aeruginosa* deploys a third unique control cycle, the so-called

“*Pseudomonas* quinolone signal” (*pqs*). The *pqs* system is only present in *Pseudomonas* and *Burkholderia* species. <sup>[67]</sup> Signal molecules of the system originate from the family of 2-alkyl-4-quinolones (AQs). <sup>[68]</sup> The main autoinducers, which interact with the receptor and trigger their own production, are 3,4-dihydroxy-2-heptylquinoline (PQS) and its precursor 4-hydroxy-2-heptylquinoline (HHQ). <sup>[69]</sup> An early precursor molecule of AQ synthesis is anthranilic acid, which is synthesized from a complex encoded by genes that are located adjacent to the *pqs* operon. <sup>[70]</sup> The *pqs* operon itself (*pqsABCDE*) contains the genes encoding for PqsA, PqsD, PqsB, and PqsC required for the synthesis of AQs. <sup>[71]</sup> The precise function of PqsE is still under discussion. Results from different studies suggest that PqsE acts as an effector of AQ execution or is a part of the AQ biosynthesis pathway. <sup>[60,72]</sup> PqsH, which is necessary for the conversion of HHQ to PQS, is not encoded within the *pqs* operon. <sup>[70]</sup> However, both signal molecules bind to *pqs* receptor (PqsR) and increase its activity as a transcription regulator. <sup>[69]</sup> This leads to activation of *pqs* operon and a direct or indirect expression of virulence factor-associated genes. <sup>[67]</sup> *Las*, *rhl*, and *pqs* are not separated from each other. On the contrary, these control cycles are able to interconnect with each other. <sup>[60]</sup> The detailed mechanism of cooperation is still not completely understood, but a rough overview can be seen in **Figure 4**. The *las* system increases the activation of the *rhl* and the *pqs* system. The *pqs* system positively regulates *rhl* in contrast to the negative feedback of *rhl* on *pqs*. <sup>[64]</sup> The overall picture is completed by a forth integrated system. The so-called “*iqs*” is able to take over the functions of other systems. <sup>[73]</sup> The main task of the control cycles (*las*, *rhl* and *pqs*) is the adaption of virulence factor production to environmental situation. Especially, the *pqs* system with its important role in the control of virulence factors and biofilm formation might be an attractive target system for a global anti-virulence therapy <sup>[74]</sup> and will be discussed in the next two chapters.

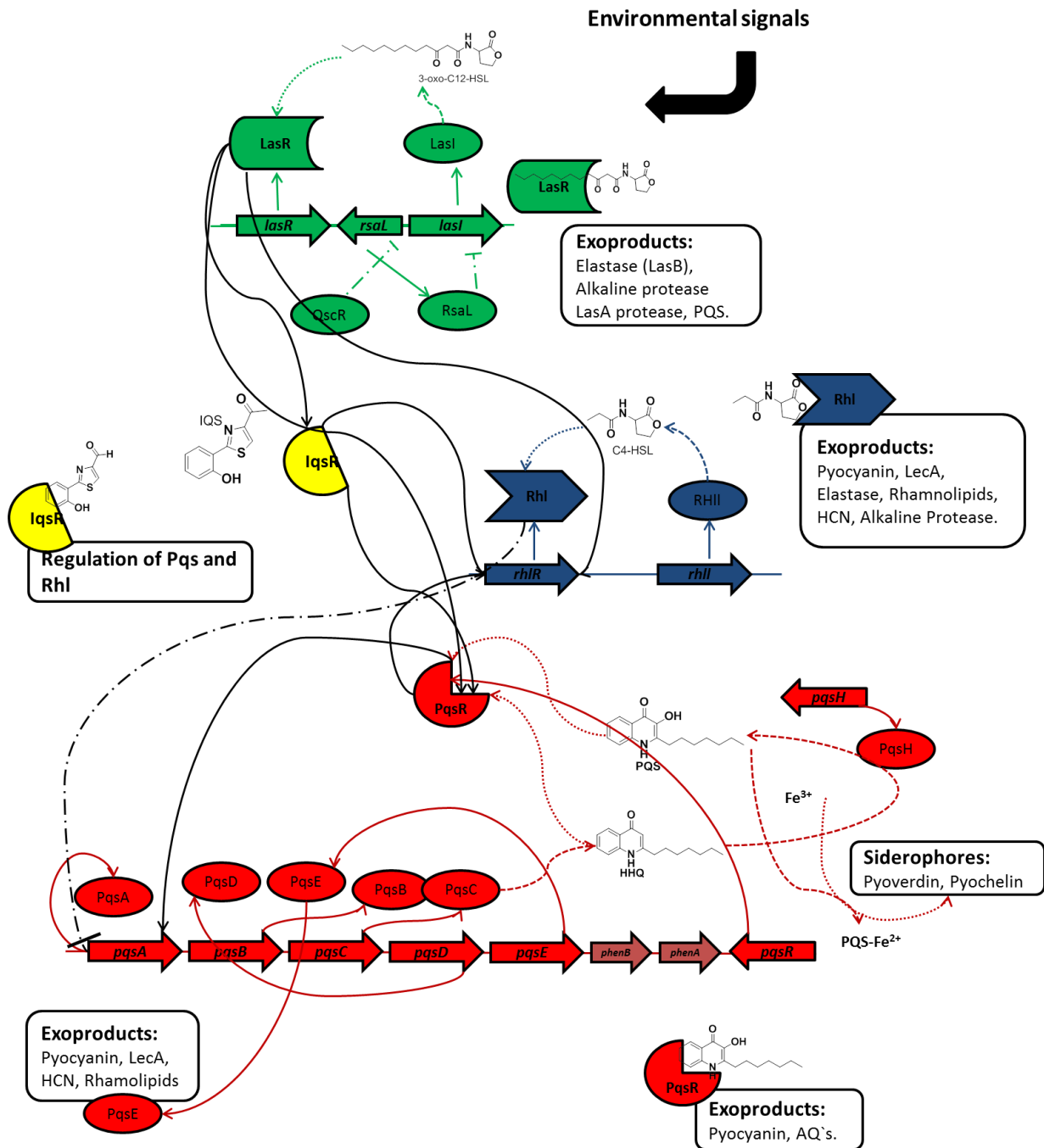


**Figure 4.** The overview represents the interconnection of the quorum sensing systems in *P. aeruginosa*. [adapted from Lee et al. and Dubern et.al.<sup>[64,67]</sup>]

### 1.2.2 The “Pseudomonas Quinolone Signal” and its influence on virulence factors and biofilm

*P. aeruginosa* produces a broad arsenal of virulence factors used for establishment in host and competition with the immune system. The *pqs* system directly and indirectly takes over control of essential virulence factors. A major virulence factor directly controlled by PqsR is pyocyanin.<sup>[71,75]</sup> This redox active blue-green pigment damages human lung epithelial cells.<sup>[76,77]</sup> A second virulence

factor regulated by PQS is elastase, also called lasB<sup>[68]</sup> This metalloprotease is capable of damaging tissues and degrading various immune components.<sup>[78]</sup> Furthermore, it was shown that production of hydrogen cyanide, a toxin that acts via blockage of the cell respiration cascade, is affected by *pqs* genes.<sup>[71]</sup> Indirectly, the *pqs* system influences the pyoverdine and rhamnolipid production by interfering with the rhl system.<sup>[71,79]</sup> Pyoverdine is an iron scavenger molecule and important for virulence in a mouse model.<sup>[80]</sup> Rhamnolipids are known to lyse several types of immune cells.<sup>[81]</sup> On top of that, PQS directly induces a downregulation of the host's immune response.<sup>[82]</sup> Besides the described influence on important virulence factors, the role of *pqs* system on biofilm formation and persister cells should not be underestimated.<sup>[74,83]</sup>

### 1.2.3 Biofilm and persistence

A biofilm is an extracellular polymeric matrix consisting of various molecular structures surrounding living bacterial cells. The biofilm embed bacteria of different species and protect them from a hostile environment like for example the immune system of a host. *P. aeruginosa* also produces biofilms in the human body.<sup>[84]</sup> The main components of a biofilm are polysaccharides (Psl, Pel, and alginate), extracellular DNA (eDNA), proteins, rhamnolipids, and surface components of bacterial cells. The biofilm maturation occurs in several steps, which are summarized in **Figure 5**.<sup>[84,85]</sup> Biofilms and persister cells play a crucial role in chronic *Pseudomonas* infections of cystic fibrosis patients.<sup>[86]</sup> Persister cells are dormant cells with a low level of metabolism and a high tolerance to antibiotics. However, these persisters can be cleared by the immune system. In contrast, biofilm does not only block several antibiotics but also protects the bacteria from the attack of the immune system. This means persister cells inside a biofilm can form a source of relapsing and chronic infections.<sup>[87]</sup>

The *pqs* system regulates the formation of different biofilm components. In a  $\Delta pqsE$  mutant, no galactophilic lectin, LecA, is produced. LecA is necessary to complete biofilm formation<sup>[88,89]</sup> Furthermore, the eDNA as a major component of a biofilm is also controlled by the *pqs* system.<sup>[83,90]</sup> Moreover, PqsR antagonists and PqsD inhibitors were shown to decrease biofilm formation.<sup>[91,92]</sup> An interesting result described in a recent study is the influence of the *pqs* system on persister cells. The blockade of PqsR results in a decreased number of *P. aeruginosa* persister cells.<sup>[74]</sup>

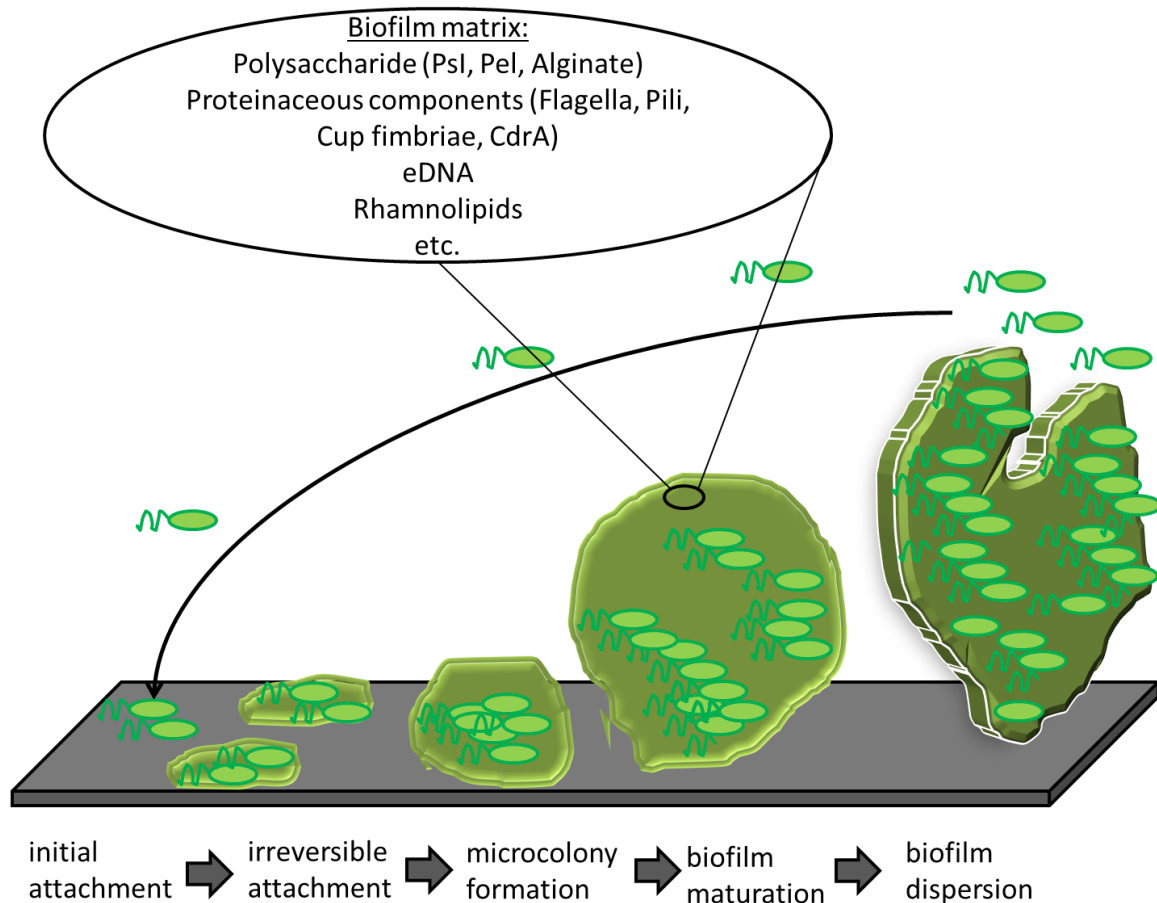


**Figure 5.** A summary of the individual biofilm components and the maturation of a biofilm population [adapted from Wei et al. <sup>[84]</sup>]

#### 1.2.4 PqsD as a key enzyme in the synthesis of HHQ and PQS

PqsD was shown to completely catalyse HHQ synthesis *in vitro* by utilizing the two precursor molecules anthraniloyl coenzyme A (ACoA) and  $\beta$ -ketodecanoic acid. However, recent results indicate a different *in cellulo* biosynthesis route. This pathway assumes that PqsD catalyses the reaction of ACoA and malonyl-CoA producing 2-aminobenzoylacetate (2-ABA). 2-ABA is further used by the PqsB/C complex to synthesize HHQ. <sup>[93]</sup> Nevertheless, both theories confirm PqsD as a key enzyme in the signal molecule synthesis (**Figure 6.**). In crystallographic studies, PqsD forms a dimer and shows a similarity to FabH and chalcone synthase, which are enzymes from fatty acid and polyketide metabolism. Especially, the polar amino acids Cys112, His257, and Asn287 in the catalytic centre represent interesting residues for possible ligand-receptor interactions. Most probably only Cys112 and His257 are involved in the first step of the enzyme reaction. <sup>[94]</sup> In this reaction anthranilic acid is transferred from ACoA to Cys112. <sup>[95]</sup> An inhibition of PqsD was shown to inhibit signal molecule (HHQ and PQS) production and biofilm formation. <sup>[91]</sup>

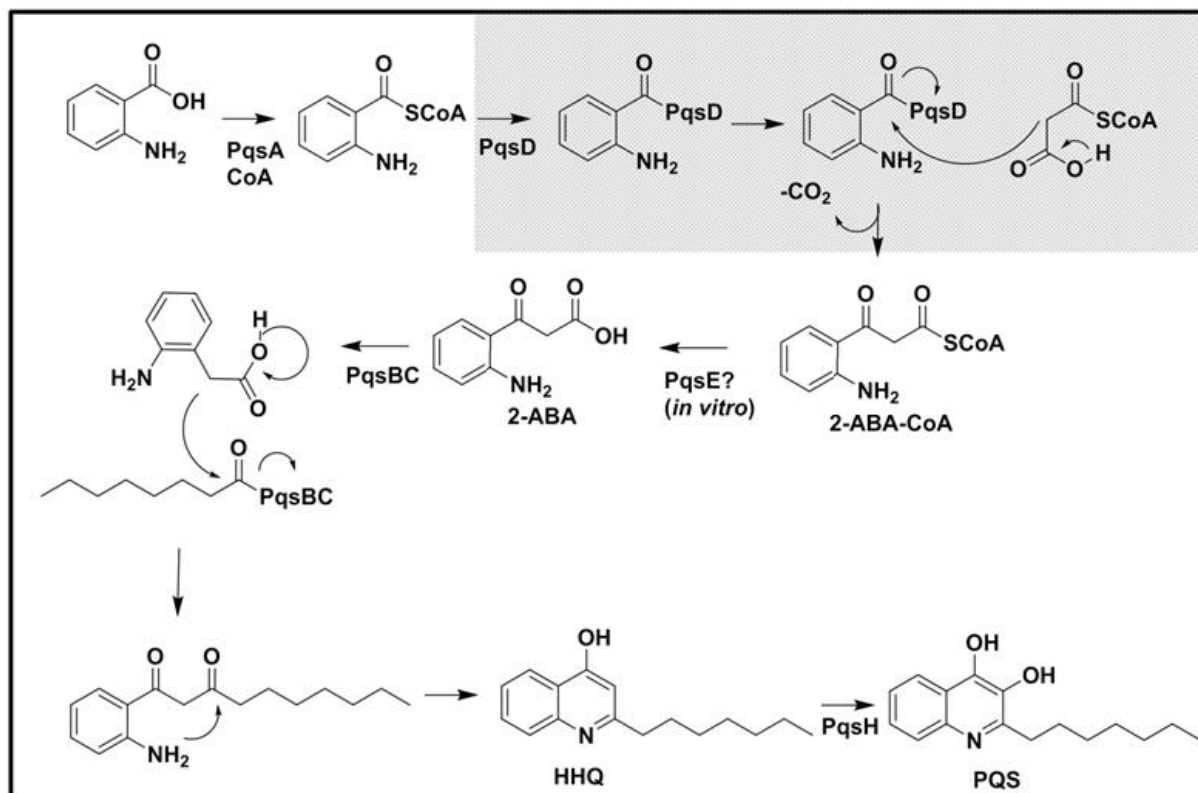


**Figure 6.** This depiction describes the biosynthesis pathway of HHQ and PQS as the major signalling molecules of the *pqs* system. The gray box highlights PqsD as a key enzyme in the system. [adapted from Dulcey et al. and Drees et al. <sup>[72,93]</sup>]

### 1.3 Rational Drug Design

The term rational drug design summarises techniques for the identification of new therapeutics under consideration of all information known about physiological and pathophysiological targets. <sup>[96]</sup> The technique can be divided into two major approaches: the ligand-based and the structure-based concept. <sup>[97]</sup>

The origin of rational drug design is deeply rooted in the early antibiotic research successes. Driven by the first theories in organic chemistry at the end of the 18<sup>th</sup> century, e.g. Avogadro's atomic hypothesis, a more directed synthesis of molecules was possible. This influenced the production of particular dyes, which were the base for Paul Ehrlich's theory of the "chemoreceptors" and, thus, for pharmacology and rational drug design. <sup>[98]</sup> From that point on, academic working groups and pharmaceutical companies made many efforts in the identification of natural and synthetic compounds with pharmacological efficiency. This early drug discovery was dominated by phenotypic screening approaches and derivatization of natural products. The first steps to modern rational drug design were made in the 1960s with the identification of receptor function and ion channels. <sup>[99]</sup> Pioneering works from researchers like Topliss and Hansch provided the basis for the so-called ligand-based approach; a



today's often used method in drug discovery. <sup>[100-102]</sup> Another ground-breaking event took place as David C. Phillips described the elucidation of the first 3D-protein structure of an enzyme in 1965. <sup>[103]</sup> This was the fundamental starting point for the structure-based design. Several years ago, Kendrew reported the first protein crystal structure originating from sperm whale myoglobin. <sup>[104]</sup> The rise of the genomic era in 1990 provided more information about reasons for the occurrence of diseases and the biochemical background. <sup>[105]</sup> Together with the better understanding of diseases, more and more techniques and approaches were invented facilitating rational drug design. <sup>[106]</sup> Examples will be discussed in the following sections.

### 1.3.1 Ligand-based approaches

The ligand-based approach relies on the knowledge of ligands that bind to the target structure. <sup>[107]</sup> It is not necessary to have information about the 3D-structure of the target. Only those chemical properties that are essential for affinity are taken into consideration. <sup>[108]</sup> In principle, the concept starts with the determination of a pharmacophore model, which is defined by IUPAC (International Union of Pure and Applied Chemistry) in the following way: "A pharmacophore is the ensemble of steric and electronic features that is necessary to ensure the optimal supramolecular interactions with a specific biological target structure and to trigger (or to block) its biological response". <sup>[109]</sup>

Early methods described for example by Hansch, Topliss, and Andrews combined statistical and experimental data to simple rules useful for rational compound evaluation and optimization. Hansch and coworkers created a tool for the comparison of biological activity and physicochemical properties to create a quantitative-structure-activity-relationship (QSAR). This resulted in a mathematical equation known as the "Hansch-Analysis". <sup>[102,110]</sup> In further studies, Topliss revealed a method that applied the Hansch-Analysis to medicinal chemistry by introduction of simple synthesis schemes. <sup>[100,101]</sup> Another method invented by Andrews to characterize a hit compound originating, for example, from an experimental screening should simplify the optimization process. <sup>[111]</sup>

Modern methods are computer-based to analyse a more complicated set of data. The aims are similar to the older approaches and include the interpretation of physicochemical properties, which are important for the desired interactions. A prominent example is the Comparative Molecular Field Analysis (CoMFA), which facilitates a QSAR in a three-dimensional room (3D-QSAR). For this purpose the method combines molecular interaction fields and physicochemical properties of the molecules without any structural information about the target. <sup>[112]</sup>

### 1.3.2 Structure-based approaches

The IUPAC defines this process roughly as drug design based on the 3D-structure of the target. <sup>[109]</sup> The aforementioned elucidation of the myoglobine and lysozyme as the first X-ray structures of proteins were basic work for this approach. <sup>[103,104]</sup> Today, structural data of the enzymes originate from X-ray crystallography, Nuclear Magnetic Resonance Spectroscopy (NMR), or homology

modelling. <sup>[111]</sup> An observed protein structure can be used in different ways as a starting point for the finding of a potential drug candidate.

Often used approaches for the finding of first hit candidates are computer methods. A pharmacophore model build up from the protein structure can be used for a virtual screening or a de novo design. <sup>[112,113]</sup> Virtual screening is a method, where a large database of compounds undergoes various docking steps based on the pocket of the target protein. Following definitions for the two terms are given by IUPAC: “Docking studies are molecular modelling studies aiming at finding a proper fit between a ligand and its binding site”; “De novo design is the design of bioactive compounds by incremental construction of a ligand model within a model of the receptor or enzyme active site, the structure of which is known from X-ray or NMR data.” <sup>[109]</sup> The procedures are followed by an experimental confirmation of the hit in a biochemical or biophysical assay. <sup>[114]</sup>

More precise information could be obtained via a co-crystallization of compounds identified by virtual or experimental screening. Depending on the quality of the structure it is possible to identify all important interactions (hydrogen bonds (H-bonds), Van-der-Waals, or electrostatic interactions etc.). This information can be used as a template for straightforward optimization. The data guide a directed targeting of important amino acids or empty site pockets at the target protein to increase affinity and selectivity of a hit compound. <sup>[106,115]</sup> The aforementioned approach is often used for hit or lead optimization. In case of fragment-based hit finding strategies, a co-crystallization is indispensable. Fragments are compounds with a molecular weight lower than 300 Da. Dependant on their structure and molecular interaction properties they can bind in different parts of the target protein. Merging or linking of these fragments guided by co-crystal structure can lead to a high-affinity ligand. <sup>[106,114]</sup> Driven by the advancements in protein crystallization new approaches combine fragment-based drug design and crystallography to an elegant screening method, which extends the applicability of structure based drug design. <sup>[116]</sup>

### 1.3.3 Biochemical and molecular biological assay systems in rational drug design

Before a rational drug design process can be applied, a biological structure has to be identified and validated as a suitable target. <sup>[117]</sup> If the target discovery is successfully completed, first hits for the selected target have to be identified. Despite technical advances in the biophysical field, a routine hit identification is based on biochemical or molecular biological screening systems. Furthermore, biological assays play an important role in subsequent hit and lead characterization steps of drug development. <sup>[117]</sup> Since the early concepts in the 1930s defined enzymes and receptors as suitable drug targets, the development of applicable biochemical test systems has been accelerated. <sup>[98]</sup> In the field of biochemical and molecular biological methods, two trends can be distinguished: cell-based or target-based assay systems. <sup>[118,119]</sup> Depending on the expected outcome both methods have their advantages and disadvantages. <sup>[120–122]</sup> Caused by the diversity of target systems and their

requirements, a lot of different assays have been developed. Widely used techniques are for example: fluorescence resonance energy transfer (FRET) coupled enzyme assays, and fluorescence polarization. These *in vitro* test systems can be divided in simple binding and functional assays. However, the latter normally provide more information about the tested compound, because natural ligand or substrate is involved in the molecular interplay.<sup>[123]</sup> During the course of an assay development or even a protocol adaption procedure, a lot of parameters have to be taken into consideration. Buffer pH, ion strength, temperature, solvent composition, and concentrations of substrate, enzyme and cofactors are crucial parameters influencing enzyme reaction.<sup>[121]</sup> One of the most commonly used metrics to assess the quality of a test system is the Z'-value. This improved the signal-to-noise ratio as a quality factor by the introduction of a positive and a negative control.<sup>[123]</sup> Special binding and functional assays, as well as cell based assay systems were used in this thesis to characterize biological behaviour of our compounds. Further descriptions of these approaches can be found in the following sections.

### 1.3.3.1 Binding assay: UV/Vis-assay for P450 enzyme interaction

A binding assay is a simple method used in drug discovery to determine the affinity of a compound to the target. The outcome of this method is typically the association constant ( $K_A$ ) or the dissociation constant ( $K_D$ ) of a ligand-target interaction.<sup>[124,125]</sup> An often used method for determination of binding to CYP enzymes is the UV/Vis spectroscopic heme coordination assay (A more detailed specification of CYP enzymes can be found in chapter: **1.1.1**). It is based on the interaction of a compound with the heme iron in the catalytic centre of the protein.<sup>[126,127]</sup> The interaction with the heme iron leads to a shift of the enzyme Soret band (Soret band: typical absorbance band of CYP enzymes at a wavelength of approximately 420 nm). A direct coordination of the heme shifts the iron from the high- to the low-spin state with a maximum between 425 – 430 nm. This behaviour is designated as “type-II-binding”. The coordination blocks binding of the substrate and hinders the first iron reduction step in the enzyme reaction. Approved CYP enzyme inhibitors that show a type II profile contain  $sp^2$ -hybridized nitrogen as a structural element (e.g., pyridine, imidazole, and triazole derivatives).<sup>[30,128–146]</sup> Type I binders shifted the maximum of the spectra to lower wavelength. This is often associated with the spectroscopic behaviour of the substrate and caused by a water-bridged coordination of the heme iron.<sup>[29]</sup> There is also an intermediate mechanism, the so-called “reversed type I” binding. This originates from an increased low-spin absorbance band at 420 nm combined with an indirect water-bridged compound-iron interaction<sup>[147,148]</sup>

UV/Vis spectroscopic heme coordination assays provide information on the binding mode and can be used for affinity determination. The  $K_D$  values are obtained by titration of the compound against the CYP enzyme (**Figure 7**).

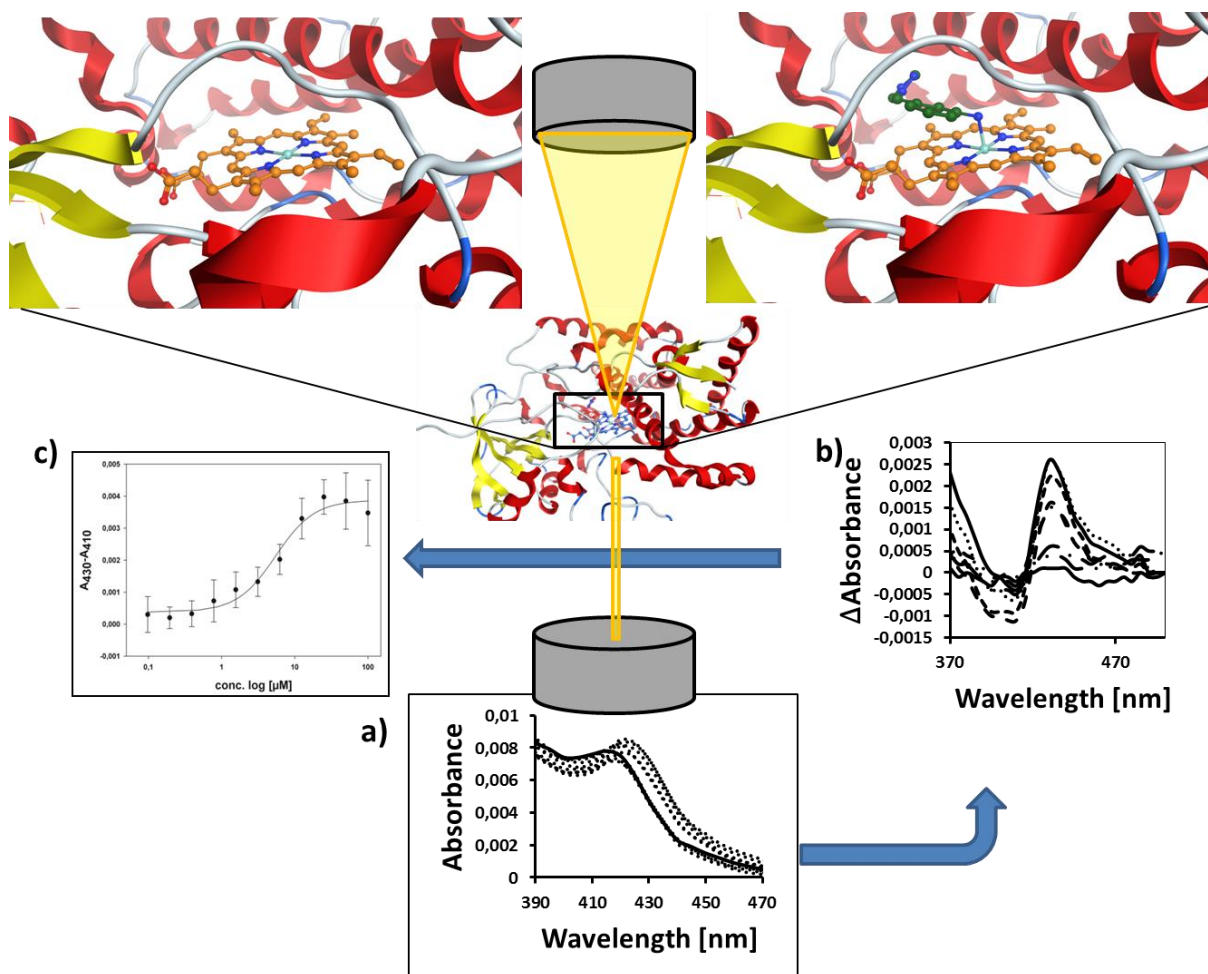


**Figure 7.** UV/Vis spectrum of CYP enzyme monitored with and without a ligand. Crystal structure of heme coordinating ligand [adapted from PDB:4G44 <sup>[32]</sup>]. **a)** Picture of the enzyme's (continues line) absorbance spectrum and ligand titrated in different concentrations against the enzyme (dotted line). **b)** Difference spectrum of native enzyme and ligand complex. **c)** Binding curve for  $K_D$  determination, calculated from the difference spectrum.

### 1.3.3.2 Functional assay: LC-MS quantification of enzyme reaction

A functional assay can directly quantify the efficiency of an enzyme inhibition by a specific compound. This provides information about the biological relevance of an inhibitor. Normally, the inhibitory strength is described as  $IC_{50}$  (defined as the concentration of inhibitor required to produce 50% inhibition of an enzyme reaction at a specific substrate concentration). <sup>[149]</sup> Nevertheless, new theories suggested that the residence time of inhibitors to their target could be a better parameter to judge biological efficiency. <sup>[150]</sup>

There is a broad arsenal of *in vitro* assays to determine effectiveness of an inhibitor. Depending on the biological system an appropriate assay has to be selected. <sup>[117]</sup> First descriptions using Liquid Chromatography (LC) or High Pressure LC (HPLC) for the detection of an enzyme reaction were

reported in the 1970s. The biggest advantage of the LC/ HPLC systems is the potential to separate different components of the enzyme reaction before the detection. The separation is based on a variable distribution of the mixture components between a mobile and a stationary phase. This is necessary in reactions composed of products and/or substrates with similar physicochemical properties. Depending on the method used for analysing the sample similar properties could interfere with the quantification process. Furthermore, the chromatography step is combinable with wide range of detection methods like, for example, spectrophotometric, fluorimetric, electrochemical, and radiometric ones. This provides a broad flexibility concerning physicochemical properties of the components in a reaction mixture. <sup>[151]</sup>

Especially, the mass spectrometry offers a good compromise between sensitivity for a quantification process and flexibility concerning compound characteristics (**Figure 8**). <sup>[152]</sup> Mass spectrometry (MS) is based on the ionization of a compound and the analysis by the mass to charge ratio. In development of functional assays using MS detection, several points have to be taken into consideration. First of all, the aforementioned parameters governing the enzyme reaction are crucial <sup>[121]</sup>, secondly, the different steps in the analytical procedure consisting of sample preparation, choice of reference and internal standards, selection of the ion source, optimization of MS parameters, and LC separation. <sup>[153]</sup>

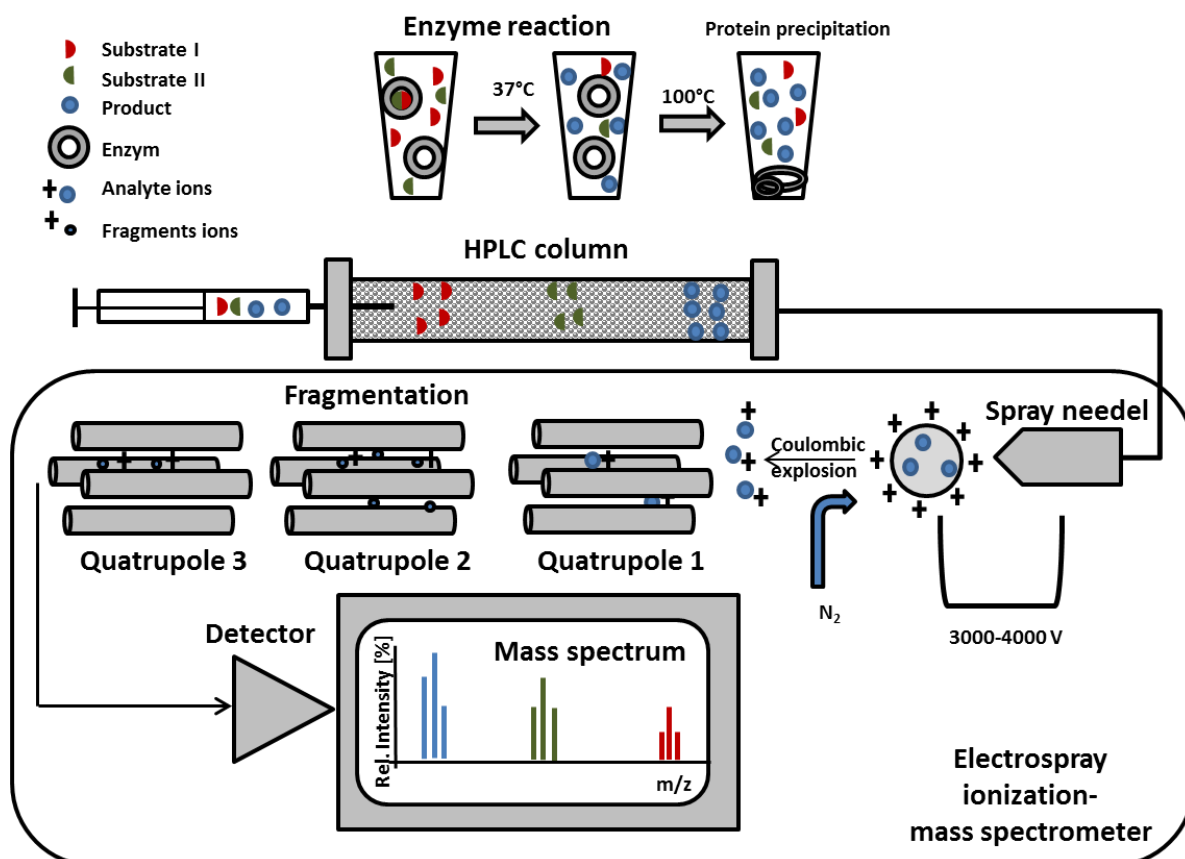


**Figure 8.** Schematic overview of HPLC-MS/MS based assay procedure [adapted from Hess, Meier, Zeeh et. al. <sup>[154]</sup>]

### 1.3.3.3 Cell-based assays part 1: Determination of cytotoxicity to eukaryotes and prokaryotes

In the development of new antibiotics, it is highly important to find selective compounds with low toxicity in human cell lines. The most antibiotics display an on target efficiency in an acceptable range. However, due to a lowered penetration through the bacterial cell membrane, antibiotic effects are often in the micromolar range. This is two to three magnitudes higher compared to drugs with eukaryotic targets. The higher doses needed to overcome this disadvantage increases the possibility of *in vivo* toxicity.<sup>[14]</sup> This emphasizes the relevance of appropriate assay systems to specify cell toxicity to both genera (eukaryotes and prokaryotes).

An often used approach to quantify the effect of an antibiotic compound on bacteria is the determination of the minimum inhibitory concentration (MIC). MIC is defined as the lowest concentration that inhibits bacterial growth.<sup>[155]</sup> Besides the common agar plate methods, the broth dilution test is the standard approach to determine MIC values (**Figure 9 b**). It is based on bacterial growth in a liquid medium under different concentrations of antibiotic. The growth is monitored by differences in turbidity of the medium (Optical density at 600 nm: OD<sub>600</sub>).<sup>[156]</sup> Depending on the growth behaviour of some bacterial strains, using OD<sub>600</sub> could be imprecise. For example, bacteria of the species *mycobacteria* tend to grow in a clumped fashion. Besides the usage of detergents, colorimetric, fluorescent, or luminescent measuring methods can be applied to circumvent this problem. One example is the alamarBlue® assay that works via the reduction of resazurin by respiratory chain metabolism of a living cell. The reaction can be monitored by colorimetry- or fluorescence- based methods. A similar system is the MTT assay, where the reduction of 3-(4,5-dimethylthiazol-2-yl)-2,5-diphenyltetrazolium bromide (MTT) to formazan can be detected by the change of the color. The third approach detects the concentration of adenosine triphosphate (ATP), which correlates with cell viability. In this protocol, an ATP/luciferase reaction produces a chemiluminescent dye.<sup>[157,158]</sup> The aforementioned methods are also suitable with regards to eukaryotic cells (**Figure 9a**). Though MTT- and ATP-based methods are simple and accurate, they could be influenced by metabolic interference. Thus, the result of such approaches should be confirmed by secondary screens based on cell death markers.<sup>[159]</sup>



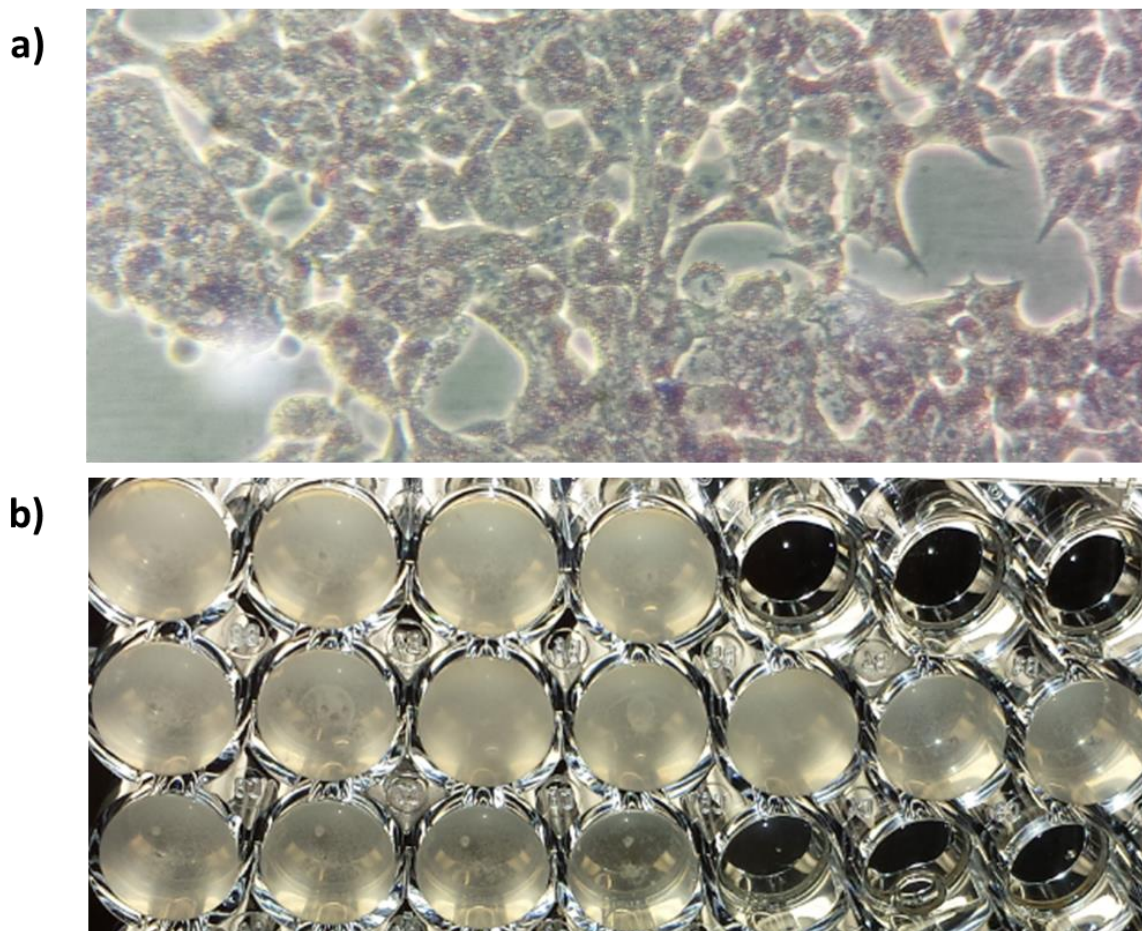


**Figure 9.** a) MTT assay of HEK293 cells to measure toxicity on human cell lines. b) MIC determination of *Mycobacterium bovis* BCGT growth under antibacterial pressure by OD<sub>600</sub> in 48-well plates.

#### 1.3.3.4 Cell-based assays part 2: Biofilm assay

As already discussed in chapter 1.2.3 biofilm plays a crucial role in the pathogenesis of *P. aeruginosa* infections, especially in chronic ones. Accordingly, a biofilm inhibition might be a good strategy for the treatment of such infections. <sup>[160,161]</sup> The efforts of finding compounds with such promising activities resulted in the development of several *in vitro*, *ex vivo*, and *in vivo* biofilm assay systems. The *in vitro* models can be divided in static (e.g., microtiter plate) and open systems (e.g., flow cell) as well as microcosms (e.g., reconstituted human epithelia). Although these are only simplified systems, they are useful to address fundamental questions. Especially, the microtiter plate approach is suitable for high throughput compound testing. <sup>[160]</sup>

The principle of the latter can be summarized as follows: bacteria are grown in plates or modified plate systems and components of the biofilm are stained by suitable dyes. Depending on the aim of the study, three modifications of assays can be performed. These include biomass assays (quantification of matrix and cells), viability assays (quantification of living cells), and matrix assays (staining of

selected matrix components).<sup>[162]</sup> A common method for the quantification of the whole biomass is the crystal violet staining. Crystal violet (CV) is a positively charged dye that binds to polysaccharides and negatively charged cell surface molecules (**Figure 10.**). Using this system it is not possible to distinguish between living and dead cells.<sup>[163]</sup> A second dye, the fluorogenic Syto9<sup>®</sup> can also be used to measure biomass volume. This is based on attachment to DNA in living and dead cells as well as to eDNA.<sup>[164]</sup> Experimental procedures such as antibiotic susceptibility assays require discrimination between living and dead cells within the biofilm. Available test systems to assess this task are described in chapter 1.3.3.3 and work via MTT, resazurin, and ATP bioluminescence. Applicability of these staining methods to biofilm scenarios was shown by Sanchez, Pettit, and Adam et al.<sup>[165–167]</sup> Another interesting modification of biofilm assay can be used for the quantification of matrix components. As mentioned before some major components of biofilm are polysaccharides and eDNA.<sup>[84]</sup> The polysaccharides are detectable via a congo red staining and 1,9-dimethyl-methylene blue (DMMB).<sup>[168,169]</sup> DMMB binds to sulphated polysaccharide forming an insoluble complex.<sup>[169]</sup> A selective staining of eDNA is possible with propidium iodide (PI), which is not able to cross the bacterial cell wall (**Figure 10.**). The dye shows a specific fluorescence after intercalation into the DNA.<sup>[83,90]</sup> Moreover, there are several examples described in literature that illustrate the combination of staining methods with confocal laser scanning microscopy (CLSM) detection. This provides a more detailed view on the composition of the biofilm.<sup>[161]</sup>

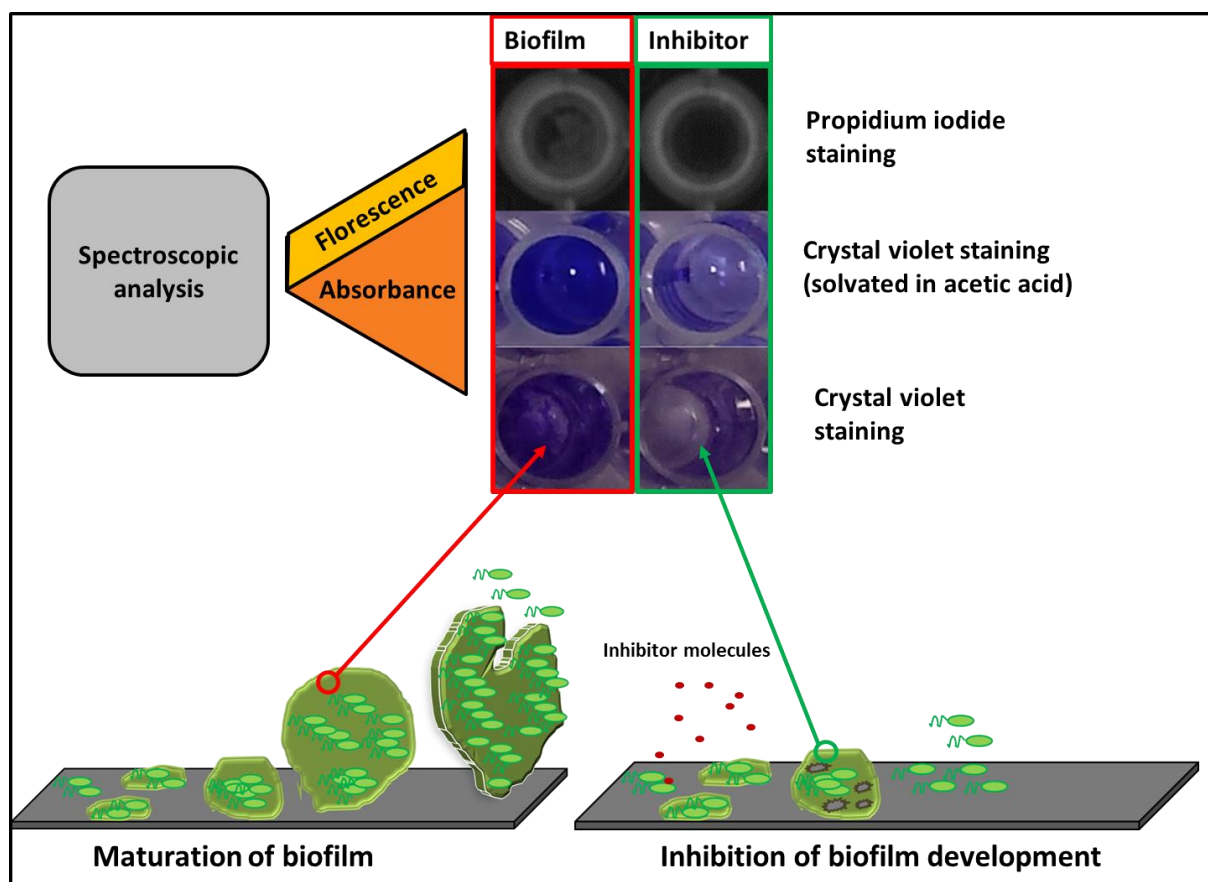




**Figure 10.** Upper part demonstrates the effect of a biofilm inhibitor on the whole biomass (CV) and specific component eDNA (PI). Lower part of the figure depicts schematically the development of biofilm with and without a biofilm inhibitor [adapted from Wei et al. <sup>[84]</sup>]. PI: propidium iodine; CV: crystal violet.

### 1.3.4 Biophysical methods in rational drug design

Besides the typical functional assays that are based on biochemical or cellular methods, biophysical test systems offer an alternative platform for evaluation of ligand-target interactions. <sup>[170]</sup> Important examples for these methods are X-ray crystallography, NMR, Isothermal Titration Calorimetry (ITC), SPR, Differential Scanning Fluorimetry (DSF), and different fluorescence-based techniques. These are widely used in hit identification and parametrization to gather information for a directed optimization process. <sup>[171]</sup>

#### 1.3.4.1 Differential scanning fluorimetry

DSF technique detects the thermal unfolding of proteins. Binding of a compound to the protein is represented by a shift of the melting temperature (defined as the temperature, at which half of the protein molecules are unfolded). A binder stabilizes the protein, which increases the temperature of unfolding (**Figure 11.**). Monitoring of the experiment is possible via a dye that shows fluorescence in a nonpolar environment. The denaturation exposes hydrophobic parts in the protein, which can then be occupied by the dye. Thus, the fluorescence level correlates with the amount of unfolded protein. The whole reaction can be quantified by the use of, for example, a real-time detection polymerase chain reaction machine (RTD-PCR). <sup>[172]</sup>

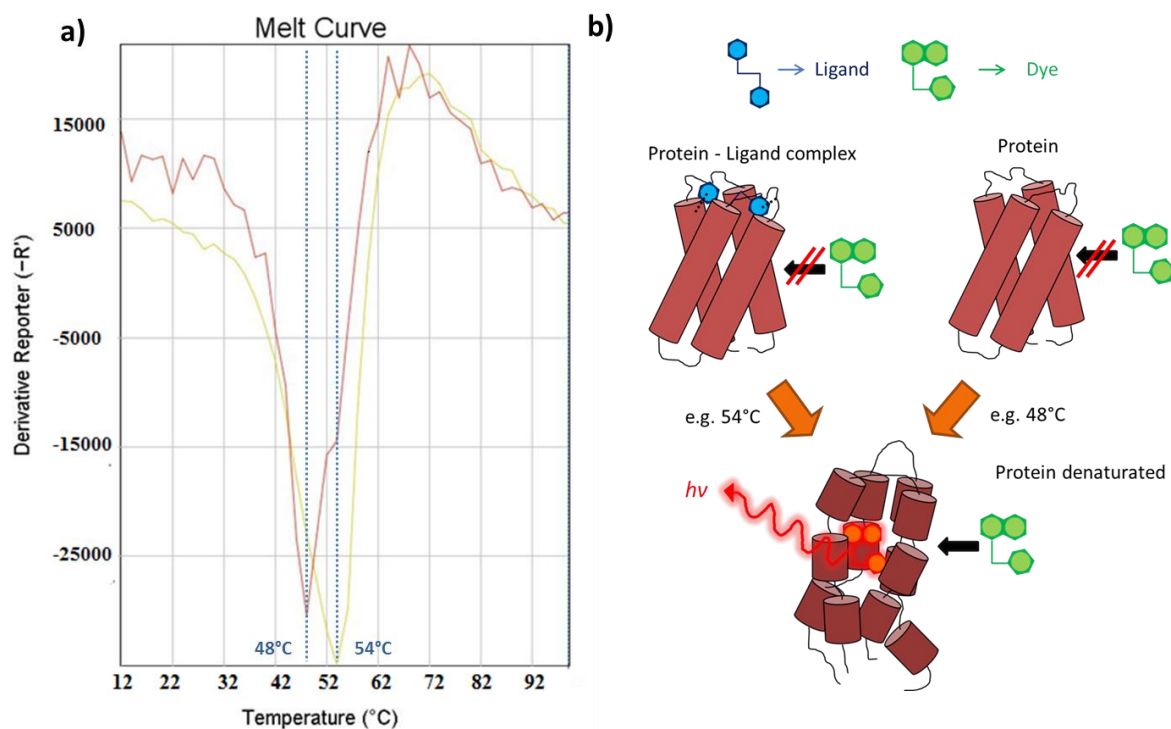


**Figure 11.** a) Interaction of 2-(Nitrophenyl)-methanol derivative and PqsD detected by differential scanning fluorimetry (unpublished results); b) Principle of DSF binding assay [adapted from Cummings et al. <sup>[173]</sup>].

### 1.3.4.2 Isothermal Titration Calorimetry

Hit finding in the pharmaceutical environment often starts with a large number of compounds. <sup>[174]</sup> In this crucial step it is often hard to make a selection on best candidate. The main focus lies here on the assessment of binding affinity. However, thermodynamically, ligand-protein interactions can be dissected in two terms, entropy and enthalpy of binding. <sup>[174]</sup> Often, a compound's affinity is dominated by entropy-driven interaction based on the hydrophobic character of the molecule. <sup>[175]</sup> These hydrophobic interactions are problematic due to the potential of making a compound unselective. Furthermore, one should keep in mind that an improvement of the enthalpy contribution of interaction is more difficult. To understand this fact it is necessary to have a closer look on the thermodynamic processes that take place during ligand binding. The interaction goes along with a loss of enthalpy (H-bonds with water molecules, i.e. desolvation enthalpy) and entropy (conformational degree), which must be compensated or overcompensated by a gain of energy (hydrogen bonds to target and release of water). The entropy term is dominated by a loss of conformational degrees of freedom and release of water molecules. These are non-directed interactions in contrast to the enthalpy term, which predominantly reflects H-bonds. Directed interactions (e.g H-bonds) are hard to generate in an optimization process as distances and angles of the bonds have to be formed in an ideal way. This

highlights the importance of a starting molecule with favourable enthalpy (**Figure 12.**). The ITC represents a tool that helps finding suitable candidates. <sup>[175]</sup>

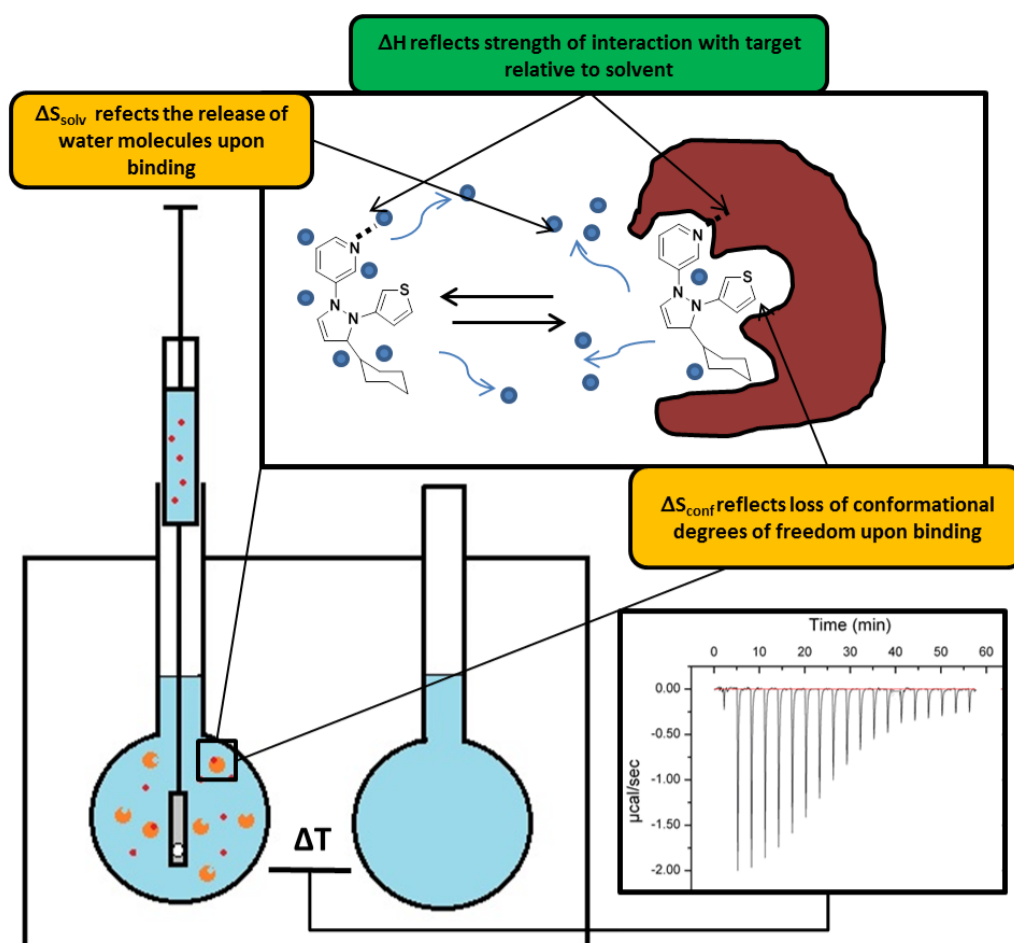


**Figure 12.** Scheme of ITC shows sample and reference cell. The ligand is titrated stepwise into the protein solution. Interaction of ligand (red) and target (orange) zoomed out for a detailed view on the single events of interaction. The interaction of an exemplary molecule and a protein (brown) is shown in the upper part. [Adapted from Freire et al. <sup>[175]</sup>]. ITC: isothermal titration calorimetry.

A typical ITC instrument consists of a sample cell filled with the target protein and a reference cell containing buffer. Both cells are thermally shielded from environmental influences. The sample is titrated stepwise to the target solution, while the solution is stirred. Differences in temperature are calculated between sample and reference cell. The ITC experiment provides information about the enthalpy ( $\Delta H$ ) of binding, the affinity of the ligand ( $K_D$ ), and the stoichiometry of the reaction ( $N$ ). With these data it is possible to calculate the free energy ( $\Delta G$ ) and the entropy ( $\Delta S$ ) using two thermodynamic equations (**Eq. 1** and **Eq. 2**) <sup>[176]</sup> (**Figure 12. and 13.**).

**Eq. 1:**  $\Delta G = \Delta H - T\Delta S$

$$\text{Eq. 2: } \Delta G = RT \ln K_A = -RT \ln K_D$$

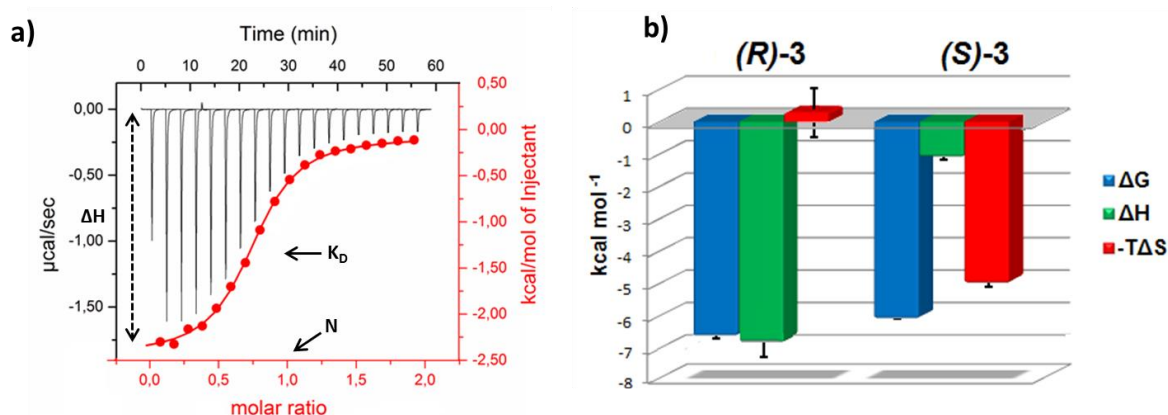


**Figure 13.** **a)** Representative example for an ITC titration curve (black) and the integrated enthalpy proportion (red). Enthalpy ( $\Delta H$ ) of binding, the affinity of the ligand ( $K_D$ ), and, the stoichiometry of the reaction ( $N$ ) can be calculated from red sigmoidal curve. Other parameters can be received via the equation (**Eq. 1** and **Eq. 2**). **b)** Example for 2 compounds with different thermodynamic profile concerning enthalpy and entropy.

### 1.3.4.3 Site-directed mutagenesis / alanine scan

The gold standard in structure-based drug design is a co-crystal structure of the inhibitor with the target protein. Despite the fact that a lot of native protein structures can be found in databases, co-crystal structures are not always available.<sup>[177,178]</sup> The so-called “alanine scan” is based on the site-directed mutagenesis of amino acids possibly involved in binding to a possible molecular interaction partner (replaced by alanine because of the less bulky and inert side chain). This is an often used tool in molecular biology to determine hot spots of interaction.<sup>[179]</sup> Combined with a suitable assay system the technique can be applied to identify structures that interact with ligands and consequently elucidate the binding modes of the molecules. That means, for example, that the exchange of serine in the catalytic pocket of an enzyme as a possible H-bond donor by an alanine should lead to a decreased affinity of an inhibitor, if there is an interaction with this motif. Accordingly, the inhibitor shows a decreased efficiency against the mutated enzyme, which indicates serine to be an important interaction partner.<sup>[177]</sup> A drawback of an enzymatic test system is given by the fact that the amino acids needed for substrate conversion have to be excluded from the study. This could be overcome by the utilization of methods only focusing on binding such as ITC or SPR.<sup>[180]</sup> Taking into account results of docking studies can increase the informational content and give new ideas for optimization (**Figure 14**).<sup>[181,182]</sup>

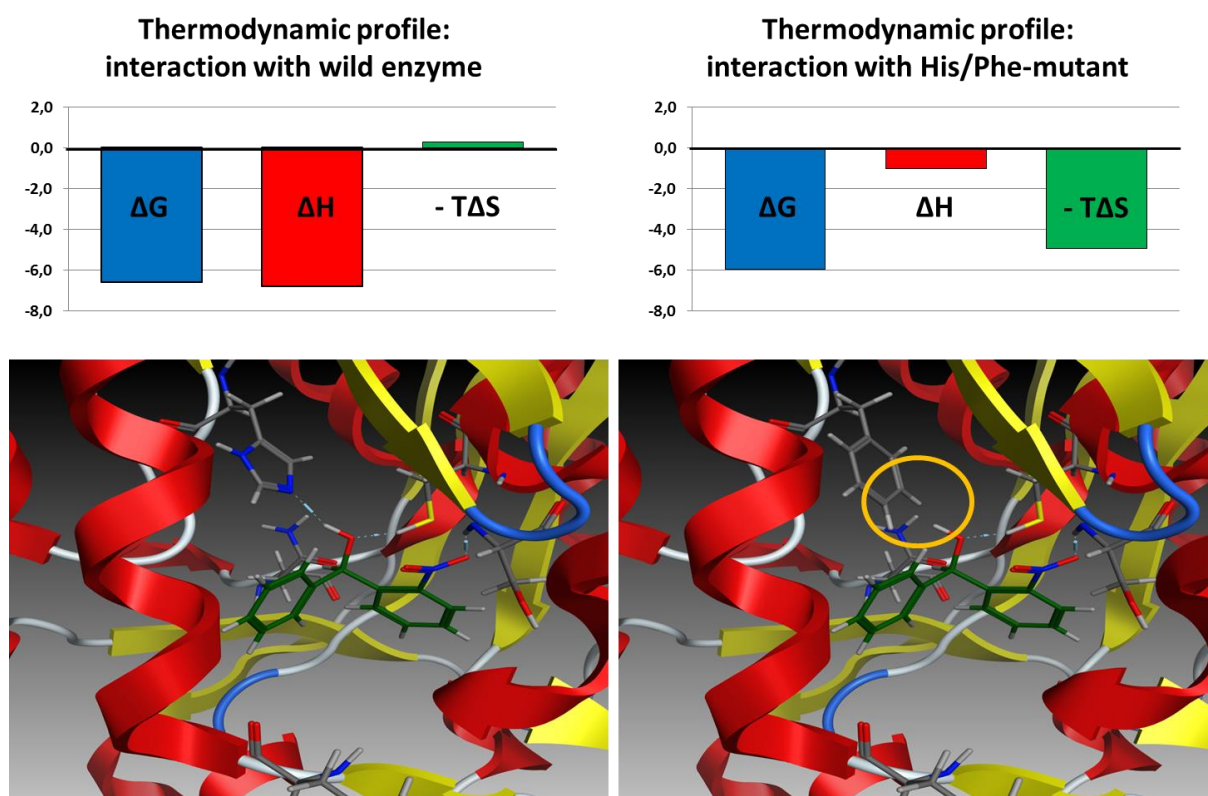


**Figure 14.** A combined analysis of ITC and site-directed mutagenesis illustrates changed compound X affinity and thermodynamic profile to mutant and wild type (wt). The loss of H-bond interaction causes a loss in enthalpy of binding. [Model of compound X bound to PqsD wt and H257F mutant]. ITC: isothermal titration calorimetry.

#### 1.3.4.4 Surface Plasmon Resonance spectroscopy

SPR is a biophysical method with a broad applicability at various steps of drug discovery. This covers the whole process from target identification to clinical phases. Here, SPR supports the discovery process in the hit screening phases as well as mode of action studies.<sup>[183]</sup> The advantage of the technology is that it is a good compromise between a high throughput screening and low material consumption.<sup>[184]</sup> Additionally, it is possible to monitor the binding event in real time and determine binding kinetics, which can in some cases be more important than the affinity itself.<sup>[150,185]</sup>

The sensing of the binding event is based on a surface plasmon wave (SPW), which means quasi-free electron plasma between gold surface (component of the sensor chip) and medium. Such SPW is extremely sensitive concerning a variation of the refractive index of the medium. An interaction of a biomolecule (e.g. protein) bound to the surface and a ligand (e.g. inhibitor) leads to an increase of the refraction index and the SPW propagation constant. This change can be measured optically by the extinction of polarized light of a laser source. Here, polarization is generated by a prism and the light is totally reflected on the surface. Depending on the sensor the binding event, this induces a difference

in refraction index and, consequently, in the SPW propagation constant, can be detected by changes in angle, wavelength, or intensity of the reflected light. <sup>[186,187]</sup> The construction of a SPR spectroscopy can be seen in **Figure 15**.

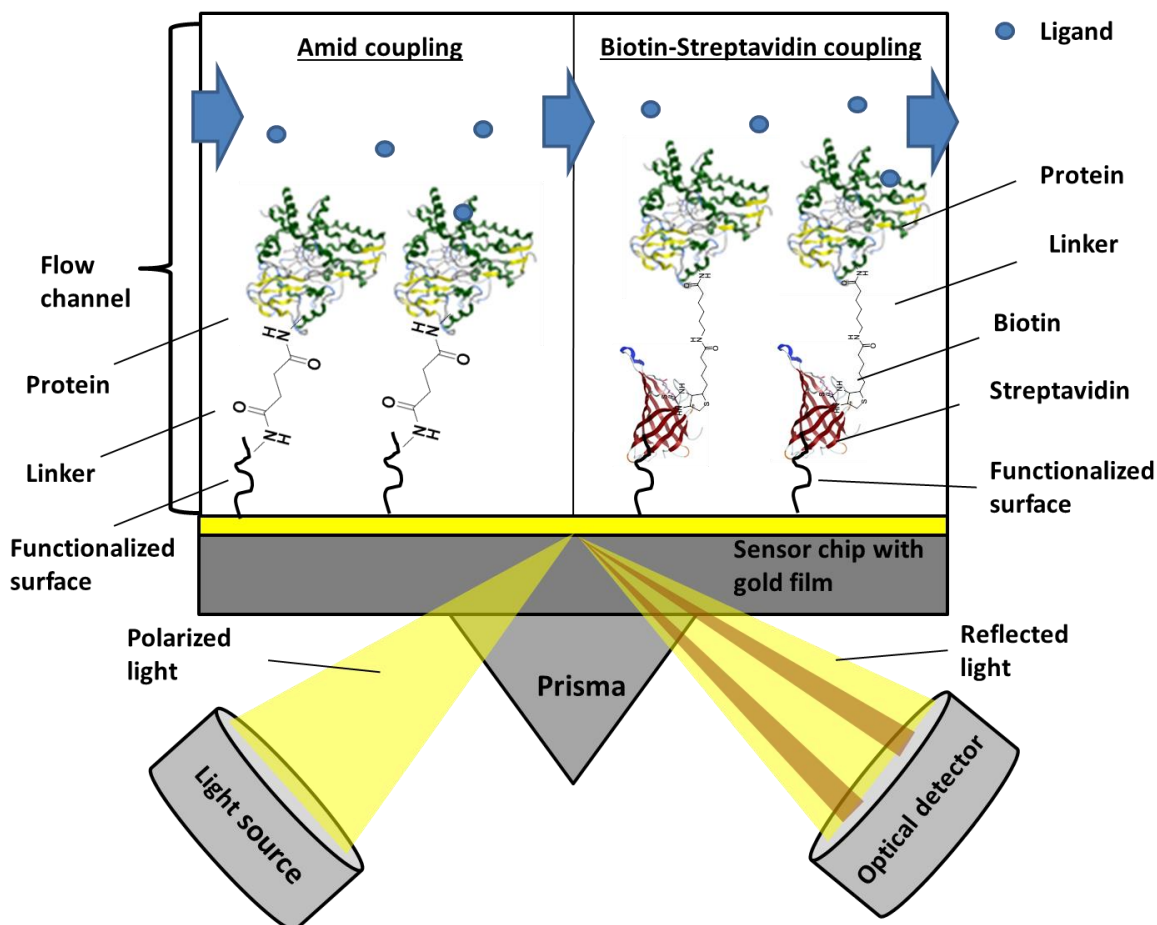


**Figure 15.** Simplified setup of two SPR experiments used for the detection of protein-small molecule interaction. The left box represents the flow channel with amino-coupled protein probe. The right one shows a protein-biotin construct immobilized via a biotin-streptavidin interaction. [adapted from Cooper et al. <sup>[183]</sup>]. SPR: surface plasmon resonance spectroscopy.

A critical step of an SPR experiment is the immobilization of the protein on the sensor chip. <sup>[183]</sup> The most common polymer coat on the chip is carboxymethyl dextran. <sup>[188]</sup> Depending on the nature of the protein several methods for coupling to the carboxymethyl dextran surface are available. Examples are: different ways of covalent attachment, biotin- or streptavidin-presenting surfaces, (**Figure 15**), monoclonal antibodies, metal-coordinating groups. <sup>[183,185,187]</sup>

After immobilization, the test compounds are flushed over the sensor chip. The result of an SPR experiment is a sensorgram, which shows the real-time response of interactions divided in four major steps (**Figure 16**).

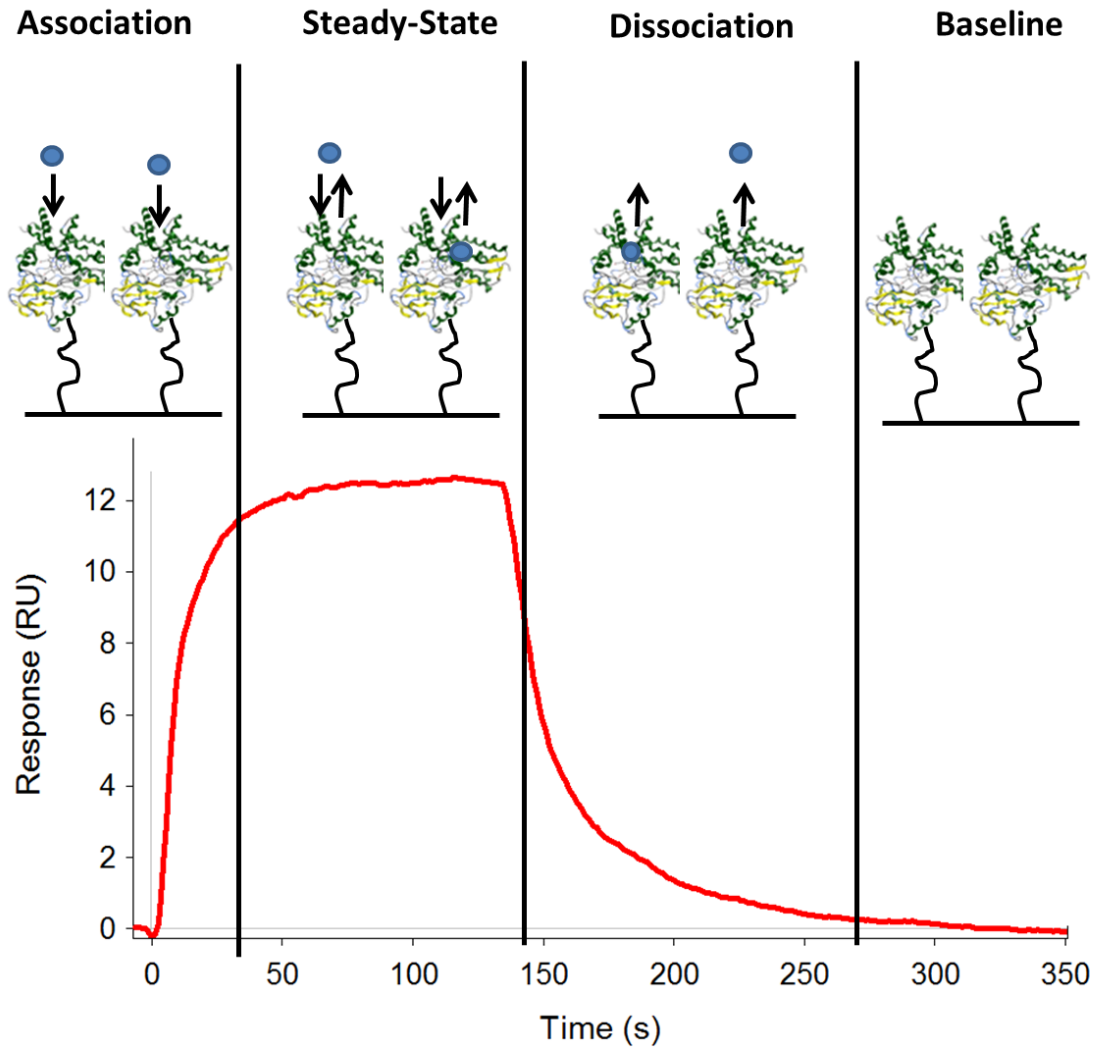


**Figure 16.** Sensogram as a result of an SPR experiment originating from an ligand-protein interaction [adapted from Cooper et al. <sup>[183]</sup>]. SPR: surface plasmon resonance spectroscopy.

The intensity of the signal is described in response units (RU). The first phase begins after injection of the ligand and describes the association to the immobilized protein ( $K_{on}$ ). At the steady-state, the protein-binding site is completely occupied by the ligand molecules. This phase could be used for the measurement of  $K_D$  values. In the dissociation phase, continuous flow of buffer removes bound ligand from the binding site ( $K_{off}$ ) until the baseline is again represented. A kinetic fit of  $K_{on}$  and  $K_{off}$  value could also be used for affinity determination. <sup>[187]</sup>

All biochemical, molecular biological and biophysical methods described in this introduction are important parts of this thesis. The methods were used in different ways depending on the scope of the corresponding manuscript or paper.



## 2 Aims of the thesis

The innovation gap in antibiotic research from 1962 to 2000 resulting from the false conviction that bacterial infections were successfully eradicated creates new challenges. A wide range of pathogenic bacteria already developed resistance towards most antibiotics in clinical use. Due to a lack of last-resort antibiotics there is an increased mortality rate in the field of infectious diseases. Furthermore, the costlines of such therapies might turn into an economical problem in the future. Thus, there is an urgent need for new therapeutic options. A possible strategy is the identification of drugs acting on a new target system. On the one hand, this approach overcomes target-dependent resistance mechanisms (point mutations). On the other hand, there is a creation of new structural space avoiding drug-dependent resistance mechanisms (efflux pumps). A second possible approach is to lower bacterial pathogenicity without affecting viability. The so-called “anti-virulence” strategy should prevent resistance development and additionally facilitate the clearance by the host’s immune system. Apart from these concepts, a third approach aims at targeting of structures, which are essential for *in vivo* detoxification. This thesis deals with the three aforementioned aspects in development of new anti-infectives.

The first part of the thesis describes the identification of compounds targeting mycobacterial CYP enzymes as a new therapeutic strategy for the treatment of tuberculosis. One aim was the identification of first selective CYP 121 inhibitors with an *in cellulo* activity to Mtb. Early studies confirmed CYP 121 to be essential for *in vitro* growth. To validate the enzyme as a drug target and create a reliable starting point for a rational optimization process, we planned a screening campaign based on a focused in-house library. Compounds out of this library bear chemical properties that privilege these structures for interaction with P450 enzymes. Binders resulting from a biochemical and biophysical screening were considered for *in cellulo* activity tests against *Mycobacterium bovis* BCG and Mtb. Further studies on selectivity and *in vitro* activity were conducted to confirm CYP121 as the main target and to exclude toxicity.

Another enzyme of interest is the mycobacterial P450 enzyme CYP125. It was shown to be essential for *in vivo* growth and is a key enzyme in cholesterol metabolism of Mtb. The aim of our studies was the identification of first high-affinity binders for the evaluation of CYP125 as a starting point for the development of antimycobacterial agents with a new mode of action. For this purpose the same in-house library used in the CYP121 screening was tested for CYP125 binding. Consequently, same biophysical and biochemical approaches proven successful in the first project were pursued for CYP125. Furthermore, we were also interested in selectivity towards human and other mycobacterial CYP enzymes to provide information for specific optimization processes.

A third strategy, we are following to overcome bacterial resistance, is the interference with quorum sensing systems. *P. aeruginosa* controls the production of major virulence factors and components of biofilm via the *pqs* communication system. Former studies confirmed that PqsD inhibitors (biosynthesis enzyme of signal molecules PQS and HHQ) sufficiently lower signal molecule



concentration and inhibit biofilm formation. A desirable aim was the determination of the PqsD inhibitors' binding mode. The lack of co-crystal structures was circumvented by the use of a straightforward approach combining biophysical methods, site directed mutagenesis, and molecular modelling. Such investigations were carried out for several inhibitor classes.

Biofilm formation plays a key role in chronic infections with *P. aeruginosa*. The objective was to establish a biofilm assay system to characterize phenotypic outcome of PqsD inhibitors (PqsD and PqsR as target structures). The use of selective staining reagents represents a suitable tool to investigate influence on various biofilm components. Furthermore, this assay enables us to perform combination experiments with quorum sensing inhibitors and antibiotic agents.



### 3 Results

#### A Biophysical Screening of a Focused Library for the Discovery of Novel Antimycobacterials targeting CYP121

#### Manuscript A

The experimental contributions to this manuscript made by the respective persons are summarized below:

Christian Brengel: He heterologously expressed CYP121 and executed the LC-MS/MS-based functional enzyme assay. He was involved in the synthesis of Mycrocyclosin. Furthermore, he performed the SPR and heme assay screening. Additionally, he determined the MIC values on *M. bovis* BCGT.

Andreas Thomann: He heterologously expressed CYP121. He performed molecular docking studies. Furthermore, he executed heme assay screening. Additionally, he determined the MIC values on *M. bovis* BCGT.

Alexander Schifrin: He measured the CO-spectra of and CYP121.

Giuseppe Allegretta: He developed LC-MS/MS method of mycrocyclosin and cYY.

Ahmed Kamal: He synthesized cYY.

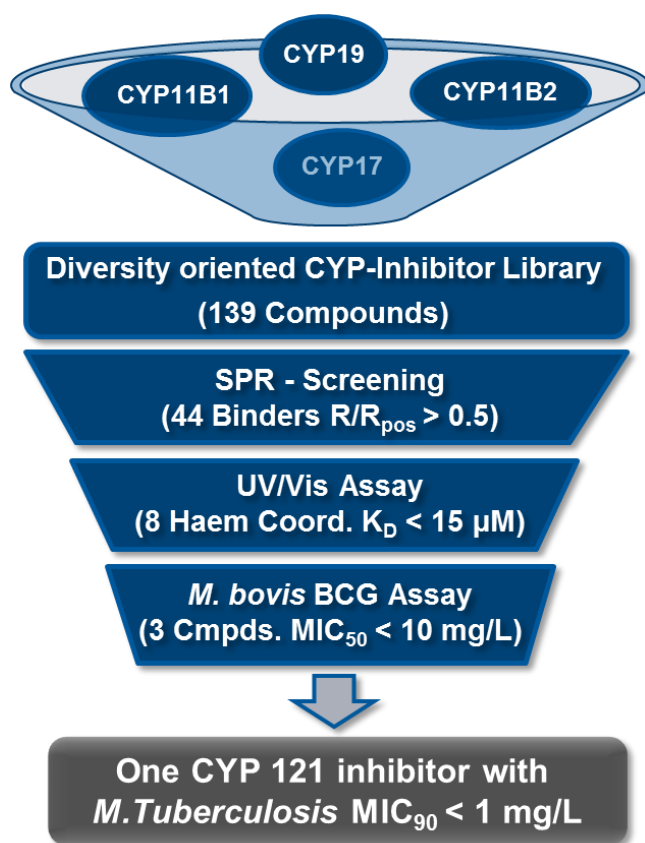
Sang Hyun Cho: He determined MIC values on *M. tuberculosis*.

**ABSTRACT:** The appearance of multi-drug resistance (MDR) combined with a generally complicated long-term treatment hamper the therapy of *Mycobacterium tuberculosis* (Mtb) infections. Therefore, the development of novel antimycobacterial agents with new modes of action is urgently required. CYP121 was shown to be a promising novel target for inhibition of mycobacterial growth. However, besides the identification of azole antifungals as molecules that interfere with this system, not many efforts have been made to develop new inhibitors. In this study, we describe the rational discovery of new CYP121 inhibitors by a systematic screening based on biophysical and microbiological methods. Best hits originating from only one structural class gave first information about molecular motifs required for binding and activity. The initial screening procedure was followed by mode of action studies and further biological characterizations. The results demonstrate a superior antimycobacterial efficacy and a reduced toxicity profile of our frontrunner compound compared to the reference econazole. Due to its low molecular weight, promising biological profile and advantageous physicochemical properties this compound displays an excellent starting point for further rational optimization.

Tuberculosis belongs to the most lethal infectious diseases caused by bacteria. According to the WHO Global Tuberculosis Report,<sup>1</sup> 1.5 million people died in 2013 due to infections caused by Mtb. This goes along with an estimated amount of 9 million new cases of Mtb infections arising each year. Despite a broad spectrum of first and second line antimycobacterial drugs, there is an antibiotic gap for the treatment of infections with multi-drug-resistant (MDR) and extensively-drug-resistant (XDR) Mtb.<sup>1</sup> Additionally, alarming reports have been published describing totally-drug-resistant Mtb (TDR-TB).<sup>2,3</sup> Moreover, tuberculosis still requires long-term treatment leading to an increased probability for non-compliance which impairs the therapeutic outcome.<sup>4</sup> Hence, there is an urgent need for new antimycobacterial agents with novel modes of action which in best case could also lead to shorter treatment periods.

Driven by the elucidation of the Mtb genome in 1998<sup>5</sup>, new potential drug targets were identified.<sup>6</sup> Interestingly, Mtb exhibits an unusual high number of twenty P450 enzymes in contrast to other bacteria. Further studies have revealed some of them to be essential for viability, survival and/or pathogenicity.<sup>7</sup> Out of these, CYP121 was shown to be essential for bacterial growth by an *in vitro* knock out study.<sup>8</sup> Moreover, the deficient strain could be revived by a complementary plasmid.<sup>8,9</sup> The first evidence of CYP121 function in Mtb was derived from its gene position which is located in an operon harboring two enzymes involved in the formation of cyclo-di-l-tyrosine (cYY).<sup>10</sup> *In vitro* studies provided proof, that CYP121 catalyzes the reaction of cYY to mycocyclosin with high substrate specificity.<sup>10,11</sup> The role of its substrate and product in the cellular setting remains to be elucidated. However, the variety of biological functions of diketopiperazines is well described e.g. as quorum sensing signals.<sup>12</sup> Thus, besides development of antimycobacterials targeting CYP121, a small selective molecule with *in cellulo* efficiency may help to understand the precise function of CYP121.

Despite the fact that CYP121 is a potential target for Mtb treatment only little efforts have been undertaken to identify potent inhibitors. Hudson *et al.* published several compounds designed for selective CYP121 binding and inhibition. However, none of them were shown to be effective against Mtb.<sup>13</sup> Fonveille *et al.* described a CYP121 inhibitory effect of cYY derivatives without data on bacterial growth.<sup>11,14</sup> Regarding compounds with cellular activity, it was shown that azole antifungals bind tightly to CYP121 and exhibit an *in vitro* and *in vivo* activity against Mtb.<sup>15-20</sup>



**Scheme 1.** Hit finding progress. The initial library (139 compounds) was built of inhibitors designed for inhibition of human CYP11B1/2, CYP17 and CYP19 with regard to structural diversity. A positive SPR screening hit was defined by the coefficient of its response divided by the response of the positive control (econazole) which had to be above 0.5 ( $R/R_{pos} > 0.5$ ). This resulted in 44 positives. From this preselection, eight compounds coordinated iron-heme with a  $K_D < 15 \mu\text{M}$ . These compounds were tested against BCGT and three showed a  $\text{MIC}_{BCGT} < 10 \text{ mg/L}$ . Finally, one compound was highly active on Mtb with a  $\text{MIC}_{Mtb} < 1 \text{ mg/L}$ .

Furthermore, the binding to the enzyme was in good correlation with the antimycobacterial effect.<sup>8,20</sup> As the azole antifungals are active on Mtb cells and effective in mice infection models they display a valuable reference for antimycobacterial CYP inhibitors.<sup>15–20</sup>

The essential role of CYP121 for Mtb survival and our expertise in developing potent and selective human steroidogenic CYP enzyme inhibitors, motivated us to identify novel CYP121 inhibitors with increased efficiency and improved properties compared to the azole antifungals.<sup>21–25</sup> Potential antimycobacterial activity could provide further evidence of target validity, drugability and stimulate development of respective inhibitors towards new therapeutic agents bearing the potential to treat MDR and XDR Mtb infections. For these reasons, we established a screening strategy based on *in vitro* and cell-based assays (Scheme 1). By the use of a small highly diverse library composed of our

CYP-inhibitors, we could identify a CYP121 inhibitor with increased antimycobacterial potency compared to positive control econazole.

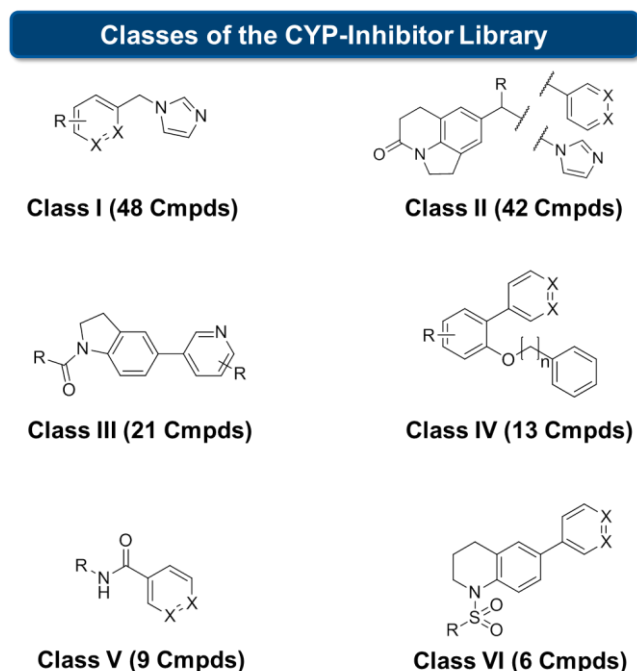


**Figure 1.** Classes of the library used for screening against CYP121 with their respective number of representatives stated in brackets. The structures represent the core scaffold of the compound where R is a substituent, X represent the position of either nitrogen or CH, and  $[\ ]_n$  the alkyl chain length of n methylene units.

This compound possesses desirable physicochemical properties, low toxicity towards human cells and high antibacterial selectivity against Mtb, rendering it an appropriate candidate for further optimization.

## RESULTS AND DISCUSSION

**Library generation.** For hit discovery we selected 139 compounds from our in-house CYP-inhibitor library designed for inhibition of CYP17, CYP19, CYP11B1 and B2 (Supporting Information). The screening library is composed of six different scaffolds to ensure a broad structural diversity (Figure 1). Additionally, known pharmacological profiles, drug-likeness, and established synthetic routes of the compounds provide an ideal starting point for future optimization. As a reference compound we chose econazole which was shown to have the highest reported affinity to CYP121 (UV/Vis heme P450 binding assay) and the strongest inhibition of mycobacterial growth in the class ofazole antifungals.<sup>17,20</sup>

**Enzyme expression, characterization and initial SPR Screening.** As starting point for SPR screening we expressed CYP121 in a heterologous host (*E. coli* K12 BL21) and purified the protein by ion affinity chromatography (IMAC). Notably, addition of 1% Triton-X-100 into the lysis buffer during purification increased the protein yield by about 10-fold.<sup>26</sup> The purity of the enzyme was determined by SDS-PAGE (Supp. Data, section 2, Figure S1).

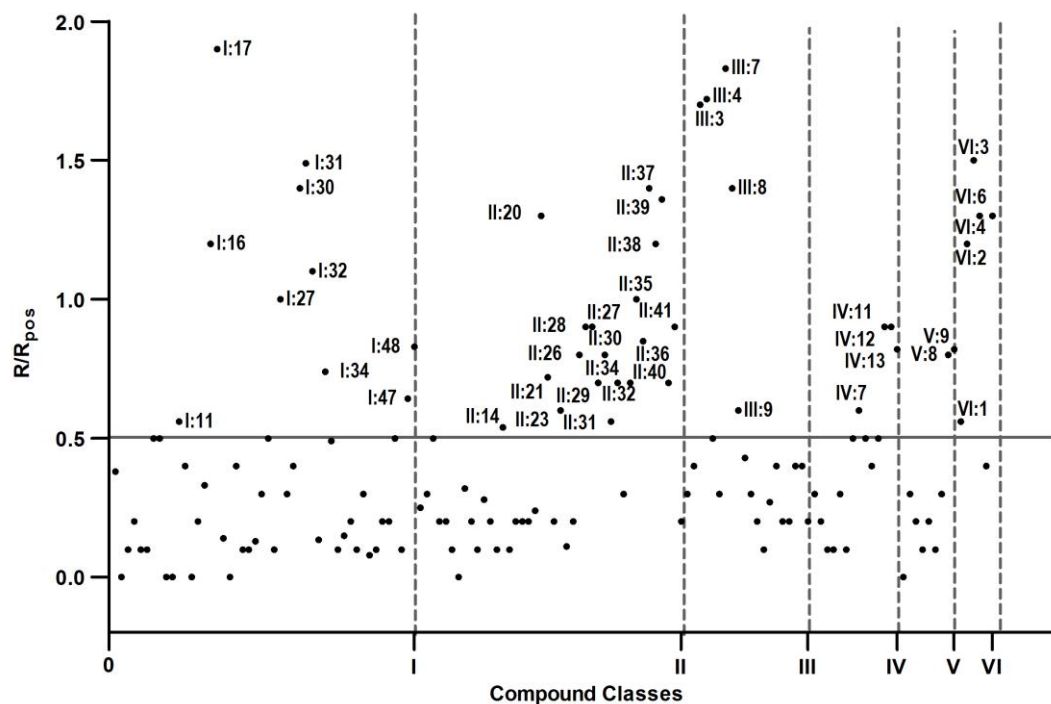


**Figure 2.** SPR screening results: compounds plotted *versus* their  $R/R_{\text{pos}}$  values. Econazole (100  $\mu\text{M}$ ) was used as a positive control and its SPR response was set to 1 ( $R_{\text{pos}}$ ). The compounds were tested at a concentration of 100  $\mu\text{M}$  and their response ( $R$ ) was divided through the response of positive control ( $R/R_{\text{pos}}$ ). Hit compounds possess  $R/R_{\text{pos}}$  values  $> 0.5$  (horizontal solid grey line). Vertical dashed lines separate the six classes.

To ensure active protein conformation we conducted enzymatic *in vitro* activity tests. A first experiment to gain information about activity of P450 enzymes is the determination of CO-binding spectra.<sup>27</sup> 50% of the expressed enzyme showed the typical P450 band of CO-bound heme after dithionate reduction (Supp. Data, section 3, Figure S2 and S3). Using the same experimental conditions but replacing sodium dithionate, we were able to identify Etp1fd (516-618) as ferredoxin and Arh1\_A18G as ferredoxin reductase, two proteins of the fungus/fission yeast *Schizosaccharomyces pombe*,<sup>28,29</sup> as suitable heterologous electron transfer system for CYP121. Additionally, utilizing the latter system, we could show conversion of cYY to mycocyclusin proving enzymatic activity of CYP121 (Supp. Data, section 4, Figure S4 and S5).



For SPR immobilization of the protein we used the biotin-streptavidin interaction.<sup>30</sup> Prior to immobilization we conjugated a biotin tag to CYP121. To confirm applicability of the SPR method, we determined a response curve of econazole to the target protein (Supp. Data, section 5, Figure S6).<sup>8</sup> The SPR signal of econazole, measured in response units (RU), was set to one ( $R_{\text{pos}}$ ). The binding event of library compounds (R) was referenced to the positive control and declared as  $R/R_{\text{pos}}$ . We defined  $R/R_{\text{pos}} > 0.5$  as the threshold for hits from SPR screening procedure. Using this approach, we identified 44 binders out of 139 compounds with representatives from all of the six classes (Figure 2). Notably, we found 17 compounds with higher responses than econazole (Supp. Data, section 6, Table S1).

**Binding mode and affinity characterization via UV/Vis heme binding assay.** The 44 SPR binders were investigated for their ability to interact with the iron(II)-heme by monitoring the shift of the characteristic absorbance band at 416 nm of CYP121 (Figure 3).<sup>8,13</sup> In addition to the 44 SPR hits, we also took two weak SPR binders into consideration (**I:1** and **I:33**,  $R/R_{\text{pos}} < 0.5$ ) to conduct a retrospective evaluation of the reliability of our SPR screening. McLean *et al.* reported that econazole has a tight-binding profile to CYP121 with a  $K_D = 0.02 \mu\text{M}$ .<sup>8</sup> However, we observed a  $K_D$  of  $3 \mu\text{M}$ . This discrepancy could be due to a difference in UV/Vis spectrometric devices used and, thus, limited sensitivity. To provide a higher throughput employing 96-well plates, we were limited to a higher enzyme concentration which impairs measurement in lower nanomolar ranges. Compounds were initially tested at a concentration of  $100 \mu\text{M}$  to identify iron-heme interactions and distinguish between type I (water bridged iron-interaction) and type II (direct iron-interaction) binding.

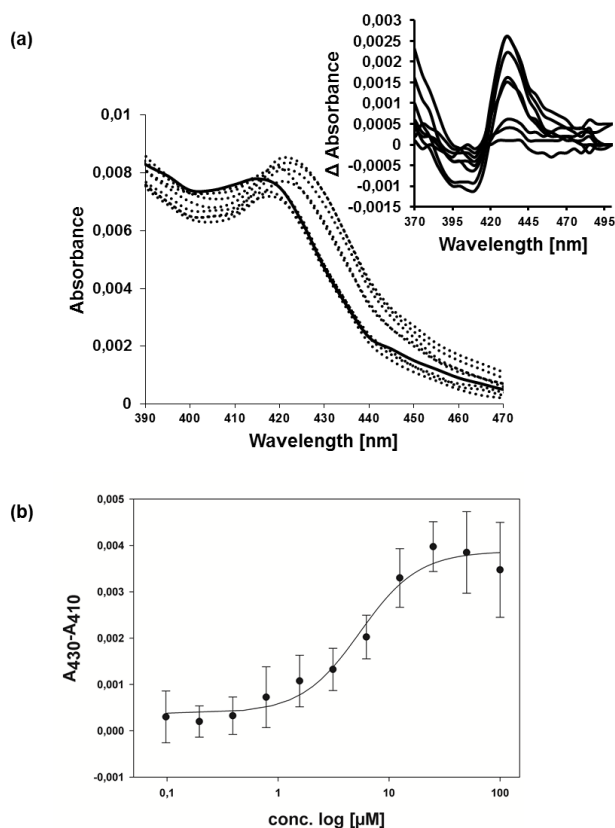


**Figure 3.** Binding of **I:47** to CYP121 as determined from heme coordination assay. **(a)**: UV/Vis spectrum (left inset) and difference spectra (upper right inset) were recorded of the enzyme in the presence of **I:47** (100, 50, 25, 12.5, 6.25, 3.13, 1.56, 0.78, 0.39, 0.20, 0.10  $\mu\text{M}$ ; dotted lines) and in the absence of **I:47** (solid line). **(b)**: The  $K_D$  value of **I:47** was derived by non-linear fitting of the data using *Equations 1* and the difference in absorption at 430 and 410 nm.

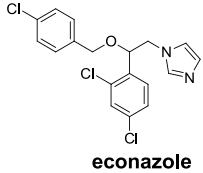
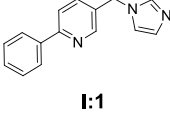
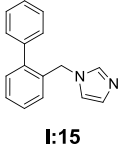
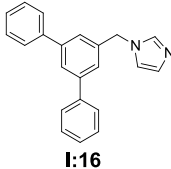
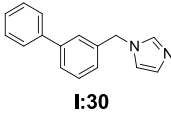
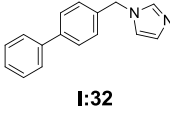
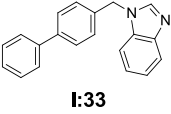
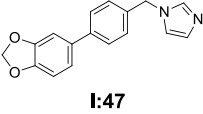
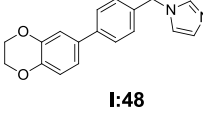
30 compounds showed a type II shift while none showed type I binding behavior. The latter compounds appear in class I, II, III and IV indicating that the catalytic center accepts imidazolyl- and pyridinyl-moieties for iron-heme coordination. **I:1** and **I:33** (weak SPR binders) did not coordinate the heme-iron which emphasizes the suitability of our SPR screening procedure. The identified type II binders were further investigated regarding their  $K_D$ . For eight binders an affinity better than 15  $\mu\text{M}$  was observed (Supp. Data, section 6, Table S1). Interestingly, this subset of compounds only arose from classes I and II. Pyridinyl (class II) as well as imidazolyl (class I) motifs were tolerated as heme coordinators while the imidazolyl ligands showed higher affinities (Supp. Data, section 6, Table S1). With regard to class I the highest affinity could be found for compounds decorated with hydrophobic and space-demanding moieties connected to the benzylimidazole substructure. This is also a structural trend in the class of antimycobacterial azoles (e.g. econazole, clotrimazole).<sup>8</sup> The most affine binder **I:16** showed three-fold improved  $K_D$  compared to econazole ( $K_D = 3 \mu\text{M}$ ) (Supp. Data, section 6, Table S1). Furthermore, two linearized, *para*-substituted biphenyl compounds of this class (**I:47** and

**I:48**) possessed a CYP121 affinity comparable to econazole. As mentioned before, molecules with linear biphenyl units bearing an *N*-methylenbenzimidazolyl moiety instead of an unsubstituted benzylimidazolyl scaffold did not bind to the heme (**I:33**). Additionally, replacement of the interconnecting phenyl group within this class by pyridinyl resulted in inactive compounds (**I:1**). Moreover, the analysis of all regioisomers of benzylimidazol scaffolds substituted with phenyl revealed that the *para*- (**I:32**) and *meta*- (**I:30**) position lead to comparable affinities. A phenyl group at the *ortho*-position (**I:15**) impairs binding. The *para*-benzodioxine substituent of **I:48** and the *para*-benzodioxole substituent of **I:47** increase the affinity by about two-to threefold (Supp. Data, section 6 Table S1). However, compared to econazole our most active compounds showed similar (e.g.: **I:47**; 5  $\mu$ M and **I:48**; 5  $\mu$ M) or slightly better  $K_D$  (**I:16**; 1  $\mu$ M) (Supp. Data, section 7, Figure S7).

**MIC determination in BCGT and Mtb.** For investigating cellular activity we focused on those compounds with a  $K_D$  lower than 15  $\mu$ M, but also added selected compounds showing low affinity to CYP121 as negative controls (Supp. Data, section 6, Table S1). In this setting, econazole was used as described antimycobacterial reference compound.<sup>31</sup> For initial screening on mycobacterial growth inhibition we used the bovine strain BCGT. The strain serves as a suitable substitute for Mtb as it carries a copy of CYP121 in its genome with an overall amino acid identity of 100% in comparison to its Mtb congener (Supp. Data, section 8, Figure S8).<sup>32</sup> Regarding the more complex situation in the cellular context, the six identified classes have to be discussed separately. In case of subset III to VI, we could only detect weak growth inhibition ( $MIC_{BCGT} > 10$  mg/L; Supp. Data, section 6, Table S1). In class II three compounds were found to have a  $K_D$  value below 15  $\mu$ M but none of them had  $MIC_{BCGT}$  below 10 mg/L (**II:20**, see Supp. Data, section 6, Table S1). For econazole, we observed a  $MIC_{BCGT} = 5.4$  mg/L which is in good correlation to previous findings.<sup>31</sup> Most active compounds were observed in class I (Supp. Data, section 9, Figure S9 and S10). The best heme-binder to CYP121 (**I:16**) with a three-fold increased affinity compared to econazole showed a  $MIC_{BCGT}$  of 1.6 mg/L. For **I:47** and **I:48** we could determine  $MIC_{BCGTs} = 0.3$  mg/L and 2 mg/L which renders **I:47** to be the most potent antimycobacterial compound in this subset. The MIC tests of negative controls out of class I (**I:1** and **I:33**) showed no significant growth inhibition. Within class I results of the MIC assay are in good correlation to the  $K_D$  values on the target enzyme CYP121 (Table 1).

To test the potency of the most effective antimycobacterial compounds against the human pathogen Mtb, we used the MABA assay system. For  $MIC_{Mtb}$  determination we chose the common laboratory strain H<sub>37</sub>Rv. In several studies the  $MIC_{Mtb}$  value of econazole was determined ranging from 0.12 mg/L to 8 mg/L.<sup>8,18</sup> To facilitate comparability of the  $MIC_{Mtb}$  values, we referenced them to results made in our assay system where a  $MIC_{Mtb}$  for econazole of 4.2 mg/L was determined previously.<sup>31</sup> The most effective compounds were **I:47** with  $MIC_{Mtb} = 0.3$  mg/L followed by **I:16** ( $MIC_{Mtb} = 1.9$  mg/L) and **I:48** ( $MIC_{Mtb} = 3.5$  mg/L, see Table 1). Notably, in terms of cellular efficiency metrics, **I:47** has an AE = 0.39 and hence, a higher AE than econazole (0.24) and rifampicin (0.16) (Supp. Data, section 10, Table S2).

**Table 1.** Structures, relative SPR responses ( $R/R_{\text{pos}}$ ), binding affinities ( $K_D$ ) and antimycobacterial activities of econazole, most active hits (**I:16**, **I:47**, **I:48**), examples for negatives (**I:1**, **I:33**) and for moderately active hits (**I:15**, **I:30**, **I:32**).

Cmpd	SPR [ $R/R_{\text{pos}}$ ]	Haem $K_D$ [ $\mu\text{M}$ ]	$\text{MIC}_{\text{BCGT}}$ [mg/L]	$\text{MIC}_{\text{BCGT}}$ [ $\mu\text{M}$ ]	$\text{MIC}_{\text{Mtb}}$ [mg/L]	$\text{MIC}_{\text{Mtb}}$ [ $\mu\text{M}$ ]
 <b>econazole</b>	1	3	5.4	14	4.2 <sup>b</sup>	11 <sup>b</sup>
 <b>I:1</b>	0.4	>100	>25	>100	-	-
 <b>I:15</b>	0.3	34	9.6	41	-	-
 <b>I:16</b>	1.2	1	1.6	5	1.9	6
 <b>I:30</b>	1.4	11	2.6	11	11.2	48
 <b>I:32</b>	1.1	14	7.0	30	9.6	41
 <b>I:33</b>	0.1	>100	>25	>100	-	-
 <b>I:47</b>	0.6	5	0.3	1	0.3	1
 <b>I:48</b>	0.6	5	2.0	7	3.5	12

<sup>a</sup> Eco = econazole, <sup>b</sup>  $\text{MIC}_{\text{Mtb}}$  determined previously.<sup>31</sup>

**Table 2.** Comparison of human cellular toxicity and anti-Mtb effect.

Compound	MIC <sub>Mtb</sub> [mg/L]	LD <sub>50</sub> HEK 293 cells [mg/L]	Toxicity factor MIC <sub>Mtb</sub> /LD <sub>50</sub> <sup>a</sup>
Eco	4.2	6.0	1.4
I:16	1.9	6.1	3.2
I:47	0.3	18.6	62.0
I:48	3.5	22.3	6.4

<sup>a</sup> Toxicity factor (MIC<sub>Mtb</sub> (Mtb) divided by LD<sub>50</sub> (HEK293)) was used to enhance comparability of compounds with regard to their antimycobacterial effect.

**Toxicity on human cell lines.** The azole antifungals are known to attenuate growth of several human cell lines.<sup>33,34</sup> To compare cellular toxicity of econazole with our three most promising hits we used HEK293 cells in a MTT-based assay.<sup>35</sup> 6.0 mg/L of econazole killed 50% of HEK 293 cell population after 48 h. Notably, the toxicity of our most active antimycobacterial compounds was lower compared to the azole antifungal drug (**I:16** LD<sub>50</sub> = 6.1 mg/L; **I:47** LD<sub>50</sub> = 18.6 mg/L; **I:48** 22.3 mg/L). For comparability reasons, we calculated the toxicity factor for **I:47** (MIC<sub>Mtb</sub>/LD<sub>50</sub>), which revealed a 44-fold improvement compared to econazole (Table 2). One of the most prominent undesirable effects of azole antifungals is their hepatotoxicity observed in mice.<sup>34,36</sup> For this reason, we also conducted toxicity experiments employing HepG2 cells. We could observe an approximately 2-fold increased toxicity for econazole (3.1 mg/L) and **I:16** (3.9 mg/L) compared to HEK293 cells. The LD<sub>50</sub> of **I:47** was 17.1 mg/L which is close to the toxicity seen in HEK cells. (*vide supra*, Supp. Data, section 11, Table S3).

**In vitro and in cellulo mode of action studies.** In addition to the binding constant, we determined inhibition of CYP121 enzymatic reaction by **I:47**. The enzyme catalyzes the formation of an intramolecular C-C bond between the carbon atoms in *ortho*-position to the hydroxyl-group of the phenol-moiety of cYY resulting in the production of mycocyclusin.<sup>10</sup> For assessing CYP121 activity we used an artificial redox-system from *Schizosaccharomyces pombe* (ferredoxin Etp1fd (516-618) and ferredoxin reductase Arh1\_A18G).<sup>29</sup> This redox-system is known for its broad applicability as electron-donor for CYP enzymatic reactions but firstly described for CYP121 herein. Indeed, we could observe an inhibition of product formation confirming **I:47** to be a potent inhibitor of mycocyclusin production by interference with CYP121 *in vitro* (Supp. Data, SI section 1).

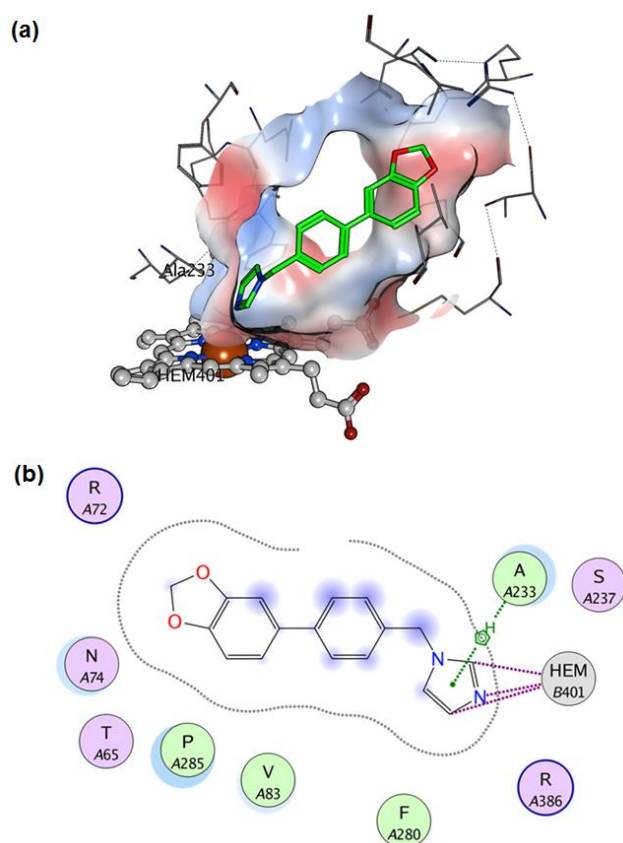


**Figure 4.** Molecular docking of **I:47** against the prepared co-crystal structure of CYP121. Heme coordination was a prerequisite for the docking process which was achieved by placing a pharmacophore feature on the interacting metal and ligand position. Resulting docking poses were sorted by score ( $E_{refine}$ ) and the highest scored pose is depicted as 3D model **(a)** and 2D-interaction chart **(b)**. **I:47** shows close van der Waals contacts to surrounding amino acids but also possibilities for compound enlargement **(b)**. The grey surface in panel **(a)** represents the van der Waals surface of the protein, which is also shown as dotted lines in panel **(b)**.

To gather further evidence for target-based mycobacterial selectivity towards other bacteria, we assessed the activity of our compounds on growth of *E. coli* TolC as a representative for Gram-negative bacteria and *S. aureus* Newmann strain for Gram-positive. The results show no significant growth inhibition of **I:47** and **I:48** against the latter bacteria ( $MIC_{Mtb} > 100\mu M$  or  $> 25\text{ mg/L}$ ). In contrast to econazole and **I:16** that showed certain inhibitory effects for *E. coli* and *S. aureus* in higher concentrations (Supp. Data, section 12, Figure S11).

**Physicochemical and selectivity profile of I:47.** The aforementioned compounds were originally designed as inhibitors of human CYP17, CYP19 and CYP11B1/2 known to be involved in steroid biosynthesis. **I:47** was initially synthesized as an inhibitor of CYP17. The compound showed only a low activity on CYP17 compared to other inhibitors with an  $IC_{50} = 3.1\ \mu M$ . Additionally, only a 48 % inhibition of aromatase at a concentration of  $25\ \mu M$  was observed.<sup>37</sup>

Regarding physicochemical properties suitable for permeation through the cellular membranes, one has to differentiate between biological barriers of human and mycobacterial origin. For humans, a guidepost for appropriate physicochemical properties is the Lipinski's rule of five for oral bioavailability of drugs (< 5 hydrogen bond donors,  $\leq 10$  hydrogen bond acceptors, MW < 500 Da,  $\log P \leq 5$ ).<sup>38</sup> Our frontrunner compound **I:47** fulfils all four criteria (0 hydrogen bond donors, 3 hydrogen bond acceptors, MW = 278 Da,  $\log P = 3.1$ ) (Supp. Data, section 13). To the best of our knowledge, akin correlations for physicochemical properties with mycobacterial membrane passage were not set up, yet. Thus, a respective guide for compound development is still missing.<sup>39</sup>

**Molecular modelling studies on the binding mode of I:47.** As a type II binding profile was observed for **I:47**, we set up a constrained docking protocol to predict its binding mode to the heme center of CYP121. Docking to the active site of CYP121 was restricted by two essential pharmacophore features reflecting the direct interaction between the coordinated iron and **I:47** (type II binding). The resulting docking poses were sorted by their predicted binding energies and the best scored docking pose was chosen for further studies (Figure 4). This modelling approach revealed new possibilities for further derivatization or rigidification. For instance, intramolecular linking of the methylene bridge at the imidazolyl unit with the *ortho*-position of phenyl using e.g. a five-membered ring should be tolerated by CYP121 and increase affinity through reduction of entropic penalties upon binding. Furthermore, the central hydrophobic aromatic moiety shows Van-der-Waals contacts to flanking hydrophobic amino acids Phe-168 and Met-62. Regarding steric factors, the ring could easily rotate in this position. This degree of rotatable freedom might be necessary to place the aforementioned phenyl in a suitable position to grant access to a large flat subpocket (composed of Met-61, Asn-84 and the backbone of Asn-83) which could then be reached by substituents at its 2-position. The 1,3-benzodioxole moiety was placed in a hydrophilic subpocket, formed by Arg-72, Asn-74 and Thr-65, which is in good accordance with the low lipophilicity of this motif ( $c\text{Log}P = 0.27$ ). Moreover, the 5-position of 1,3-benzodioxole holds great potential for further enlargement of the molecule, as it directly points to another subpocket which is decorated with several hydrophobic amino acids, namely Leu-73, Phe-280, Leu-284 and the sidechain of Gln-385.

## CONCLUSION

Despite the fact that CYP121 had been reported to be a potential target for the treatment of Mtb infections, not many inhibitors with cellular activity had been discovered. Herein we have presented a rational screening approach to address CYP121 by a small library focused on privileged scaffolds for CYP enzyme inhibition. The identified compounds could help to clarify the hitherto unknown role of CYP121 in Mtb metabolism and provide a good starting point for a drug optimization program.

Our search for new inhibitors of CYP121 started with an initial SPR screen of the aforementioned focused library. As the compounds were designed for P450 inhibition we observed a high number of binders (32%). The identified compound classes differed highly with regard to their structures.

Obviously, the large pocket of CYP121 (1350 Å<sup>3</sup>) which is necessary for the sterically demanding enzyme reaction can accept a large variety of differently shaped molecules.<sup>8,10,40,41</sup> However, it has to be noted that the SPR method does not exclude compound attachment outside the enzymes active site.

For rational design approaches it is of high interest to clarify the binding mode and affinity of our hit compounds. A common method for P450 enzymes to address this issue is the heme coordination assay.<sup>8</sup> All SPR-binders from classes III, IV, V and VI had only weak affinity to the heme-iron ( $K_D > 100\mu\text{M}$ ). **IV:13** is the only compound from this subset that could be titrated and gave a  $K_D$  of 62  $\mu\text{M}$  (Supp. Data, section 6, Table 1). Therefore, we conclude that most of the compounds from these classes do not bind directly to heme but address another unknown site. This information could, however, be valuable for fragment-linking approaches at a later stage of drug development. For classes I and II we identified eight compounds with  $K_D$  values below 15  $\mu\text{M}$ . Notably, the best compounds of class II (**II:20** and **II:34**) contained a space-demanding trityl-moiety. It was discussed for a crystal structure of CYP121 (PDB-ID: 1N40) that Arg-386 may restrict access of voluminous moieties to the iron-heme.<sup>40</sup> Nevertheless, we observed that the enzyme can accommodate space-demanding molecules at the heme-site as shown by our UV/Vis experiments. Binders with the best affinity were found in class I. A comparison of compound structures and binding efficiencies within this class gave first evidence for properties needed to gain affinity towards CYP121. Imidazolyl head group linked by an methylene bridge to a hydrophobic core can be considered as an important basic structure for a good binding efficiency (**I:16**, **I:47** and **I:48**). In case of the linearized compounds, an *N*-methylenbenzimidazolyl head group (**I:33**), *ortho*-substituted biphenyl system (**I:15**), and an interconnecting pyridinyl (**I:1**) ring had unfavorable binding properties. In a hit optimization process these structural characteristics should be avoided. In contrast to this observation, a *para*-benzodioxine substituent (**I:48**) and a *para*-benzodioxole substituent (**I:47**) linked to the biphenyl system increases affinity. This might provide a possible position for further derivatization. Our docking study supports this result as this motif was predicted to be placed in a subpocket having a great potential for new interactions.

A straightforward approach for target validation is to correlate on-target potency and cellular activity. Although it has to be noted, that such a correlation can be flawed by the fact that compounds might also be inefficient due to e.g. poor membrane penetration. We hypothesized that class II might be a prime example for compounds that poorly permeate the membrane of mycobacteria and, thus, cannot reach their intracellular target. This could be an explanation for the lack of *in cellulo* activity although a moderate affinity to the target was measured.

Class I is the most remarkable of the six classes showing reasonable affinity towards CYP121 and, more importantly, also high activity *in cellulo* against Mtb and BCGT. Furthermore, the on-target affinity of class I compounds directly correlates with their activity on mycobacteria which provides further evidence of a CYP121-dependent effect. In detail, on-target inactive compounds like **I:1** and **I:33** had no activity against BCGT, while moderate binders e.g. **I:15**, **I:30** and **I:32** had low



antimycobacterial effects. Finally, compounds with highest affinity (**I:16**, **I:47**, **I:48**) were the most potent in the cellular setting. Especially, compounds **I:16**, **I:47**, and **I:48** are even more effective on mycobacteria than the positive control, econazole, although no optimization has been undertaken, yet (Table 1). In terms of antibacterial efficiency (AE), **I:47** is superior to econazole and the first-line drug rifampicin indicating an excellent optimization potential of this novel inhibitor class. Moreover, we could provide data that **I:47** does not only bind to CYP121 but does also inhibit the enzyme reaction (Supp. Data, section 4). The correlation between MIC and  $K_D$  bares minor inconsistencies, which might be due to poor penetration through the mycobacterial cell wall of some compounds (see e.g. **I:47** and econazole). A highly lipophilic molecule (e.g. econazole  $cLogP = 5.3$  vs. **I:47**  $cLogP = 3.1$ ) might be trapped in this lipophilic barrier containing mycolic acids and slowly or only partially released into the mycobacterial cytoplasm. This results in lower cellular activity than expected from on-target affinities. A second explanation for the differences in MIC and  $K_D$ , at least for econazole, is its promiscuous behavior in different growth inhibition assays. This suggests that there are additional targets for econazole. An explanation for the antibacterial activity of econazole against *E. coli* and *S. aureus* was already provided before. In these studies econazole was described as an inhibitor of Flavohemoglobin.<sup>42,43</sup> Further possible target systems of azole antifungals within Mtb metabolism have also been described.<sup>44-46</sup> However, evaluation of **I:47** and **I:48** leads to the conclusion that these novel structures are of improved selectivity towards Mtb with a good correlation of CYP121 affinity and antimycobacterial activity. Furthermore, the two compounds possess lower toxicity against human cells than determined for econazole. Although toxicity to hepatocytes was low, it is of high interest to clarify potential inhibition of metabolizing CYP enzymes (e.g. CYP3A4). These results further underline the target-based mycobacterial specificity of our compounds, at least in the subset of bacterial and human cells tested. Taken together the *in vitro* and cell-based studies conducted herein, CYP121 is most certainly the major target of **I:47** and **I:48**.

In summary, we have reported a biophysical screening procedure employing a focused library of privileged scaffolds, which ultimately lead to the discovery of novel CYP121 inhibitors. From this process, **I:47** turned out to be the most promising hit compound pairing convincing antimycobacterial activity and bacterial selectivity with a good toxicity profile. Furthermore, this compound exhibits a fragment-like molecular weight and preferable physiochemical properties that fulfil the Lipinski rules for oral bioavailability (Supp. Data, section 13). Thus, **I:47** is an excellent starting point for rational structure-based drug discovery. Our *in silico* studies revealed several possible modifications to be investigated in future optimization steps. Additionally, the inhibitor might be a suitable candidate for an *in vivo* proof-of-concept study towards validation of CYP121 as a drug target.

## METHODS

**SPR-Screening:** SPR binding studies were performed using a Reichert SR7500DC instrument optical biosensor (Reichert Technologies, Munich, DE) and SAD500m sensor chips obtained from XanTec Bioanalytics.

CYP121 was immobilized on a SAD500m sensor chip at 12 °C using standard biotin-streptavidin complexation. The surface of both channels was quenched by a 3 min injection of 0.003 mg/mL biotin. CYP121 was immobilized at densities between 5000 and 6000 RU for binding studies.

**UV/Vis heme P450 binding assay.** Optical titration experiments were performed in 96 well plates (Greiner, Kremsmünster, AT; transparent round bottom). The data were recorded using Tecan infinite M200Pro Nano Quant (Tecan Groupe Ltd., Männedorf, DE). Absorbance of enzyme and enzyme-inhibitor complex was measured between 350 and 500 nm in 1 nm steps with 10 flashes. Compounds were titrated from DMSO stock solutions maintaining a final DMSO concentration of 1%. CYP121 was used in a concentration of 0.25 µM. Data were plotted as optical shift *versus* ligand concentration. Equation 1 (Eq. 1) was used for non-linear regression of the resulting dose–response curves employing the Levenberg–Marquardt algorithm of Sigma Plot 12 (Systat Software GmbH, Erkrath, DE).

$$f = y_{min} + \frac{y_{max} - y_{min}}{1 + \left(\frac{x}{K_D}\right)^{-slope}}$$

*Equation 1.*  $f$  is the observed difference in absorbance at wavelengths 410 nm and 430 nm within the difference spectrum (see Figure 3) at ligand concentration  $x$ . This difference spectrum is obtained by subtracting the pure heme absorption spectrum from those with ligand present.  $y_{max}$  refers to the absorbance change at ligand saturation,  $y_{min}$  is the extrapolated minimal difference in absorbance;  $K_D$  refers to the dissociation constant of the CYP121 ligand complex.<sup>20</sup>

**Determination of BCGT MIC<sub>BCGT</sub> by OD<sub>600</sub> assay.** A pre-culture of BCGT was grown in 7H9 medium supplemented with ADC Enrichment for 10 days. The assay was performed in 48 well plates (Greiner, Kremsmünster, AT). Prior to culture addition, compounds were serially diluted in DMSO to fit a final DMSO concentration of 1%. For compound susceptibility the pre-culture was diluted 1:100 with fresh medium (7H9 + ADC enrichment). After 168 h of incubation at 37 °C and 80% air moisture, bacterial growth was measured by determination of OD<sub>600</sub>. Absorption data was recorded on a Polarstar Omega Multidetector Plate Reader (BMG LABTECH, Ortenberg, DE). Graphs were plotted with GraphPad Prism using OneSite Log IC<sub>50</sub> model provided by the software. MIC<sub>BCGT</sub> was defined as the concentration at which 50 percent of growth was detected in accordance with previous methods used.<sup>31</sup>

In analogy to ligand efficiency, which relates activity of compounds to their number of heavy atoms, a new metric has been introduced: antibacterial efficiency (AE).<sup>47,48</sup> This coefficient was developed for better comparability of antimicrobial compounds differing in molecular weight (Eq.2).

$$AE = -\ln\left(\frac{MIC}{NHA}\right)$$

*Equation 2.* *AE* refers to the antibacterial efficiency, *MIC* is the minimal inhibitory concentration, and *NHA* equals the number of heavy atoms in a given compound.

**Human cytotoxicity assay.** HEK 293 cells ( $2 \times 10^5$  cells per well) were seeded in 24-well, flat-bottomed plates (Greiner Bioscience, Kremsmünster, AT). Culturing of cells, incubations and OD measurements were performed as described previously<sup>35</sup> with minor modifications. 24 h after seeding of the cells the incubation was started by the addition of the compounds from DMSO stock solutions to a final DMSO concentration of 1%. The living cell mass was determined 48 h after addition of the compounds and was followed by the calculation of LD<sub>50</sub> values. The calculation of the LC<sub>50</sub> values was performed by plotting the percent inhibition vs. the concentration of inhibitor on a semi-logarithmic plot. From this, the molar concentration causing 50% reduction of the living cell mass was calculated. At least three independent experiments were performed for each compound.

## ASSOCIATED CONTENT

**Supporting Information.** The Supporting Information is available free of charge on the ACS

Publications website at DOI:

Including: Chemical synthesis of cYY and Mycocyclosin, SDS-PAGE of His-tagged CYP121, Activity of CYP121/ CO Spectra, LC-MS analysis of in vitro CYP121 enzyme reaction and effect of I:47, Surface Plasmon Resonance Sensorgram of econazole, Screening overview, K<sub>D</sub> determination by UV-VIS Heme coordination assay, Protein Blast of Mtb H<sub>37</sub>R<sub>V</sub> CYP121 (Rv2276) and *M. bovis* BCG Pasteur CYP121 (BCG\_2293), MIC<sub>BCGT</sub> determination against *Mycobacterium bovis*, Calculation of antimicrobial efficiency, Toxicity assessment against human cancer cell lines HEK293 and HepG2, MIC against *Escherichia coli* and *Staphylococcus aureus* in comparison to growth inhibition against *Mycobacterium bovis* BCG, Physicochemical data.

## AUTHOR INFORMATION

### Corresponding Author

\*E-mail: rolf.hartmann@helmholtz-hzi.de, Phone: +49 681 98806 2000; Fax: +49 681 98806-2009.

### Author Contributions

‡ These authors contributed equally.

### Notes

The authors declare no competing financial interest.

## ACKNOWLEDGMENT

Many thanks go to Jeannine Jung, Mellissa Meng, Isabell Schnorr and Phil Servatius for their experimental support. We also want to thank Prof. Munro (University of Manchester) for kindly providing us the plasmid harboring *cyp121* gene (pHAT2/*cyp121*) and Prof. Bernhardt (Saarland University) for the kind gift of the purified ferredoxin Etp1fd (516-618) and ferredoxin reductase Arh1\_A18G.

## REFERENCES

- (1) World Health Organization (2014) Global tuberculosis report 2014. *Available at: <http://www.who.int/tb/>*.
- (2) Udawadia, Z. F., Amale, R. A., Ajbani, K. K., and Rodrigues, C. (2012) Totally drug-resistant tuberculosis in India. *Clin. Infect. Dis.* 54, 579–581.
- (3) Velayati, A. A., Masjedi, M. R., Farnia, P., Tabarsi, P., Ghanavi, J., Ziazarifi, A. H., and Hoffner, S. E. (2009) Emergence of new forms of totally drug-resistant tuberculosis bacilli: super extensively drug-resistant tuberculosis or totally drug-resistant strains in iran. *Chest* 136, 420–425.
- (4) Connolly, L. E., Edelstein, P. H., and Ramakrishnan, L. (2007) Why is long-term therapy required to cure tuberculosis? *PLoS Med.* 4, e120.
- (5) Cole, S. T., Brosch, R., Parkhill, J., Garnier, T., Churcher, C., Harris, D., Gordon, S. V., Eiglmeier, K., Gas, S., Barry, C. E., Tekaia, F., Badcock, K., Basham, D., Brown, D., Chillingworth, T., Connor, R., Davies, R., Devlin, K., Feltwell, T., Gentles, S., Hamlin, N., Holroyd, S., Hornsby, T., Jagels, K., Krogh, A., McLean, J., Moule, S., Murphy, L., Oliver, K., Osborne, J., Quail, M. A., Rajandream, M. A., Rogers, J., Rutter, S., Seeger, K., Skelton, J., Squares, R., Squares, S., Sulston, J. E., Taylor, K., Whitehead, S., and Barrell, B. G. (1998) Deciphering the biology of *Mycobacterium tuberculosis* from the complete genome sequence. *Nature* 393, 537–544.
- (6) Duncan, K. (2004) Identification and validation of novel drug targets in tuberculosis. *Curr. Pharm. Des.* 10, 3185–3194.
- (7) McLean, K. J., Clift, D., Lewis, D. G., Sabri, M., Balding, P. R., Sutcliffe, M. J., Leys, D., and Munro, A. W. (2006) The preponderance of P450s in the *Mycobacterium tuberculosis* genome. *Trends Microbiol.* 14, 220–228.
- (8) McLean, K. J., Carroll, P., Lewis, D. G., Dunford, A. J., Seward, H. E., Neeli, R., Cheesman, M. R., Marsollier, L., Douglas, P., Smith, W. E., Rosenkrands, I., Cole, S. T., Leys, D., Parish, T., and Munro, A. W. (2008) Characterization of active site structure in CYP121. A cytochrome P450 essential for viability of *Mycobacterium tuberculosis* H37Rv. *J. Biol. Chem.* 283, 33406–33416.
- (9) Tsolaki, A. G., Hirsh, A. E., DeRiemer, K., Enciso, J. A., Wong, M. Z., Hannan, M., Goguet de la Salmoniere, Yves-Olivier L, Aman, K., Kato-Maeda, M., and Small, P. M. (2004) Functional and evolutionary genomics of *Mycobacterium tuberculosis*: insights from genomic deletions in 100 strains. *Proc. Natl. Acad. Sci. U.S.A.* 101, 4865–4870.

- (10) Belin, P., Le Du, Marie H el ene, Fielding, A., Lequin, O., Jacquet, M., Charbonnier, J.-B., Lecoq, A., Thai, R., Cour on, M., Masson, C., Dugave, C., Genet, R., Pernodet, J.-L., and Gondry, M. (2009) Identification and structural basis of the reaction catalyzed by CYP121, an essential cytochrome P450 in *Mycobacterium tuberculosis*. *Proc. Natl. Acad. Sci. U.S.A.* *106*, 7426–7431.
- (11) Fonvielle, M., Le Du, M.-H., Lequin, O., Lecoq, A., Jacquet, M., Thai, R., Dubois, S., Grach, G., Gondry, M., and Belin, P. (2013) Substrate and reaction specificity of *Mycobacterium tuberculosis* cytochrome P450 CYP121: insights from biochemical studies and crystal structures. *J. Biol. Chem.* *288*, 17347–17359.
- (12) Martins, M. B., and Carvalho, I. (2007) Diketopiperazines: biological activity and synthesis. *Tetrahedron* *63*, 9923–9932.
- (13) Hudson, S. A., McLean, K. J., Surade, S., Yang, Y.-Q., Leys, D., Ciulli, A., Munro, A. W., and Abell, C. (2012) Application of fragment screening and merging to the discovery of inhibitors of the *Mycobacterium tuberculosis* cytochrome P450 CYP121. *Angew. Chem. Int. Ed. Engl.* *51*, 9311–9316.
- (14) Belin, P., Lecoq, A., Beaurepaire Ledu, M.-H., Gondry, M., and Pernodet, J.-L. (2009). *Patent EP2088143A1*.
- (15) Ahmad, Z., Sharma, S., Khuller, G. K., Singh, P., Faujdar, J., and Katoch, V. M. (2006) Antimycobacterial activity of econazole against multidrug-resistant strains of *Mycobacterium tuberculosis*. *Int. J. Antimicrob. Agents* *28*, 543–544.
- (16) Ahmad, Z., Sharma, S., and Khuller, G. K. (2006) Azole antifungals as novel chemotherapeutic agents against murine tuberculosis. *FEMS Microbiol. Lett.* *261*, 181–186.
- (17) Ahmad, Z., Sharma, S., and Khuller, G. K. (2006) The potential of azole antifungals against latent/persistent tuberculosis. *FEMS Microbiol. Lett.* *258*, 200–203.
- (18) Ahmad, Z., Sharma, S., and Khuller, G. K. (2005) In vitro and ex vivo antimycobacterial potential of azole drugs against *Mycobacterium tuberculosis* H37Rv. *FEMS Microbiol. Lett.* *251*, 19–22.
- (19) Byrne, S. T., Denkin, S. M., Gu, P., Nuermberger, E., and Zhang, Y. (2007) Activity of ketoconazole against *Mycobacterium tuberculosis* in vitro and in the mouse model. *J. Med. Microbiol.* *56*, 1047–1051.
- (20) McLean, K. J., Marshall, K. R., Richmond, A., Hunter, I. S., Fowler, K., Kieser, T., Gurcha, S. S., Besra, G. S., and Munro, A. W. (2002) Azole antifungals are potent inhibitors of cytochrome P450 mono-oxygenases and bacterial growth in mycobacteria and streptomycetes. *Microbiology* *148*, 2937–2949.
- (21) L ez e, M.-P., Le Borgne, M., Pinson, P., Paluszczak, A., Duflos, M., Le Baut, G., and Hartmann, R. W. (2006) Synthesis and biological evaluation of 5-[(aryl)(1H-imidazol-1-yl)methyl]-1H-indoles: potent and selective aromatase inhibitors. *Bioorg. Med. Chem. Lett.* *16*, 1134–1137.

- (22) Bayer, H., Batzl, C., Hartman, R. W., and Mannschreck, A. (1991) jm00113a004 // New aromatase inhibitors. Synthesis and biological activity of pyridyl-substituted tetralone derivatives. *J. Med. Chem.* 34, 2685–2691.
- (23) Leroux, F., Hutschenreuter, T. U., Charrière, C., Scopelliti, R., and Hartmann, R. W. (2003) N-(4-Biphenylmethyl)imidazoles as Potential Therapeutics for the Treatment of Prostate Cancer: Metabolic Robustness Due to Fluorine Substitution? *HCA* 86, 2671–2686.
- (24) Voets, M., Antes, I., Scherer, C., Müller-Vieira, U., Biemel, K., Marchais-Oberwinkler, S., and Hartmann, R. W. (2006) Synthesis and evaluation of heteroaryl-substituted dihydronaphthalenes and indenes: potent and selective inhibitors of aldosterone synthase (CYP11B2) for the treatment of congestive heart failure and myocardial fibrosis. *J. Med. Chem.* 49, 2222–2231.
- (25) Lucas, S., Heim, R., Ries, C., Schewe, K. E., Birk, B., and Hartmann, R. W. (2008) In vivo active aldosterone synthase inhibitors with improved selectivity: lead optimization providing a series of pyridine substituted 3,4-dihydro-1H-quinolin-2-one derivatives. *J. Med. Chem.* 51, 8077–8087.
- (26) McLean, K. J., Cheesman, M. R., Rivers, S. L., Richmond, A., Leys, D., Chapman, S. K., Reid, G. A., Price, N. C., Kelly, S. M., Clarkson, J., Smith, W., and Munro, A. W. (2002) Expression, purification and spectroscopic characterization of the cytochrome P450 CYP121 from *Mycobacterium tuberculosis*. *J. Inorg. Biochem.* 91, 527–541.
- (27) Omura, T., and Sato, R. (1964) The Carbon Monoxide-binding Pigment of Liver Microsomes. *J. Biol. Chem.* 239, 2379–2385.
- (28) Ewen, K. M., Schiffler, B., Uhlmann-Schiffler, H., Bernhardt, R., and Hannemann, F. (2008) The endogenous adrenodoxin reductase-like flavoprotein arh1 supports heterologous cytochrome P450-dependent substrate conversions in *Schizosaccharomyces pombe*. *FEMS Yeast Res.* 8, 432–441.
- (29) Müller, J. J., Hannemann, F., Schiffler, B., Ewen, K. M., Kappl, R., Heinemann, U., and Bernhardt, R. (2011) Structural and thermodynamic characterization of the adrenodoxin-like domain of the electron-transfer protein Etp1 from *Schizosaccharomyces pombe*. *J. Inorg. Biochem.* 105, 957–965.
- (30) Morgan, H., and Taylor, D. M. (1992) A surface plasmon resonance immunosensor based on the streptavidin-biotin complex. *Biosens Bioelectron* 7, 405–410.
- (31) Franzblau, S. G., DeGroote, M. A., Cho, S. H., Andries, K., Nuermberger, E., Orme, I. M., Mdluli, K., Angulo-Barturen, I., Dick, T., Dartois, V., and Lenaerts, A. J. (2012) Comprehensive analysis of methods used for the evaluation of compounds against *Mycobacterium tuberculosis*. *Tuberculosis (Edinb)* 92, 453–488.
- (32) Altaf, M., Miller, C. H., Bellows, D. S., and O'Toole, R. (2010) Evaluation of the *Mycobacterium smegmatis* and BCG models for the discovery of *Mycobacterium tuberculosis* inhibitors. *Tuberculosis (Edinb)* 90, 333–337.
- (33) Benko, I., Hernádi, F., Megyeri, A., Kiss, A., Somogyi, G., Tegye, Z., Kraicsovits, F., and Kovács, P. (1999) Comparison of the toxicity of fluconazole and other azole antifungal drugs to

murine and human granulocyte-macrophage progenitor cells in vitro. *J. Antimicrob. Chemother.* 43, 675–681.

(34) Korashy, H. M., Shayeganpour, A., Brocks, D. R., and El-Kadi, Ayman O S (2007) Induction of cytochrome P450 1A1 by ketoconazole and itraconazole but not fluconazole in murine and human hepatoma cell lines. *Toxicol. Sci* 97, 32–43.

(35) Haupenthal, J., Baehr, C., Zeuzem, S., and Piiper, A. (2007) RNAse A-like enzymes in serum inhibit the anti-neoplastic activity of siRNA targeting polo-like kinase 1. *Int. J. Cancer* 121, 206–210.

(36) Liu, C.-F., Lin, C.-H., Lin, C.-C., Lin, Y.-H., Chen, C.-F., Lin, C.-K., and Lin, S.-C. (2004) Antioxidative natural product protect against econazole-induced liver injuries. *Toxicology* 196, 87–93.

(37) Wachall, B. G., Hector, M., Zhuang, Y., and Hartmann, R. W. (1999) Imidazole substituted biphenyls: A new class of highly potent and in vivo active inhibitors of P450 17 as potential therapeutics for treatment of prostate cancer. *Bioorg. Med. Chem.* 7, 1913–1924.

(38) Lipinski, C. A., Lombardo, F., Dominy, B. W., and Feeney, P. J. (2001) Experimental and computational approaches to estimate solubility and permeability in drug discovery and development settings. *Adv. Drug Deliv. Rev.* 46, 3–26.

(39) Koul, A., Arnoult, E., Lounis, N., Guillemont, J., and Andries, K. (2011) The challenge of new drug discovery for tuberculosis. *Nature* 469, 483–490.

(40) Leys, D., Mowat, C. G., McLean, K. J., Richmond, A., Chapman, S. K., Walkinshaw, M. D., and Munro, A. W. (2003) Atomic structure of Mycobacterium tuberculosis CYP121 to 1.06 Å reveals novel features of cytochrome P450. *J. Biol. Chem.* 278, 5141–5147.

(41) Tanford, C. (1978) The hydrophobic effect and the organization of living matter. *Science* 200, 1012–1018.

(42) Nobre, L. S., Todorovic, S., Tavares, Ana Filipa N, Oldfield, E., Hildebrandt, P., Teixeira, M., and Saraiva, L. M. (2010) Binding of azole antibiotics to Staphylococcus aureus flavohemoglobin increases intracellular oxidative stress. *J. Bacteriol.* 192, 1527–1533.

(43) Helmick, R. A., Fletcher, A. E., Gardner, A. M., Gessner, C. R., Hvitved, A. N., Gustin, M. C., and Gardner, P. R. (2005) Imidazole Antibiotics Inhibit the Nitric Oxide Dioxygenase Function of Microbial Flavohemoglobin. *Antimicrob. Agents Chemother.* 49, 1837–1843.

(44) Guardiola-Diaz, H. M., Foster, L.-A., Mushrush, D., and Vaz, A. D. (2001) Azole-antifungal binding to a novel cytochrome P450 from Mycobacterium tuberculosis: implications for treatment of tuberculosis. *Biochem. Pharmacol.* 61, 1463–1470.

(45) Boshoff, Helena I M, Myers, T. G., Copp, B. R., McNeil, M. R., Wilson, M. A., and Barry, C. E. (2004) The transcriptional responses of Mycobacterium tuberculosis to inhibitors of metabolism: novel insights into drug mechanisms of action. *J. Biol. Chem.* 279, 40174–40184.

(46) Milano, A., Pasca, M. R., Provvedi, R., Lucarelli, A. P., Manina, G., Ribeiro, Ana Luisa de Jesus Lopes, Manganelli, R., and Riccardi, G. (2009) Azole resistance in Mycobacterium tuberculosis is mediated by the MmpS5-MmpL5 efflux system. *Tuberculosis* 89, 84–90.

(47) Hopkins, A. L., Groom, C. R., and Alex, A. (2004) Ligand efficiency: a useful metric for lead selection. *Drug Discov. Today* 9, 430–431.

(48) Czaplewski, L. G., Collins, I., Boyd, E. A., Brown, D., East, S. P., Gardiner, M., Fletcher, R., Haydon, D. J., Henstock, V., Ingram, P., Jones, C., Noola, C., Kennison, L., Rockley, C., Rose, V., Thomaides-Brears, H. B., Ure, R., Whittaker, M., and Stokes, N. R. (2009) Antibacterial alkoxybenzamide inhibitors of the essential bacterial cell division protein FtsZ. *Bioorg. Med. Chem. Lett.* 19, 524–527.

**Supporting Information: Appendix 7.1 A**



**B Discovery and biophysical evaluation of first low nanomolar hits targeting CYP125 of *M. tuberculosis***

**Manuscript B**

The experimental contributions to this manuscript made by the respective persons are summarized below:

Christian Brengel: He heterologously expressed CYP121, CP125, and CYP142. Furthermore, he executed the SPR measurement, heme assay and the MTT assay.

Andreas Thomann: He heterologously expressed CYP121, CP125. Furthermore, he executed heme assay.

Alexander Schifrin: He measured the CO-spectra of CYP125 and CYP121

**Abstract:** Tuberculosis which is predominantly caused by *Mycobacterium tuberculosis* (Mtb) is still the most lethal bacterial infection with 1.5 million casualties in 2014. Moreover, appearance of resistant mutants and the long term treatment being coupled with economic problems of developing countries hamper an efficient therapy. The interference with the essential cholesterol metabolism of Mtb could be a promising novel strategy to fight Mtb infections. CYP125, a P450 enzyme in Mtb, was shown to play an important role in this metabolic pathway. For this reason, we used a combined screening approach of surface plasmon resonance spectroscopy (SPR) and heme coordination assay to identify new CYP125 binders employing a focused P450-inhibitor library. We could identify first hits with high affinity and favourable ligand efficiencies (LE). Furthermore, frontrunner compounds showed also selectivity towards CYP121 specific to Mtb and required for its survival. To date, these are the first compounds targeting CYP125 with low nanomolar affinity.

## Introduction

Since the discovery of first drugs for the therapy of tuberculosis (TB) in the 1940's many new compounds and therapeutic regimes have been developed to improve treatment of TB.<sup>[1,2]</sup> Despite these great successes, the World Health Organization (WHO) registered 9 million new infections and 1.5 million cases of death caused by the disease in 2014.<sup>[3]</sup> Key problems are the long term treatment of at least 6 months, resistance development against anti-TB drugs and co-infections with *human immunodeficiency virus* (HIV). In this respect, new anti-TB drugs, should address these circumstances and most preferably reduce hospitalization and increase therapeutic success of treatment-resistant TB.<sup>[2,4]</sup> For these reasons, there is an urgent need for new drug targets with novel modes of action to improve the portfolio of anti-TB drugs.

In 2007 Chang et al. identified an interesting sequence in the genome of Mtb which is required for mycobacterial growth in macrophages. The so called “*igr*” operon (derived from “intracellular growth”) was also confirmed to be essential for Mtb's full virulence in an *in vivo* scenario.<sup>[5]</sup> In subsequent studies it could be shown that the respective operon is involved in cholesterol metabolism of Mtb. Therein, a  $\Delta$ *igr* mutant was not able to grow on cholesterol and the supplementation of an additional source of nutrition demonstrated only insufficient recovery of growth. These findings suggested an intoxicating effect caused by the sterol.<sup>[6]</sup> In the same year CYP125, a P450 enzyme encoded in the *igr* operon, was reported to efficiently metabolize cholesterol.<sup>[7]</sup> Capyk et al. could generate a  $\Delta$ *cyp125* knock-out strain of *M. bovis* BCG which was unable to survive on cholesterol supplemented medium indicating the CYP-enzyme to be a key player for cholesterol detoxification. However, this finding could not be confirmed by a  $\Delta$ *cyp125* mutant of *M. tuberculosis* H<sub>37</sub>R<sub>v</sub>.<sup>[8]</sup> Further investigations explained this observation with the presence of a compensatory enzyme, namely CYP142 in the laboratory strain H<sub>37</sub>R<sub>v</sub>. However, the latter enzyme is not present in the clinical isolate CDC1551, questioning the clinical relevance of this bypass.<sup>[9,10]</sup> Moreover, in this study the previous

results found for BCG were corroborated which still render CYP125 as a key enzyme for cholesterol metabolism.<sup>[9]</sup>

As metabolism of cholesterol plays an essential role in persistence and virulence of Mtb, interference with the key player CYP125 could be a new promising strategy for TB treatment.<sup>[6,9,11]</sup> Until today, besides the azole-antifungals, there is only one inhibitor of CYP125 described: **LP10**.<sup>[7,12]</sup> Interestingly, **LP10** was not designed for inhibition of CYP125 but was discovered as an inhibitor of CYP51 from *Trypanosoma cruzi*.<sup>[13]</sup> CYP125 inhibition was only moderate which was explained with its lower affinity compared to the substrate cholest-4-en-3-one (**CHN**).<sup>[12]</sup>

Herein, we employed a combined biophysical screening approach for the discovery of new CYP125 binders with increased affinity and favorable Ligand Efficiency (LE).<sup>[14]</sup> The compounds discovered showed 7 to 70 times higher affinity for CYP125 than its substrate **CHN** rendering promising starting points for future drug optimization campaigns.

## Results and Discussion

### Library generation

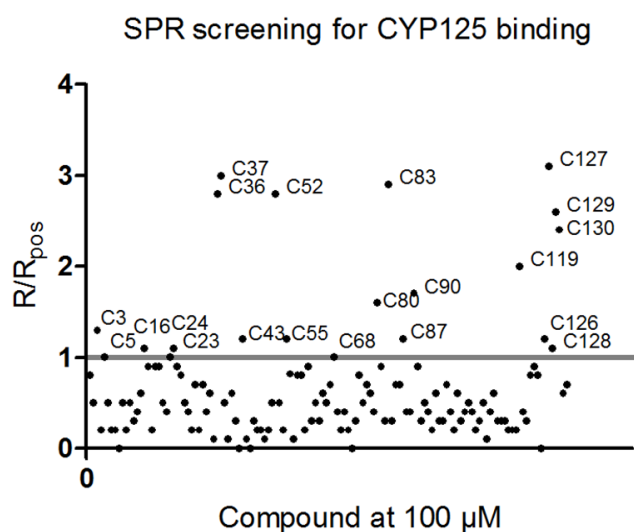


**Figure 1.** Result of the SPR screening. 22 out of 132 compounds were hits with  $R/R_{\text{pos}} \geq 1$  with  $R$  = response of econazole (**Eco**),  $R_{\text{pos}}$  = response of library compound.

For the SPR guided identification of CYP125 binders we started with a hand-picked selection of 132 compounds from our in-house CYP inhibitor library focusing on structural diversity. The library contains compounds designed for inhibition of human steroidal P450 enzymes, especially CYP17, CYP11B1/2 and CYP19.<sup>[15–36]</sup> These inhibitors are privileged to interact with P450 enzymes because of their nitrogen containing heterocycle enabling coordination to the iron(II) center of the heme.<sup>[15]</sup> In

general huge benefits arise from the use of focused libraries: the hit rates are usually much higher, the biological activities are already known for the compounds and derivatization is often easy as synthetic routes are already established. Thus, for our compounds inhibition data for steroidogenic and hepatic CYP enzymes as well as cytotoxicity data were available.

For the evaluation of our library compounds, two described inhibitors of CYP125, namely econazole (**Eco**) and **LP10** served as reference compounds.<sup>[7,12]</sup>

#### *SPR screening*

CYP125 used for *in vitro* experiments was expressed in the heterologous host *E.coli* BL21 DE3 and was purified by affinity chromatography. The correct folding and function of the enzyme was confirmed with carbon monoxide binding spectra.<sup>[37]</sup> In these studies we were also able to identify a new heterologous electron transfer system composed of Etp1fd (516-618) as ferredoxin and Arh1\_A18G as reductase.<sup>[38,39]</sup> Biotinylated CYP125 was bound to the streptavidine labelled SPR sensor-chip.<sup>[40]</sup>

The reference compound **Eco** is reported to form a type II complex with CYP125's heme-iron.<sup>[7]</sup> For initial validation of our SPR technique, we confirmed **Eco** binding at a concentration of 100  $\mu\text{M}$  to immobilized CYP125. (SI Figure 1) For all library compounds the binding response of **Eco** ( $R_{\text{pos}}$ ) was set to 1. The compounds were tested in the same concentration (100  $\mu\text{M}$ ) and their binding response ( $R$ ) was referenced to the response of the positive control ( $R/R_{\text{pos}}$ ). All compounds with an  $R/R_{\text{pos}}$  value  $\geq 1$  were regarded as hits in the following experiments and defined as SPR binders. The screening of the in-house library consisting of 132 compounds resulted in 22 binders which showed a broad structural variety. The observed hit rate (approximately 17%) is high confirming our initial hypothesis that choosing privileged structures results in lower attrition rates (Figure 1).

#### *UV-VIS heme P450 binding assay*

To derive detailed information of compound binding behavior we chose the UV-Vis heme coordination assay for P450 enzyme interaction.<sup>[41]</sup> The assay was used to determine the binding affinity and the putative binding mode of our SPR hits. Such experiments, employing CYP125 are already described for **Eco**, the substrate **CHN** and **LP10**.<sup>[7,9,12]</sup> In our study, we selected these three compounds as positive- and three weak SPR binders (**C25**, **C53**, **C59**) as negative controls ( $R/R_{\text{pos}} < 1$ , SI Table 1, Figure 2).<sup>[7]</sup> **LP10** and **CHN** bound as previously reported to CYP125 with slight differences in the  $K_D$  values ( $K_D$  **CHN** = 6.1  $\mu\text{M}$ ,  $K_D$  **LP10** = 4.6  $\mu\text{M}$ ;  $K_D$  **CHN**<sub>lit</sub> = 1.2  $\mu\text{M}$ ,  $K_D$  **LP10**<sub>lit</sub> = 1.7  $\mu\text{M}$ ).<sup>[9,12]</sup> For **LP10** an increase in absorbance of the low spin band at 420 nm is described (such compounds are defined as reverse type I binders), which we could confirm in our experiments.<sup>[12]</sup> Interestingly, for econazole we observed a type I binding behavior with a  $K_D$  of 0.94  $\mu\text{M}$  which differs from the type II profile with a  $K_D$  of 11  $\mu\text{M}$  described by McLean et al.<sup>[7]</sup> Notably, the co-crystal structure of econazole bound to CYP125 (PDB-ID: 3IW2) shows a water-

bridge interaction with the iron-heme which supports our finding.<sup>[7]</sup> From the initial 22 SPR binders, we identified 14 compounds that showed binding to the CYP125 heme with a  $K_D < 30 \mu\text{M}$  (SI Table 1). It is described, that the iron of the native enzyme is in equilibrium between low spin and high spin.<sup>[7]</sup> Thus, a reverse type I binding as seen for **LP10** might be possible for some of our compounds as well.<sup>[12]</sup> Out of the 14 heme coordinators, nine show a characteristic type II or reverse type I profile. Their binding resulted in an absorbance maximum at a higher wavelength compared to **LP10** (SI Table 2) and, hence, a type II interaction might be more plausible than a reverse type I. Nevertheless, a precise binding mode determination might require an analysis of the co-crystal structure of our hits and CYP125. For convenience we use in the following the term type II shift profile.

With regard to type I binding behavior, we could identify further seven compounds fulfilling this profile. Five SPR hits do not seem to exhibit a heme coordination behavior (SI Table 1). The binders with highest affinity, **C24** (type I:  $0.26 \mu\text{M}$ ) as well as **C127**, **C128**, and **C130** (type II: **C127** =  $0.85 \mu\text{M}$ ; **C128** =  $0.084 \mu\text{M}$ ; **C130** =  $0.17 \mu\text{M}$ ) displayed a  $K_D$  in the nanomolar range which, to the best of our knowledge, renders them the most affine compounds to CYP125 described to date (SI Table 1). The weak SPR binders ( $R/R_{\text{pos}} < 1$ ) with a high structural relationship to strong binders were chosen for SPR screening procedure validation (SI Table 1; **C25**, **C59**, **C53**):

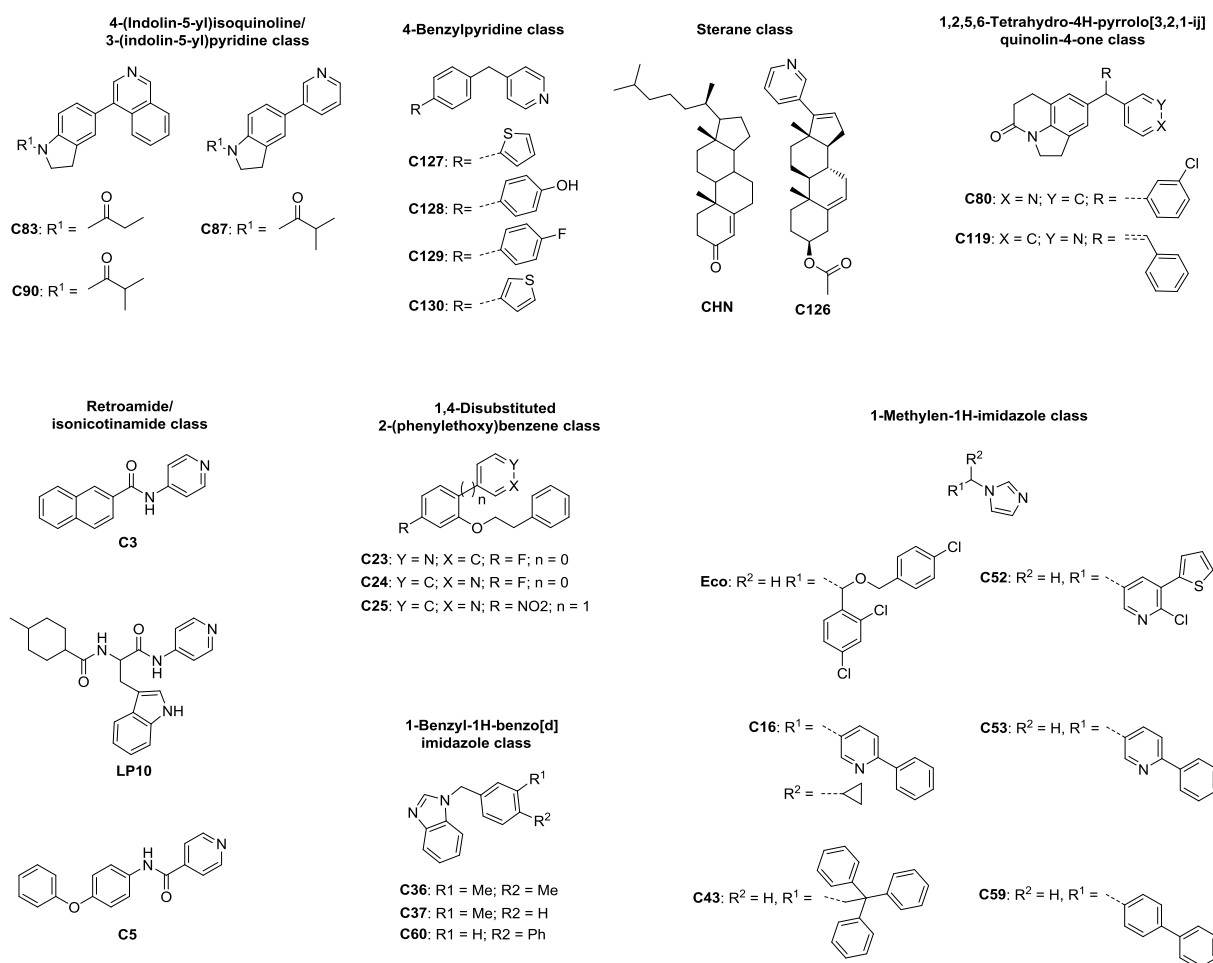


**Figure 2.** Chemical structures of the 22 SPR hits.

**C25** is an example for a weak binder which is structurally strongly related to the strong SPR and heme binders **C23** and **C24** (Figure 2). As expected, **C25** did not interact with the heme iron (SI Table 1). Furthermore, **C53** and **C59** showing distinct structural analogy to **Eco** had exhibited low affinity in the SPR experiment. Thus, we were interested whether these compounds were false positives and tested them for heme coordination. Again, none of these compounds showed binding to CYP125 in the UV/VIS assay which validates our initial screen. Notably, we obtained several compounds (SI Table 1; **C45**, **C52**, **C83**, **C87**, **C90**, and **C119**) with a stronger SPR response than **Eco** ( $R/R_{\text{pos}} \geq 1$ ) that did not interact with the heme iron. Such compounds are expected to bind to other binding sites of the protein without interacting with the iron in the catalytic center. They were excluded from the screening procedure but are still interesting as they might function as fragments in merging or linking strategies with type I or type II binders. However, with the information of the respective binding modes, one can faster and more rationally decide how to modify the binders or even combine given structures to generate inhibitors of higher activity.

The gathered data from the two binding assays provide fundamental information for preliminary structure binding relationships (Table 1 and SI Table 1). The ligand efficiency (LE) as a classification index is not only indicative of the affinity of a compound but takes also its molecular weight into consideration: the LE is the free energy contribution for binding (expressed in kcal) per heavy atom (HA) of the molecule.<sup>[14]</sup> These data were calculated to give estimation if a compound is suitable for efficient drug discovery with regard to its size and affinity (LE > 0.3). Having a look at the head groups needed for interaction with the heme iron a first SAR observation can be made. In case of the methylene-bridged imidazole residues only **Eco** binds in the nanomolar range (SI Table 1).

**Table 1.** Heme binding affinity data, binding profiles and selectivity factors of CYP125 binders against Mtb CYP121 and the bypass enzyme CYP142.

Cmpd	CYP125			CYP142			CYP121		SF <sup>[a]</sup>	
	type	K <sub>D</sub> [μM]	LE [kcal/mol]	type	K <sub>D</sub> [μM]	LE [kcal/mol]	type	K <sub>D</sub> [μM]	142 vs. 125	121 vs. 125
<b>C3</b> <sup>[19]</sup>	II	19	0.35	II	0.893	0.45	weak	>100	0.047	>5.26
<b>C5</b> <sup>[18]</sup>	II	28	0.29	II	6.265	0.14	weak	>100	0.224	>3.57
<b>C16</b> <sup>[17]</sup>	I	16	0.32	I	19.71	0.31	II	>100	1.232	>6.25
<b>C23</b> <sup>[21]</sup>	I	1.5	0.37	I	1.789	0.17	II	7.20	1.193	4.80
<b>C24</b> <sup>[21]</sup>	I	0.26	0.42	I	1.533	0.18	II	11.7	5.896	45.00
<b>C36</b> <sup>[27,28]</sup>	I	1.3	0.46	I	3.428	0.19	no	>100	2.637	>76.92
<b>C37</b> <sup>[27,28]</sup>	I	1.1	0.49	no	100	0.33	no	>100	90.909	>90.91
<b>C43</b> <sup>[27,28]</sup>	II	13.1	0.26	II	0.143	0.37	II	8.8	0.011	0.67
<b>C60</b> <sup>[27,28]</sup>	I	0.28	0.42	I	0.183	0.43	no	>100	0.654	>357.14
<b>C126</b> <sup>[20]</sup>	II	2.1	0.27	no	>100	---	no	>100	>47.619	>47.62
<b>C127</b> <sup>[20]</sup>	II	0.85	0.47	II	0.096	0.55	II	2.6	0.113	3.06
<b>C128</b> <sup>[20]</sup>	II	0.084	0.50	II	0.008	0.57	II	1.33	0.095	15.83
<b>C129</b> <sup>[20]</sup>	II	1.34	0.41	II	0.062	0.50	II	2.5	0.046	1.87
<b>C130</b> <sup>[20]</sup>	II	0.174	0.53	II	0.252	0.51	II	1.8	1.448	10.34
<b>LP10</b> <sup>[12]</sup>	II	6.1	0.24	II	5.02	0.25	II	34.3	0.823	5.62
<b>Eco</b> <sup>[b]</sup> <sup>[7]</sup>	I	0.941	0.35	II	0.767	0.36	II	2.8	0.815	2.98
<b>CHN</b> <sup>[c]</sup> <sup>[7]</sup>	I	4.6	0.27	I	0.948	0.30	no	>100	1.896	>200.00

[a] SF = selectivity factor, [b] Eco = econazole, [c] CHN = Cholest-4-en-3-one

All other compounds containing such a structure were only weak binders or did not show any heme iron coordination respectively. (**C16**, **C43**, **C52**). In contrast to this, most of pyridinyl and benzimidazolyl head groups linked to different core structures are tolerated by the enzyme. In these subgroups, we identified type I as well as type II binders depending on the core structure. Notably, all benzimidazolyl-substituted compounds showed binding to CYP125 in both test systems (Figure 2), especially **C60**, with a K<sub>D</sub> value of 0.28 μM and a LE of 0.42 kcal/HA. The two derivatives of this subset having the phenyl residue replaced by a methyl group showed an even higher LE score (**C36**: 0.46 kcal/HA, **C37**: 0.49 kcal/HA) (SI Table 1). This underlines the potential of the 1-benzyl-1*H*-benzo[*d*]imidazole class as a promising starting point for hit optimization, as these compounds are still in the molecular weight range of fragments (< 300 Da). The SPR screening yielded various compounds bearing a pyridinyl head group linked to different core structures (Figure 2). In general, compounds with an 4-(indolin-5-yl)isoquinoline or 3-(indolin-5-yl)pyridine scaffold did not show heme interaction at the tested concentrations and were therefore excluded from further investigations.



The isonicotinamid and corresponding retroamid compounds (**C3**, **C5**) share some degree of structural similarity to literature described CYP125 inhibitor **LP10**. Both compounds generate a type II shift.  $K_D$  values and LE (**LP10**: 6.1  $\mu\text{M}$  and 0.24 kcal/HA; **C5**: 28  $\mu\text{M}$  and 0.29 kcal/HA) are in an acceptable range but lower than seen for other high affinity ligands from the focused library. These structures should be regarded as second choice if the more affine compounds fail in a subsequent optimization process. The binders found in the 1,2,5,6-tetrahydro-4H-pyrrolo[3,2,1-ij]quinolin-4-one class were of moderate affinity with a type II binding profile (Table 1). Because of their low affinity combined with their high molecular weight, **C80** and **C119** are not suitable for structural optimization regarding CYP125 inhibition. High affinity binders were identified in the 1,4-disubstituted 2-(phenylethoxy)benzene and 4-benzylpyridine substituted subset (Figure 2). The latter derivatives bind in a type I mode to the enzyme. Interestingly, repositioning of the coordinating nitrogen from *para* to *meta* in the heteroaromatic ring of this compound class results in a 6-fold increase in binding affinity for **C24** ( $K_D = 0.26 \mu\text{M}$ ) compared to **C23** ( $K_D = 1.5 \mu\text{M}$ ) (Table 1). A reason for this increase could be a privileged angle for interaction of nitrogen with the coordinating water molecule linked to the heme iron or a more favorable interaction with other residues of the protein. With a LE score of 0.42 kcal/HA **C24** provides a considerable potential for further optimization. Most interestingly, highly activate compounds could also be observed in the group of 4-benzylpyridines. Three of the four compounds bind with low micromolar to nanomolar affinity to CYP125 (**C127**: 0.85  $\mu\text{M}$ ; **C128**: 0.085  $\mu\text{M}$ ; **C129**: 1.34  $\mu\text{M}$ ; **C130**: 0.17  $\mu\text{M}$ ). Moreover, the low molecular weight of these compounds results in remarkable LE scores (**C127**: 0.47 kcal/HA; **C128**: 0.50 kcal/HA; **C129**: 0.41 kcal/HA; **C130**: 0.53 kcal/HA.). The *p*-hydroxyphenyl residue increases the affinity in comparison to the *p*-fluorophenyl group. Presumably, an electron rich aromatic system is preferred or the hydroxyl-group undergoes additional interactions with the target. Regarding five-membered heterocycles, the electron-rich thiophene compounds (**C127**, **C130**) showed also high affinity. In particular, we observed a difference between the thiophene regional isomers in the class of the aforementioned derivatives whereby the 2-substituted **C127** compound is superior in terms of affinity over the 3-substituted congener **C130** (Table 2). From the 132 initially tested compounds, **C128** was the one with the highest affinity to CYP125 and is the most affine compound described in literature to date. With a 55-fold lower  $K_D$  value than the substrate CHN ( $K_D = 4.6 \mu\text{M}$ ), **C128** should be a highly efficient inhibitor of the enzyme reaction.

#### *Selectivity among P450 enzymes*

As the library compounds were originally designed for the inhibition of human steroidogenic enzymes it was important to compare their activities towards human steroidogenic and hepatic as well as bacterial CYP enzymes (Table 2). Most compounds from our library are active in the nanomolar range against their respective target.<sup>[15-36]</sup> From our 14 heme-binders we selected five, based on their LE score, to be the most promising hits (**C24**, **C60**, **C127**, **C128**, **C130**) for further selectivity evaluation.

Compounds out of the 2-(phenylethoxy)benzene class are potent inhibitors of CYP11B1 and CYP11B2. Although **C24** showed good binding affinity to CYP125 ( $K_D = 0.26 \mu\text{M}$ ), an improvement of selectivity towards CYP11B1 and CYP11B2 enzymes is necessary ( $IC_{50}$  CYP11B1:  $51 \mu\text{M}$ ,  $IC_{50}$  CYP11B2:  $84 \mu\text{M}$ ). The frontrunner compound of the 1-benzyl-1*H*-benzo[*d*]imidazole class, that is **C60** ( $K_D = 0.28 \mu\text{M}$ ), was not active against CYP17 (6% inhibition at  $2 \mu\text{M}$ ) and CYP19 (2% inhibition at  $0.5 \mu\text{M}$ ) and showed only a weak inhibition of CYP11B2. The  $IC_{50}$  against CYP11B1 ( $IC_{50} = 0.197 \mu\text{M}$ ) is in a similar range as the  $K_D$  value against CYP125. However, it should be noted that  $K_D$  values are typically lower than  $IC_{50}$  values.<sup>[42]</sup> Looking at the activity of 4-substituted 4-benzylpyridines we observed similar values for **C127** and **C130** on CYP125, CYP17 and CYP11B1 and CYP11B2 but with **C128** an exception, as it showed a moderate selectivity over CYP17, CYP19, CYP11B1, CYP11B2 and CYP3A4 (Table 2).

As the basis of our strategy is to interfere with a crucial function during host adaptation of *Mtb* we were interested to study whether the herein found inhibitors might also bind to an essential consistently expressed CYP enzyme of *Mtb*.

**Table 2.** Selectivity profile of most affine CYP125 heme ligands ( $K_D < 1 \mu\text{M}$ ) versus human CYP enzymes.

Cmpd.	CYP125	CYP17	CYP11B1	CYP11B2	CYP19	CYP3A4
	$K_D$ [nM]	$IC_{50}$ [nM]	$IC_{50}$ [nM]	$IC_{50}$ [nM]	$IC_{50}$ [nM]	$IC_{50}$ [nM]
<b>C24</b>	260	-	51	84	-	-
<b>C60</b>	280	6% at 2000	197	1903	2% at 500	-
<b>C127</b>	850	577	422	331	-	-
<b>C128</b>	84	248	251	341	3070	3210
<b>C130</b>	174	647	415	796	-	-

We chose CYP121, an enzyme essential for *Mtb in vitro*, for the latter mentioned counter screen. In addition, we incorporated CYP142, the bypass enzyme of the CYP125 enzyme-reaction in *Mtb* H<sub>37</sub>R<sub>v</sub>, to study the possibility of a dual target strategy.<sup>[10,43]</sup> Here we determined selectivity factors (SF) to enhance comparability. When looking at the compounds with nanomolar binding affinity to CYP125 we obtained different profiles depending on the compound class (Table 1). **C24** is a selective binder of CYP125, with regard to CYP142, showing less selectivity to CYP121 ( $SF_{CYP142}$ : 6;  $SF_{CYP121}$ : 45). In contrast to **C60** which also binds tightly to the bypass enzyme CYP142 and is a much weaker inhibitor of CYP121 ( $SF_{CYP142}$ : 0.6;  $SF_{CYP121}$  > 350). With regard to CYP142, selectivity might not be desirable as blockage of the bypass could increase the effectivity of cholesterol metabolism targeted approach, at least in the lab strain H<sub>37</sub>R<sub>v</sub>. In general, the 4-benzylpyridines **C127**, **C128**, **C130** possess a tight binding profile and convincing LE scores on CYP142 and selectivity towards CYP121 with **C128** being the most promising compound overall (**C128**:  $SF_{CYP142}$ : 1;  $SF_{CYP121}$ : 16, Table 1).

## Conclusions

In this study, 132 compounds of a focused CYP inhibitor library were subsequently screened using two biophysical assays to identify nanomolar binders to CYP125. This procedure led to the identification of 22 hit-compounds with high structural diversity. Further investigations employing a UV/Vis heme coordination assay characterized five compounds as type I and nine as type II binders with  $K_D$  values below 30  $\mu\text{M}$ . Five out of these compounds (type II: **C127** = 0.85  $\mu\text{M}$ , **C128** = 0.085  $\mu\text{M}$ , and **C130** = 0.174  $\mu\text{M}$ ; type I: **C24** = 0.26  $\mu\text{M}$ , **C60** = 0.28  $\mu\text{M}$ ) bind in the nanomolar range to the heme site of CYP125. Thereby, their affinity is higher than the affinity of the

substrate **CHN** which makes them interesting candidates with a possibly high inhibitory potential. Furthermore, these compounds showed a 7 to 70-fold increased affinity to CYP125 in comparison to the reported inhibitor **LP10**. Frontrunner compound **C128** is - to the best of our knowledge - the first described low nanomolar CYP125 binder. In addition, this compound tightly binds to the bypass enzyme of CYP125 (CYP142) providing a good starting point for *in cellulo* proof of principle studies in Mtb lab strain H<sub>37</sub>R<sub>v</sub>. The selectivity among human (CYP11B1/B2, CYP19, CYP17, CYP3A4) and another essential Mtb P450 enzyme (CYP121) is given for some inhibitors investigated in this study. However, an improvement of selectivity is important to circumvent potential later stage side effects originated from blockage of steroid and/or xenobiotic metabolism by CYP enzymes in humans. Moreover, compounds identified in this study might be also useful as scientific tools to further support the investigation of the intensively discussed cholesterol metabolism in Mtb as some of them block both enzymes known for **CHN** transformation (CYP125 and CYP142). Furthermore, due to their low molecular weight, excellent water solubility, and high LE the herein reported compounds are promising first hits for the development of novel antimycobacterial drugs targeting an essential metabolic pathway in Mtb.

### Acknowledgements

We thank Prof. Ortiz de Montellano for kindly providing plasmids pCWori/*cyp125* and pCWori/*cyp142A1*<sup>[9]</sup> and Prof Munro for kindly providing pHAT2/*cyp121* harboring plasmid. We thank Prof. Bernhard for fruitful discussions, for providing plasmids harbouring Arh1\_A18G and Etp1fd and for the possibility to characterize the enzymes by UV/VIS in her laboratory.

### Experimental Section

**Bacterial strains and growth conditions.** Bacterial strain used in this study was *E. coli* K12 BL21 DE3 for protein expression.

**Chemical synthesis and analytical characterization.** Compounds for testing (**LP10**, econazole (**Eco**) and choleste-3-en-4-one (**CHN**)) were purchased from commercial suppliers and used without further purification. Procedures for the synthesis of library compounds were reported before.<sup>[15-36]</sup> Detailed information can be found in SI section 6.

**Protein expression, purification and biotinylation.** *E. coli* K12 BL21 DE3 cells were transformed with plasmid harbouring *cyp125* gene (CYP125A1/pCWori).<sup>[9]</sup> The previously described enzyme expression and purification method was slightly modified and used for CYP125, CYP142 and CYP121 constructs.<sup>[7,44]</sup> His<sub>6</sub>-tagged protein was expressed in *E. coli* K12 BL21 DE3 and purified using a single affinity chromatography step. Briefly, *E. coli* K12 BL21 DE3 cells containing the plasmid were grown in terrific broth medium containing 100 µg/mL ampicillin at 37 °C until an OD<sub>600</sub>

of approximately 0.8 mAU was reached. Protein expression was then induced by the addition of 0.5 mM IPTG and 0.5 mM  $\delta$ -aminolevulinic acid and the bacteria were grown for additional 36 h at 25 °C and 200 rpm. The cells were harvested by centrifugation (5000 rpm, 10 min, 4 °C), and the cell pellet was resuspended in 100 mL of binding buffer containing 1% Triton-X-100 (50 mM tris-HCl, 300 mM NaCl, 20 mM imidazol, 10% glycerol, pH = 7.2) and lysed by sonication for a total process time of 2.5 min. Cellular debris was removed by centrifugation (18500 rpm, 40 min, 4 °C), and the supernatant was filtered through a syringe filter (0.2  $\mu$ m). The clear lysate was immediately applied to a Ni-NTA affinity column, washed with binding buffer, and eluted with an one-step gradient of 500 mM imidazole. The protein containing fractions were buffer-exchanged to storage buffer (140 mM NaCl, 10 mM Na<sub>2</sub>HPO<sub>4</sub>, 2.7 mM KCl, 1.8 mM KH<sub>2</sub>PO<sub>4</sub> and 10% glycerol (v/v), pH = 7.2), using a PD10 column (GE Healthcare) and judged pure by SDS-PAGE analysis. Protein was stored in aliquots at -80 °C at a final concentration of 50  $\mu$ M. Before SPR streptavidin immobilization CYP125 was biotinylated. For biotinylation, EZ-linked Sulfo-NHS-LC-LC-Biotin (Thermo Science) was dissolved in storage buffer (140 mM NaCl, 10 mM Na<sub>2</sub>HPO<sub>4</sub>, 2.7 mM KCl, 1.8 mM KH<sub>2</sub>PO<sub>4</sub> and 10% glycerol (v/v)) with CYP125 in 1:1 molar ratio. The solution was incubated on ice for 2 h and mixed carefully every 30 minutes. The biotinylated CYP 121 was purified by size exclusion column using storage buffer and stored at -80 °C at a final concentration of 10  $\mu$ M.<sup>[40]</sup>

**Spectroscopic characterization of enzyme activity.** Ferredoxin Etp1fd (516-618) and ferredoxin reductase Arh1\_A18G from the fission yeast *Schizosaccharomyces pombe* were expressed and purified as described previously.<sup>[38,39]</sup> Functionality of CYP125 and electron transfer was assayed by the occurrence of the characteristic peak at ~450 nm, related to the reduced, CO-bound heme complex. The assay was conducted as described with slight modifications.<sup>[37]</sup> CYP125 (2  $\mu$ M) was reduced through the addition of a few grains of sodium dithionite or incubation with NADPH (100  $\mu$ M), Etp1fd (516618) (40  $\mu$ M), and Arh1\_A18G (2  $\mu$ M) and divided in two cuvettes to record a baseline. One of the samples was saturated with carbon monoxide for 60 s and difference spectra were recorded until the peak at ~450 nm reached saturation.

**SPR-Screening.** SPR binding studies were performed using a Reichert SR7500DC instrument optical biosensor (Reichert Technologies) and SAD500m sensor chips obtained from XanTec Bioanalytics. CYP125 was immobilized on a SAD500m sensor chip at 12 °C using standard biotin-streptavidin complexation. The surface of both channels was quenched by a 3 min injection of 3  $\mu$ g/mL biotin. CYP125 was immobilized at densities between 5000 and 6000 RU for binding studies.

**UV-VIS Heme P450 binding assay.** Optical titration experiments were performed in 96 well plates (Greiner; transparent round-bottom). The data were recorded using Tecan infinite M200Pro (Nano Quant). Absorbance of enzyme and enzyme-inhibitor complex was measured between 350 and 500 nm in 1 nm steps with 10 flashes. Compounds were titrated from DMSO stock solutions to a final DMSO

concentration of 1%. CYP125, CYP121, and CYP142 were used in a concentration of 0.25  $\mu\text{M}$ . Data were plotted by optical shift versus ligand concentration. Variable slope model was used for nonlinear regression of resulting dose–response curves employing GraphPad Prism 5.

**Keywords:** CYP-Inhibitors • *Mycobacterium tuberculosis* • Screening • Anti-infectives • Biophysical Methods

- [1] M. D. Iseman, *European Respiratory Journal* **2002**, *20*, 87S.
- [2] A. Zumla, P. Nahid, S. T. Cole, *Nature reviews. Drug discovery* **2013**, *12*, 388–404.
- [3] World Health Organization **2014**.
- [4] A. Koul, E. Arnoult, N. Lounis, J. Guillemont, K. Andries, *Nature* **2011**, *469*, 483–490.
- [5] J. C. Chang, N. S. Harik, R. P. Liao, D. R. Sherman, *The Journal of infectious diseases* **2007**, *196*, 788–795.
- [6] J. C. Chang, M. D. Miner, A. K. Pandey, W. P. Gill, N. S. Harik, C. M. Sasseti, D. R. Sherman, *Journal of bacteriology* **2009**, *191*, 5232–5239.
- [7] K. J. McLean, P. Lafite, C. Levy, M. R. Cheesman, N. Mast, I. A. Pikuleva, D. Leys, A. W. Munro, *The Journal of biological chemistry* **2009**, *284*, 35524–35533.
- [8] J. K. Capyk, R. Kalscheuer, G. R. Stewart, J. Liu, H. Kwon, R. Zhao, S. Okamoto, W. R. Jacobs, L. D. Eltis, W. W. Mohn, *The Journal of biological chemistry* **2009**, *284*, 35534–35542.
- [9] H. Ouellet, S. Guan, J. B. Johnston, E. D. Chow, P. M. Kells, A. L. Burlingame, J. S. Cox, L. M. Podust, de Montellano, Paul R Ortiz, *Molecular microbiology* **2010**, *77*, 730–742.
- [10] J. B. Johnston, H. Ouellet, Ortiz de Montellano, Paul R, *The Journal of biological chemistry* **2010**, *285*, 36352–36360.
- [11] A. K. Pandey, C. M. Sasseti, *Proceedings of the National Academy of Sciences of the United States of America* **2008**, *105*, 4376–4380.
- [12] H. Ouellet, P. M. Kells, Ortiz de Montellano, Paul R, L. M. Podust, *Bioorganic & medicinal chemistry letters* **2011**, *21*, 332–337.
- [13] C.-K. Chen, P. S. Doyle, L. V. Yermalitskaya, Z. B. Mackey, Ang, Kenny K H, J. H. McKerrow, L. M. Podust, *PLoS neglected tropical diseases* **2009**, *3*, e372.
- [14] C. Abad-Zapatero, J. T. Metz, *Drug. Discov. Today*. **2005**, *10*, 464–469.
- [15] L. Yin, S. Lucas, F. Maurer, U. Kazmaier, Q. Hu, R. W. Hartmann, *Journal of medicinal chemistry* **2012**, *55*, 6629–6633.
- [16] B. G. Wachall, M. Hector, Y. Zhuang, R. W. Hartmann, *Bioorganic & medicinal chemistry* **1999**, *7*, 1913–1924.
- [17] J. Emmerich, Q. Hu, N. Hanke, R. W. Hartmann, *Journal of medicinal chemistry* **2013**, *56*, 6022–6032.
- [18] M. Balcells, J. Avilla, J. Profitos, R. Canela, *Journal of Agricultural and Food Chemistry* **2000**, *48*, 83–87.

- [19] S. S. Gunatilleke, C. M. Calvet, J. B. Johnston, C.-K. Chen, G. Erenburg, J. Gut, J. C. Engel, Ang, Kenny K H, J. Mulvaney, S. Chen et al., *PLoS neglected tropical diseases* **2012**, *6*, e1736.
- [20] Q. Hu, C. Jagusch, U. E. Hille, J. Haupenthal, R. W. Hartmann, *Journal of medicinal chemistry* **2010**, *53*, 5749–5758.
- [21] Q. Hu, J. Kunde, N. Hanke, R. W. Hartmann, *European journal of medicinal chemistry* **2015**, *96*, 139–150.
- [22] Q. Hu, M. Negri, K. Jahn-Hoffmann, Y. Zhuang, S. Olgen, M. Bartels, U. Müller-Vieira, T. Lauterbach, R. W. Hartmann, *Bioorganic & medicinal chemistry* **2008**, *16*, 7715–7727.
- [23] Q. Hu, L. Yin, C. Jagusch, U. E. Hille, R. W. Hartmann, *Journal of medicinal chemistry* **2010**, *53*, 5049–5053.
- [24] Pinto-Bazurco Mendieta, Mariano A E, M. Negri, Q. Hu, U. E. Hille, C. Jagusch, K. Jahn-Hoffmann, U. Müller-Vieira, D. Schmidt, T. Lauterbach, R. W. Hartmann, *Archiv der Pharmazie* **2008**, *341*, 597–609.
- [25] C. Jagusch, M. Negri, U. E. Hille, Q. Hu, M. Bartels, K. Jahn-Hoffmann, Pinto-Bazurco Mendieta, Mariano A E, B. Rodenwaldt, U. Müller-Vieira, D. Schmidt et al., *Bioorganic & medicinal chemistry* **2008**, *16*, 1992–2010.
- [26] U. E. Hille, Q. Hu, C. Vock, M. Negri, M. Bartels, U. Müller-Vieira, T. Lauterbach, R. W. Hartmann, *European journal of medicinal chemistry* **2009**, *44*, 2765–2775.
- [27] U. E. Hille, C. Zimmer, C. A. Vock, R. W. Hartmann, *ACS medicinal chemistry letters* **2011**, *2*, 2–6.
- [28] U. E. Hille, C. Zimmer, J. Haupenthal, R. W. Hartmann, *ACS medicinal chemistry letters* **2011**, *2*, 559–564.
- [29] C. Zimmer, M. Hafner, M. Zender, D. Ammann, R. W. Hartmann, C. A. Vock, *Bioorganic & medicinal chemistry letters* **2011**, *21*, 186–190.
- [30] L. Yin, Q. Hu, R. W. Hartmann, *Journal of medicinal chemistry* **2013**, *56*, 460–470.
- [31] L. Yin, Q. Hu, J. Emmerich, M. M.-C. Lo, E. Metzger, A. Ali, R. W. Hartmann, *Journal of medicinal chemistry* **2014**, *57*, 5179–5189.
- [32] M. Voets, I. Antes, C. Scherer, U. Müller-Vieira, K. Biemel, S. Marchais-Oberwinkler, R. W. Hartmann, *Journal of medicinal chemistry* **2006**, *49*, 2222–2231.
- [33] M.-P. Lézé, M. Le Borgne, P. Pinson, A. Paluszczak, M. Duflos, G. Le Baut, R. W. Hartmann, *Bioorganic & medicinal chemistry letters* **2006**, *16*, 1134–1137.
- [34] H. Bayer, C. Batzl, R. W. Hartman, A. Mannschreck, *Journal of medicinal chemistry* **1991**, *34*, 2685–2691.
- [35] F. Leroux, T. U. Hutschenreuter, C. Charrière, R. Scopelliti, R. W. Hartmann, *Helvetica Chimica Acta* **2003**, *86*, 2671–2686.
- [36] W. Zhu, Q. Hu, N. Hanke, van Koppen, Chris J, R. W. Hartmann, *Journal of medicinal chemistry* **2014**, *57*, 7811–7817.

- [37] T. Omura, R. Sato, *Journal of Biological Chemistry* **1964**, 239, 2379–2385.
- [38] K. M. Ewen, B. Schiffler, H. Uhlmann-Schiffler, R. Bernhardt, F. Hannemann, *FEMS yeast research* **2008**, 8, 432–441.
- [39] J. J. Müller, F. Hannemann, B. Schiffler, K. M. Ewen, R. Kappl, U. Heinemann, R. Bernhardt, *Journal of inorganic biochemistry* **2011**, 105, 957–965.
- [40] K. Hüsecken, S. Hinsberger, Elgaher, Walid A M, J. Hauptenthal, R. W. Hartmann, *Future medicinal chemistry* **2014**, 6, 1551–1565.
- [41] a) B. J. Wilson, S. Orrenius, *Biochimica et Biophysica Acta (BBA) - General Subjects* **1972**, 261, 94–101; b) J. B. Schenkman, H. Remmer, R. W. Estabrook, *Molecular pharmacology* **1967**, 3, 113–123.
- [42] M. Saecker, B. T. Burlingham, T. S. Widlanski, *J. Chem. Educ.* **2003**, 80, 214.
- [43] K. J. McLean, P. Carroll, D. G. Lewis, A. J. Dunford, H. E. Seward, R. Neeli, M. R. Cheesman, L. Marsollier, P. Douglas, W. E. Smith et al., *J. Biol. Chem.* **2008**, 283, 33406–33416.
- [44] a) H. Ouellet, L. M. Podust, de Montellano, Paul R Ortiz, *The Journal of biological chemistry* **2008**, 283, 5069–5080; b) H. Ouellet, J. Lang, M. Couture, Ortiz de Montellano, Paul R, *Biochemistry* **2009**, 48, 863–872.

#### **Supporting Information: Appendix 7.1 B**



**C Biochemical and Biophysical Analysis of a Chiral PqsD Inhibitor Revealing Tight-Binding Behavior and Enantiomers with Contrary Thermodynamic Signatures**

Michael P. Storz\*, Christian Brenzel\*, Elisabeth Weidel, Michael Hoffmann, Klaus Hollemeyer, A. Steinbach, Rolf Müller, Martin Empting, and Rolf W. Hartmann

\*These authors contributed equally

Reprinted with permission from *ACS Chem. Biol.* **2013**, (8), 2794-2801.

Copyright (2013) American Chemical Society.

DOI: 10.1021/cb400530d

## ABSTRACT

Anti-virulence strategies addressing bacterial pathogenicity without exhibiting growth inhibition effects represent a novel approach to overcome today's crisis in antibiotic development. In recent studies, we examined various inhibitors of PqsD, an enzyme involved in formation of *Pseudomonas aeruginosa* cell-to-cell signaling molecules, and observed desired cellular effects for 2-nitrophenyl derivatives. Herein, we investigated the binding characteristics of this interesting compound class using several biochemical and biophysical methods. The inhibitors showed time-dependent activity, tight-binding behavior and interactions with the catalytic center. Furthermore, isothermal titration calorimetry (ITC) experiments with separated enantiomers revealed contrary thermodynamic signatures showing either enthalpy- or entropy-driven affinity. A combination of site-directed mutagenesis and thermodynamic profiling was used to identify key residues involved in inhibitor binding. This information allowed the proposal of experimentally confirmed docking poses. Although originally designed as transition state analogs, our results suggest an altered position for both enantiomers. Interestingly, the main difference between stereoisomers was found in the orientation of the hydroxyl group at the stereogenic center. The predicted binding modes are in accordance with experimental data and, thus, allow future structure-guided optimization.

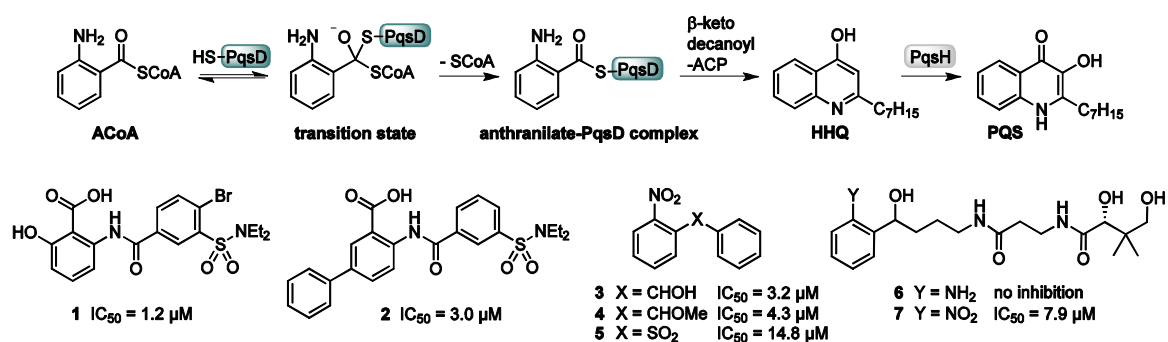
## INTRODUCTION

Antimicrobial resistance is a worldwide emerging problem since current treatment becomes more and more inefficient (1). In *P. aeruginosa*, which is considered as the major cause of mortality in cystic fibrosis patients (2), several resistance mechanisms against commonly used antibiotics are known. For example, the limited permeability of the outer membrane (3) in combination with broad spectrum multidrug efflux systems (4) can result in a dramatically lowered intracellular drug concentration. Thus, it is all the more important that the compound blocks its target efficiently providing sufficient drug residence time to achieve the desired effects. In the case of competitive inhibitors interacting with the same binding site as the substrate, effectiveness can be drastically diminished by mass-action competition with the substrate. Thus, it was proposed to avoid this unfavorable situation through (pseudo-) irreversible inhibition (5).

Bacteria apply cell-to-cell communication to coordinate group behavior, a phenomenon which became known as quorum sensing (QS). Thereby, small diffusible signal molecules are produced by bacterial cells and released into the environment. The extracellular concentration reflects the cell density of the population, which can be in turn measured by single members of the colony. Once a special threshold is reached, the population collectively alters its gene expression pattern. Multiple QS systems based on

various signal molecules are present in beneficial as well as pathogenic bacteria. *P. aeruginosa* utilizes the quinolone-based *pqs* system, which is characteristic for particular *Pseudomonas* and *Burkholderia* species (6). The *pqs* system is reported to have crucial influence on biofilm formation and virulence factor production (7, 8). In this regard, inhibition of the *pqs* system is an attractive strategy to overcome biofilm mediated resistance. Furthermore, QS inhibitors might ideally address pathogenicity without affecting bacterial cell viability. Hence, compared to the current treatment by bactericidal and bacteriostatic antibiotics, less selection pressure to develop resistance against this novel mode of action is expected (9). Another advantage of *pqs* inhibitors is the absence of quinolone signals in beneficial bacteria, and therefore, the natural microbial flora should not be affected.

PqsD is a key enzyme in the biosynthesis of the *pqs* signal molecules 2-heptyl-4-hydroxyquinoline (HHQ) and 2-heptyl-3-hydroxy-4-quinolone (*Pseudomonas* quinolone signal, PQS) (Scheme 1) (10). For this reason, we consider PqsD as an attractive target for the development of novel anti-infectives (11). We have identified the first PqsD inhibitors by testing known inhibitors of FabH, a structurally and functionally related enzyme (10). Structural optimization decreased IC<sub>50</sub> values to 1.2 μM (Scheme 1, **1** and **2**) (12). However, these compounds were not capable of potently reducing the extracellular signal molecule levels in *P. aeruginosa* PA14 (unpublished data).



**Scheme 1.** PqsD mediated formation of HHQ and PQS and structures of known PqsD inhibitors<sup>a</sup>

<sup>a</sup>IC<sub>50</sub> values were taken from refs. (11) and (12) and were measured using the screening procedure described in the methods section.

Recently, we have identified 2-nitrophenyl derivatives as potent PqsD inhibitors in a ligand-based approach (Scheme 1, **3-5**, **7**) (11). The most active compound of this series **3** was capable of reducing the HHQ and PQS levels as well as the biofilm volume in *P. aeruginosa* PA14 without affecting cell viability. In our original concept, (2-aminophenyl)methanol derivative **6** was designed as transition state analog of the reaction between PqsD and its primary substrate anthraniloyl-CoA (ACoA) (Scheme 1). Since transition states are the most tightly bound species of a catalytic reaction, transition state analogs are a reasonable strategy to achieve high potency (13). But unexpectedly, no activity was

observed for **6**, while the corresponding nitro compound **7** effectively inhibited PqsD. Thus, it is open to question how the optimized nitro compound **3** interacts with PqsD on a molecular level.

To address this question, we conducted a surface plasmon resonance (SPR) competition experiment to validate the binding site. Various modifications of the *in vitro* assay were used to elucidate time dependency of inhibition as well as functional reversibility. Mass spectrometry was applied to investigate the nature of interaction between the protein and the inhibitors. Site-directed mutagenesis in combination with ITC analysis revealed key interaction features responsible for affinity and astonishing differences in the thermodynamic profile of the separated enantiomers. This information was used to deduce plausible binding modes, which may explain the efficacy of the compound class.

## RESULTS AND DISCUSSION

**Binding site analysis by SPR.** To investigate whether our compounds bind in the active site, we performed binding experiments using SPR. Compound **2**, which was described as a channel blocker interacting in the upper part of the tunnel (*12*) and **3** were separately added to PqsD immobilized on an SPR sensor chip. Figures 1A/B show the resulting response curves, indicating affinity to the enzyme for both compounds.

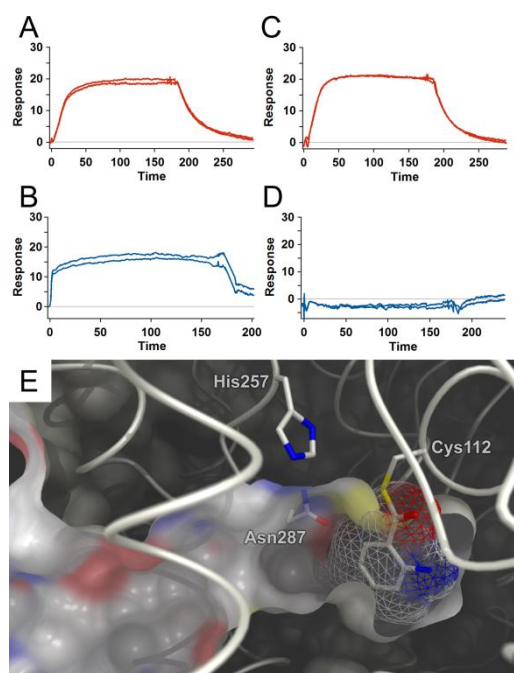


**Figure 1.** Elucidation of the binding site by SPR. Addition of inhibitor to native PqsD leads to response curves (A) and (B) for compounds **2** and **3**, respectively. In contrast to compound **2** (C), no response curve for **3** (D) is observed after addition to PqsD pretreated with ACoA. (E) Binding pocket of PqsD and space-filling model of covalent anthranilate adduct (wireframe). Picture was generated using the crystal structure [Protein Data Bank (PDB) entry 3H77] (14).

In a second experiment, the first substrate of PqsD, ACoA, was added until saturation of all active-site Cys112 by formation of an anthranilate thioester was reached (Figure 1E). Noteworthy, the X-ray structure of this key intermediate shows no significant conformational changes compared to untreated PqsD (14), which eliminates the possibility of allosteric effects. Addition of inhibitors **2** or **3** was subsequently repeated. In the case of **2**, response curves were very similar to those obtained using unmodified enzyme (Figure 1C). Thus, affinity of **2** is not affected by covalently bound anthranilate, which is consistent with previous results (12). In contrast, no response was observed for **3** (Figure 1D), indicating that the binding site of **3** is blocked by anthranilate. Moreover, this experiment shows that the binding pocket around Cys112 is the only target site of **3**. This is supported by a 1:1 interaction stoichiometry determined in the ITC experiment (11).

To gather further evidence for the proposed binding site, we preincubated PqsD with ACoA prior to continuation of the original assay procedure. In the case of the FabH inhibitor-derived compounds **1** and **2**, no significant differences in  $IC_{50}$  values determined by both procedures were observed ( $IC_{50,mod}$  values in Supplementary Table S2). In contrast to this, the  $IC_{50}$  values of **3-5** were increased at least

threefold when PqsD was preincubated with the substrate. This provides further evidence that nitrophenyl derivatives and the anthraniloyl moiety share a common binding site.

**Time-dependent inhibition and reversibility.** To investigate the time dependency of PqsD inhibition by **3**, the protein was added to a mixture of substrates and inhibitor before HHQ formation was measured at different time points. Figure 2A (blue) shows decreasing HHQ production over time compared to the untreated control, indicating slow binding kinetics for **3**. For reference compound **2** (red), a nearly constant HHQ formation rate is observed, which is due to a rapid establishment of binding equilibrium with the enzyme.

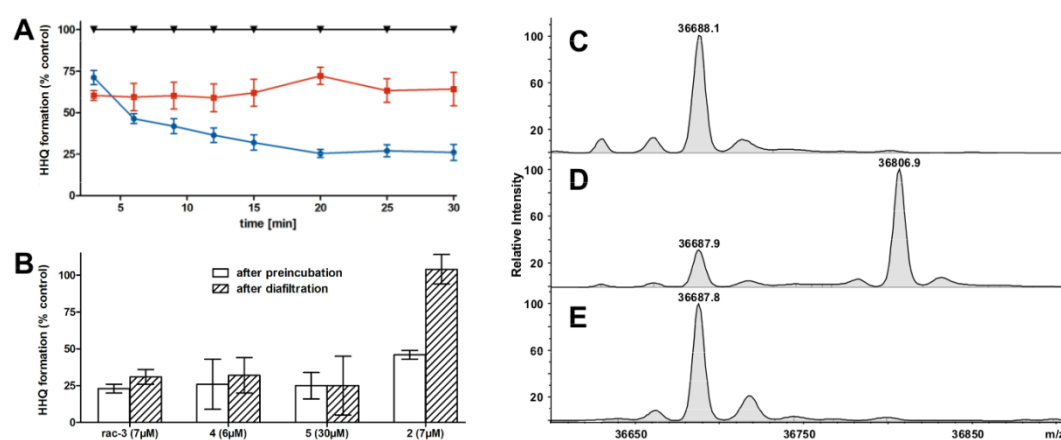


**Figure 2.** Mode of action analysis. (A) Time dependency of PqsD inhibition by 3 μM of FabH inhibitor-derived compound **2** (■) and 6 μM of 2-nitrophenyl derivative **3** (●) compared to untreated control (▼). Values are given in the supporting information. (B) Reversibility of PqsD inhibition by compounds **2-5**. Centrifugal filter devices with a molecular weight limit of 10k were used to remove at least 95% inhibitor by three diafiltration steps as controlled by HPLC analysis, while PqsD was retained. (C-E) HPLC-ESI mass spectra of untreated PqsD (C) and after preincubation with 5 mM ACoA (D) or 2.5 mM of compound **3** (E), respectively.

Inhibition by **3** has not reached the equilibrium after 10 min, which is the standard preincubation time in the *in vitro* assay. Consequently,  $IC_{50}$  data and structure-activity relationships derived in this compound class are dependent on the rate of complex formation. Furthermore, the potency is underestimated compared to the FabH inhibitor-derived compound class. This becomes apparent when the preincubation period was extended from 10 min ( $IC_{50}$ ) to 30 min ( $IC_{50,ext}$  values in Supplementary Table S2). While the inhibitory potency of **1** and **2** did not increase, the  $IC_{50,ext}$  of **3-5** showed significantly lowered values. This effect is most pronounced for the alcohol **3**, which is probably due to the slowest binding kinetics.

There are two general modes of interaction between enzyme and inhibitor resulting in time-dependent inhibition. First, the enzyme inactivation is practically irreversible, for example by covalent binding. As the reaction progresses, enzyme inhibition will be increased. In the second case, slow binding kinetics can lead to an equilibrium establishment of a reversible inhibition, which is slow compared to enzyme turnover. To address this issue, we examined the reversibility by modification of our *in vitro* functional assay. Therefore, PqsD was preincubated with inhibitor and the remaining HHQ formation was quantified with and without removal of unbound inhibitor by diafiltration. After preincubation with 7  $\mu\text{M}$  of the FabH inhibitor-derived compound **2**, 46% of HHQ formation remained compared to the untreated control. After removal of unbound inhibitor, PqsD activity was fully restored, since binding of the inhibitor is non-permanent (Figure 2B). In the case of the 2-nitrophenyl derivatives **3-5**, PqsD activity was not significantly increased. But providing reversible inhibition, HHQ formation should be very sensitive to changes in inhibitor concentration, since the dose-inhibition curves are very steep at the concentrations used (Supplementary Figure S1 for compound **3**). Hence, inhibition by this compound class is apparently irreversible. However, it should be mentioned that the time available for dissociation between the diafiltration steps is limited due to enzyme denaturation ( $t_{1/2} \approx 100$  min at room temperature). Thus, the irreversible behavior of **3-5** may be restricted to the time period which is covered by the experiment.

To distinguish between irreversible inhibition by formation of a covalent bond or tight-binding characterized by slow off-rates, mass spectrometry (MS) techniques were applied. First, PqsD was incubated with or without ACoA as well as compound **3**, and the samples were subjected to HPLC-ESI analysis (Figure 2C). In absence of any additives, the main signal was observed at  $m/z = 36688.1$ , which corresponds to the calculated average mass of PqsD (36688.1 Da). Formation of the anthranilate-PqsD complex by addition of the substrate led to the expected mass shift of + 119.2 towards 36806.9 (calculated: 36807.2). In presence of a 100 fold excess of inhibitor **3** no covalent adduct or oxidation product was observed. This was also the case, when any reductive reagents were avoided (Supplementary Figure S2). Thus, we exclude a redox-based inhibition mechanism.

To exclude a possible dissociation during HPLC, we also analyzed PqsD with or without compound **3** by Maldi-TOF after tryptic digestion. In the case of unmodified PqsD, more than 99% of the sequence was covered by the peptides observed in the mass spectra. (Results are shown and discussed in detail in the Maldi-TOF section of the Supporting Information.) Thus, apart from 6 of 340 amino acids, which are unlikely to be involved in inhibitor binding, the modification should be captured by this technique. However, no novel signal appeared after preincubation of PqsD with compound **3** (Supplementary Table S4). The only difference compared to untreated PqsD is the disappearance of one fragment, which is not involved in substrate or inhibitor binding, since it is located far away from the active site. This fragment is also unresolved in the X-ray structure of PqsD, which is probably due to conformational flexibility. Thus, possible allosteric effects are unlikely. Considering both experiments, we exclude covalent binding, simultaneously denoting **3** as a tight-binding inhibitor.

**Elucidation of the binding mode.** The data presented so far were obtained using a racemic mixture of **3** since we have already shown that both enantiomers possess very similar  $IC_{50}$  values (11). The SPR experiment using the separated stereoisomers revealed that both enantiomers bind near the active site residues deep in the binding channel and in an exclusive manner with respect to one another (Supplementary Figures S9). Furthermore, (*R*)-**3** and (*S*)-**3** showed the same behavior as the racemic mixture **3** in the diafiltration experiment (Supplementary Figure S10). But when we analyzed the thermodynamic profile of binding to PqsD by ITC, surprising differences between both enantiomers were observed, even though very similar values for  $\Delta G$  were determined (Figure 3 and Table 1).

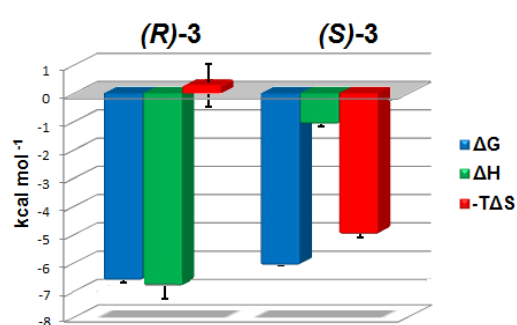


**Figure 3.** ITC analysis of thermodynamic profiles of enantiomers binding to PqsD wild-type.

Whereas the affinity of (*R*)-**3** is driven enthalpically, (*S*)-**3** shows a pronounced entropic binding profile. The combination of the values obtained for both enantiomers is in accordance with the balanced profile determined for their racemic mixture ( $\Delta H = -3.47$  kcal mol<sup>-1</sup>,  $-T\Delta S = -3.20$  kcal mol<sup>-1</sup>). The differences in the thermodynamic profiles are evident, even if uncertainties in  $\Delta H$ , and thus also in  $T\Delta S$ , of ~24% have to be expected for the technique (value determined by an interlaboratory comparison) (16).

With respect to the dissimilar thermodynamic profiles, we were interested whether differences in the interaction with the amino acid residues are detectable. Because of a lack in co-crystal structure, we decided to execute a combined approach of site-directed mutagenesis and ITC as a promising method to identify specific spots of interaction (17). Due to the SPR results, the binding site of both enantiomers should be located near the catalytic triad characterized by Cys112, His257 and Asn287. Furthermore, the adjacent Ser317 represents another possible interaction partner. Thus, we mutated the aforementioned amino acids. Only S317A possessed catalytic activity comparable to the wild-type. C112S retained 8% activity, whereas all other mutations led to inactivity (Supplementary Table S1). However, the aforementioned PqsD variants allowed to investigate the contribution of the respective residue side chains to inhibitor binding.



ITC analyses using (*R*)-**3** revealed Cys112 and His257 as mainly interacting residues, since mutation led to a loss of affinity by more than factor 2.3, as measured by deterioration in  $\Delta G$  by more than  $0.5 \text{ kcal mol}^{-1}$  (Table 1). Binding affinity of (*S*)-**3** does not seem to be significantly changed by any of these mutations with the exception of a small loss in affinity for both Ser317 mutants. For C112A standard deviations in  $\Delta G$  are too high for a reliable interpretation.

	<i>(R)</i> - <b>3</b> <sup>b</sup>			<i>(S)</i> - <b>3</b> <sup>b</sup>		
	$\Delta G$ [kcal mol <sup>-1</sup> ]	$\Delta H$ [kcal mol <sup>-1</sup> ]	$-T\Delta S$ [kcal mol <sup>-1</sup> ]	$\Delta G$ [kcal mol <sup>-1</sup> ]	$\Delta H$ [kcal mol <sup>-1</sup> ]	$-T\Delta S$ [kcal mol <sup>-1</sup> ]
<b>WT</b>	-6.56±0.14	-6.99±1.02	0.43±1.15	-6.13±0.20	-1.11±0.34	-5.02±0.18
	$\Delta\Delta G$ [kcal mol <sup>-1</sup> ]	$\Delta\Delta H$ [kcal mol <sup>-1</sup> ]	$-T\Delta\Delta S$ [kcal mol <sup>-1</sup> ]	$\Delta\Delta G$ [kcal mol <sup>-1</sup> ]	$\Delta\Delta H$ [kcal mol <sup>-1</sup> ]	$-T\Delta\Delta S$ [kcal mol <sup>-1</sup> ]
	<b>C112A</b>	-0.82±0.11 <sup>c</sup>	-5.36±0.60 <sup>c</sup>	4.54±0.86 <sup>c</sup>	0.10±0.40	-0.30±0.53
<b>C112S</b>	-0.75±0.14 <sup>c</sup>	-5.87±0.78 <sup>c</sup>	5.12±0.86 <sup>c</sup>	-0.03±0.10	-0.39±0.36	0.36±0.36
<b>S317F</b>	-0.58±0.14 <sup>c</sup>	-6.09±0.72 <sup>c</sup>	5.51±0.86 <sup>c</sup>	-0.30±0.10 <sup>c</sup>	-0.78±0.22 <sup>c</sup>	0.40±0.20
<b>S317A</b>	0.10±0.10	-1.10±0.67	1.26±0.76	-0.22±0.10 <sup>c</sup>	0.14±0.36	-0.36±0.36
<b>N287A</b>	-0.18±0.10	-1.16±0.61	0.98±0.70	-0.02±0.10	-0.02±0.20	-0.01±0.20
<b>H257F</b>	-0.61±0.30 <sup>c</sup>	-5.83±0.67 <sup>c</sup>	5.22±0.76 <sup>c</sup>	0.03±0.30	-0.19±0.36	0.22±0.36

**Table 1.** Effects of mutated amino acids on thermodynamic profiles of the enantiomers of **3**<sup>a</sup>

<sup>a</sup> $\Delta\Delta G$ ,  $\Delta\Delta H$ , and  $-T\Delta\Delta S$  are  $\Delta G_{WT} - \Delta G_{mutant}$ ,  $\Delta H_{WT} - \Delta H_{mutant}$ , and  $-T(\Delta S_{WT} - \Delta S_{mutant})$ , respectively. Negative values indicate a loss; positive values, a gain compared to wild-type. Significance: effect of the mutations on thermodynamic parameters of ligand binding compared to wild-type indicates a difference in interaction. <sup>b</sup>Absolute configurations were derived from measurement of the optical rotation and comparison to literature (15). <sup>c</sup> $p < 0.05$ .

Based on these results, we docked both enantiomers to propose binding poses. Calculation of the protonation state revealed that the Cys112 and His257 residues exist in a neutral form at physiological pH. In all high-ranked docking poses, the scaffold of both enantiomers had the same position, whereas one phenyl ring was located directly adjacent to the bottom of the channel and the other oriented towards the tunnel entrance (Figure 4A). For *(R)*-**3**, the nitro group was observed at both phenyl rings. But since both enantiomers retained comparable inhibitory activity even for elongated substituents instead of phenyl (data not shown), we concluded that the nitro-phenyl moiety is apparently located at the bottom of the channel. Thereby, the nitro group forms an asymmetrical bifurcated hydrogen bond (2.85 and 3.10 Å) to the backbone NH of Ser317 (Figure 4B) (18). The hydroxyl group is involved in a hydrogen bond network between the side chains of Cys112 (3.07 Å) and His257 (2.90 Å). The observed distances are typical for weak hydrogen bonds (19, 20), which explains the loss in affinity

and enthalpy for the C112A and H257F mutants. The C112S mutant showed strongly reduced affinity, which is probably due to the shorter van der Waals radius of oxygen compared to sulfur (21), leading to an interruption of the hydrogen bond network. No interaction was observed with the side chains of Asn287 and Ser317, which is in accordance with the collected ITC data (Table 1). However, introduction of a bulky phenyl ring in S317F probably results in sterical hindrance.

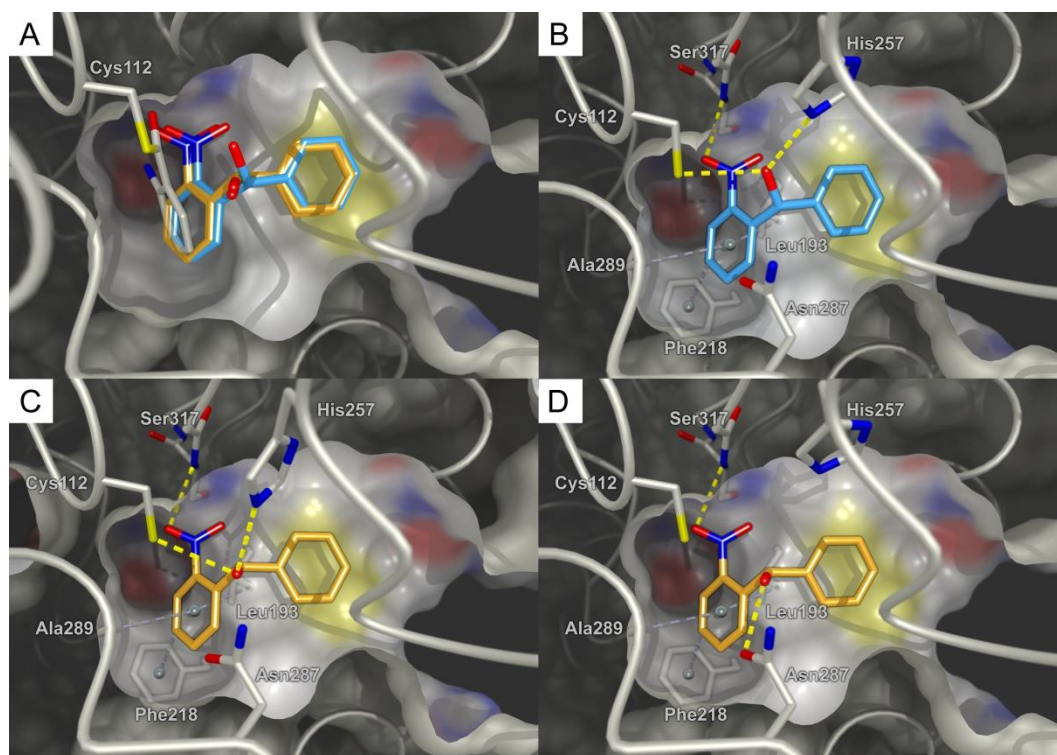


**Figure 4.** (A) Superimposition of the covalent anthranilate-PqsD complex (PDB entry 3H77) and docking poses for both enantiomers. Observed hydrogen bonds and CH- $\pi$  interactions of *R*-enantiomer (B) and the *S*-enantiomer (C/D) of compound **3** in PqsD wild-type. Nitrogen: blue, oxygen: red, sulfur: yellow, carbons of PqsD: grey, carbons of *R*-enantiomer: light blue, carbons of *S*-enantiomer: orange, hydrogen left out for clarity.

In the case of (*S*)-**3**, docking results were unambiguous with respect to the positioning of the nitro group, since in all high-ranked poses a short hydrogen bond between NO<sub>2</sub> and NH of Ser317 was observed (Figure 4C/D). However, the hydroxyl group was involved in different interactions, either facing towards Asn287 or His256/Cys112. We speculate that no singular mutation of the aforementioned residues significantly reduced affinity, since the hydroxyl group is able to switch to an alternative interaction mode. Noteworthy, this is not possible for the *R*-enantiomer due to the different orientation of the OH functionality.

Recently, two enantiomers with similar binding affinity for acetylcholinesterase but different thermodynamic profiles were reported (22). X-ray co-crystal structures revealed multiple

conformations stabilized by weak interactions for one enantiomer, leading to a gain in  $T\Delta S$  of 2.4 kcal mol<sup>-1</sup> compared to its counterpart. A similar effect might be contributing to the significant change in  $T\Delta S$  of 5.3 kcal mol<sup>-1</sup> for our compounds. Furthermore, a gain in entropy is characteristic for the classical hydrophobic effect (23). Thereby, the release of ordered water from well-solvated hydrophobic pockets upon ligand binding increases the water molecules degree of freedom (24). However, we were not able to identify such a displacement of water when comparing our docking results with the published X-ray structures.

Since small changes in structure without significant effect on  $\Delta G$  can lead to large changes in  $\Delta H$  and  $T\Delta S$ , the phenomenon of entropy-enthalpy compensation may also help to explain the contrary thermodynamic profiles of the enantiomers (25). The physical origin of the compensation is still not fully understood and it has been repeatedly discussed whether a structural interpretation is even possible (25, 26). According to this, the altered position of OH may well be the source of the shift in thermodynamic contributions.

Nevertheless, besides the interpretation of the thermodynamic profile, the proposed models should enable us to perform structure-guided optimization. Thus, the docking poses have to be in accordance with previous structure-activity relationship observations (11). Firstly, as soon as the amino group of **6** was substituted by nitro, the compounds turned active. As has been described above, (2-nitrophenyl)(phenyl)methanol **3** was originally designed as transition state analog. However, in the transition state, which has formed by attack of Cys112 on the thioester bond of ACoA, the generated oxyanion is stabilized by backbone nitrogen atoms of Cys112 and Ser317 (14). In our model, this position is in each case rather occupied by the nitro group (Figure 4A), which cannot be mimicked by the corresponding amine geometrically and spatially. As a consequence, this compound does not interact with PqsD as expected for a transition state analog. Furthermore, it is noteworthy that the nitrophenyl moiety aligns quite accurately with the benzoate moiety in an X-ray structure of anthranilate bound to a C112A mutant (14). This indicates the preference for this kind of isoelectronic groups at this point of the channel. Secondly, a carbonyl linker between both phenyl rings, which conjugates the  $\pi$ -systems, leads to inactivity. This can now be explained, as the banana-shaped bottom of the channel is not able to accommodate the planar molecule anymore. Furthermore, substitution of the methylene-H abolished inhibitory activity, either due to a steric clash with Asn287 (*R*), or because a substitution is followed by a twist of the molecule, which destabilizes the biological active conformation (*S*). Hence, the experimental results are in good accordance with our binding model.

**Conclusions.** 2-Nitrophenyl derivatives and FabH inhibitor-derived compounds show similar  $IC_{50}$  values, but only congeners of the former class are capable of significantly reducing signal molecule production and biofilm formation in *P. aeruginosa* PA14. We have shown that both inhibitor classes possess fundamentally different profiles regarding binding site, time-dependent inhibition and

reversibility. And besides possible advantages in cell permeability of the (2-nitrophenyl)methanol derivatives due to their low molecular weight, the deeply buried binding site at the bottom of the substrate channel and the apparent irreversibility could be crucial factors for their intracellular efficacy.

Furthermore, the calorimetric characterization of two enantiomers revealed remarkable differences in their thermodynamic signatures. The detailed binding modes were examined by a combined approach using site-directed mutagenesis, ITC, and docking. This enabled us to propose binding poses for both enantiomers only differing in the position of the hydroxyl group. Notably, the nitro group occupies the oxyanion hole forming strong interactions with the enzyme backbone. However, this site was expected to accommodate the aforementioned hydroxyl group. Hence, the position of the scaffold is altered compared to the transition state (Figure 4A). The predicted enzyme-inhibitor complexes explain the reported structure-activity relationship and, therefore, enable the structure-guided design of PqsD inhibitors towards improved inhibitory activity.

## METHODS

**Preparation of PqsD Mutants.** PqsD mutants were generated using the QuikChange Site-Directed Mutagenesis Kit (Stratagene) according to the manufacturer's instructions using the pET28b(+)/*pqsD* plasmid as a template. Briefly, *pqsD* gene was amplified through 16 cycles of PCR. After treatment with *DpnI*, the PCR product was transformed into *E. coli* strain XL1-Blue. Plasmid DNA was purified using the GenElute™ HP Plasmid Miniprep Kit (Sigma-Aldrich) and sequenced to confirm the site-directed mutations. For the primer sequence of the mutations see Supporting Information.

**Expression and Purification of Recombinant PqsD Wild-type and Mutants in *E. coli*.** *E. coli* BL21 ( $\lambda$ DE3) cells were transformed with plasmid harboring PqsD (pET28b(+)/*pqsD*) (10). Overexpression, purification, and storage of the His<sub>6</sub>-tagged PqsD was performed as described recently (11).

**Screening Assay Procedures for *In Vitro* PqsD Inhibition.** The standard assay for determination of IC<sub>50</sub> values was performed monitoring the enzyme activity by measuring the HHQ concentration as described recently (10). PqsD was preincubated with inhibitor for 10 min prior to addition of the substrates ACoA and  $\beta$ -ketodecanoic acid. The concentration of PqsD applied in the assay was 0.1  $\mu$ M. Quantification of HHQ was performed analogously, but with some modifications: The flow rate was set to 750  $\mu$ l min<sup>-1</sup> and an Accucore RP-MS column, 150 x 2.1 mm, 2.6  $\mu$ m, (Thermo Scientific) was used. All test compound reactions were performed in sextuplicate. Synthesis of ACoA and  $\beta$ -ketodecanoic acid was performed as described in the Supporting Information. In the modified protocol used for the determination of IC<sub>50,mod</sub>, PqsD and the first substrate ACoA were preincubated for 30 min prior to adding them to the test compounds. Then,  $\beta$ -ketodecanoic acid was added and the further steps

were performed identical to the standard protocol.  $IC_{50,ext}$  values were determined analogously to the normal  $IC_{50}$  values, with the sole exception that PqsD was preincubated with inhibitor for 30 min.

**Surface Plasmon Resonance (SPR) Spectrometry.** SPR binding studies were performed using a Reichert SR7500DC instrument optical biosensor (Reichert Technologies) and CMD500M sensor chips obtained from XanTec Bioanalytics. PqsD was immobilized on a CMD500M (carboxymethyl-dextran-coated) sensor chip at 12°C using standard amine coupling conditions according to the manufacturers' instructions. PqsD was diluted with sodium acetate buffer (10 mM, pH 4.5) to a final concentration of 100  $\mu\text{g ml}^{-1}$ . PqsD was immobilized at densities of 2217 RU and 2918 RU.

**SPR Competition Study.** The binding studies were performed at a constant flow rate of 50  $\mu\text{l min}^{-1}$  in instrument running buffer (50 mM MOPS, pH 8.0, 150 mM NaCl, 5% DMSO (v/v), 0.1% Triton X-100 (v/v)). 10 mM stock solutions of compounds **2** and **3** in DMSO were directly diluted to a concentration of 500  $\mu\text{M}$  (50 mM MOPS, pH 8.0, 150 mM NaCl, 0.1% Triton X-100 (v/v)) and then diluted to a final concentration of 100  $\mu\text{M}$  (**3**) and 20  $\mu\text{M}$  (**2**) in running buffer. Before the compounds were injected, 6 warm-up blank injections were performed. Buffer blank injections and DMSO calibration were included for double referencing. The compounds were injected for 180 s association and 300 s dissociation times. Experiments were performed twice with two independently prepared PqsD coated CMD500M sensor chips. Scrubber software was used for processing and analyzing the data.

Compounds **2** and **3** were first tested in the absence of ACoA. In the second experiment ACoA (100  $\mu\text{M}$ ) was injected for 40 minutes with a constant flow of 5  $\mu\text{l min}^{-1}$  to reach saturation of the active-site Cys112. After this, the flow rate was increased to 50  $\mu\text{l min}^{-1}$  for 30 minutes in order to remove residual reagents. Once the baseline signal was stable, additional ACoA (10  $\mu\text{M}$ ) was injected to assure that the anthranilate binding site is completely saturated (no additional signal was observed). Afterwards compounds **2** (20  $\mu\text{M}$ ) and **3** (100  $\mu\text{M}$ ) were consecutively injected.

**Elucidation of Time-Dependent PqsD Inhibition.** The assay was performed analogously to the screening assay procedure for *in vitro* PqsD inhibition described above, except that inhibitor and substrate were mixed and the reaction was started by addition of enzyme. The reactions were stopped after 3, 6, 9, 12, 15, 20, 25 and 30 min by addition of methanol containing 1  $\mu\text{M}$  amitriptyline as internal standard. Percentage of inhibition was determined as the mean value of duplicates and HHQ concentrations measured without inhibitor at each time point were set to 100%. The uncertainty was calculated assuming uncorrelated standard deviations of the HHQ levels with or without inhibitor using a first-order Taylor series expansion. Percentages of inhibition are given in the Supporting Information.

**Examination of Reversibility by Diafiltration.** The diafiltration experiment was performed using identical conditions as for the screening assay procedure, but with doubled enzyme concentration (0.2

$\mu\text{M}$ ). PqsD was preincubated with inhibitor for 10 min and the solutions were divided into two fractions. While the first one was stored under  $4^\circ\text{C}$ , the second was diafiltrated (3x) at 1200 g for 6 min at  $4^\circ\text{C}$  using Nanosep® Centrifugal Devices equipped with a Omega™ membrane (MWCO = 10K), which were obtained from Pall Corporation. Between diafiltration steps, the samples were diluted from 30  $\mu\text{l}$  to 500  $\mu\text{l}$  with buffer (identical chemical composition as used for preincubation). The enzyme inhibitor complex was allowed to dissociate for 1 min at room temperature. Afterwards, the substrates ACoA and  $\beta$ -ketodecanoic acid were added to both fractions and the assay was continued as described in the screening assay procedure.

**HPLC-ESI Experiment.** PqsD (25  $\mu\text{M}$ ) was preincubated with compound **9** (2.5 mM) for 60 min at  $37^\circ\text{C}$  in Tris-HCl buffer (50 mM, pH 8.0) with 0.5% DMSO (v/v). Dithiothreitol was added and the samples were analyzed by HPLC-ESI. All ESI-MS-measurements were performed on a Dionex Ultimate 3000 RSLC system using an Aeris Widepore XB-C8, 150 x 2.1 mm, 3.6  $\mu\text{m}$  dp column (Phenomenex). Separation of 2  $\mu\text{l}$  samples were achieved by a linear gradient from (A)  $\text{H}_2\text{O}$  + 0.05% TFA (v/v) to (B) ACN + 0.05% TFA (v/v) at a flow rate of 250  $\mu\text{l min}^{-1}$  and  $45^\circ\text{C}$ . The gradient was initiated by a 1.0 min isocratic step at 15% B, followed by an increase to 80% B within 4.5 min to end up with a 6 min step at 80% B before re-equilibration with initial conditions. UV spectra were recorded by a DAD in a range from 200 to 600 nm. The LC flow was split to 75  $\mu\text{l min}^{-1}$  before entering the maXis 4G hr-ToF mass spectrometer (Bruker Daltonics) using the standard Bruker ESI source. In the source region, the temperature was set to  $180^\circ\text{C}$ , the capillary voltage was 4000 V, the dry-gas flow was 6.0 l  $\text{min}^{-1}$  and the nebulizer was set to 1.1 bar. Mass spectra were acquired in positive ionization mode ranging from 600 to 1800 m/z at 2.5 Hz scan rate. Protein masses were deconvoluted using the Maximum Entropy algorithm (Copyright 1991–2004 Spectrum Square Associates, Inc.).

**Maldi-TOF Experiment.** PqsD (10  $\mu\text{M}$ ) was preincubated with compound **3** (2.5 mM) for 60 min at  $37^\circ\text{C}$  using identical buffer composition as in the screening assay procedure (50 mM MOPS, pH 7.0 with 0.005% (v/v) Triton X-100 and 0.5% DMSO (v/v)). The buffer was exchanged by an  $\text{NH}_4\text{HCO}_3$  buffer (50 mM, pH 8.1) in three diafiltration steps. Diafiltration was performed at 1200 g for 6 min at  $4^\circ\text{C}$  in Nanosep® Centrifugal Devices (MWCO = 10K) of Pall Corporation. The protein was digested with trypsin overnight and dithiothreitol was added.  $\alpha$ -Cyano-4-hydroxycinnamic acid was used as matrix component. Analysis of the peptides were performed on a 4800 TOF/TOF Analyzer mass spectrometer (Applied Biosystems) in positive reflector mode using a pulsed 200 Hz solid state Nd:YAG laser with a wavelength of 355 nm. Laser energy was set to 2000–2300 units for standards and to 2700–3200 units for real samples. Source 1 voltage was set to 20 kV with a grid voltage of 16 kV. Reflector detector voltage was 2.19 kV. Spectra of standard peptides used for wide range calibration ranging from 0.8 to 4 kDa (des-arg1-bradykinin, angiotensin I, glu1-fibrinopeptide B, ACTH 1–17 clip, ACTH 18–39 clip and ACTH 7–38 clip) were measured with a delay time of 600 ns. One single mass spectrum was formed from 20 subspectra per spot using 25 accepted laser impulses

each. From the standard peptides exclusively monoisotopic ions were used with a minimum signal-to-noise (S/N) ratio of 20 and a resolution >10000. Mass tolerance was set to 0.3 Da with maximum outlier of 5 ppm. Accepted calibration settings were used to measure real sample spectra in the range of 1 to 3.5 kDa with a minimum S/N range of 10 and a resolution >8000. An internal algorithm defined the isotope cluster area subsequently named intensity (I), based on the peptides' molecular weight and their general elemental composition. MALDI-TOF MS resulted in pmfs consisting of mass-intensity spectra ( $m/z-I_{\text{abs, ai}}$ ).

**Isothermal Titration Calorimetry (ITC).** ITC experiments were carried out using an ITC200 instrument (Microcal Inc., GE Healthcare). Final ligand concentrations were obtained by dilution 1:20 (v/v) in the experimental buffer resulting in a final DMSO concentration of 5% (v/v). Protein concentration was determined by measuring the absorbance at 280 nm using a theoretical molarity extinction coefficient of  $17,780 \text{ M}^{-1} \text{ cm}^{-1}$ . DMSO concentration in the protein solution was adjusted to 5% (v/v). ITC measurements were routinely performed at 25°C in PBS-buffer, pH 7.4, 10% glycerol (v/v), 5% DMSO (v/v). The titrations were performed on 83–102  $\mu\text{M}$  PqsD-His<sub>6</sub> and mutants-His<sub>6</sub> in the 200  $\mu\text{l}$  sample cell using 2  $\mu\text{l}$  injections of 3.5 mM ligand solution every 180 s. Raw data were collected and the area under each peak was integrated. To correct for heats of dilution and mixing, the final baseline consisting of small peaks of the same size at the end of the experiment was subtracted. The experimental data were fitted to a theoretical titration curve (one site binding model) using MicroCal Origin 7 software, with  $\Delta H$  (enthalpy change in  $\text{kcal mol}^{-1}$ ),  $K_A$  (association constant in  $\text{M}^{-1}$ ), and  $N$  (number of binding sites) as adjustable parameters. Thermodynamic parameters were calculated from equation

$$\Delta G = \Delta H - T\Delta S = RT \ln K_A = -RT \ln K_D$$

where  $\Delta G$ ,  $\Delta H$ , and  $\Delta S$  are the changes in Gibbs free energy, enthalpy, and entropy of binding, respectively.  $T$  is the absolute temperature, and  $R = 1.98 \text{ cal mol}^{-1} \text{ K}^{-1}$ . For every mutant, three independent experiments were performed.

**In Silico Experiments.** Docking poses of PqsD inhibitors (*R*)-**3** and (*S*)-**3** were generated with YASARA structure (YASARA Biosciences) using the AMBER03 force field on an Intel® Core™ i7-2600 workstation with 8 virtual cores (27, 28). Receptor coordinates were prepared using a crystal structure of the PqsD-anthraniloyl complex (PDB entry 3H77)(14).

First, the covalent and non-covalent ligands were removed without altering the dihedral angle of the Cys112 side chain and protonation states were assigned automatically at pH 7.4. Then, a grid box of  $27 \times 20 \times 20 \text{ \AA}^3$  was set up around the residues forming the active site tunnel of PqsD. Finally, the binding mode of the ligands was calculated using the flexible local docking procedure of the implemented AutoDock 4 algorithm with 999 docking runs (29). In every case, at least the 5 highest-ranked poses were found to belong to one cluster. Predicted PqsD-inhibitor complexes were further refined by an additional energy minimization step with fixed receptor backbone atoms and then analysed using MOE 2012 (Chemical Computing Group)(30).



## ASSOCIATED CONTENT

### Supporting Information

Primer sequence of mutations and catalytic activity; synthesis of the substrates used in the enzymatic inhibition assays; percentages of inhibition of the time dependency experiment; detailed analysis of the Maldi-TOF experiment; additional HPLC-ESI MS, diafiltration and SPR experiments; separation and purity of the enantiomers; representative ITC curves. This material is available free of charge *via* the Internet at <http://pubs.acs.org>.

## AUTHOR INFORMATION

### Corresponding Author

\* E-mail: [rolf.hartmann@helmholtz-hzi.de](mailto:rolf.hartmann@helmholtz-hzi.de); Phone: +49 681 302 70300; Fax: +49 681 302 70308.

### Author Contributions

‡ These authors contributed equally.

### Notes

The authors declare no competing financial interest.

## ACKNOWLEDGEMENTS

We thank S. Amann and C. Scheid for their help in performing all HPLC-MS/MS-based assays.

## REFERENCES

1. Levy, S. B., Marshall, B. (2004) Antibacterial resistance worldwide: Causes, challenges and responses, *Nature Medicine*, 10, S122–S129.
2. Govan, J. R., Deretic, V. (1996) Microbial pathogenesis in cystic fibrosis: Mucoid *Pseudomonas aeruginosa* and *Burkholderia cepacia*, *Microbiol. Rev.* 60, 539–574.
3. Nikaido, H. (1989) Outer membrane barrier as a mechanism of antimicrobial resistance, *Antimicrob. Agents Chemother.* 33, 1831–1836.
4. Poole, K. (2001) Multidrug efflux pumps and antimicrobial resistance in *Pseudomonas aeruginosa* and related organisms, *J. Mol. Microbiol. Biotechnol.* 3, 255–264.
5. Stewart, P. S., Costerton, J. W. (2001) Antibiotic resistance of bacteria in biofilms, *Lancet* 358, 135–138.

6. Copeland, R. A., Pompliano, D. L., Meek, T. D. (2006) Drug-target residence time and its implications for lead optimization, *Nat. Rev. Drug. Discov.* 5, 730–739.
5. Swinney, D. C. (2004) Biochemical mechanisms of drug action: What does it take for success?, *Nature Rev. Drug. Disc.* 3, 801–808.
6. Diggle, S. P., Lumjiaktase, P., Dipilato, F., Kunakorn, M., Barrett, D. A., Chhabra, S. R.; Camara, M., Williams, P. (2006) Functional genetic analysis reveals a 2-alkyl-4-quinolone signaling system in the human pathogen *Burkholderia pseudomallei* and related bacteria, *Chem. Biol.* 13, 701–710.
7. Yang, L., Nilsson, M., Gjermansen, M., Givskov, M., Tolker-Nielsen, T. (2009) Pyoverdine and PQS mediated subpopulation interactions involved in *Pseudomonas aeruginosa* biofilm formation, *Mol. Microbiol.* 74, 1380–1392.
8. Summarized in: Dubern, J.-F., Diggle, S. P. (2008) Quorum sensing by 2-alkyl-4-quinolones in *Pseudomonas aeruginosa* and other bacterial species, *Mol. BioSyst.* 4, 882–888.
9. Hentzer, M., Wu, H., Andersen, J. B., Riedel, K., Rasmussen, T. B., Bagge, N., Kumar, N., Schembri, M. A., Song, Z., Kristoffersen, P., Manefield, M., Costerton, J. W., Molin, S., Eberl, L., Steinberg, P., Kjelleberg, S., Hoiby, N., Givskov, M. (2003) Attenuation of *Pseudomonas aeruginosa* virulence by quorum sensing inhibitors, *EMBO J.* 22, 3803–3815.
10. Pistorius, D., Ullrich, A., Lucas, S., Hartmann, R. W., Kazmaier, U., Müller, R. (2011) Biosynthesis of 2-alkyl-4(1*H*)-quinolones in *Pseudomonas aeruginosa*: Potential for therapeutic interference with pathogenicity, *ChemBioChem* 12, 850–853.
11. Storz, M. P., Maurer, C. K., Zimmer, C., Wagner, N., Brengel, C., de Jong, J. C., Lucas, S., Müsken, M., Häussler, S., Steinbach, A., Hartmann, R. W. (2012) Validation of PqsD as an anti-biofilm target in *Pseudomonas aeruginosa* by development of small-molecule inhibitors, *J. Am. Chem. Soc.* 134, 16143–16146.
12. Weidel, E., de Jong, J. C., Brengel C., Storz, M. P., Braunshausen, A., Negri, M., Plaza, A., Steinbach, A., Müller, R., Hartmann, R. W. (2013) Structure optimization of 2-benzamidobenzoic acids as PqsD inhibitors for *Pseudomonas aeruginosa* infections and elucidation of binding mode by SPR, STD NMR and molecular docking, *J. Med. Chem.*, in press

13. Schloss, J. V. (1988) Significance of slow-binding enzyme inhibition and its relationship to reaction-intermediate analogues, *Acc. Chem. Res.* *21*, 348–353.
14. Bera, A. K., Atanasova, V., Robinson, H., Eisenstein, E., Coleman, J. P., Pesci, E. C., Parsons, J. F. (2009) Structure of PqsD, a *Pseudomonas* quinolone signal biosynthetic enzyme, in complex with anthranilate, *Biochemistry* *48*, 8644–8655.
15. Duan, H.-F., Xie, J.-H., Shi, W.-J., Zhang, Q., Zhou, Q.-L. (2006) Enantioselective rhodium-catalyzed addition of arylboronic acids to aldehydes using chiral spiro monophosphite ligands, *Organic Letters* *8*, 1479–1481.
16. Myszka, D. G., Abdiche, Y. N., Arisaka, F., Byron, O., Eisenstein, E., Hensley, P., Thomson, J. A., Lombardo, C. R., Schwarz, F., Stafford, W., Doyle, M. L. (2003) The ABRF-MIRG'02 study: Assembly state, thermodynamic, and kinetic analysis of an enzyme/inhibitor interaction, *J. Biomol. Tech.* *14*, 247–269.
17. Ciulli, A., Williams, G., Smith, A. G., Blundell, T. L., and Abell, C. (2006) Probing hot spots at protein–ligand binding sites: A fragment-based approach using biophysical methods, *J. Med. Chem.* *49*, 4992–5000.
18. Allen, F. H., Baalham, C. A., Lommerse, J. P. M., Raithby, P. R., Sparr, E. (1997) Hydrogen-bond acceptor properties of nitro-O atoms: A combined crystallographic database and *ab initio* molecular orbital study, *Acta Cryst.* *B53*, 1017–1024.
19. Allen, F. H., Bird, C. M., Rowland, R. X., Raithby, P. R. (1997) Hydrogen-bond acceptor and donor properties of divalent sulfur (Y-S-Z and R-S-H), *Acta Cryst.* *B53*, 696–701.
20. Vianello, L., Kovačević, B., Ambrožič, G., Mavri, J., Maksić, Z. B. (2004) Hydrogen bonding in complex of serine with histidine: Computational and spectroscopic study of model compounds, *Chem. Phys. Lett.* *400*, 117–121.
21. Bondi, A. (1964) Van der Waals volumes and radii, *J. Phys. Chem.* *68*, 441–451.
22. Berg, L., Niemiec, M. S., Qian, W., Andersson, C. D., Wittung-Stafshede, P., Ekström, F., Linusson, A. (2012) Similar but different: Thermodynamic and structural characterization of a pair of enantiomers binding to acetylcholinesterase, *Angew. Chem. Int. Ed.* *51*, 12716–12720.

23. Tanford, C. (1978) The hydrophobic effect and the organization of living matter, *Science* 200, 1012–1018.
24. Biela, A., Sielaff, F., Terwesten, F., Heine, A., Steinmetzer, T., Klebe F. (2012) Ligand binding stepwise disrupts water network in thrombin: Enthalpic and entropic changes reveal classical hydrophobic effect, *J. Med. Chem.* 55, 6094–6110.
25. Bissantz, C., Kuhn, B., Stahl, M. (2010) A medicinal chemist's guide to molecular interactions, *J. Med. Chem.* 53, 5061–5084.
26. Chodera, J. D., Mobley, D. L. (2013) Entropy-enthalpy compensation: Role and ramifications in biomolecular ligand recognition and design, *Annu. Rev. Biophys.* 42, 121–142.
27. Krieger, E., Koraimann, G., Vriend, G. (2002) Increasing the precision of comparative models with YASARA NOVA—a self-parameterizing force field, *Proteins* 47, 393–402.
28. Duan, Y., Wu, C., Chowdhury, S., Lee, M. C., Xiong, G., Zhang, W., Yang, R., Cieplak, P., Luo, R., Lee, R. (2003) A point-charge force field for molecular mechanics simulations of proteins based on condensed-phase quantum mechanical calculations, *J. Comput. Chem.* 24, 1999–2012.
29. Morris, G. M., Goodsell, D. S., Halliday, R. S., Huey, R., Hart, W. E., Belew, R. K. Olson, A. J. (1998) Automated docking using a Lamarckian genetic algorithm and empirical binding free energy function, *J. Comput. Chem.* 19, 1639–1662.
30. *Molecular Operating Environment (MOE)*, 2012.10; Chemical Computing Group Inc., 1010 Sherbooke St. West, Suite #910, Montreal, QC, Canada, H3A 2R7, (2012)

### Supporting Information: Appendix 7.1

**D Combining in Silico and Biophysical Methods for the Development of Pseudomonas aeruginosa Quorum Sensing Inhibitors: An Alternative Approach for Structure-Based Drug Design**

J. Henning Sahner\*, Christian Brengel\*, Michael P. Storz, Matthias Groh, Alberto Plaza, Rolf Müller, and Rolf W. Hartmann

\*These authors contributed equally

Reprinted with permission from *J. Med. Chem.* **2013**, 56(21), 8656–8664.

Copyright (2013) American Chemical Society.

DOI: 10.1021/jm401102

## ABSTRACT

The present work deals with the optimization of an inhibitor of PqsD, an enzyme essential for *Pseudomonas aeruginosa* quorum sensing apparatus. Molecular docking studies, supported by biophysical methods (surface plasmon resonance, isothermal titration calorimetry, saturation transfer difference NMR), were used to illuminate the binding mode of the 5-aryl-ureidothiophene-2-carboxylic acids. Enabled to make profound predictions, structure-based optimization led to increased inhibitory potency. Finally a covalent inhibitor was obtained. Binding to the active site was confirmed by LC-ESI-MS and MALDI-TOF-MS experiments. Following this rational approach, potent PqsD inhibitors were efficiently developed within a short period of time. This example shows that a combination and careful application of *in silico* and biophysical methods represents a powerful complement to co-crystallography.

## INTRODUCTION

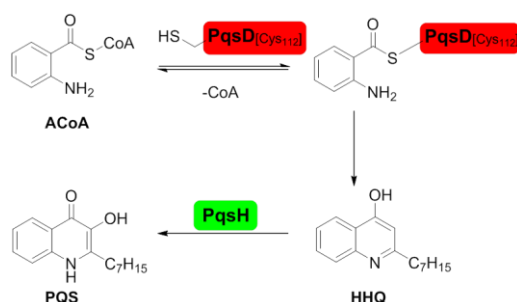
Structure-based drug design is a rational strategy to develop bioactive molecules without the necessity of performing many rounds of modifications to derive structure activity relationships (SAR). Frequently data from X-ray co-crystallography are used to accelerate the lead optimization process. Although this method is undeniably efficient, there are some drawbacks: a co-crystal structure does not necessarily represent the biological state, as it results in a single “frozen” conformation that is affected by the crystallization conditions.<sup>1,2</sup> Furthermore, especially the ligand may not be well defined even at high resolution.<sup>3</sup> In some cases, attempts of co-crystallizing ligands and their targets were not successful forcing the research groups to make use of alternative strategies. The described problems can be overcome by the use of biophysical methods such as surface plasmon resonance (SPR), nuclear magnetic resonance (NMR) and isothermal titration calorimetry (ITC). An advantage of SPR, NMR and ITC is that they can be performed in aqueous solution, which can be considered almost “physiological” conditions.

In the forefront of this work, compound **1** (Figure 1a) was identified as an inhibitor of PqsD. The target protein PqsD, is a key player in the quorum sensing system of *P. aeruginosa*. It mediates the formation of heptyl-4-hydroxy-quinoline (HHQ) which is the precursor of *Pseudomonas* quinolone signal (PQS) (Scheme 1). Both molecules are potent virulence factors and function as signal molecules of *P. aeruginosa*, coordinating group behavior like the formation of biofilms.<sup>4,5</sup> The substrate channel of PqsD is about 15 Å long and rather narrow.<sup>6</sup> The channel can be divided into three parts. A positively charged entrance followed by a mainly hydrophobic middle segment, ending in a polar bottom part. The latter is delimited by the catalytic residues Cys112, His257 and Asp287. Suppression of PqsD activity has been shown recently by our group to inhibit biofilm formation.<sup>7</sup> This makes PqsD

an attractive target for the therapy of chronic *P. aeruginosa* infections, especially in immunosuppressed individuals.<sup>8–10</sup>

Herein, we report on the optimization of **1** supported by biophysical methods and molecular docking. The approach described in the following, represents a hit to lead optimization process that does not involve co-crystallographic structure determination.

**Scheme 1. Biosynthesis of signaling molecules HHQ and PQS in *Pseudomonas aeruginosa*.**<sup>a</sup>

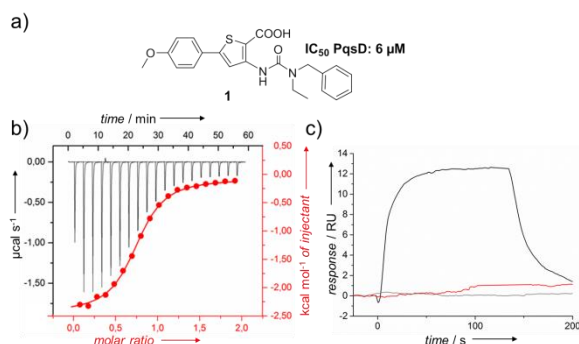


<sup>a</sup> Anthranilate is transferred to PqsD *via* thio-esterification of ACoA with Cys112. The next step is a condensation with acetyl carrier protein (ACP) bound  $\alpha$ -ketodecanoic acid to form HHQ, which is finally transformed to PQS by PqsH.

## RESULTS AND DISCUSSION

The IC<sub>50</sub> value of compound **1** (Figure 1a) against PqsD was determined in a functional enzyme assay<sup>11</sup> to be 6  $\mu$ M. The same compound has recently been reported as a weak inhibitor of bacterial RNA polymerase (IC<sub>50</sub>: 241  $\mu$ M)<sup>12</sup>, a classical target for antibacterial therapy. While targeting quorum sensing an antibacterial effect is not desired to avoid selection pressure inevitably leading to the development of resistant strains.<sup>13</sup> Thus, other potential hit candidates from the 5-aryl-ureidothiophene-2-carboxylic acid class, displaying poor selectivity, were not considered for further optimization (see Table S1 in Supporting Information).

**Figure 1.** a) Compound **1**. Biophysical characterization of **1**: b) Thermogram (red) and titration curve (black) obtained from ITC of PqsD with **1**; c) SPR experiment: ACoA binds to PqsD (black). ACoA binding is inhibited by preincubation with **1** (red). The reference signal is shown in grey.



Attempts to obtain a co-crystal-structure of **1** and PqsD, using soaking techniques, were not successful. Therefore, a combination of biophysical methods and molecular docking was used to elucidate the binding mode of **1**. To exclude a non-specific binding behavior (e.g. *via* aggregation), **1** was examined in an isothermal titration calorimetry (ITC) experiment to ensure stoichiometric binding. Thereby an equimolar binding ratio ( $0.82 \pm 0.05$ ) with a  $K_D$  of  $6.3 \pm 2.6 \mu\text{M}$  was determined (Figure 1b), confirming that the discovered class of compounds represents a promising starting point for further optimization.

In order to clarify the binding site on PqsD, SPR experiments were conducted. It was shown, that the natural substrate ACoA can no longer bind to the enzyme when PqsD was preincubated with **1** (Figure 1c). This result indicates that **1** binds inside the ACoA-channel, thus blocking the first step of the catalytic reaction.

From docking simulations with **1**, two putative binding modes with similar scoring values but reverse orientations were obtained. In the first pose (Figure 2; orange), the ureido *N*-ethyl-benzyl moiety points to the bottom of the pocket (delimited by Cys112, His257 and Asn287), whereas in the second pose (Figure 2; green), the methoxy-group is placed in this position.



**Figure 2.** Docking poses of **1** within the ACoA channel of PqsD: (orange; Vina-Score: 8.3 kcal mol<sup>-1</sup>) (green; Vina-Score: 8.2 kcal mol<sup>-1</sup>).

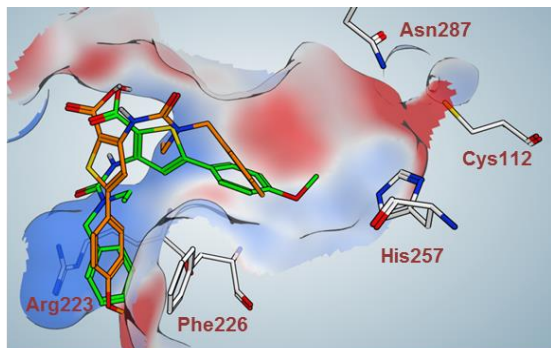
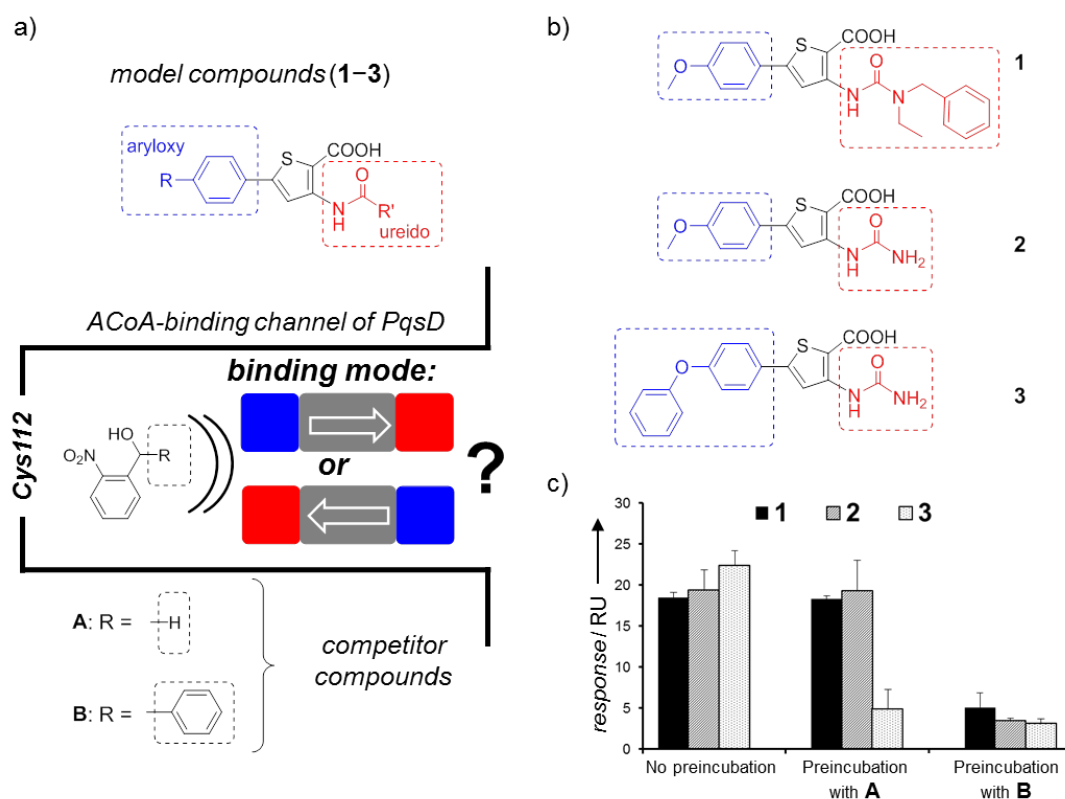


**Figure 3. a)** Schematic illustration of the SPR competition experiments: PqsD was preincubated with competitor compounds **A** and **B** binding to the ACoA-channel, delimited by Cys112. The model compounds **1–3** were subsequently added and the influence of **A** or **B** on their binding behaviors was investigated. The results shed light on the binding mode of the aryl-ureidothiophene-2-carboxylic acids. **b)** Structures of the model compounds **1–3** **c)** Results from SPR-competition experiments suggest the aryloxy-moiety to point into the pocket.

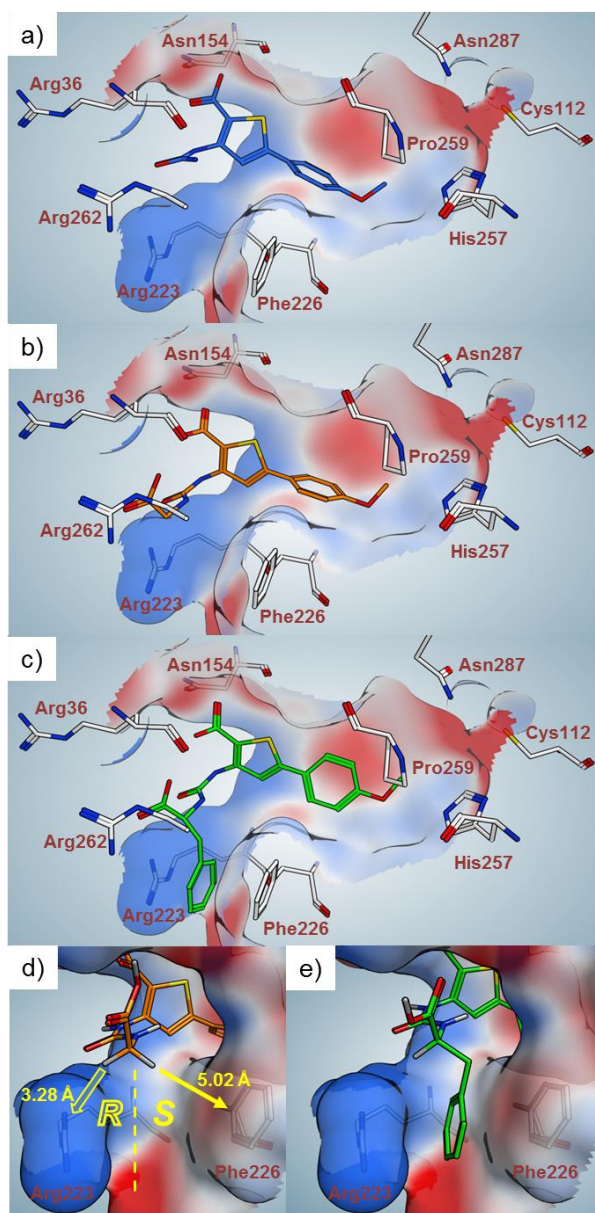


To get a reliable starting point for a structure-based optimization, discrimination between the two poses was necessary. Therefore, we designed an SPR competition experiment with model compounds **1–3** from the 5-aryl-ureidothiophene-2-carboxylic acid class, differently substituted in the ureido and aryloxy parts (Figure 3b). As competitor compounds the 2-nitrophenyl-methanols **A** and **B** were used (Figure 3a). They were recently reported as PqsD inhibitors<sup>7</sup> and were shown to interact with the catalytic residues, especially Cys112, at the bottom of the ACoA-channel.<sup>14</sup>

As illustrated in Figure 3a, the presence of **A** and **B** should influence the binding of the ureidothiophene model compounds depending on their substitution pattern. Compared with **2**, **1** bears a large substituent at the ureido part, whereas **3** is elongated in the aryloxy part, at the opposite site. If the ureido part points to the bottom of the pocket, one would expect that **1** is more sterically hindered than **2** and **3**, when the competitors are present. In contrast, the longer aryloxy part of **3** should lead to a reduced binding if the ureidothiophenes bind in the reversed orientation. In the absence of a competitor compound, **1–3** displayed comparable responses (Figure 3c). When the sterically less demanding 2-nitrophenyl-methanol derivative **A** was present, a reduction of affinity was observed exclusively for **3** bearing a bulky phenyl substituent in the aryloxy part. In contrast, the ethyl-benzyl moiety at the ureido motif of **1** did not prevent a binding. These results fit to the docking prediction with the aryloxy part pointing into the pocket (Figure 2, green). In competition with **B**, the binding affinity of all three compounds was reduced as expected from the docking results. (see Figure S1 and S2) Thus a deeper insight into the position of the new inhibitors in the binding channel was provided.

As the starting point for structure activity exploration compound **2** was chosen, a truncated derivative of the initial hit **1**. It displays comparable ligand efficiency (LE, Table 1) whilst being more suitable for further modification at the ureido motif. The docking pose of **2** (Figure 4a) suggests an anchoring of the ureido moiety by interaction of the carbonyl oxygen with Arg223. To validate this assumption, binding of **2** to the R223A mutant, that should display weaker affinity, was investigated by SPR. The response of compound **2** was reduced to 6 response units (RU) in comparison to 25 RU for the wild type enzyme (see Figure S4), confirming this hypothesis. Arg262, placed in the upper part of the binding pocket, should be a potential interaction partner for a negatively charged moiety. The introduction of a carboxylate resulting in compounds **4** and **5** (Table 1) indeed led to an increased activity, confirming this prediction. In the docking pose, the introduced carboxylic acid moiety of **4** is located closely to Arg262 enabling the formation of a new interaction (Figure 4b). Based on the finding that **4** is more active than **5**, we concluded that a methylene linker is more appropriate than a longer spacer unit. This allowed making use of  $\alpha$  amino acids for simple variations in the next steps, taking advantage of their hydrophilicity to increase the polarity of the inhibitors, as low lipophilicity is an important requirement for drugs targeting Gram negative bacteria. A study of O'Shea et al. shows that almost all antibiotics, effective against *P. aeruginosa*, possess a  $\text{clogD}_{7.4}$  value below 0.<sup>15</sup> While our hit compound **1** ( $\text{logD}_{7.4}$ : 2.58) did not meet this criterion, amino acid derivative **4** ( $\text{logD}_{7.4}$ : -1.62) did.

**Figure 4.** a) Docking pose of **2**, the starting point for structure-based optimization. b) Docking pose of glycine derivative **4**. c) Docking pose of optimized compound **7**. d) Illustration of the limited space in the narrow cleft formed by Arg223 and Phe226. e) Close-up of the benzyl moiety of **7**, perfectly fitting into the narrow cleft.



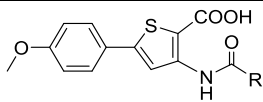
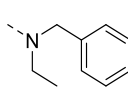
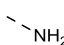
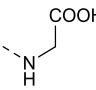
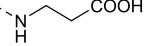
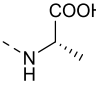
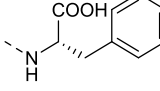
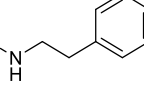
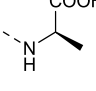
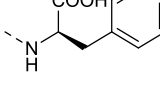
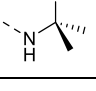
As illustrated in Figure 4b, docking simulations predict that the glycine derivative **4** is anchored by an interaction of the carboxylate group with Arg262. The narrow cleft, subjacent to the  $\alpha$ -position of **4** and delimited by Arg223 and Phe226, is supposed to be addressable by expansion of **4**. A targeted approach should replace the *pro-S* hydrogen since the space adjacent to the *pro-R* hydrogen is blocked by Arg223, which could lead to a sterical clash (Figure 4d). Following this strategy, the introduction of *S*-amino acid residues improved the activity resulting in up to submicromolar  $IC_{50}$  values in case of the

*S*-alanine and *S*-phenylalanine derivative **6** and **7** (Figure 4b–e). Compound **8**, the counterpart of **7** that lacks the COOH group next to the ureido moiety displays a significantly weaker inhibition. This again highlights the importance of the carboxylic acid group, which is in accordance with our binding hypothesis.

In order to complete the picture, the *R*-enantiomers **9** and **10** were investigated. In both cases the activity decreased dramatically. These data corroborate the highly selective three-dimensional interaction formed by the *S*-enantiomeric moieties with the target enzyme. To evaluate whether the decreased activity of the *R*-enantiomer **9** is due to a sterical clash, as expected, or associated with the absence of the *S*-methyl group of **6**, the dimethyl compound **11** was investigated. The fact that **11** was less active than **4** and **6** confirms the prediction of a sterical collision.

To test for selectivity towards bacterial RNA polymerase, the most potent derivatives **6** and **7** were tested for inhibition of this enzyme. Both displayed only slight inhibitory potency (~10–20%) at a concentration of 200  $\mu$ M.

**Table 1. Inhibition of PqsD *in vitro*, ligand efficiencies and clogD<sub>7.4</sub> values of compounds 1–11**

				
Cpd	R	IC <sub>50</sub> PqsD	LE <sup>[a]</sup>	clogD <sub>7.4</sub> <sup>[b]</sup>
1		6 μM	0.25	2.58
2		170 μM	0.26	0.15
4		7 μM	0.30	-1.62
5		37 μM	0.25	-1.47
6		2 μM	0.32	-1.27
7		0.5 μM	0.28	0.59
8		58 μM	0.21	2.61
9		54 μM	0.24	-1.27
10		26 μM	0.19	0.59
11		56 μM	0.23	-0.93

<sup>[a]</sup> Ligand efficiency calculated as  $LE = 1.4 \times (\text{pIC}_{50}/\text{HAC})$

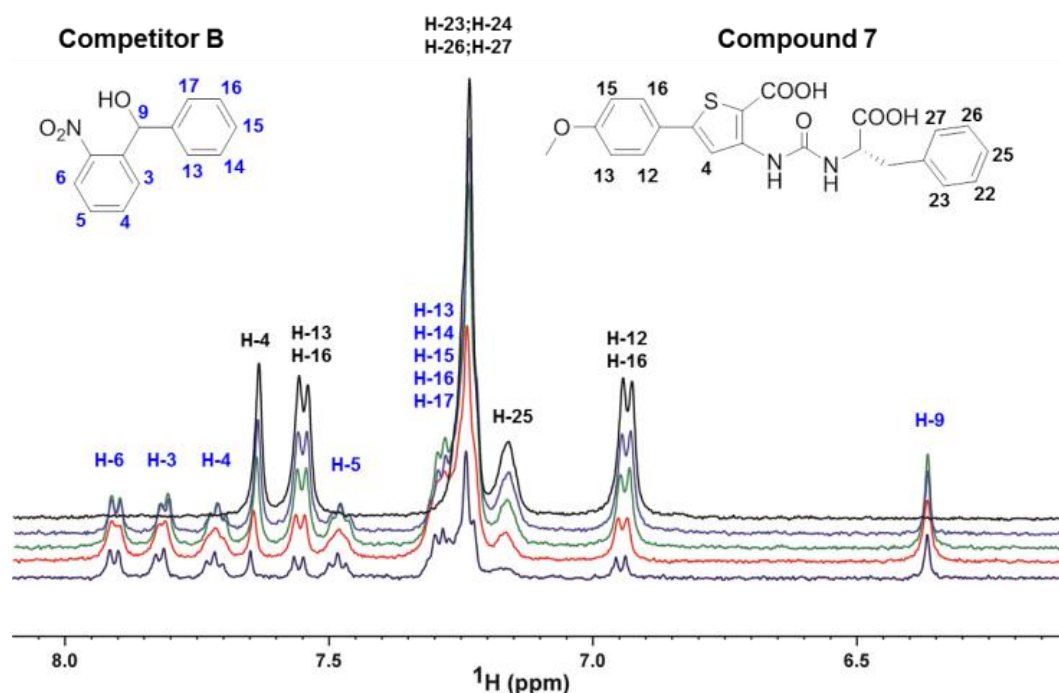
<sup>[b]</sup> clogD<sub>7.4</sub> calculated with ACDLabs Percepta 2012

Saturation transfer difference (STD) NMR<sup>16</sup> was used to identify the binding epitopes of **7** (Figure S5). Strong STD enhancements were observed for all protons of **7** with the methylene linker protons exhibiting the strongest enhancements. This is consistent with the docking simulations, which predict these methylene protons to be positioned at the entrance of the narrow subpocket delimited by Arg223

and Phe226. Moreover, the fact that the other protons of **7** also displayed strong STD enhancements suggests that **7** is nearly completely surrounded by PqsD.

To confirm that the optimized inhibitors bind in a similar way as the model compounds **1–3**, the SPR-competition experiment with **A** and **B** was conducted for compound **7**. As expected, the binding response was only significantly reduced in the presence of **B** (Figure S3). In addition, we performed an STD-NMR competition experiment to validate the SPR results. Increasing amounts of compound **B** were added to a 100:1 complex of **7**/PqsD (Figure 5). Difference spectra were monitored for a change in intensity of signals belonging to either **7** or **B** during titration. As seen in the spectral expansions showing the aromatic region, stepwise addition of up to 3.0 equivalents of **B** with respect to **7** resulted in a uniform decrease in intensity for signals corresponding to **7** while signals ascribable to **B** appeared and steadily increased. This confirms that **7** binds deep inside the ACoA-channel of PqsD.

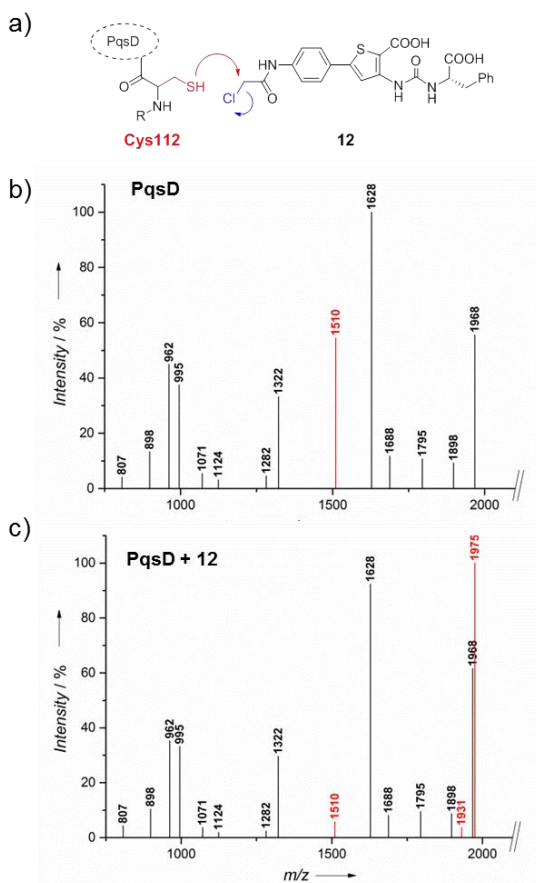
**Figure 5.** Competition of **7** and **B** binding to PqsD by STD NMR. Expanded  $^1\text{H}$  STD NMR spectrum of **7** (1 mM) in the presence of PqsD (10  $\mu\text{M}$ ) (black curve). STD NMR spectra recorded on the same sample after addition of 0.5 (purple), 1.0 (green), 2.0 (red) and 3.0 (blue) equivalents of compound **B**. Signals of **7** are labeled in black, from **B** in blue.



Finally, we focused on the substituted 5-aryl ring that is predicted to be located near the active site within the ACoA channel (Figure 4). As already shown with phenoxy compound **3** ( $\text{IC}_{50} = 20 \mu\text{M}$ ), larger substituents are tolerated in this part of the binding pocket. As Cys112 is pivotal for the catalytic activity of PqsD, a covalent trapping of this amino acid should lead to an effective blockade of the

enzymatic machinery. For that purpose a  $\beta$ -chloroacetyl moiety was introduced, as an “electrophilic warhead”,<sup>17</sup> at the appropriate position, linked to the 5-aryl ring *via* an amide function (Figure 6a).

**Figure 6. a)** Schematic illustration of the proposed trapping of Cys112 by the introduced electrophilic warhead of **12**. MALDI-TOF-MS after tryptic digestion. The mass of the fragment containing Cys112 is highlighted in red **b)** PqsD **c)** PqsD after incubation with **12**. Signals below 3% intensity were removed for the sake of clarity (raw data is shown in Figure S6 and S7).



The resulting compound **12** ( $\text{clogD}_{7.4}$ : -0.59) displays an  $\text{IC}_{50}$  value of 2  $\mu\text{M}$ . The covalent binding of **12** to PqsD was demonstrated by LC-ESI-MS. The PqsD peak ( $m/z = 36687.5$   $[\text{M}+\text{H}]^+$ ) shifted after preincubation with **12** to the calculated adduct mass ( $m/z = 37153.1$   $[\text{M}+\text{H}]^+$ ) (Figure S8). To evaluate whether indeed Cys112 is targeted by **12**, the tryptically digested protein was analyzed by MALDI-TOF-MS. The signal of the fragment containing Cys112, with a calculated  $m/z = 1510.8$   $[\text{M}+\text{H}]^+$ , was found in the reference sample without inhibitor. In the sample treated with **12**, this signal was absent while two new peaks at  $m/z = 1975.9$  and  $1931.9$   $[\text{M}+\text{H}]^+$  appeared (Figure 6b,c). The former fits to the Cys112 fragment with covalently bound **12**. The latter refers to its fragmentation product missing a carboxylic acid moiety. Taking into account that a long residence time at the active site is considered important for *in vivo* potency of the inhibitor,<sup>18</sup> covalently binding compound **12** carries the potential of strong biological effects.

## CONCLUSIONS

In conclusion, we optimized the PqsD inhibitor **1**, following a novel approach. First, an equimolar binding behavior to the target protein PqsD was determined by ITC. The binding mode was elucidated by examination of three model compounds (**1–3**) in SPR competition experiments. To the best of our knowledge, this is the first example of such an approach. These findings allowed profound docking calculations guiding our subsequent structure-based optimization process. This approach culminated in an irreversible inhibitor, which covalently binds to the active site of PqsD as predicted. The optimization of activity was accompanied by reduced lipophilicity (Table 1), caused by the introduction of amino acids at the ureido motif. According to the literature, this should facilitate permeation into Gram negative cells.<sup>15</sup>

For several drug targets, inhibitors with known binding sites and the protein crystal structures are available. In such cases, the presented approach of determining the binding mode can be helpful to guide a structure-based design of new inhibitors, especially if co-crystallization fails.

While we mainly focused on the inhibitory potency at this early point of development, structural variations leading to more drug-like properties (e.g. bio-isosteric exchange of the carboxylic groups) remains a challenging task and will be an element of future work. Additional efforts will also include studies on intracellular activity and inhibition of biofilm formation in *P. aeruginosa*. In the present study, shortcomings of *in silico* docking simulations (prediction of multiple binding modes) were compensated by the use of biophysical methods. This rational approach represents a powerful complement to X-ray co-crystallography and should be applicable to many drug targets with known ligands.

## EXPERIMENTAL SECTION

**Materials and Methods.** Starting materials were purchased from commercial suppliers and used without further purification. Column flash chromatography was performed on silica gel (40–63  $\mu\text{M}$ ), and reaction progress was monitored by TLC on TLC Silica Gel 60 F<sub>254</sub> (Merck). All moisture-sensitive reactions were performed under nitrogen atmosphere using oven-dried glassware and anhydrous solvents. <sup>1</sup>H and <sup>13</sup>C NMR spectra were recorded on Bruker Fourier spectrometers (500/300 or 176/126/75 MHz) at ambient temperature with the chemical shifts recorded as  $\delta$  values in ppm units by reference to the hydrogenated residues of deuteriated solvent as internal standard. Coupling constants (*J*) are given in Hz and signal patterns are indicated as follows: s, singlet; d, doublet; dd, doublet of doublets; t, triplet; m, multiplet, br., broad signal. The purity of the final compounds was >95% except for **12** (90%) measured by HPLC. The Surveyor LC system consisted of a pump, an autosampler, and a PDA detector. Mass spectrometry was performed on a MSQ electrospray mass spectrometer (ThermoFisher, Dreieich, Germany). The system was operated by the standard software Xcalibur. A RP C18 NUCLEODUR 100-5 (125 mm x 3 mm) column (Macherey-Nagel GmbH,



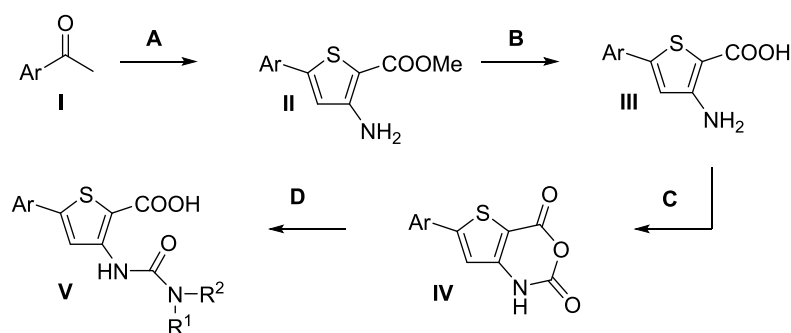
Dühren, Germany) was used as the stationary phase. All solvents were HPLC grade. In a gradient run the percentage of acetonitrile (containing 0.1% trifluoroacetic acid) was increased from an initial concentration of 0% at 0 min to 100% at 15 min and kept at 100% for 5 min. The injection volume was 10  $\mu\text{L}$ , and flow rate was set to 800  $\mu\text{L}/\text{min}$ . MS analysis was carried out at a spray voltage of 3800 V and a capillary temperature of 350  $^{\circ}\text{C}$  and a source CID of 10 V. Spectra were acquired in positive mode from 100 to 1000  $m/z$  at 254 nm for the UV trace.

## Chemistry

### General synthesis procedures.

Experimental details on synthesis of **12** can be found in the Supporting Information.

### Scheme S1: Synthesis of 5-aryl-3-ureidothiophene-2-carboxylic acids.



*Method A, general procedure for the synthesis of 5-aryl-3-amino-2-carboxylic acid methylester (II):*<sup>19</sup> POCl<sub>3</sub> (26.1 g, 0.17 mol) was added dropwise to DMF (24.9 g, 0.34 mol) maintaining the temperature below 25  $^{\circ}\text{C}$  (cooling in ice bath) and stirred for additional 15 min. The acetophenone **I** (85.0 mmol) was added slowly and the temperature was kept between 40 and 60  $^{\circ}\text{C}$ . After complete addition, the mixture was stirred for 30 minutes at room temperature. Hydroxylamine hydrochloride (23.6 g, 0.34 mol) was carefully added portionwise (exothermic reaction!) and the reaction was stirred for additional 30 min without heating. After cooling to room temperature, the mixture was poured into ice water (300 mL). The precipitated  $\beta$ -chloro-cinnamionitrile was collected by filtration, washed with H<sub>2</sub>O (2 x 50 mL) and dried under reduced pressure over CaCl<sub>2</sub>. In the next step sodium (1.93 g, 84.0 mmol) was dissolved in MeOH (85 mL) and methylthioglycolate (6.97 g, 65.6 mmol) was added to the stirred solution. The  $\beta$ -chloro-cinnamionitrile (61.1 mmol) was added and the mixture was heated to reflux for 30 min. After cooling to room temperature, the mixture was poured in ice water (300 mL). The precipitated solid was collected by filtration, washed with H<sub>2</sub>O (2 x 50 mL) and dried under reduced pressure over CaCl<sub>2</sub>. If necessary, recrystallisation was performed from EtOH.

*Method B, general procedure for the synthesis of 5-aryl-3-amino-2-carboxylic acid (III):*

The 5-aryl-3-amino-2-carboxylic acid methyl ester **II** (16.6 mmol) was added to a solution of KOH (60 mL, 0.6M in H<sub>2</sub>O) and MeOH (60 mL). The mixture was heated to reflux for 3 h, concentrated, and washed with EtOAc (2 x 50 mL). The aqueous layer was cooled with ice and acidified with a

saturated aqueous solution of  $\text{KHSO}_4$ . The precipitated solid was collected by filtration, washed with  $\text{H}_2\text{O}$  (2 x 30 mL) and dried under reduced pressure over  $\text{CaCl}_2$ .

*Method C, general procedure for the synthesis of 5-aryl-2-thiaisatoic-anhydrid (IV).*<sup>20,21</sup>

To a solution of the 5-aryl-3-amino-2-carboxylic acid (**III**) (5.28 mmol) in THF (50 mL) a solution of phosgene (6.10 mL, 20 wt% in toluene, 11.6 mmol) was added dropwise over a period of 30 min. The reaction mixture was stirred for 2 h at room temperature, followed by the addition of saturated aqueous solution of  $\text{NaHCO}_3$  (30 mL) and  $\text{H}_2\text{O}$  (50 mL). The resulting mixture was extracted with EtOAc/THF (1:1, 3 x 100 mL). The organic layer was washed with saturated aqueous NaCl (100 mL), dried ( $\text{MgSO}_4$ ) and concentrated. The crude material was suspended in a mixture of *n*-hexane/EtOAc (2:1, 50 mL) heated to 50 °C and after cooling to room temperature separated *via* filtration.

*Method D, general procedure for the synthesis of 5-aryl-3-ureidothiophene-2-carboxylic acid (V).*<sup>22</sup>

The 5-aryl-2-thiaisatoic-anhydrid (**IV**) (0.46 mmol) was suspended in water (7.5 mL) and the appropriate amine (4.60 mmol) was added. The reaction mixture was stirred, heated to 100 °C and then cooled to room temperature. The reaction mixture was poured into a mixture of concentrated HCl and ice (1:1) and extracted with EtOAc/THF (1:1, 60 mL). The organic layer was washed with aqueous HCl (2M), followed by saturated aqueous NaCl (2 x 50 mL), dried ( $\text{MgSO}_4$ ) and concentrated. The crude material was suspended in a mixture of *n*-hexane/EtOAc (2:1, 20 mL) heated to 50 °C and after cooling to room temperature separated *via* filtration.

Spectroscopic data of final compounds and intermediates can be found in the Supporting Information. Compound **7** is presented as example.

(*S*)-3-(3''-(1-Carboxy-2-phenylethyl)ureido)-5-(4'-methoxyphenyl)thiophene-2-carboxylic acid (**7**).

$^1\text{H}$  NMR ( $\text{DMSO-}d_6$ , 300 MHz):  $\delta$  = 12.84 (br. s., 2 H, COOH), 9.42 (s, 1 H), 8.15 (d,  $J$  = 7.9 Hz, 1 H), 8.09 (s, 1 H), 7.69–7.51 (m,  $J$  = 8.8 Hz, 2 H), 7.37–7.25 (m, 4 H), 7.25–7.17 (m, 1 H), 7.03–6.97 (m,  $J$  = 8.8 Hz, 2 H), 4.56–4.28 (m, 1 H), 3.79 (s, 3 H,  $\text{OCH}_3$ ), 3.11 (dd,  $J$  = 13.9, 4.6 Hz, 1 H), 2.88 (dd,  $J$  = 13.9, 9.8 Hz, 1 H) ppm.

$^{13}\text{C}$  NMR ( $\text{DMSO-}d_6$ , 75 MHz):  $\delta$  = 173.6, 164.6, 160.1, 153.7, 147.1, 145.9, 137.7, 129.0, 128.2, 127.1, 126.4, 125.4, 116.7, 114.7, 105.8, 55.3, 54.4, 36.9 ppm.

## Biology and Biophysics

**General procedure for expression and purification of recombinant PqsD WT and R223A mutant in *E. coli*.** His6-tagged PqsD (H6-PqsD) and mutants were expressed in *E. coli* and purified using a single affinity chromatography step. Briefly, *E. coli* BL21 ( $\lambda\text{DE3}$ ) cells containing the pET28b(+)/pqsD (kindly provided by Prof. Rolf Müller) were grown in LB medium containing 50  $\mu\text{g}/\text{mL}$  kanamycin at 37 °C to an  $\text{OD}_{600}$  of approximately 0.8 units and induced with 0.2 mM IPTG for

16 h at 16 °C. The cells were harvested by centrifugation (5,000 rpm, 10 min, 4 °C) and the cell pellet was resuspended in 100 mL binding buffer (10 mM Na<sub>2</sub>HPO<sub>4</sub>, 2 mM KH<sub>2</sub>PO<sub>4</sub> pH 7.4, 3 mM KCl, 137 mM NaCl, 20 mM imidazole, 10% glycerol (v/v)) and lysed by sonication for a total process time of 2.5 min. Cell debris were removed by centrifugation (18500 rpm, 40 min, 4 °C) and the supernatant was filtered through a syringe filter (0.20 µm). The clarified lysate was immediately applied to a Ni-NTA column, washed with binding buffer and eluted with 500 mM imidazole. The protein containing fractions were buffer-exchanged into 125 mM Na<sub>2</sub>HPO<sub>4</sub>, 50 mM KH<sub>2</sub>PO<sub>4</sub> pH 7.6, 50 mM NaCl, 10% glycerol (v/v), using a PD10 column and judged pure by SDS-PAGE analysis. Then protein was stored in aliquots at -80 °C.

**Screening assay procedure for *in vitro* PqsD inhibition.**<sup>11</sup> The assay was performed monitoring enzyme activity by measuring HHQ formed by condensation of anthraniloyl-CoA and β-ketodecanoic acid. The reaction mixture contained MOPS buffer (0.05 M, pH 7.0) with 0.005% (w/v) Triton X-100, 0.1 µM of the purified enzyme and inhibitor. The test compounds were dissolved in DMSO and diluted with buffer. The final DMSO concentration was 0.5%. After 10 min preincubation at 37 °C, the reaction was started by the addition anthraniloyl-CoA to a final concentration of 5 µM and β-ketodecanoic acid to a final concentration of 70 µM. Reactions were stopped by addition of MeOH containing 1 µM amitriptyline as internal standard for LC/MS-MS analysis. HHQ was quantified using a HPLC-MS/MS mass spectrometer (ThermoFisher, Dreieich, Germany) in ESI mode. Ionization of HHQ and the internal standard amitriptyline was optimized in each case. The solvent system consisted of 10 mM ammonium acetate (A) and acetonitrile (B), both containing 0.1% trifluoroacetic acid. The initial concentration of B in A was 45%, increasing the percentage of B to 100% in 2.8 min and keeping it at 98% for 0.7 min with a flow of 500 µL/min. The column used was a NUCLEODUR-C18, 100-3/125-3 (Macherey & Nagel, Dueren, Germany). Control reactions without the inhibitor, but including identical amounts of DMSO, were performed in parallel and the amount of HHQ produced was set to 100%. All reactions were performed in triplicates.

**RNAP-transcription assay.** *E. coli* RNA polymerase holo enzyme was purchased from Epicentre Biotechnologies (Madison, WI). Final concentrations in a total volume of 30 µL were one unit of RNA polymerase (0.5 µg) which were used along with 60 nCi of [5,6-<sup>3</sup>H]-UTP, 400 µM of ATP, CTP and GTP as well as 100 µM of UTP, 20 units of RNase inhibitor (RiboLock, Fermentas), 10 mM DTT, 40 mM Tris-HCl (pH 7.5), 150 mM KCl, 10 mM MgCl<sub>2</sub> and 0.1% CHAPS. As a DNA template 3500 ng of religated pcDNA3.1/V5-His-TOPO were used per reaction.<sup>23</sup> Prior to starting the experiment, the compounds were dissolved in DMSO (final concentration during experiments: 2%). Dilution series of compounds were prepared using a liquid handling system (Janus, Perkin Elmer, Waltham, MA). The components described above (including the inhibitors) were preincubated in absence of NTPs and DNA for 10 min at 25 °C. Transcription reactions were started by the addition of a mixture containing

DNA template and NTPs and incubated for 10 min at 37 °C. The reaction was stopped by the addition of 10% TCA, followed by a transfer of this mixture to a 96 well Multiscreen GFB plate (Millipore, Billerica, MA) and incubation for 45 min at 4 °C. The plate underwent several centrifugation and washing steps with 10% TCA and 95% ethanol to remove residual unincorporated  $^3\text{H}$ -UTP. After that the plate was dried (30 min, 50 °C) and 30  $\mu\text{L}$  of scintillation fluid (Optiphase Supermix, Perkin Elmer) was added to each well. After 10 min the wells were assayed for presence of  $^3\text{H}$ -RNA by counting using a Wallac MicroBeta TriLux system (Perkin Elmer). To obtain inhibition values for each sample, their counts were related to DMSO controls.

**Surface plasmon resonance.** SPR binding studies were performed using a Reichert SR7500DC instrument optical biosensor (Reichert Technologies, Depew, NY, USA) and CMD500M (carboxymethyl dextrane-coated) sensor chips obtained from XanTec (XanTec Bioanalytics, Düsseldorf, Germany).

*Immobilization of wild type PqsD and R223A mutant.* PqsD was immobilized on a CMD500M sensor chip at 12 °C using standard amine coupling analogous to the manufacturers' instructions. PqsD was diluted into sodium acetate buffer (10 mM, pH 4.5) to a final concentration of 100  $\mu\text{g}/\text{mL}$ . PqsD was immobilized at densities between 5000-6000 RU for binding studies and for mutagenesis studies. The PqsD mutant was immobilized analogously to the wild type.

*Competition studies.* The competition studies were performed at a constant flow rate of 50  $\mu\text{L}/\text{min}$  in instrument running buffer (50 mM MOPS, pH 8.0, 150 mM NaCl, 5% DMSO (v/v), 0.1% Triton X 100 (v/v)). 10 mM stock solutions of compounds **1**, **2** and **3** in DMSO were directly diluted to a concentration of 500  $\mu\text{M}$  (50 mM MOPS, pH 8.0, 150 mM NaCl, 0.1% Triton X-100 (v/v)) and then diluted to a final concentration of 100  $\mu\text{M}$  in running buffer (50 mM MOPS, pH 8.0, 150 mM NaCl, 5% DMSO (v/v), 0.1% Triton X 100 (v/v)). Final concentration of DMSO was retained at 5% (v/v). Before the compounds were injected, 6 warm-up blank injections were performed. Buffer blank injections and DMSO calibration were included for double referencing.

*ACoA competition.* PqsD was preincubated with compound **1**, therefore **1** was added to the running buffer (100  $\mu\text{M}$ ). The sensor chip surface was flushed for several hours at a constant flow rate of 50  $\mu\text{L}/\text{min}$  until the baseline was stable. Afterwards the flow rate was decreased to 10  $\mu\text{L}/\text{min}$  and ACoA was injected (100  $\mu\text{M}$ ) twice for 120 s association and 15 min dissociation times.

*Competitor competition.* PqsD was preincubated with compounds **A** or **B**, therefore the competitor compound was added to the running buffer (100  $\mu\text{M}$ ). The sensor chip surface was flushed for several hours at a constant flow rate of 50  $\mu\text{L}/\text{min}$  until the baseline was stable. Afterwards the flow rate was decreased to 10  $\mu\text{L}/\text{min}$  and compound **1**, **2** or **3** were injected (100  $\mu\text{M}$ ) twice for 120 s association and 300 s dissociation times. Due to a slow  $k_{\text{off}}$  rate of the competitor compounds,  $k_{\text{D}}$  values referring to the concentrations do not play a decisive role during the competition experiment.

*Studies with R223A mutant.* The experiments were performed at a constant flow rate of 50  $\mu\text{L}/\text{min}$  in instrument running buffer (50 mM MOPS, pH 8.0, 150 mM NaCl, 5% DMSO (v/v), 0.1% Triton X 100 (v/v)) at 12  $^{\circ}\text{C}$ . 10 mM stock solutions of compounds **1** or **2** in DMSO were diluted to a concentration of 100  $\mu\text{M}$  analogous to the binding studies. Before the compound was injected, twelve warm-up blank injections were performed. The obtained data were referenced against blank injections and DMSO calibration. The compounds were injected twice for 120 s association and 300 s dissociation time. Scrubber software was used for processing and analysing data.

**Isothermal titration calorimetry.** ITC experiments were carried out using an ITC200 instrument (Microcal Inc., GE Healthcare). Concentration of the ligand in DMSO stock solutions was 20 mM. Final ligand concentrations were achieved by diluting 1:20 (v/v) in the experimental buffer resulting in a final DMSO concentration of 5% (v/v). Protein concentration was determined by measuring the absorbance at 280 nm using a theoretical molarity extinction coefficient of  $17,780 \text{ M}^{-1} \text{ cm}^{-1}$ . DMSO concentration in the protein solution was adjusted to 5% (v/v). ITC measurements were routinely performed at 25  $^{\circ}\text{C}$  in PBS-buffer, pH 7.4, 10% glycerol (v/v), 5% DMSO (v/v). The titrations were performed on 100  $\mu\text{M}$  PqsD-His6 in the 200  $\mu\text{L}$  sample cell using 2  $\mu\text{L}$  injections of 1.0 mM ligand solution every 180 s. Raw data were collected and the area under each peak was integrated. To correct for heats of dilution and mixing the final baseline consisting of small peaks of the same size at the end of the experiment was subtracted. The experimental data were fitted to a theoretical titration curve (one site binding model) using MicroCal Origin 7 software, with  $\Delta\text{H}$  (enthalpy change in  $\text{kcal mol}^{-1}$ ),  $K_{\text{A}}$  (association constant in  $\text{M}^{-1}$ ), and  $N$  (number of binding sites) as adjustable parameters. Thermodynamic parameters were calculated from equation:

$$\Delta\text{G} = \Delta\text{H} - T\Delta\text{S} = RT \ln K_{\text{A}} = -RT \ln K_{\text{D}}$$

where  $\Delta\text{G}$ ,  $\Delta\text{H}$ , and  $\Delta\text{S}$  are the changes in free energy, enthalpy, and entropy of binding, respectively,  $T$  is the absolute temperature, and  $R = 1.98 \text{ cal mol}^{-1} \text{ K}^{-1}$ . For compound **1** four independent experiments were performed.

**Saturation transfer difference NMR.** All NMR data were recorded at 298 K on a Bruker Avance 500 NMR instrument equipped with a cryogenically cooled z-shielded gradient probe. Experiments were recorded with the carrier set at -2 ppm for on-resonance irradiation and 40 ppm for off-resonance irradiation. Control spectra were recorded under identical conditions on samples containing free compound **7** to test for artifacts. Selective protein saturation (3 s) was accomplished using a train of 50 ms Gauss-shaped pulses, each separated by a 1 ms delay, at an experimental determined optimal power (50 dB on our probe); a T1 $\rho$  filter (15 ms) was incorporated to suppress protein resonances. Experiments were recorded using a minimum of 512 scans and 32K points. On- and off-resonance spectra were processed independently, and subtracted to provide a difference spectrum. Samples

containing **7** and PqsD at final concentrations of 1 mM and 10  $\mu$ M, respectively, were prepared in 20 mM sodium phosphate, 50 mM NaCl, and 5 mM MgCl<sub>2</sub>, pH 7.0.

**LC-ESI-MS.** PqsD (25  $\mu$ M) was preincubated with compound **12** (25  $\mu$ M) for 30 min at 37°C in Tris-HCl buffer (0.05 M, pH 8.0) with 0.5% DMSO. Dithiothreitol was added and the samples were analyzed by HPLC-ESI. All ESI-MS-measurements were performed on a Dionex Ultimate 3000 RSLC system using an Aeris Widepore XB-C8, 150 x 2.1 mm, 3.6  $\mu$ m dp column (Phenomenex, USA). Separation of 2  $\mu$ l sample was achieved by a linear gradient from (A) H<sub>2</sub>O + 0.05% TFA to (B) ACN + 0.05% TFA at a flow rate of 250  $\mu$ l/min and 45 °C. The gradient was initiated by a 1.0 min isocratic step at 15% B, followed by an increase to 80% B in 4.5 min to end up with a 6 min step at 80% B before re-equilibration with initial conditions. UV spectra were recorded by a DAD in the range from 200 to 600 nm. The LC flow was split to 75  $\mu$ l/min before entering the maXis 4G hr-ToF mass spectrometer (Bruker Daltonics, Bremen, Germany) using the standard Bruker ESI source. In the source region, the temperature was set to 180°C, the capillary voltage was 4000 V, the dry-gas flow was 6.0 l/min and the nebulizer was set to 1.1 bar. Mass spectra were acquired in positive ionization mode ranging from 600 – 1800 m/z at 2.5 Hz scan rate. Protein masses were deconvoluted by using the Maximum Entropy algorithm (Copyright 1991-2004 Spectrum Square Associates, Inc.).

**MALDI-TOF-MS.** PqsD (10  $\mu$ M) was preincubated with compound **12** (10  $\mu$ M) for 60 min at 37°C using identical buffer composition as in the screening assay procedure (0.05 M MOPS, pH 7.0 with 0.005 % (w/v) Triton X-100 and 0.5 % DMSO). The buffer was exchanged by an NH<sub>4</sub>HCO<sub>3</sub> buffer (0.05 M, pH 8.1) in three diafiltration steps. Diafiltration was performed at 1200 g for 6 min at 4°C in Nanosep® Centrifugal Devices (MWCO = 10K) of Pall Corporation (Port Washington, NY, USA). The protein was digested with trypsin overnight and dithiothreitol was added.  $\alpha$ -Cyano-4-hydroxycinnamic acid was used as matrix component. Analyzes of the peptides were performed on a 4800 TOF/TOF Analyzer mass spectrometer (Applied Biosystems, Darmstadt, Germany) in positive reflector mode using a pulsed 200 Hz solid state Nd:YAG laser with a wavelength of 355 nm. Laser energy was set to 2000–2300 units for standards and to 2700–3200 units for real samples. Source 1 voltage was set to 20 kV with a grid voltage of 16 kV. Reflector detector voltage was 2.19 kV. Spectra of standard peptides used for wide range calibration ranging from 0.8 to 4 kDa (des-arg1-bradykinin, angiotensin I, glu1-fibrinopeptide B, ACTH 1–17 clip, ACTH 18–39 clip and ACTH 7–38 clip) were measured with a delay time of 600 ns. One single mass spectrum was formed from 20 subspectra per spot using 25 accepted laser impulses each. From the standard peptides exclusively monoisotopic ions were used with a minimum signal-to-noise (S/N) ratio of 20 and a resolution >10000. Mass tolerance was set to 0.3 Da with maximum outlier of 5 ppm. Accepted calibration settings were used to measure real sample spectra in the range of 1 to 3.5 kDa with a minimum S/N range of 10 and a resolution >8000. An internal algorithm defined the isotope cluster area subsequently named intensity (I), based

on the peptides' molecular weight and their general elemental composition. MALDI-TOF-MS resulted in pmfs consisting of mass-intensity spectra ( $m/z$ - $I_{\text{abs, ai}}$ ).

### Molecular Modeling

**Docking.** Inhibitors were built in Molecular Operating Environment (MOE).<sup>24</sup> The receptor was derived from the co-crystal structure of anthraniloyl coenzyme A with PqsD (PDB Code: 3H77)<sup>6</sup> ACoA, the covalently bound anthranilate and H<sub>2</sub>O were removed and Cys112 was restored considering its conformation in 3H76.<sup>6</sup> AutoDockTools V.1.5.6 was used to add polar hydrogens and to save the protein in the appropriate file format for docking with Vina. For docking AutoDockVina was used.<sup>25</sup> The docking parameters were kept at their default values. The docking grid was sized 18 Å x 24 Å x 24 Å, covering the entire ACoA channel.

### ASSOCIATED CONTENT

**Supporting Information.** Further experimental procedures, analytical data and <sup>13</sup>C NMR spectra, selectivity data (PqsD vs. RNAP) and more details concerning mutagenesis, SPR-competition, MALDI-TOF-MS and LC-ESI-MS investigations. This material is available free of charge *via* the Internet at <http://pubs.acs.org>

### AUTHOR INFORMATION

#### Corresponding Author

\* Phone: +(49) 681 302 70300. E-mail: [rolf.hartmann@helmholtz-hzi.de](mailto:rolf.hartmann@helmholtz-hzi.de).

#### Author Contributions

The manuscript was written through contributions of all authors. / All authors have given approval to the final version of the manuscript. / ‡These authors contributed equally.

### ACKNOWLEDGMENT

The authors thank Carina Scheid for technical assistance, Patrick Fischer for his help performing the synthesis, Dr. K. Hollemeyer for MALDI-TOF investigations and Michael Hoffmann for LC-ESI-MS measurements. J.H. Sahner gratefully acknowledges a scholarship from the Stiftung der Deutschen Wirtschaft (SDW).

### ABBREVIATIONS

ACN, acetonitrile; ACoA, anthraniloyl coenzyme A; CHAPS, 3-[(3-Cholamidopropyl)dimethylammonio]-1-propanesulfonate hydrate; CMD, carboxymethyl

dextrane, cytidine triphosphate; EtOAc, ethylacetate; EtOH, ethanol; GTP, guanosine triphosphate; HAC, heavy atom count; HHQ, heptyl-4-hydroxy-quinoline; ITC, isothermal titration calorimetry; MeOH, methanol; MOE, Molecular Operating Environment; MOPS, **4-Morpholinepropanesulfonic acid**; NTA, nitrilotriacetic acid; NTP, nucleotide triphosphate; PDA, photodiode array; PQS, *Pseudomonas* quinolone signal; RNAP, RNA polymerase; RP, reversed phase; RU, response unit; SPR, surface plasmon resonance, STD, saturation transfer difference; UTP, uridine triphosphate

## REFERENCES

- (1) Wagner, G.; Hyberts, S. G.; Havel, T. F. NMR structure determination in solution: a critique and comparison with X-ray crystallography. *Annu. Rev. Biophys. Biomol. Struct.* **1992**, *21*, 167–198.
- (2) Davis, A. M.; Teague, S. J.; Kleywegt, G. J. Application and limitations of X-ray crystallographic Data in structure-based ligand and drug design. *Angew. Chem. Int. Ed.* **2003**, *42*, 2718–2736.
- (3) Boström, J. Reproducing the conformations of protein-bound ligands: a critical evaluation of several popular conformational searching tools. *J. Comp-Aided Mol. Des.* **2001**, *15*, 1137–1152.
- (4) Xiao, G.; Dézièl, E.; He, J.; Lépine, F.; Lesic, B.; Castonguay, M.-H.; Milot, S.; Tampakaki, A. P.; Stachel, S. E.; Rahme, L. G. MvfR, a key *Pseudomonas aeruginosa* pathogenicity LTTR-class regulatory protein, has dual ligands. *Mol. Microb.* **2006**, *62*, 1689–1699.
- (5) For a recent review see: Dubern, J.-F.; Diggle, S. P. Quorum sensing by 2-alkyl-4-quinolones in *Pseudomonas aeruginosa* and other bacterial species. *Mol. Biosyst.* **2008**, *4*, 882–888.
- (6) Bera, A.K.; Atanasova, V.; Robinson, H.; Eisenstein, E.; Coleman, J. P.; Pesci, E. C.; Parsons, J. F. Structure of PqsD, a *Pseudomonas* quinolone signal biosynthetic enzyme, in complex with anthranilate. *Biochemistry* **2009**, *48*, 8644–8655.
- (7) Storz, M. P.; Maurer, C. K.; Zimmer, C.; Wagner, N.; Brengel, C.; de Jong, J. C.; Lucas, S.; Müsken, M.; Häussler, S.; Steinbach, A.; Hartmann, R. W. Validation of PqsD as an anti-biofilm target in *Pseudomonas aeruginosa* by development of small-molecule inhibitors. *J. Am. Chem. Soc.* **2012**, *134*, 16143–16146.
- (8) Gomez, M. I.; Prince, A. Opportunistic infections in lung disease: *Pseudomonas* infections in cystic fibrosis. *Curr. Opin. Pharmacol.* **2007**, *7*:244–251.
- (9) Hakki, M.; Limaye, A. P.; Kim, H. W.; Kirby, K. A.; Corey, L.; Boeckh, M. Invasive *Pseudomonas aeruginosa* infections: high rate of recurrence and mortality after hematopoietic cell transplantation. *Bone Marrow Transpl.* **2007**, *39*, 687–693.
- (10) Asboe, D.; Gant, V.; Aucken, H. M.; Moore, D. A.; Umasankar, S.; Bingham, J. S.; Kaufmann, M. E.; Pitt, T. L. Persistence of *Pseudomonas aeruginosa* strains in respiratory infection in AIDS patients. *AIDS* **1998**, *12*, 1771–1775.



- (11) Pistorius, D.; Ullrich, A.; Lucas, S.; Hartmann, R. W.; Kazmaier, U.; Müller, R. Biosynthesis of 2-alkyl-4(1H)-quinolones in *Pseudomonas aeruginosa*: potential for therapeutic interference with pathogenicity. *ChemBioChem* **2011**, *12*, 850–853.
- (12) Sahner, J. H.; Groh, M.; Negri, M.; Hauptenthal, J.; Hartmann, R. W. Novel small molecule inhibitors targeting the “switch region” of bacterial RNAP: structure-based optimization of a virtual screening hit. *Eur. J. Med. Chem.* **2013**, *65*, 223–231.
- (13) Hentzer, M.; Givskov, M. Pharmacological inhibition of quorum sensing for treatment of chronic bacterial infections. *J. Clin. Invest.* **2003**, *112*, 1300–1307.
- (14) Storz, M. P.; Brengel, C.; Weidel, E.; Hoffmann, M.; Empting, M.; Steinbach, A.; Müller, R.; Hartmann, R. W. unpublished results.
- (15) O’Shea, R.; Moser, H.E. Physicochemical properties of antibacterial compounds: implications for drug discovery. *J. Med. Chem.* **2008**, *51*, 2871–2878.
- (16) Mayer, M.; Meyer, B. Characterization of ligand binding by saturation transfer difference NMR spectroscopy. *Angew. Chem. Int. Ed.* **1999**, *38*, 1784–1788.
- (17) Henise, J. C.; Taunton, J. Irreversible Nek2 kinase inhibitors with cellular activity. *J. Med. Chem.* **2011**, *54*, 4133–4146.
- (18) Copeland, R. A.; Pompliano, D. L.; Meek, T. D. Drug-target residence time and its implications for lead optimization. *Nat. Rev. Drug Discov.* **2006**, *5*, 730–739.
- (19) Hartmann, H.; Liebscher, J. A simple method for the synthesis of 5-aryl-3-amino-2-alkoxycarbonylthiophenes. *Synthesis* **1984**, 275–276.
- (20) Fabis, F.; Jolivet-Fouchet, S.; Robba, M.; Landelle, H.; Rault, S. Thiaisatoic anhydrides: efficient synthesis under microwave heating conditions and study of their reactivity. *Tetrahedron* **1998**, *54*, 10789–10800.
- (21) Foulon, L.; Braud, E.; Fabis, F.; Lancelot, J.C.; Rault, S. Synthesis and combinatorial approach of the reactivity of 6-and 7-arylthieno [3, 2-d][1, 3] oxazine-2, 4-diones. *Tetrahedron* **2003**, *59*, 10051–10057.
- (22) Le Foulon, F.X.; Braud, E.; Fabis, F.; Lancelot, J.C.; Rault, S. Solution-phase parallel synthesis of a 1140-member ureidothiophene carboxylic acid library. *J. Comb. Chem.* **2005**, *7*, 253–257.
- (23) Hauptenthal, J.; Hüsecken, K.; Negri, M.; Maurer, C.K.; Hartmann, R.W. Influence of DNA template choice on transcription and inhibition of *E. coli* RNA polymerase. *Antimicrob. Agents Ch.* **2012**, *56*, 4536–4539.
- (24) Molecular Operating Environment (MOE), 2010.10; Chemical Computing Group Inc., 1010 Sherbooke St. West, Suite #910, Montreal, QC, Canada, H3A 2R7, **2010**.
- (25) Trott, O.; Olson, A. J. AutoDock Vina: improving the speed and accuracy of docking with a new scoring function, efficient optimization, and multithreading. *J. Comput. Chem.* **2009**, *31*, 455–461.

**Supporting Information: Appendix 7.1 D**

**E Structure Optimization of 2-Benzamidobenzoic Acids as PqsD Inhibitors for Pseudomonas aeruginosa Infections and Elucidation of Binding Mode by SPR, STD NMR, and Molecular Docking**

Elisabeth Weidel\*, Johannes C. de Jong\*, Christian Brengel, Michael P. Storz, Andrea Braunshausen, Matthias Negri, Alberto Plaza, Anke Steinbach, Rolf Müller, and Rolf W. Hartmann

\*These authors contributed equally

Reprinted with permission from *J. Med Chem.* **2013**, 56(15), 6146-6155.

Copyright (2013) American Chemical Society.

DOI: 10.1021/jm4006302

## ABSTRACT

*Pseudomonas aeruginosa* employs a characteristic *pqs* quorum sensing (QS) system that functions via the signal molecules PQS and its precursor HHQ. They control the production of a number of virulence factors and biofilm formation. Recently, we have shown that sulfonamide substituted 2-benzamidobenzoic acids, which are known FabH inhibitors, are also able to inhibit PqsD, the enzyme catalyzing the last and key step in the biosynthesis of HHQ. Here, we describe the further optimization and characterization of this class of compounds as PqsD inhibitors. Structural modifications showed that both the carboxylic acid *ortho* to the amide and 3'-sulfonamide are essential for binding. Introduction of substituents in the anthranilic part of the molecule resulted in compounds with IC<sub>50</sub> values in the low micromolar range. Binding mode investigations by SPR with wild-type and mutated PqsD revealed that this compound class does not bind into the active center of PqsD, but in the ACoA channel preventing the substrate from accessing the active site. This binding mode was further confirmed by docking studies and STD NMR.

## INTRODUCTION

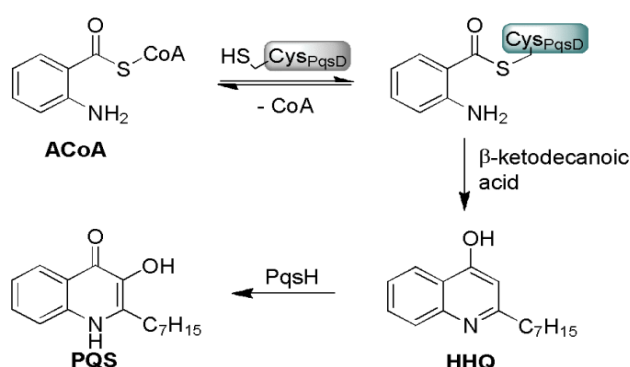
The Gram-negative bacterium *Pseudomonas aeruginosa* is an opportunistic pathogen that is commonly associated with hospital-acquired life-threatening infections. Especially patients with severe burns and immunocompromised individuals,<sup>1</sup> like those undergoing chemotherapy or having HIV/AIDS<sup>2</sup> are highly susceptible to infections with *P. aeruginosa*. A wide variety of infection sites can be observed, such as ocular, ear, urinary tract, bloodstream, skin and soft tissue infections, and hospital-acquired pneumonia. Furthermore it is the dominant cause of chronic lung infections in the majority of people with cystic fibrosis (CF).<sup>3-5</sup> Due to the high intrinsic resistance of *P. aeruginosa* to many antimicrobial agents, antimicrobial therapy is challenging. The resistance arises from the combination of low outer membrane permeability and resistance mechanisms such as efficient multidrug efflux pumps and  $\beta$ -lactamases.<sup>6</sup> Treatment is further hampered when the bacterium is growing in biofilms.<sup>7,8</sup> As a consequence infections caused by bacterial biofilms are generally chronic and very difficult to eradicate.<sup>9</sup> Due to the rising levels of resistance to conventional antibiotics, there is an urgent need for new therapeutic options.

The production of several virulence factors as well as biofilm formation<sup>10,11</sup> is coordinated by a cell density dependent mechanism termed quorum sensing (QS) using a number of QS signal molecules.<sup>12,13</sup> This mechanism of communication enables bacteria to coordinate the regulation of gene expression with subsequent effects on metabolism, protein synthesis and virulence.<sup>14</sup> Three different QS systems are known for *P. aeruginosa*. The *las*<sup>15,16</sup> and *rhl*<sup>17,18</sup> systems use 3-oxo-C12-HSL (*N*-(3-oxododecanoyl) homoserine lactone) and C4-HSL (*N*-butyryl homoserine lactone), respectively, as

signal molecules, whereas the *pqs* system utilizes the 2-heptyl-3-hydroxy-4(1*H*)-quinolone, called *Pseudomonas* Quinolone Signal (PQS) and its immediate precursor 2-heptyl-4-quinolone (HHQ).<sup>19, 20</sup> Both PQS and HHQ bind to the transcriptional regulator PqsR, the receptor of the *pqs* system. Among other factors, this system is involved in the regulation of multiple virulence determinants<sup>21, 22</sup> such as elastase, rhamnolipids and pyocyanin and also influences biofilm formation.<sup>23, 24</sup> Therefore PqsD is considered as an attractive therapeutic target for drug development and treatment of *P. aeruginosa* infections. It is believed that disrupting the cell-to-cell communication instead of killing the bacteria will result in less selective pressure than with conventional antibacterial agents such as antibiotics<sup>25</sup> and thus will circumvent the problem of resistance.

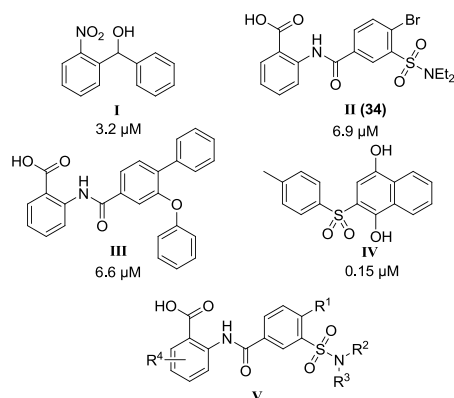
Using a ligand-based approach we developed the first highly potent competitive PqsR antagonists, which were able to reduce the production of the virulence factor pyocyanin.<sup>26, 27</sup> As HHQ and PQS activate PqsR, inhibition of their synthesis should lead to a decrease of virulence factor production without interfering with bacterial growth.<sup>28, 29</sup> PqsD is an essential enzyme in the biosynthesis of HHQ and PQS as it catalyzes the last step in HHQ formation, the condensation of anthraniloyl-CoA (ACoA) with  $\beta$ -ketodecanoic acid (Scheme 1).<sup>30</sup>

**Scheme 1.** Biosynthesis of signal molecules HHQ and PQS



Recently we have shown for the first time that inhibition of PqsD with a small molecule (compound **I**, Scheme 2) leads to a strong reduction of extracellular HHQ and PQS levels and a significant reduction of biofilm volume.<sup>31</sup> Structurally, PqsD most closely resembles  $\beta$ -ketoacyl-ACP synthase (FabH) having the same catalytic triad consisting of Cys112, His257 and Asn287. Therefore, we postulated that inhibitors of FabH might also act as PqsD inhibitors. For three FabH inhibitors (compound **II**, **III** and **IV**, Scheme 2)<sup>30, 32, 33</sup>, two of them were anthranilic acid derived, we could demonstrate that they indeed inhibit PqsD.

**Scheme 2.** Structures of the PqsD inhibitor **I** and the FabH inhibitors **II**, **III** and **IV** as well as the according PqsD IC<sub>50</sub> values. **V** represents the general structure of synthesized compounds.

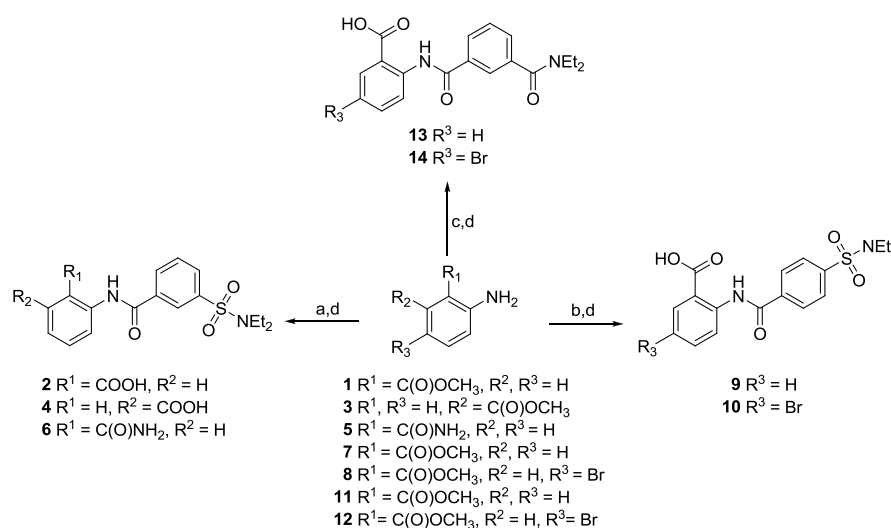


In the current work, we report about the optimization of compound **II** for which a series of 3-sulfonamide substituted benzamidobenzoic acids (general structure **V**) were synthesized. The binding mode of the potent inhibitors was investigated using surface plasmon resonance spectroscopy (SPR), molecular docking studies and saturation transfer difference nuclear magnetic resonance (STD NMR).

## RESULTS AND DISCUSSION

**Chemistry** Reaction of amines **1**, **3**, **7-8** and **11-12** with the appropriate acid chloride afforded the amides **2a**, **4a**, **9a-10a** and **13a-14a** (see SI). Subsequent basic hydrolysis of the carboxylic ester groups yielded the corresponding acids **2**, **4**, **9-10** and **13-14**. Carboxamide **6** was prepared from 2-aminobenzamide (**5**) and 3-(*N,N*-diethylsulfamoyl)benzoyl chloride (Scheme 3).

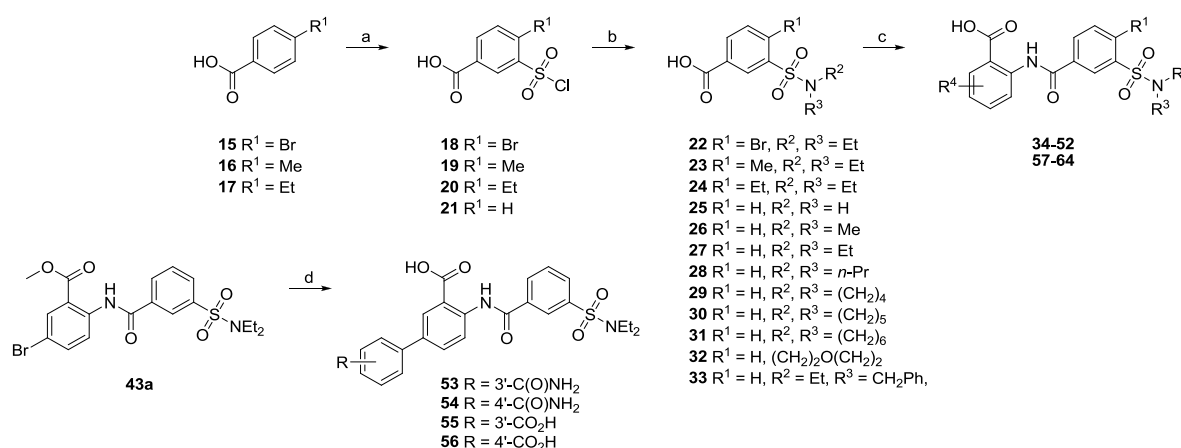
Scheme 3. Reaction of benzoyl chlorides with methyl aminobenzoates and 2-aminobenzamide<sup>a</sup>



<sup>a</sup>Reagents and conditions: (a) 3-(*N,N*-diethylsulfamoyl)benzoyl chloride **1**, **3**:  $K_2CO_3$ , *N*-methylimidazole, TMEDA,  $CH_3CN$ ; **5**: toluene; (b) 4-(*N,N*-diethylsulfamoyl)benzoyl chloride;  $K_2CO_3$ , *N*-methylimidazole, TMEDA,  $CH_3CN$ ; (c) 3-(diethylcarbamoyl)benzoyl chloride,  $K_2CO_3$ , *N*-methylimidazole, TMEDA,  $CH_3CN$ ; (d) 1N NaOH (aq.), MeOH, THF (not **5**).

As outlined in Scheme 4 the synthesis of 3-sulfamoylbenzoic acids 22-33 started from *para*-substituted benzoic acids 15-17, which were converted into 3-(chlorosulfonyl)benzoic acids 18-20 by reaction with chlorosulfonic acid at 100 °C in 82-88% yield.

Scheme 4. Synthesis of 3'-sulfonamide substituted benzamidobenzoic acids and their intermediates<sup>a</sup>



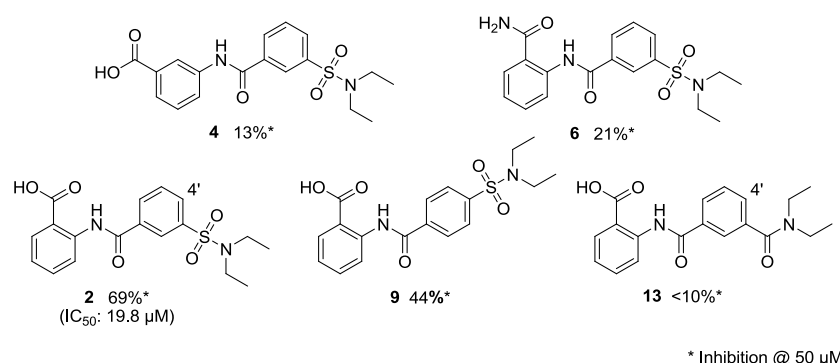
<sup>a</sup>Reagents and conditions: (a) ClSO<sub>3</sub>H, 100 °C, overnight; (b) HNR<sup>2</sup>R<sup>3</sup>, CH<sub>2</sub>Cl<sub>2</sub>; (c) (i) SOCl<sub>2</sub>, DMF (cat.), CH<sub>2</sub>Cl<sub>2</sub>, overnight or SOCl<sub>2</sub>, DMF (cat.), toluene, 80 °C, 4h; (ii) methyl anthranilate; (iii) 1N NaOH (aq.), MeOH, THF, rt; (d) phenylboronic acid, cesium carbonate, DME/water 1/1, 100 °C, 3.5 h.

Compound **21** was commercially available. The sulfonyl chlorides **18-21** were then reacted with ammonia or a secondary amine to afford 3-sulfamoylbenzoic acids **22-33**. Reaction of the carboxylic acids with thionyl chloride, either in dichloromethane at room temperature or in toluene at 80 °C gave the corresponding acid chlorides, which were reacted under standard conditions with the methyl ester of anthranilic acids. The resulting compounds **34a-52a** and **57a-64a** (see SI) were hydrolyzed with a mixture of 1N NaOH (aq.), MeOH and THF, yielding the corresponding 2-(3'-(sulfamoyl)benzamido) benzoic acids **34-52** and **57-64**. Phenyl substituted compounds **53-56** were obtained in 60-76% yield by means of a Suzuki reaction of methyl 5-bromo-2-(3-(*N,N*-diethylsulfamoyl) benzamido) benzoate (**43a**) with phenylboronic acids. Under the reaction conditions used, the intermediate methyl esters were already hydrolyzed to the desired carboxylic acids.

**PqsD inhibition** In order to investigate the importance of the carboxylic acid and the sulfonamide moiety of the 3'-sulfonamide substituted benzamidobenzoic acids (general structure **V**) 2-(3'-(*N,N*-diethylsulfamoyl)benzamido)benzoic acid (**2**) and two regioisomers (**4** and **9**) were synthesized.

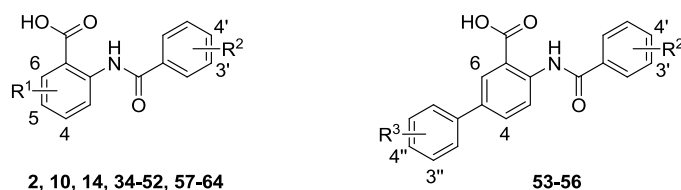
Furthermore, the carboxylic acid and sulfonamide were replaced by a carboxamide (**6** and **13**, Scheme 5).

Scheme 5. Influence of sulfonamide and benzoic acid modifications on PqsD inhibition.



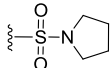
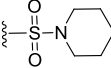
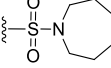
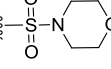
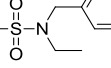
Compound **2** lacking the Br substituent showed reduced activity compared to **34** ( $IC_{50} = 19.8$  vs  $6.9$  μM). The carboxylic acid *ortho* to the NH turned out to be essential for activity. Changing the position of the carboxylic acid to the *meta* position (**4**) as well as replacement with a carboxamide (**6**) led to a dramatic loss in activity. Shifting the *N,N*-diethylsulfamoyl group from 3'-position to 4'-position<sup>34</sup> (**9**) also resulted in reduced activity, whereas replacement with an *N,N*-diethylcarboxamide (**13**) gave an inactive compound. As the structure of compound **2**, having a carboxylic group next to the amide and with the sulfonamide in 3'-position, seemed to be optimal, we turned our attention to the introduction of additional substituents on both aromatic rings (Table 1).

**Table 1.** PqsD inhibition by compounds **10**, **14** and 2-(3'-sulfamoyl)benzamido)benzoic acids **2** and **34-64**.



Compd	R <sup>1</sup>	R <sup>2</sup>	R <sup>3</sup>	IC <sub>50</sub> (μM)
2	H	3'-SO <sub>2</sub> NEt <sub>2</sub>		19.8 ± 4.5
34	H	4'-Br, 3'-SO <sub>2</sub> NEt <sub>2</sub>		6.9 ± 0.8
35	H	4'-Me, 3'-SO <sub>2</sub> NEt <sub>2</sub>		27.3 ± 1.9
36	H	4'-Et, 3'-SO <sub>2</sub> NEt <sub>2</sub>		39%*
37	4-Cl	3'-SO <sub>2</sub> NEt <sub>2</sub>		9.4 ± 1.3
38	4-F	3'-SO <sub>2</sub> NEt <sub>2</sub>		8.0 ± 1.2
39	4-NO <sub>2</sub>	3'-SO <sub>2</sub> NEt <sub>2</sub>		6.3 ± 1.1
40	5-Me	3'-SO <sub>2</sub> NEt <sub>2</sub>		18.4 ± 3.2



41	5-CF <sub>3</sub>	3'-SO <sub>2</sub> NEt <sub>2</sub>		12.4 ± 3.0
42	5-F	3'-SO <sub>2</sub> NEt <sub>2</sub>		11.4 ± 1.9
43	5-Br	3'-SO <sub>2</sub> NEt <sub>2</sub>		9.9 ± 2.1
44	5-CN	3'-SO <sub>2</sub> NEt <sub>2</sub>		26.2 ± 10.4
45	5-NO <sub>2</sub>	3'-SO <sub>2</sub> NEt <sub>2</sub>		8.9 ± 1.8
10	5-Br	4'-SO <sub>2</sub> NEt <sub>2</sub>		13.0 ± 1.8
14	5-Br	3'-C(O)NEt <sub>2</sub>		25.5 ± 5.5
46	5-F	4'-Br, 3'-SO <sub>2</sub> NEt <sub>2</sub>		6.6 ± 0.1
47	5-Br	4'-Br, 3'-SO <sub>2</sub> NEt <sub>2</sub>		3.8 ± 1.0
48	5-Ph	3'-SO <sub>2</sub> NEt <sub>2</sub>		3.0 ± 0.7
49	6-OMe	3'-SO <sub>2</sub> NEt <sub>2</sub>		44 %*
50	6-Cl	3'-SO <sub>2</sub> NEt <sub>2</sub>		39.0 ± 1.9
51	6-F	3'-SO <sub>2</sub> NEt <sub>2</sub>		24.9 ± 4.0
52	6-OH	3'-SO <sub>2</sub> NEt <sub>2</sub>		1.2 ± 0.1
53		3'-SO <sub>2</sub> NEt <sub>2</sub>	3''-C(O)NH <sub>2</sub> -	3.8 ± 0.4
54		3'-SO <sub>2</sub> NEt <sub>2</sub>	4''-C(O)NH <sub>2</sub>	1.9 ± 0.1
55		3'-SO <sub>2</sub> NEt <sub>2</sub>	3''-CO <sub>2</sub> H	1.5 ± 0.3
56		3'-SO <sub>2</sub> NEt <sub>2</sub>	4''-CO <sub>2</sub> H	2.7 ± 0.3
57	H	3'-SO <sub>2</sub> NH <sub>2</sub>		43.6 ± 1.3
58	H	3'-SO <sub>2</sub> NMe <sub>2</sub>		35%*
59	H	3'-SO <sub>2</sub> N( <i>n</i> -Pr) <sub>2</sub>		5.4 ± 1.0
60	H			47%*
61	H			14.4 ± 2.4
62	H			14.8 ± 2.4
63	H			16%*
64	H			16.5 ± 3.8

Data shown are mean ± SD, n = 3. \* Inhibition at 50 μM

### Binding mode characterization

**SPR measurements** In order to gain some insight into the binding mode of the potent inhibitors SPR experiments were performed. At first compounds **43** and **48** were tested in absence of ACoA and strong interactions with PqsD were observed (Figure 1A). In a second experiment the PqsD loaded sensor chip was first treated with ACoA. Nucleophilic attack of Cys112 to the thioester of ACoA and subsequent elimination of CoA is known to result in an anthranilate-PqsD complex,<sup>36</sup> in which the catalytic center is occupied by the covalent bound anthranilate. Subsequent injection of compounds **43** and **48** resulted in Figure 1B showing comparable signals for the ACoA-treated and the -untreated PqsD. This indicates that the compounds do not occupy the catalytic site of PqsD. These results are in contrast to what was observed for the sulfone (**IV**) (Figure 1C and 1D). Performing the experiment in the same way no signal for **IV** was observed when injected after preincubation with ACoA, indicating that this compound is competing with anthranilate for the same binding site.

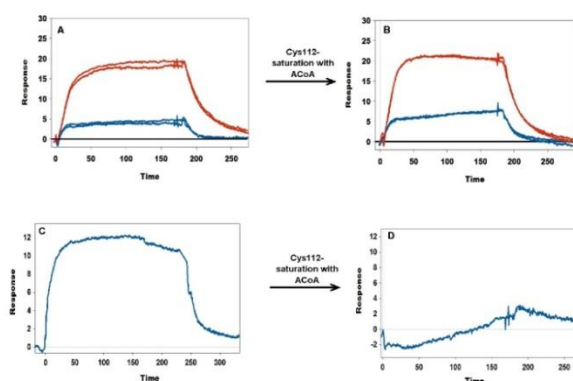


**Figure 1.** SPR binding studies of compounds **43**, **48** and **IV**. A) Binding of **43** (blue) and **48** (red) to PqsD. B) Binding of **43** (blue) and **48** (red) after pretreatment of the chip with ACoA, which results in a covalent anthranilate-Cys112-PqsD complex with part of the active site being blocked. C-D) Same experiments performed with **IV**.

This also means that the two inhibitor classes have different modes of action: compound **IV** is competing with the catalytic triad, whereas the anthranilic acid derivatives are “channel blockers”. Another SPR experiment was performed inverting the compound order. PqsD was preincubated with **48** and ACoA was injected subsequently. The finding that in contrast to the untreated surface no binding of ACoA to PqsD was observed indicates that **48** blocks the ACoA channel and prevents ACoA from reaching its binding site.

Further support for this mode of action comes from our screening assay. In the standard procedure purified PqsD is first incubated with test compound. After 10 minutes ACoA and  $\beta$ -ketodecanoic acid are added and the enzyme activity is monitored by measuring the amount of HHQ being formed during 40 minutes reaction time. In a modified assay procedure, a 30 min preincubated enzyme / ACoA mixture is first added to the test compound. After 10 minutes, the reaction is started by addition

of  $\beta$ -ketodecanoic acid and the enzyme activity is monitored as mentioned before. In contrast to experiments with compound **IV**, very similar  $IC_{50}$  values were observed in both settings, indicating that the benzamidobenzoic acids do not compete in the active site of PqsD with the covalently bound anthranilate (Table 2).

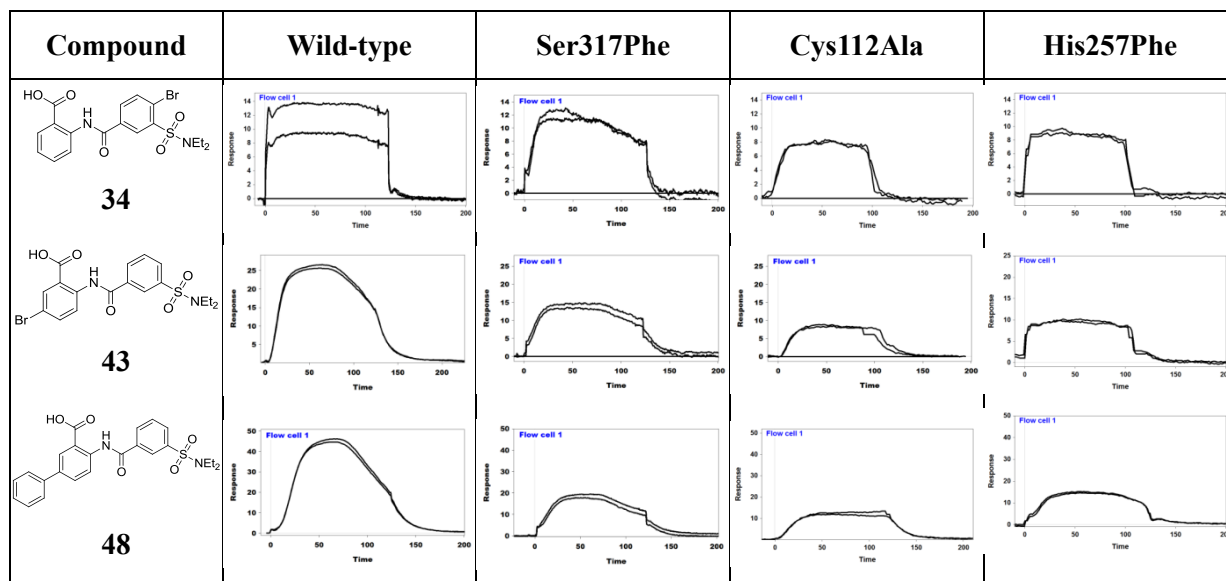
**Table 2.** Comparison of  $IC_{50}$  values obtained with standard procedure (SP) and modified procedure (MP).

Compd	$IC_{50}$ [ $\mu$ M] SP	$IC_{50}$ [ $\mu$ M] MP
<b>IV</b>	$0.15 \pm 0.1$	$1.1 \pm 0.1$
<b>2</b>	$19.8 \pm 4.5$	$19.4 \pm 0.8$
<b>43</b>	$9.9 \pm 2.1$	$7.0 \pm 0.4$
<b>48</b>	$3.0 \pm 0.7$	$4.2 \pm 0.3$
<b>52</b>	$1.2 \pm 0.1$	$1.1 \pm 0.2$
<b>55</b>	$1.5 \pm 0.3$	$1.6 \pm 0.1$
<b>56</b>	$2.7 \pm 0.3$	$2.0 \pm 0.2$
<b>64</b>	$16.5 \pm 3.8$	$12.9 \pm 0.1$

Data shown are mean  $\pm$  SD, n = 3.

For further binding mode investigation, additional SPR experiments were performed with compounds **34**, **43** and **48** differing in the size of the substituents in position 5 of the anthranilate. To investigate how deep they reach into the channel the compounds were tested on wild-type and on three PqsD mutants in which active site residues were exchanged (Ser317Phe, Cys112Ala and His257Phe). Notably, different binding behaviors were observed. For compound **34** no differences in binding signals were seen, indicating that the binding is not influenced by the amino acid exchanges. Increasing the size of the substituent (H to Br, **43**) resulted in slightly decreased binding signals compared to wild-type PqsD. This observation is more pronounced for compound **48**, where the additional phenyl ring leads to strongly reduced binding signals (Table 3).

**Table 3.** SPR based binding studies with wild-type and mutated PqsD (Ser317Phe, Cys112Ala, and His257Phe), for compounds **34**, **43** and **48** (n=2).



These results suggest that bulky substituents on the anthranilate are likely to reach the active center potentially interacting with Ser317, Cys112 and His257. The decreased binding signals observed in the mutants might either be due to missing interactions caused by amino acid replacement or due to conformational changes in the active site. The fact that the three investigated compounds are differently influenced by the amino acid exchanges is very likely to be caused by the size of the substituents the more bulky ones reaching deeper into the catalytic center.

**Docking studies** In order to rationalize the SPR experiments and to establish a basis to explain the SAR of the PqsD inhibitors molecular docking studies were performed with selected compounds. For compound **2** three main binding clusters were found all localized within the ACoA channel (Figure 2 and S1). In binding mode I (Figure 2I) **2** is placed deep into the channel: it is stabilized by hydrogen bonds to Cys112 (carboxylic acid) and Arg262 (sulfonamide oxygens), CH- $\pi$  interactions to Leu193 (anthranilic ring) and Asn260 (*N,N*-diethylsulfonamidebenzene moiety), and hydrophobic interactions with further amino acids. In binding mode II (Figure 2II) the inhibitor is placed more central in the channel: hydrogen bonds are formed to Asn287 (carboxylic acid) and Arg36/Arg223 (sulfonamide oxygens),  $\pi$ -stackings to Pro259/Met225 (anthranilic ring) and Met220 and Arg262 (sulfonamidebenzene), and additional hydrophobic interactions. In mode III (Figure 2III) **2** is rotated 180 degrees placing the anthranilic ring at the channel entrance: the carboxylic acid binds to Arg262 and Arg36, while CH- $\pi$  interactions with Thr37, Pro259 and Ile263 stabilize the aromatic scaffold. The *N,N*-diethyl group is buried into to the catalytic center forming hydrophobic interactions

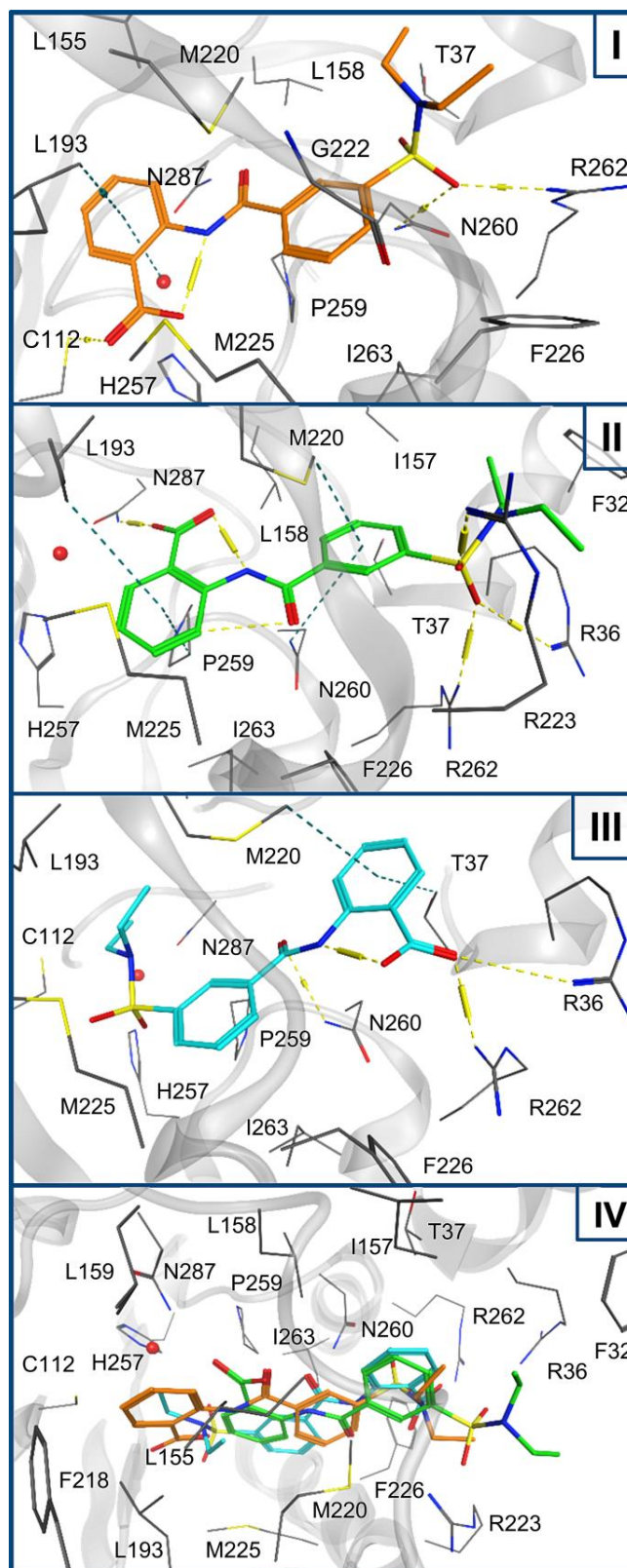


**Figure 2.** Three main binding modes I, II and III of compound **2** in the ACoA channel of PqsD and (IV) superimposition of the three main binding modes of compound **2** shown as orange (binding mode I), green (binding mode II) and cyan (binding mode III) sticks. The main interacting amino acids are shown as lines and key interactions are highlighted as dotted lines (polar in yellow, hydrophobic in dark cyan).

In the most common pose of compound **48** the phenyl ring in position 5 is sandwiched between Met225 and Pro259, as seen for the anthranilic ring of compound **2** in binding mode II. The rest of the molecule is slightly pushed outwards (Figure 3 and S1) with the anthranilate forming hydrogen bonds to Arg262, Asn154 or Asn260. In contrast to compound **2** no hydrogen bonds are found to the sulfonamide oxygens.  $\pi$ -Stacking with Phe226 (anthranilic ring) and Phe32 (diethyl-sulfonamide-benzene) and hydrophobic interactions (Figure S1) further stabilize the inhibitor.

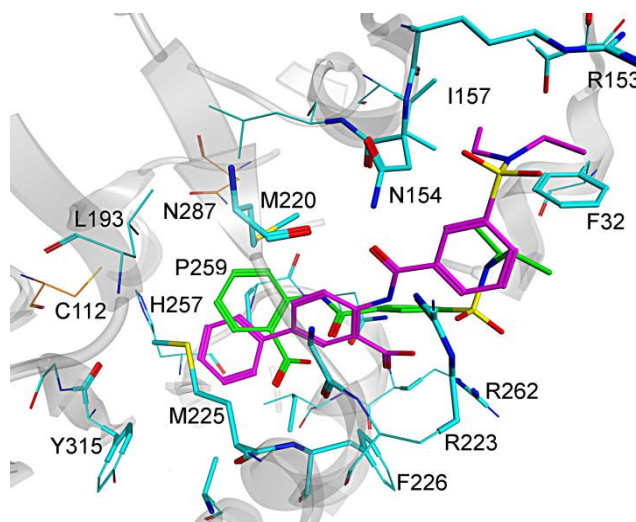


**Figure 3.** Docking pose of compound **2** (binding mode II; green) and **48** (magenta).

For compound **48** a dissociation constant ( $K_D$ ) of 5.2  $\mu\text{M}$  was determined by ITC (Figure 4). An explanation for these results could be that the main interactions for this compound are hydrophobic. The low value of enthalpy could be due to a desolvation penalty ( $\Delta G = -7.2$  kcal/mol,  $\Delta H = -2.3$  kcal/mol,  $-T\Delta S = -5.0$  kcal/mol). In two of the PqsD structures (3H76 and 3H78) a water molecule is present bridging to the catalytic residues Cys112, His257 and Asn287. When this water molecule was included in the docking process as part of the protein compound **52** was found deeper in the channel. The OH group forms an intramolecular hydrogen bond to the carboxylic acid (maintaining its planarity), which binds to Asn287, but also interacts via the structural water molecule with Cys112 and His257 (Figure S2). This would explain the strong increase in activity and is further supported by the fact that for the methoxy derivative less than 50% inhibition at 50  $\mu\text{M}$  is observed.

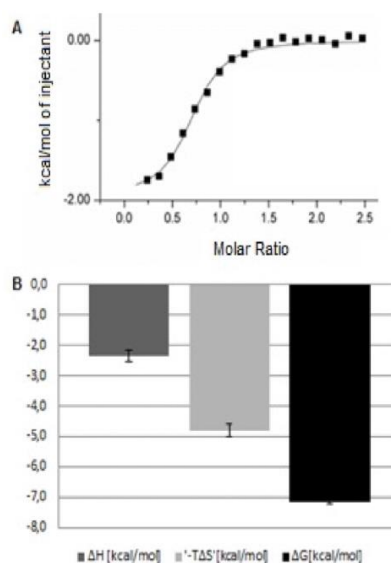


**Figure 4.** ITC experiments with compound **48** and wild-type PqsD. A: Integrated heats (black squares) plotted against the molar ratio of the reactants. B: Thermodynamic profile of **48**. Data shown are mean  $\pm$  SD,  $n = 3$ .

**STD NMR studies** To identify the orientation and mode of binding to PqsD, we recorded Saturation Transfer Difference (STD) NMR<sup>37</sup> spectra of **2**, **48**, **52**, and **64** in the presence of PqsD (Figure 5 and S4-S7). STD NMR is a powerful technique that allows the precise definition of binding epitopes on small molecule ligands. Samples contained an 80-fold excess of the compounds relative to PqsD with respective concentrations of 0.8 mM and 10  $\mu$ M were recorded at 298 K. As seen in Figure 5 for compound **2**, normalization of the signal of greatest intensity (H-6) in the difference spectrum (red) to the one of the reference spectrum (black) showed signals for the anthranilate protons H-5 (95%), H-4 (86%), and H-3 (81%) to display the strongest enhancements. Signals for the benzene protons H-2' and H-4', H-5', and H-6' showed enhancements of  $\sim$ 70% while significantly reduced enhancements were observed for the methylene (42%) and methyl protons (39%, Figure S4). These results indicate that the protons of the anthranilic acid ring of **2** are in closer contact to the protein.

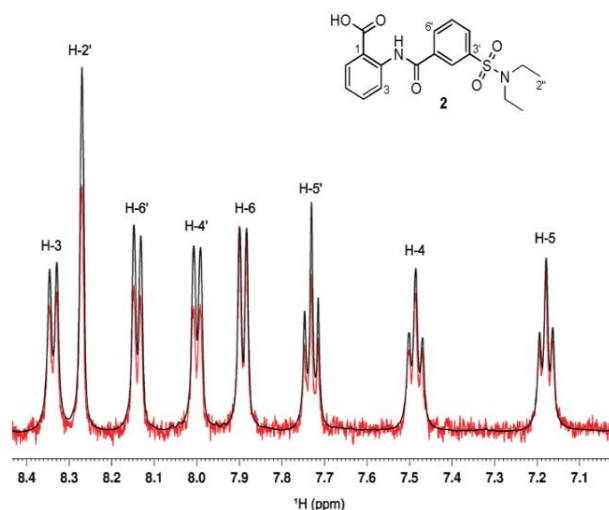


**Figure 5.** Reference (black) and STD NMR difference (red) spectra of **2** in complex with PqsD. Samples contained an 80-fold excess of the compounds relative to PqsD with respective concentrations of 0.8 mM and 10  $\mu$ M were recorded at 298 K. Overlaid spectra were normalized to the signal for H-6 ( $\delta$  7.90), which gave the strongest enhancement.

Similar epitope binding profiles were observed for **52** where once again the anthranilate protons showed the strongest enhancements (Figure S5). The STD NMR spectrum of **64** in presence of PqsD (Figure S6) displayed the strongest enhancements for anthranilate protons H-6 (100%), H-4 (99%), and H-3 (90%), for benzene proton H-5' (93%), and for the N-benzylic proton H-4'''(90%). It is worthwhile to note that enhancements of 87 and 80% were observed for methylene protons H-1'' and methyl protons H-2'', respectively. The spectra of **2**, **52** and **64** revealed a similar binding mode for all compounds, which is independent of the substitution on the anthranilic acid ring or on the sulfonamide moiety. Low signal to noise ratio and spectral overlap did not allow to integrate individual peaks corresponding to the benzene protons of **48** in the STD NMR spectrum (Figure S7). However, it was clear that the benzene protons together with the methylene protons showed the highest intensities.

The results of SPR, STD NMR and docking as presented are consistent with binding mode II, where the methylene protons are within van der Waals contact distances (2,5- 3,5 Å) to Pro259 and Met225. In particular, the SPR experiment with ACoA injection after pretreatment with inhibitor clearly speaks in favor of a channel-blocking mechanism for these inhibitors. Further, NMR results exclude binding mode III, where the anthranilic ring is almost exposed at the entrance of the ACoA channel (no correspondence between the intense signals and close enough residues), and disfavor binding mode I, where the methyl groups are predicted to be in closer contact to the protein.



## SAR Discussion

From binding mode II of **2** it becomes apparent that an important interaction partner is the carboxylic acid group in *ortho* position to the NH, which forms hydrogen bonds with Asn 287. Shifting to *meta* position (**4**) as well derivatization to carboxamide (**6**) strongly reduces activity (Scheme 5), as this interaction can no longer be sustained. Also of high importance is the 3-position of the *N,N*-diethylsulfamoyl group to perfectly fit into the channel, and which must not be exchanged by *N,N*-diethylcarboxamide as only the sulfur oxygens can establish hydrogen bonds with Arg 36 and Arg 223 (compounds **9** and **13**, respectively, Scheme 5).

The finding that the sulfonamides lacking the diethyl residues (**57**- **64**) exhibit weak or no inhibition can be explained by the strong interactions between the methylene and methyl protons with the protons of the protein as shown in the NMR experiments. Introduction of substituents in **2** resulted in different effects which are in accordance with the proposed binding mode II. An example is the Br substitution *ortho* to the sulfonamide group, which showed improved binding (**34**, **46** - **47**) compared to the unsubstituted parent compounds. In binding mode II the benzene ring is oriented in a way in which the Br can build orthogonal halogen bonds with amino acids of the protein backbone for example with Arg36 and Thr37 (Figure S8). A reduced activity depending on the size of the substituents is observed when they were introduced into the 6-position of the anthranilic acid ring (**49** - **51**). This is possibly due to a steric interference with the carboxylic acid group, which in turn can no longer optimally interact with Asn287. **52** is an exception, where introduction of OH in 6-position leads to a high inhibitory activity. As shown above, a plausible reason for this could be the ability of the OH group to build a hydrogen bond network with the carboxylic acid group and the amino acid residues of the active site (ITC and docking results). The introduction of small substituents in 4 and 5 position of the anthranilic acid ring leads to increased PqsD inhibition (**37** - **47**). As shown in the SPR experiments with mutated PqsD, the docking results and NMR experiments the anthranilic acid ring is oriented towards the active center, whereby substituents at positions 4 and 5 reach deeper into the channel and thus can form additional interactions. This effect is more pronounced for **48**, where a phenyl ring is attached in 5-position, leading to a slight shift in the binding mode compared to compound **2** (see above). Obviously, the gain in binding activity by the phenyl ring sandwiched between Met225 and Pro259 is higher than the loss of binding activity due to the missing interactions of the sulfonamide ethyl groups. The introduction of an amide or carboxylic acid group in *meta* or *para*-position (**53**-**56**) to address Asn 287 and His257 however, led only to slightly improved inhibition compared to the parent compound **48**.

## CONCLUSION

In summary, we synthesized a series of sulfonamide substituted 2-benzamidobenzoic acids which inhibit PqsD in the low  $\mu\text{M}$  range. The carboxylic acid was essential for activity. Systematic variation of substituents in 4- and 5-position of the 2-aminobenzoic acid part of the scaffold resulted in the most potent PqsD inhibitors. Activity was reduced significantly when substituents were introduced in 6-position. However, introduction of a hydroxyl group in this position resulted in a compound with increased potency ( $\text{IC}_{50} = 1.2 \mu\text{M}$ ). SPR, ITC, modeling, and NMR experiments suggest these inhibitors to bind within the ACoA channel of PqsD, thereby acting as entropy-driven channel-blockers that prevent ACoA from reaching the catalytic site. Further biological evaluation of our compounds is under investigation.

## EXPERIMENTAL SECTION

**Chemical Synthesis.** *General Methods.* Chemicals were purchased from commercial sources and used without further purification.  $^1\text{H}$  NMR spectra were recorded on a Bruker DRX-500 (500 MHz) and a Bruker Fourier 300 (300 MHz) spectrometer. Chemical shifts are given in parts per million (ppm) with the solvent resonance as internal standard. Data are reported as follows; chemical shift, multiplicity (s = singlet, d = doublet, t = triplet, q = quartet, m = multiplet, bs = broad signal or as a combination of these, e.g. dd, dt, etc.), coupling constants (Hz) and integration.  $^{13}\text{C}$  NMR spectra were recorded on a Bruker DRX-500 (125 MHz) with complete proton decoupling. Chemical shifts are given in parts per million (ppm) with the solvent resonance as internal standard. Mass spectrometry (HPLC/MS) was performed on a MSQ<sup>®</sup> electro spray mass spectrometer (Thermo Fisher). The system was operated by the standard software Xcalibur<sup>®</sup>. A RP C18 NUCLEODUR<sup>®</sup> 100-5 (125  $\times$  3 mm) column (Macherey - Nagel GmbH) was used as stationary phase. The mobile phase was a mixture of  $\text{CH}_3\text{CN}$  (0.1% TFA) and  $\text{H}_2\text{O}$  (0.1% TFA). All solvents were HPLC grade. Flash chromatography was performed on silica gel 60, 70-230 mesh (Fluka) and the reaction progress was determined by thin-layer chromatography (TLC) analyses on silica gel 60, F<sub>254</sub> (Merck). Visualization was accomplished with UV light and staining with basic potassium permanganate ( $\text{KMnO}_4$ ). Melting points were determined in open capillaries using a SMP3 melting point apparatus of Bibby Sterilin Ltd with a gradient of 2  $^\circ\text{C}/\text{min}$ . The reported yields are the actual isolated yields of purified material, unless stated otherwise, and are not optimized. Purities of all test compounds used in the biological assays were determined by HPLC/MS using the area percentage method on the UV trace recorded at a wave length of 254 nm. All compounds were found to have  $\geq 95\%$  purity. Yields and characterization of all compounds are provided in the Supporting Information.

*General Procedure A for the Preparation of 3-Sulfamoylbenzoic Acids.* At 0  $^\circ\text{C}$  the amine (30.0 mmol) was added to a stirred solution of 3-(chlorosulfonyl)benzoic acid (2.21 g, 10.0 mmol) in dichloromethane (25 mL). After stirring overnight at room temperature 1N HCl (aq., 25 mL) was

added. The organic solvent was removed by evaporation under reduced pressure. The solid was isolated by suction filtration, washed thoroughly with water and dried under reduced pressure at 50 °C. *General Procedure B for the Preparation of 3-Sulfamoylbenzoyl Chlorides.* Thionyl chloride (2.9 mL, 40.0 mmol) was added slowly to a stirred solution of 3-sulfamoylbenzoic acid (4.00 mmol) in dichloromethane (25 mL) followed by 1-2 drops of DMF. After stirring overnight at room temperature the solution was evaporated under reduced pressure. The crude 3-sulfamoylbenzoyl chloride was used without further purification.

*General Procedures C for the Preparation of 2-Benzamidobenzoic Acid Methyl Esters. Procedure C1.* 3-(*N,N*-Diethylsulfamoyl)benzoyl chloride (1.00 mmol) was added to a stirred solution of anthranilic acid methyl ester (1.00 mmol) in pyridine (4 mL). After stirring overnight the solvent was removed by evaporation under reduced pressure. The residue was stirred with 1N HCl (aq., 4 mL). The solid was isolated by suction filtration, washed with water and heated briefly with a small amount of methanol. After cooling to room temperature the product was isolated by suction filtration, washed with some methanol and dried under reduced pressure at 50 °C.

*Procedure C2.* 3-(*N,N*-Diethylsulfamoyl)benzoyl chloride (1.50 mmol) was added to a stirred suspension of anthranilic acid methyl ester (1.00 mmol), potassium carbonate (207 mg, 1.50 mmol) *N*-methylimidazole (8 mg, 0.10 mmol) and *N,N,N',N'*-tetramethylethylenediamine (12 mg, 0.10 mmol) in acetonitrile (1 mL). After stirring for 2.5 h at room temperature 1N HCl (aq.) was added. The solid was isolated by suction filtration, washed thoroughly with water and heated briefly with a small amount of methanol (2 mL). After cooling to room temperature the product was isolated by suction filtration, washed with some methanol and dried under reduced pressure at 50 °C.

*Procedure C3.* A solution of 3-(*N,N*-diethylsulfamoyl)benzoyl chloride (3.00 mmol) and anthranilic acid methyl ester (3.00 mmol) in toluene (10 mL) was heated to reflux for 1.5 h. The solvent was evaporated under reduced pressure and the residue was heated briefly with a small amount of methanol. After cooling to room temperature the solid was isolated by suction filtration, washed with some methanol and dried under reduced pressure at 50 °C.

*General Procedure D for the Hydrolysis of 2-Benzamidobenzoic Acid Methyl Esters.* A mixture of 2-benzamidobenzoic acid methyl ester (1.30 mmol), THF/MeOH 2/1 (9 mL) and 1N NaOH (aq., 2.6 mL, 2.6 mmol) was stirred overnight at room temperature. 1N HCl (aq., 2.6 mL, 2.6 mmol) was added and the solid was isolated by suction filtration, washed with water and dried under reduced pressure.

*Procedure for the Synthesis of compound IV.* 1,4-Naphthoquinone (31.6 mmol) was dissolved in DCM (45 mL). Then TFA (2.45 mL) and *p*-toluenesulfinate (33.18 mmol) dissolved in water (30 mL) were added and the mixture was stirred for 1 hour. Solid precipitates were obtained. The solution was purified over a column and stirred for additional 5 hours. The solid was filtered off and washed several times with water and DCM.<sup>32,38</sup>

**Screening assay procedure for *in vitro* PqsD inhibition.** The assay was performed monitoring the enzyme activity by measuring the HHQ formation as described by Storz and coworkers<sup>31</sup>.

Quantification of HHQ was performed analogous to Storz *et al.*,<sup>31</sup> but with some modifications: the flow rate amounted 750  $\mu\text{L}/\text{min}$  and an Accucore RP-MS column, 150 x 2.1 mm, 2.6  $\mu\text{m}$  (Thermo Scientific, Waltham, Massachusetts, USA), was used. All test compound reactions were performed in triplicate in three independent runs. In the modified protocol, PqsD and the first substrate were preincubated for 30 min prior to adding them to the test compounds. Then  $\beta$ -ketodecanoic acid was added and the further steps were performed analogous to the standard protocol.

**Surface Plasmon Resonance.** SPR binding studies were performed using a Reichert SR7500DC instrument optical biosensor (Reichert Technologies, Depew, NY, USA) and CMD500M sensor chips obtained from XanTec (XanTec Bioanalytics, Düsseldorf, Germany). Scrubber software was used for processing and analyzing data.

*Preparation of PqsD mutants.* Ser317Phe, Cys112Ala and His257Phe PqsD mutants were generated using the QuikChange Site-Directed Mutagenesis Kit (Stratagene, La Jolla, CA) according to the manufacturer's instructions using the pET28b(+)/*pqsD* plasmid as a template. Briefly, *pqsD* gene was amplified through 16 cycles of PCR. After treatment with *DpnI*, the PCR product was transformed into *E. coli* strain XL1-Blue. Plasmid DNA was purified using the GenElute™ HP Plasmid Miniprep Kit (Sigma-Aldrich, St. Louis, MO) and sequenced to confirm the site-directed mutations. For the primer sequence of the mutations see Supporting Information.

*Expression and purification of recombinant PqsD wild-type and mutants in E. coli.* *E. coli* BL21 ( $\lambda$ DE3) cells were transformed with plasmid harboring PqsD (pET28b(+)/*pqsD*).<sup>30</sup> Overexpression, purification and storage of the His<sub>6</sub>-tagged PqsD was performed as described by Storz *et al.*<sup>31</sup> The expression and purification of recombinant PqsD used for the NMR-studies is described in SI

*Immobilization of His<sub>6</sub>-PqsD.* PqsD (38 kDA, >90% pure based on SDS-PAGE) was immobilized on a CMD500M (carboxymethyl-dextran-coated) sensor chip at 12 °C analogous to the method described by Henn and coworkers.<sup>39</sup> The PqsD immobilization levels were 2217 RU for the binding studies with ACoA and 3085 RU in the mutagenesis studies to serve as reference. The PqsD mutants were immobilized analogous to the wild-type at densities of 6789 RU (Ser317Phe), 3903 RU (Cys112Ala) and 4272 RU (His257Phe).

*Binding studies.* The binding studies were performed at a constant flow rate of 50  $\mu\text{L}/\text{min}$  in instrument running buffer (50 mM MOPS, pH 8.0, 150 mM NaCl, 5% DMSO (v/v), 0.1% Triton-X 100 (v/v)). **IV** (100  $\mu\text{M}$ ), **43** and **48** (20  $\mu\text{M}$ ) were injected consecutively for 180 s association and 300 s dissociation times. Experiments were performed twice. In the second experiment ACoA (100  $\mu\text{M}$ ) was injected for 40 minutes with a constant flow of 5  $\mu\text{L}/\text{min}$  to reach saturation of the ACoA binding site. Afterwards the flow rate was increased to 50  $\mu\text{L}/\text{min}$  (30 min) in order to flush all CoA away. Once the baseline signal is stable additional ACoA (10  $\mu\text{M}$ ) was injected to assure that the anthraniloyl binding site is completely saturated (no additional signal was observed). Afterwards **IV** (100  $\mu\text{M}$ ), **43** and **48** (20  $\mu\text{M}$ ) were consecutively injected.

In the experiment with inverted compound order PqsD was preincubated with compound **48**, therefore the compound was added to the running buffer (20  $\mu\text{M}$ ). The sensor chip surface was flushed for several hours at a constant flow rate of 50  $\mu\text{L}/\text{min}$  until the baseline was stable. Afterwards the flow rate was decreased to 10  $\mu\text{L}/\text{min}$  and ACoA was injected (100  $\mu\text{M}$ ) twice for 120 s association and 15 min dissociation. The binding studies with PqsD mutants were performed analogously to the wild-type experiments. The compounds were injected twice for 120 s association and 300 s dissociation time.

**Molecular Docking.** Molecular docking studies were performed by means of GOLDv5.0<sup>40, 41</sup> using the CHEMPLP scoring function. 100 runs per molecule were performed. Default GOLD parameters were used with carbons, halogens, and non-polar sulfur atoms matching hydrophobic regions. All three 3D-structures of PqsD (PDB-id 3H76, 3H77, 3H78) were used. For 3H77 (anthranilate-Cys112) and 3H78 (Ala112) the residue 112 of both chain A and B was mutated back into wild-type Cys112. Before docking geometry optimization of the enzymes has been performed using the LigX module of Molecular Operating Environment (MOE).<sup>42</sup> The active site was determined including all residues within 8 Å of the co-crystallized ACoA molecule of 3H77.

**Saturation-Transfer Difference NMR.** Experiments were recorded with the carrier set at -2 ppm for on-resonance irradiation and 40 ppm for off-resonance irradiation. Control spectra were recorded under identical conditions on samples containing free compound **2** to test for artifacts. Selective protein saturation (2 s) was accomplished using a train of 50 ms Gauss-shaped pulses, each separated by a 1 ms delay, at an experimentally determined optimal power (60 dB on our probe); a  $T_{1\rho}$  filter (25 ms) was incorporated to suppress protein resonances. Experiments were recorded using a minimum of 2048 scans and 32K points. On- and off-resonance spectra were processed independently, and subtracted to provide a difference spectrum. The expression and purification of recombinant PqsD from *E. coli* for STD NMR analysis is described in Supporting Information.

**Isothermal Titration Calorimetry.** ITC experiments were carried out using an ITC200 instrument (Microcal Inc., GE Healthcare). ITC measurements were routinely performed at 25 °C in PBS-buffer, pH 7.4, 10% glycerol (v/v), 5% DMSO (v/v). The titrations were performed on 83-102  $\mu\text{M}$  His<sub>6</sub>-PqsD in the 200  $\mu\text{L}$  sample cell using 2  $\mu\text{L}$  injections of 1.0 mM ligand solution every 180 s. Raw data were collected and the area under each peak was integrated. To correct for heats of dilution and mixing the final baseline consisting of small peaks of the same size at the end of the experiment was subtracted. The experimental data were fitted to a theoretical titration curve (one site binding model) using MicroCal Origin 7 software, with  $\Delta\text{H}$  (enthalpy change in kcal mol<sup>-1</sup>),  $K_{\text{A}}$  (association constant in M<sup>-1</sup>), and N (number of binding sites) as adjustable parameters. Thermodynamic parameters were calculated from equation;

$$\Delta\text{G} = \Delta\text{H} - \text{T}\Delta\text{S} = \text{RT} \ln K_{\text{A}} = -\text{RT} \ln K_{\text{D}}$$

where  $\Delta G$ ,  $\Delta H$ , and  $\Delta S$  are the changes in free energy, enthalpy, and entropy of binding, respectively,  $T$  is the absolute temperature, and  $R = 1.98 \text{ cal mol}^{-1} \text{ K}^{-1}$ . For compound **48** four independent experiments were performed.

## ASSOCIATED CONTENT

### Supporting Information

Additional figures docking study and STD NMR, ITC measurement, experimental details, biological methods and compound characterizations. This material is available free of charge via the Internet at <http://pubs.acs.org>.

## AUTHOR INFORMATION

### Corresponding Author

\*Phone: +49 681 302 70300; fax: +49 681 302 70308; e-mail: [rolf.hartmann@helmholtz-hzi.de](mailto:rolf.hartmann@helmholtz-hzi.de).

### Present addresses

<sup>1</sup> Syncom, Kadijk 3, 9747 AT Groningen, The Netherlands

### Author Contributions

‡ These authors contributed equally.

## ACKNOWLEDGMENT

We thank Dr. Claudia Henn for preparing the Ser317Phe and His257Phe mutants of PqsD, Dr. Simon Lucas for the synthesis of compound **IV**, Simone Amann for her help in performing the PqsD assay and Dr. Joseph Zapp for NMR analyses.

## ABBREVIATIONS

ACoA, anthraniloyl-CoA; HHQ, 2-heptyl-4-quinolone, ITC, isothermal titration calorimetry; PQS, *Pseudomonas* quinolone signal; QS, quorum sensing; SPR, surface plasmon resonance; STD saturation transfer difference.

## REFERENCES

1. Hakki, M.; Limaye, A. P.; Kim, H. W.; Kirby, K. A.; Corey, L.; Boeckh, M. Invasive *Pseudomonas aeruginosa* infections: high rate of recurrence and mortality after hematopoietic cell transplantation. *BMT* **2007**, *39*, 687-693
2. Asboe, D.; Gant, V.; Aucken, H. M.; Moore, D. A.; Umasankar, S.; Bingham, J. S.; Kaufmann, M. E.; Pitt, T. L. Persistence of *Pseudomonas aeruginosa* strains in respiratory infection in AIDS patients. *Aids* **1998**, *12*, 1771-1775

3. Govan, J. R. W.; Deretic, V. Microbial pathogenesis in cystic fibrosis: Mucoid *Pseudomonas aeruginosa* and *Burkholderia cepacia*. *Microbiol. Rev.* **1996**, *60*, 539-574
4. Gomez, M. I.; Prince, A. Opportunistic infections in lung disease: *Pseudomonas* infections in cystic fibrosis. *Curr. Opin. Pharmacol.* **2007**, *7*, 244-251
5. Wagner, V. E.; Iglewski, B. H. *P. aeruginosa* Biofilms in CF Infection. *Clin. Rev. Allergy Immunol.* **2008**, *35*, 124-134
6. Hancock, R. E. W.; Speert, D. P. Antibiotic resistance in *Pseudomonas aeruginosa*: mechanisms and impact on treatment. *Drug Resist. Updat.* **2000**, *3*, 247-255
7. Høiby, N.; Bjarnsholt, T.; Givskov, M.; Molin, S.; Ciofu, O. Antibiotic resistance of bacterial biofilms. *Int. J. Antimicrob. Agents* **2010**, *35*, 322-332
8. Ciofu, O.; Fusing, V.; Bagge, N.; Koch, C.; Høiby, N. Characterization of paired mucoid/non-mucoid *Pseudomonas aeruginosa* isolates from Danish cystic fibrosis patients: antibiotic resistance, beta-lactamase activity and RiboPrinting. *J. Antimicrob. Chemo.* **2001**, *48*, 391-396
9. Costerton, J. W.; Stewart, P. S.; Greenberg, E. P. Bacterial biofilms: A common cause of persistent infections. *Sci.* **1999**, *284*, 1318-1322
10. Williams, P.; Camara, M.; Hardman, A.; Swift, S.; Milton, D.; Hope, V. J.; Winzer, K.; Middleton, B.; Pritchard, D. I.; Bycroft, B. W. Quorum sensing and the population-dependent control of virulence. *Phil. Trans. R. Soc. Lond. B.* **2000**, *355*, 667-680
11. Rumbaugh, K. P.; Griswold, J. A.; Hamood, A. N. The role of quorum sensing in the in vivo virulence of *Pseudomonas aeruginosa*. *Microb. Infect.* **2000**, *2*, 1721-1731
12. Van Delden, C.; Iglewski, B. H. Cell-to-cell signaling and *Pseudomonas aeruginosa* infections. *Emerg. Infect. Dis.* **1998**, *4*, 551-560
13. Swift, S.; Downie, J. A.; Whitehead, N. A.; Barnard, A. M. L.; Salmond, G. P. C.; Williams, P. Quorum sensing as a population-density-dependent determinant of bacterial physiology. *Adv. Microb. Physiol.* **2001**, *45*, 199-270
14. Antunes, L. C. M.; Ferreira, R. B. R.; Buckner, M. M. C.; Finlay, B. B. Quorum sensing in bacterial virulence. *Microbiol. Sgm.* **2010**, *156*, 2271-2282
15. Gambello, M. J.; Iglewski, B. H. Cloning and Characterization of the *Pseudomonas-Aeruginosa LasR* Gene, a Transcriptional Activator of Elastase Expression. *J. Bacteriol.* **1991**, *173*, 3000-3009
16. Passador, L.; Cook, J. M.; Gambello, M. J.; Rust, L.; Iglewski, B. H. Expression of *Pseudomonas-Aeruginosa* Virulence Genes Requires Cell-to-Cell Communication. *Sci.* **1993**, *260*, 1127-1130
17. Ochsner, U. A.; Koch, A.; Fiechter, A.; Reiser, J. Isolation and Characterization of a Regulatory Gene Affecting Rhamnolipid Biosurfactant Synthesis in *Pseudomonas-Aeruginosa*. *J. Bacteriol.* **1994**, *176*, 2044-2054

18. Ochsner, U. A.; Reiser, J. Autoinducer-Mediated Regulation of Rhamnolipid Biosurfactant Synthesis in *Pseudomonas-Aeruginosa*. *Proc. Natl. Acad. Sci.* **1995**, *92*, 6424-6428
19. Xiao, G. P.; Deziel, E.; He, J. X.; Lepine, F.; Lesic, B.; Castonguay, M. H.; Milot, S.; Tampakaki, A. P.; Stachel, S. E.; Rahme, L. G. MvfR, a key *Pseudomonas aeruginosa* pathogenicity LTTR-class regulatory protein, has dual ligands. *Molecular Microbiology* **2006**, *62*, 1689-1699
20. Pesci, E. C.; Milbank, J. B. J.; Pearson, J. P.; McKnight, S.; Kende, A. S.; Greenberg, E. P.; Iglewski, B. H. Quinolone signaling in the cell-to-cell communication system of *Pseudomonas aeruginosa*. *Proc. Natl. Acad. Sci.* **1999**, *96*, 11229-11234
21. Déziel, E.; Gopalan, S.; Tampakaki, A. P.; Lépine, F.; Padfield, K. E.; Saucier, M.; Xiao, G. P.; Rahme, L. G. The contribution of MvfR to *Pseudomonas aeruginosa* pathogenesis and quorum sensing circuitry regulation: multiple quorum sensing-regulated genes are modulated without affecting *lasRI*, *rhlRI* or the production of *N*-acyl-L-homoserine lactones. *Mol. Microbiol.* **2005**, *55*, 998-1014
22. Gallagher, L. A.; McKnight, S. L.; Kuznetsova, M. S.; Pesci, E. C.; Manoil, C. Functions required for extracellular quinolone signaling by *Pseudomonas aeruginosa*. *Journal of Bacteriology* **2002**, *184*, 6472-6480
23. Müsken, M.; Di Fiore, S.; Dötsch, A.; Fischer, R.; Häussler, S. Genetic determinants of *Pseudomonas aeruginosa* biofilm establishment. *Microbiology-Sgm* **2010**, *156*, 431-441
24. Diggle, S. P.; Winzer, K.; Chhabra, S. R.; Chhabra, S. R.; Worrall, K. E.; Camara, M.; Williams, P. The *Pseudomonas aeruginosa* quinolone signal molecule overcomes the cell density-dependency of the quorum sensing hierarchy, regulates *rhl*-dependent genes at the onset of stationary phase and can be produced in the absence of LasR. *Molecular Microbiology* **2003**, *50*, 29-43
25. Hentzer, M.; Givskov, M. Pharmacological inhibition of quorum sensing for the treatment of chronic bacterial infections. *J. Clin. Invest.* **2003**, *112*, 1300-1307
26. Klein, T.; Henn, C.; de Jong, J. C.; Zimmer, C.; Kirsch, B.; Maurer, C. K.; Pistorius, D.; Müller, R.; Steinbach, A.; Hartmann, R. W. Identification of Small-Molecule Antagonists of the *Pseudomonas aeruginosa* Transcriptional Regulator PqsR: Biophysically Guided Hit Discovery and Optimization. *ACS Chem. Biol.* **2012**, *7*, 1496-1501
27. Lu, C. B.; Kirsch, B.; Zimmer, C.; de Jong, J. C.; Henn, C.; Maurer, C. K.; Müsken, M.; Häussler, S.; Steinbach, A.; Hartmann, R. W. Discovery of Antagonists of PqsR, a Key Player in 2-Alkyl-4-quinolone-Dependent Quorum Sensing in *Pseudomonas aeruginosa*. *Chem. Biol.* **2012**, *19*, 381-390
28. Suga, H.; Smith, K. M. Molecular mechanisms of bacterial quorum sensing as a new drug target. *Curr. Opin. Chem. Biol.* **2003**, *7*, 586-591



29. Rasmussen, T. B.; Givskov, M. Quorum-sensing inhibitors as anti-pathogenic drugs. *Int. J. Med. Microbiol.* **2006**, *296*, 149-161
30. Pistorius, D.; Ullrich, A.; Lucas, S.; Hartmann, R. W.; Kazmaier, U.; Müller, R. Biosynthesis of 2-Alkyl-4(1H)-Quinolones in *Pseudomonas aeruginosa*: Potential for Therapeutic Interference with Pathogenicity. *Chembiochem* **2011**, *12*, 850-853
31. Storz, M. P.; Maurer, C. K.; Zimmer, C.; Wagner, N.; Brengel, C.; de Jong, J. C.; Lucas, S.; Müsken, M.; Häussler, S.; Steinbach, A.; Hartmann, R. W. Validation of PqsD as an Anti-biofilm Target in *Pseudomonas aeruginosa* by Development of Small-Molecule Inhibitors. *J. Am. Chem. Soc.* **2012**, *134*, 16143-16146
32. Alhamadsheh, M. M.; Waters, N. C.; Sachdeva, S.; Lee, P.; Reynolds, K. A. Synthesis and biological evaluation of novel sulfonyl-naphthalene-1,4-diols as FabH inhibitors. *Bioorg. Med. Chem. Lett.* **2008**, *18*, 6402-6405
33. Nie, Z.; Perretta, C.; Lu, J.; Su, Y.; Margosiak, S.; Gajiwala, K. S.; Cortez, J.; Nikulin, V.; Yager, K. M.; Appelt, K.; Chu, S. S. Structure-based design, synthesis, and study of potent inhibitors of beta-ketoacyl-acyl carrier protein synthase III as potential antimicrobial agents. *J. Med. Chem.* **2005**, *48*, 1596-1609
34. Larsen, S. D.; Hester, M. R.; Ruble, J. C.; Kamilar, G. M.; Romero, D. L.; Wakefield, B.; Melchior, E. P.; Sweeney, M. T.; Marotti, K. R. Discovery and initial development of a novel class of antibacterials: Inhibitors of *Staphylococcus aureus* transcription/translation. *Bioorg. Med. Chem. Lett.* **2006**, *16*, 6173-6177
35. Stiff, C. M.; Zhong, M.; Sarver, R. W.; Gao, H.; Ho, A. M.; Sweeney, M. T.; Zurenko, G. E.; Romero, D. L. Correlation of carboxylic acid pK(a) to protein binding and antibacterial activity of a novel class of bacterial translation inhibitors. *Bioorg. Med. Chem. Lett.* **2007**, *17*, 5479-5482
36. Bera, A. K.; Atanasova, V.; Robinson, H.; Eisenstein, E.; Coleman, J. P.; Pesci, E. C.; Parsons, J. F. Structure of PqsD, a *Pseudomonas* Quinolone Signal Biosynthetic Enzyme, in Complex with Anthranilate. *Biochem.* **2009**, *48*, 8644-8655
37. Mayer, M.; Meyer, B. Group epitope mapping by saturation transfer difference NMR to identify segments of a ligand in direct contact with a protein receptor. *J. Am. Chem. Soc.* **2001**, *123*, 6108-6117
38. Bruce, J. M.; Lloydwilliams, P. Benzoquinones and Related-Compounds .6. Addition of Benzenesulfinic Acid to Substituted 1,4-Quinones. *Journal of the Chemical Society-Perkin Transactions 1* **1992**, 2877-2884
39. Henn, C.; Boettcher, S.; Steinbach, A.; Hartmann, R. W. Catalytic enzyme activity on a biosensor chip: Combination of surface plasmon resonance and mass spectrometry. *Analytical Biochemistry* **2012**, *428*, 28-30

40. Jones, G.; Willett, P.; Glen, R. C.; Leach, A. R.; Taylor, R. Development and validation of a genetic algorithm for flexible docking. *J. Mol. Biol.* **1997**, 267, 727-748
41. Verdonk, M. L.; Cole, J. C.; Hartshorn, M. J.; Murray, C. W.; Taylor, R. D. Improved protein-ligand docking using GOLD. *Proteins Struct. Funct. Genet.* **2003**, 52, 609-623
42. Molecular Operating Environment (MOE) 2010.10; Chemical Computing Group Inc. Sherbrooke St. W, S. M., Quebec, Canada H3A 2R7, 2010

**Supporting Information: Appendix 7.1 E**

**F Application of dual inhibition concept within looped autoregulatory system  
toward antivirulence agents against *Pseudomonas aeruginosa* infections**

Andreas Thomann\*, Antonio G. G. de Mello Martins\*, Christian Brengel, Martin Empting,  
and Rolf W. Hartmann

\*These authors contributed equally

Reprinted with permission from *ACS Chem. Biol.* **2016**, 11, 1279–1286

Copyright (2016) American Chemical Society.

DOI: 10.1021/acscchembio.6b00117

**Publication F**

**ABSTRACT:** The *Pseudomonas aeruginosa* quorum-sensing (QS) is a sophisticated network of genome-wide regulation triggered in response to population density. A major component is the self-inducing pseudomonas quinolone signal (PQS) QS system that regulates the production of several non-vital virulence- and biofilm-related determinants. Hence, QS circuitry is an attractive target for anti-virulence agents with lowered resistance development potential and a good model to study the concept of polypharmacology in auto-loop regulated systems per se. Based on the finding that a combination of PqsR antagonist and PqsD inhibitor synergistically lowers pyocyanin, we have developed a dual-inhibitor compound of low molecular weight and high solubility that targets PQS transcriptional regulator (PqsR) and PqsD, a key enzyme in the biosynthesis of PQS-QS signal molecules (HHQ and PQS). *In vitro*, this compound markedly reduced virulence factor production and biofilm formation accompanied by a diminished content of extracellular DNA (eDNA). Additionally, co-administration with ciprofloxacin increased susceptibility of PA14 to antibiotic treatment under biofilm conditions. Finally, disruption of pathogenicity mechanisms was also assessed *in vivo*, with significantly increased survival of challenged larvae in a *Galleria mellonella* infection model. Favorable physicochemical properties and effects on virulence/biofilm establish a promising starting point for further optimization. In particular, the ability to address two targets of the PQS auto-induction cycle at the same time with a single compound holds great promise in achieving enhanced synergistic cellular effects while potentially lowering rates of resistance development.

Polypharmacology, or addressing two or more disease-related targets at the same time, has proven to have a significant impact on the treatment efficacy of e.g. cancer,<sup>1,2</sup> bacterial<sup>3,4</sup> and viral infections,<sup>5</sup> high blood pressure,<sup>6</sup> asthma<sup>7</sup> and hormone-related diseases<sup>8</sup> in clinical setups. These multi-target effects are in most cases achieved by a combination of selective single target agents. Drug combinations can either act synergistically, whereby the combined effect is greater than the sum of their separate responses, or additively, when the resulting activity is the outcome of their combined individual effects. Both of which are shown to have favorable outcomes on lowered resistance development in cancer,<sup>9</sup> and microbial<sup>10</sup> infections.<sup>11</sup> Unfortunately, such multi-drug cocktails may incur in several drawbacks, such as undesired drug-drug interactions and increasingly complex dosing schemes resulting in a lesser compliance of patients to follow the prescribed intake schedules.<sup>12</sup> To reduce those problems, development of multi-target drugs is a worthwhile endeavor. In many of the abovementioned intricate systems self-inducing auto-loop cycles can be found. In this study we describe the concept of such multi-target approach in positively regulated auto-loop systems to achieve beneficial and synergistic inhibitory effects against *Pseudomonas aeruginosa* (PA) infections. Auto-inducing pathways are widely spread in mammalian,<sup>13</sup> plant<sup>14</sup> and bacterial kingdoms<sup>15</sup> and regulate vital functions in a variety of organisms.

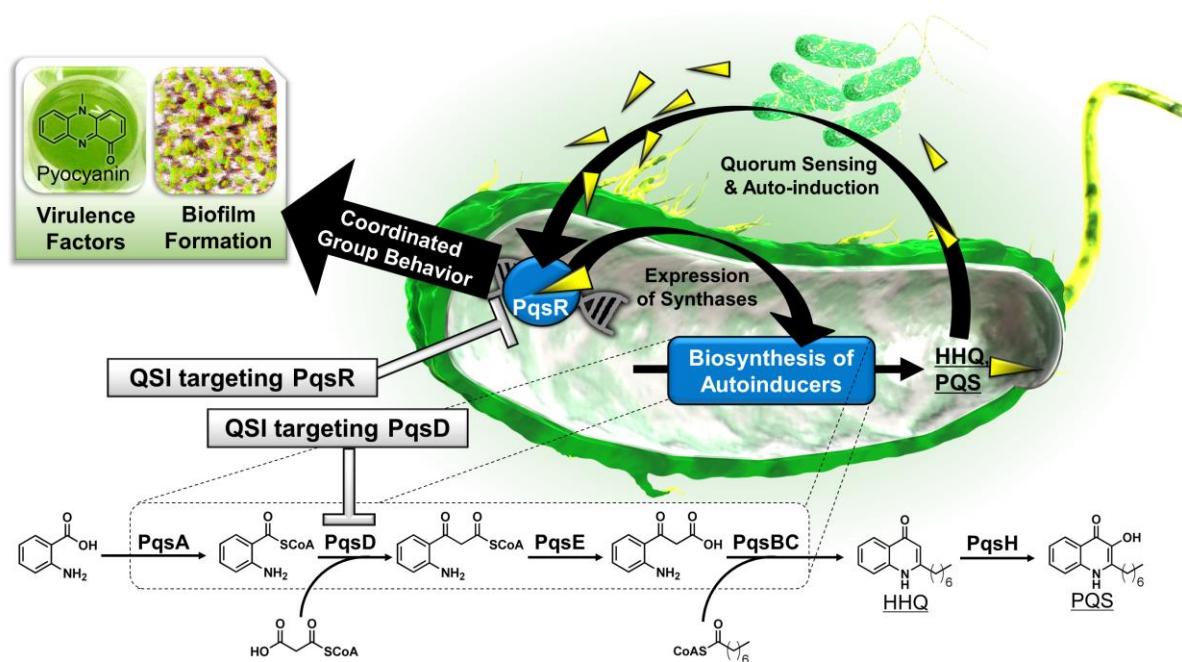


**Figure 1.** Schematic representation of the *Pseudomonas* quinolone signal (PQS) quorum-sensing system, involved in virulence factor production and biofilm formation. Anthranilate is converted by the *pqsABCDE* gene products into 2-heptyl-4-quinolone (HHQ), which can be converted intracellularly into PQS by the action of PqsH. HHQ and PQS are ligands of the Pqs Receptor (PqsR). Simultaneous inhibition of PQS synthesis (e.g. through PqsD) and interference with the auto-loop transcriptional regulator PqsR lead to increased reduction of pathogenicity-associated biomarkers.

As one model system to provide proof of this concept we chose the cell density-dependent<sup>16</sup> *Pseudomonas* quinolone signal quorum-sensing system (PQS-QS) of *Pseudomonas aeruginosa* which was intensively studied by us in the past.<sup>17-19</sup> In PA, PQS and 2-heptyl-4-quinolone (HHQ) are the natural agonists of PqsR which is the transcriptional regulator of the *pqsABCDE* operon (Figure 1).<sup>20</sup> This operon harbors the genes encoding for the synthases responsible for PQS production. Thus, as soon as PQS and/or HHQ activate PqsR they induce their own production and the concentration of signal molecules rise exponentially (Figure 1).<sup>21</sup> Interference experiments, combined with mutational analysis, revealed PqsR and PqsD to be attractive drug targets for reducing pathogenicity of PA *in vivo*.<sup>17,22</sup> Thus, PQS-QS displays an ideal and relevant model to study the concept of polypharmacology in such positive feedback loops with the possibility to directly transfer the results herein towards other similarly controlled biological systems. Furthermore, we directly put the lessons learned from drug combination experiments to an application for the straightforward rational design of the first drug-like dual-target PqsD/R inhibitors. Additionally, an optimized compound was achieved that shows promising reduction of two major virulence factors and biofilm inhibition *in vitro*. Finally, this optimized dual inhibitor displayed convincing activity in an *in vivo* acute PA infection model.

## RESULTS AND DISCUSSION

**Combination of PqsD inhibitor and PqsR antagonist prominently reduces relevant marker pyocyanin through synergistic activity.** As proof of principle to assess the amenability of the PQS-QS system to dual-target inhibition with improved outcome, we initially investigated the combinatorial effect of a PqsD inhibitor and a PqsR antagonist on a QS-dependent PA-exclusive secondary metabolite, pyocyanin.<sup>23,24</sup> Pyocyanin is one of PA's most prominent virulence factors with distinct roles in acute infection establishment and biofilm formation. Pyocyanin also substantially contributes to the generation of reactive oxygen species (ROS) by inhibiting the activity of catalase in eukaryotic cells. ROS is one of pseudomonas' adaptations to environmental competition against other microbes and is the cause for its cytotoxicity towards eukaryotic cells.<sup>25</sup> As a consequence, pyocyanin production is linked to increased inflammation, modulation of iron metabolism and tissue necrosis.<sup>26</sup> Its important physiological role in diseased states and correlation with the QS system suggest that by monitoring pyocyanin levels we may gain relevant insights into the suitability of dual inhibition that efficiently targets PA virulence.

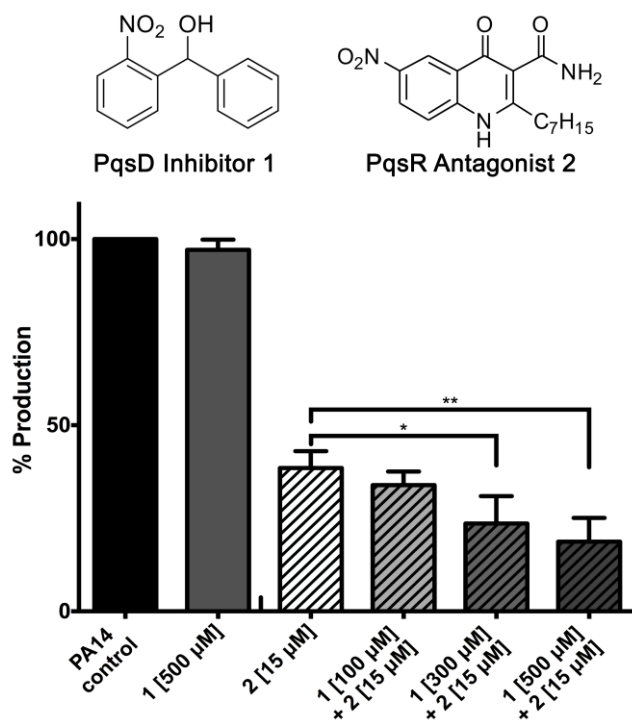


**Figure 2.** Synergistic activity of PqsD inhibitor 1 and PqsR antagonist 2 on pyocyanin inhibition in PA14 wild type. Treatment with 500  $\mu\text{M}$  of 1 alone did not alter pyocyanin production. However, basal pyocyanin production under inhibition with 15  $\mu\text{M}$  of 2 is significantly increased upon combinatorial titrated administration of 1 (100  $\mu\text{M}$ , 300  $\mu\text{M}$  and 500  $\mu\text{M}$ , respectively), indicative of synergistic activity. All values are relative to a control without inhibitors. Error bars represent the standard deviation of three independent experiments ( $n = 3$ ). \* =  $p < 0.05$ , \*\* =  $p < 0.005$ .

We cultured *P. aeruginosa* (PA14) wild type in the presence of different concentrations of a PqsD inhibitor **1**<sup>19</sup> and PqsR antagonist **2**,<sup>17</sup> as single treatment or combination therapy. As seen in Figure 2, 500  $\mu\text{M}$  of **1** alone does not influence the production of pyocyanin but, interestingly, when added in combination with 15  $\mu\text{M}$  of **2**, we observed a dose-dependent decrease in pyocyanin production. Notably, from 38% (**2** alone) to 34%, 23% and 18% (**2** added of 100  $\mu\text{M}$ , 300  $\mu\text{M}$  and 500  $\mu\text{M}$  of **1**, respectively) that is highly significant at higher concentrations of **1**, corroborating the synergistic activity of two PQS-QS inhibitors with different modes of action. These results further demonstrate that a biomarker negative synthase inhibitor (e.g. compound **1**) can indirectly increase the potency of a receptor antagonist (e.g. **2**) presumably by decreasing the natural ligand concentration and thus lowering competition to the receptor's binding site. However, when extending the exposure of PA14 to PqsD inhibitor **1**, we observed a slight, yet significant, reduction of pyocyanin after 48 h of incubation (see Supporting Information, section IIc). Obviously, a continuous attenuation of PQS/HHQ production through PqsD inhibition can result in an antivirulence effect.

**Application of concept study towards the rational design of dual PqsD/R inhibitors.** Having demonstrated the potential of combining synthase inhibition and receptor antagonism, we searched

through our in-house inhibitor library with regard to structural similarity of selective PqsD and PqsR inhibitors. From this search, we found compound **3** which was designed as a PqsR antagonist ( $IC_{50}$  = 26  $\mu$ M) with good activity on PA's virulence factor pyocyanin (Figure 3) and a quite similar compound, **4**, which was designed to target PqsD ( $IC_{50}$  = 1.7  $\mu$ M) based on SPR screening results recently reported by us (Figure 3).<sup>27</sup> As for **1**, compound **4** displayed no inhibitory activity on pyocyanin even at the maximum soluble concentration.

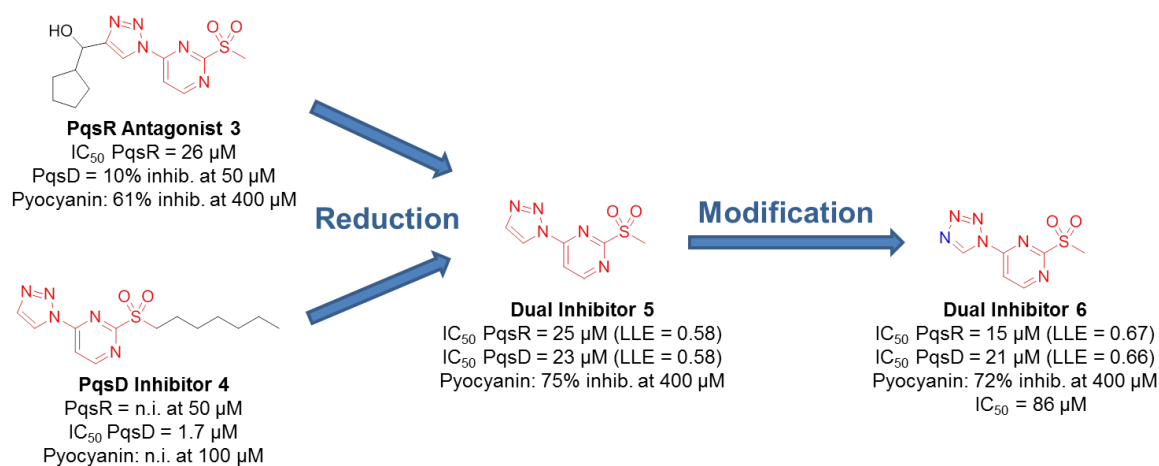


**Figure 3.** Reduction of structurally related PqsR antagonist **3** and PqsD inhibitor **4** to the common molecular core resulting in the first dual-active compound **5** (red). In comparison to **3**, **5** shows higher activity on pyocyanin, although being similarly active on PqsR, corroborating the findings of the combination experiments (Figure 2). Bioisosteric modification (blue) led to dual inhibitor **6** with improved physicochemical properties as shown by its increased ligand lipophilicity efficiency (LLE).



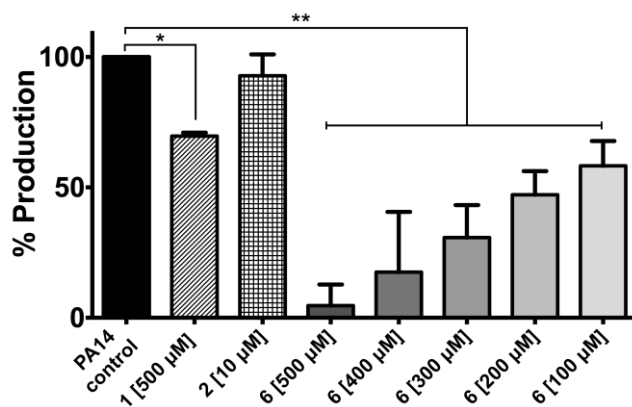


**Figure 4.** Effects of compounds 1, 2, and 6 on pyoverdine production. Compound 6 showed a prominent, significant decrease in pyoverdine levels in a concentration-dependent manner. At the highest concentration of 500  $\mu\text{M}$ , pyoverdine production was almost completely arrested (5%  $\pm$  8), and halved at the lowest inhibitor concentration of 100  $\mu\text{M}$  (58%  $\pm$  10). All values are relative to a control without inhibitors. Error bars represent standard deviation of three independent experiments ( $n = 3$ ). \* =  $p < 0.05$ , \*\* =  $p < 0.005$ .

Although, both compounds are selective for their respective targets, they share the same molecular scaffold: a pyrimidine core decorated with a triazole and a sulfone moiety (Figure 3). Thus, we decided to synthesize compound **5** and assess its biological activity, as it represents a simplified molecule consisting only of the shared structural features. Notably, the obtained compound **5** showed inhibition of both targets. Moreover, in very good accordance to our conceptual studies (*vide supra*), compound **5** showed a stronger reduction of pyocyanin compared to the equipotent PqsR selective precursor **3** (Figure 3). These results indicate that the concept of dual inhibition with combination experiments and the observed synergism can be directly combined in one compound. With regard to ligand lipophilicity efficiency (LLE), a metric used in medicinal chemistry to evaluate the activity of a compound based on its molecular weight and lipophilicity for further drug design, **5** showed a LLE = 0.56 on both targets which is above the suggested minimum score of 0.3.<sup>28</sup> To further improve the potential of **5** based on its LLE we decided to modify it via a bioisosteric replacement of C4 at the triazole substituent. Introducing a nitrogen at this site yielded the tetrazole congener **6** (Figure 3). To confirm the regiochemistry of the introduced tetrazole moiety we crystallized intermediate **6a**<sup>29</sup> and verified the structure by X-ray analysis (CCDC-No.: 1432241, Supporting Information, section Ib.). As expected for the tetrazole substituent, lipophilicity of **6** dropped compared to **5** leading to an increase of the LLE score (PqsR = 0.67; PqsD = 0.66) and better solubility. Notably, activity on PqsR was slightly increased while activity on PqsD was retained resulting in an overall  $\text{IC}_{50}$  on pyocyanin of 86  $\mu\text{M}$  (Figure 3).

Dual inhibitor affects not only pyocyanin production, but also modulates the generation of a second virulence factor, pyoverdine (PVD). Pyoverdines are *Pseudomonas*' primary siderophores. These

fluorescent signaling molecules are used by the bacterium in iron scavenging and metabolism, and are closely related to the production of other virulence factors in acute infections, as well as the correct architectural construction of biofilms.<sup>30,31</sup> Since absence of PVD in deficient mutants has shown to drastically reduce infection ability,<sup>32</sup> and iron acquisition *in vitro* is linked to biofilm formation,<sup>33</sup> PVD metabolism provides a connection between acute pathogenicity and biofilm-related severe infections. The intrinsic relationship of PQS and PVD signaling pathways in iron metabolism and virulence has been shown to be mutual: on one hand PQS induces the expression of genes involved in the biosynthesis of PVD,<sup>34</sup> on the other PvdS, one of the major regulators in the biosynthesis of PVD, controls the expression of PqsR.<sup>35,36</sup> Hence, we investigated whether our PQS dual inhibitor would have a beneficial effect on PVD inhibition by targeting PQS biosynthesis. We grew PA14 wild-type cultures in the presence of increasing concentrations of **6** (Figure 4). In accordance with our assumption, **6** was able to decrease PVD significantly in all tested concentrations (500  $\mu$ M to 100  $\mu$ M). Production of the siderophore was essentially blocked at the highest tested concentration of **6**, while compounds **1** and **2** had only moderate or low effects in this assay (69.7%  $\pm$  1.3 and 92.8%  $\pm$  8.2, respectively). Thus, dual inhibitor **6** is not only able to target pyocyanin biosynthesis, but also addresses PVD production, disrupting iron metabolism and virulence factor production, ultimately reducing the environmental competitive advantage of *Pseudomonas*, as well as its pathogenicity to lower levels that better respond to treatment. These beneficial cellular effects may contribute to attenuation of biofilm formation and establishment - a scenario that we further investigated in our next experiments.

**Compound 6 reduces biofilm formation and restores antibiotic efficacy.** Biofilms are one of the major clinically relevant resistance mechanisms of PA against antibiotic treatment,<sup>37</sup> immune responses,<sup>38</sup> and antimicrobial peptides<sup>39</sup> in particular. Thus, reduction of biofilm mass holds the potential to enable immunological clearance of the pathogen and restore antibiotic activity, features of undoubtedly high interest. The development of biofilms is dependent on the PQS Quorum sensing network as shown in previous knock out studies.<sup>40</sup> Recently we showed that PqsD inhibitor **1** reduces PA biofilms at high concentrations (reduction of biofilm volume to 62 % at 500  $\mu$ M).<sup>19</sup> Furthermore, anti-biofilm activities have been reported for PqsR antagonists designed on the basis of the natural ligand HHQ,<sup>41</sup> the biological precursor of PQS (Figure 1), and we observed a reduction in biofilm volume by compound **2** to 84.8%  $\pm$  4.7 at 15  $\mu$ M (see Supplementary Figure 5). These target-related effects and the reduction of the biofilm-associated virulence factor PVD (*vide supra*) motivated us to test whether our dual target compound **6** was also active on preventing biofilm formation. Indeed, **6** displayed prominent effects on biofilm development with an IC<sub>50</sub> of 100  $\mu$ M (Figure 5A, circles). This is in good accordance with previously obtained data regarding biofilm inhibition targeting either PqsR or PqsD.<sup>19,41,42</sup>

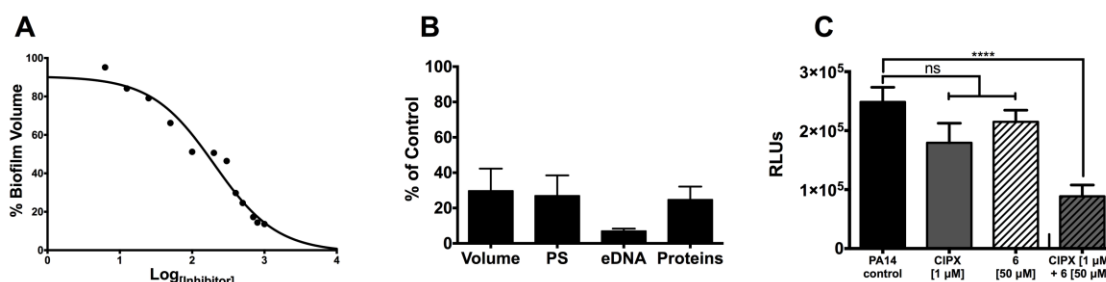


**Figure 5.** Dose-dependent reduction of biofilm in PA14 wild type cultures treated with compound **6** (A). Pronounced reduction of extracellular DNA (eDNA), polysaccharides (PS) and proteins of the biofilm matrix (Volume) was found at 400  $\mu$ M of **6** (B). Activity of 1  $\mu$ M ciprofloxacin (CIPX) was increased by a combination of the antibiotic with 50  $\mu$ M of **6** under biofilm conditions (C). Error bars represent standard error of at least two independent experiments. ns = not significant, \*\*\*\* =  $p < 0.0001$ .

We concluded that the dual inhibition concept might not only pronouncedly reduce pyocyanin formation, but might also result in stronger inhibition of PA biofilm. To further validate the target of **6** under biofilm-conditions we assessed whether the dual inhibitor is still active on a PqsR deficient mutant strain of PA. We observed a reduced activity of about 1 log unit of the  $\Delta pqsR$  mutant strain compared to wild type PA. This result on the one hand underlines the target-related activity but also shows that the compound has an additional target involved in biofilm formation. A biofilm is a heterogeneous matrix composed of different components e.g. polysaccharides (PS), proteins, lipopolysaccharides (LPS) and extracellular DNA (eDNA).<sup>43</sup> The latter has been described as responsible for resistance development against aminoglycoside<sup>44</sup> and fluoroquinolone antibiotics<sup>45</sup> as well as increased tolerance against host defensins.<sup>46</sup> Moreover, release of eDNA is directly regulated by the presence of pyocyanin<sup>47</sup> and PQS.<sup>48</sup> Hence, we were curious how **6** affects the components of the biofilm (Figure 5B). Our results demonstrate that **6** significantly inhibited eDNA release under biofilm conditions (7%  $\pm$  2 residual eDNA detected) which is in good accordance with the previous findings described above. Moreover, we observed a marked attenuation of PS and protein BF constituents down to 27%  $\pm$  20 and 25%  $\pm$  13, respectively. As a targeted decrease of eDNA might lead to higher efficacy of antibiotics on biofilm cultures of PA, we tested the susceptibility of PA14 against the fluoroquinolone-based antibiotic ciprofloxacin, which activity has been described to be hindered in the presence of eDNA.<sup>45</sup> Under biofilm conditions no significant inhibition of PA viability by ciprofloxacin was observed (Figure 5C). However, combination with **6**, which alone had no effect on the viability of PA, antibiotic activity could be restored under biofilm conditions that mimic a chronic infection *in vitro*. Furthermore, these findings complement published data regarding the application of PqsR antagonists in acute infection models.<sup>42</sup> Thus, therapy of QSIs in combination with antibiotic treatment in acute and chronic PA infections holds great promise for future anti-infective drug discovery focusing on quorum sensing inhibition.

**Compound 6 reduces pathogenicity of PA14 *in vivo*.** Until today a variety of *in vivo* models to assess the pathogenicity of PA were developed. We chose an animal infection model employing *Galleria mellonella* larvae which has been previously shown to have a high correlation with mouse PA infection models<sup>49</sup> and was also used by us to validate a PqsR antagonist *in vivo*.<sup>17</sup> To determine efficacy of our dual-target compound **6**, *G. mellonella* larvae were inoculated with the agent in the presence and absence of PA. Interestingly, **6** was able to increase the survival rate of larvae in a dose-dependent manner with 53% survival at 1.25 nmol and 29% survival at 0.5 nmol applied dose (Figure 6). The susceptibility of larvae was described to be 50% if infected by one cell of PA.<sup>49</sup> Notably, in our experiments one larva was challenged with 10-13 PA cells, resulting in a very high bacterial load and hurdle to be taken by an anti-infective treatment. Regarding the average hemeolymph and body weight (450  $\mu$ l and 450 mg)<sup>17</sup> of each larvae most beneficial protective effect was observed at a dosage of 1.25 nmol, correspondent to a final *in vivo* concentration of 2.7  $\mu$ M or 0.63 mg kg<sup>-1</sup>. Most interestingly, when assessing toxicity of **6** in *G. mellonella* we could show that even a 4 times higher concentration (5 nmol) than the effective dose was well tolerated with no observable disparity with PBS control.

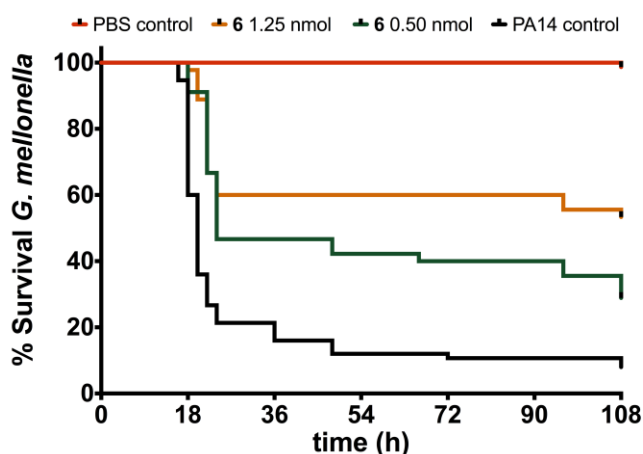


**Figure 6.** Dose-dependent *in vivo* protective effect of **6** on the survival of *Pseudomonas aeruginosa* PA14-challenged larvae of *Galleria mellonella*. Survival rate was significantly higher for treated larvae (0.5 nmol or 1.25 nmol) compared to the untreated control (0.5 and 1.25 nmol applied doses:  $p < 0.0001$ ; log-rank test).

## CONCLUSION

In this study, we demonstrated the applicability of dual synergistic inhibition within the frame of positive feedback auto-loop systems as a novel concept for the development of quorum sensing inhibitors. We chose the model PQS-QS system of *Pseudomonas aeruginosa* to demonstrate that an enzyme inhibitor **1** can increase the potency of the associated receptor antagonist **2** regarding virulence factor production. Presumably, this beneficial effect is due to lowered signal molecule levels and,

therefore, less competition at the receptor's binding site. We successfully exploited this concept of dual inhibition in a rational design strategy to achieve the first dual-active inhibitor **5** targeting the PQS-QS system. This compound was further improved by bioisosteric replacement, culminating in inhibitor **6** with enhanced efficiency/lipophilicity profile. This compound effectively reduced pyocyanin and pyoverdine, two major virulence factors of PA, in a dose-dependent manner without affecting bacterial growth. Importantly, **6** had a strong effect on PA biofilm assembly and restored the efficacy of ciprofloxacin, presumably due to hindering of eDNA release. Finally, dual inhibitor **6** was also active *in vivo* protecting *G. mellonella* larvae from lethal PA infections. Taken together, the presented dual inhibition strategy holds great potential to effectively interfere with intricate cellular systems. Via this promising approach we achieved an enhanced bioactivity profile through synergistic action at two points-of-intervention (PqsD and PqsR) within a positive feedback loop (the PQS-QS system). Hence, this strategy might be a powerful tool for devising new treatment options for diseases related to complex or compensatory metabolic pathways similar to the one investigated in this study.

## METHODS

**Pyocyanin Assay.** Pyocyanin formation was assessed as previously described<sup>18,23,50</sup> with minor modifications. Single colony was removed from agar plates after 16 h of growth at 37 °C and transferred into 25 mL Erlenmeyer flasks with 10 mL of PPGAS medium. Following 19 h of aerobic growth with shaking at 200 rpm and 37 °C, cultures were centrifuged at 7.450 g, washed once with 10 mL of fresh PPGAS medium, and resuspended to a final volume of 5 mL. Cultures were then diluted to a final OD<sub>600</sub> of 0.02, and distributed into test tubes in 1.2 mL aliquots. Compounds **1** and **2** were added in 1:100 dilutions with a final DMSO concentration of 1% (v/v). Treated and untreated cultures were incubated for additional 17 h under aerobic conditions as mentioned above. Pyocyanin was extracted by adding 900 µL of chloroform to 900 µL of overnight culture, and subsequently re-extracted with 250 µL of 0.2 M HCl from the organic phase. OD<sub>520</sub> was measured in the aqueous phase. Pyocyanin formation values were normalized to corresponding OD<sub>600</sub> of respective sample.

**Pyoverdine Assay.** For the analysis of pyoverdine formation, culture work-up and stock solution of compounds **1**, **2**, and **6** were performed as described above (Pyocyanin Assay). Treated and untreated cultures were incubated in 200 µL PPGAS medium for 8 h under aerobic conditions in black 96-well plates with glass bottom. This allowed for the simultaneous measurements of pyoverdine (fluorescent light units with excitation at 400 ± 10 and emission at 460 ± 10) and bacterial growth at OD<sub>600</sub>. Inhibition of pyoverdine was normalized to OD<sub>600</sub> values.

***Galleria mellonella* virulence assay.** An infection model of *G. mellonella* was used to determine disruption of virulence mechanisms *in vivo* as described in the works of Lu et al.<sup>17</sup> Treatment conditions of larvae included: a) Sterile PBS solution; b) PA14 suspension; c) 0.50 nmol of compound **6** in “b”); d) 1.25 nmol of compound **6** in “b”). For each treatment, data from at least three independent experiments were combined.

**Biofilm Assay.** Commonly used crystal violet (CV) assay procedures<sup>51–53</sup> were adapted for determination of biofilm mass. For the cultivation of biofilm in 96 well plates biofilm, the protocol described by Frei et al.<sup>53</sup> was slightly modified by replacement of medium and *Pseudomonas* strain used. The experiment was performed using *P. aeruginosa* PA14 strain (including  $\Delta$ pqsR mutant, kindly provided by S. Häussler) and M63 medium.<sup>54</sup> CV staining was used to detect compound effects on the overall biofilm biomass. Impact on eDNA was assessed by incubation of biofilm with propidium iodine solution (0,05 mg ml<sup>-1</sup>) for 3 h and detection of specific fluorescence at 620 nm after a thorough washing step with 18M $\Omega$  H<sub>2</sub>O.<sup>55</sup> Polysaccharide levels in biofilm were specified by congo red staining described by Ghafoor et al.<sup>56</sup> For this purpose, a 20 mg ml<sup>-1</sup> congo red solution was incubated with the matured biofilm for 3 hours, followed by a washing step with water and the concentration measurement at 490 nm. For the detection of protein levels, Bradford reagent was diluted 1:5 (Roti®-Quant, Carl Roth) and incubated with the washed biofilm for 5 minutes.<sup>57</sup> 18M $\Omega$  H<sub>2</sub>O was used to remove unbound dye. The amount of proteins was determined by absorbance measurement at 595 nm. To investigate killing efficacy of ciprofloxacin in combination with QS inhibitor on biofilm-encapsulated bacteria, biofilm was grown in the same conditions used for CV assay. At first, biofilm growth was initiated under QS inhibitor treatment (50  $\mu$ M) or DMSO control. After washing steps, matured biofilm was incubated with 4  $\mu$ g ml<sup>-1</sup> ciprofloxacin dissolved in M63 medium and grown for further 24 hours. Viability of bacteria in biofilm was determined by BacTiter-Glo™ Assay using black plates.<sup>58</sup>

**Chemical Synthesis and Analytical Characterization.** NMR spectra were recorded on a Avance AV 300 or a Bruker DRX 500. The residual proton, <sup>1</sup>H, or carbon <sup>13</sup>C resonances of the >99 % deuterated solvents were used for internal reference of all spectra acquired. (CDCl<sub>3</sub> <sup>1</sup>H 7.260 ppm, <sup>13</sup>C 77.16 ppm; DMSO-*d*<sub>6</sub>, <sup>1</sup>H 2.500 ppm, <sup>13</sup>C 39.52 ppm). Electrospray ionization (ESI) mass spectrometry and LC-UV purity determination were recorded with a Surveyor LC system MSQ electrospray mass spectrometer (ThermoFisher) LC-MS couple and acetonitrile/water gradient in positive mode (+), if not indicated otherwise. 1% TFA was added if necessary. Compound **6** was analyzed using a setup produced by Waters Corporation containing a 2767 Sample Manager, a 2545 binary gradient pump, a 2998 PDA detector and a 3100 electron spray mass spectrometer. Water containing 0.1 % formic acid and acetonitrile containing 0.1 % formic acid were used as solvents for the analysis. A Waters X-Bridge column (C18, 150 x 4.6 mm, 5  $\mu$ M) has been used with a flow of 1 mL min<sup>-1</sup> starting with 10% acid containing acetonitrile to 95% acid containing acetonitrile. All final compounds were of  $\geq$  95% purity. Unless otherwise stated, all reagents used were purchased from commercial vendors and used without further purification.

#### ASSOCIATED CONTENT

**Supporting Information Available.** Spectra (<sup>1</sup>H COSY, <sup>13</sup>C NMR, LC-MS, X-ray crystallography) and synthetic procedures of described new compounds, and details on PqsD-, PqsR-Assays. Growth

curves, and IC<sub>50</sub> determination on Pyocyanin with **6**, LLE calculations, and antibiofilm effects of **2**. This material is available free of charge via the Internet at <http://pubs.acs.org>.

## AUTHOR INFORMATION

### Corresponding Author

\* rolf.hartmann@helmholtz-hzi.de

\* martin.empting@helmholtz-hzi.de

### Author Contributions

‡These authors contributed equally.

### Notes

The authors declare no competing financial interest.

### ACKNOWLEDGMENT

We thank C. Maurer, S. Amann and C. Scheidt for performing and supervising the PqsD, PqsR and pyocyanin assays. Many thanks go to V. Huch for recording the X-ray structure of compound **6a** and B. Kirsch for helpful discussions and introduction to the *Galleria mellonella* assay. We thank C. Börger for LC-MS analysis of compound **6**.

### FUNDING SOURCES

This project was funded by BMBF through grant 1616038B.

### ABBREVIATIONS

PQS, Pseudomonas Quinolone Signal; QS, Quorum Sensing; PA, Pseudomonas aeruginosa

### References

- (1) Tolaney, S. M., Barry, W. T., Dang, C. T., Yardley, D. A., Moy, B., Marcom, P. K., Albain, K. S., Rugo, H. S., Ellis, M., Shapira, I., Wolff, A. C., Carey, L. A., Overmoyer, B. A., Partridge, A. H., Guo, H., Hudis, C. A., Krop, I. E., Burstein, H. J., and Winer, E. P. (2015) Adjuvant paclitaxel and trastuzumab for node-negative, HER2-positive breast cancer. *N. Engl. J. Med.* 372, 134–141.
- (2) Robert, C., Karaszewska, B., Schachter, J., Rutkowski, P., Mackiewicz, A., Stroiakovski, D., Lichinitser, M., Dummer, R., Grange, F., Mortier, L., Chiarion-Sileni, V., Drucis, K., Krajsova, I., Hauschild, A., Lorigan, P., Wolter, P., Long, G. V., Flaherty, K., Nathan, P., Ribas, A., Martin, A.-M., Sun, P., Crist, W., Legos, J., Rubin, S. D., Little, S. M., and Schadendorf, D. (2015) Improved overall survival in melanoma with combined dabrafenib and trametinib. *N. Engl. J. Med.* 372, 30–39.
- (3) Diacon, A. H., Pym, A., Grobusch, M., Patientia, R., Rustomjee, R., Page-Shipp, L., Pistorius, C., Krause, R., Bogoshi, M., Churchyard, G., Venter, A., Allen, J., Palomino, J. C., Marez, T. de, van Heeswijk, Rolf P G, Lounis, N., Meyvisch, P., Verbeeck, J., Parys, W., Beule, K. de, Andries, K., and Mc Neeley, David F (2009) The diarylquinoline TMC207 for multidrug-resistant tuberculosis. *N. Engl. J. Med.* 360, 2397–2405.

- (4) Hilf, M., Yu, V. L., Sharp, J., Zuravleff, J. J., Korvick, J. A., and Muder, R. R. (1989) Antibiotic therapy for *Pseudomonas aeruginosa* bacteremia: Outcome correlations in a prospective study of 200 patients. *Am. J. Med.* 87, 540–546.
- (5) Gandhi, M., and Gandhi, R. T. (2014) Single-pill combination regimens for treatment of HIV-1 infection. *N. Engl. J. Med.* 371, 248–259.
- (6) Sever, P. S., and Messerli, F. H. (2011) Hypertension management 2011: optimal combination therapy. *Eur. Heart J.* 32, 2499–2506.
- (7) Kerstjens, Huib A M, Engel, M., Dahl, R., Paggiaro, P., Beck, E., Vandewalker, M., Sigmund, R., Seibold, W., Moroni-Zentgraf, P., and Bateman, E. D. (2012) Tiotropium in asthma poorly controlled with standard combination therapy. *N. Engl. J. Med.* 367, 1198–1207.
- (8) Vilar, L., Naves, L. A., Machado, M. C., and Bronstein, M. D. (2015) Medical combination therapies in Cushing's disease. *Pituitary* 18, 253–262.
- (9) Samanta, D., Gilkes, D. M., Chaturvedi, P., Xiang, L., and Semenza, G. L. (2014) Hypoxia-inducible factors are required for chemotherapy resistance of breast cancer stem cells. *Proc. Natl. Acad. Sci. U. S. A.* 111, E5429-38.
- (10) Worthington, R. J., and Melander, C. (2013) Combination approaches to combat multidrug-resistant bacteria. *Trends Biotechnol.* 31, 177–184.
- (11) Elisabeth Buirra, Angeles Jaen (2015) Impact of Fixed-Dose Combinations of Antiretrovirals on Prevalence Trends of HIV Resistance: A 7 Year Follow-Up Study. *J. AIDS Clin. Res.* 06.
- (12) Anighoro, A., Bajorath, J., and Rastelli, G. (2014) Polypharmacology: challenges and opportunities in drug discovery. *J. Med. Chem.* 57, 7874–7887.
- (13) Bombeli, T., and Spahn, D. R. (2004) Updates in perioperative coagulation: physiology and management of thromboembolism and hemeorrhage. *Br. J. Anaesth.* 93, 275–287.
- (14) Petruzzelli, L., Coraggio, I., and Leubner-Metzger, G. (2000) Ethylene promotes ethylene biosynthesis during pea seed germination by positive feedback regulation of 1-aminocyclopropane-1-carboxylic acid oxidase. *Planta* 211, 144–149.
- (15) van Hoek, M., and Hogeweg, P. (2007) The effect of stochasticity on the lac operon: an evolutionary perspective. *PLoS Comput. Biol.* 3, e111.
- (16) Swift, S., Allan Downie, J., Whitehead, N. A., Barnard, A. M., Salmond, G. P., and Williams, P. (2001) Quorum sensing as a population-density-dependent determinant of bacterial physiology. *Adv. Microb. Physiol.* 45, 199–270.
- (17) Lu, C., Maurer, C. K., Kirsch, B., Steinbach, A., and Hartmann, R. W. (2014) Overcoming the unexpected functional inversion of a PqsR antagonist in *Pseudomonas aeruginosa*: an in vivo potent antivirulence agent targeting pqs quorum sensing: An In Vivo Potent Antivirulence Agent Targeting pqs Quorum Sensing. *Angew. Chem. Int. Ed. Engl.* 53, 1109–1112.
- (18) Klein, T., Henn, C., de Jong, Johannes C, Zimmer, C., Kirsch, B., Maurer, C. K., Pistorius, D., Müller, R., Steinbach, A., and Hartmann, R. W. (2012) Identification of small-molecule



- antagonists of the *Pseudomonas aeruginosa* transcriptional regulator PqsR: biophysically guided hit discovery and optimization. *ACS Chem. Biol.* 7, 1496–1501.
- (19) Storz, M. P., Maurer, C. K., Zimmer, C., Wagner, N., Brengel, C., de Jong, Johannes C, Lucas, S., Müssen, M., Häussler, S., Steinbach, A., and Hartmann, R. W. (2012) Validation of PqsD as an anti-biofilm target in *Pseudomonas aeruginosa* by development of small-molecule inhibitors. *J. Am. Chem. Soc.* 134, 16143–16146.
- (20) Rutherford, S. T., and Bassler, B. L. (2012) Bacterial quorum sensing: its role in virulence and possibilities for its control. *Cold Spring Harb. Perspect. Med.* 2.
- (21) Déziel, E., Gopalan, S., Tampakaki, A. P., Lépine, F., Padfield, K. E., Saucier, M., Xiao, G., and Rahme, L. G. (2005) The contribution of MvfR to *Pseudomonas aeruginosa* pathogenesis and quorum sensing circuitry regulation: multiple quorum sensing-regulated genes are modulated without affecting lasRI, rhlRI or the production of N-acyl-L-homoserine lactones. *Mol. Microbiol.* 55, 998–1014.
- (22) Gallagher, L. A., McKnight, S. L., Kuznetsova, M. S., Pesci, E. C., and Manoil, C. (2002) Functions Required for Extracellular Quinolone Signaling by *Pseudomonas aeruginosa*. *J. Bacteriol.* 184, 6472–6480.
- (23) O'Loughlin, C. T., Miller, L. C., Siryaporn, A., Drescher, K., Semmelhack, M. F., and Bassler, B. L. (2013) A quorum-sensing inhibitor blocks *Pseudomonas aeruginosa* virulence and biofilm formation. *Proc. Natl. Acad. Sci. U. S. A.* 110, 17981–17986.
- (24) Recinos, D. A., Sekedat, M. D., Hernandez, A., Cohen, T. S., Sakhtah, H., Prince, A. S., Price-Whelan, A., and Dietrich, Lars E P (2012) Redundant phenazine operons in *Pseudomonas aeruginosa* exhibit environment-dependent expression and differential roles in pathogenicity. *Proc. Natl. Acad. Sci. U. S. A.* 109, 19420–19425.
- (25) Mavrodi, D. V., Parejko, J. A., Mavrodi, O. V., Kwak, Y.-S., Weller, D. M., Blankenfeldt, W., and Thomashow, L. S. (2013) Recent insights into the diversity, frequency and ecological roles of phenazines in fluorescent *Pseudomonas* spp. *Environ. Microbiol.* 15, 675–686.
- (26) Priyaja, P., Jayesh, P., Philip, R., and Bright Singh, I S (2014) Pyocyanin induced in vitro oxidative damage and its toxicity level in human, fish and insect cell lines for its selective biological applications. *Cytotechnology*. DOI: 10.1007/s10616-014-9765-5.
- (27) Weidel, E., Negri, M., Empting, M., Hinsberger, S., and Hartmann, R. W. (2014) Composing compound libraries for hit discovery--rationality-driven preselection or random choice by structural diversity? *Future Med. Chem.* 6, 2057–2072.
- (28) Mortenson, P. N., and Murray, C. W. (2011) Assessing the lipophilicity of fragments and early hits. *J. Comput. Aided Mol. Des.* 25, 663–667.
- (29) Thomann, A., Börger, C., Empting, M., and Hartmann, R. (2014) Microwave-Assisted Synthesis of 4-Substituted 2-Methylthiopyrimidines. *Synlett* 25, 935–938.

- (30) Banin, E., Vasil, M. L., and Greenberg, E. P. (2005) Iron and *Pseudomonas aeruginosa* biofilm formation. *Proc. Natl. Acad. Sci. U. S. A.* 102, 11076–11081.
- (31) Cézard, C., Farvacques, N., and Sonnet, P. (2015) Chemistry and biology of pyoverdines, *Pseudomonas* primary siderophores. *Curr. Med. Chem.* 22, 165–186.
- (32) Stanners, C. P., and Goldberg, V. J. (1975) On the mechanism of neurotropism of vesicular stomatitis virus in newborn hamsters. Studies with temperature-sensitive mutants. *J. Gen. Virol.* 29, 281–296.
- (33) Visca, P., Imperi, F., and Lamont, I. L. (2007) Pyoverdine siderophores: from biogenesis to biosignificance. *Trends Microbiol.* 15, 22–30.
- (34) Diggle, S. P., Matthijs, S., Wright, V. J., Fletcher, M. P., Chhabra, S. R., Lamont, I. L., Kong, X., Hider, R. C., Cornelis, P., Cámara, M., and Williams, P. (2007) The *Pseudomonas aeruginosa* 4-quinolone signal molecules HHQ and PQS play multifunctional roles in quorum sensing and iron entrapment. *Chem. Biol.* 14, 87–96.
- (35) Bredenbruch, F., Geffers, R., Nimtz, M., Buer, J., and Häussler, S. (2006) The *Pseudomonas aeruginosa* quinolone signal (PQS) has an iron-chelating activity. *Environ. Microbiol.* 8, 1318–1329.
- (36) Jimenez, P. N., Koch, G., Thompson, J. A., Xavier, K. B., Cool, R. H., and Quax, W. J. (2012) The multiple signaling systems regulating virulence in *Pseudomonas aeruginosa*. *Microbiol Mol Biol Rev.* 76, 46–65.
- (37) Drenkard, E. (2003) Antimicrobial resistance of *Pseudomonas aeruginosa* biofilms. *Microb. Infect.* 5, 1213–1219.
- (38) Alhede, M., Bjarnsholt, T., Givskov, M., and Alhede, M. (2014) *Pseudomonas aeruginosa* biofilms: mechanisms of immune evasion. *Adv. Appl. Microbiol.* 86, 1–40.
- (39) Lewenza, S. (2013) Extracellular DNA-induced antimicrobial peptide resistance mechanisms in *Pseudomonas aeruginosa*. *Front. Microbiol.* 4, 21.
- (40) Müsken, M., Di Fiore, S., Dötsch, A., Fischer, R., and Häussler, S. (2010) Genetic determinants of *Pseudomonas aeruginosa* biofilm establishment. *Microbiology* 156, 431–441.
- (41) Ilangovan, A., Fletcher, M., Rampioni, G., Pustelny, C., Rumbaugh, K., Heeb, S., Cámara, M., Truman, A., Chhabra, S. R., Emsley, J., and Williams, P. (2013) Structural basis for native agonist and synthetic inhibitor recognition by the *Pseudomonas aeruginosa* quorum sensing regulator PqsR (MvfR). *PLoS Pathog.* 9, e1003508.
- (42) Starkey, M., Lepine, F., Maura, D., Bandyopadhyaya, A., Lesic, B., He, J., Kitao, T., Righi, V., Milot, S., Tzika, A., and Rahme, L. (2014) Identification of anti-virulence compounds that disrupt quorum-sensing regulated acute and persistent pathogenicity. *PLoS Pathog.* 10, e1004321.
- (43) Wei, Q., and Ma, L. Z. (2013) Biofilm matrix and its regulation in *Pseudomonas aeruginosa*. *Int. J. Mol. Sci.* 14, 20983–21005.

- (44) Chiang, W.-C., Nilsson, M., Jensen, P. Ø., Høiby, N., Nielsen, T. E., Givskov, M., and Tolker-Nielsen, T. (2013) Extracellular DNA shields against aminoglycosides in *Pseudomonas aeruginosa* biofilms. *Antimicrob. Agents. Chemother.* 57, 2352–2361.
- (45) Johnson, L., Horsman, S. R., Charron-Mazenod, L., Turnbull, A. L., Mulcahy, H., Surette, M. G., and Lewenza, S. (2013) Extracellular DNA-induced antimicrobial peptide resistance in *Salmonella enterica* serovar Typhimurium. *BMC microbiol.* 13, 115.
- (46) Jones, E. A., McGillivray, G., and Bakaletz, L. O. (2013) Extracellular DNA within a nontypeable *Haemophilus influenzae*-induced biofilm binds human beta defensin-3 and reduces its antimicrobial activity. *J. Innate Immun.* 5, 24–38.
- (47) Das, T., and Manefield, M. (2012) Pyocyanin promotes extracellular DNA release in *Pseudomonas aeruginosa*. *PloS one* 7, e46718.
- (48) Häussler, S., and Becker, T. (2008) The *Pseudomonas* quinolone signal (PQS) balances life and death in *Pseudomonas aeruginosa* populations. *PLoS Pathog.* 4, e1000166.
- (49) Jander, G., Rahme, L. G., and Ausubel, F. M. (2000) Positive correlation between virulence of *Pseudomonas aeruginosa* mutants in mice and insects. *J. Bacteriol.* 182, 3843–3845.
- (50) Essar, D. W., Eberly, L., Hadero, A., and Crawford, I. P. (1990) Identification and characterization of genes for a second anthranilate synthase in *Pseudomonas aeruginosa*: interchangeability of the two anthranilate synthases and evolutionary implications. *J. Bacteriol.* 172, 884–900.
- (51) Christensen, G. D., Simpson, W. A., Younger, J. J., Baddour, L. M., Barrett, F. F., Melton, D. M., and Beachey, E. H. (1985) Adherence of coagulase-negative staphylococci to plastic tissue culture plates: a quantitative model for the adherence of staphylococci to medical devices. *J. Clin. Microbiol.* 22, 996–1006.
- (52) O'Toole, G. A., Pratt, L. A., Watnick, P. I., Newman, D. K., Weaver, V. B., and Kolter, R. (1999) Genetic approaches to study of biofilms. *Methods Enzymol.* 310, 91–109.
- (53) Frei, R., Breitbach, A. S., and Blackwell, H. E. (2012) 2-Aminobenzimidazole derivatives strongly inhibit and disperse *Pseudomonas aeruginosa* biofilms. *Angew. Chem. Int. Ed. Engl.* 51, 5226–5229.
- (54) Elbing, K., and Brent, R. (2002) Media preparation and bacteriological tools, in. *Curr. Protoc. Mol Biol.* (Taylor, G. P., Ed.), pp 1.1.1-1.1.7, John Wiley & Sons, New York.
- (55) Allesen-Holm, M., Barken, K. B., Yang, L., Klausen, M., Webb, J. S., Kjelleberg, S., Molin, S., Givskov, M., and Tolker-Nielsen, T. (2006) A characterization of DNA release in *Pseudomonas aeruginosa* cultures and biofilms. *Mol. Microbiol.* 59, 1114–1128.
- (56) Ghafoor, A., Hay, I. D., and Rehm, Bernd H A (2011) Role of exopolysaccharides in *Pseudomonas aeruginosa* biofilm formation and architecture. *Appl. Environ. Microbiol.* 77, 5238–5246.

- (57) Lembre, P., Lorentz, C., Di, Martino, P. (2012) Exopolysaccharides of the Biofilm Matrix: A Complex Biophysical World, in *The Complex World of Polysaccharides* (Karunaratne, D. N., Ed.) 1<sup>st</sup> ed., pp 371–392, InTech, Rijeca.
- (58) Sule, P., Wadhawan, T., Wolfe, A. J., and Prüß, B. M. (2008) Promega Notes. *Promega Notes* ([www.promega.de](http://www.promega.de)) 99.

**Supporting Information: Appendix 7.1 F**

## 4 Final Discussion

A large number of concepts to evade antibacterial resistance are under discussion in the scientific community. The present work aimed at the identification and validation of compounds addressing new target systems. In this context, the main focus lies on three strategies. Firstly, resistance should be overcome by targeting new essential metabolic pathways (Mtb CYP121). Secondly, the host's clearance mechanism should be supported via *in vivo* intoxication of the pathogen (Mtb CYP125). Third, the emergence of resistant mutants should be avoided by the usage of an anti-virulence strategy based on the interruption of bacterial communication systems (*P. aeruginosa* *pqs* system).

### 4.1 Targeting bacterial of CYP enzymes

Most prominent CYP enzymes in context of drug discovery are human subspecies involved in xenobiotics and steroid hormone metabolism<sup>[189,190]</sup> However, the targeting of bacterial P450 enzymes is a promising new strategy for discovery of new anti-infective agents.<sup>[29,191]</sup> Especially, in case of Mtb, where a high content of these enzymes is presented, this approach could be fruitful. Manuscript **A** and **B** describe the discovery of compounds that address CYP121 and CYP125 as new potential anti-Mtb drug targets.

#### 4.1.1 Targeting CYP121 as a new antimycobacterial strategy (Manuscript A)

As described in the introduction CYP121 is essential for Mtb growth *in vitro*.<sup>[34]</sup> However, all compounds reported to bind to the enzyme have no *in cellulo* activity or show shortcomings in their pharmacokinetic or toxicity profile.<sup>[32,41,43,44,192]</sup> As **A: econazole** was shown to bind tightly to CYP121 and eradicate Mtb *in vitro* and *in vivo* it was used as a suitable positive control. Manuscript **A** aimed at the identification of compounds with an improved inhibitory profile compared to **A: econazole** as a reliable starting point for the development of new antimycobacterial agents. For this purpose a screening of an in-house CYP inhibitor library was undertaken. This library originates from projects focusing on the development of CYP17, CYP19, CYP11B1, and CYP11B2 inhibitors which are important enzymes in the human steroid hormone synthesis.<sup>[130–146]</sup> The library should accelerate the screening progress as the included compounds have privileged structure for the inhibition of CYP enzymes. A structural key element is the heterocycle with a sp<sup>2</sup>-hybridized nitrogen that is essential to coordinate the heme iron and, thus, increase affinity. Such iron coordinators are known to inhibit first steps in enzyme activation.<sup>[30,128,129]</sup> Additionally, this library provides benefits for future drug optimization, namely established synthetic routes, known pharmacological profiles, and a given drug-likeness of the compounds. The experimental work was started with the heterologous expression of CYP121 in *E. coli* K12 BL21. The correct folding was confirmed by the so-called CO-binding spectra.<sup>[193]</sup> This approach was used to identify a surrogate reductase system composed of Etp1fd (516-618) as ferredoxin and Arh1\_A18G as ferredoxin reductase. The two proteins originate

from the fungi *Schizosaccharomyces pombe*.<sup>[194,195]</sup> However, the functional HPLC-MS/MS based enzyme assay was only suitable for a qualitative prediction because of an insufficient substrate conversion. As an alternative method for the screening of the library, SPR assay was chosen. To simplify hit finding steps the compounds were divided into six classes and examples for each compound class were picked under consideration of a broad structural diversity. **A: econazole** as a literature-described tight binder to CYP121 with activity against Mtb was applied as a positive control.<sup>[34]</sup> SPR screening resulted in 44 binders with a similar affinity to CYP121 than that of **A: econazole**, which is in accordance with a hit rate of 33%. (Manuscript **A: Figure 2.**) This high hit rate could be due to fact that CYP121 has a large substrate pocket (1350 Å<sup>3</sup>).<sup>[34]</sup> This favours the binding of a high diversity of structures. However, with this SPR screening, a binding outside of the pocket could not be excluded. To further characterize binding behaviour the heme binding assay was used. Only compounds out of classes I and II coordinated to the heme iron and showed a type II binding (Manuscript **A: SI Table 1.**). The results indicate a binding of the other classes in a different orientation to the enzyme. This could be used for future optimization e.g. linking of two classes. As heme coordination is correlated with an inhibition of the enzyme activation steps and high affinity further investigations are focused on heme coordinators.<sup>[30]</sup> This fact increases the chance of identifying an inhibitor in a more streamlined process. On top of that, this information was used in a docking of the best heme coordinator to gather information about the binding position in the pocket. The best compounds concerning affinity were identified in class I (**A: I:16** K<sub>D</sub> = 1 μM). In class II, most compounds only showed a moderate K<sub>D</sub>. A more detailed look at the results guided a first prediction of the relationship between binding and ligand structure. In case of the linearized class I compounds, an exchange of the interconnecting phenyl groups by a pyridinyl ring resulted in a non-binder (**A: I:1**). The same observation was made for the replacement of the heme-coordinating imidazolyl group by a benzimidazolyl (**A: I:33**). In addition, regioisomers show differences in their affinity (**A: I:15**, **A: I:30**, **A: I:32**). The *para*-benzodioxine substituent of **A: I:48** and the *para*-benzodioxole substituent of **A: I:47** increased affinity. The same was true for the two phenyl substituents linked to the middle ring (**A: I:16**) (**Figure 17.**). Docking of **A: I:47** suggested that the 1,3-benzodioxol motif is oriented into a hydrophilic subpocket. A further narrow subpocket near to the 1,3-benzodioxol provides opportunity for a possible extension of the molecule (Manuscript **A: Figure 4.**) These results can support further optimization as they give first information about the tolerated chemical space of CYP121.

To check for *in cellulo* activity *Mycobacterium bovis* BCG (BCG) was chosen as a literature-described surrogate for Mtb.<sup>[196]</sup> Both organisms share 100% identity in the CYP121 amino acid sequence (Manuscript **A: SI section 14**). In the cellular setting, compound class II showed almost no activity. This could be due to unexpected problems with the penetration or efflux. These findings are in contrast to the results of class I, where a correlation between binding to CYP121 and activity towards BCG could be observed (Manuscript **A: Table 1**). Non-binders show no (**A: I:1**, **A: I:33**), moderate

binders a moderate (**A: I:15**, **A: I:30**, **A: I:32**), and strong binders high antimycobacterial activity in the assay (**A: I:16**, **A: I:47**, **A: I:48**). This gave a first evidence for CYP121 as the main target for class I compounds. As the results for human pathogen Mtb and BCG surrogate correlated well, suitability of the model organism was confirmed. **A: I:16**, **A: I:47** and **A: I:48** were identified to be more active than the positive control **A: econazole**. The frontrunner compound **A: I:47** was measured with an MIC (BCG assay: 50% inhibition) value on BCG of 0.3  $\mu\text{g/mL}$  and an MIC (Mtb assay: 90% inhibition) value on Mtb of 0.3  $\mu\text{g/mL}$  (Manuscript **A: Table 1**). Furthermore, inhibition of CYP121 enzyme reaction by **A: I:47** could be confirmed in an LC-MS/MS-based assay strengthening CYP121 inhibition as mode of action.

A structural similarity between class I compounds and **A: econazole** is obvious. As **I:47**, **I:48** and **I: 16** have improved efficiency against Mtb it could be interesting whether there are additional advantages in the toxicity and selectivity profiles. **A: I:47** showed a 45-fold decreased toxicity to HEK293 cells and Hep2G cells. This underlines the improved pharmacological profile of **A: I:47** towards **A: econazole**. To get more information about mode of action and selectivity, compounds were also examined for their antimicrobial activity on bacteria lacking CYP enzymes (*E. coli* TolC and *S. aureus* Newman).<sup>[30,33]</sup> Almost no activity was observed for **A: I:47** and **A: I:48**. Here, selectivity for mycobacteria was demonstrated, which emphasises CYP-targeting strategy. The weak antibiotic effect of **A: econazole** and **A: I:16** could be explained by a possible inhibition of flavohemoglobin and indicates a possible unselectivity of a space-demanding, lipophilic residue.<sup>[197]</sup> As **A: I:47** showed almost no inhibition of aromatase (CYP19) and only a moderate IC<sub>50</sub> on CYP17 the compound seems to be a good starting point for selectivity optimization towards human CYP enzymes. The combination of promising biological activities, high ligand efficiency (LE: value that correlates affinity with the size of a compound to predict the potential of this ligand for optimization<sup>[198]</sup>), and physicochemical properties that fulfil “Lipinski” criteria makes **A: I:47** a candidate for future development processes.

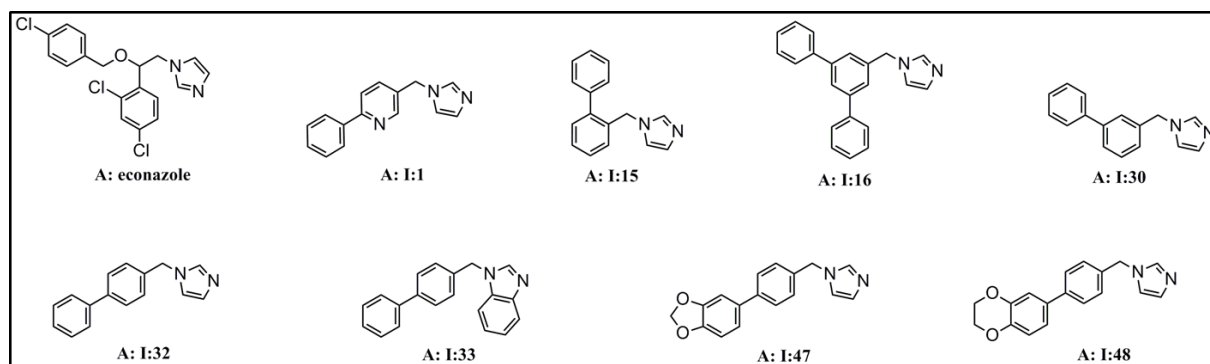


**Figure 17.** Structures of important class I compounds used for the determination of simple structure-binding-relationship and *in vitro* – *in cellulo* correlation. (Source code of the compounds - first: letter of publication/manuscript; second: structure description in the publication/manuscript)

#### 4.1.2 Blockage of cholesterol metabolism induces *in vivo* intoxication (CYP125) (Manuscript B)

CYP125 catalyses the conversion of **B: cholest-4-en-3-one** as a toxic intermediate in the cholesterol metabolism of Mtb. An inhibition of its conversion leads to an intoxication of Mtb inside of macrophages, which promotes a lower *in vivo* pathogenicity and persistence.<sup>[52]</sup> However, proof of principle for pharmacological intervention using a specific compound has not been reported until now. To support reliability of this strategy and identify antimycobacterials with a new mode of action the identification of the first compounds with high affinity to CYP125 is described in Manuscript B. This serves as a promising starting point for further studies. Initial SPR screening was performed using aforementioned in-house library and **B: econazole** as positive control.<sup>[131,133–138,142–146,199]</sup> The SPR screening resulted in a hit rate of 17% (**Figure 18.**).

More detailed hit characterization (Binding mode and  $K_D$  values) was made by UV/Vis heme binding assay system. **B: LP10** was included as a weak CYP125 inhibitor with a special reversed type I binding profile. Reversed type I spectra result from an increased low-spin absorbance band at 420 nm combined with an indirect compound-iron interaction.<sup>[148]</sup> In contrast to results observed for CYP121, so called “type I binders” were identified here as well. These are known to interact with heme iron via a water-bridged mechanism.<sup>[30]</sup> It was hard to differentiate between type II and reversed type I binders as only slight differences in absorbance maxima were observed. To facilitate discussion the compounds were named “type II binders”. Further studies should include necessarily X-ray crystallography or more sensitive spectroscopy to elucidate true binding mode of these compounds. Binders with the lowest  $K_D$  values were obtained in the phenylethoxybenzene (**B: C24**: type I,  $K_D = 0.260 \mu\text{M}$ ), 4-benzylpyridine (**B: C127**: type II,  $K_D = 0.850 \mu\text{M}$ ; **B: C128**: type II,  $K_D = 0.084 \mu\text{M}$ ; **B: C130**: type II,  $K_D = 0.174 \mu\text{M}$ ) and 1-benzyl-1*H*-benzo[*d*]imidazole (**B: C60**: type I,  $K_D = 0.280 \mu\text{M}$ ) class (Manuscript B; **Table 1.**). These compounds demonstrate a higher affinity than positive control **B: LP10** ( $K_D = 6.1 \mu\text{M}$ ) and **B: econazole** ( $K_D = 0.941 \mu\text{M}$ ). Furthermore, there is also a tighter binding compared to natural substrate **B: cholest-4-en-3-one** ( $K_D = 4.6 \mu\text{M}$ ). This indicates a sufficient inhibition of enzyme reaction by these compounds. Having a look at the SPR and the heme assay data it is possible to define simple structure-binding-relationships for the different classes. (Manuscript B; **SI Table 1.**) The 4-(indolin-5-yl)isoquinoline/ 3-(indolin-5-yl)pyridine are non-coordinators and seem to interact with the enzyme at a different binding site. In case of 3,4-dihydroquinolin-2(1*H*)-one two SPR binders could be identified but only **B: C 80** is a weak heme interactor. Isonicotinamide/ retroamide class compounds have certain similarity to **B: LP10** but possess a lower affinity to CYP125. The imidazolyl head group of methylimidazole seems not to be favourable for a CYP125 interaction with exception of **B: econazole** ( $K_D = 0.941 \mu\text{M}$ ). A comparison of **B: C23** and **B: C24** shows that a different position of the head group nitrogen results in a 5-fold increased activity of **B: C24**. It could be suggested that an unfavourable angle or distance to the interacting water leads to a loss of affinity in the phenylethoxybenzene class. In the 1-benzyl-1*H*-benzo[*d*]imidazole class, the highest affinities were obtained for **B: C60**. The replacement of the



methyl substituent by a phenyl ring may introduce a new interaction or lead to an entropy gain by the release of unfavourable water molecules. **B: C128** could be found as best binder in the 4-benzylpyridine class. Here the p-hydroxyphenyl (**B: C128**:  $K_D = 0.084 \mu\text{M}$ ) showed increased binding affinity in comparison to p-fluorophenyl group (**B: C129**:  $K_D = 1.340 \mu\text{M}$ ). Probably, the hydroxyl group forms a new interaction or an electron-rich aromatic system is preferred.

To get a reliable starting point for the proof of principle the compounds have to be selective for CYP125. However, in Mtb lab strain, a bypass enzyme, CYP142, was found.<sup>[49]</sup> In an experimental setup based on the the latter strain, this enzyme has to be included in the considerations and a dual inhibition of CYP125 and CYP142 would be desirable. A CYP121 inhibition could be interesting for a dual inhibitor strategy but is undesired for a proof of principle study. First of all, comparing the hits of CYP125 SPR screening with the results from the CYP121 project, differences in the structures are clearly recognizable. Hence, it could be concluded that CYP125 binding pocket accepts different structures as binders than CYP121 does. This offers a good starting point for a selectivity optimization. Furthermore, hit compounds tested in the UV/ Vis assay showed different selectivity profiles towards CYP142 and CYP121 (Manuscript **B**; **Table 1**). Best hit **B: C128** binds in the low nanomolar range to CYP142 (**B: C128**:  $K_D = 0.008 \mu\text{M}$ ), which most likely leads to complete inhibition of the cholesterol metabolism. For a prospective hit optimization process, it was important to compare the selectivity against human P450. **B: C128** inhibits CYP17 ( $IC_{50} = 0.248 \mu\text{M}$ ), CYP11B1 ( $IC_{50} = 0.928 \mu\text{M}$ ), CYP11B2 ( $IC_{50} = 0.515 \mu\text{M}$ ), and CYP3A4 ( $IC_{50} = 0.668 \mu\text{M}$ ) in the high nanomolar range. The  $K_D$  values on the Mtb enzymes are lower than the  $IC_{50}$  values to the human P450 (Manuscript **B**; **Table 2**). However,  $K_D$  values are typically lower than  $IC_{50}$  and variations in the test systems must be taken into account.<sup>[200]</sup> The results should be treated as a first hint for selectivity and have to be investigated more intensively. As physicochemical properties of **B: C128** are in accordance to Lipinski's rule of five and the compound combines good LE with promising biological profile they could be a good starting point for a new therapeutic strategy. Nevertheless, it has to be mentioned that the proof of principle is still not finalized.

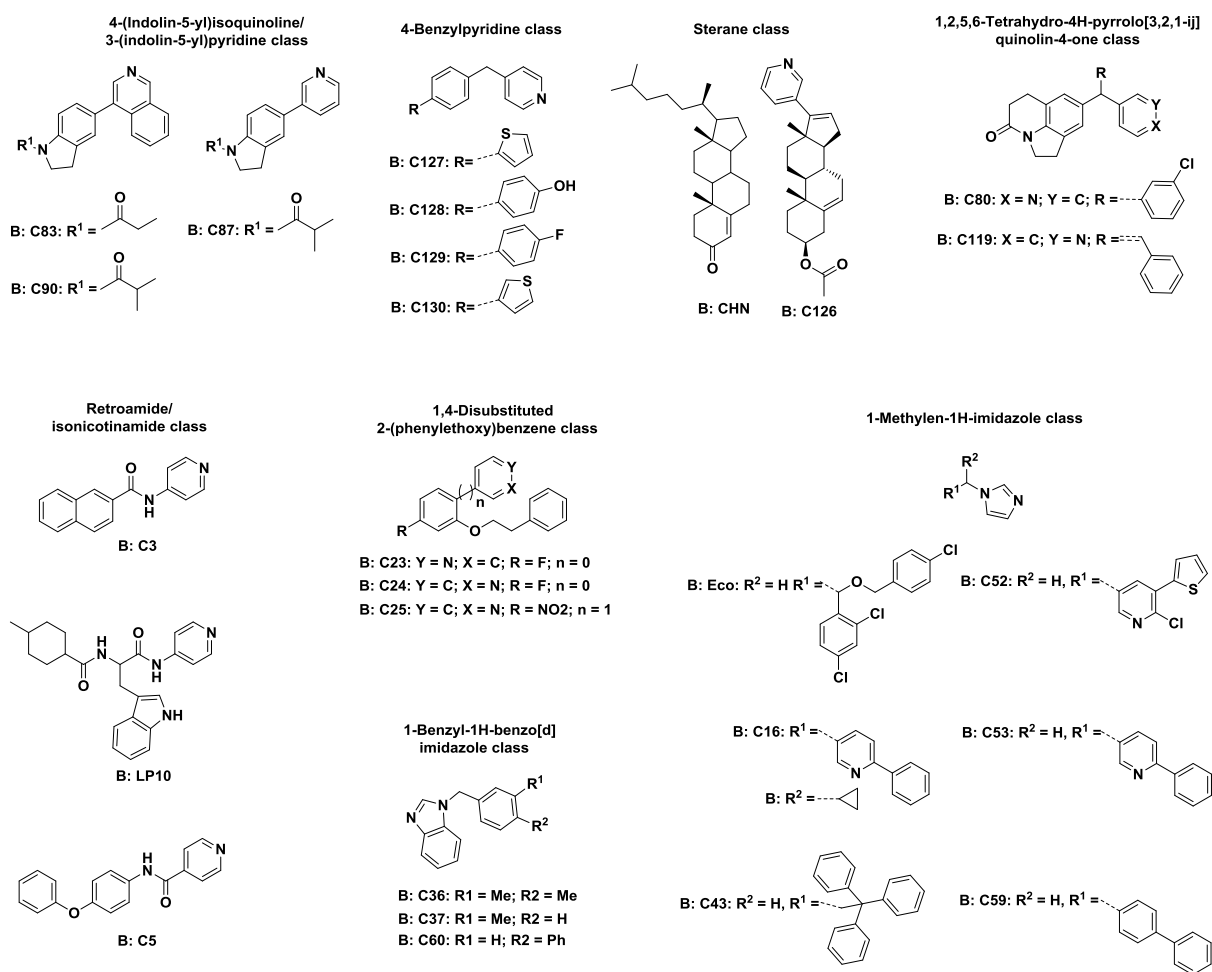


**Figure 18.** Hit compounds identified in the SPR screening of CYP125. The compounds are sorted in 8 classes considering structural similarities (Source code of the compounds - first: letter of publication/manuscript; second: structure description in the publication/manuscript)

## 4.2 Interrupting pqs system as anti-virulence and -biofilm strategy (Publications: C-E)

Targeting the *pqs* system as a strategy to lower pathogenicity without affecting viability was widely discussed as a suitable approach to avoid and overcome *P. aeruginosa* resistance. PqsD is a key enzyme in the biosynthesis of the major *pqs* signalling molecules HHQ and PQS.<sup>[93]</sup> An interruption of the signal molecule production was shown to lower *in vivo* pathogenicity of *P. aeruginosa*.<sup>[201]</sup> These findings motivated design of four PqsD inhibitors classes (2-benzamidoic acid derivatives, (2-nitrophenyl)methanol derivatives, ureidothiophene-2-carboxylic acids; 2-sulfonylpyrimidines) (**Figure 19a**). The (2-nitrophenyl)methanol derivatives as a prime example were shown to inhibit signal molecule production and biofilm formation without affecting cell viability.<sup>[91]</sup> In accordance to the latter group of PqsD inhibitors, the 2-sulfonylpyrimidines showed promising effects on *P. aeruginosa* biofilm. These are *in vitro* inhibitors of the enzyme reaction and block biofilm formation (Submitted to ChemMedChem.: Manuskript is not included in the Thesis).

An additional strategy to block the influence of the *pqs* system on virulence factor expression is to antagonize the receptor (PqsR) function (**Figure 19c**). Here, three classes of antagonists were identified, which inhibit pyocyanin production and lower signal molecule biosynthesis. The 2-amino-oxadiazoles originating from fragment screening showed effects on PQS signalling and interrupted pyocyanin production.<sup>[202]</sup> Same effects were observed for a second fragment derived from hydroxamic acid.<sup>[180]</sup> Both compound classes were potent antagonists of PqsR in a reporter gene assay indicating the receptor to be the main target.<sup>[180,202]</sup> The most potent compound was obtained by the modification of signal molecules.<sup>[203]</sup> This compound did not only inhibit virulence factor production in the low micro-molar range but also lowered the pathogenicity of *P. aeruginosa* in a *Galleria mellonella* infection model.<sup>[204]</sup> However, the quinolone derivatives suffer from a poor solubility.<sup>[205]</sup> Results of other working groups demonstrated the efficiency of PqsR antagonists in mouse models achieving lower persister cell formation and blocking biofilm development.<sup>[74,92]</sup> Publication **F** depicts the development of first dual PqsD/PqsR inhibitors as compounds providing a broad spectrum of biological effects on *P. aeruginosa*. Those compounds derived from the 2-sulfonylpyrimidines class did not only inhibit pyocyanin production but also pyoverdinin and biofilm formation (**Figure 19b**). Furthermore, a decreased virulence of *P. aeruginosa* in the aforementioned *G. mellonella* infection model was observed.

All these findings justify a more detailed investigation on PqsD, PqsR, and dual inhibitors. Publications contributing to this thesis described binding mode analysis of PqsD inhibitors (2-benzamidoic acid derivatives, (2-nitrophenyl)methanol derivatives, ureidothiophene-2-carboxylic acids) in chapter **4.4.1** (Publication: **C – E**) and biofilm interference of dual inhibitors (2-sulfonylpyrimidines) in chapter **4.4.2** (Publication: **F**).

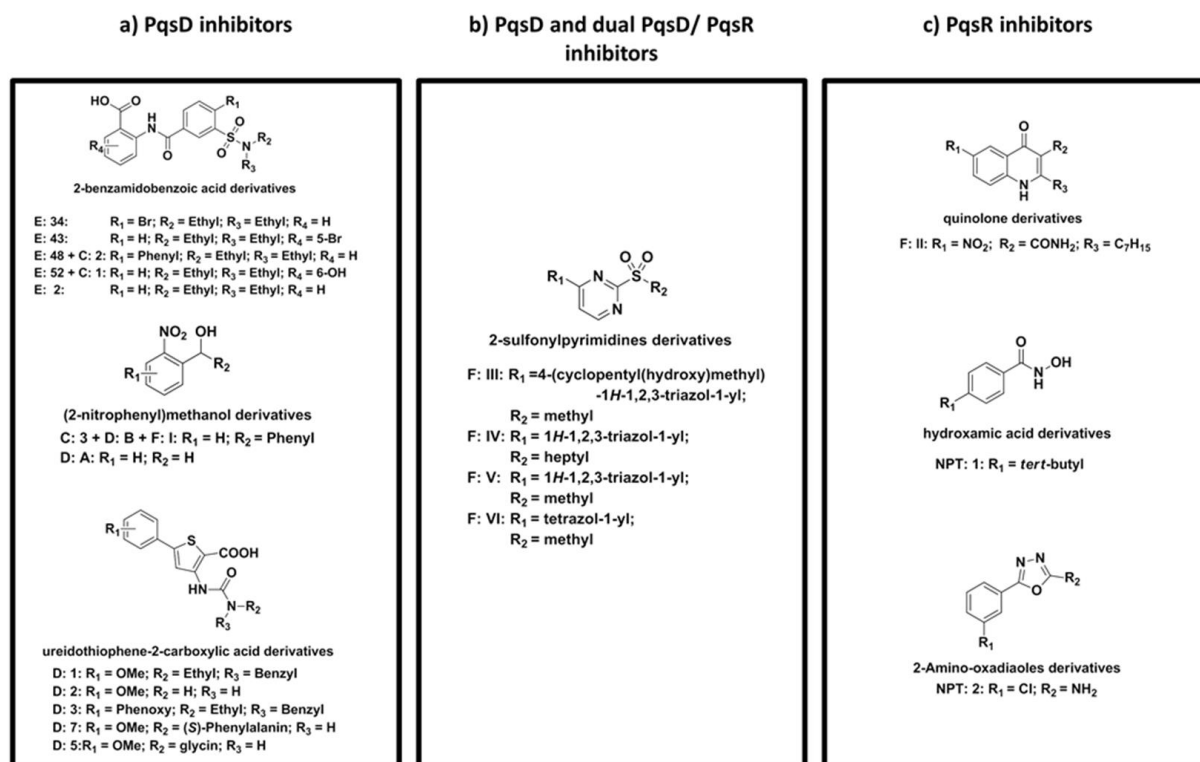


**Figure 19.** Overview of compounds designed to interfere with the *pqs* system and discussed as a part of the thesis. (Source code of the compounds - first: letter of publication; second: structure description in the publication)

#### 4.2.1 Biophysical methods in the prediction of binding modes

Publications C - E describe in detail, how a combination of biophysical methods and site-directed mutagenesis can be used to validate docking poses of PqsD inhibitors. Although crystal structures of PqsD, a PqsD (Cys112Ala) mutant and co-crystal structures with ACoA were available, it was not possible to co-crystallize the enzyme with an inhibitor.<sup>[95]</sup> This fact makes a structure-based optimization process more complicated. This prompted us to use the aforementioned combinatorial approach consisting of biophysical methods, site-directed mutagenesis, and molecular docking as an alternative solution. Similar approaches were already described in our working group.<sup>[180]</sup> Following chapters discuss the different PqsD inhibitor classes in detail with a focus on prediction of their binding modes. As these approaches helped to elucidate binding mode of 2-benzamidoic acid derivatives, (2-nitrophenyl)methanols, and ureidothiophene-2-carboxylic acids they could be used for further classes of PqsD inhibitors. Furthermore, the utilized techniques have a broad applicability (see Introduction) and thus, these studies can be exemplary for other target enzymes. Although such techniques cannot entirely replace a co-crystal structure, they have some advantages. For example in comparison to X-ray crystallography, all experiments are performed in solution, which is closer to the real biological state.<sup>[206,207]</sup>

#### 4.2.1.1 2-benzamidobenzoic acids (Publication: E)

The benzoic acid derivatives were previously described to be inhibitors of FabH.<sup>[208]</sup> Thus, the aforementioned homology of PqsD and FabH assumed this compound class to inhibit both enzymes. This could be confirmed in an *in vitro* assay resulting in compound **E: 34** as a starting point for optimization.<sup>[209]</sup> Here, binding mode was investigated by the combination of SPR, ITC, NMR, and site-directed mutagenesis. The starting point was a binding pose prediction of compound **E: 2** (unsubstituted derivative of **E: 34**) by molecular docking that suggested three possible orientations of the molecule in the PqsD substrate pocket. First binding pose defined a positioning of the benzoic acid moiety within the catalytic centre (pose 1), the second pushed this moiety more in the substrate channel (pose 2), and a third pose rotated the compound by 180 degrees in the pocket (pose 3) (Publication: **E (Figure 16.)**). To define the most probable position, a specific application of the aforementioned methods was necessary. First, PqsD was linked to an SPR chip. This was followed by incubation with substrate to form the covalent anthraniloyl-PqsD-complex, which blocks amino acid residues of the catalytic centre. As a result, the 2-benzamidobenzoic acids were still able to bind to this complex. The simple experiment excludes interactions with the amino acids near the catalytic residues and, therefore, the docking pose 1. In a second experiment, three derivatives (**E: 34**, **E: 43**, and **E: 48**) decorated with substituents differing in size at 5-position of the benzoic acid were tested for their affinity to three PqsD mutants (Ser317Phe, Cys112Ala, and His257Phe). The mutated amino acids include residues of the catalytic centre. Only for compounds with a space-demanding substituent (**E: 43**: 5-Br, **E: 48**: 5-Phen), the SPR binding response decreased. This confirms the binding of benzoic acids in the substrate channel and excludes docking pose 3. The result was verified via a so-called saturation-transfer difference (STD)-NMR experiment, which determines distances from the ligand's protons to the pocket.<sup>[210]</sup> The ethyl groups in R<sub>1</sub> and R<sub>2</sub> possess the weakest contacts to the enzyme pocket indicating an interaction of these groups with amino acids near the pocket edge. Altogether, these studies gave evidence for pose 2 to be the most likely one (**Figure 20. c, d**). In the following optimization processes, this docking pose should facilitate compound derivatization. Furthermore, an ITC experiment using **E: 48** showed a more pronounced entropic binding to PqsD ( $\Delta G = -7.2$  kcal/mol,  $\Delta H = -2.3$  kcal/mol,  $-T\Delta S = -5.0$  kcal/mol). The determined K<sub>D</sub> value (5.0  $\mu$ M) correlates with the IC<sub>50</sub> value (3.0  $\mu$ M) of the compound and a confirmed 1:1 stoichiometry. This excludes a binding by, for example, an accumulation. All in all, 64 derivatives were synthesized in 2-benzamidoic acids class resulting in compound **E: 52** as the frontrunner compound with an IC<sub>50</sub> of 1.2  $\mu$ M. However, this class was not able to efficiently reduce signal molecule production *in cellulo*. The observation could be explained by an insufficient cell penetration, a compound efflux, or an enzymatic modification by *P. aeruginosa* enzymes, as observed for other QSIs.<sup>[204]</sup>

#### 4.2.1.2 (2-nitrophenyl)methanols (Publication: C)

In contrast to the benzamidoic acids, the (2-nitrophenyl)methanol derivatives were shown to exhibit an *in cellulo* effect. The latter compounds arose from an approach, which aimed at the development of

transition state analogues. However, only compounds with a nitrophenyl moiety were able to inhibit PqsD enzyme reaction *in vitro*. Most efficient enzyme inhibitor **C: 3** with an  $IC_{50}$  of 3.2  $\mu\text{M}$  also showed a reduction of HHQ and PQS at 250  $\mu\text{M}$  in a whole cell setup and block the formation of *P. aeruginosa* biofilm at a concentration of 500  $\mu\text{M}$  without having an effect on cell viability.<sup>[91]</sup>

For a more straightforward optimization and to find an explanation for the different *in cellulose* profiles of the two PqsD inhibitor classes ((2-nitrophenyl)methanol, 2-benzamidoic acid derivatives) investigations on binding mode and inhibition kinetics were made. In the kinetic studies, **C: 2**, **C: 1**, and **C: 3** were included to consider both classes. These selected structures only slightly differ in their *in vitro*  $IC_{50}$  values (**C: 2** = 3  $\mu\text{M}$ , **C: 1** = 1.2  $\mu\text{M}$ , and **C: 3** = 3.2  $\mu\text{M}$ ), whereas only **C: 3** possesses an *in cellulose* activity. Interestingly, the kinetic experiment demonstrated obvious differences in their inhibitory profiles. Compound **C: 3** shows a time dependency of inhibition in contrast to **C: 1** and **C: 2**. In detail, a longer pre-incubation period decreases its  $IC_{50}$  value. Furthermore, recovery of enzymatic activity via filtration experiment was not possible. Such profiles indicate an irreversible or a tight binding characteristic. To exclude a covalent complex between **C: 3** and PqsD, an HPLC – ESI (electrospray ionization) – MS and a MALDI–TOF (Matrix-Assisted Laser Desorption/Ionization - Time Of Flight) experiment after tryptic digestion were performed. Both MS experiments excluded a covalent binding. The results could be important for further optimization as, in medicinal chemistry, there is always a concern about covalent inhibitors and a possible unselective binding to various biomolecular structures. This could lead to severe side effects of the compound depending on the reactivity of the functional groups.<sup>[211]</sup> Differences in the kinetic results give a hint that the (pseudo)-irreversible behaviour of (2-nitrophenyl)methanols could be important for *in cellulose* activity. Literature reports indicate a good correlation between the residence time on the target and the pharmacological outcome.<sup>[150]</sup> Nevertheless, it has to be considered that the two inhibitor classes completely differ in physicochemical properties and structure, which can have influence, for example, on the cell permeability and metabolism. A tight binding mechanism could indicate a transition state binding mode.<sup>[212]</sup>

The determination of the **C: 3** binding mode was a second part of Publication: C. Here, we primary focused on a combination of ITC, site-directed mutagenesis, and molecular docking. A previous SPR experiment using a covalent anthraniloyl – PqsD complex suggested (2-nitrophenyl)methanols to bind near the catalytic residues (Cys112 and His257). Therefore, the focus was set on amino acid mutants with polar side chains at the bottom of the pocket (Cys112Ala, Cys112Ser, Ser317Phe, Ser317Ala, Asn287Ala and His257Phe). The side chain is easier to target with mutagenesis approach as backbone interaction could only be blocked by the replacement through a proline. A negative effect of this mutation could be an influence on enzyme folding. Compound **C: 3** was always considered as a racemate ( $\Delta H = -3.47 \text{ kcal/mol}^{-1}$  and  $-T\Delta S = -3.20 \text{ kcal/mol}^{-1}$ ). As the respective enantiomers could bind in different ways we decided to separate them for the binding studies.<sup>[213]</sup> Earlier investigations concerning PqsD inhibition showed  $IC_{50}$  values of (*R*) - and (*S*) – enantiomers to be almost similar.<sup>[91]</sup>

Surprisingly, the enantiomers differed in their thermodynamic profile. Here, we could distinguish between the more enthalpy-driven binding of the (*R*) – enantiomer ( $\Delta H = -6.99 \text{ kcal/mol}^{-1}$  and  $-T\Delta S = -0.43 \text{ kcal/mol}^{-1}$ ) the entropy-driven binding of (*S*) – enantiomer ( $\Delta H = -1.11 \text{ kcal/mol}^{-1}$  and  $-T\Delta S = -5.02 \text{ kcal/mol}^{-1}$ ). However, the overall Gibbs free energy, which directly correlates with the  $K_D$ , was similar for both compounds. This can explain comparability of the  $IC_{50}$  values. A detailed overview of the results gathered from the titration of the enantiomers and mutants can be seen in Publication C (Table 1.). For the (*R*) – enantiomer a significant loss of enthalpy and Gibbs free energy can be observed measuring the interaction with Cys112Ala, Cys112Ser, Ser317Phe and His257Phe mutant. In case of Cys112 and His257, the decreased affinity can be explained with a loss of interaction partner. A decrease of  $-4$  to  $-5 \text{ kcal/mol}^{-1}$  in enthalpy could be correlated with the interruption of approximately one H-bond.<sup>[175]</sup> However, such interpretations should be made carefully as these parameters are often influenced by multiple factors.<sup>[214]</sup> The low affinity in case of the Ser317Phe mutant could be explained with a sterical hindrance as the Ser317Ala mutant shows no significant difference in the interaction profile to the wild type. This result emphasizes binding close to the serine residue. Interestingly, for all mutants leading to differences in the interaction profile the phenomenon of enthalpy-entropy compensation was observed. In theory, it could be explained by a gain of degrees of freedom after loss of a binding partner. This goes along with the compensation of a decreased enthalpy by an increased entropy contribution.<sup>[215]</sup> Such a phenomenon is often reported in literature, but its significance is still under discussion.<sup>[214]</sup> Looking at the (*S*) – enantiomer more favourable entropy upon binding was observed. The interaction profile is hard to interpret as the only significant difference could be obtained for Ser317 mutants. Docking of the (*S*) – enantiomer gives a possible explanation for the experimental results (Figure 20. b), d). The enantiomers occupy the same position in the pocket with a different orientation of the hydroxyl group (Publication: C (Figure 4.)). The nitro group forms an H-bond to the backbone of Ser317. This result is conclusive as the ITC study indicates a narrow orientation of the compound to this amino acid without having a direct interaction to the serine's hydroxyl group. Respectively, both enantiomers form a weak H-bond network to Cys112 and His257 with their hydroxyl groups.<sup>[216,217]</sup> For the (*R*) – enantiomer this is in good correlation with the experimental results. The absence of thermodynamic differences in case of the (*S*) – enantiomer when binding to the Cys112 and His257 mutant can be explained by the docking pose. The orientation of the hydroxyl group favours a compensatory interaction with Asn287, if the other amino acids are mutated. With these models in hands, a binding mode similar to a transition state mimic can be excluded (Publication C (Figure 4.)). This offers a good starting point for a structure based optimization of (2-nitrophenyl)methanol derivatives. However, as the correlation of *in vitro* and *in cellulo* activities in this class seems to be difficult further investigations have to be done to figure out the best optimization strategy.<sup>[218]</sup>

#### 4.2.1.3 Ureidothiophene-2-carboxylic acids (Publication: **D**)

Applicability of (2-nitrophenyl)methanol derivatives as a scientific tools was confirmed in the binding mode determination of the ureidothiophene-2-carboxylic acid class. This inhibitor class originates from compounds that were initially designed to inhibit RNA polymerase (RNAP). As in our anti-virulence strategy an antimicrobial effect is not desirable compound **D: 1** with R<sub>1</sub> methoxymoiety was chosen being selective to PqsD (**D: 1**: IC<sub>50</sub> (RNAP): 241 μM; IC<sub>50</sub> (PqsD): 6 μM)<sup>[219]</sup>. Binding in the substrate channel of PqsD was verified via SPR competition experiment with the ACoA. Furthermore, 1:1 stoichiometry was confirmed by ITC. Both results suggested that a docking of **D: 1** to catalytic pocket could help to predict a binding mode that might be useful for compound optimization. (Publication: **D**, **Figure 1. b**), **c**)) However, two docking poses with a similar score but reverse compound orientation were observed.

At this point, a simple SPR competition experiment including two (2-nitrophenyl)methanol derivatives (**D: B** and **D: A**) and three ureidothiophene-2-carboxylic acid derivatives (**D: 1**, **D: 2** and **D: 3**) elucidated the correct orientation (Publication: **D**, **Figure 2**). The ureidothiophene-2-carboxylic acid derivatives differ in the size of their substituents linked to methoxy or ureido moiety. As **D: 3** showed a lowered affinity to the SPR-immobilized PqsD – **D: A** - complex in contrast to compounds **D: 1** and **D: 2**, a clash of phenoxy group with **D: A** can be concluded. An additional experiment performed with the PqsD – **D: B** – complex gave more information on the distance of the methoxy - moiety to the bottom of the pocket. Competition experiment results confirm the docking pose indicating for methoxy moiety orientated towards pocket bottom. The pose was additionally validated by an SPR binding experiment with an Arg223Ala mutant indicating an interaction of this residue with the ureido moiety. Despite similarity to literature-described experiments, this approach is innovative in its particular design.<sup>[220]</sup> As co-crystal structures are not available for PqsD inhibitors this approach could help validating further docking poses of new compound classes. The validated docking pose of **D: 1** supported a structure-based optimization of this class.

Compound **D: 2** was chosen as a starting point due to promising LE. As the docking pose indicated possible interaction partners on the top of the channel, substituents linked to the ureido part of the molecule were subsequently introduced. Different (*S*)-configured α – amino acids showed decreased IC<sub>50</sub> values in comparison to starting compound **D: 1**. This is especially observed in case of **D: 7** with an IC<sub>50</sub> of 0.5 μM (**Figure 20. a**), **d**)). Our docking pose revealed Arg262 as the possible interaction partner, which is positioned in close proximity to the ureido moiety. The introduction of a carboxylic acid with a methylene linker decreased IC<sub>50</sub> from 170 μM (**D: 2**) to 7 μM (**D: 5**). Here, the docking pose confirmed the establishment of an interaction with Arg262. A narrow cleft provided potential to increase affinity using substituents that sufficiently occupy this part of the protein. As predicted in the docking pose, only (*S*) - amino acids were able to target this position leading to an affinity gain. The improved IC<sub>50</sub> of compound **D: 7** was most likely achieved by the formation of a sandwich complex between Arg223, Phe226, and the phenylalanine moiety (Publication: **D**, **Figure 4. c**)). In an STD-



NMR experiment using compound **D: B** and **D: 7**, it was shown that the (2-nitrophenyl)methanol derivatives could be displaced by the ureidothiophene-2-carboxylic acid class confirming the initially determined binding mode also for the optimized compound. An additional benefit of the amino acid derivatives is the decreased  $\text{clogD}_{7,4}$  value (**D: 7**:  $\text{clogD}_{7,4} = 0.59$ ), which could possibly improve permeation into Gram-negative bacterial cells.<sup>[221]</sup>

All in all, the experimentally validated docking pose supported a more straightforward improvement of this class. For example, a covalent binder that selectively targets Cys112 could be synthesised based on the docking. This could possibly help to gain *in cellulosa* activity via optimized kinetic behaviour. Furthermore, a linkage of the (2-nitrophenyl)methanols and ureidothiophene-2-carboxylic acids increasing *in vitro* efficiency was possible due to detailed docking pose. However, all optimizations concerning *in cellulosa* activity were not successful.<sup>[219]</sup>

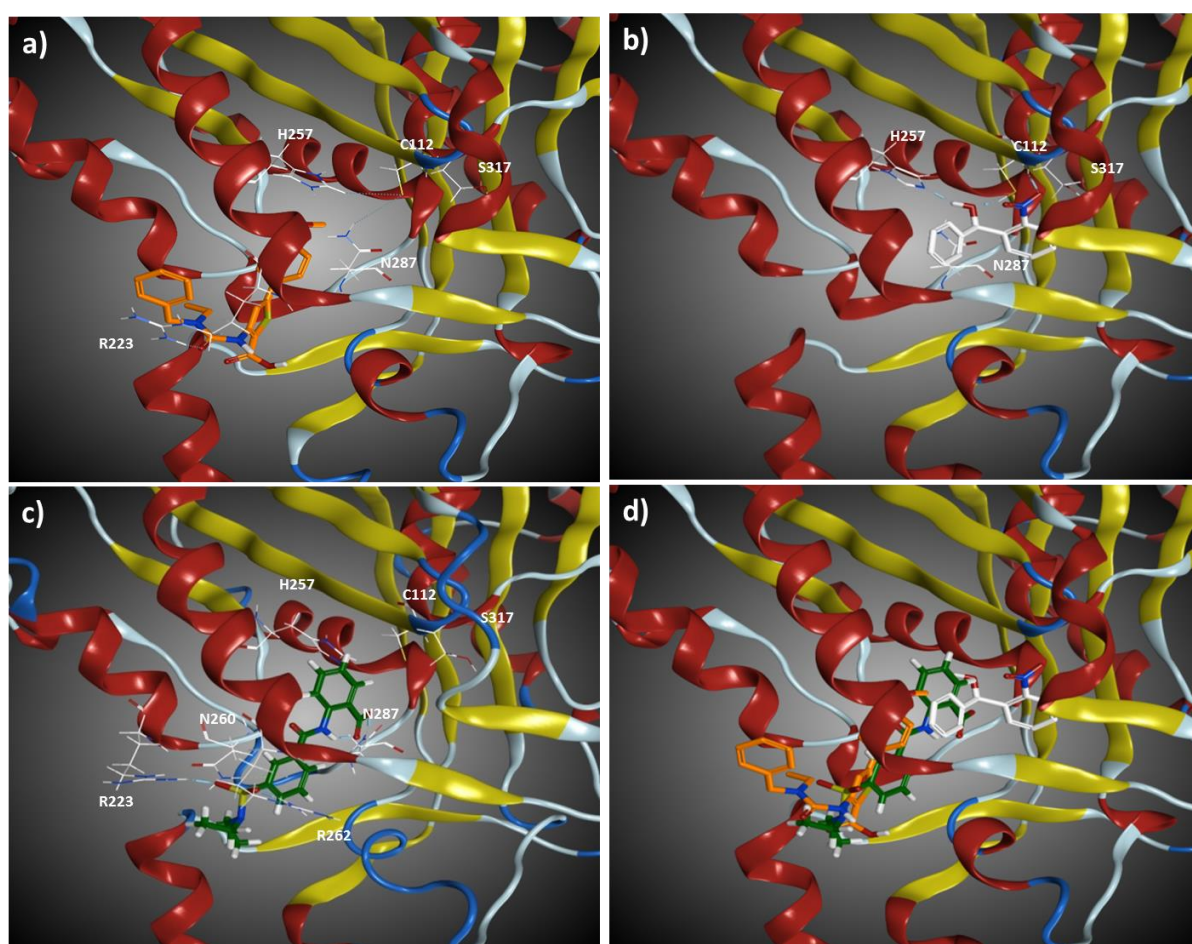


**Figure 20.** All figures represent experimentally validated docking poses of different PqsD inhibitor classes. **a)** Ureidothiophene-2-carboxylic acids (Publication: **D**); **b)** (2-nitrophenyl)methanols (Publication: **C**); **c)** 2-benzamidobenzoic acids (Publication: **E**); **d)** Overlay of the three docking poses.

#### 4.2.2 Targeting biofilm as a bacterial lifestyle in chronic infections (Publication: **F**)

Other in-house PqsD, PqsR, and dual PqsD/PqsR inhibitor classes showed improved *in cellulosa* activity profiles. PqsR antagonists like **F: II** ( $\text{IC}_{50}$  (pyocyanin) = 2  $\mu\text{M}$ ), **NPT: 1** ( $\text{IC}_{50}$  (pyocyanin) = 87  $\mu\text{M}$ ),

and **NPT: 2** (IC<sub>50</sub> (pyocyanin) ~ 250 μM) inhibit the production of pyocyanin, an important virulence factor. <sup>[180,202,204,222,223]</sup> Additionally, compound **F: II** blocks the formation of the signal molecules HHQ and PQS, which is in agreement with the auto loop theory. <sup>[204]</sup> However, influence on biofilm formation was only observed for **F: I** at a high concentration. <sup>[91]</sup> As described in the introduction, biofilm in combination with persister cell formation plays a crucial role in chronic *P. aeruginosa* infections. Furthermore, the *pqs* system is known to have a control function on biofilm development. <sup>[83,88–90]</sup> In preliminary studies, compounds **F: II**, **NPT: 1**, and **NPT: 2** showed certain effects on biomass and eDNA (data not shown).

However, here, the focus is on the 2-sulfonpyrimidine derivatives, which were described in Publications **F** and **G**. The development of dual PqsD/ PqsR inhibitors originated from the observation that a combination of **F: I** with **F: II** enhances the inhibitory efficiency on pyocyanin even though **F: I** displays no anti-pyocyanin effects. Two library compounds out of the 2-sulfonpyrimidine class selective for PqsR antagonism (**F: III** IC<sub>50</sub> on PqsR: 26 μM; 10% PqsD inhib. at 50 μM; 61% pyocyanin inhib. at 400 μM) and PqsD inhibition (**F: IV**: no PqsR antagonism at 50 μM; IC<sub>50</sub> on PqsD: 1.7 μM; no pyocyanin inhib. at 100 μM) were merged to a dual inhibitor (**F: V**: IC<sub>50</sub> on PqsR: 25 μM; IC<sub>50</sub> on PqsD: 23 μM; 75% pyocyanin inhib. at 400 μM). A further optimization step resulted in compound **F: VI** (IC<sub>50</sub> on PqsR: 15 μM; IC<sub>50</sub> on PqsD: 21 μM; IC<sub>50</sub> on pyocyanin: 86 μM). Besides the inhibitory potential on pyocyanin, compound **F: VI** was also able to reduce production of pyoverdine, another virulence factor that plays a crucial role in iron acquisition and acute pathogenicity of *P. aeruginosa*. <sup>[79,224]</sup> In accordance to the reduced production of virulence factors *in vitro*, compound **F: VI** shows a concentration-dependent decrease of pathogenicity in an *in vivo* *G. mellonella* model. <sup>[225]</sup> The model is mostly correlated to the acute stage of *P. aeruginosa* infection. <sup>[226]</sup>

A second major issue is the chronic *P. aeruginosa* infection, which is linked to a biofilm lifestyle. That reason makes it interesting to see whether the compounds have an effect on biofilm. Thus, a crystal violet (CV) assay system was established to determine the whole biomass in a 96 well set-up. <sup>[227]</sup> Both, the  $\Delta PqsR$  and the  $\Delta PqsA$  mutant, showed approximately 60% decreased biofilm volume (data not shown). For the best hit **F: VI**, an IC<sub>50</sub> of 100 μM was observed on wild type biofilm (Publication **F**, **Figure 5 A**). The effects on a  $\Delta PqsR$  mutant were determined to exclude a biofilm inhibition that is unspecifically triggered by a system other than *pqs*. A weak influence on the mutant's biofilm confirmed that the major effect is *pqs*-dependent. CV assay was extended by selective staining approaches of polysaccharides using congo red, proteins by Bradford staining, and eDNA with propidium iodide, <sup>[83,168,228]</sup> as the major components of the biofilm. <sup>[84,85]</sup> As they have various roles in biofilm stability, immune evasion, and antibiotic resistance it could be interesting to see the influence of our compounds on every single constituent. <sup>[84]</sup> At a concentration of 100 μM, **F: VI** attenuated polysaccharide, protein, and eDNA formation in biofilm down to 27±20%; 25 ±13% and 7 ±2%. Polysaccharide components are known to protect the bacteria against the influence of antibiotics and

the immune system. <sup>[229–231]</sup> Proteins like lectins are important for stability of the biofilm structure. <sup>[232]</sup> Apart from that, the most prominent effect of **F: VI** was observed on eDNA. This component shields the bacteria from an attack by antimicrobial peptides from the host, blocks aminoglycosides, and seems to play a role in fluoroquinolone resistance. <sup>[233–235]</sup> Similar effects on biomass and eDNA were shown for PqsD inhibitors of 2-sulfonpyrimidine derivatives class ((Submitted to ChemMedChem.: Manuskript is not included in the Thesis)). Furthermore, the results are in agreement with the described influence of *pqs* mutants on eDNA production. <sup>[83,90]</sup> As **F: VI** has a significant effect on all of the components, this strategy might bear the potential of making the biofilm more susceptible to environmental influences and, therefore, better to handle in a chronic infection scenario. Thus, the third variation of the assay was based on the determination of cell viability via an ATP-luciferase reaction. <sup>[236]</sup> The staining was used to check for susceptibility of biofilm to antibiotic compounds after treatment with the QS inhibitors. Bacterial life style represents a major challenge for antibiotic therapy as the biofilm is capable of decreasing the penetration rate of antibiotics. More importantly, the reduced rate of metabolism lowered the efficiency of the compounds to bacteria. For this reason an improvement of antibiotic susceptibility by a biofilm-blocking agent is desirable. <sup>[237]</sup> Ciprofloxacin (CIP) as a clinically used antibiotic to treat *P. aeruginosa* infections was included in our experimental set-up. <sup>[238]</sup> However, effects of this antibiotic on *P. aeruginosa* biofilms are controversially discussed. Gopal et al. observed a decreased effect of CIP against biofilm-encapsulated bacteria. <sup>[239]</sup> In contrast, Tanaka et al. reported a strong effect of CIP to bacteria inside of a biofilm. <sup>[240]</sup> Furthermore, there are additional results indicating a physical blockage of CIP by the biofilm. <sup>[241]</sup> In our experiment, CIP had no significant effect on *P. aeruginosa* biofilm at a concentration of 1  $\mu\text{M}$ . The **F: VI**-pre-treated biofilm, which was shown to be hindered in maturation, turned out to be more susceptible to CIP. To decide, which factor is the most crucial one for these results, more experiments have to be performed. All in all, the strategy of targeting the *pqs* system to lower biofilm formation and support antibiotic treatment seems to be reasonable.

### 4.3 New antimicrobial targets and anti-virulence strategy

Apart from the fact that the fight against resistant bacteria should begin with a more careful use of antibiotics, several strategies can be used to evade already existing resistances. <sup>[8]</sup> Three strategies were applied and discussed in this thesis. The most common approach is focusing on new targets. The goal is to overcome target – related (e.g., mutations, bypass systems) and compound-dependent (e.g., efflux, metabolism, and penetration) resistances. <sup>[10]</sup> The development of CYP121 inhibitors deals with this strategy, although a proof of principle still has to be demonstrated. In future, such a compound has to be used more prudentially to circumvent rising of new resistant mutants. <sup>[8]</sup> An important criterion is already fulfilled as the CYP121 inhibitors are specific for mycobacteria. This prevents the transfer of resistance mechanisms between different bacterial species. Furthermore, toxicity to human cells and an adverse effect on symbiotic bacterial flora is excluded. <sup>[14]</sup>

With the compounds targeting CYP125, a combined approach of viability reduction and anti-virulence effects is pursued.<sup>[52]</sup> However, there are no compounds with biological effects described for this target. To estimate the relevance of the system on the resistance development and persistence more intensive investigations have to be undertaken.

The anti-*pqs* strategy aims at reducing the virulence of the bacteria without exerting a selection pressure. This approach should prevent development of new resistances. Two major problems occurred in the development of the PqsD inhibitors. These are related to phenomena often observed in anti-infective drug discovery. Firstly, compound discovery based on *in vitro* approaches can result in structures lacking *in cellulo* activity. As common rules for eukaryotic cells systems (e.g. “Lipinski’s rule of five”, which is used to estimate oral bioavailability) are not applicable to bacteria it is difficult to predict cell permeability based on physicochemical properties. Same observations were made in high throughput campaigns of pharmaceutical industry.<sup>[11]</sup> A second phenomenon was the missing effect on pyocyanin in case of the (2-nitrophenyl)methanol derivatives, although a knock-out mutant of PqsD was defective in pyocyanin production.<sup>[71]</sup> This can be explained by an insufficient activity or unknown pathways/bypass in the *pqs* system.<sup>[242]</sup> The PqsR antagonist or the dual target strategy seems to be more promising as the efficiency was proven in an *in vivo* scenario (Publication: **F**).<sup>[74,204]</sup> Whether this strategy prevents resistance development or lowers the rate of resistant mutants remains to be seen. This is a widely discussed subject in different publications as, up to now, the results are ambivalent. Reports by Gerdt et al. support the theory that the strategy of targeting quorum sensing is robust to resistance.<sup>[243]</sup> In contrast, Maeda et al. reported resistance development to a quorum sensing inhibitor.<sup>[244]</sup> Further observations support the theories of a possible resistance to quorum sensing inhibition. Whether and if they do, to what extent such mutations influence a therapy in a clinical environment has to be clarified.<sup>[245]</sup>

#### 4.4 Outlook

With the CYP121 inhibitor **A: I:47** of class I, an efficient anti-Mtb agent exhibiting a decreased toxicity and a selectivity against mycobacteria was identified. As a lot of derivatives of class I were not considered in the present study (Manuscript **A**) their efficiency to CYP121 and Mtb has to be tested. This should support the determination of a structure-activity-relationship and gather more information on the *in vitro* / *in cellulo* correlation. In this context, an advancement of the LC-MS/MS-based functional assay can support this process. The results out of such studies could be used for compound optimization especially concerning selectivity towards human P450 and affinity to CYP121. Mutation studies on **A: I:47** and other derivatives can further evaluate CYP121 as the main target and give information about the mutation rate. This could prove CYP121 as a target with beneficial properties. As first tests on **A: I:47** toxicity were successful further *in vitro* pharmacokinetic and pharmacodynamic experiments, e.g. metabolic stability and permeability into macrophages, have

to be performed to get reliable starting points for a *in vivo* study with mice. In the beginning, the compounds should be tested for their efficiency to lower Mtb burden in mouse lungs as an initial experiment. Later, the compounds or an optimized derivative has to demonstrate reduction of the long term treatment in a chronic infection model.

In case of CYP125, the best hits (**B: C24**, **B: C60**, **B: C127**, **B: C128**, and **B: C130**) have to be tested for their biological effects, i.e. an *in vitro* blockage of cholest-4-en-3-one conversion, an *in cellulo* intoxication by cholesterol, and an increased clearance in infected macrophages. Further pharmacokinetic and toxicity studies have to be performed before planning an *in vivo* proof of principle in a mouse model. Selectivity optimization towards human P450 enzymes and affinity to CYP125 could be supported by testing derivatives of these compounds and obtaining a structure–activity-relationship.

Since the PqsD inhibitors are not able to sufficiently block virulence factor production, further development does not seem to be promising. However, the efficacy of a dual inhibitor strategy (2-sulfonylpyrimidines) justifies further investigations. Structural data of the different PqsD inhibitor classes can support optimization of the dual target compounds. More precisely, the approaches used for binding mode elucidation can be transferred to 2-sulfonylpyrimidines. The same applies to the biofilm assay, which can be used for testing other compound classes for activity in this important bacterial life style. Deeper investigations on the influence of biofilm blockers in chronic infection models should prove the relevance of the assay system and anti-biofilm agents.

## 5 References

- [1] Aminov R.I. *Frontiers in microbiology* (2010):134.
- [2] Ehrlich P., Hata S. Berlin: Springer (1910):978-3-642-64926-4.
- [3] Fleming A. *Bulletin of the World Health Organization* (2001):780–790.
- [4] Chopra I., Hesse L., O'Neill A. *Pharmacochemistry Library* (2002):213–225.
- [5] Daniels N. Cambridge, New York: Cambridge University Press (2008):978-0-521-69998-3.
- [6] Nussbaum F. von, Brands M., Hinzen B. et al. *Angewandte Chemie* (2006):5072–5129.
- [7] Levy S. *The Lancet* (1982):83–88.
- [8] Levy S.B., Marshall B. *Nature medicine* (2004):122–129.
- [9] WHO: World Health Organization (2014):ISBN: 978 92 4 156474 8.
- [10] Silver L.L. *Clinical microbiology reviews* (2011):71–109.
- [11] Clatworthy A.E., Pierson E., Hung D.T. *Nature chemical biology* (2007):541–548.
- [12] Alanis A.J. *Archives of Medical Research* (2005):697–705.
- [13] Fischbach M.A., Walsh C.T. *Science* (2009):1089–1093.
- [14] Lewis K. *Nature reviews. Drug discovery* (2013):371–387.
- [15] Payne D.J., Gwynn M.N., Holmes D.J. et al. *Nature reviews. Drug discovery* (2007):29–40.
- [16] Silver L.L., Bostian K.A. *Antimicrobial agents and chemotherapy* (1993):377–383.
- [17] Tripathi R.P., Tewari N., Dwivedi N. et al. *Medicinal research reviews* (2005):93–131.
- [18] Smith I. *Clinical microbiology reviews* (2003):463–496.
- [19] Sakamoto K. *Veterinary pathology* (2012):423–439.
- [20] Gengenbacher M., Kaufmann, S.H.E. *FEMS microbiology reviews* (2012):514–532.
- [21] Zumla A., Nahid P., Cole S.T. *Nature reviews. Drug discovery* (2013):388–404.
- [22] Lienhardt C., Vernon A., Raviglione M.C. *Current opinion in pulmonary medicine* (2010):186–193.
- [23] WHO: World Health Organization (2014):978-92-4-156480-9.
- [24] Connolly L.E., Edelstein P.H., Ramakrishnan L. *PLoS medicine* (2007):e120.
- [25] Lutge E., Lewin S., Volmink J. et al. *Trials* (2013):154.
- [26] Velayati A.A., Masjedi M.R., Farnia P. et al. *Chest* (2009):420–425.
- [27] Cole S.T., Brosch R., Parkhill J. et al. *Nature* (1998):537–544.
- [28] McLean K.J., Clift D., Lewis D.G. et al. *Trends in microbiology* (2006):220–228.
- [29] Ouellet H., Johnston J.B., Ortiz de Montellano P.R. *Archives of biochemistry and biophysics* (2010):82–95.
- [30] Ortiz de Montellano P. R. New York: Kluwer Academic/Plenum Publishers (2005):0-306-48324-6.
- [31] Munro A.W., Girvan H.M., Mason A.E. et al. *Trends in biochemical sciences* (2013):140–150.
- [32] Hudson S.A., McLean K.J., Surade S. et al. *Angewandte Chemie* (2012):9311–9316.
- [33] McLean K.J., Marshall K.R., Richmond A. et al. *Microbiology* (2002):2937–2949.

- [34] McLean K.J., Carroll P., Lewis D.G. et al. *The Journal of biological chemistry* (2008):33406–33416.
- [35] Belin P., Le Du M.H., Fielding A. et al. *Proceedings of the National Academy of Sciences of the United States of America* (2009):7426–7431.
- [36] Fonvielle M., Le Du M.-H., Lequin O. et al. *The Journal of biological chemistry* (2013):17347–17359.
- [37] Judd C., Engelhard D., Handsheer R. et al. *Bone marrow transplantation* (1991):295–300.
- [38] Ahmad Z., Sharma S., Khuller G.K. *FEMS microbiology letters* (2006):181–186.
- [39] Ahmad Z., Sharma S., Khuller G.K. et al. *International journal of antimicrobial agents* (2006):543–544.
- [40] Ahmad Z., Sharma S., Khuller G.K. *FEMS microbiology letters* (2006):200–203.
- [41] Korashy H.M., Shayeganpour A., Brocks D.R. et al. *Toxicological sciences an official journal of the Society of Toxicology* (2007):32–43.
- [42] Liu C.F., Lin C.H., Lin C.C. et al. *Toxicology* (2004):87–93.
- [43] Dvorak Z. *Toxicology letters* (2011):129–132.
- [44] Wood A.J.J., Como J.A., Dismukes W.E. *New England Journal of Medicine* (1994):263–272.
- [45] Sasseti C.M., Rubin E.J. *Proceedings of the National Academy of Sciences of the United States of America* (2003):12989–12994.
- [46] Rengarajan J., Bloom B.R., Rubin E.J. *Proceedings of the National Academy of Sciences of the United States of America* (2005):8327–8332.
- [47] Chang J.C., Harik N.S., Liao R.P. et al. *The Journal of infectious diseases* (2007):788–795.
- [48] Chang J.C., Miner M.D., Pandey A.K. et al. *Journal of Bacteriology* (2009):5232–5239.
- [49] Ouellet H., Guan S., Johnston J.B. et al. *Molecular microbiology* (2010):730–742.
- [50] Capyk J.K., Kalscheuer R., Stewart G.R. et al. *The Journal of biological chemistry* (2009):35534–35542.
- [51] Johnston J.B., Singh A.A., Clary A.A. et al. *Bioorganic & medicinal chemistry* (2012):4064–4081.
- [52] Ouellet H., Johnston J.B., Ortiz de Montellano P.R. *Trends in microbiology* (2011):530–539.
- [53] Pandey A.K., Sasseti C.M. *Proceedings of the National Academy of Sciences of the United States of America* (2008):4376–4380.
- [54] van Delden C., Iglewski B.H. *Emerging infectious diseases* (1998):551–560.
- [55] Gellatly S.L., Hancock, Robert E W. *Pathogens and disease* (2013):159–173.
- [56] Mesaros N., Nordmann P., Plésiat P. et al. *Clinical microbiology and infection the official publication of the European Society of Clinical Microbiology and Infectious Diseases* (2007):560–578.
- [57] Lister P.D., Wolter D.J., Hanson N.D. *Clinical microbiology reviews* (2009):582–610.
- [58] Hurley M.N., Cámara M., Smyth A.R. *The European respiratory journal* (2012):1014–1023.
- [59] Morris N., Cross A.S. *Critical care* (2008):196.

- [60] Williams P., Cámara M. *Current opinion in microbiology* (2009):182–191.
- [61] Neelson K.H., Hastings J.W. *Microbiological Reviews* (1979):496–518.
- [62] Fuqua W.C., Winans S.C., Greenberg E.P. *Journal of Bacteriology* (1994):269–275.
- [63] Miller M.B., Bassler B.L. *Annual review of microbiology* (2001):165–199.
- [64] Lee J., Zhang L. *Protein & cell* (2015):26–41.
- [65] Latifi A., Foglino M., Tanaka K. et al. *Molecular microbiology* (1996):1137–1146.
- [66] Schuster M., Greenberg E.P. *International journal of medical microbiology* (2006):73–81.
- [67] Dubern J.F., Diggle S.P. *Molecular bioSystems* (2008):882–888.
- [68] Pesci E.C., Milbank, Jared B J, Pearson J.P. et al. *Proceedings of the National Academy of Sciences of the United States of America* (1999):11229–11234.
- [69] Xiao G., Déziel E., He J. et al. *Molecular microbiology* (2006):1689–1699.
- [70] Déziel E., Lépine F., Milot S. et al. *Proceedings of the National Academy of Sciences of the United States of America* (2004):1339–1344.
- [71] Gallagher L.A., McKnight S.L., Kuznetsova M.S. et al. *Journal of Bacteriology* (2002):6472–6480.
- [72] Drees S.L., Fetzner S. *Chemistry & Biology* (2015):611–618.
- [73] Lee J., Wu J., Deng Y. et al. *Nature chemical biology* (2013):339–343.
- [74] Starkey M., Lepine F., Maura D. et al. *PLoS pathogens* (2014):e1004321.
- [75] Zaborina O., Lepine F., Xiao G. et al. *PLoS pathogens* (2007):e35.
- [76] Rada B., Leto T.L. *Immunologic research* (2009):198–209.
- [77] Rada B., Leto T.L. *Trends in microbiology* (2013):73–81.
- [78] Wretling B., Pavlovskis O.R. *Reviews of Infectious Diseases* (1983):S998.
- [79] Diggle S.P., Matthijs S., Wright V.J. et al. *Chemistry & Biology* (2007):87–96.
- [80] Meyer J.M., Neely A., Stintzi A. et al. *Infection and Immunity* (1996):518–523.
- [81] Gennip M. Van, Christensen L.D., Alhede M. et al. *Acta pathologica, microbiologica, et immunologica Scandinavica* (2009):537–546.
- [82] Kim K., Kim Y.U., Koh B.H. et al. *Immunology* (2010):578–588.
- [83] Allesen-Holm M., Barken K.B., Yang L. et al. *Molecular microbiology* (2006):1114–1128.
- [84] Wei Q., Ma L.Z. *International journal of molecular sciences* (2013):20983–21005.
- [85] Mann E.E., Wozniak D.J. *Federation of European Microbiological Societies microbiology reviews* (2012):893–916.
- [86] Alkawash M.A., Soothill J.S., Schiller N.L. *Acta pathologica, microbiologica, et immunologica Scandinavica* (2006):131–138.
- [87] Lewis K. *Annual review of microbiology* (2010):357–372.
- [88] Diggle S.P., Winzer K., Chhabra S.R. et al. *Molecular microbiology* (2003):29–43.
- [89] Diggle S.P., Stacey R.E., Dodd C. et al. *Environmental microbiology* (2006):1095–1104.
- [90] Yang L., Barken K.B., Skindersoe M.E. et al. *Microbiology* (2007):1318–1328.



- [91] Storz M.P., Maurer C.K., Zimmer C. et al. *Journal of the American Chemical Society* (2012):16143–16146.
- [92] Ilangovan A., Fletcher M., Rampioni G. et al. *PLoS pathogens* (2013):e1003508.
- [93] Dulcey C.E., Dekimpe V., Fauvelle D.A. et al. *Chemistry & Biology* (2013):1481–1491.
- [94] Hutter M.C., Brengel C., Negri M. et al. *Journal of molecular modeling* (2014):2255.
- [95] Bera A.K., Atanasova V., Robinson H. et al. *Biochemistry* (2009):8644–8655.
- [96] Madsen U., Krogsgaard-Larsen P., Liljefors T. London: Taylor & Francis (2002):0-203-30137-4.
- [97] Merz K. M., Ringe D., Reynolds C. H. Cambridge U.K.: Cambridge University Press (2010):978-0521887236.
- [98] Drews J. *Science* (2000):1960–1964.
- [99] Takenaka T. *British journal of urology International* (2001):7–10.
- [100] Topliss J.G. *Journal of medicinal chemistry* (1972):1006–1011.
- [101] Topliss J.G. *Journal of medicinal chemistry* (1977):463–469.
- [102] Hansch C. *Accounts of Chemical Research* (1969):232–239.
- [103] Blake C.C., Koenig D.F., Mair G.A. et al. *Nature* (1965):757–761.
- [104] Kendrew J.C., Bodo G., Dintzis H.M. et al. *Nature* (1958):662–666.
- [105] Swinney D.C., Anthony J. *Nature reviews. Drug discovery* (2011):507–519.
- [106] Klebe G. Heidelberg: Spektrum Akademischer Verlag (2009):978-3-8274-2046-6.
- [107] Lee C.H., Huang H.C., Juan H.F. *International journal of molecular sciences* (2011):5304–5318.
- [108] Kurogi Y., Guner O. *Current Medicinal Chemistry* (2001):1035–1055.
- [109] Wermuth C.G., Ganellin C.R., Lindberg P. et al. *Pure and Applied Chemistry* (1998):1129–1143.
- [110] Hansch C., Maloney P.P., Fujita T. et al. *Nature* (1962):178–180.
- [111] Andrews P.R., Craik D.J., Martin J.L. *Journal of medicinal chemistry* (1984):1648–1657.
- [112] Sliwoski G., Kothiwale S., Meiler J. et al. *Pharmacological reviews* (2014):334–395.
- [113] Schneider G., Fechner U. *Nature reviews. Drug discovery* (2005):649–663.
- [114] Verlinde C.L., Hol W.G.J. *Structure* (1994):577–587.
- [115] Whittle P.J., Blundell T.L. *Annual review of biophysics and biomolecular structure* (1994):349–375.
- [116] Chilingaryan Z., Yin Z., Oakley A.J. *International journal of molecular sciences* (2012):12857–12879.
- [117] Hughes J.P., Rees S., Kalindjian S.B. et al. *British journal of pharmacology* (2011):1239–1249.
- [118] Schenone M., Dančik V., Wagner B.K. et al. *Nature chemical biology* (2013):232–240.
- [119] Fox S., Farr-Jones S., Sopchak L. et al. *Journal of biomolecular screening* (2006):864–869.
- [120] Zang R., Li D., Tang I.C. et al. *International Journal of Biotechnology for Wellness Industries* (2012):31–51.
- [121] Bisswanger H. *Perspectives in Science* (2014):41–55.

- [122] Michelini E., Cevenini L., Mezzanotte L. et al. *Analytical and bioanalytical chemistry* (2010):227–238.
- [123] Walters W.P., Namchuk M. *Nature reviews. Drug discovery* (2003):259–266.
- [124] Sittampalam G.S., Kahl S.D., Janzen W.P. *Current Opinion in Chemical Biology* (1997):384–391.
- [125] Jong L.A.A. de, Uges D.R.A., Franke J.P. et al. *Journal of chromatography. B, Analytical technologies in the biomedical and life sciences* (2005):1–25.
- [126] Schenkman J.B., Estabrook R.W., Remmer H. *Molecular Pharmacology* (1967):113–123.
- [127] Kries J.P. von, Warriar T., Podust L.M. *Current protocols in microbiology* (2010):Unit17.4.
- [128] Vaz A.D., Coon M.J., Peegel H. et al. *Drug Metabolism and Disposition* (1992):108–112.
- [129] Locuson C.W., Hutzler J.M., Tracy T.S. *Drug metabolism and disposition: the biological fate of chemicals* (2007):614–622.
- [130] Bayer H., Batzl C., Hartmann R.W. et al. *Journal of medicinal chemistry* (1991):2685–2691.
- [131] Wachall B.G., Hector M., Zhuang Y. et al. *Bioorganic & medicinal chemistry* (1999):1913–1924.
- [132] Leroux F., Hutschenreuter T.U., Charrière C. et al. *Helvetica Chimica Acta* (2003):2671–2686.
- [133] Hille U.E., Hu Q., Vock C. et al. *European journal of medicinal chemistry* (2009):2765–2775.
- [134] Hille U.E., Hu Q., Pinto-Bazurco Mendieta, Mariano A.E. et al. *Comptes Rendus Chimie* (2009):1117–1126.
- [135] Hille U.E., Zimmer C., Vock C.A. et al. *ACS medicinal chemistry letters* (2011):2–6.
- [136] Hille U.E., Zimmer C., Hauptenthal J. et al. *ACS medicinal chemistry letters* (2011):559–564.
- [137] Jagusch C., Negri M., Hille U.E. et al. *Bioorganic & medicinal chemistry* (2008):1992–2010.
- [138] Pinto-Bazurco M.M.A.E., Negri M., Hu Q. et al. *Archiv der Pharmazie* (2008):597–609.
- [139] Lézé M.-P., Le Borgne M., Pinson P. et al. *Bioorganic & medicinal chemistry letters* (2006):1134–1137.
- [140] Voets M., Antes I., Scherer C. et al. *Journal of medicinal chemistry* (2006):2222–2231.
- [141] Lucas S., Heim R., Ries C. et al. *Journal of medicinal chemistry* (2008):8077–8087.
- [142] Zimmer C., Hafner M., Zender M. et al. *Bioorganic & medicinal chemistry letters* (2011):186–190.
- [143] Yin L., Hu Q., Hartmann R.W. et al. *PloS one* (2012):e48048.
- [144] Yin L., Lucas S., Maurer F. et al. *Journal of medicinal chemistry* (2012):6629–6633.
- [145] Yin L., Hu Q., Hartmann R.W. *Journal of medicinal chemistry* (2013):460–470.
- [146] Yin L., Hu Q., Emmerich J. et al. *Journal of medicinal chemistry* (2014):5179–5189.
- [147] Shimada T., Tanaka K., Takenaka S. et al. *Chemical research in toxicology* (2009):1325–1333.
- [148] Ouellet H., Kells P.M., Ortiz de Montellano P.R. et al. *Bioorganic & medicinal chemistry letters* (2011):332–337.
- [149] Yung-Chi C., Prusoff W.H. *Biochemical Pharmacology* (1973):3099–3108.
- [150] Shadwell J., Copeland R.A., Pompliano D.L. et al. *Nature reviews. Drug discovery* (2006):730–739.

- [151] Lambeth D.O., Muhonen W.W. *Journal of Chromatography B: Biomedical Sciences and Applications* (1994):143–157.
- [152] Greis K.D. *Mass spectrometry reviews* (2007):324–339.
- [153] Božović A., Kulasingam V. *Clinical biochemistry* (2013):444–455.
- [154] Hesse M., Meier H., Zeeh B. Stuttgart: Thieme (2002):3-13-576106-1.
- [155] Andrews J.M. *Journal of Antimicrobial Chemotherapy* (2001):5–16.
- [156] Jorgensen J.H., Ferraro M.J. *Clinical infectious diseases* (2009):1749–1755.
- [157] Franzblau S.G., DeGroot M.A., Cho S.H. et al. *Tuberculosis* (2012):453–488.
- [158] Kairo S.K., Bedwell J., Tyler P.C. et al. *Vaccine* (1999):2423–2428.
- [159] Kepp O., Galluzzi L., Lipinski M. et al. *Nature reviews. Drug discovery* (2011):221–237.
- [160] Lebeaux D., Chauhan A., Rendueles O. et al. *Pathogens* (2013):288–356.
- [161] Müsken M., Di Fiore S., Römling U. et al. *Nature protocols* (2010):1460–1469.
- [162] Peeters E., Nelis H.J., Coenye T. *Journal of microbiological methods* (2008):157–165.
- [163] Li X., Yan Z., Xu J. *Microbiology* (2003):353–362.
- [164] Boulos L., Prévost M., Barbeau B. et al. *Journal of microbiological methods* (1999):77–86.
- [165] Sanchez M., Llama-Palacios A., Marin M. et al. *Medicina Oral Patología Oral y Cirugía Bucal* (2013):e86.
- [166] Pettit R.K., Weber C.A., Kean M.J. et al. *Antimicrobial agents and chemotherapy* (2005):2612–2617.
- [167] Adam B., Baillie G.S., Douglas L.J. *Journal of medical microbiology* (2002):344–349.
- [168] Ghafoor A., Hay I.D., Rehm, Bernd H A. *Applied and environmental microbiology* (2011):5238–5246.
- [169] Barbosa I., Garcia S., Barbier-Chassefière V. et al. *Glycobiology* (2003):647–653.
- [170] Kemp M.M., Weïwer M., Koehler A.N. *Bioorganic & medicinal chemistry* (2012):1979–1989.
- [171] Renaud J.P., Delsuc M.A. *Current opinion in pharmacology* (2009):622–628.
- [172] Niesen F.H., Berglund H., Vedadi M. *Nature protocols* (2007):2212–2221.
- [173] Cummings M.D., Farnum M.A., Nelen M.I. *Journal of biomolecular screening* (2006):854–863.
- [174] Ladbury J.E., Klebe G., Freire E. *Nature reviews. Drug discovery* (2010):23–27.
- [175] Freire E. *Drug discovery today* (2008):869–874.
- [176] Freire E. *Drug Discovery Today: Technologies* (2004):295–299.
- [177] Lounnas V., Ritschel T., Kelder J. et al. *Computational and Structural Biotechnology Journal* (2013):1–14.
- [178] Weiss G.A., Watanabe C.K., Zhong A. et al. *Proceedings of the National Academy of Sciences* (2000):8950–8954.
- [179] Morrison K.L., Weiss G.A. *Current Opinion in Chemical Biology* (2001):302–307.
- [180] Klein T., Henn C., de Jong, Johannes C. et al. *ACS chemical biology* (2012):1496–1501.
- [181] Storz M.P., Brengel C., Weidel E. et al. *ACS chemical biology* (2013):2794–2801.

- [182] Weidel E., de Jong, Johannes C., Brengel C. et al. *Journal of medicinal chemistry* (2013):6146–6155.
- [183] Cooper M.A. *Nature reviews. Drug discovery* (2002):515–528.
- [184] Perspicace S., Banner D., Benz J. et al. *Journal of biomolecular screening* (2009):337–349.
- [185] Schuck P. *Annual review of biophysics and biomolecular structure* (1997):541–566.
- [186] Homola J. *Analytical and bioanalytical chemistry* (2003):528–539.
- [187] Patching S.G. *Biochimica et biophysica acta* (2014):43–55.
- [188] Löfas S., Johnsson B. *Journal of the Chemical Society, Chemical Communications* (1990):1526.
- [189] Zanger U.M., Schwab M. *Pharmacology & therapeutics* (2013):103–141.
- [190] Bruno R.D., Njar V.C.O. *Bioorganic & medicinal chemistry* (2007):5047–5060.
- [191] Munro A.W., Lindsay J.G. *Molecular microbiology* (1996):1115–1125.
- [192] Benkoo I. *Journal of Antimicrobial Chemotherapy* (1999):675–681.
- [193] Omura T., Sato R. *The Journal of biological chemistry* (1964):2370–2378.
- [194] Ewen K.M., Schiffler B., Uhlmann-Schiffler H. et al. *Federation of European Microbiological Societies yeast research* (2008):432–441.
- [195] Müller J.J., Hannemann F., Schiffler B. et al. *Journal of inorganic biochemistry* (2011):957–965.
- [196] Altaf M., Miller C.H., Bellows D.S. et al. *Tuberculosis* (2010):333–337.
- [197] Nobre L.S., Todorovic S., Tavares A.F.N. et al. *Journal of Bacteriology* (2010):1527–1533.
- [198] Hopkins A.L., Groom C.R., Alex A. *Drug discovery today* (2004):430–431.
- [199] McLean K.J., Lafite P., Levy C. et al. *The Journal of biological chemistry* (2009):35524–35533.
- [200] Saecker M., Burlingham B.T., Widlanski T.S. *Journal of Chemical Education* (2003):214.
- [201] Lesic B., Lépine F., Déziel E. et al. *PLoS pathogens* (2007):1229–1239.
- [202] Zender M., Klein T., Henn C. et al. *Journal of medicinal chemistry* (2013):6761–6774.
- [203] Lu C., Kirsch B., Zimmer C. et al. *Chemistry & Biology* (2012):381–390.
- [204] Lu C., Maurer C.K., Kirsch B. et al. *Angewandte Chemie* (2014):1127–1130.
- [205] Lu C., Kirsch B., Maurer C.K. et al. *European journal of medicinal chemistry* (2014):173–183.
- [206] Wagner G., Hyberts S.G., Havel T.F. *Annual review of biophysics and biomolecular structure* (1992):167–198.
- [207] Davis A.M., Teague S.J., Kleywegt G.J. *Angewandte Chemie* (2003):2718–2736.
- [208] Nie Z., Perretta C., Lu J. et al. *Journal of medicinal chemistry* (2005):1596–1609.
- [209] Pistorius D., Ullrich A., Lucas S. et al. *Chembiochem a European journal of chemical biology* (2011):850–853.
- [210] Mayer M., Meyer B. *Angewandte Chemie International Edition* (1999):1784–1788.
- [211] Park B.K., Boobis A., Clarke S. et al. *Nature reviews. Drug discovery* (2011):292–306.
- [212] Schloss J.V. *Accounts of Chemical Research* (1988):348–353.
- [213] Berg L., Niemiec M.S., Qian W. et al. *Angewandte Chemie* (2012):12716–12720.
- [214] Geschwindner S., Ulander J., Johansson P. *Journal of medicinal chemistry* (2015):6321–6335.

- [215] Chodera J.D., Mobley D.L. *Annual review of biophysics* (2013):121–142.
- [216] Allen F.H., Bird C.M., Rowland R.S. et al. *Acta Crystallographica Section B Structural Science* (1997):696–701.
- [217] Vianello R., Kovačević B., Ambrožič G. et al. *Chemical Physics Letters* (2004):117–121.
- [218] Storz M.P., Allegretta G., Kirsch B. et al. *Organic & biomolecular chemistry* (2014):6094–6104.
- [219] Sahner J.H., Empting M., Kamal A. et al. *European journal of medicinal chemistry* (2015):14–21.
- [220] Gozalbes R., Mosulén S., Ortí L. et al. *Bioorganic & medicinal chemistry* (2013):1944–1951.
- [221] O'Shea R., Moser H.E. *Journal of medicinal chemistry* (2008):2871–2878.
- [222] Mavrodi D.V., Parejko J.A., Mavrodi O.V. et al. *Environmental microbiology* (2013):675–686.
- [223] Priyaja P., Jayesh P., Philip R. et al. *Cytotechnology* (2014):143–155.
- [224] Visca P., Imperi F., Lamont I.L. *Trends in microbiology* (2007):22–30.
- [225] Jander G., Rahme L.G., Ausubel F.M. *Journal of Bacteriology* (2000):3843–3845.
- [226] Lorè N.I., Cigana C., Fino I. de et al. *PloS one* (2012):e35648.
- [227] Frei R., Breitbach A.S., Blackwell H.E. *Angewandte Chemie* (2012):5226–5229.
- [228] Karunaratne D. N. Rijeka: InTech (2012):978-953-51-0819-1.
- [229] Colvin K.M., Gordon V.D., Murakami K. et al. *PLoS pathogens* (2011):e1001264.
- [230] Yang L., Hu Y., Liu Y. et al. *Environmental microbiology* (2011):1705–1717.
- [231] Leid J.G., Willson C.J., Shirliff M.E. et al. *The Journal of Immunology* (2005):7512–7518.
- [232] Tielker D., Hacker S., Loris R. et al. *Microbiology* (2005):1313–1323.
- [233] Lewenza S. *Frontiers in microbiology* (2013):21.
- [234] Johnson L., Horsman S.R., Charron-Mazenod L. et al. *BMC microbiology* (2013):115.
- [235] Chiang W.C., Nilsson M., Jensen P.Ø. et al. *Antimicrobial agents and chemotherapy* (2013):2352–2361.
- [236] Sule P., Wadhawan T., Carr N.J. et al. *Letters in applied microbiology* (2009):299–304.
- [237] Davies D. *Nature reviews. Drug discovery* (2003):114–122.
- [238] Zelenitsky S., Ariano R., Harding G. et al. *Antimicrobial agents and chemotherapy* (2005):4009–4014.
- [239] Gopal, Agarwal G., Kapil A. et al. *The National medical journal of India* (2005):184–186.
- [240] Tanaka G., Shigeta M., Komatsuzawa H. et al. *Chemotherapy* (1999):28–36.
- [241] Suci P.A., Mittelman M.W., Yu F.P. et al. *Antimicrobial agents and chemotherapy* (1994):2125–2133.
- [242] Sams-Dodd F. *Drug discovery today* (2005):139–147.
- [243] Gerdt J.P., Blackwell H.E. *ACS chemical biology* (2014):2291–2299.
- [244] Maeda T., García-Contreras R., Pu M. et al. *The International Society for Microbial Ecology journal* (2012):493–501.
- [245] Ruer S., Pinotsis N., Steadman D. et al. *Chemical biology & drug design* (2015):379–399.

## 6 Acknowledgements

An erster Stelle möchte ich Prof. Dr. Rolf Hartmann danken, für die Aufnahme in seinen Arbeitskreis und die sehr gute Betreuung der Arbeit. Vielen Dank für das interessante Thema, das Sie mir gegeben haben, die Unterstützung und Diskussionsbereitschaft in wissenschaftlichen Belangen, sowie Freiräume um meine Ideen zu entfalten.

Weiteren Personen möchte ich einen herzlichen und aufrichtigen Dank aussprechen:

Herrn Prof. Dr. Lehr für die Übernahme meines Koreferats und seine Rolle als wissenschaftlicher Begleiter

Dres. Christina Zimmer, Anke Steinbach und Martin Empting für die Leitung des pqs Projekts, insbesondere für eure Unterstützung, kreative Vorschläge und alle Diskussionen.

Danke an das ganze pqs Team, Dr. Michael Storz, Zender Michael, Dr. Christine Maurer, Benjamin Kirsch, Andreas Thomann, Andreas Kany, Dr. Cenbin Lu, Dr. Matthias Negri, Ahmed Kamal, Giuseppe Allegretta, Antonia Martins, Dr. Johannes de Jong, Dr. Claudia Henn, Dr. Tobias Klein, Dr. Elisabeth Weidel und Dr. Carsten Börger für die gute Zusammenarbeit.

Dres. Dr. Jörg Hauptenthal, Jens Eberhardt und Martin Empting für die Leitung des cyp Projekts, insbesondere für eure Unterstützung, kreative Vorschläge und alle Diskussionen.

Danke an das ganze cyp Team, Andreas Thomann und unsere Praktikanten für die gute Zusammenarbeit.

Vielen Dank an Dr. Jan Henning Sahner, Dr. Michael Storz und Andreas Thomann für die gute Zusammenarbeit in unseren gemeinsamen Projekten.

Simone Amann, Jeannine Jung und Carina Scheid für die Hilfe bei der Durchführung der biologischen Experimente.

Dr. Tobias Klein und Dr. Matthias Negri für die Einarbeitung in den Laborbereich und die Betreuung in Projektplanung und Doktorarbeit zu Beginn der Doktorarbeit.

Dr. Martin Frotscher, Dr. Matthias Negri, Dr. Christian Schmitt und Andreas Thomann für die gute Zusammenarbeit bei der Betreuung der studentischen Praktika.

Katrin Schmitt für die Organisation im Sekretariat.

Lothar Jager für alle technischen Problemlösungen.

Michael Hoffmann für die Hilfe bei besonders diffizilen HPLC/MS Messungen.

Dr. Stefan Böttcher für seine Unterstützung in allen Fragen zu HPLC/MS Experimenten.

Dr. Alberto Plaza für seine Unterstützung in allen Fragen zu NMR Experimenten.

Alle Personen die ich hier nicht namentlich genannt habe danke ich für ihre Kollegialität und Unterstützung während meiner Promotion

Ein ganz wichtiger Dank gilt aber auch den Leuten ohne die meine Promotionszeit wohl lange nicht so schön gewesen wäre und mich nicht nur arbeitstechnisch sondern auch in allen anderen Bereichen dieses Lebensabschnitts unterstützt haben:

Vielen Dank an die „Gute Leute Gruppe“: Andreas Thomann, Daniel Wiegemann, Benjamin Kirsch, Martin Empting, Martina Fruth, Michael Storz, Michael Zender, Stefan Hinsberger, Stefan Böttcher, Nina Hanke, Juliette Emmerich, Christine Maurer, Elisabeth Weidel, Ines Joachim und Kristina Hüsecken für unterhaltsame Pausen und den Ausgleich zur Arbeit durch verschiedenste Freizeitunternehmungen.

Vielen Dank an das Carré: Andreas Thomann, Andreas Kany, Jan Henning Sahner und Michael Zender, inclusive externe Unterstützung: Michael Storz, für die gute Arbeitsatmosphäre in unserem Büro.

Meiner Familie, meinen Freunden und Fußballkameraden danke ich für den nötigen Ausgleich zum stressigen Arbeitsalltag und für die Geduld wenn ich mal wieder keine Zeit hatte.

Ein ganz besonderer Dank gilt meinen Eltern Astrid und Rudolf, sowie Großeltern Emma und Rudolf, weil sie mich in allen Lebenslagen unterstützt und hinter mir gestanden haben.

Und meiner Martina, dass sie mir die letzten Jahre meiner Promotion um so viel leichter gemacht hat und mir den Rücken gestärkt hat, wenn es mal etwas stressiger wurde.





## 7 Appendix

### 7.1 Supporting Informations

#### **A Biophysical Screening of a Focused Library for the Discovery of Novel Antimycobacterials targeting CYP121**

Christian Brengel, Andreas Thomann, Alexander Schifrin, Giuseppe Allegretta, Ahmed Kamal, Jörg Hauptenthal, Sang Hyun Cho, Scott G. Franzblau, Jens Eberhard, and Rolf W. Hartmann

*Manuscript in preperation*

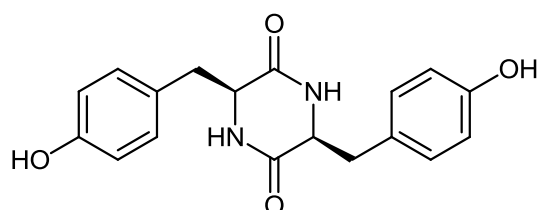
## Supplementary Data

### Chemical synthesis cYY and Mycocyclusin:

#### Synthesis of cyclo-di-*L*-tyrosine (cYY)

#### cyclo-di-*L*-tyrosine (cYY):

cYY was synthesized as previously described.<sup>1</sup>

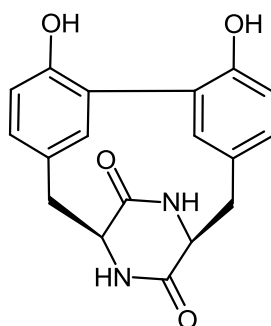


cYY was synthesized as previously described.<sup>1</sup> Spectral data is in accordance with the previously published results:<sup>1</sup>

<sup>1</sup>H NMR (300 MHz, DMSO-*d*<sub>6</sub>) δ 9.19 (s, 1H), 7.75 (d, *J* = 2.6 Hz, 1H), 7.05 – 6.78 (m, 2H), 6.78 – 6.55 (m, 2H), 3.85 (s, 1H), 2.54 (dd, *J* = 4.6 Hz, 1H), 2.11 (dd, *J* = 13.7, 6.5 Hz, 1H); <sup>13</sup>C NMR (75 MHz, DMSO) δ 166.7, 156.5, 131.2, 127.0, 115.5, 56.2, 39.3; ESI-MS(+) = *m/z* 327.1 [M+H]<sup>+</sup>.

### 1.2 Synthesis of mycocyclusine

#### Mycocyclusine:



Mycocyclusine was synthesized as previously described.<sup>1,2</sup> Spectral data is in accordance with the previously published results:<sup>1</sup>

$^1\text{H}$  NMR (300 MHz,  $\text{DMSO-}d_6$ )  $\delta$  7.98 (s, 1H), 6.84 (dd,  $J = 2.51, 7.9$  Hz, 1H), 6.62 (d,  $J = 8.1$  Hz, 1H), 6.58 (d,  $J = 2.4$  Hz, 1H), 4.32 (d,  $J = 4.8$  Hz, 1H), 3.46 (d,  $J = 15.7$  Hz, 1H), 2.64 (dd,  $J = 5.73, 15.6$  Hz, 1H).

### SDS-PAGE of His-tagged CYP121

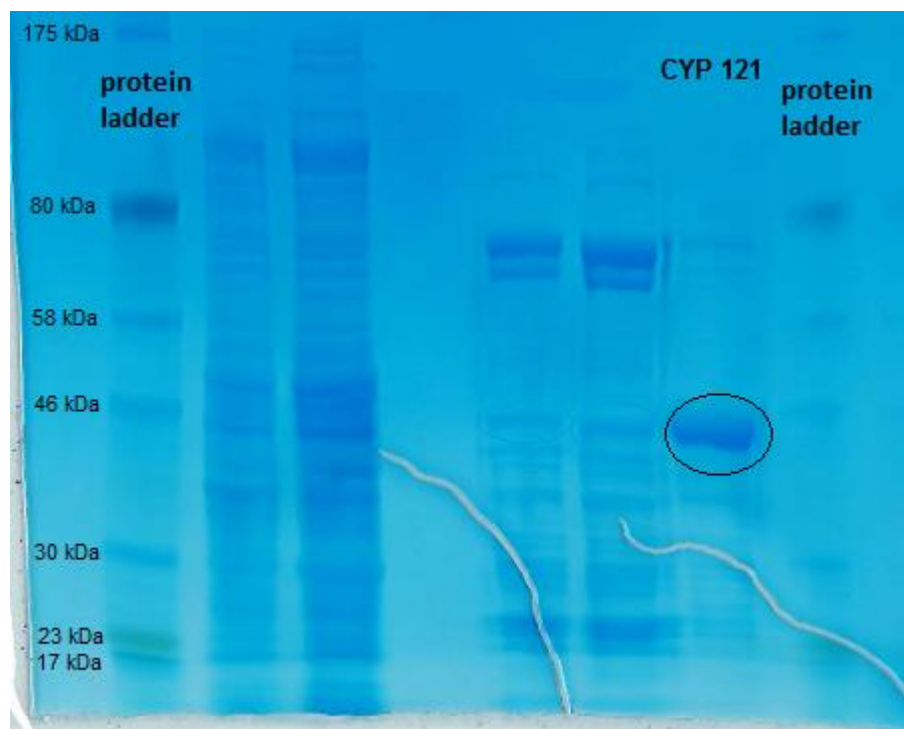


**Figure S1.** SDS-PAGE of Ni-NTA purified heterologous expressed CYP121. The band corresponds to a molecular mass of  $> 46000$  Da which is in good accordance with the calculated protein mass of 43256 Da.

## Activity of CYP121/ CO Spectra

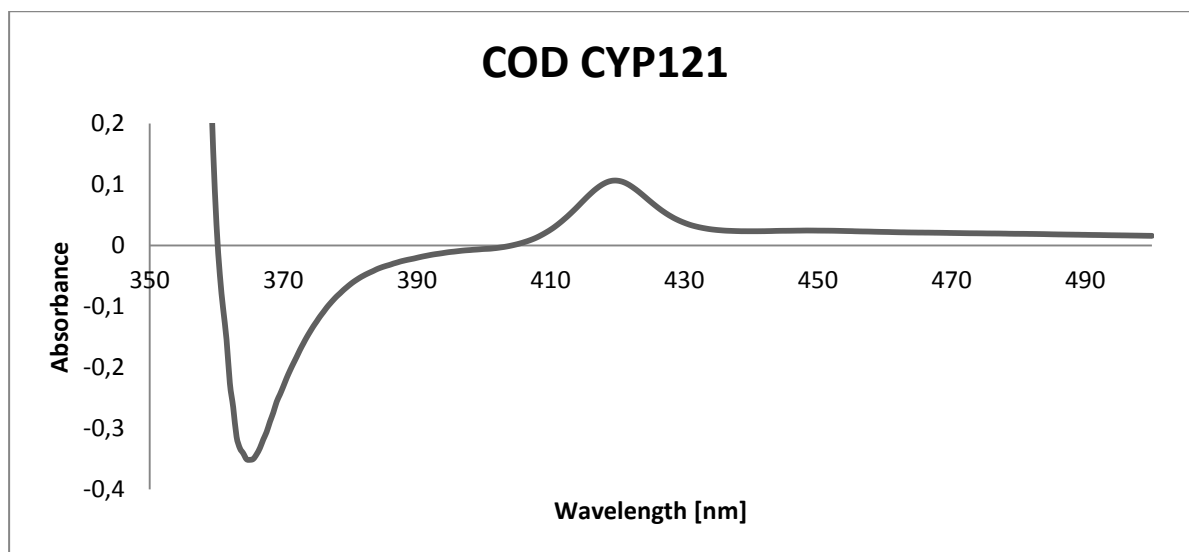


**Figure S2.** UV-VIS carbonmonoxide difference spectra (COD) of CYP121 after treatment with sodium sulfide and carbonmonoxide. The characteristic band at ~420 nm shows CO coordination to the reduced iron-heme.

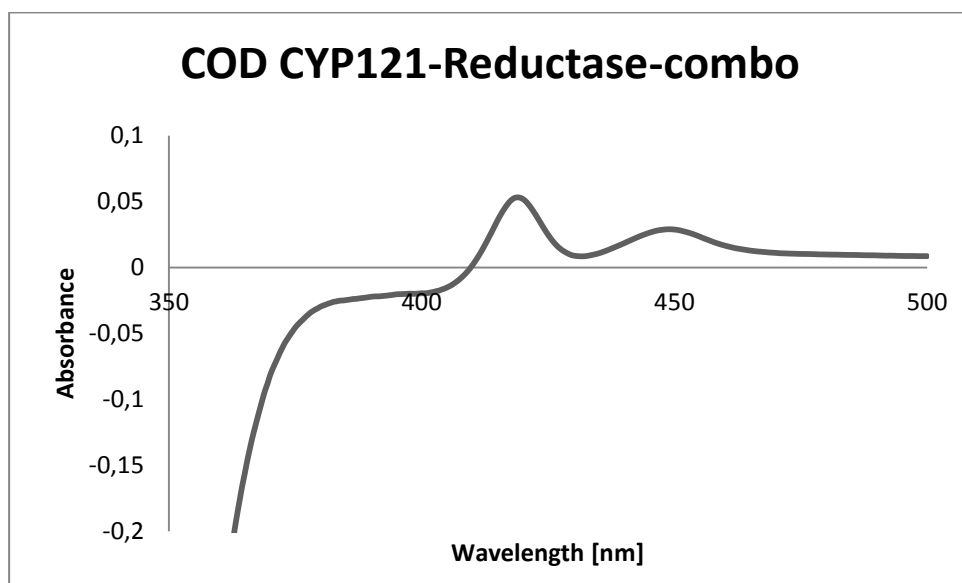


**Figure S3.** UV-VIS carbonmonoxide difference spectra (COD) of CYP121 after incubation with reductase Arh1\_A18G and ferredoxin Etp1fd (516-618) followed by carbonmonoxide treatment. The characteristic band at ~420 nm shows CO coordination to the reduced iron-heme

LC-MS analysis of *in vitro* CYP121 enzyme reaction and effect of I:47

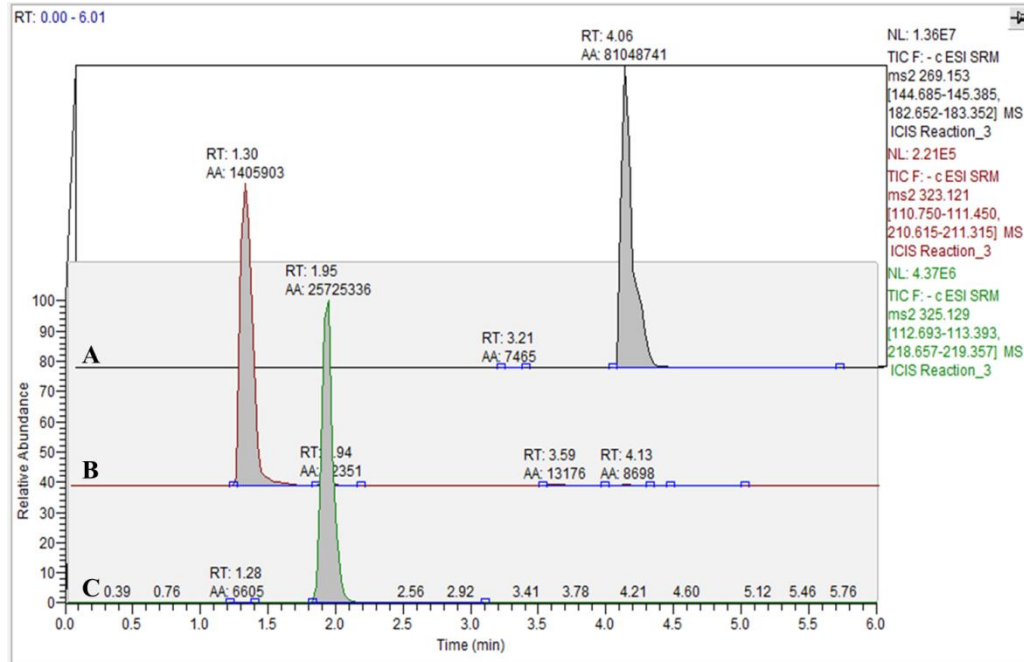


**Figure S4.** LC-MS/MS quantification of CYP121 enzyme reaction: internal standard estrone  $t_R = 4.05$  min (A); mycocyclusin  $t_R = 1.30$  min (B); cYY  $t_R = 1.95$  min (C).

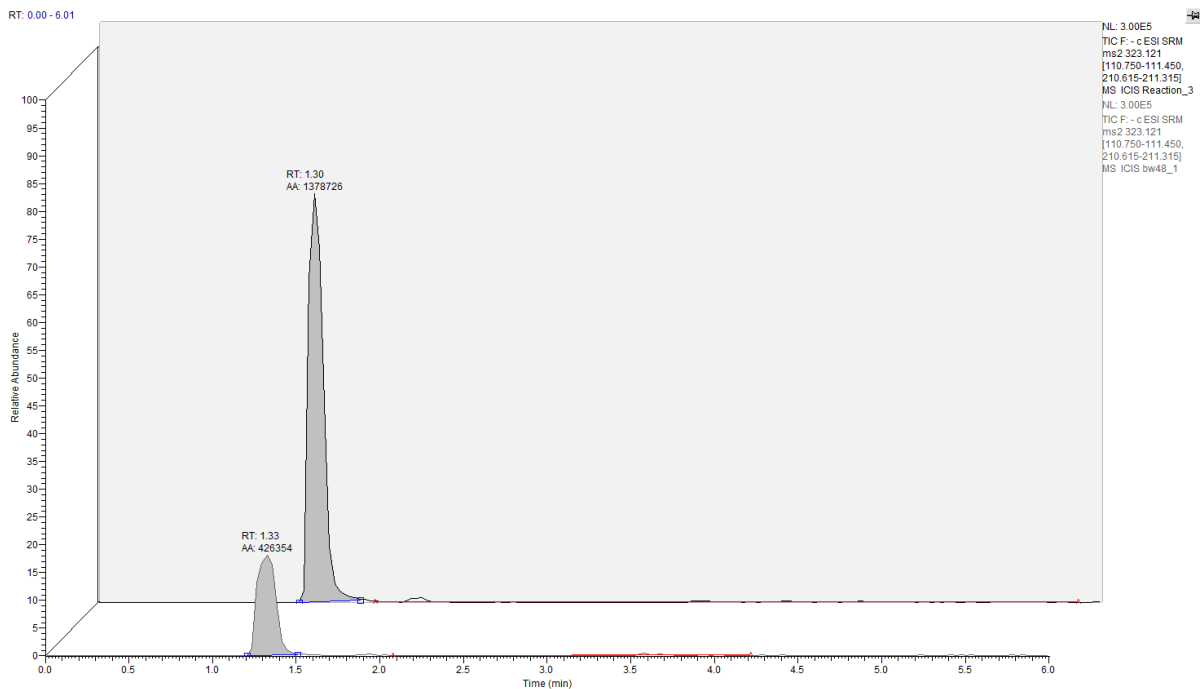


**Figure S5.** LC-MS/MS based quantification of CYP121 *in vitro* enzyme reaction product mycocyclusin with addition of **I:47** (100  $\mu$ M, lower chromatogram) and without the presence of the inhibitor (upper chromatogram).

## Surface Plasmon Resonance Sensorgram of econazole

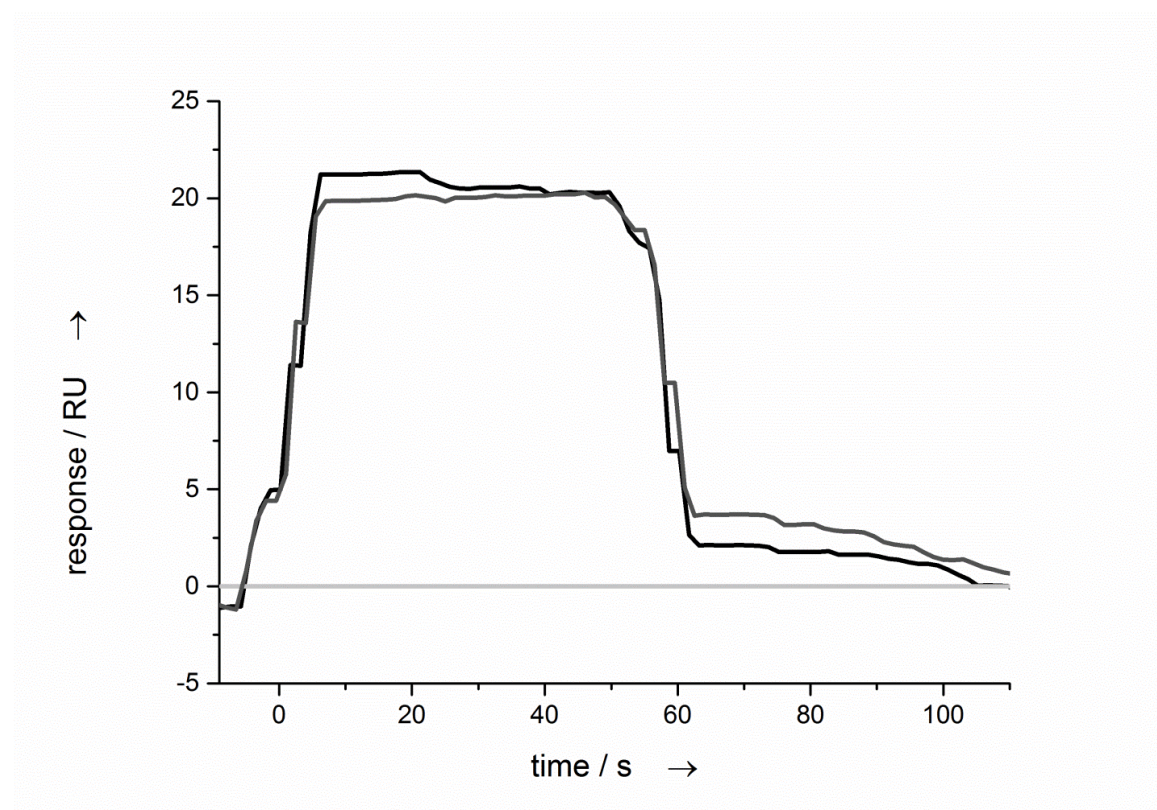


**Figure S6.** Representative example for SPR binding curve of econazole to CYP121 injected from 100  $\mu\text{M}$  sample.

## Screening overview

**Table S1.** Overview of the results of SPR screening, Heme binding assay, BCG and Mtb growth inhibition and MIC determination

Cmpd	SPR [R/Rpos]	Heme coord. <sup>a</sup>	Heme- K <sub>D</sub> [μM]	BCGT Inhibition @ 100 μM [%]	MIC <sub>BCGT</sub> [μM]	MIC <sub>Mtb</sub> [μM]
I:1	0.4	N		10		
I:2	0					
I:3	0.1					
I:4	0.2					
I:5	0.1					
I:6	0.1					
I:7	0.5					
I:8	0.5					
I:9	0					
I:10	0					
I:11	0.6	N				
I:12	0.4					
I:13	0					
I:14	0.2					
I:15	0.3	Y (T-II)	34	87	41	
I:16	1.2	Y (T-II)	1	78	5	6
I:17	1.9	Y (T-II)	3	65	38	
I:18	0.1					
I:19	0					
I:20	0.4					
I:21	0.1					
I:22	0.1					
I:23	0.1					
I:24	0.3					
I:25	0.5					
I:26	0.1					
I:27	1.0	Y (T-II)	weak			
I:28	0.3					
I:29	0.4					



<b>I:30</b>	1.4	Y (T-II)	11	94	11	48
<b>I:31</b>	1.5	N				
<b>I:32</b>	1.1	Y (T-II)	14	85	30	41
<b>I:33</b>	0.1	N		0		
<b>I:34</b>	0.7	Y (T-II)	29	25		
<b>I:35</b>	0.5					
<b>I:36</b>	0.1					
<b>I:37</b>	0.2					
<b>I:38</b>	0.2					
<b>I:39</b>	0.1					
<b>I:40</b>	0.3					
<b>I:41</b>	0.1					
<b>I:42</b>	0.1					
<b>I:43</b>	0.2					
<b>I:44</b>	0.2					
<b>I:45</b>	0.5					
<b>I:46</b>	0.1					
<b>I:47</b>	0.6	Y (T-II)	5	87	1	1
<b>I:48</b>	0.8	Y (T-II)	5	88	7	12
<hr/>						
<b>II:1</b>	0.3					
<b>II:2</b>	0.3					
<b>II:3</b>	0.5					
<b>II:4</b>	0.2					
<b>II:5</b>	0.2					
<b>II:6</b>	0.1					
<b>II:7</b>	0.0					
<b>II:8</b>	0.3					
<b>II:9</b>	0.2					
<b>II:10</b>	0.1					
<b>II:11</b>	0.3					
<b>II:12</b>	0.2					
<b>II:13</b>	0.1					
<b>II:14</b>	0.5	N				
<b>II:15</b>	0.1					
<b>II:16</b>	0.2					
<b>II:17</b>	0.2					
<b>II:18</b>	0.2					

<b>II:19</b>	0.2			
<b>II:20</b>	1.3	Y (T-II)	9	48
<b>II:21</b>	0.7	Y (T-II)	31	
<b>II:22</b>	0.2			
<b>II:23</b>	0.6	N		
<b>II:24</b>	0.1			
<b>II:25</b>	0.2			
<b>II:26</b>	0.8	Y (T-II)	16	
<b>II:27</b>	0.9	Y (T-II)	20	
<b>II:28</b>	0.9	Y (T-II)	19	
<b>II:29</b>	0.7	Y (T-II)	62	
<b>II:30</b>	0.8	Y (T-II)	weak	
<b>II:31</b>	0.6	Y (T-II)	weak	
<b>II:32</b>	0.7	Y (T-II)	weak	
<b>II:33</b>	0.3			
<b>II:34</b>	0.7	Y (T-II)	12	0
<b>II:35</b>	1.0	Y (T-II)	weak	
<b>II:36</b>	0.9	Y (T-II)	16	
<b>II:37</b>	1.4	Y (T-II)	50	
<b>II:38</b>	1.2	Y (T-II)	weak	
<b>II:39</b>	1.4	N		
<b>II:40</b>	0.7	Y (T-II)	27	
<b>II:41</b>	0.9	Y (T-II)	13	7
<b>II:42</b>	0.2			
<hr/>				
<b>III:1</b>	0.3			
<b>III:2</b>	0.4			
<b>III:3</b>	1.7	Y (T-II)	weak	20
<b>III:4</b>	1.7	N		20
<b>III:5</b>	0.5			
<b>III:6</b>	0.3			
<b>III:7</b>	1.8	N		18
<b>III:8</b>	1.4	Y (T-II)	weak	5
<b>III:9</b>	0.6	Y (T-II)	weak	
<b>III:10</b>	0.4			
<b>III:11</b>	0.3			
<b>III:12</b>	0.2			
<b>III:13</b>	0.1			

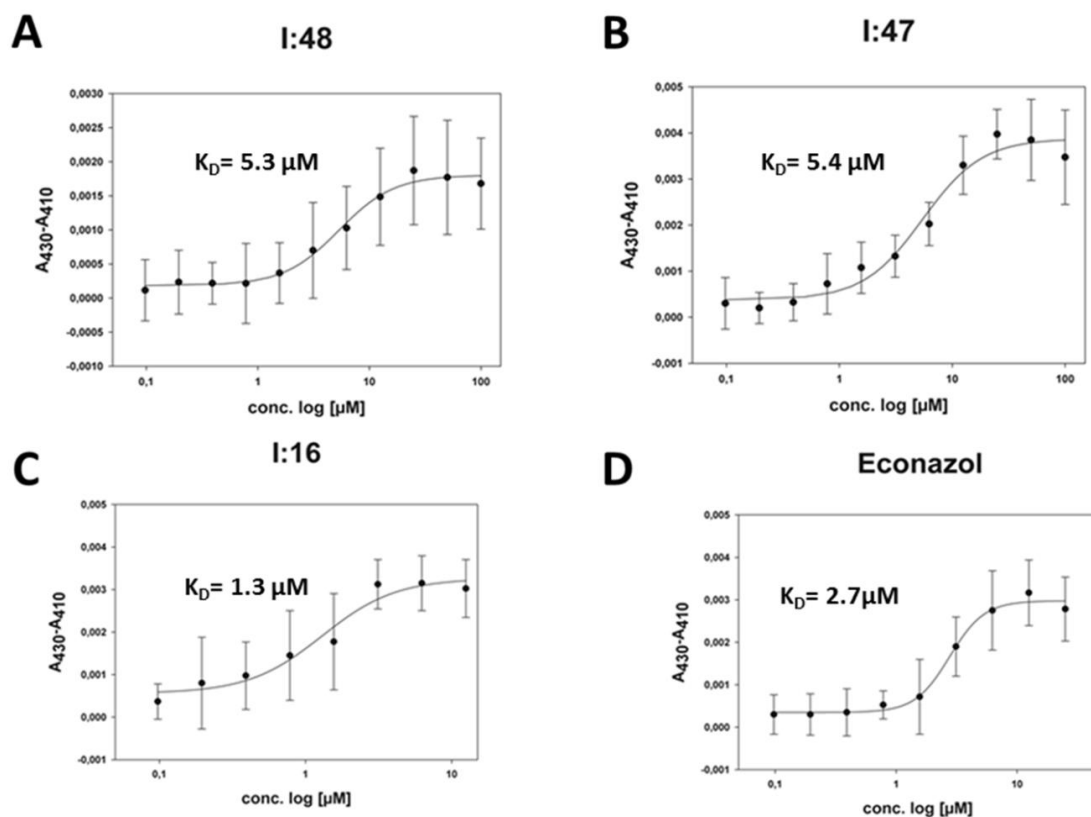
<b>III:14</b>	0.3					
<b>III:15</b>	0.4					
<b>III:16</b>	0.2					
<b>III:17</b>	0.2					
<b>III:18</b>	0.4					
<b>III:19</b>	0.4					
<b>III:20</b>	0.2					
<b>III:21</b>	0.3					
<hr/>						
<b>IV:1</b>	0.2					
<b>IV:2</b>	0.1					
<b>IV:3</b>	0.1					
<b>IV:4</b>	0.3					
<b>IV:5</b>	0.1	N				
<b>IV:6</b>	0.5					
<b>IV:7</b>	0.6	N				
<b>IV:8</b>	0.5					
<b>IV:9</b>	0.4					
<b>IV:10</b>	0.5			60		
<b>IV:11</b>	0.9	Y (T-II)	weak			
<b>IV:12</b>	0.9	N				
<b>IV:13</b>	0.8	Y (T-II)	62			
<hr/>						
<b>V:1</b>	0.0					
<b>V:2</b>	0.3					
<b>V:3</b>	0.2					
<b>V:4</b>	0.1					
<b>V:5</b>	0.2					
<b>V:6</b>	0.1					
<b>V:7</b>	0.3					
<b>V:8</b>	0.8	N				
<b>V:9</b>	0.8	N				
<hr/>						
<b>VI:1</b>	0.6	N		50		
<b>VI:2</b>	1.2	N				
<b>VI:3</b>	1.5	N				
<b>VI:4</b>	1.3	N				
<b>VI:5</b>	0.4					
<b>VI:6</b>	1.3	N				
<hr/>						
<b>Eco<sup>b</sup></b>	1.0	Y (T-II)	3	71	14	11 <sup>3</sup>

---

<b>cYY<sup>c</sup></b>	<b>Y (T-I)</b>	<b>12</b>
------------------------	----------------	-----------

---

<sup>a</sup>n= no, y= yes, T-I = type I binding profile, T-II = type II binding profile, <sup>b</sup>Eco = econazole,  
cYY = cyclo-di-*L*-tyrosine

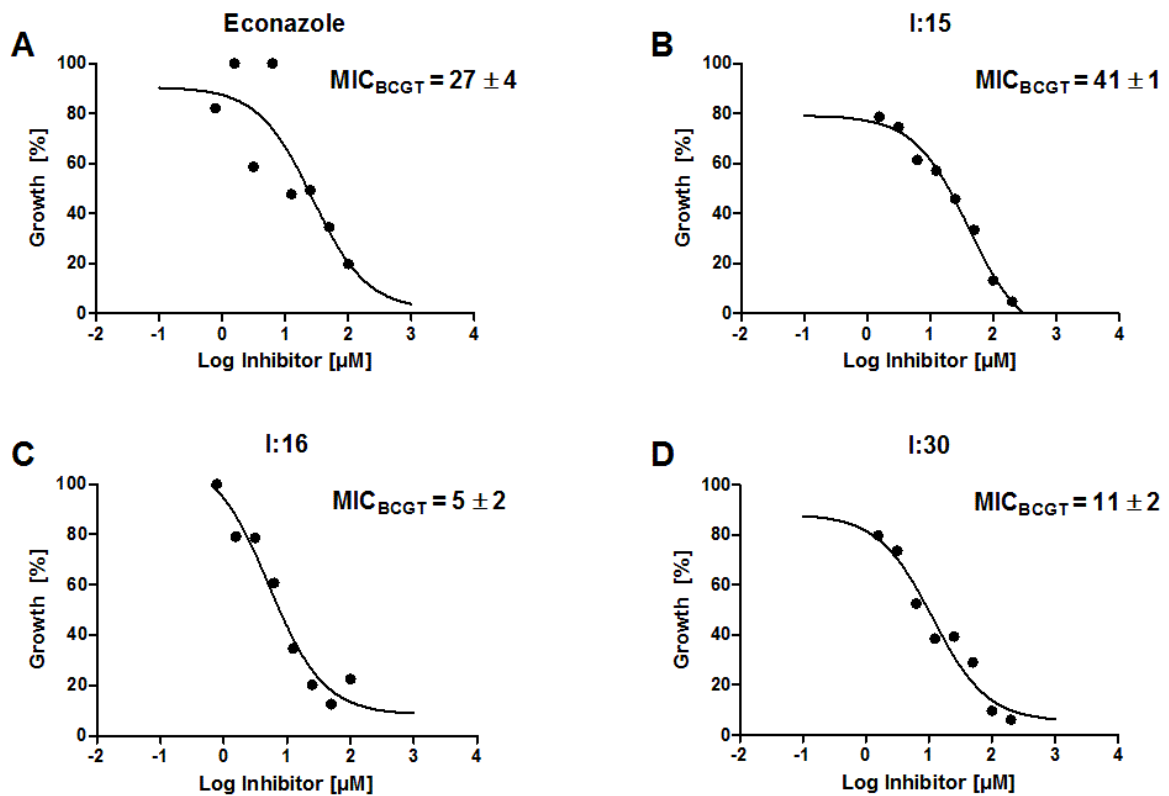
**K<sub>D</sub>** determination by UV-VIS Heme coordination assay

**Figure S7.** Determination of  $K_D$ 's by titration of **I:48** (A), **I:47** (B), **I:16** (C) and **econazole** (D) and monitoring the difference between the absorption at 430 nm minus absorption at 410 nm in the presence of CYP121. Graphs were plotted with SigmaPlot using Marquardt - Levenberg algorithm.

Protein Blast of Mtb H<sub>37</sub>R<sub>v</sub> CYP121 (Rv2276) and M. bovis BCG Pasteur CYP121 (BCG\_2293)

Range 1: 1 to 396		<a href="#">Graphics</a>		▼ Next Match ▲ Previous Match	
Score	Expect	Method	Identities	Positives	Gaps
800 bits(2066)	0.0	Compositional matrix adjust.	396/396(100%)	396/396(100%)	0/396(0%)
Query 1		MTATVLLLEVPFSARGDRIPDAVAELRTREPIRKVRTITGAEAWLVSSYALCTQVLEDRRF			60
Sbjct 1		MTATVLLLEVPFSARGDRIPDAVAELRTREPIRKVRTITGAEAWLVSSYALCTQVLEDRRF			60
Query 61		SMKETAAAGAPRLNALTVPEVVNMGNIADAGLRKAVMKAITPKAPGLEQFLRDTANSL			120
Sbjct 61		SMKETAAAGAPRLNALTVPEVVNMGNIADAGLRKAVMKAITPKAPGLEQFLRDTANSL			120
Query 121		LDNLITEGAPADLRNDFADPLATALHCKVLGIPQEDGPKLFRSLSI AFMS SADPIPAAKI			180
Sbjct 121		LDNLITEGAPADLRNDFADPLATALHCKVLGIPQEDGPKLFRSLSI AFMS SADPIPAAKI			180
Query 181		NWDRDIEYMAGILENPNITTGLMGELSRLRKDPAYSHVSDLEFATIGVTFFGAGVISTGS			240
Sbjct 181		NWDRDIEYMAGILENPNITTGLMGELSRLRKDPAYSHVSDLEFATIGVTFFGAGVISTGS			240
Query 241		FLTTALISLIQRPQLRNLLHEKPELIPAGVEELLRINLSFADGLPRLATADIQVGDVLR			300
Sbjct 241		FLTTALISLIQRPQLRNLLHEKPELIPAGVEELLRINLSFADGLPRLATADIQVGDVLR			300
Query 301		KGELVLVLLLEGANFDPEHFPNPGSIELDRPNPTSHLAFGRGQHFCPGSALGRRHAQIGIE			360
Sbjct 301		KGELVLVLLLEGANFDPEHFPNPGSIELDRPNPTSHLAFGRGQHFCPGSALGRRHAQIGIE			360
Query 361		ALLKKMPGVDLAVPIDQLVWRTRFQRRIPERLPVLW	396		
Sbjct 361		ALLKKMPGVDLAVPIDQLVWRTRFQRRIPERLPVLW	396		

**Figure S8.** Results of the Protein Blast of Mtb CYP121 (upper sequence) and BCGT CYP121 (lower sequence) showing 100% amino acid identity between both proteins.

MIC<sub>BCGT</sub> determination against *Mycobacterium bovis*

**Figure S9.** Growth inhibition of BCG *versus* control (%) of econazole (A), I:15 (B), I:16 (C), I:30 (D) of concentrations ranging from 100-1.56 µM of the respective compounds. Endpoint optical density was measured at 600 nm. MIC<sub>BCGT</sub> were determined by GraphPad Prism using OneSite Log IC<sub>50</sub> model provided by the software.

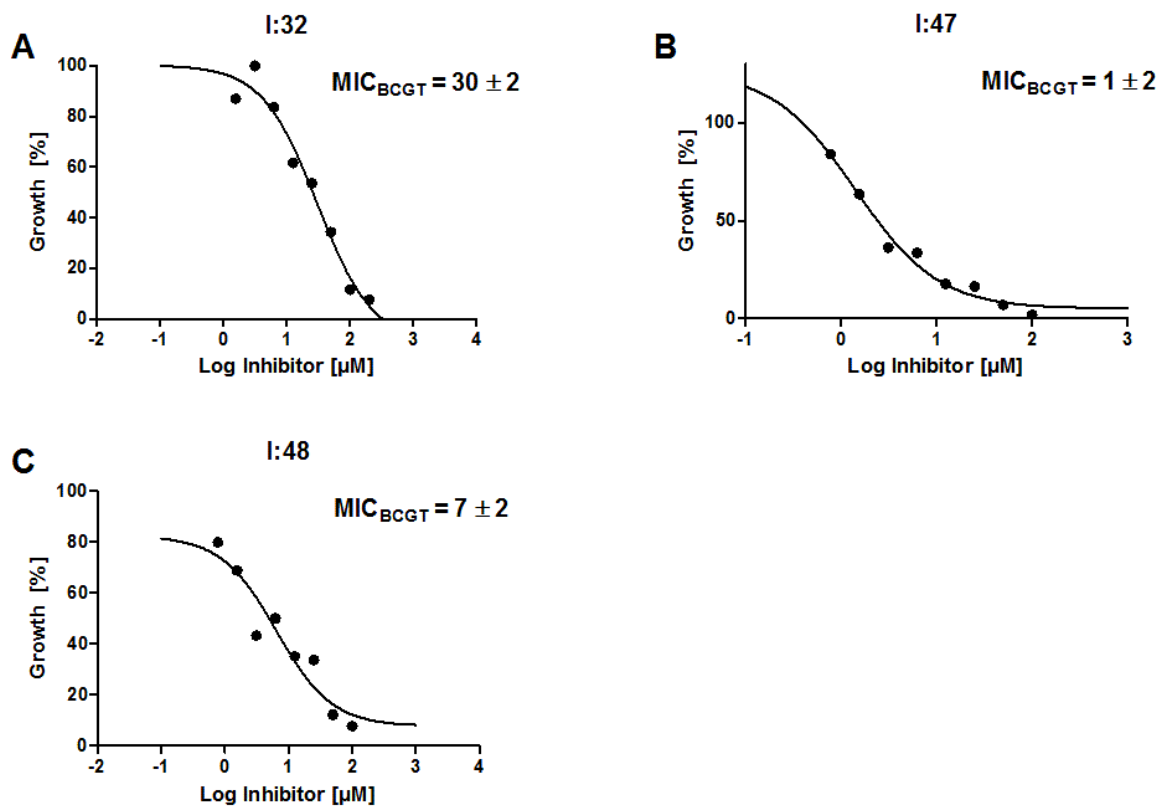


**Figure S10.** Growth inhibition of BCG *versus* control (%) of **I:32** (A), **I:47** (B), **I:48** (C) of concentrations ranging from 100-1.56  $\mu\text{M}$  of the respective compounds. Endpoint optical density was measured at 600 nm. MIC<sub>BCGT</sub> were determined by GraphPad Prism using OneSite Log IC<sub>50</sub> model provided by the software.



## Calculation of antimicrobial efficiency

$$\text{Antibacterial Efficiency} = -\ln\left(\frac{\text{MIC}}{\text{NHA}}\right)$$

**Table S2.** Antimicrobial efficiency <sup>4</sup> of **I:16, I:30, I:32, I:47, I:48, econazole, isoniazide** and **rifampicine** calculated for effects on *Mycobacterium tuberculosis*.

<b>Cmpd.</b>	<b>MIC [mg/L]</b>	<b>MW</b>	<b>NHA<sup>a</sup></b>	<b>Antibacterial Efficiency</b>
<b>I:16</b>	1.90	310	24	0.26
<b>I:30</b>	11.20	234	18	0.25
<b>I:32</b>	9.60	234	18	0.26
<b>I:47</b>	0.30	278	21	0.39
<b>I:48</b>	3.50	292	22	0.26
<b>Eco</b>	4.20	382	23	0.24
<b>INH<sup>b</sup></b>	0.05	137	10	0.99
<b>Rif<sup>c</sup></b>	0.11	823	57	0.16

<sup>a</sup>NHA = number of heavy atoms, INH = isoniazide <sup>3</sup>, Rif = rifampicine <sup>3</sup>.

**Toxicity assessment against human cancer cell lines HEK293 and HepG2**

**SI Table 3.** Toxicity data against human cancer cell lines HEK293 and HepG2 of **I:47**, **I:16** and econazole (Eco).

<b>Compounds</b>	<b>LD<sub>50</sub></b> <b>HEK293</b> <b>[μM]</b>	<b>SD</b>	<b>LD<sub>50</sub></b> <b>HEK293</b> <b>[mg/L]</b>	<b>LD<sub>50</sub> HepG2</b> <b>[μM]</b>	<b>SD</b>	<b>LD<sub>50</sub></b> <b>HepG2</b> <b>[mg/L]</b>
<b>I:47</b>	66.9	5.3	18.6	47.5	8.1	17.1
<b>I:16</b>	19.6	3.8	6.1	12.1	2.8	3.9
<b>Eco</b>	15.6	3.8	6.0	11.8	4.3	3.1

**MIC against *Escherichia coli* and *Staphylococcus aureus* in comparison to growth inhibition against *Mycobacterium bovis* BCG**

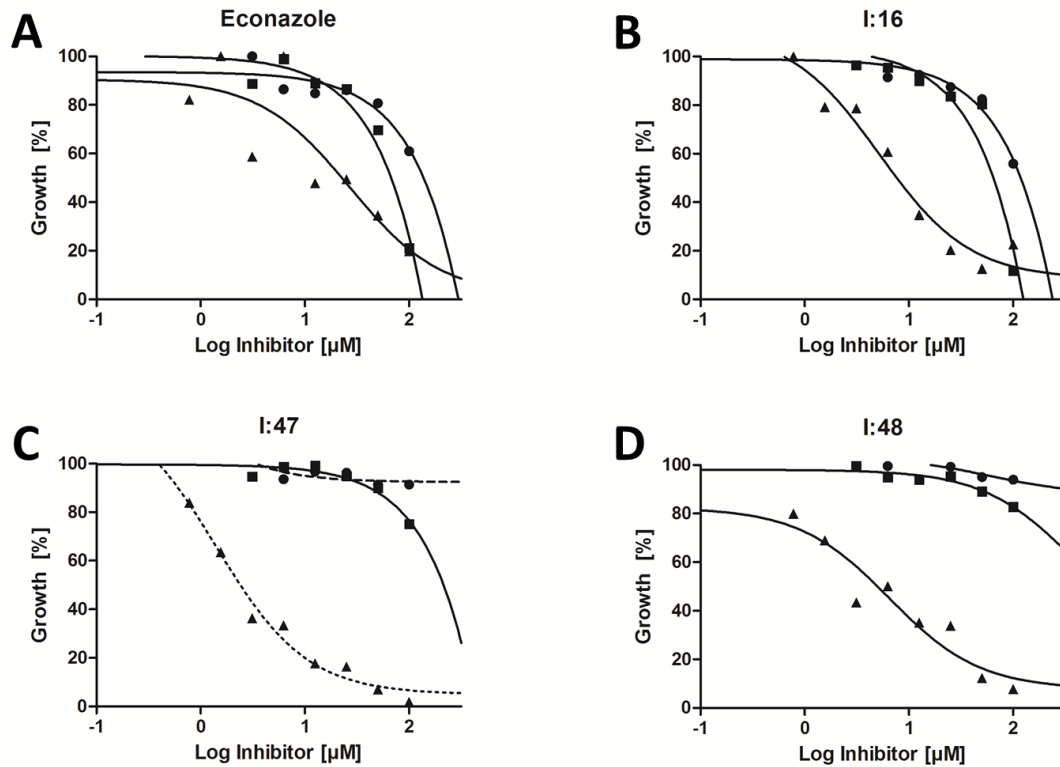


**Figure S11.** Comparison of growth inhibition of **econazole** (A), **I:16** (B), **I:47** (C) and **I:48** (D) against *M. bovis* (▲,  $c = 1.56 - 100 \mu\text{M}$ ), *E. Coli* (■,  $c = 3.125 - 100 \mu\text{M}$ ), *S. aureus* (●,  $c = 3.125 - 100\mu\text{M}$ ) of concentrations ranging from 100-0.725  $\mu\text{M}$  of the respective compounds. Endpoint optical density was measured at 600 nm. Graphs were plotted with GraphPad Prism using OneSite Log  $\text{IC}_{50}$  model provided by the software.

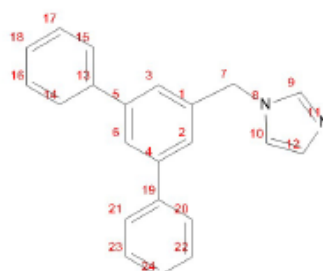
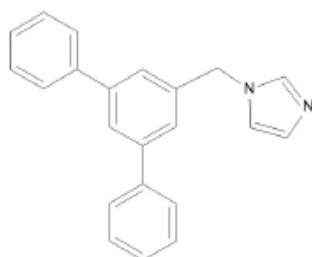
**Physicochemical data:***I:16***ACD/Labs**  
*ACD/LogP Classic Module Report*

Date: February 17, 2015 9:47 AM

Software name and version: ACD/Percepta 14.0.0 (Build 2203)

Compound name:

Structure:



Calculated LogP: 5,26 +- 0,35

**LogP Calculation Protocol:**

Increments of the functional groups:

1. -1,86 (experimental value), atom(s) number: 9, 11, 8

Increments of the Carbon atoms:

2. +0,53 (experimental value), atom(s) number: 7
3. +0,37 (experimental value), atom(s) number: 10
4. +0,37 (experimental value), atom(s) number: 12
5. -0,08 (experimental value), atom(s) number: 1
6. -0,08 (experimental value), atom(s) number: 5
7. -0,08 (experimental value), atom(s) number: 4
8. -0,08 (experimental value), atom(s) number: 19
9. -0,08 (experimental value), atom(s) number: 13
10. +0,37 (experimental value), atom(s) number: 3
11. +0,37 (experimental value), atom(s) number: 2
12. +0,37 (experimental value), atom(s) number: 6
13. +0,37 (experimental value), atom(s) number: 21
14. +0,37 (experimental value), atom(s) number: 20
15. +0,37 (experimental value), atom(s) number: 15
16. +0,37 (experimental value), atom(s) number: 14
17. +0,37 (experimental value), atom(s) number: 23
18. +0,37 (experimental value), atom(s) number: 22
19. +0,37 (experimental value), atom(s) number: 17
20. +0,37 (experimental value), atom(s) number: 16
21. +0,37 (experimental value), atom(s) number: 24
22. +0,37 (experimental value), atom(s) number: 18

Interactions through aromatic system:

- 8-9 +0,29 (experimental value), atom(s) number: 19, 4, 6, 5, 13

Interactions through aliphatic system:

- 1-5 +0,28 (experimental value), atom(s) number: 1, 7, 8

Increments of the ring interactions

Increments of the ring interactions

Increments of the ring interactions



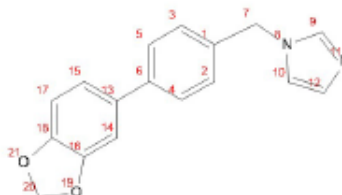
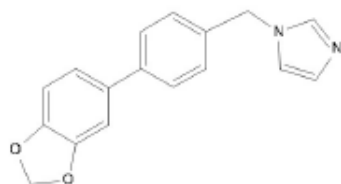
**ACD/Labs**  
*ACD/LogP Classic Module Report*

Date: February 17, 2015 9:59 AM

Software name and version: ACD/Percepta 14.0.0 (Build 2203)

Compound name:

Structure:



Calculated LogP: 3.08 ± 0.37

**LogP Calculation Protocol:**

Increments of the functional groups:

1. +0,43 (experimental value), atom(s) number: 20, 21, 19
2. -1,86 (experimental value), atom(s) number: 9, 11, 8

Increments of the Carbon atoms:

3. +0,53 (experimental value), atom(s) number: 7
4. +0,37 (experimental value), atom(s) number: 10
5. +0,37 (experimental value), atom(s) number: 12
6. +0,08 (experimental value), atom(s) number: 16
7. +0,08 (experimental value), atom(s) number: 18
8. -0,08 (experimental value), atom(s) number: 1
9. -0,08 (experimental value), atom(s) number: 13
10. -0,08 (experimental value), atom(s) number: 6
11. +0,37 (experimental value), atom(s) number: 14
12. +0,37 (experimental value), atom(s) number: 17
13. +0,37 (experimental value), atom(s) number: 3
14. +0,37 (experimental value), atom(s) number: 2
15. +0,37 (experimental value), atom(s) number: 15
16. +0,37 (experimental value), atom(s) number: 5
17. +0,37 (experimental value), atom(s) number: 4

Interactions through aromatic system:

- 1-10 0,00 (approximated value), atom(s) number: 19, 16, 14, 13, 6

Interactions through aliphatic system:

- 2-8 +0,28 (experimental value), atom(s) number: 1, 7, 8

Increments of the ring interactions

Increments of the ring interactions

*Econazole*

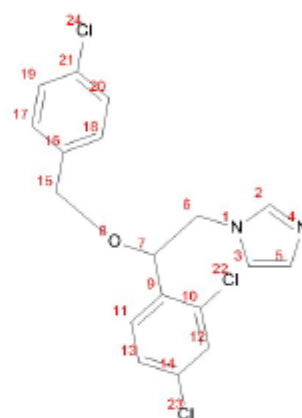
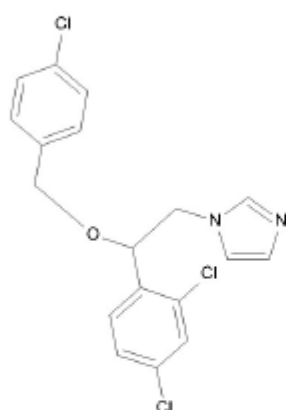
ACD/Labs  
ACD/LogP Classic Module Report

Date: February 17, 2015 10:16 AM

Software name and version: ACD/Percepta 14.0.0 (Build 2203)

Compound name: Econazole

Structure:



Calculated LogP: 5,32 +- 0,55



**LogP Calculation Protocol:**

Increments of the functional groups:

1. -1,86 (experimental value), atom(s) number: 2, 4, 1
2. +1,04 (experimental value), atom(s) number: 22
3. +1,04 (experimental value), atom(s) number: 23
4. +1,04 (experimental value), atom(s) number: 24
5. -1,90 (experimental value), atom(s) number: 8

Increments of the Carbon atoms:

6. +0,53 (experimental value), atom(s) number: 15
7. +0,53 (experimental value), atom(s) number: 6
8. -0,03 (experimental value), atom(s) number: 7
9. +0,37 (experimental value), atom(s) number: 3
10. +0,37 (experimental value), atom(s) number: 5
11. -0,08 (experimental value), atom(s) number: 10
12. -0,08 (experimental value), atom(s) number: 14
13. -0,08 (experimental value), atom(s) number: 21
14. -0,08 (experimental value), atom(s) number: 9
15. -0,08 (experimental value), atom(s) number: 16
16. +0,37 (experimental value), atom(s) number: 12
17. +0,37 (experimental value), atom(s) number: 13
18. +0,37 (experimental value), atom(s) number: 20
19. +0,37 (experimental value), atom(s) number: 19
20. +0,37 (experimental value), atom(s) number: 11
21. +0,37 (experimental value), atom(s) number: 18
22. +0,37 (experimental value), atom(s) number: 17

Interactions through aromatic system:

- 2-3 +0,01 (experimental value), atom(s) number: 22, 10, 12, 14, 23

Interactions through aliphatic system:

- 14-15 -0,05 (experimental value), atom(s) number: 16, 15, 8, 7, 9
- 1-14 -0,01 (experimental value), atom(s) number: 9, 7, 6, 1
- 1-5 +0,64 (experimental value), atom(s) number: 1, 6, 7, 8
- 5-14 +0,65 (experimental value), atom(s) number: 9, 7, 8
- 5-15 +0,65 (experimental value), atom(s) number: 16, 15, 8
- 1-15 +0,10 (approximated value), atom(s) number: 16, 15, 8, 7, 6, 1

Referenced data:



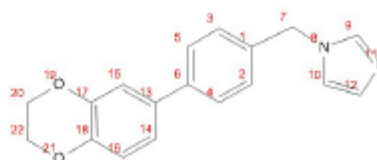
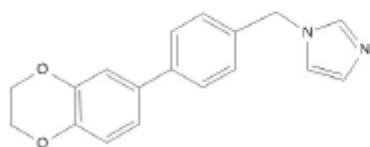
ACD/Labs  
ACD/LogP Classic Module Report

Date: February 17, 2015 10:03 AM

Software name and version: ACD/Percepta 14.0.0 (Build 2203)

Compound name:

Structure:



Calculated LogP: 2.63 ± 0.39

**LogP Calculation Protocol:**

Increments of the functional groups:

1. -1,86 (experimental value), atom(s) number: 9, 11, 8
2. -0,55 (experimental value), atom(s) number: 19
3. -0,55 (experimental value), atom(s) number: 21

Increments of the Carbon atoms:

4. +0,56 (experimental value), atom(s) number: 20
5. +0,56 (experimental value), atom(s) number: 22
6. +0,53 (experimental value), atom(s) number: 7
7. +0,37 (experimental value), atom(s) number: 10
8. +0,37 (experimental value), atom(s) number: 12
9. +0,08 (experimental value), atom(s) number: 17
10. +0,08 (experimental value), atom(s) number: 18
11. -0,08 (experimental value), atom(s) number: 1
12. -0,08 (experimental value), atom(s) number: 13
13. -0,08 (experimental value), atom(s) number: 6
14. +0,37 (experimental value), atom(s) number: 15
15. +0,37 (experimental value), atom(s) number: 16
16. +0,37 (experimental value), atom(s) number: 3
17. +0,37 (experimental value), atom(s) number: 2
18. +0,37 (experimental value), atom(s) number: 14
19. +0,37 (experimental value), atom(s) number: 5
20. +0,37 (experimental value), atom(s) number: 4

Interactions through aromatic system:

- 3-13 -0,10 (experimental value), atom(s) number: 6, 13, 14, 16, 18, 21
- 2-13 -0,15 (experimental value), atom(s) number: 6, 13, 15, 17, 19
- 2-3 -0,09 (experimental value), atom(s) number: 19, 17, 18, 21

Interactions through aliphatic system:

- 2-3 +0,29 (experimental value), atom(s) number: 21, 22, 20, 19
- 1-11 +0,28 (experimental value), atom(s) number: 1, 7, 8

Increments of the ring interactions

Increments of the ring interactions

**Bacterial strains and growth conditions.**

Bacterial strains used in this study were *Mycobacterium bovis* DSM-43990 (BCGT), *Mycobacterium tuberculosis* H<sub>37</sub>Rv (Mtb), *Escherichia coli* TolC acr A/B deficient, *Staphylococcus aureus* (Newman strain) and *E. coli* K12 BL21. Mammalian cell lines for cytotoxicity evaluation were HEK293 (human embryonic kidney) and Hep2G (human liver carcinoma cells) cells. Mycobacteria were cultured in 7H9GC-Tween<sup>5</sup> or Middlebrook 7H9 broth complemented with ADC Enrichment (Middlebrook). *E. coli* TolC and *S. aureus* tests were performed in lysogenic broth (LB) and LB plus ADC Enrichment.

**Chemical synthesis and analytical characterization. Chemicals were purchased from commercial suppliers and used without further purification.**

Column flash chromatography was performed on silica gel (40–63 μm), and reaction progress was monitored by TLC on TLC Silica Gel 60 F<sub>254</sub> plates (Merck, Darmstadt, Germany). All moisture-sensitive reactions were performed under nitrogen atmosphere using anhydrous solvents. <sup>1</sup>H and <sup>13</sup>C NMR spectra were recorded on Bruker Fourier spectrometers (300 MHz) at ambient temperature with the chemical shifts recorded as δ values in ppm units by reference to the hydrogenated residues of deuterated solvent as internal standard. Coupling constants (J) are given in Hertz (Hz), and signal patterns are indicated as follows: s, singlet; d, doublet; dd, doublet of doublets; t, triplet; m, multiplet, br, broad signal. The purity of the final compounds was >95% measured by HPLC with UV detection at 254 nm. The SpectraSystem LC system consisted of a pump, an autosampler, and a UV/Vis detector (ThermoFisher, Dreieich, Germany). Mass spectrometry was performed on an LC-coupled Surveyor MSQ electrospray mass spectrometer (ThermoFisher, Dreieich, Germany). The system was operated by the Xcalibur software. An RP C18 NUCLEODUR ec 100-5 125×3 mm 5 μm column (Macherey-Nagel GmbH, Düren, Germany) was used as the stationary phase. All solvents were HPLC grade. In a gradient run, the percentage of acetonitrile (containing 0.1 % trifluoroacetic acid) was increased from an initial concentration of 0 % at 0 min to 100 % at 15 min and kept at 100 % for 5 min. The injection volume was 10 μL, and flow rate was set to 800 μL/min. MS analysis was carried out at a spray voltage of 3800 V, a source CID of 10 V and a capillary temperature of 350 °C. Spectra were acquired in positive mode from 100 to 1000 m/z.

cYY and mycocyclosin were synthesized as described.<sup>6–8</sup> Experimental details on modification of cYY and mycocyclosin synthesis and analytical data can be found in the Supplementary Data (Supp. Data, section 1).

The synthesis of library compounds has been described previously: class I<sup>9–14</sup>, class II<sup>15,16</sup>, class III<sup>17</sup>, class IV<sup>18</sup>, class V<sup>19</sup>, and class VI<sup>20</sup>.

### Protein expression, purification and biotinylation.

*E. coli* K12 BL21 (DE3) cells were transformed with plasmid harboring *cyp121* gene (pHAT2/*cyp121*).<sup>21</sup>

The previously described<sup>22</sup> enzyme expression and purification method was slightly modified: His<sub>6</sub>-tagged CYP121 (H<sub>6</sub>-CYP121) was expressed in *E. coli* K12 BL21 and purified using a single affinity chromatography step. Briefly, *E. coli* K12 BL21 cells containing the pHAT2/*cyp121* were grown in terrific broth medium containing 100 µg/mL ampicillin at 37 °C until an OD<sub>600</sub> of approximately 0.8 units was reached, followed by induction with 0.5 mM IPTG and 0.5 mM δ-aminolevulinic acid for 36 h at 25 °C and 200 rpm. The cells were harvested by centrifugation (5000 rpm, 10 min, 4 °C), and the cell pellet was resuspended in 100 mL of binding buffer containing 1% Triton-X-100 (50 mM tris-HCl, 300 mM NaCl, 20 mM imidazole, 10% glycerol, pH = 7.2) and lysed by sonication for a total process time of 2.5 min. Cellular debris was removed by centrifugation (18,500 rpm, 40 min, 4 °C), and the supernatant was filtered through a syringe filter (0.2 µm). The clear lysate was immediately applied to a Ni-NTA affinity column, washed with binding buffer, and eluted with a one-step gradient of 500 mM imidazole. The protein containing fractions were buffer-exchanged into storage buffer (140 mM NaCl, 10 mM Na<sub>2</sub>HPO<sub>4</sub>, 2.7 mM KCl, 1.8 mM KH<sub>2</sub>PO<sub>4</sub> and 10% glycerol (v/v), pH = 7.2), using a PD10 column (GE Healthcare, Little Chalfont, UK) and judged to be pure by SDS-PAGE analysis. Then protein was stored in aliquots at -80 °C in a final concentration of 50 µM.<sup>22</sup>

Before SPR streptavidin immobilization CYP121 was biotinylated. For biotinylation, Sulfo-NHS-LC-LC-Biotin (Thermo Science, Waltham, US) was dissolved in storage buffer (140 mM NaCl, 10 mM Na<sub>2</sub>HPO<sub>4</sub>, 2.7 mM KCl, 1.8 mM KH<sub>2</sub>PO<sub>4</sub> and 10% glycerol (v/v)) with CYP121 in 1:1 molar ratio. The solution was incubated on ice for 2 h and mixed carefully every 30 min. The biotinylated CYP121 was purified by size exclusion chromatography using the storage buffer and subsequently stored at -80 °C at a final concentration of 10 µM.<sup>23</sup>

### In silico binding mode.

*In silico* studies were performed with the X-ray co-crystal structure of a type II inhibitor and CYP121 (PDB-ID: 4G44) using MOE software package (Chemical Computing Group).<sup>24</sup> Prior to modelling, a pharmacophore model was created, placing a feature for an interacting metal on the heme iron (ML2, R = 1) and a second feature for a metal ligand (ML, R = 1) on the iron-coordinating nitrogen of the co-crystallized ligand. Both features were set to be essential and constrained (Atoms/Projections). Before energy minimization with LigX the solvent and the ligand was deleted from the structure. For LigX, an AMBER10:EHT forcefield with the default parameters were used but the solvation model was changed to R-Field as recommended by the manufacturer. For docking experiments the following parameters were used: Protocols = induced fit, Receptor = Receptor+Solvent, Site = Selected Atoms (these consisted of the heme and the surrounding amino acids in 4.5 Å proximity), Pharmacophore =

File (as described above), Ligand = MDB File (Database file with **I:47**, energy minimized with MMFF94x), Placement = Pharmacophore, Rescoring 1 = London dG, Refinement = Forcefield, Rescoring 2 = GBVI/WSA dG. 30 poses were retained within the placement and refinement step. The resulting poses were sorted by their *E\_refine* score and the first (best) pose was selected for further evaluation.

### **Physicochemical properties.**

Physicochemical properties were calculated using ACD/Percepta version 2012 (Build 2203, 29 jan. 2013), ACD/Labs.

### **Cyp121 *in vitro* enzyme inhibition assay.**

The enzyme inhibition assay was performed in 200 mL PBS buffer pH 7.2. Compounds were used in a concentration of 100  $\mu\text{M}$  and incubated with 1  $\mu\text{M}$  CYP121 for 30 minutes at 30 °C. The final DMSO concentration did not exceed 2%. After incubation the electron transfer system Arh1\_A18G (5  $\mu\text{M}$ ), Etp1fd (15  $\mu\text{M}$ ) and NADPH+H<sup>+</sup> (200  $\mu\text{M}$ ) was added. The reaction was started with the addition of cYY (50  $\mu\text{M}$ ) and stopped after 30 min by addition of 200  $\mu\text{l}$  methanol with internal standard estrone (1  $\mu\text{M}$  final concentration, addition included).

The characterization of CYP121 activity was conducted by a UHPLC-MS/MS analysis carried out on a TSQ Quantum Access Max mass spectrometer equipped with an HESI-II source and a triple quadrupole mass detector (Thermo Scientific, Dreieich, Germany). Compounds were separated on an Accucore RP-MS 150 $\times$ 2.1 mm 2.6  $\mu\text{m}$  column (Thermo Fisher, Waltham, US) by a methanol/water gradient (from 1.4 min - 3.5 min 50% methanol to 3.5 min - 5.0 min 90% methanol) with a flow of 550  $\mu\text{L}/\text{min}$ . Compounds were ionized in negative mode by electrospray ionization. Ionization was assisted by a post-column addition of 2 mM ammonia in methanol with an automated syringe at 1.25  $\mu\text{L}/\text{min}$ . Monitored ions were (mother ion [m/z], product ion [m/z], scan time [s], scan width [m/z], collision energy [V], tube lens offset [V], polarity): mycrocyclosin: 323.101, 111.100, 0.3, 0.7, 28, negative; cYY: 325.129, 113.043, 0.3, 0.7, 29, negative; internal standard (estrone): 269.153, 145.035, 0.3, 0.7, 42, negative. Samples were injected in a volume of 25  $\mu\text{L}$ . Xcalibur software was used for data acquisition. For quantification, the ratios of the area under the curve of the educt and the product were used.

### Determination MIC<sub>Mtb</sub> using MABA.

The assay for determination of minimal inhibition concentration against *Mtb* was performed as previously described.<sup>5</sup>

### MIC<sub>Eco</sub> *E. coli* TolC and MIC<sub>Sa</sub> *S.aureus* Newman

MIC<sub>Eco</sub> /MIC<sub>Sa</sub> values were performed for econazole, **I:16**, **I:47**, **I:48** in *E. coli* TolC and *S. aureus* Newman. A start OD<sub>600</sub> of 0.03 was used in a total volume of 200 mL in lysogeny broth (LB) + ACD enrichment containing the compounds predissolved in DMSO. Final compound concentrations were prepared from serial dilutions ranging from 1.56 to 100 μM in duplicates. The maximal DMSO concentration in the experiment was 1%. The recorded OD<sub>600</sub> values were determined after addition of the compounds and again after incubation for 18 h at 37 °C and 50 rpm in a 96-well plate (Sarstedt, Nümbrecht, Germany) using a FLUOStar Omega (BMG Labtech, Ortenberg, Germany). Given MIC<sub>Eco</sub> /MIC<sub>Sa</sub> values are means of two independent experiments (two different clones) and are defined as concentrations at which no bacterial growth was detectable.

### Spectroscopic characterization of enzyme activity.

Recombinant CYP121 from *Mycobacterium tuberculosis* as well as ferredoxin Etp1fd (516-618) and ferredoxin reductase Arh1\_A18G from the fission yeast *Schizosaccharomyces pombe* were expressed and purified as described previously.<sup>25,26</sup>

Functionality of CYP121 and electron transfer were assayed by the occurrence of the characteristic absorbance maximum at  $\lambda \cong 450$  nm, related to the reduced, CO-bound heme complex. The assay was conducted following the method of Omura and Sato<sup>27</sup> with slight modifications. CYP121 (2 μM) was reduced through the addition of a few grains of sodium dithionite or incubation with NADPH (100 μM), ferredoxin Etp1fd(516-618) (40 μM), and Arh1\_A18G ferredoxin reductase (2 μM) and divided in two cuvettes to record a baseline. One of the samples was saturated with carbon monoxide for 60 s and difference spectra were recorded until the absorbance at  $\lambda \cong 450$  nm was constant.

### References

- (1) Cochrane, J. R., White, J. M., Wille, U., and Hutton, C. A. (2012) Total synthesis of mycrocyclosin. *Organic letters* 14, 2402–2405. DOI: 10.1021/ol300831t.
- (2) Jung, M. E., and Rohloff, J. C. (1985) Organic chemistry of L-tyrosine. 1. General synthesis of chiral piperazines from amino acids. *J. Org. Chem.* 50, 4909–4913. DOI: 10.1021/jo00224a051.
- (3) Franzblau, S. G., DeGroote, M. A., Cho, S. H., Andries, K., Nuermberger, E., Orme, I. M., Mdluli, K., Angulo-Barturen, I., Dick, T., Dartois, V., and Lenaerts, A. J. (2012) Comprehensive

analysis of methods used for the evaluation of compounds against *Mycobacterium tuberculosis*.

*Tuberculosis* 92, 453–488. DOI: 10.1016/j.tube.2012.07.003.

(4) Brzostek, A., Dziadek, B., Rumijowska-Galewicz, A., Pawelczyk, J., and Dziadek, J. (2007) Cholesterol oxidase is required for virulence of *Mycobacterium tuberculosis*. *FEMS microbiology letters* 275, 106–112. DOI: 10.1111/j.1574-6968.2007.00865.x.

(5) Collins, L., and Franzblau, S. G. (1997) Microplate alamar blue assay versus BACTEC 460 system for high-throughput screening of compounds against *Mycobacterium tuberculosis* and *Mycobacterium avium*. *Antimicrob. Agents Chemother.* 41, 1004–1009.

(6) Hauptenthal, J., Baehr, C., Zeuzem, S., and Piiper, A. (2007) RNase A-like enzymes in serum inhibit the anti-neoplastic activity of siRNA targeting polo-like kinase 1. *Int. J. Cancer* 121, 206–210. DOI: 10.1002/ijc.22665.

(7) Fonvielle, M., Le Du, M.-H., Lequin, O., Lecoq, A., Jacquet, M., Thai, R., Dubois, S., Grach, G., Gondry, M., and Belin, P. (2013) Substrate and reaction specificity of *Mycobacterium tuberculosis* cytochrome P450 CYP121: insights from biochemical studies and crystal structures. *J. Biol. Chem.* 288, 17347–17359. DOI: 10.1074/jbc.M112.443853.

(8) Cochrane, J. R., White, J. M., Wille, U., and Hutton, C. A. (2012) Total synthesis of mycrocyclosin. *Org. Lett.* 14, 2402–2405. DOI: 10.1021/ol300831t.

(9) Wachall, B. G., Hector, M., Zhuang, Y., and Hartmann, R. W. (1999) Imidazole substituted biphenyls: A new class of highly potent and in vivo active inhibitors of P450 17 as potential therapeutics for treatment of prostate cancer. *Bioorg. Med. Chem.* 7, 1913–1924. DOI: 10.1016/S0968-0896(99)00160-1.

(10) Hille, U. E., Zimmer, C., Vock, C. A., and Hartmann, R. W. (2011) First Selective CYP11B1 Inhibitors for the Treatment of Cortisol-Dependent Diseases. *ACS Med. Chem. Lett.* 2, 2–6. DOI: 10.1021/ml100071j.

(11) Jagusch, C., Negri, M., Hille, U. E., Hu, Q., Bartels, M., Jahn-Hoffmann, K., Pinto-Bazurco Mendieta, Mariano A E, Rodenwaldt, B., Müller-Vieira, U., Schmidt, D., Lauterbach, T., Recanatini, M., Cavalli, A., and Hartmann, R. W. (2008) Synthesis, biological evaluation and molecular modelling studies of methyleneimidazole substituted biaryls as inhibitors of human 17 $\alpha$ -hydroxylase-17,20-lyase (CYP17). Part I: Heterocyclic modifications of the core structure. *Bioorg. Med. Chem.* 16, 1992–2010. DOI: 10.1016/j.bmc.2007.10.094.

(12) Pinto-Bazurco Mendieta, Mariano A E, Negri, M., Hu, Q., Hille, U. E., Jagusch, C., Jahn-Hoffmann, K., Müller-Vieira, U., Schmidt, D., Lauterbach, T., and Hartmann, R. W. (2008) CYP17 inhibitors. Annulations of additional rings in methylene imidazole substituted biphenyls: synthesis, biological evaluation and molecular modelling. *Arch. Pharm.* 341, 597–609. DOI: 10.1002/ardp.200700251.

(13) Hille, U. E., Hu, Q., Vock, C., Negri, M., Bartels, M., Müller-Vieira, U., Lauterbach, T., and Hartmann, R. W. (2009) Novel CYP17 inhibitors: synthesis, biological evaluation, structure-activity



relationships and modelling of methoxy- and hydroxy-substituted methyleneimidazolyl biphenyls.

*Eur. J. Med. Chem.* 44, 2765–2775. DOI: 10.1016/j.ejmech.2009.01.002.

(14) Hille, U. E., Zimmer, C., Haupenthal, J., and Hartmann, R. W. (2011) Optimization of the First Selective Steroid-11 $\beta$ -hydroxylase (CYP11B1) Inhibitors for the Treatment of Cortisol Dependent Diseases. *ACS Med. Chem. Lett.* 2, 559–564. DOI: 10.1021/ml100283h.

(15) Yin, L., Lucas, S., Maurer, F., Kazmaier, U., Hu, Q., and Hartmann, R. W. (2012) Novel imidazol-1-ylmethyl substituted 1,2,5,6-tetrahydropyrrolo[3,2,1-ij]quinolin-4-ones as potent and selective CYP11B1 inhibitors for the treatment of Cushing's syndrome. *J. Med. Chem.* 55, 6629–6633. DOI: 10.1021/jm3003872.

(16) Yin, L., Hu, Q., and Hartmann, R. W. (2013) Tetrahydropyrroloquinolinone type dual inhibitors of aromatase/aldosterone synthase as a novel strategy for breast cancer patients with elevated cardiovascular risks. *J. Med. Chem.* 56, 460–470. DOI: 10.1021/jm301408t.

(17) Yin, L., Hu, Q., Emmerich, J., Lo, M. M.-C., Metzger, E., Ali, A., and Hartmann, R. W. (2014) Novel pyridyl- or isoquinoliny-substituted indolines and indoles as potent and selective aldosterone synthase inhibitors. *Journal of medicinal chemistry* 57, 5179–5189. DOI: 10.1021/jm500140c.

(18) Hu, Q., Kunde, J., Hanke, N., and Hartmann, R. W. (2015) Identification of 4-(4-nitro-2-phenethoxyphenyl)pyridine as a promising new lead for discovering inhibitors of both human and rat 11 $\beta$ -Hydroxylase. *Eur. J. Med. Chem.* 96, 139–150. DOI: 10.1016/j.ejmech.2015.04.013.

(19) Zimmer, C., Hafner, M., Zender, M., Ammann, D., Hartmann, R. W., and Vock, C. A. (2011) N-(Pyridin-3-yl)benzamides as selective inhibitors of human aldosterone synthase (CYP11B2). *Bioorg. Med. Chem. Lett.* 21, 186–190. DOI: 10.1016/j.bmcl.2010.11.040.

(20) Zhu, W., Hu, Q., Hanke, N., van Koppen, Chris J, and Hartmann, R. W. (2014) Potent 11 $\beta$ -hydroxylase inhibitors with inverse metabolic stability in human plasma and hepatic S9 fractions to promote wound healing. *J. Med. Chem.* 57, 7811–7817. DOI: 10.1021/jm501004t.

(21) Hudson, S. A., McLean, K. J., Surade, S., Yang, Y.-Q., Leys, D., Ciulli, A., Munro, A. W., and Abell, C. (2012) Application of fragment screening and merging to the discovery of inhibitors of the Mycobacterium tuberculosis cytochrome P450 CYP121. *Angew. Chem., Int. Ed.* 51, 9311–9316. DOI: 10.1002/anie.201202544.

(22) McLean, K. J., Cheesman, M. R., Rivers, S. L., Richmond, A., Leys, D., Chapman, S. K., Reid, G. A., Price, N. C., Kelly, S. M., Clarkson, J., Smith, W., and Munro, A. W. (2002) Expression, purification and spectroscopic characterization of the cytochrome P450 CYP121 from Mycobacterium tuberculosis. *J. Inorg. Biochem.* 91, 527–541. DOI: 10.1016/S0162-0134(02)00479-8.

(23) Hüsecken, K., Hinsberger, S., Elgaher, Walid A M, Haupenthal, J., and Hartmann, R. W. (2014) Surface plasmon resonance--more than a screening technology: insights in the binding mode of  $\sigma$ 70:core RNAP inhibitors. *Future Med. Chem.* 6, 1551–1565. DOI: 10.4155/fmc.14.105.

(24) *Molecular Operating Environment (MOE) (Version 2013.08)* (2015), Chemical Computing Group Inc., 1010 Sherbooke St. West, Suite #910, Montreal, QC, Canada, H3A 2R7.

(25) Ewen, K. M., Schiffler, B., Uhlmann-Schiffler, H., Bernhardt, R., and Hannemann, F. (2008) The endogenous adrenodoxin reductase-like flavoprotein arh1 supports heterologous cytochrome P450-dependent substrate conversions in *Schizosaccharomyces pombe*. *FEMS Yeast Res.* 8, 432–441. DOI: 10.1111/j.1567-1364.2008.00360.x.

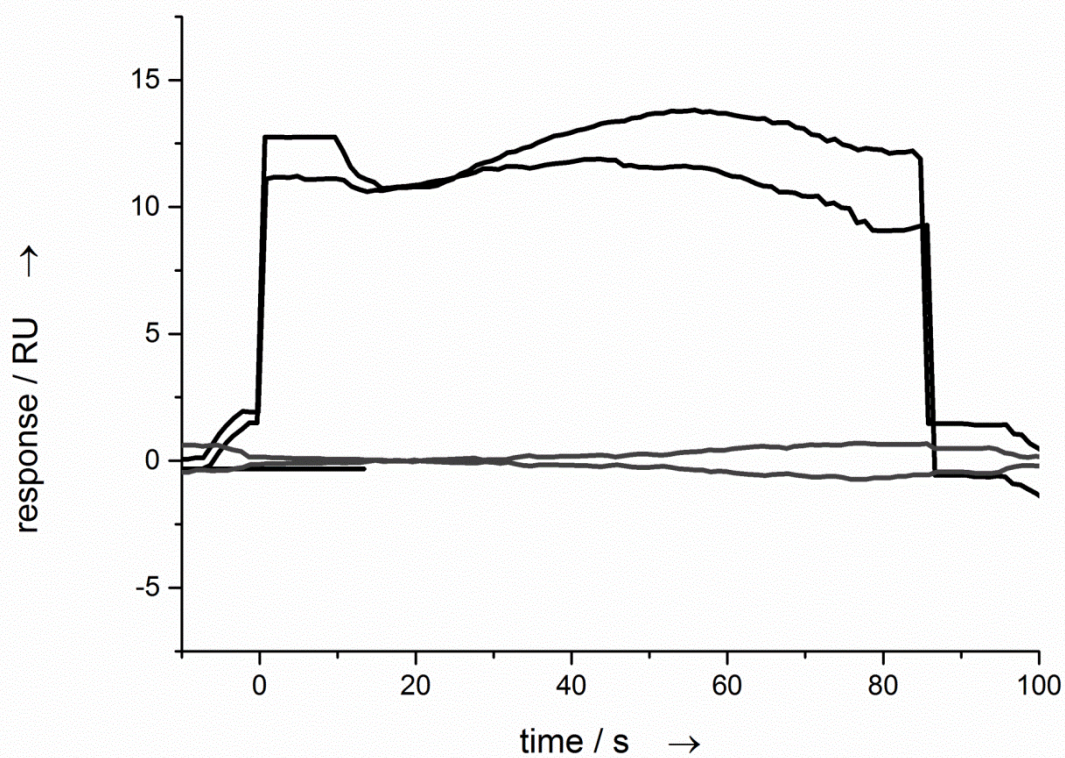
(26) Müller, J. J., Hannemann, F., Schiffler, B., Ewen, K. M., Kappl, R., Heinemann, U., and Bernhardt, R. (2011) Structural and thermodynamic characterization of the adrenodoxin-like domain of the electron-transfer protein Etp1 from *Schizosaccharomyces pombe*. *J. Inorg. Biochem.* 105, 957–965. DOI: 10.1016/j.jinorgbio.2011.04.001.

(27) Omura, T., and Sato, R. (1964) THE CARBON MONOXIDE-BINDING PIGMENT OF LIVER MICROSOMES. II. SOLUBILIZATION, PURIFICATION, AND PROPERTIES. *J. Biol. Chem.* 239, 2379–2385.

**B      Discovery and biophysical evaluation of first low nanomolar hits targeting CYP125 of M. tuberculosis**

Christian Brengel, Andreas Thomann, Jens Eberhard, and Rolf W. Hartmann

*Manuscript in preparation*

**SPR Response Curve of Econazole (positive control)**

**SI Figure 1.** SPR response curve of 100  $\mu$ M econazole (eco, black, positive binder) and baseline (grey) recorded against biotin labeled CYP125 immobilized on a streptavidine coated sensorchip.

### Comparison of CYP125 from *M. tuberculosis* and *M. bovis* BCG

unnamed protein product

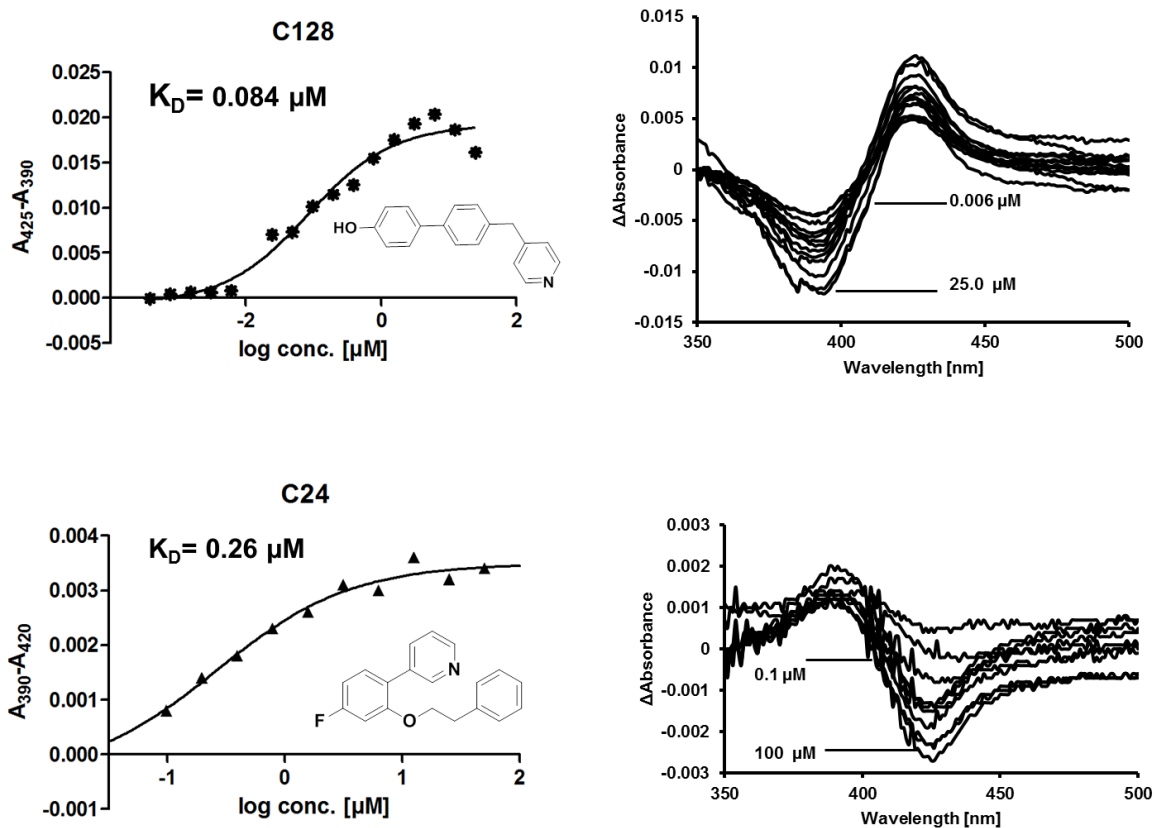
Sequence ID: lc|Query\_152585 Length: 433 Number of Matches: 1

Range 1: 1 to 433 [Graphics](#)

▼ Next Match ▲ Previous Match

Score	Expect	Method	Identities	Positives	Gaps
901 bits(2329)	0.0	Compositional matrix adjust.	433/433(100%)	433/433(100%)	0/433(0%)
Query 1		MSWNHQSV EIAVRRRTTVPSNLPPGFDFDPAIYAERLPVAEFAELRSAAPIIWMNGQDPG			60
Sbjct 1		MSWNHQSV EIAVRRRTTVPSNLPPGFDFDPAIYAERLPVAEFAELRSAAPIIWMNGQDPG			60
Query 61		KGGGFHDGGFWAITKLN DVKEISRHSDFVSSYENGVIPRFKNDIARE DIEVQRFVMLNMD			120
Sbjct 61		KGGGFHDGGFWAITKLN DVKEISRHSDFVSSYENGVIPRFKNDIARE DIEVQRFVMLNMD			120
Query 121		APHHTRLRK IISRGFTPR AVGRLHDELQERAQKIAAEAAAAGSGDFVEQVSC ELPLQAIA			180
Sbjct 121		APHHTRLRK IISRGFTPR AVGRLHDELQERAQKIAAEAAAAGSGDFVEQVSC ELPLQAIA			180
Query 181		GLLGV PQEDRGKLFHWSNEMTG NEDPEYAHIDPKASSAELIGYAMKMAEEKAKNPADDIV			240
Sbjct 181		GLLGV PQEDRGKLFHWSNEMTG NEDPEYAHIDPKASSAELIGYAMKMAEEKAKNPADDIV			240
Query 241		TQLIQADIDG EKLSDD EFGFFV VMLAVAGNETTRNSITQGMMAFAEHPDQWEL YKKVRPE			300
Sbjct 241		TQLIQADIDG EKLSDD EFGFFV VMLAVAGNETTRNSITQGMMAFAEHPDQWEL YKKVRPE			300
Query 301		TAADEIVRWATPV TAFQRTALRDYELSGVQIKKQQRVVMFYRSANFDEEVFQDP PTFNIL			360
Sbjct 301		TAADEIVRWATPV TAFQRTALRDYELSGVQIKKQQRVVMFYRSANFDEEVFQDP PTFNIL			360
Query 361		RNP NPHVGFGGTGAHYCIGANL ARMTINLIFNAVADHMPDLKPI SAPERLRSGWLN GIKH			420
Sbjct 361		RNP NPHVGFGGTGAHYCIGANL ARMTINLIFNAVADHMPDLKPI SAPERLRSGWLN GIKH			420
Query 421		WQVDYTGRC PVAH 433			
Sbjct 421		WQVDYTGRC PVAH 433			

**SI Figure 2.** Result of the Protein BLAST of CYP125 from *M. tuberculosis* (gene-ID: Rv3545c) and *M. bovis* BCG (gene-ID: BCG\_3609c) showing 100% amino acid identity of both proteins.

Representative  $K_D$  Dose Response Curves and Difference Spectra

SI Figure 3. Representative  $K_D$  dose response curves (left) and difference spectra (right) of a type I (C24, lower spectra) and a type II (C128, upper spectra) CYP125 heme ligands.

### Summary of Binding Constants, Profile and Ligand Efficiency Indices of SPR Hits

**SI Table 1.** Relative responses of SPR hits ( $R/R_{\text{pos}}$ ) and their respective heme binding profiles, binding affinities ( $K_D$ ) and Ligand efficiency scores (LE) against CYP125.

Compound	SPR [ $R/R_{\text{pos}}$ ]	Heme assay Binding Type <sup>c</sup>	Heme assay $K_D$ [ $\mu\text{M}$ ]	Ligand efficiency [kcal/HA]
Econazole (Eco = $R_{\text{pos}}$ )	1.0	I	0.94	0.36
CHN <sup>a</sup>	-	I	4.6	-
LP10 <sup>b</sup>	-	rI	6.1	0.24
C3	1.3	II	19	0.35
C5	1.0	II	28	0.29
C16	1.1	I	16	0.32
C23	1.0	I	1.5	0.37
C24	1.1	I	0.26	0.42
C25	0.9	no	-	-
C36	2.8	I	1.3	0.46
C37	3	I	1.1	0.49
C42	0.0	no	-	-
C43	1.2	II	13.1	0.26
C52	2.8	no	-	-
C53	0.5	-	-	-
C55	1.2	II	38.7	0.29
C59	0.8	-	-	-
C60	1.1	I	0.28	0.42
C68	1.0	II	38.7	0.34
C80	1.6	II	39.6	0.22

<b>C83</b>	2.9	no	-	-
<b>C87</b>	1.2	no	-	-
<b>C90</b>	1.7	no	-	-
<b>C119</b>	2.0	no	-	-
<b>C126</b>	1.2	II	2.1	0.27
<b>C127</b>	3.1	II	0.85	0.47
<b>C128</b>	1.1	II	0.084	0.50
<b>C129</b>	2.6	II	1.34	0.41
<b>C130</b>	2.4	II	0.174	0.53

<sup>a</sup> CHN = Cholest-4-en-3-one; <sup>b</sup> LP10 =  $\alpha$ -[(4-methylcyclohexyl)carbonyl amino]-*N*-4-pyridinyl-1*H*-indole-3-propanamide; <sup>c</sup> I = Type I binding profile, II = Type II binding profile, rI = reverse Type II binding profile no = no binding profile observed at the highest tested concentration (100  $\mu$ M).

#### Absorbance maximum in Heme assay

**SI Table 2.** Binding affinities ( $K_D$ ) and absorbance maxima of selected compounds against CYP125.

Compound	Heme $K_D$ [ $\mu$ M]	Heme assay Absorbance maximum [nm]
<b>LP10</b>	6.1	419
<b>C127</b>	0.85	421
<b>C128</b>	0.08	420
<b>C129</b>	1.34	422
<b>C130</b>	0.17	421

#### Synthesis, analytical and biological data of the screening compounds and their derivatives

**C1**,<sup>[1]</sup> **C2**,<sup>[1]</sup>, **C3**,<sup>[2]</sup> **C4**,<sup>[1]</sup> **C5**,<sup>[3]</sup> **C6**,<sup>[1]</sup> **C7** - **C10**,<sup>[5]</sup> **C11** - **C18**,<sup>[4]</sup> **C19** - **C27**,<sup>[5]</sup> **C28** - **C29**,<sup>[1]</sup> **C30** - **C33**,<sup>[6]</sup> **C34** - **C74**,<sup>[7]</sup> **C75** - **C121**,<sup>[8]</sup> **C122** - **C125**,<sup>[9]</sup> **C127** - **C130**.<sup>[10]</sup>



- [1] C. Zimmer, M. Hafner, M. Zender, D. Ammann, R. W. Hartmann, C. A. Vock, *Bioorganic & medicinal chemistry letters* **2011**, *21*, 186–190.
- [2] S. S. Gunatilleke, C. M. Calvet, J. B. Johnston, C.-K. Chen, G. Erenburg, J. Gut, J. C. Engel, Ang, Kenny K H, J. Mulvaney, S. Chen et al., *PLoS neglected tropical diseases* **2012**, *6*, e1736.
- [3] M. Balcells, J. Avilla, J. Profitos, R. Canela, *Journal of Agricultural and Food Chemistry* **2000**, *48*, 83–87.
- [4] J. Emmerich, Q. Hu, N. Hanke, R. W. Hartmann, *Journal of medicinal chemistry* **2013**, *56*, 6022–6032.
- [5] Q. Hu, J. Kunde, N. Hanke, R. W. Hartmann, *European journal of medicinal chemistry* **2015**, *96*, 139–150.
- [6] a) R. Heim, S. Lucas, C. M. Grombein, C. Ries, K. E. Schewe, M. Negri, U. Müller-Vieira, B. Birk, R. W. Hartmann, *Journal of medicinal chemistry* **2008**, *51*, 5064–5074; b) S. Lucas, M. Negri, R. Heim, C. Zimmer, R. W. Hartmann, *Journal of medicinal chemistry* **2011**, *54*, 2307–2319; c) Q. Hu, L. Yin, R. W. Hartmann, *Journal of medicinal chemistry* **2012**, *55*, 7080–7089.
- [7] a) U. E. Hille, Q. Hu, C. Vock, M. Negri, M. Bartels, U. Müller-Vieira, T. Lauterbach, R. W. Hartmann, *European journal of medicinal chemistry* **2009**, *44*, 2765–2775; b) U. E. Hille, C. Zimmer, C. A. Vock, R. W. Hartmann, *ACS medicinal chemistry letters* **2011**, *2*, 2–6; c) U. E. Hille, C. Zimmer, J. Hauptenthal, R. W. Hartmann, *ACS medicinal chemistry letters* **2011**, *2*, 559–564.
- [8] a) L. Yin, Q. Hu, R. W. Hartmann, *Journal of medicinal chemistry* **2013**, *56*, 460–470; b) L. Yin, Q. Hu, J. Emmerich, M. M.-C. Lo, E. Metzger, A. Ali, R. W. Hartmann, *Journal of medicinal chemistry* **2014**, *57*, 5179–5189; c) L. Yin, S. Lucas, F. Maurer, U. Kazmaier, Q. Hu, R. W. Hartmann, *Journal of medicinal chemistry* **2012**, *55*, 6629–6633.
- [9] W. Zhu, Q. Hu, N. Hanke, van Koppen, Chris J, R. W. Hartmann, *Journal of medicinal chemistry* **2014**, *57*, 7811–7817.
- [10] Q. Hu, C. Jagusch, U. E. Hille, J. Hauptenthal, R. W. Hartmann, *Journal of medicinal chemistry* **2010**, *53*, 5749–5758.

**C Biochemical and Biophysical Analysis of a Chiral PqsD Inhibitor Revealing Tight-Binding Behavior and Enantiomers with Contrary Thermodynamic Signatures**

Michael P. Storz, Christian Brengel, Elisabeth Weidel, Michael Hoffmann, Klaus Hollemeyer, Anke Steinbach, Rolf Müller, Martin Empting, and Rolf W. Hartmann

ACS Chem. Biol. 2013, 8, 2794-2801.

## Supporting information

### Contents:

- 1) Primer Sequence of Mutations
- 2) Table S1: Catalytic Activity of PqsD Wild-type and Mutants
- 3) Synthesis of Substrates Used in the Enzymatic Inhibition Assays
- 4) Table S2: Comparison of IC<sub>50</sub> Values Determined by Different Assay Procedures
- 5) Percentages of Inhibition and Uncertainty of the Time Dependency Experiment
- 6) Figure S1: Dose-response Curve of PqsD Inhibition by Compound **3**
- 7) Further HPLC-ESI MS Experiments
- 8) Maldi-TOF Analysis
- 9) Separation of **3** into the Enantiomers (*R*)-**3** and (*S*)-**3** by Chiral-HPLC
- 10) Figure S9: Binding site analysis of (*R*)-**3** and (*S*)-**3** by SPR
- 11) Figure S10: Reversibility of PqsD Inhibition by the Enantiomers (*R*)-**3** and (*S*)-**3**
- 12) Representative ITC Curves
- 13) References

## 1) Primer Sequence of Mutations

Mutant	Primer	
	forward 5' → 3'	reverse 3' → 5'
<b>S317F</b>	GCTGGTCCTGACCTACGGT <u>TTT</u> GGCG CGACCTGGGGCG	CGCCCCAGGTTCGCGCCAA <u>AA</u> ACCGTA GGTCAGGACCAGC
<b>C112A</b>	GCTGGATATCCGGGCACAG <u>GCG</u> AGC GGGTTGCTGTACG	CGTACAGCAACCCGCT <u>CGC</u> CTGTGCC CGGATATCCAGC
<b>H257F</b>	CGACCATGTGATCTGCT <u>TTT</u> CAACCGA ACCTGC	GCAGGTTTCGGTTGAAAGCAGATCAC ATGGTCG
<b>C112S</b>	GCTGGATATCCGGGCACAG <u>AGC</u> AGC GGGTTGCTGTACG'	CGTACAGCAACCCGCT <u>GCT</u> CTGTGCC CGGATATCCAGC
<b>S317A</b>	GCTGGTCCTGACCTACGGT <u>GCG</u> GGCG CGACCTGGGGCG	CGCCCCAGGTTCGCGCC <u>CGC</u> ACCGTA GGTCAGGACCAGC
<b>N287A</b>	CGTCTGGG <u>GCG</u> GATGGCTTCGGCC	GGCCGAAGCCAT <u>GCG</u> CCAGACG

2) Table S1: Catalytic Activity of PqsD Wild-type and Mutants<sup>a</sup>

	wild-type	S317F	C112A	H257F	C112S	S317A	N287A
<b>Formed HHQ [nM]</b>	2154	15	1	18	171	2182	7

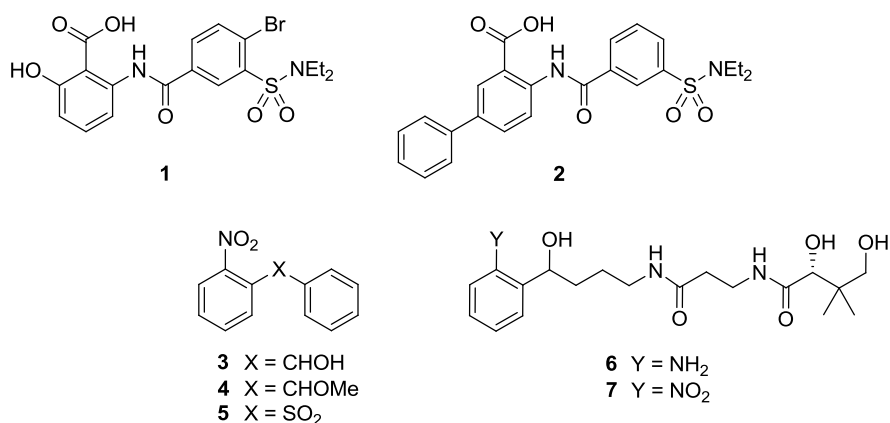
<sup>a</sup>Reactions were performed according to the screening assay procedure described in the Methods Section using 1.0 μM of *P. aeruginosa* PqsD.

### 3) Synthesis of Substrates Used in the Enzymatic Inhibition Assays

**Synthesis of anthraniloyl-S-CoA thioester (SI1).** Anthraniloyl-CoA (ACoA) was synthesized from isatoic anhydride and coenzyme A (CoA) using a previously described method. ACoA was purified by HPLC (Agilent 1200 series consisting of a quaternary pump, a fraction collector and an MWD; Agilent Technologies) after freeze drying of the aqueous reaction mixture (25 ml) and resuspending of the dried residue in 3 ml of a mixture of 50% methanol and water (v/v). A 10  $\mu\text{m}$  RP C18 150-30 column (30 x 100 mm, Agilent) was used along with a mobile phase consisting of water containing 1% TFA (A) and acetonitrile containing 1% TFA (B) with a flow rate of 5 ml min<sup>-1</sup>. The following gradient was used: 0–35 min, linear gradient 10% – 100% B (v/v); 35–42 min, 100% B; 42–43 min, 10% B (v/v) (initial conditions). ACoA containing fractions were pooled and freeze dried.

**Synthesis of  $\beta$ -ketodecanoic acid (SI2).** Ethyl 3-oxodecanoate (300 mg, 1.4 mmol) was stirred with NaOH (56 mg, 1.4 mmol) in 2 ml of water overnight. Any remaining ester was removed by washing with Et<sub>2</sub>O (10 ml). The aqueous layer was cooled and acidified with 32% HCl (w/v) to pH = 6. After filtration the 3-oxodecanoic acid was dried *in vacuo* and obtained as white solid (100 mg, 38%). <sup>1</sup>H-NMR (500 MHz, CDCl<sub>3</sub>)  $\delta$  0.86 (t, *J* = 7.0, 3H), 1.25–1.29 (m, 8H), 1.58 (m, 2H), 2.54 (t, *J* = 7.5, 2H), 3.49 (s, 2H). LC/MS (ESI) *m/z* 242.0, 99% (UV).

**Synthesis of ethyl 3-oxodecanoate (SI3).** To a THF solution of 2 M LDA (20 ml, 40 mmol) was added ethyl acetoacetate (2.16 g, 16.6 mmol) at 0°C. The deep yellow clear solution was stirred at 0°C for 1 h. To this solution the 1-iodohexane was added (4.20 g, 19.81 mmol) at -78°C. The temperature was allowed to reach an ambient temperature over 14 h and the solution was stirred at room temperature for 2 h. To the solution was added 200 ml of 10% HCl (v/v) and the mixture was extracted with Et<sub>2</sub>O (4 x 250 ml). The combined organic layers were dried over Na<sub>2</sub>SO<sub>4</sub>, filtered, and the filtrate was concentrated *in vacuo*. The residue was purified by column chromatography (*n*-hexane/ethyl acetate, 30/1) to give ethyl 3-oxodecanoate as a yellow oil (1.98 g, 55%). <sup>1</sup>H-NMR (500 MHz, CDCl<sub>3</sub>)  $\delta$  0.84 (t, *J* = 7.0, 3H), 1.23–1.28 (m, 11H), 1.54 (m, 2H), 2.49 (t, *J* = 7.0, 2H), 3.39 (s, 2H), 4.16 (m, 2H). LC/MS (ESI) *m/z* 458.0, 87% (UV).

4) Table S2: Comparison of IC<sub>50</sub> Values Determined by Different Assay Procedures

Compd	IC <sub>50</sub> [μM] <sup>ab</sup>	IC <sub>50,mod</sub> [μM] <sup>ac</sup>	IC <sub>50,ext</sub> [μM] <sup>ad</sup>
1	1.2 ± 0.1	1.1 ± 0.2	1.8 ± 0.4
2	3.0 ± 0.7	4.2 ± 0.3	7.6 ± 1.5
3	3.2 ± 0.1	24.6 ± 6.2	1.0 ± 0.4
4	4.3 ± 1.0	19.7 ± 8.9	2.6 ± 0.5
5	14.8 ± 2.9	>50	9.7 ± 1.4
6	n.i.	n.d.	n.d.
7	7.9 ± 0.7	n.d.	n.d.

<sup>a</sup>*P. aeruginosa* PqsD (0.1 μM), recombinantly expressed in *Escherichia coli*; anthraniloyl-CoA (5 μM), and β-ketodecanoic acid (70 μM); n.i. no inhibition (<10% at 50 μM); n.d. not determined.

<sup>b</sup>PqsD and inhibitor were preincubated for 10 min prior to addition of the substrates. <sup>c</sup>Modified procedure including additional preincubation of enzyme and ACoA. <sup>d</sup>Preincubation time of PqsD/inhibitors was extended to 30 min.

### 5) Percentages of Inhibition and Uncertainty of the Time Dependency Experiment

Compound 2:

<b>time</b>	<b>control</b> [%]	<b>Cmpd. 2,</b> <b>3 <math>\mu</math>M [%]</b>	<b>uncertainty</b> [%]
3 min	100	60.37	2.95
6 min	100	59.36	8.27
9 min	100	60.21	8.09
12 min	100	58.95	8.34
15 min	100	61.99	8.16
20 min	100	72.15	5.19
25 min	100	63.28	7.17
30 min	100	64.18	10.05

Compound 3:

<b>time</b>	<b>control</b> [%]	<b>Cmpd. 3,</b> <b>6 <math>\mu</math>M [%]</b>	<b>uncertainty</b> [%]
3 min	100	71.17	4.33
6 min	100	46.38	2.91
9 min	100	41.85	4.49
12 min	100	36.40	4.36
15 min	100	31.98	4.58
20 min	100	25.39	2.41
25 min	100	27.01	3.60
30 min	100	26.07	4.82

**Table S3.** HHQ formation in presence of compounds 2 and 3 relative to untreated control.

## 6) Figure S1: Dose-response Curve of PqsD Inhibition by Compound 3

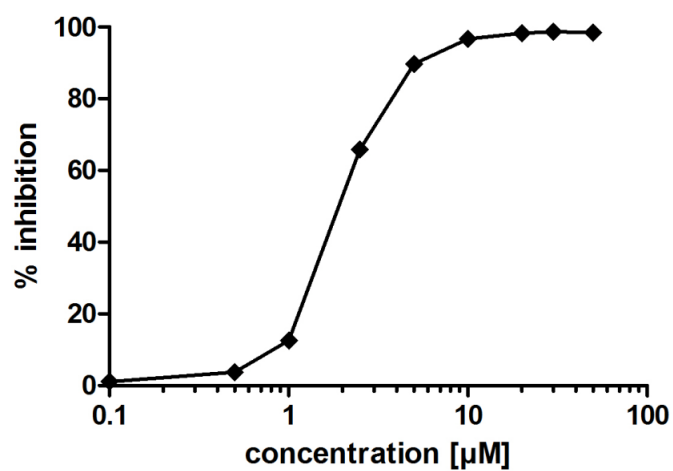


**Figure S1.** Inhibition of PqsD by compound **3** is plotted against the concentration (log scale). Data were generated using the screening assay procedure for *in vitro* PqsD inhibition as described above. Compounds **4** and **5** show similar curve shapes (data not shown).



## 7) Further HPLC-ESI MS Experiments

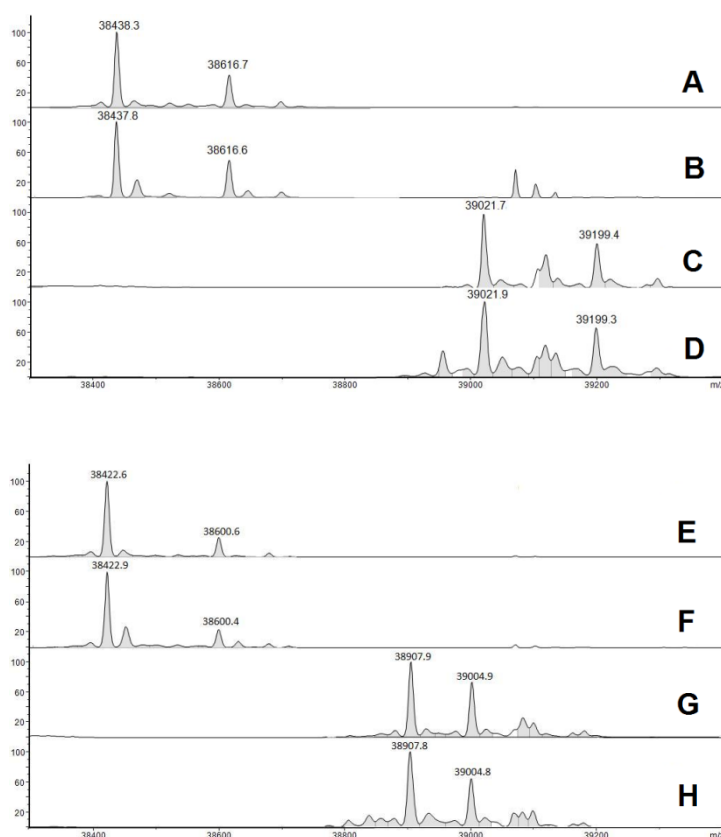


**Figure S2.** (A-D) PqsD containing a His<sub>6</sub>-tag was incubated in absence (A) or in presence (B) of compound **3**. Thereby, no anti-oxidative reagent was present. Samples were subjected to HPLC-ESI MS analysis, whereas no relevant amounts of oxidation products were observed. Subsequent addition of an excess of maleimid resulted in a shift of +582 (corresponding to a 6-fold addition of the labeling agent regardless of the presence of compound **3** (C: PqsD; D: PqsD pretreated with compound **3**). Maleimid labels all available cystein residues present in PqsD, indicating that no cystein was oxidized previously. (E-H) C112S mutant containing a His<sub>6</sub>-tag was treated in absence (E) or in presence (F) of compound **3** using the same procedure as described above. Subsequent addition of an excess of maleimid resulted in a shift of +485 (corresponding to a 5-fold addition of the labeling agent regardless of the presence of compound **3** (G: PqsD; H: PqsD pretreated with compound **3**). In all spectra, signals with a shift of +178 Da were observed. This is probably due to spontaneous  $\alpha$ -N-6-Phosphogluconoylation of the His<sub>6</sub>-tag in *E. coli* (SI4).

## 8) Maldi-TOF Analysis

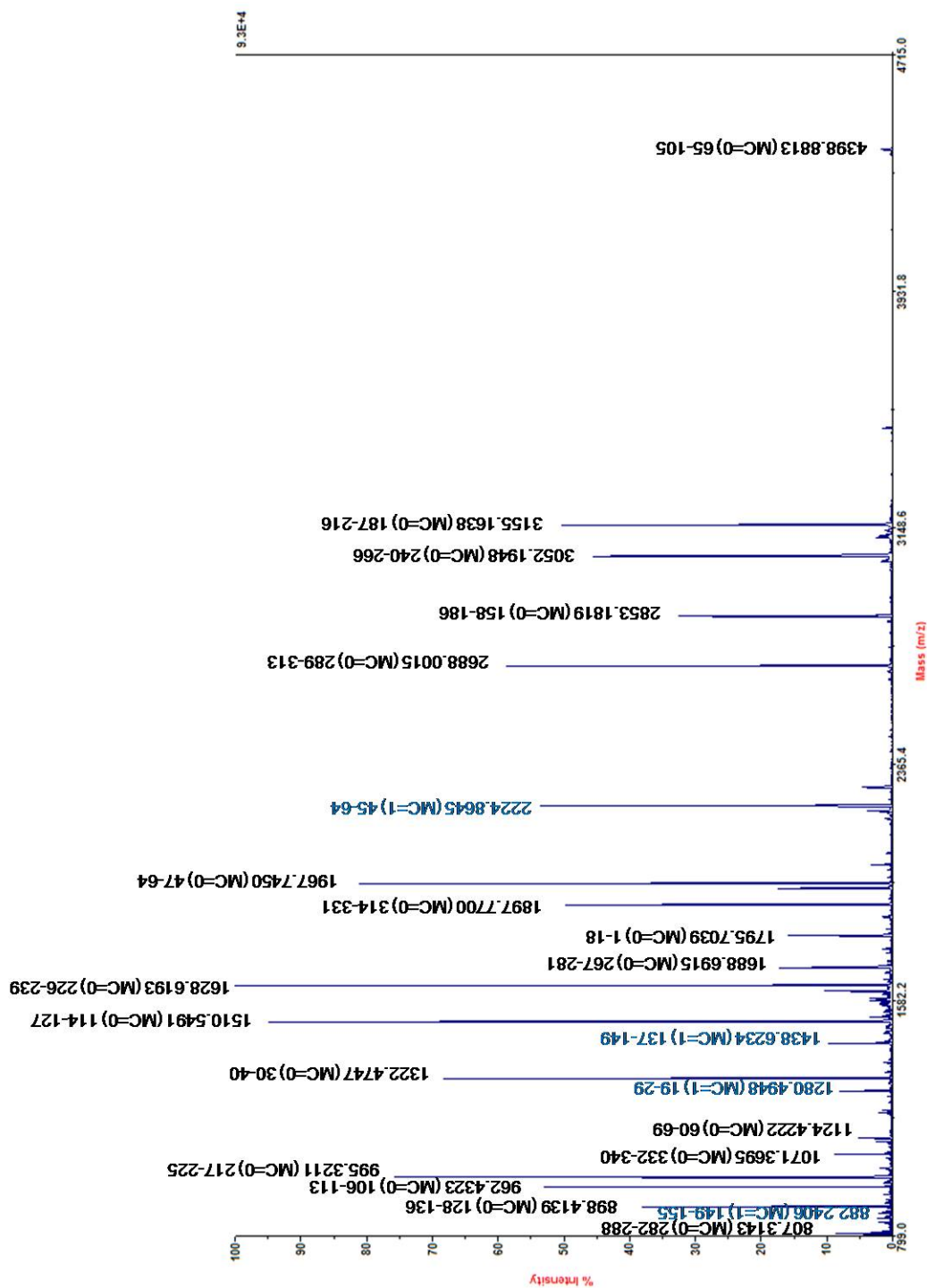


**Figure S3.** Maldi-TOF spectra of PqsD after tryptic digestion. The blue labeled fragments bear one missed cleavage (MC). Fragments generated by complete digestion (MC=0) are labeled in black. Together, 334 of 340 amino acids are visible in at least one fragment.

```

      10           20           30           40           50           60
GSHMGNPILA GLGFSLPKRQ VSNHDLVGR I NTSDEFIVER TGVRTRYHVE PEQAVSALMV

      70           80           90           100          110          120
PAARQAIEAA GLLPEDIDLL LVNTLSPDHH DPSQACLIQP LLGLRHIPVL DIRAQCSGLL

      130          140          150          160          170          180
YGLQMARGQI LAGLARHVLV VCGEVLSKRM DCSDRGRNLS ILLGDGAGAV VVSAGESLED

      190          200          210          220          230          240
GLLDLRLGAD GNYFDLLMTA APGSASPTFL DENVLREGGG EFLMRGRPMF EHASQTLVRI

      250          260          270          280          290          300
AGEMLVAHEL TLDDIDHVIC HQPNLRILDA VQEQLGIPQH KFAVTVDRLG NMASTPVT

      310          320          330          340
LAMFWPDIQP GQRVLVLTYG SGATWGAALY RKPEEVNRPC

```

**Figure S4.** Sequence of the PqsD construct used in the study. Green and blue letters represent amino acids, which are present in peptides (MC=0 and MC=1, respectively) observed by Maldi-TOF, when native PqsD has been digested. Together, 334 of 340 amino acids are visible in at least one fragment. Amino acids not observed in the experiment are Thr41, Gly42, Val43, Arg44, Gly156 and Arg157. (Numbering refers to the amino acid sequence used in the experiment; in the X-ray structure denoted as Thr37, Gly38, Val39, Arg40, Gly152, Arg153 (*SI5*.)

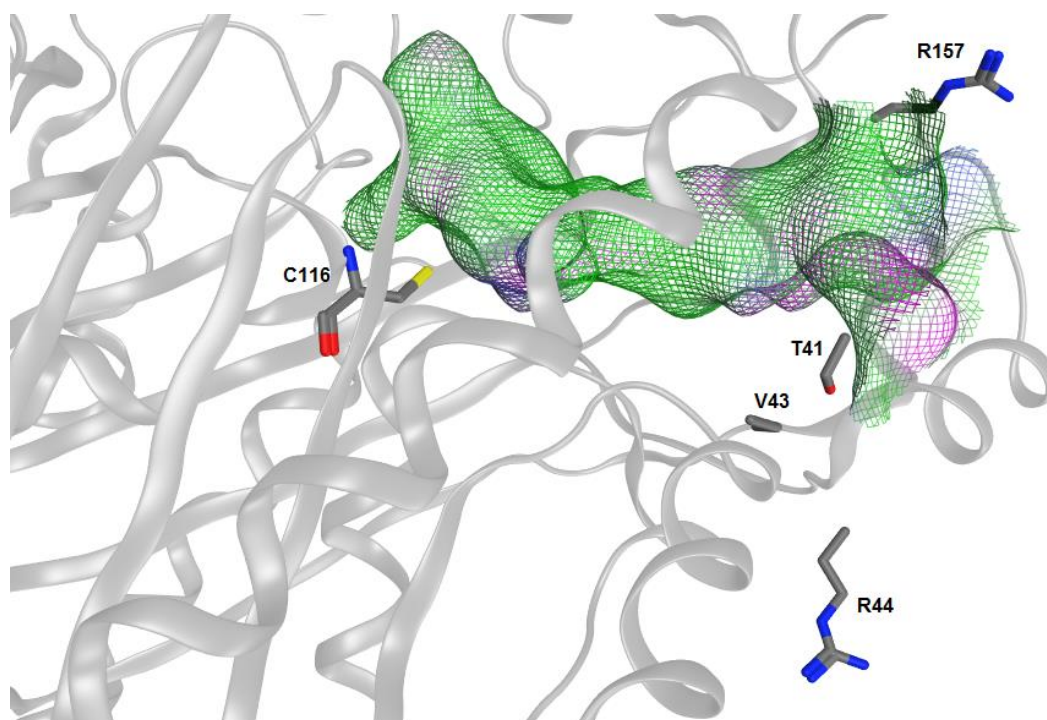


**Figure S5.** Molecular surface of the PqsD binding channel and side chains of the uncaptured amino acids Thr41, Gly42, Val43, Arg44, Gly156 and Arg157. The alkyl residues of Gly42, Val43 and Gly156 are unable to form covalent bonds. Thr41, Arg44 and Arg157 are located at the tunnel entrance, too far away from the binding site of compound **3**, which is located deep in the active site near the catalytically active Cys116 (in the construct used for X-ray analysis denoted as Cys112).

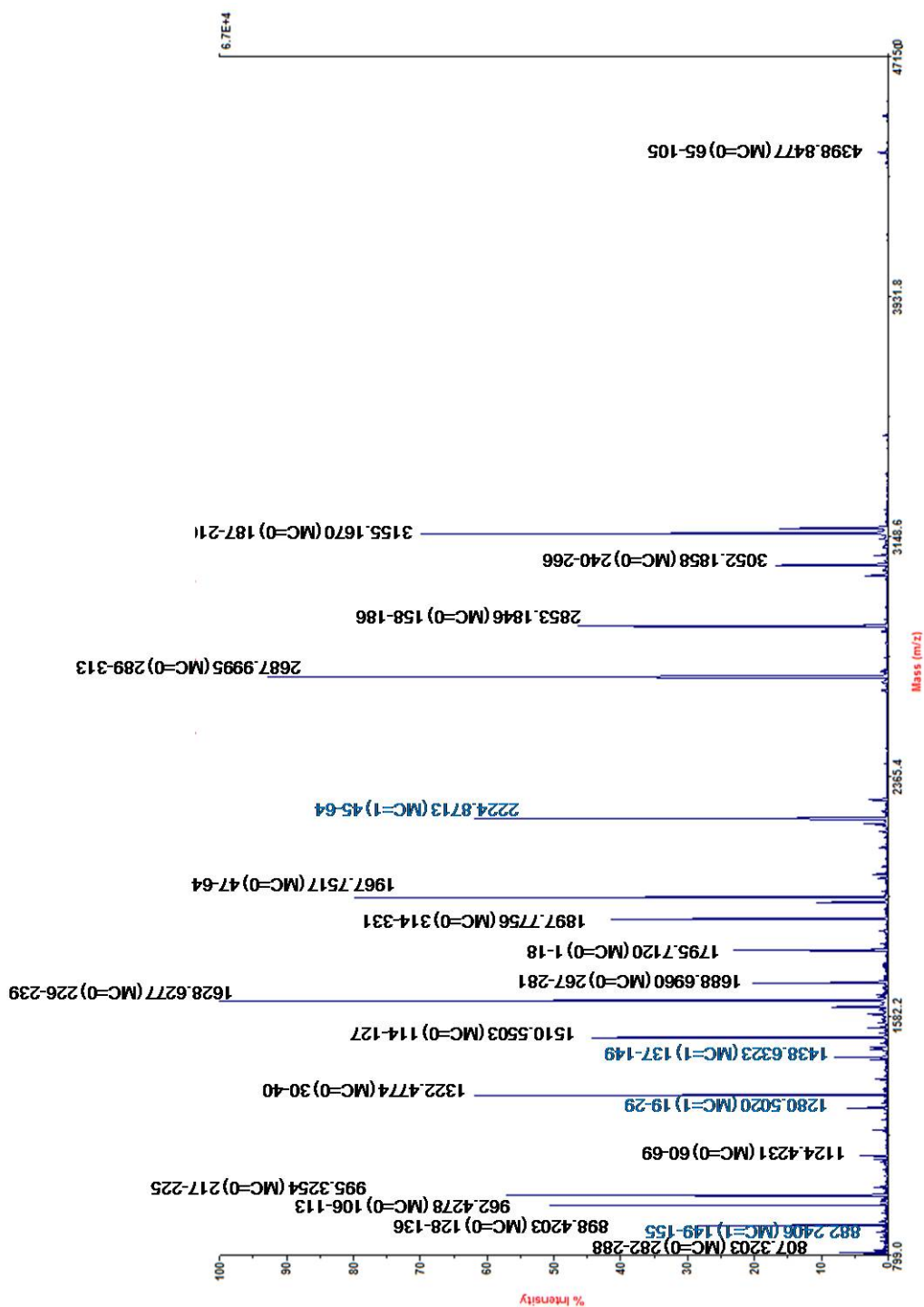


**Figure S6.** Maldi-TOF spectra of PqsD/compound **3** after tryptic digestion. The blue labeled fragments bear one missed cleavage (MC). Fragments generated by complete digestion (MC=0) are labeled in black. Compared to untreated PqsD the only difference is the disappearance of the peptide m/z of 1071.

10 20 30 40 50 60  
 GSHMGNPILA GLGFSLPKRQ VSNHDLVGRI NTSDEFIVER TGVRTRYHVE PEQAVSALMV  
 70 80 90 100 110 120  
 PAARQAIEAA GLLPEDIDLL LVNTLSPDHH DPSQAQLIQP LLGLRHIPVL DIRAQCSGLL  
 130 140 150 160 170 180  
 YGLQMARGQI LAGLARHVLV VCGEVLSKRM DCSDRGRNLS ILLGDGAGAV VVSAGESLED  
 190 200 210 220 230 240  
 GLLDLRLGAD GNYFDLLMTA APGSASPTFL DENVLREGGG EFLMRGRPMF EHASQTLVRI  
 250 260 270 280 290 300  
 AGEMLVAHEL TLDDIDHVIC HQPNLRILDA VQEQLGIPQH KFAVTVDRLG NMASASTPVT  
 310 320 330 340  
 LAMFWPDIQP GQRVLVLTYG SGATWGAALY RKPEEVNRPC

**Figure S7.** Amino acids observed after preincubation of PqsD with compound **3**. Compared to untreated PqsD the red labeled peptide at the C-terminus disappeared, maybe because of an oxidation of the terminal Cys340.

m/z (PqsD) calculated	m/z (PqsD) measured	m/z (PqsD+3) cmpd. measured	Position (Number of missed)	peptide sequence
4399.3329	4398.8813	4398.8477	65–105 (MC=0)	QAIEAAGLLPEDIDLLLVTLSPDHH DPSQACLIQPLLGLR
3155.5353	3155.1638	3155.1670	187–216 (MC=0)	LGADGNYFDLLMTAAPGSASPTFLD ENVLR
3052.5342	3052.1948	3052.1858	240–216 (MC=0)	IAGEMLVVAHELTLDDIDHVIHQPN LR
2853.5203	2853.1819	2853.1846	158–186 (MC=0)	NLSILLGDGAGAVVVSAGESLEDGL LDLR
2688.3272	2688.0015	2687.9995	289–313 (MC=0)	LGNMASASTPVTLAMFWPDIQPGQ R
2225.1495	2224.8645	2224.8713	45–64 (MC=1)	TRYHVEPEQAVSALMVPAAR
1968.0007	1967.7450	1967.7517	47–64 (MC=0)	YHVEPEQAVSALMVPAAR
1898.0170	1897.7700	1897.7756	314–331 (MC=0)	VLVLTYGSGATWGAALYR
1795.9523	1795.7039	1795.7120	1–18 (MC=0)	GSHMGNPILAGLGFSLPK
1688.9329	1688.6915	1688.6960	267–281 (MC=0)	ILDAVQEQLGIPQHK
1628.8325	1628.6193	1628.6277	226–239 (MC=0)	GRPMFEHASQTLVR
1510.7505	1510.5491	1510.5503	114–127 (MC=0)	AQCSEGLLYGLQMAR
1438.8198	1438.6234	1438.6323	137–149 (MC=1)	HVLVVCGEVLSK
1322.6586	1322.4747	1322.4774	30–40 (MC=0)	INTSDEFIVER
1282.7187	-	-	137–148 (MC=0)	HVLVVCGEVLSK
1280.6818	1280.4948	1280.5020	19–29 (MC=1)	RQVSNHDLVGR
1124.5807	1124.4222	1124.4231	60–69 (MC=0)	QVSNHDLVGR
1071.5251	1071.3695	-	332–340 (MC=0)	KPEEVNRPC
995.4615	995.3211	995.3254	217–225 (MC=0)	EGGGEFLMR
962.5781	962.4323	962.4278	106–113 (MC=0)	HIPVLDIR
898.5468	898.4139	898.4203	128–136 (MC=0)	GQILAGLAR
882.3556	882.2406	882.2174	149–155 (MC=1)	RMDCSDR
807.4359	807.3143	807.3203	282–288 (MC=0)	FAVTVDR

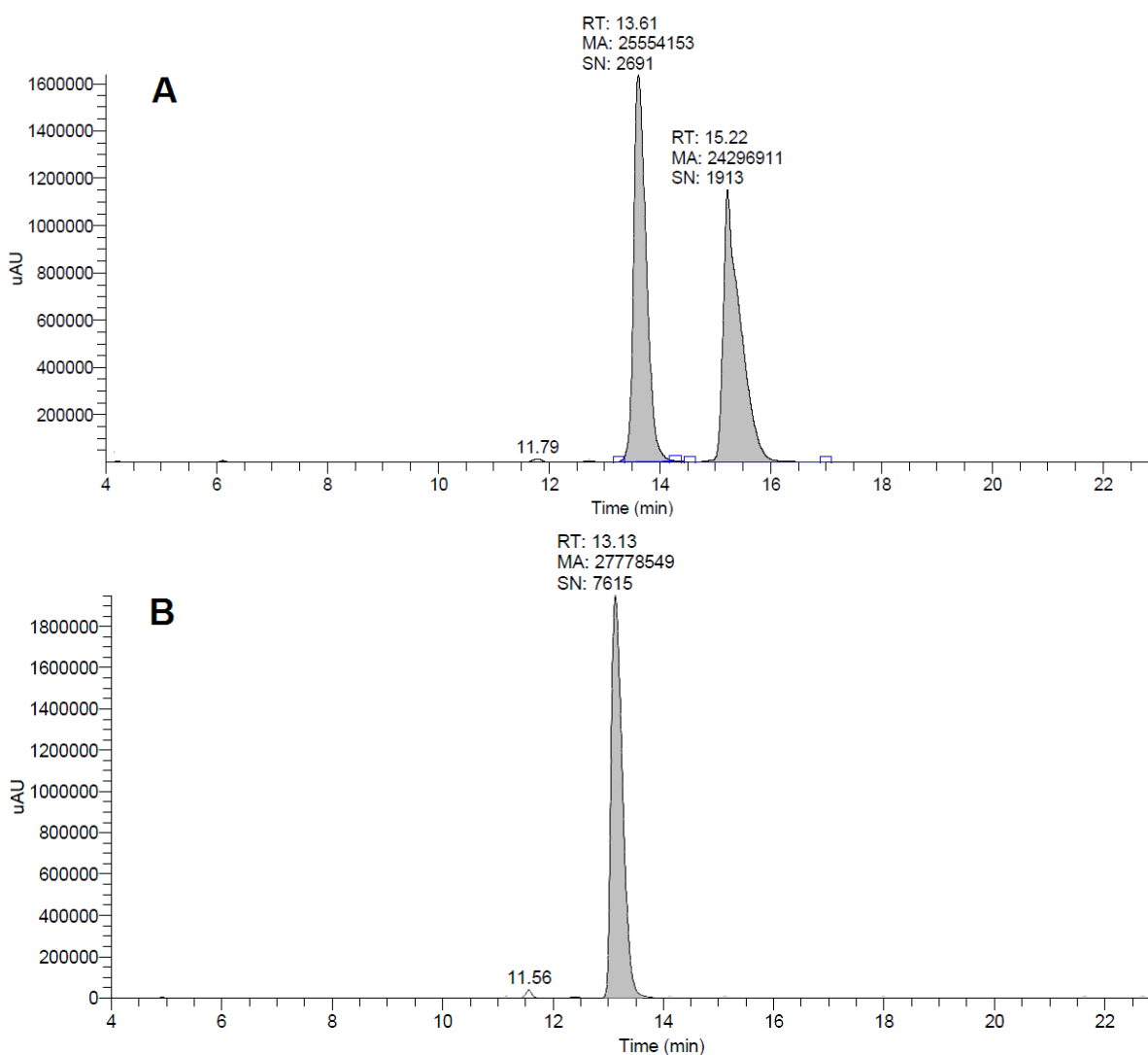
**Table S4.** Comparison of peptide masses (calculated and observed by Maldi-TOF analysis) formed by tryptic digestion of untreated PqsD and PqsD treated with compound **3**. All fragments without missed cleavages (MC=0) with  $m/z > 800$  are listed. Fragments with MC=1 contributing to coverage of the amino acid sequence are added in blue.

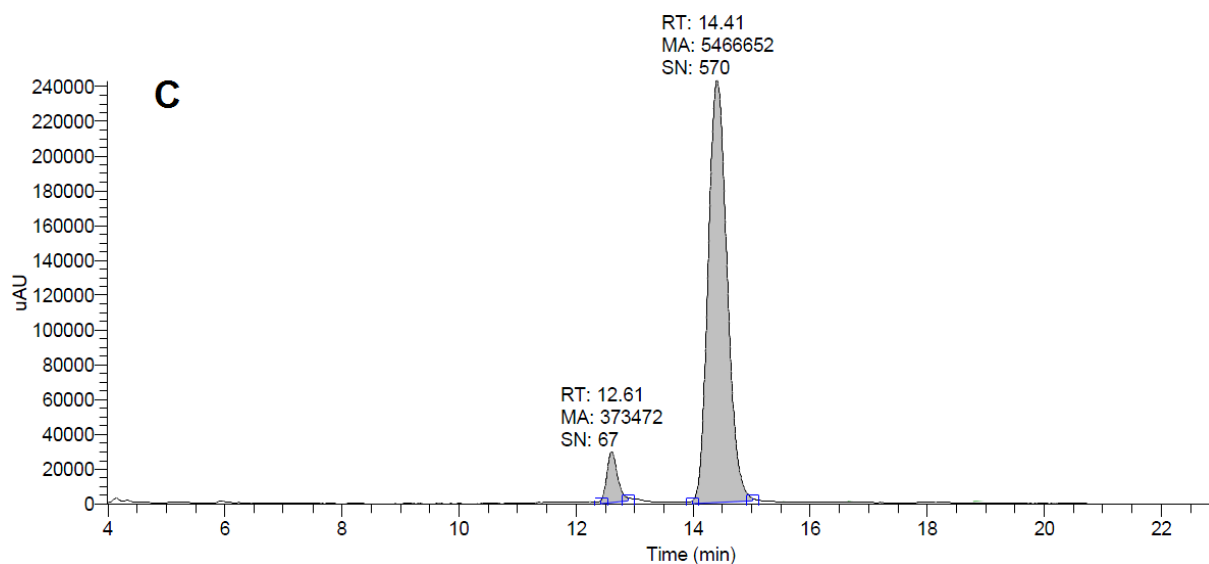


### 9) Separation of **3** into the Enantiomers (*R*)-**3** and (*S*)-**3** by Chiral-HPLC

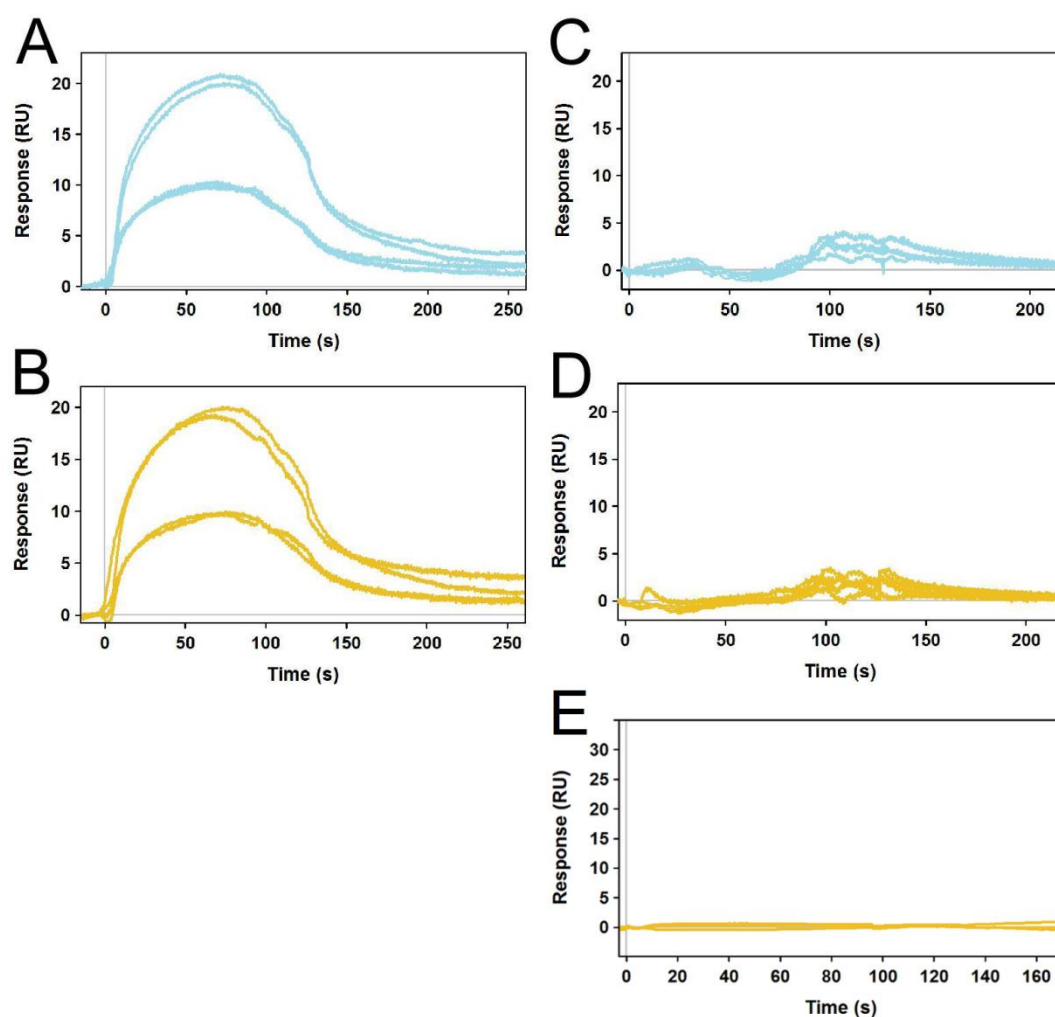
The separation was performed using an Agilent 1200 HPLC system equipped with an MWD triggering an automated fraction collector (**Agilent Technologies**) in “time based” mode. ChemStation® software was used for control and report. The sample was manually injected. A Chiralpak IE® 5 $\mu$ m (250 / 10 mm) column (DAICEL Corporation) was used as stationary phase. The solvent system consisted of *n*-hexane (A) and *iso*-propanol (B). HPLC-Method: Flow rate 2.4 ml min<sup>-1</sup>. Isocratic run of 7% of B in A (v/v).

Determination of enantiomeric excess was performed using a Chiralpak IE® 5 $\mu$ m (250 / 4.6 mm) column (DAICEL Corporation) as stationary phase. The solvent system consisted of *n*-heptane (A) and *iso*-propanol (B). HPLC-Method: Flow rate 1 ml min<sup>-1</sup>. Isocratic run of 7% of B in A (v/v). The % ee of (*R*)-**9** and (*S*)-**9** was determined using the relative peak areas in the MWD trace.

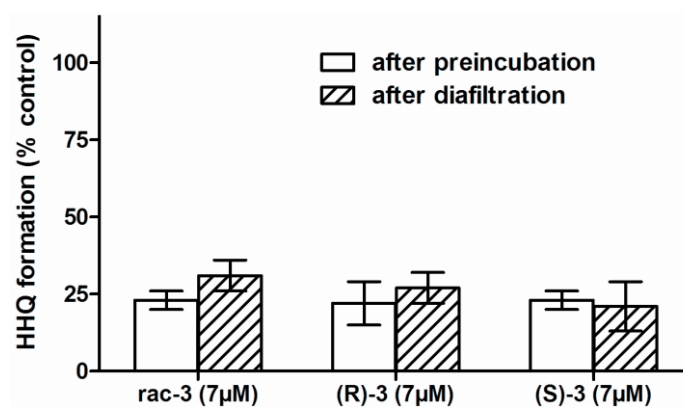




**Figure S8.** HPLC analysis of enantiomeric purity. (A) Racemic mixture **9**, (B) *S*-enantiomer (–) of **9** (>99.9% ee) and (C) *R*-enantiomer (+) of **9** (87.2% ee). Absolute configurations were derived from measurement of the optical rotation and comparison to literature (*SI6*).

10) Figure S9: Binding site analysis of (*R*)-**3** and (*S*)-**3** by SPR

**Figure S9.** SPR experiment using 250 and 125  $\mu$ M of (*R*)-**3** (blue) or (*S*)-**3** (orange), respectively. Compounds were added to native PqsD and response curves (A) and (B) were recorded. No response was observed when identical concentrations of (*R*)-**3** (C) or (*S*)-**3** (D) were added to PqsD pretreated with ACoA. Furthermore, when (*R*)-**3** was added until saturation of the SPR signal, subsequent addition of (*S*)-**3** did not affect the observed response (E). The results indicate that the binding sites of both enantiomers are blocked by anthranilate.

**11) Figure S10: Reversibility of PqsD inhibition by the Enantiomers (*R*)-3 and (*S*)-3**

**Figure S10.** PqsD was preincubated with enantiomers (*R*)-3 and (*S*)-3 and the remaining HHQ formation was quantified with and without removal of unbound inhibitor by diafiltration. Centrifugal filter devices with a molecular weight limit of 10k were used to remove at least 95% inhibitor by three diafiltration steps as controlled by HPLC analysis, while PqsD was retained.

## 12) Representative ITC Curves

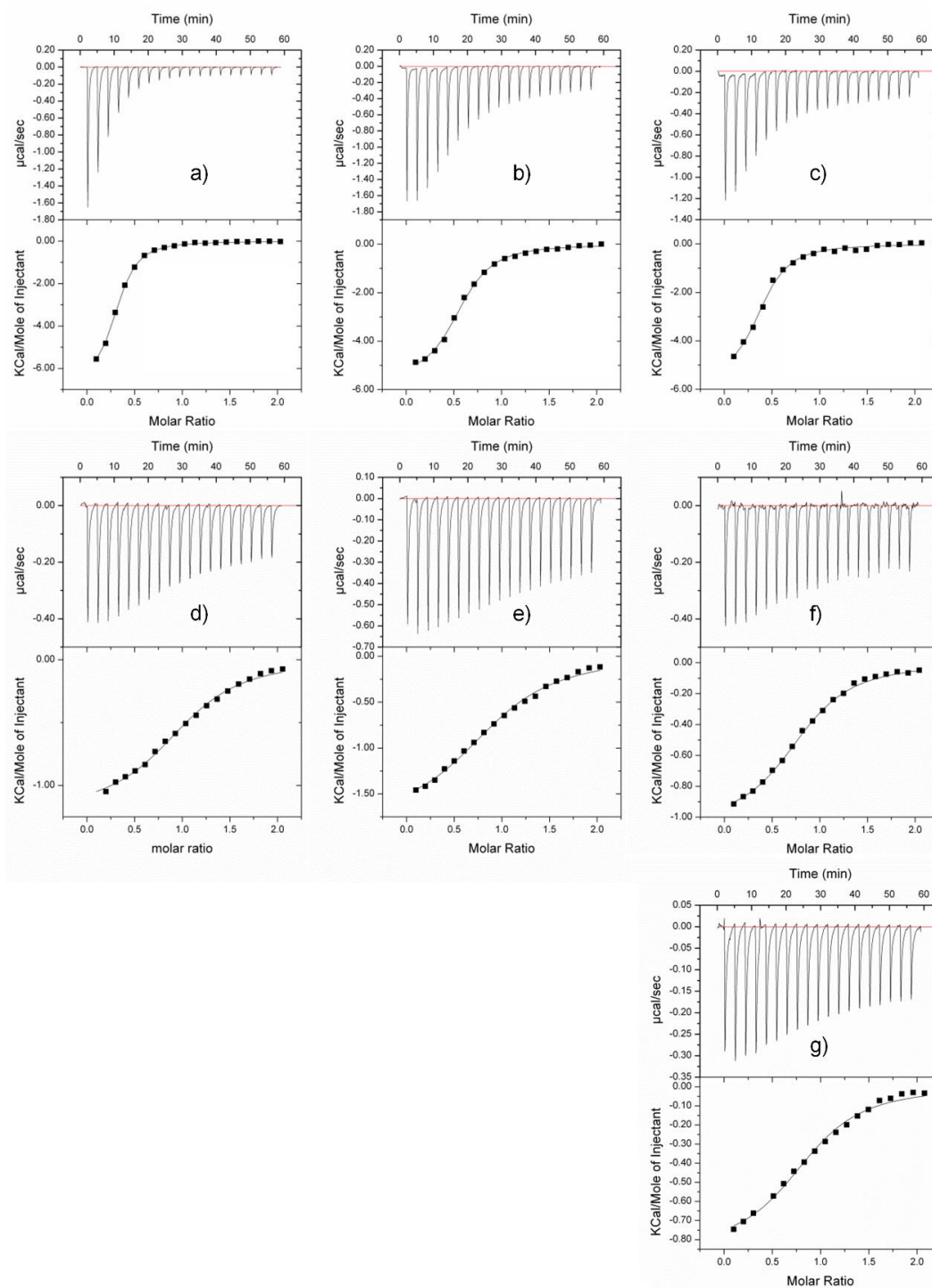
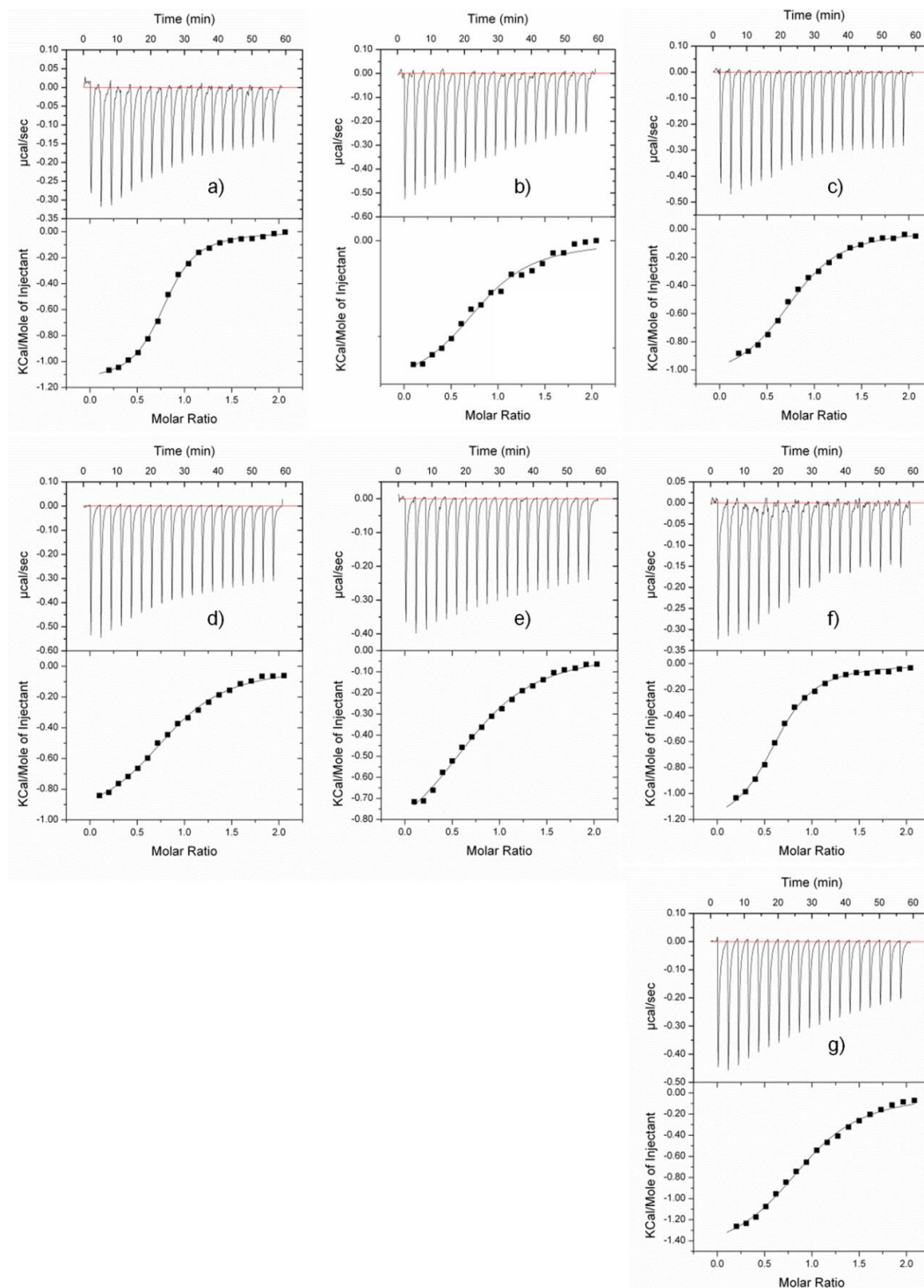


**Figure S11 (above).** Representative ITC titrations of *R*-enantiomer against PqsD wild-type and mutants. 3500  $\mu\text{M}$  of compound against: a) PqsD wild-type (347 $\mu\text{M}$ ), b) S317A (351 $\mu\text{M}$ ), c) N287A (347 $\mu\text{M}$ ), d) C112A (350 $\mu\text{M}$ ), e) C112S (354 $\mu\text{M}$ ), f) H257F (352 $\mu\text{M}$ ), g) S317F (345 $\mu\text{M}$ ). The recorded change in heat is shown in units of  $\mu\text{cal sec}^{-1}$  as a function of time for successive injections of the ligand (upper panel). Integrated heats (black squares) plotted against the molar ratio of the binding reaction. The continuous line represents the results of the non-linear least squares fitting of the data to a binding model (lower panel).

**Figure S12 (below).** Representative ITC titrations of *S*-enantiomer against PqsD wild-type and mutants. 3500  $\mu\text{M}$  of compound against: a) PqsD wild-type (347 $\mu\text{M}$ ), b) S317A (351 $\mu\text{M}$ ), c) N287A (347 $\mu\text{M}$ ), d) C112A (350 $\mu\text{M}$ ), e) C112S (354 $\mu\text{M}$ ), f) H257F (352 $\mu\text{M}$ ), g) S317F (345 $\mu\text{M}$ ). The recorded change in heat is shown in units of  $\mu\text{cal sec}^{-1}$  as a function of time for successive injections of the ligand (upper panel). Integrated heats (black squares) plotted against the molar ratio of the binding reaction. The continuous line represents the results of the non-linear least squares fitting of the data to a binding model (lower panel).



### 13) References

- SI1. Simon, E. J., Shemin, D. (1953) The preparation of *S*-succinyl coenzyme A, *J. Am. Chem. Soc.* 75, 2520.
- SI2. Cook, L., Ternai, B., Ghosh, P. (1987) Inhibition of human sputum elastase by substituted 2-pyrones, *J. Med. Chem.* 30, 1017.
- SI3. Nguyen, V. T. H., Bellur, E., Appel, B., Langer, P. (2006) Synthesis of 4-alkyl- and 4-( $\omega$ -chloroalkyl)-3-hydroxy-5-alkylidenebutenolides based on cyclizations of 4-alkyl- and 4-( $\omega$ -chloroalkyl)-1,3-bis(trimethylsilyloxy)buta-1,3-dienes with oxalyl chloride, *Synthesis* 17, 2865.
- SI4. Geoghegan, K. F., Dixon, H. B. F., Rosner, P. J., Hoth, L. R., Lanzetti, A. J., Borzilleri, K. A., Marr, E. S., Pezzullo, L. H., Martin, L. B., LeMotte, P. K., McColl, A. S., Kamath, A. V., Stroh, J. G. (1999) Spontaneous  $\alpha$ -N-6-Phosphogluconoylation of a "His Tag in *Escherichia coli*: The Cause of Extra Mass of 258 or 178 Da in Fusion Proteins, *Analytical Biochemistry* 267, 169.
- SI5. Bera, A. K., Atanasova, V., Robinson, H., Eisenstein, E., Coleman, J. P., Pesci, E. C., Parsons, J. F. (2009) Structure of PqsD, a *Pseudomonas* quinolone signal biosynthetic enzyme, in complex with anthranilate, *Biochemistry* 48, 8644.
- SI6. Duan, H.-F., Xie, J.-H., Shi, W.-J., Zhang, Q., Zhou, Q.-L. (2006) Enantioselective Rhodium-Catalyzed Addition of Arylboronic Acids to Aldehydes Using Chiral Spiro Monophosphite Ligands, *Organic Letters* 8, 1479

**D Combining in Silico and Biophysical Methods for the Development of Pseudomonas aeruginosa Quorum Sensing Inhibitors: An Alternative Approach for Structure-Based Drug Design**

J. Henning Sahner, Christian Brengel, Michael P. Storz, Matthias Groh, Alberto Plaza, Rolf Müller, and Rolf W. Hartmann

J. Med. Chem. 2013, 56, 8656-8664.



## Supporting information

### Content

s:

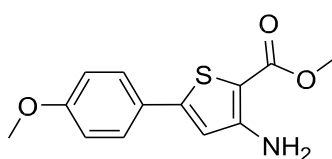
1. Experimental procedures
  - 1.1 Chemistry
    - 1.1.1 Synthesis and spectroscopic data of compounds **1–12**
    - 1.1.2  $^{13}\text{C}$  NMR spectra of compounds **1–12**
  - 1.2. Biology and biophysics
    - 1.2.1 SPR – mutagenesis study
2. Selectivity data for hit compounds: PqsD- vs. RNAP inhibition
3. Results of SPR experiments
  - 3.1 Competition experiments for identification of the binding mode
  - 3.2 Experiment with R223A mutant
4. STD-NMR spectrum of **7**
5. MALDI-ToF-MS spectra
  - 5.1 PqsD
  - 5.2 PqsD + **12**
6. LC-ESI-MS spectra
7. HPLC purities

## 1. Experimental procedures

### 1.1. Chemistry

#### 1.1.1 Synthesis and spectroscopic data of compounds 1–12

##### Methyl 3-amino-5-(4'-methoxyphenyl)thiophene-2-carboxylate (IIa).

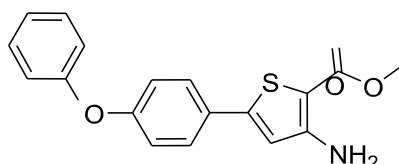


The title compound was prepared from 4'-methoxyacetophenone according to general procedure A and used directly in the next step without further purification.

$^1\text{H}$  NMR (DMSO- $d_6$ , 500 MHz):  $\delta$  = 7.56 (d,  $J$  = 8.8 Hz, 2 H), 7.00 (d,  $J$  = 8.8 Hz, 2 H), 6.86 (s, 1 H), 6.56 (br. s, 2 H), 3.79 (s, 3 H, OCH<sub>3</sub>), 3.72 (s, 3 H, OCH<sub>3</sub>) ppm.

$^{13}\text{C}$  NMR (DMSO- $d_6$ , 126 MHz):  $\delta$  = 163.9, 160.0, 155.7, 147.7, 127.0, 125.3, 114.9, 114.6, 95.7, 55.3, 50.8 ppm.

##### Methyl 3-amino-5-(4'-phenoxyphenyl)thiophene-2-carboxylate (IIb).

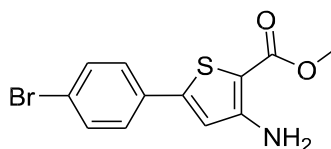


The title compound was prepared from 4'-phenoxyacetophenone according to general procedure A and used directly in the next step without further purification.

$^1\text{H}$  NMR (DMSO- $d_6$ , 500 MHz):  $\delta$  = 7.64 (d,  $J$  = 8.8 Hz, 2 H), 7.46–7.40 (m, 2 H), 7.22–7.17 (m, 1 H), 7.11–7.06 (m, 2 H), 7.04 (d,  $J$  = 8.8 Hz, 2 H), 6.91 (s, 1 H), 6.59 (br. s, 2 H), 3.72 (s, 3 H, OCH<sub>3</sub>) ppm.

$^{13}\text{C}$  NMR (DMSO- $d_6$ , 126 MHz):  $\delta$  = 163.9, 157.7, 155.9, 147.0, 130.2, 127.8, 127.4, 124.1, 119.3, 118.7, 115.7, 96.2, 50.9 ppm.

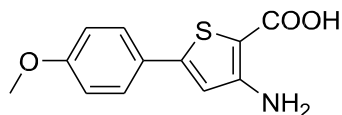
**Methyl 3-amino-5-(4'-bromophenyl)thiophene-2-carboxylate (IIc).**



The title compound was prepared from 4'-bromoacetophenone according to general procedure A.

$^1\text{H}$  NMR (CDCl<sub>3</sub>, 300 MHz):  $\delta$  = 7.51 (d,  $J$  = 8.0 Hz, 2 H), 7.43 (d,  $J$  = 8.0 Hz, 2 H), 6.75 (s, 1 H), 5.49 (br. s., 2 H), 3.85 (s, 3 H, OCH<sub>3</sub>) ppm.

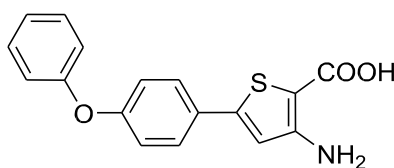
$^{13}\text{C}$  NMR (CDCl<sub>3</sub>, 75 MHz):  $\delta$  = 164.8, 154.2, 147.6, 132.3, 132.1, 127.3, 123.0, 115.8, 100.7, 51.3 ppm.

**3-Amino-5-(4'-methoxyphenyl)thiophene-2-carboxylic acid (IIIa).**

The title compound was prepared from **IIa** according to general procedure **B**.

$^1\text{H}$  NMR (DMSO- $d_6$ , 300 MHz):  $\delta$  = 7.55 (d,  $J$  = 8.8 Hz, 2 H), 6.99 (d,  $J$  = 8.8 Hz, 2 H), 6.84 (s, 1 H), 3.79 (s, 3 H, OCH<sub>3</sub>) ppm.

$^{13}\text{C}$  NMR (DMSO- $d_6$ , 75 MHz):  $\delta$  = 165.3, 159.9, 155.3, 147.0, 127.0, 125.6, 115.0, 114.6, 97.1, 55.3 ppm.

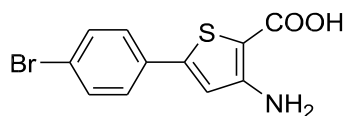
**3-Amino-5-(4'-phenoxyphenyl)thiophene-2-carboxylate (IIIb).**

The title compound was prepared from **IIb** according to general procedure **B**.

$^1\text{H}$  NMR (DMSO- $d_6$ , 500 MHz):  $\delta$  = 7.63 (d,  $J$  = 8.8 Hz, 2 H), 7.47–7.38 (m, 2 H), 7.23–7.16 (m, 1 H), 7.08 (d,  $J$  = 8.8 Hz, 2 H), 7.06–6.99 (m, 2 H), 6.90 (s, 1 H) ppm.

$^{13}\text{C}$  NMR (DMSO- $d_6$ , 126 MHz):  $\delta = 165.2, 157.5, 155.9, 146.3, 130.2, 128.1, 127.3, 124.0, 119.2, 118.7, 115.8, 97.7$  ppm.

**3-Amino-5-(4'-bromophenyl)thiophene-2-carboxylic acid (IIIc).**

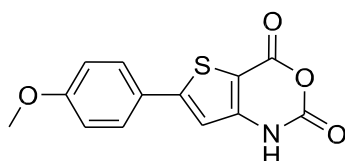


The title compound was prepared from **IIc** according to general procedure **B**.

$^1\text{H}$  NMR (DMSO- $d_6$ , 500 MHz):  $\delta = 7.63$  (d,  $J = 8.8$  Hz, 2 H),  $7.57$  (d,  $J = 8.8$  Hz, 2 H),  $6.98$  (s, 1 H) ppm.

$^{13}\text{C}$  NMR (DMSO- $d_6$ , 126 MHz):  $\delta = 165.2, 155.1, 145.3, 132.2, 132.1, 127.5, 122.0, 116.8, 98.5$  ppm.

**6-(4'-Methoxyphenyl)-2,4-dihydro-1H-thieno[3,2-d][1,3]oxazine-2,4-dione (IVa).**

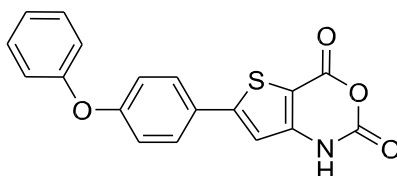


The title compound was prepared from **IIIa** according to general procedure **C**.

$^1\text{H}$  NMR (DMSO- $d_6$ , 300 MHz):  $\delta$  = 12.28 (s, 1 H), 7.74 (d,  $J$  = 8.9 Hz, 2 H), 7.12 (s, 1 H), 7.04 (d,  $J$  = 8.9 Hz, 2 H), 3.82 (s, 3 H, OCH<sub>3</sub>) ppm.

$^{13}\text{C}$  NMR (DMSO- $d_6$ , 75 MHz):  $\delta = 161.1, 155.5, 155.0, 149.6, 148.6, 127.9, 124.1, 114.8, 111.2, 103.1, 55.4$  ppm.

**6-(4'-Phenoxyphenyl)-2,4-dihydro-1H-thieno[3,2-d][1,3]oxazine-2,4-dione (IVb).**

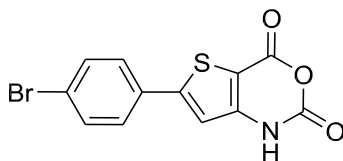


The title compound was prepared from **IIIb** according to general procedure C.

$^1\text{H}$  NMR (DMSO- $d_6$ , 500 MHz):  $\delta = 12.33$  (br. s., 1 H), 7.83 (d,  $J = 8.8$  Hz, 2 H), 7.48–7.43 (m, 2 H), 7.23 (t,  $J = 7.4$  Hz, 1 H), 7.18 (s, 1 H), 7.13–7.10 (m, 2 H), 7.08 (d,  $J = 8.8$  Hz, 2 H) ppm.

$^{13}\text{C}$  NMR (DMSO- $d_6$ , 126 MHz):  $\delta = 158.9, 155.4, 155.0, 154.8, 149.6, 148.5, 130.3, 128.4, 126.4, 124.4, 119.6, 118.6, 112.1, 103.8$  ppm.

**6-(4'-Bromophenyl)-2,4-dihydro-1H-thieno[3,2-d][1,3]oxazine-2,4-dione (IVc).**

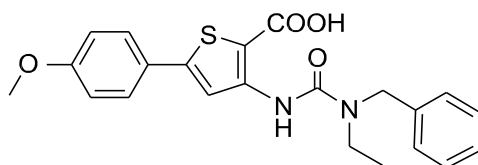


The title compound was prepared from **IIIc** according to general procedure **C**.

$^1\text{H}$  NMR (DMSO-*d*<sub>6</sub>, 500 MHz):  $\delta$  = 12.39 (br. s., 1 H), 7.77 (d,  $J$  = 8.8 Hz, 2 H), 7.70 (d,  $J$  = 8.8 Hz, 2 H), 7.29 (s, 1 H) ppm.

$^{13}\text{C}$  NMR (DMSO-*d*<sub>6</sub>, 126 MHz):  $\delta$  = 155.1, 153.5, 149.7, 148.6, 132.4, 130.8, 128.3, 123.8, 113.4, 104.7 ppm.

**3-(3''-Benzyl-3''-ethylureido)-5-(4'-methoxyphenyl)thiophene-2-carboxylic acid (1).**

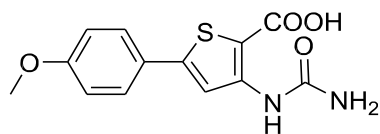


The title compound was prepared from **IVa** according to general procedure **D**.

$^1\text{H}$  NMR (DMSO-*d*<sub>6</sub>, 300 MHz):  $\delta$  = 13.21 (br. s, 1 H, COOH), 10.10 (s, 1 H), 8.17 (s, 1 H), 7.63 (d,  $J$  = 8.9 Hz, 2 H), 7.38–7.29 (m, 5 H), 7.02 (d,  $J$  = 8.9 Hz, 2 H), 3.80 (s, 3 H, OCH<sub>3</sub>), 3.39 (q,  $J$  = 7.1 Hz, 2 H), 1.16 (t,  $J$  = 7.1, 3 H) ppm.

$^{13}\text{C}$  NMR (DMSO-*d*<sub>6</sub>, 75 MHz):  $\delta$  = 165.8, 160.2, 153.1, 147.9, 147.0, 138.1, 128.5, 127.2, 127.1, 127.1, 125.3, 116.1, 114.7, 105.6, 55.3, 49.3, 41.8, 13.1 ppm.

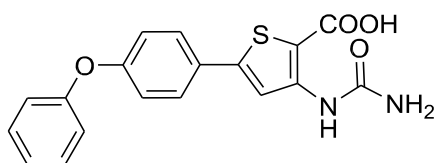


**5-(4'-Methoxyphenyl)-3-ureidothiophene-2-carboxylic acid (2).**

The title compound was prepared from **IVa** according to general procedure **D**.

$^1\text{H}$  NMR (DMSO-*d*, 300 MHz):  $\delta$  = 12.92 (br. s., 1 H, COOH), 9.30 (s, 1 H), 8.15 (s, 1 H), 7.60 (d,  $J$  = 8.8 Hz, 2 H), 7.01 (d,  $J$  = 8.8 Hz, 2 H), 6.81 (br. s, 2 H), 3.76 (s, 3 H, OCH<sub>3</sub>) ppm.

$^{13}\text{C}$  NMR (DMSO-*d*, 75 MHz):  $\delta$  = 164.8, 160.0, 154.7, 147.1, 146.6, 127.1, 125.4, 116.7, 114.7, 105.4, 55.3 ppm.

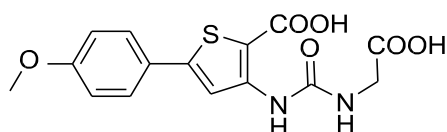
**5-(4'-Phenoxyphenyl)-3-ureidothiophene-2-carboxylic acid (3).**

The title compound was prepared from **IVb** according to general procedure **D**.

$^1\text{H}$  NMR (DMSO-*d*, 300 MHz):  $\delta$  = 12.99 (br. s., 1 H, COOH), 9.30 (s, 1 H), 8.21 (s, 1 H), 7.68 (d,  $J$  = 8.8 Hz, 2 H), 7.49–7.38 (m, 2 H), 7.25–7.14 (m, 1 H), 7.13–7.02 (m, 4 H), 6.90–6.60 (m, 2 H) ppm.

$^{13}\text{C}$  NMR (DMSO-*d*<sub>6</sub>, 75 MHz):  $\delta$  = 164.7, 157.7, 155.9, 154.6, 146.5, 146.4, 130.2, 127.9, 127.5, 124.1, 119.3, 118.8, 117.5, 106.1 ppm.

**3-(3''-(Carboxymethyl)ureido)-5-(4'-methoxyphenyl)thiophene-2-carboxylic acid (4).**

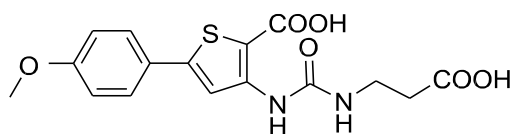


The title compound was prepared from **IVa** according to general procedure **D**.

$^1\text{H}$  NMR (DMSO-*d*<sub>6</sub>, 300 MHz):  $\delta$  = 12.79 (br. s., 2 H, COOH), 9.47 (s, 1 H), 8.13 (s, 1 H), 8.08 (t,  $J$  = 5.6 Hz, 1 H), 7.61 (d,  $J$  = 8.8 Hz, 2 H), 7.01 (d,  $J$  = 8.8 Hz, 2 H), 3.83–3.77 (m, 2 H) 3.80 (s, 3 H, OCH<sub>3</sub>) ppm.

$^{13}\text{C}$  NMR (DMSO-*d*<sub>6</sub>, 75 MHz):  $\delta$  = 171.9, 164.7, 160.1, 154.1, 147.2, 146.1, 127.1, 125.4, 116.7, 114.7, 105.7, 55.3, 41.3 ppm.

**3-(3''-(2-Carboxyethyl)ureido)-5-(4'-methoxyphenyl)thiophene-2-carboxylic acid (5).**

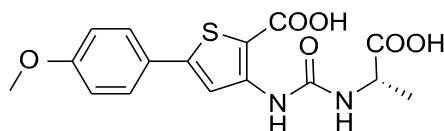


The title compound was prepared from **IVa** according to general procedure **D**.

$^1\text{H}$  NMR (DMSO-*d*, 300 MHz):  $\delta$  = 12.58 (br. s., 2 H, COOH), 9.34 (s, 1 H), 8.16 (s, 1 H), 7.90–7.72 (m, 1 H), 7.60 (d,  $J$  = 8.4 Hz, 2 H), 7.01 (d,  $J$  = 8.4 Hz, 2 H), 3.80 (s, 3 H, OCH<sub>3</sub>), 3.33–3.24 (m, 2 H), 2.44 (t,  $J$  = 6.2 Hz, 2 H) ppm.

$^{13}\text{C}$  NMR (DMSO-*d*, 75 MHz)  $\delta$  = 173.0, 164.7, 160.1, 153.8, 147.1, 146.3, 127.1, 125.4, 116.7, 114.7, 105.4, 55.3, 35.6, 34.3 ppm.

**(S)-3-(3''-(1-Carboxyethyl)ureido)-5-(4'-methoxyphenyl)thiophene-2-carboxylic acid (6).**

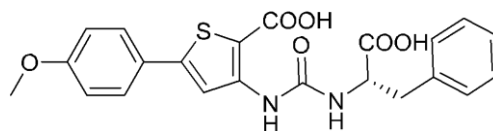


The title compound was prepared from **IVa** according to general procedure **D**

$^1\text{H}$  NMR (DMSO-*d*, 300 MHz):  $\delta$  = 12.76 (br. s., 2 H, COOH), 9.43 (s, 1 H), 8.14 (s, 1 H), 8.09 (d,  $J$  = 7.1 Hz, 1 H), 7.61 (d,  $J$  = 8.8 Hz, 2 H), 7.03 (d,  $J$  = 8.8 Hz, 2 H), 4.22–4.08 (m, 1 H), 3.81 (s, 3 H, OCH<sub>3</sub>), 1.32 (d,  $J$  = 7.30 Hz, 3 H, CH<sub>3</sub>) ppm.

$^{13}\text{C}$  NMR (DMSO-*d*, 75 MHz):  $\delta$  = 174.7, 164.7, 160.1, 153.5, 147.2, 146.1, 127.1, 125.4, 116.6, 114.7, 105.6, 55.3, 48.3, 17.4 ppm.

**(S)-3-(3''-(1-Carboxy-2-phenylethyl)ureido)-5-(4'-methoxyphenyl)thiophene-2-carboxylic acid (7).**

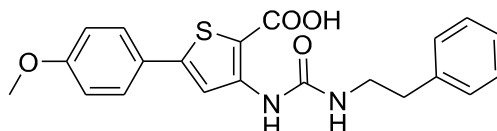


The title compound was prepared from **IVa** according to general procedure **D**.

$^1\text{H}$  NMR (DMSO-*d*, 300 MHz):  $\delta$  = 12.84 (br. s., 2 H, COOH), 9.42 (s, 1 H), 8.15 (d,  $J$  = 7.9 Hz, 1 H), 8.09 (s, 1 H), 7.69–7.51 (m,  $J$  = 8.8 Hz, 2 H), 7.37–7.25 (m, 4 H), 7.25–7.17 (m, 1 H), 7.03–6.97 (m,  $J$  = 8.8 Hz, 2 H), 4.56–4.28 (m, 1 H), 3.79 (s, 3 H, OCH<sub>3</sub>), 3.11 (dd,  $J$  = 13.9, 4.6 Hz, 1 H), 2.88 (dd,  $J$  = 13.9, 9.8 Hz, 1 H) ppm.

$^{13}\text{C}$  NMR (DMSO-*d*, 75 MHz):  $\delta$  = 173.6, 164.6, 160.1, 153.7, 147.1, 145.9, 137.7, 129.0, 128.2, 127.1, 126.4, 125.4, 116.7, 114.7, 105.8, 55.3, 54.4, 36.9 ppm.

**5-(4'-Methoxyphenyl)-3-(3''-phenethylureido)thiophene-2-carboxylic acid (8).**

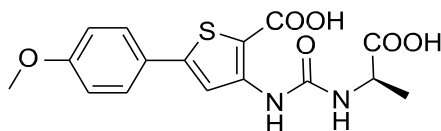


The title compound was prepared from **IVa** according to general procedure **D**.

$^1\text{H}$  NMR (DMSO-*d*, 300 MHz):  $\delta$  = 12.96 (br. s., 1 H, CCOH), 9.33 (s, 1 H), 8.18 (s, 1 H), 7.84–7.70 (m, 1 H), 7.61 (d,  $J$  = 8.3 Hz, 2 H), 7.39–7.13 (m, 5 H), 7.02 (d,  $J$  = 8.3 Hz, 2 H), 3.80 (s, 3 H, OCH<sub>3</sub>), 3.42–3.26 (m, 2 H), 2.90–2.67 (m, 2 H) ppm.

$^{13}\text{C}$  NMR (DMSO-*d*<sub>6</sub>, 75 MHz):  $\delta$  = 164.8, 160.0, 153.8, 147.2, 146.5, 139.5, 128.6, 128.3, 127.1, 126.1, 125.4, 116.7, 114.7, 105.2, 55.3, 41.0, 35.5 ppm.

**(R)-3-(3''-(1-Carboxyethyl)ureido)-5-(4'-methoxyphenyl)thiophene-2-carboxylic acid (9).**

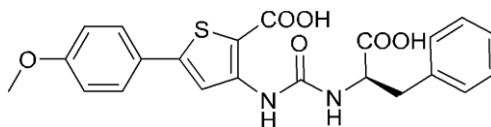


The title compound was prepared from **IVa** according to general procedure **D**.

$^1\text{H}$  NMR (DMSO-*d*<sub>6</sub>, 300 MHz):  $\delta$  = 12.76 (br. s., 2 H, CCO), 9.43 (s, 1 H), 8.14 (s, 1 H), 8.09 (d,  $J$  = 7.1 Hz, 1 H), 7.61 (d,  $J$  = 8.9 Hz, 2 H), 7.01 (d,  $J$  = 8.9 Hz, 2 H), 4.22–4.08 (m, 1 H), 3.80 (s, 3 H, OCH<sub>3</sub>), 1.31 (d,  $J$  = 7.4 Hz, 3 H, CH<sub>3</sub>) ppm.

$^{13}\text{C}$  NMR (DMSO-*d*<sub>6</sub>, 75 MHz):  $\delta$  = 174.7, 164.7, 160.1, 153.5, 147.2, 146.1, 127.1, 125.4, 116.6, 114.7, 105.6, 55.3, 48.3, 17.4 ppm.

**(R)-3-(3''-(1-Carboxy-2-phenylethyl)ureido)-5-(4'-methoxyphenyl)thiophene-2-carboxylic acid (10).**

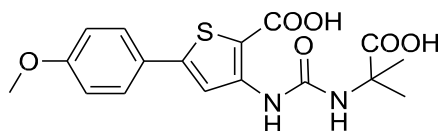


The title compound was prepared from **IVa** according to general procedure **D**.

$^1\text{H}$  NMR (DMSO-*d*, 300 MHz):  $\delta$  = 12.84 (br. s., 2 H, CCOH), 9.42 (s, 1 H), 8.15 (d,  $J$  = 7.9 Hz, 1 H), 8.09 (s, 1 H), 7.59 (d,  $J$  = 8.8 Hz, 2 H), 7.37–7.25 (m, 4 H), 7.25–7.17 (m, 1 H), 7.00 (d,  $J$  = 8.8 Hz, 2 H), 4.56–4.28 (m, 1 H), 3.79 (s, 3 H, OCH<sub>3</sub>), 3.11 (dd,  $J$  = 13.9, 4.6 Hz, 1H), 2.88 (dd,  $J$  = 13.9, 9.8 Hz, 1 H) ppm.

$^{13}\text{C}$  NMR (DMSO-*d*, 75 MHz):  $\delta$  = 173.6, 164.6, 160.1, 153.7, 147.1, 145.9, 137.7, 129.0, 128.2, 127.1, 126.4, 125.4, 116.7, 114.7, 105.8, 55.3, 54.4, 36.9 ppm.

**3-(3''-(2-Carboxypropan-2-yl)ureido)-5-(4'-methoxyphenyl)thiophene-2-carboxylic acid (11).**



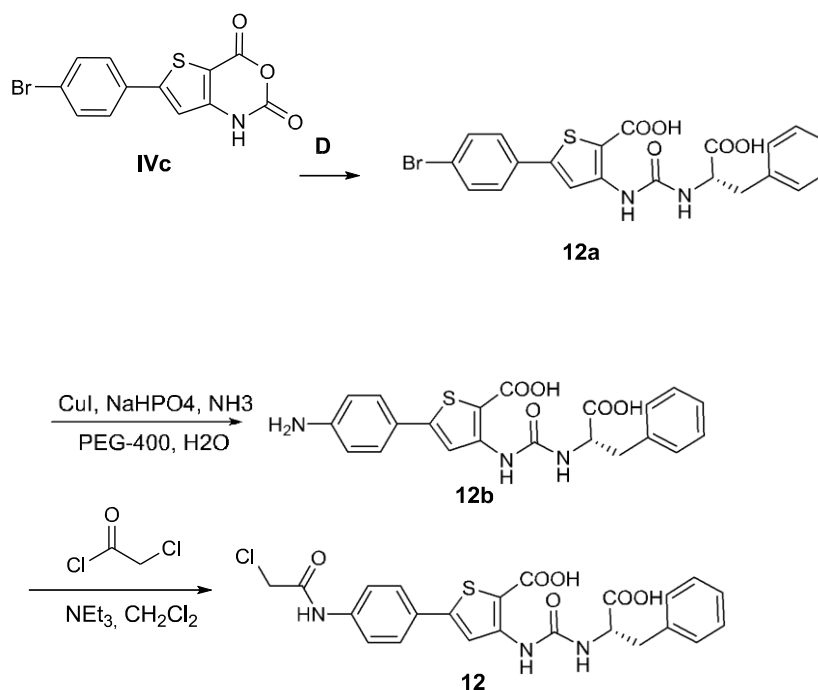
The title compound was prepared from **IVa** according to general procedure **D**.

$^1\text{H}$  NMR (DMSO-*d*, 300 MHz):  $\delta$  = 12.59 (br. s., 2 H, CCOH), 9.37 (s, 1 H), 8.13 (s, 1 H), 8.01 (s, 1 H), 7.61 (d,  $J$  = 8.8 Hz, 2 H), 7.00 (d,  $J$  = 8.8 Hz, 2 H), 3.80 (s, 3 H, OCH<sub>3</sub>), 1.40 (s, 6 H, (CH<sub>3</sub>)<sub>2</sub>) ppm.

$^{13}\text{C}$  NMR (DMSO-*d*, 75 MHz):  $\delta$  = 176.0, 164.7, 160.0, 153.0, 147.2, 146.1, 127.1, 125.4, 116.5, 114.7, 105.4, 55.3, 54.9, 25.3 ppm.

**(S)-3-(3''-(1-Carboxy-2-phenylethyl)ureido)-5-(4'-(2-chloroacetamido)phenyl) thiophene-2-carboxylic acid (12).**

## Scheme S2: Synthesis of compound 12.



(*S*)-3-(3''-(1-Carboxy-2-phenylethyl)ureido)-5-(4'-bromophenyl)thiophene-2-carboxylic acid (**12a**) was prepared from **IVc** according to general procedure **D**.

$^1\text{H}$  NMR (DMSO-*d*<sub>6</sub>, 300 MHz):  $\delta$  = 12.93 (br. s., 2 H, CCOH), 9.42 (s, 1 H), 8.23 (s, 1 H), 8.17 (d,  $J$  = 7.9 Hz, 1 H), 7.70–7.54 (m, 4 H), 7.38–7.14 (m, 5 H), 4.47–4.30 (m, 1 H), 3.11 (dd,  $J$  = 13.9, 4.8 Hz, 1 H), 2.88 (dd,  $J$  = 13.9, 9.7 Hz, 1 H) ppm.

$^{13}\text{C}$  NMR (DMSO-*d*<sub>6</sub>, 75 MHz):  $\delta$  = 173.5, 164.5, 153.7, 145.7, 145.4, 137.7, 132.2, 132.0, 129.0, 128.2, 127.6, 126.4, 122.3, 118.5, 107.3, 54.4, 37.0 ppm.

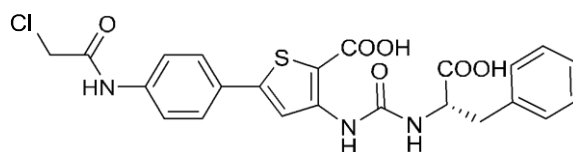
**(S)-3-(3''-(1-Carboxy-2-phenylethyl)ureido)-5-(4'-aminophenyl)thiophene-2-carboxylic acid (12b)** was prepared from **12a** according to the following procedure:

CuI (10 mg, 5.30  $\mu\text{mol}$ ), **12a** (127 mg, 0.26 mmol),  $\text{Na}_3\text{PO}_4 \cdot 12 \text{H}_2\text{O}$  (100 mg, 0.26 mmol), 25–28% aqueous ammonia (0.5 mL) and PEG-400 (1 mL) were added to a sealed tube. The reaction was stirred at 100 °C for 24 h, cooled to 0 °C and cautiously acidified with 1 M HCl to pH 4–5. The resulting mixture was extracted with EtOAc (3 x 50 mL). The combined organic layers were washed with water (50 mL) and brine (50 mL), dried over  $\text{MgSO}_4$  and concentrated to afford the title compound. The crude product was used in the next step without further purification.

**(S)-3-(3''-(1-Carboxy-2-phenylethyl)ureido)-5-(4'-(2-chloroacetamido)phenyl) thiophene -2-carboxylic acid (12)**

was prepared from **12b** according to the following procedure:

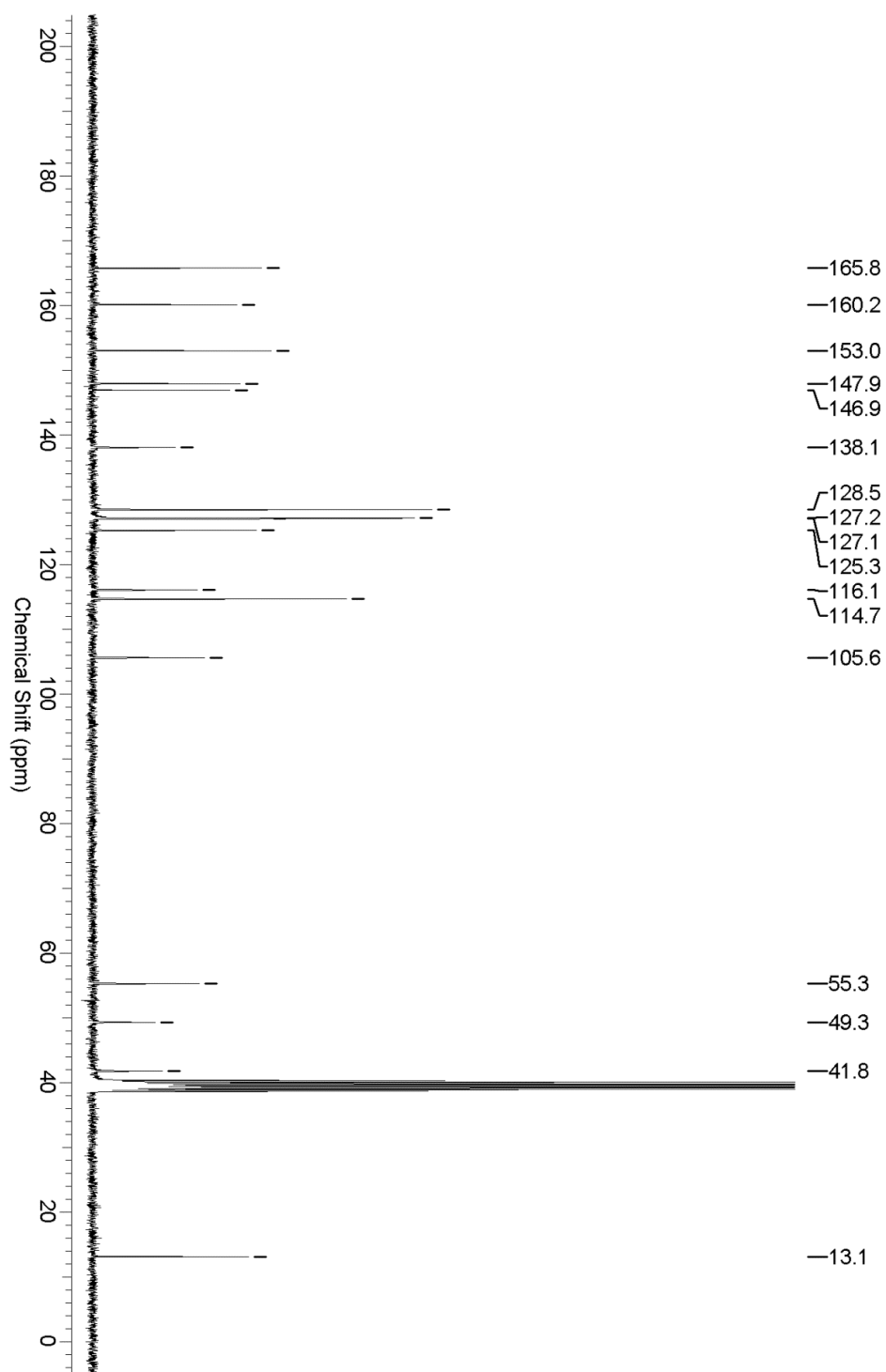
A solution of **12b** (142 mg, 1.10 mmol) and triethylamine (142 mg, 1.10 mmol) in  $\text{CH}_2\text{Cl}_2$  (6 mL) was stirred at –78 °C under stream of nitrogen. 2-Chloroacetyl chloride in  $\text{CH}_2\text{Cl}_2$  (4 mL) was added slowly and stirring was continued for 1 h at –78 °C, 1 h at 0 °C and 1 h at room temperature. The solution was diluted with ice water (30 mL) and acidified with a saturated solution of  $\text{KHSO}_4$ . The resulting mixture was extracted with EtOAc (3 x 50 mL). The combined organic layers were then washed with water (50 mL) and brine (50 mL), dried over  $\text{MgSO}_4$  and concentrated *in vacuo*. The crude material was purified via preparative HPLC (RP18, acetonitrile/ $\text{H}_2\text{O}$  50%  $\rightarrow$  95%) to yield the title compound as a light green solid. (Purity: 90%)

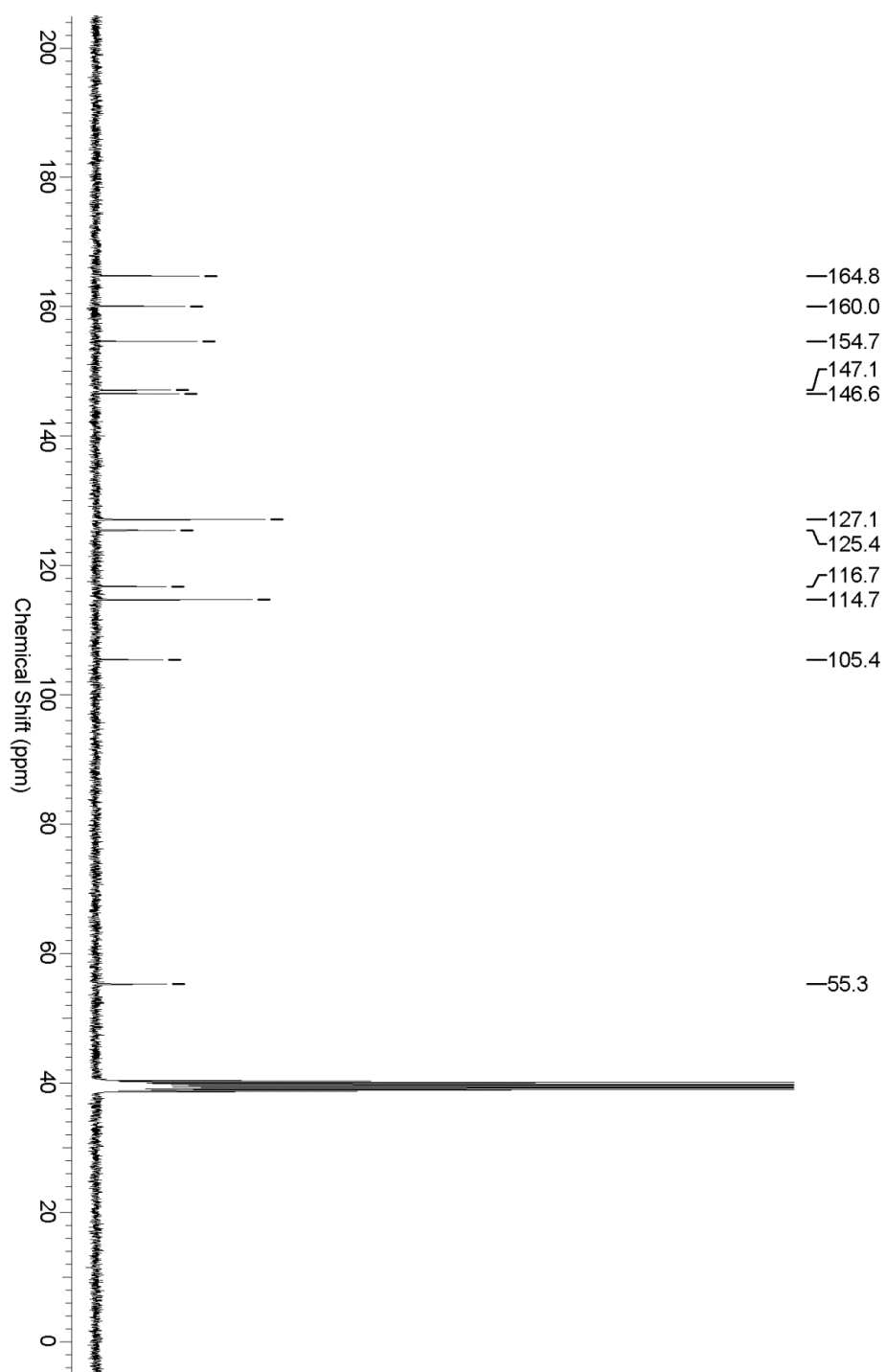


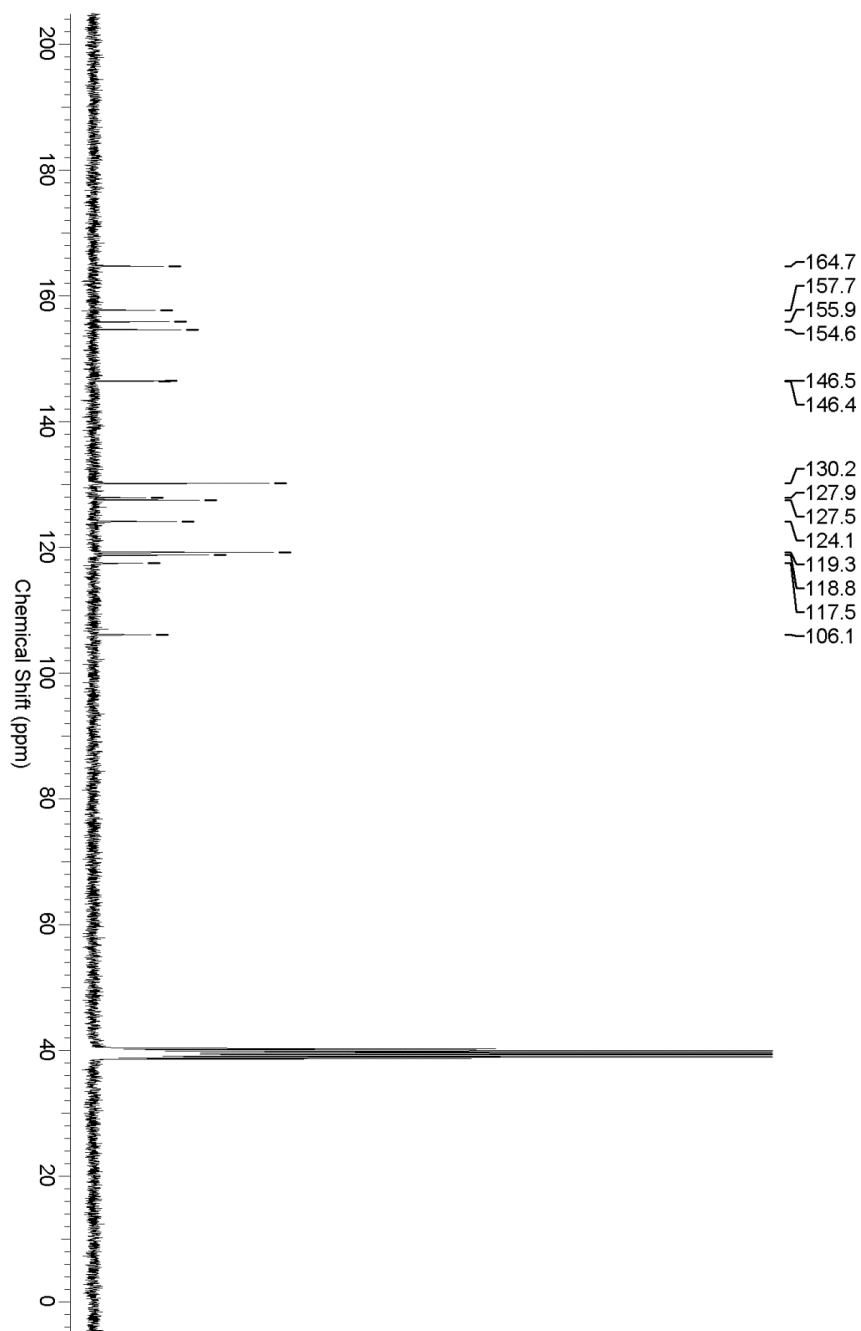


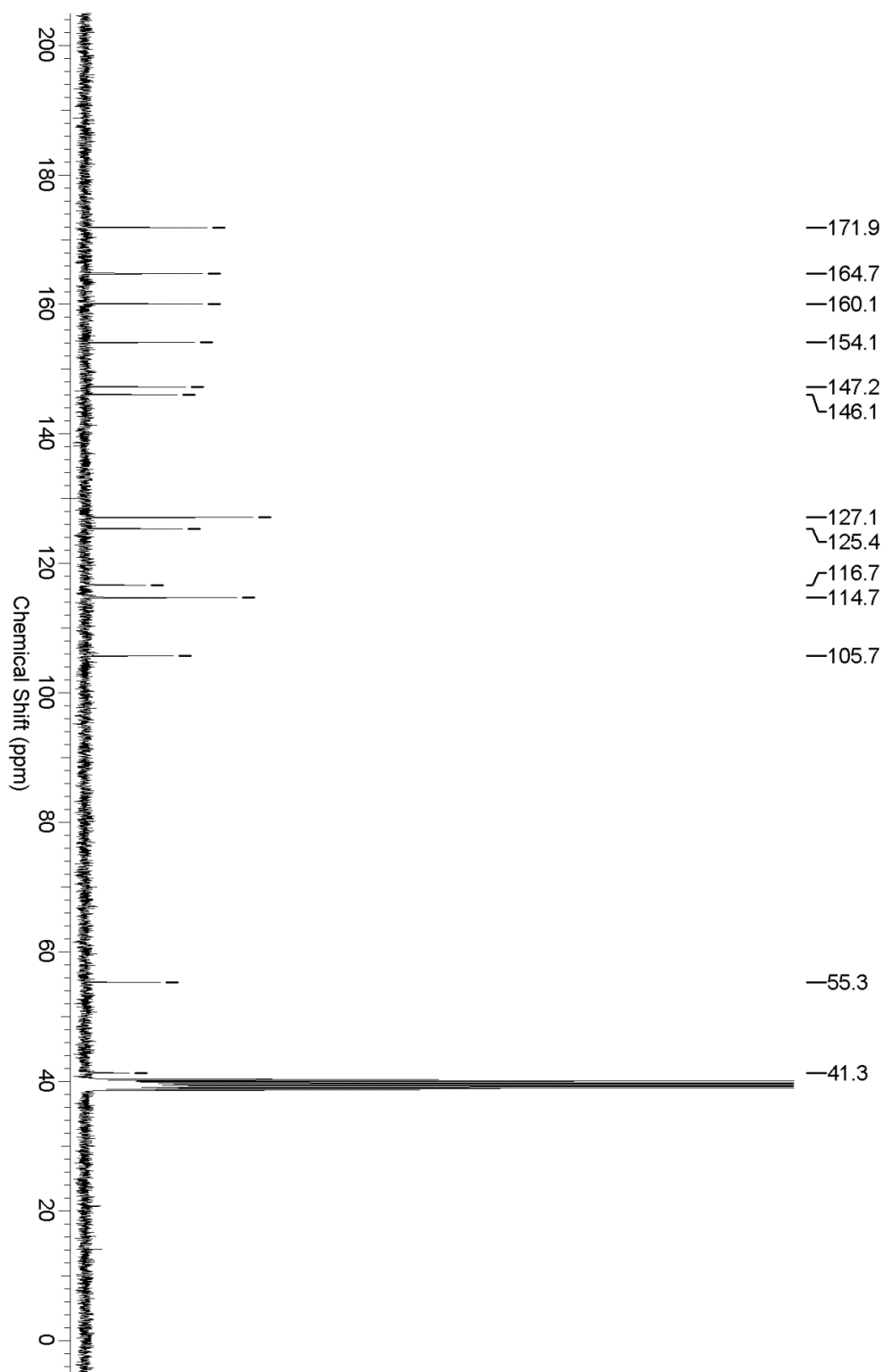
$^1\text{H}$  NMR (DMSO-*d*, 300 MHz):  $\delta$  = 12.89 (br. s., 2 H, CCOH), 10.48 (s, 1 H), 9.41 (s, 1 H), 8.16 (d,  $J$  = 7.8 Hz, 1 H), 8.15 (s, 1 H), 7.73–7.62 (m, 4 H), 7.33–7.20 (m, 5 H), 4.43–4.34 (m, 1 H), 4.27 (s, 2 H, CH<sub>2</sub>Cl), 3.14–3.07 (m, 1 H), 2.92–2.84 (m, 1 H) ppm.

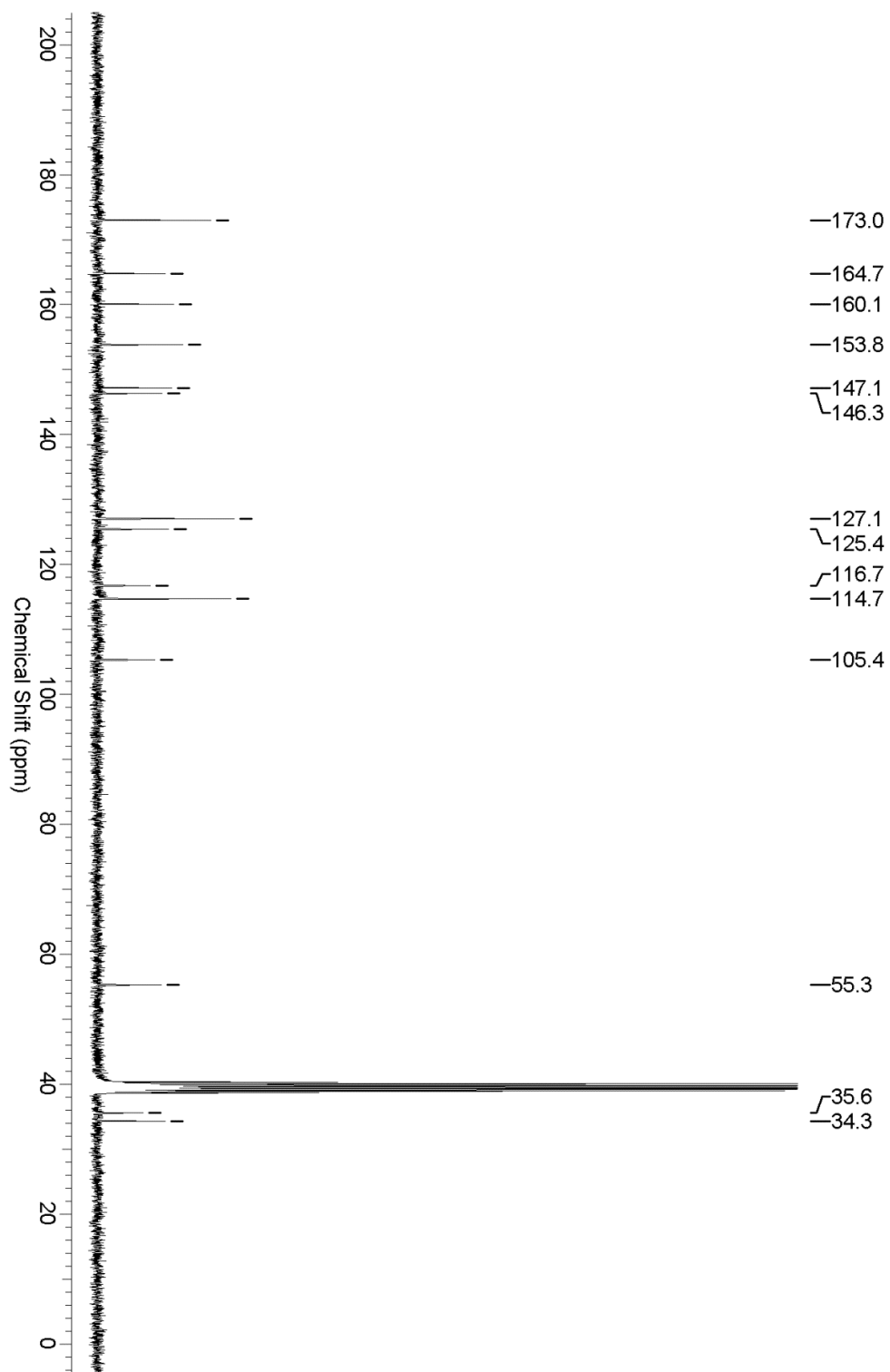
$^{13}\text{C}$  NMR (DMSO-*d*, 176 MHz):  $\delta$  = 173.7, 164.9, 164.7, 153.8, 146.8, 145.9, 139.4, 137.8, 129.1, 128.3, 128.2, 126.5, 126.4, 119.8, 117.3, 106.3, 54.5, 43.6, 36.9 ppm.

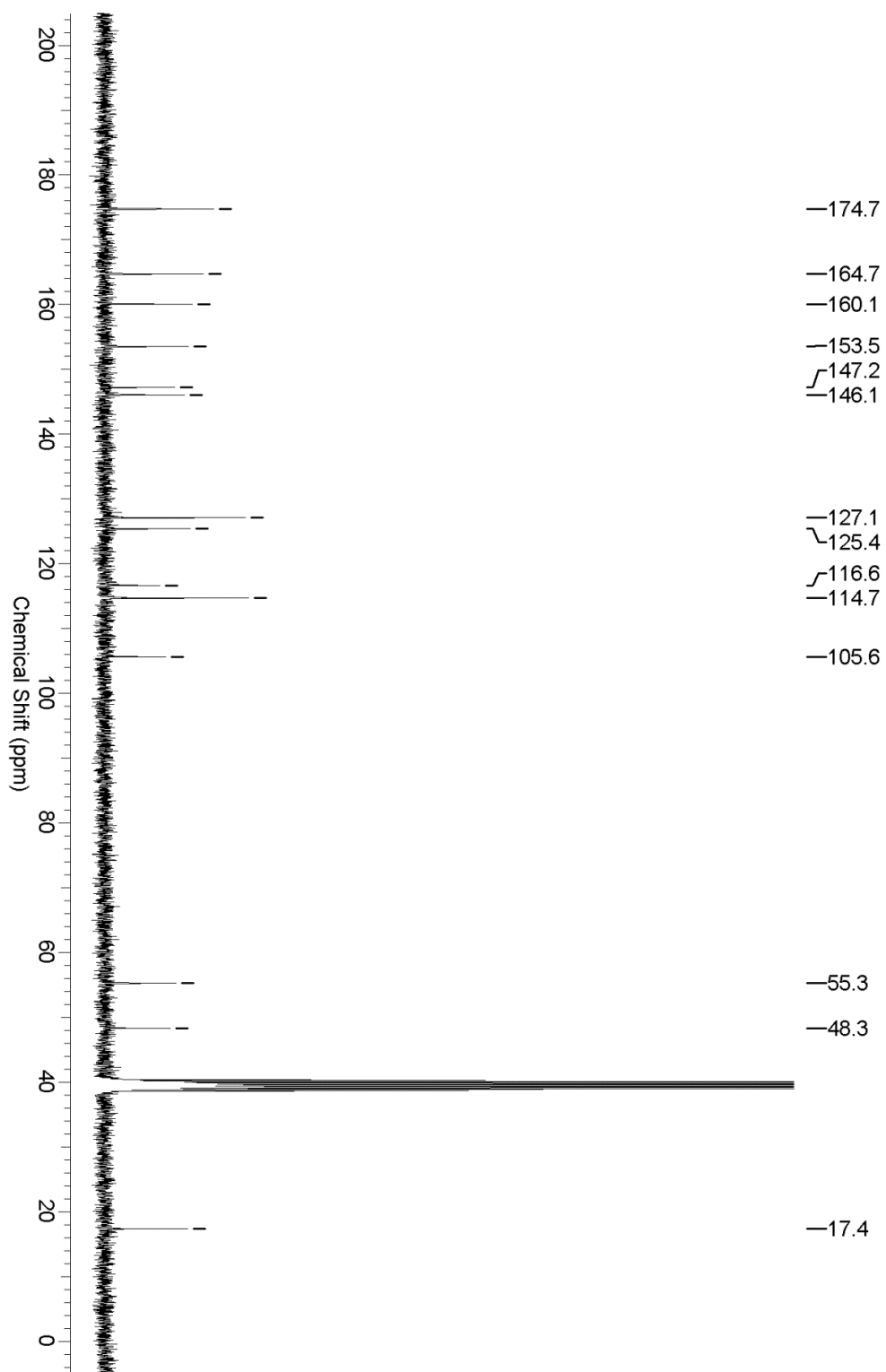
1.1.2.  $^{13}\text{C}$  NMR spectra of compounds 1–12 $^{13}\text{C}$  NMR spectrum of compound 1.

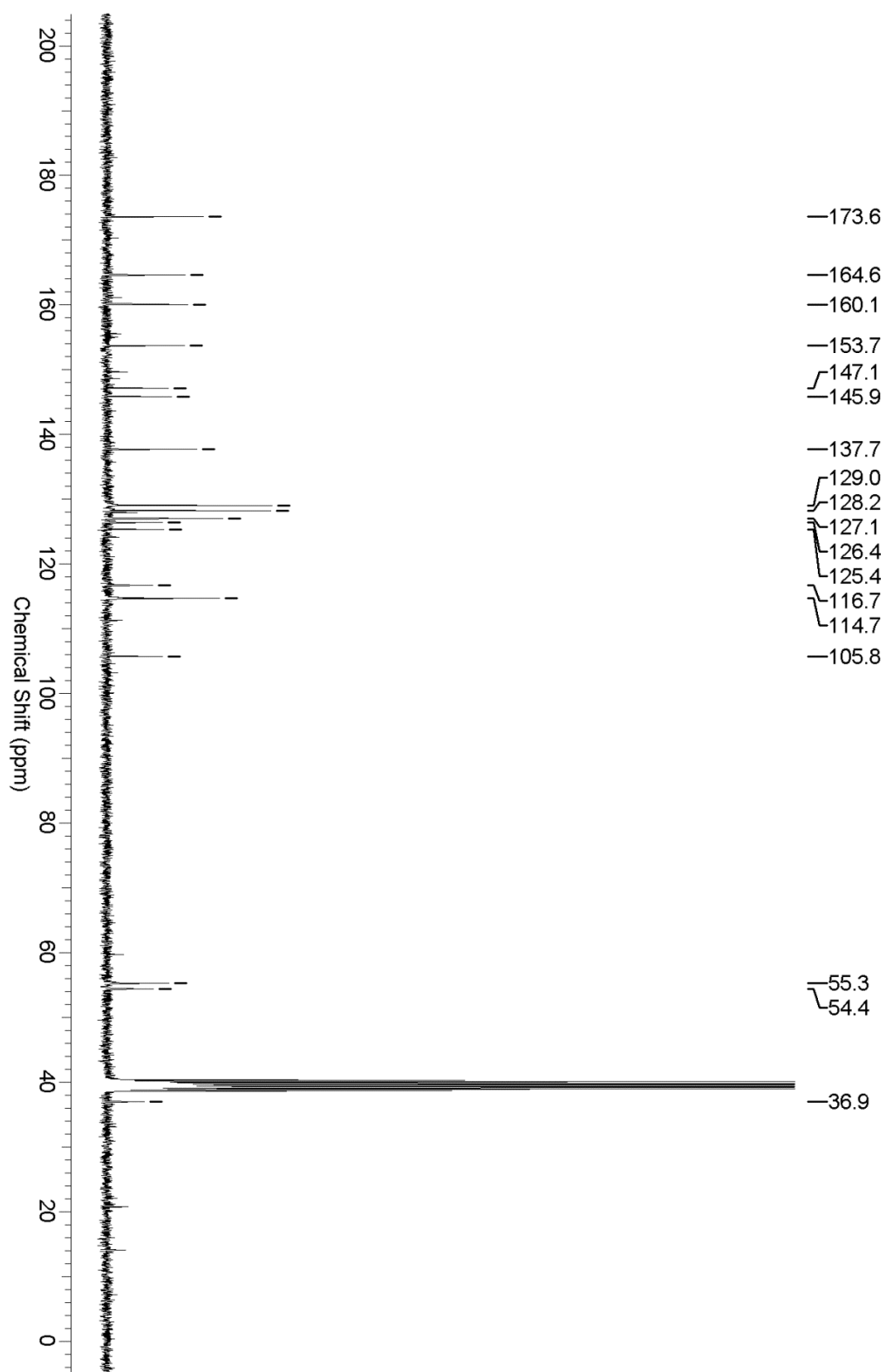




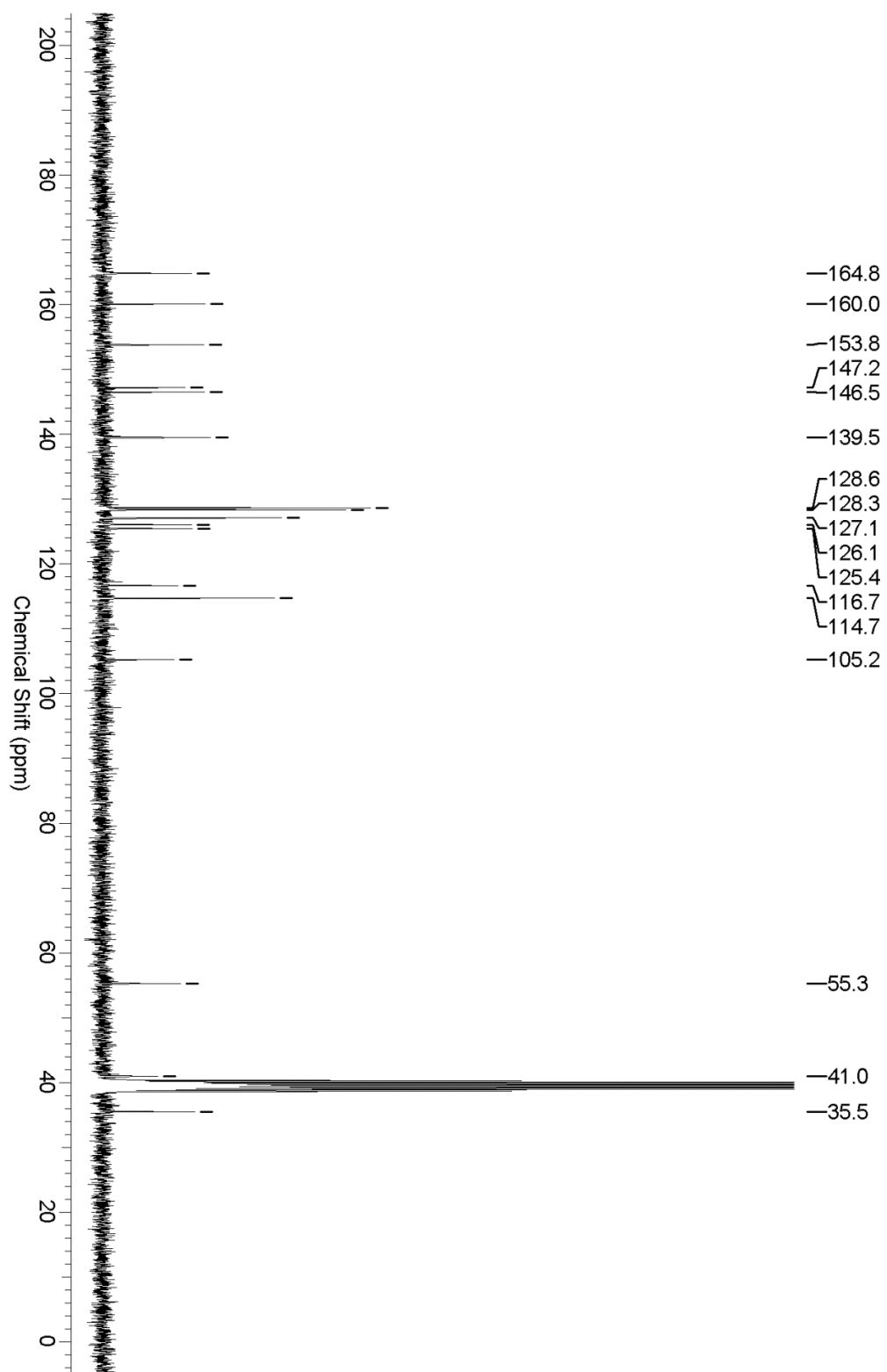


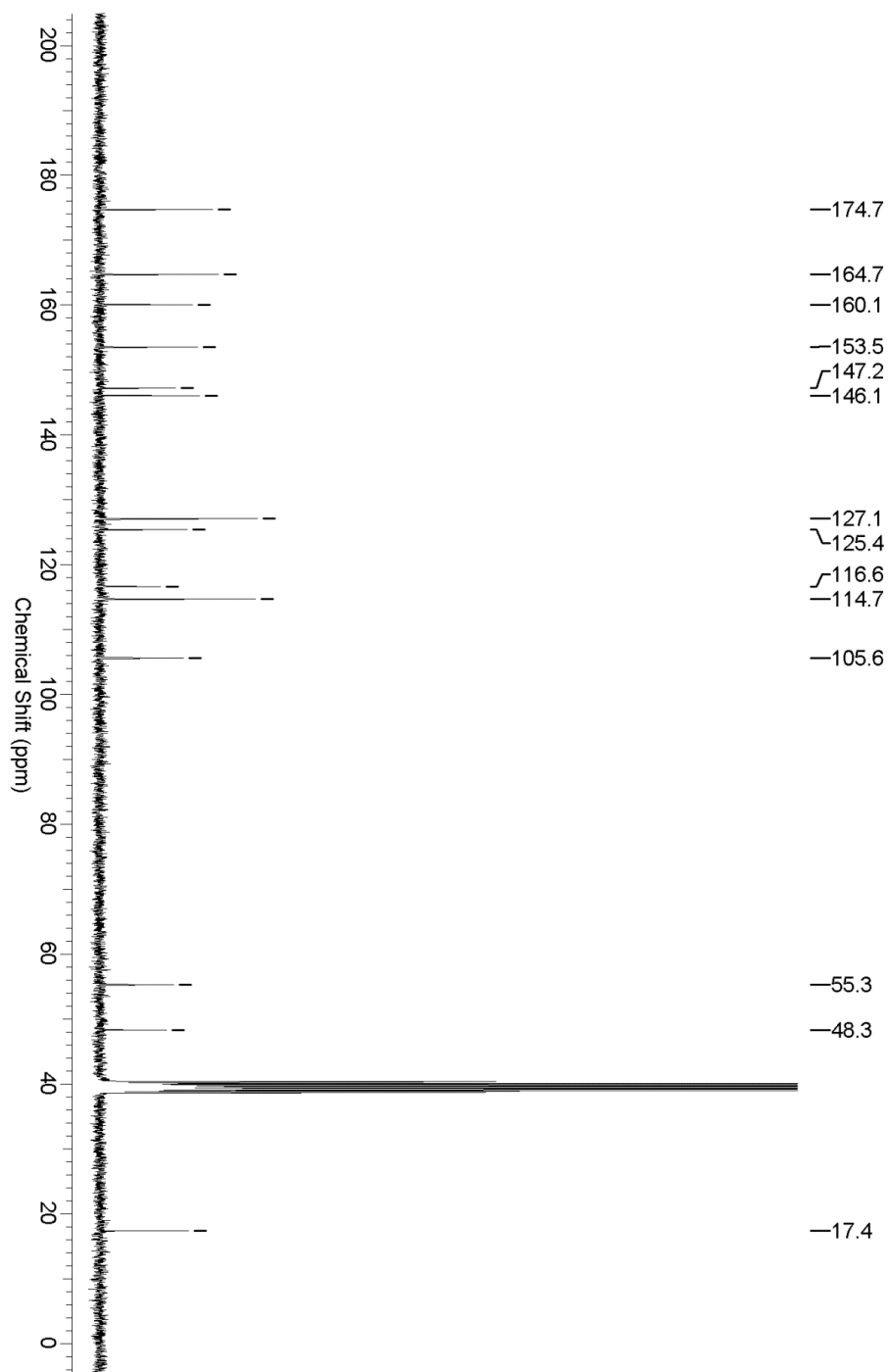


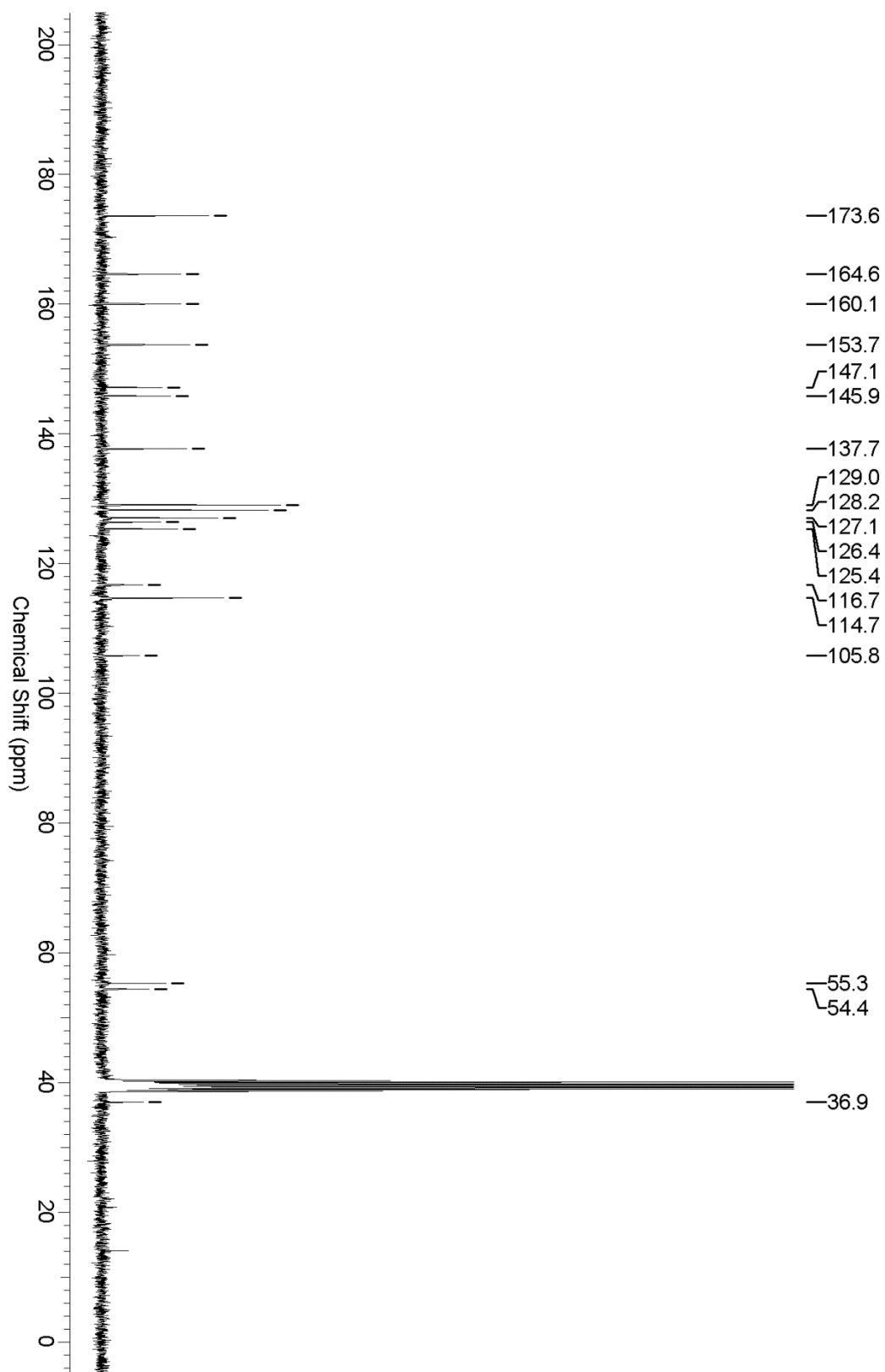


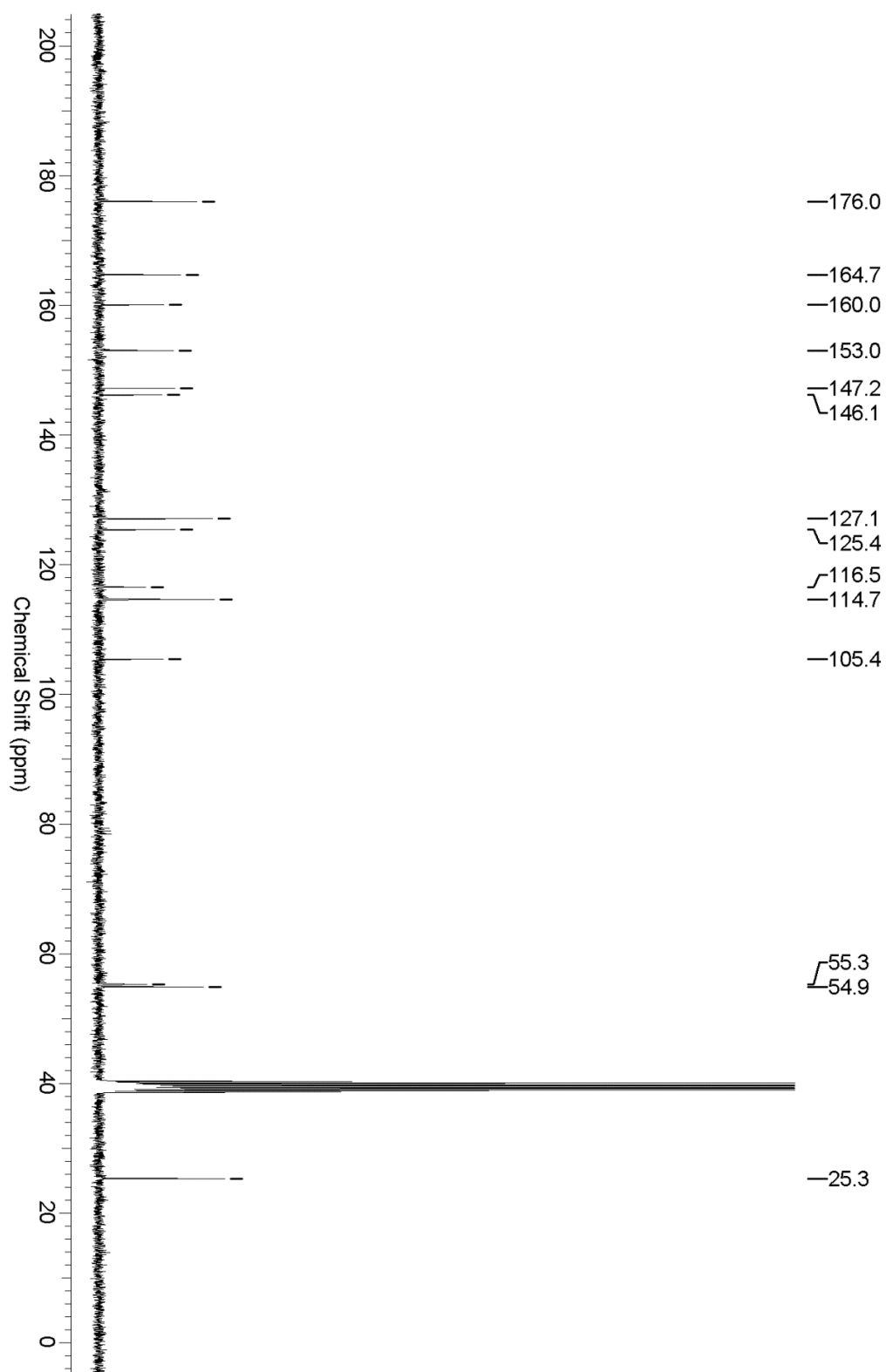


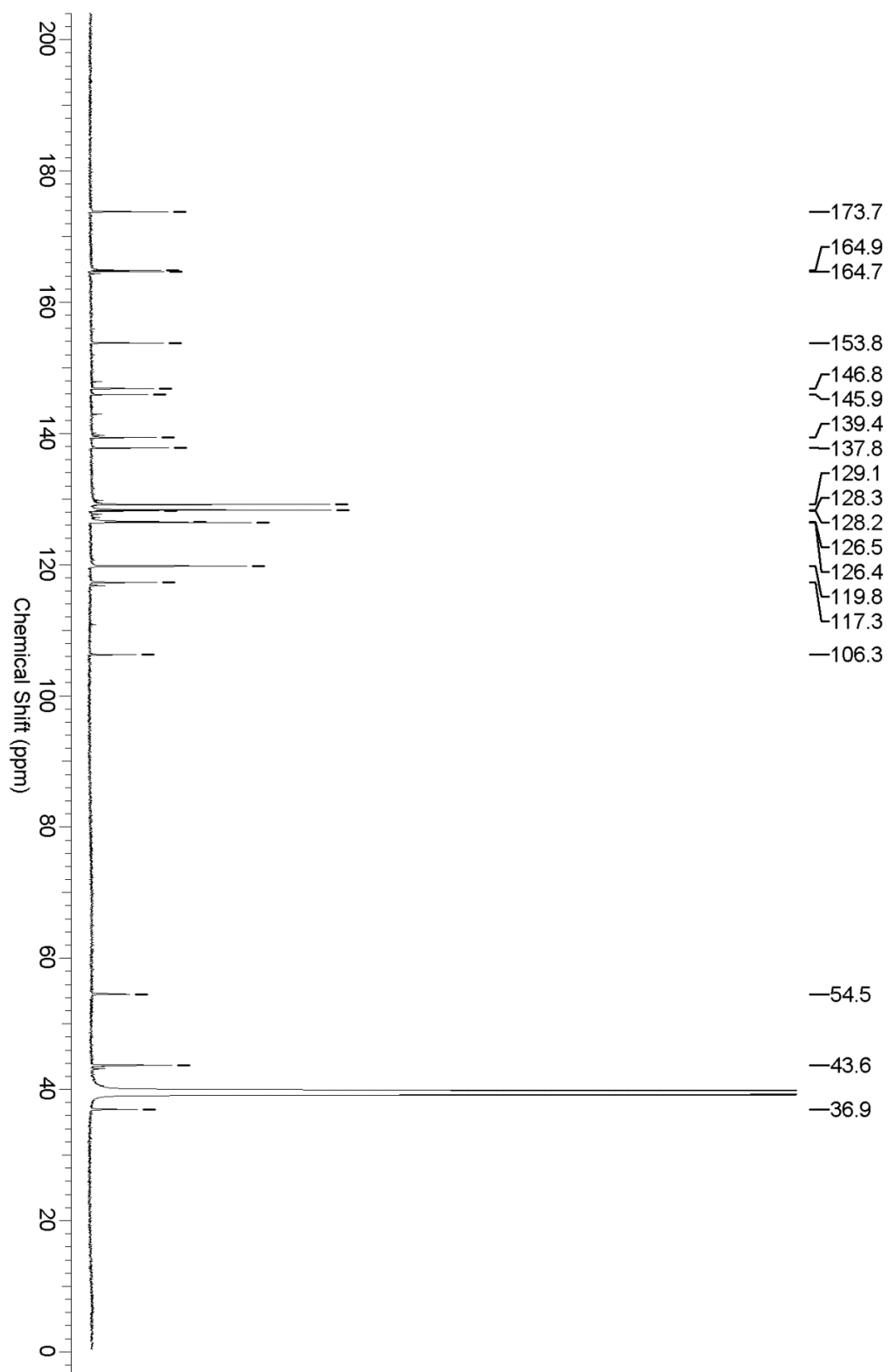












## 1.2 Biology and biophysics

### 1.2.1. SPR - studies with R223A mutant of PqsD

#### *Preparation of PqsD mutant*

R223A PqsD mutant was generated using the QuikChange Site-Directed Mutagenesis Kit (Stratagene, La Jolla, CA) according to the manufacturer's instructions using the pET28b(+)/pqsD plasmid as a template. Briefly, pqsD gene was amplified through 16 cycles of PCR. After treatment with DpnI, the PCR product was transformed into *E. coli* strain XL1-Blue. Plasmid DNA was purified using the GenElute™ HP Plasmid Miniprep Kit (Sigma-Aldrich, St. Louis, MO) and sequenced to confirm the site-directed mutations. The primer sequence of the mutations:

Primer-  
design:

Arg223Ala-  
Mutante:

Wild:		5'
GCGAGTTCCTCATGCGCGGCCGCGCCGATGTTCGAG		
C	3'	Mut: 5'
GCGAGTTCCTCATGCGCGGCCGCGCCGATGTTCGAG		
C	3'	

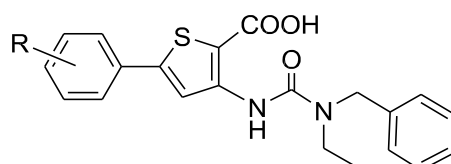
Sequence of the

Primer:

R223A_PqsD_Forward:	5'
GCGAGTTCCTCATGCGCGGCCGCGCCGATGTTCGAGC	3'
R223A_PqsD_Reverse:	5'
GCTCGAACATCGGCGCGCCGCGCATGAGGAACTCGC	3'

## 2. Selectivity data for hit compounds: PqsD vs. RNAP inhibition

**Table S1.** Inhibitory activities of hit compounds against PqsD and RNAP and the derived selectivity factors.



R	IC <sub>50</sub> PqsD [ $\mu$ M]	IC <sub>50</sub> RNAP [ $\mu$ M]	Selectivity factor <sup>[a]</sup>
4-	6	24	40
3,4-	4	2	5.5
3-CF <sub>3</sub> , 4-Cl	3	2	7.0
2,5-	9	3	4.0
4-	1	7	7.3
4-	8	5	6.4
4-	9	4	5.0
H	5	29	6.0

<sup>[a]</sup> Selectivity factor was calculated as  $IC_{50}(RNAP) IC_{50}(PqsD)^{-1}$

### 3. Results from SPR experiments

#### 3.1 Competition experiments for identification of the binding mode

**Figure S1.** SPR-competition experiments with model compounds **1–3** competitor compounds **A** (black) and **B** (red) from the 2-nitrophenyl methanol class. Reference without competition is shown in blue. A reduced response in competition with **A** can be observed exclusively for compound **3**. The reference signal is shown in grey.

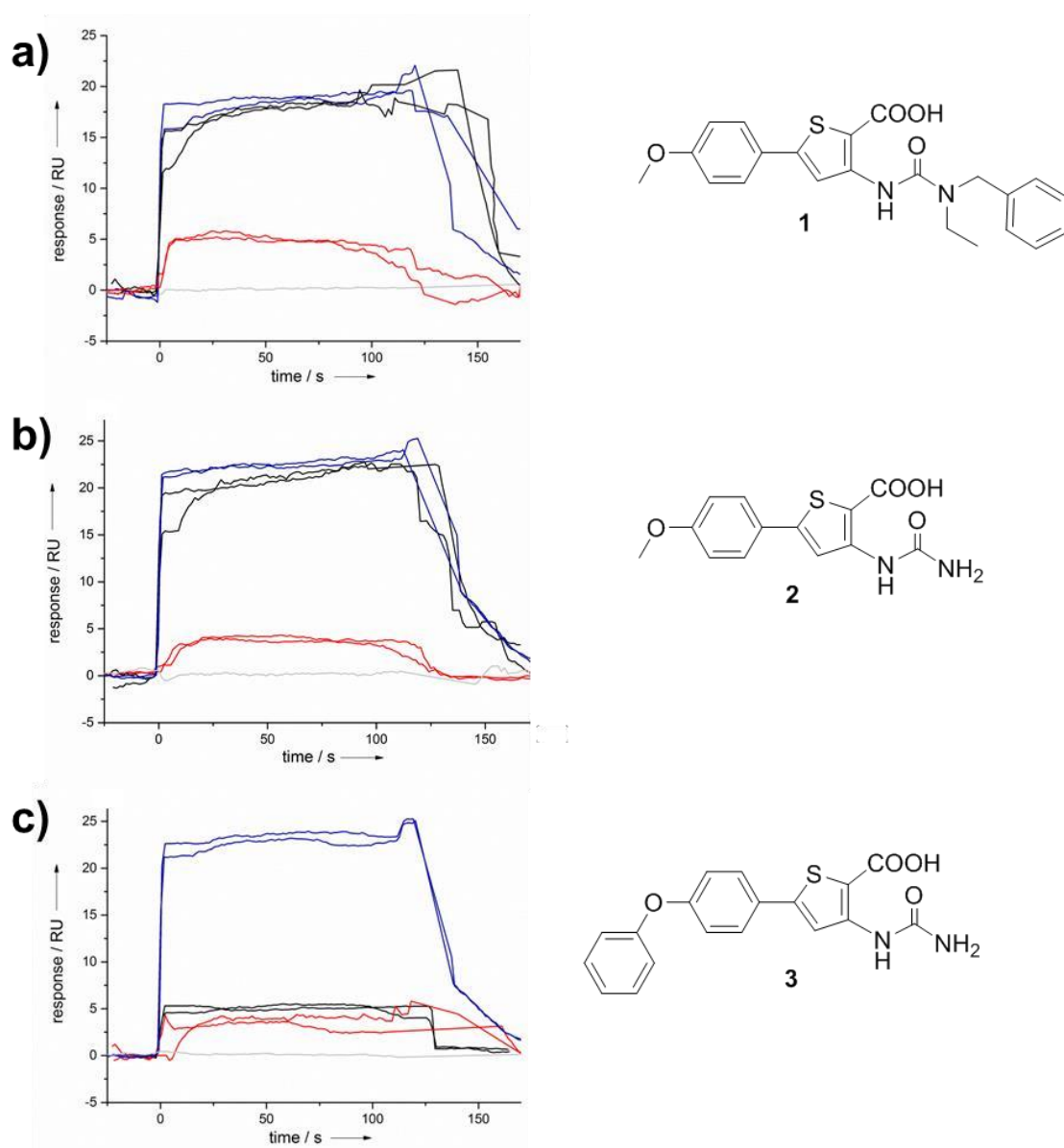




**Figure S2.** Visualization of the SPR-competition results shown in Figure S1. Competitor **A** (yellow), competitor **B** (magenta) a) **A** does not affect the binding of **1** (green). b) **B** leads to sterical clash with methoxy group of **1** (green). c) **A** does not affect the binding of **2** (blue). d) **B** leads to sterical clash with methoxy group of **2** (blue). e) **A** leads to sterical clash with phenoxy group of **3** (turquoise). f) **B** leads to sterical clash with phenoxy group of **3** (turquoise).

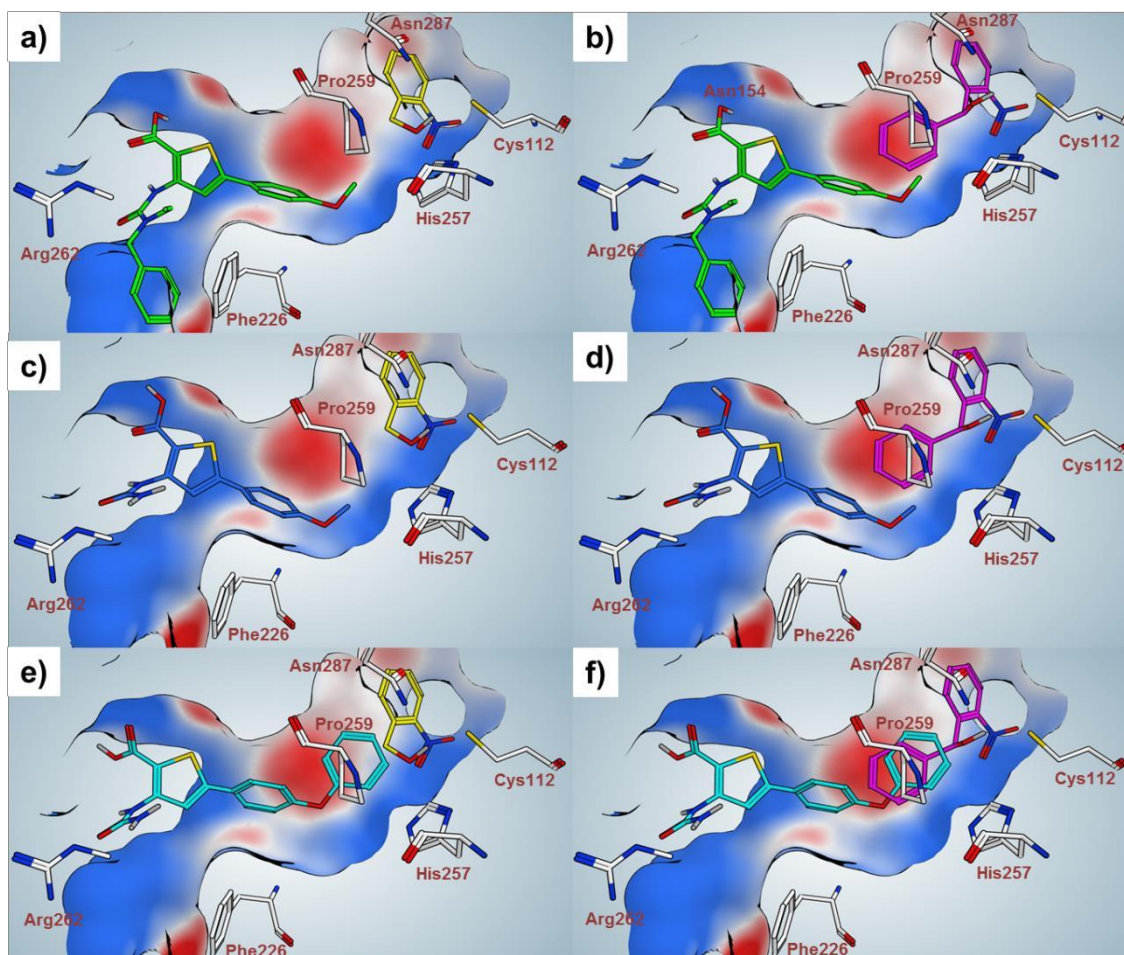
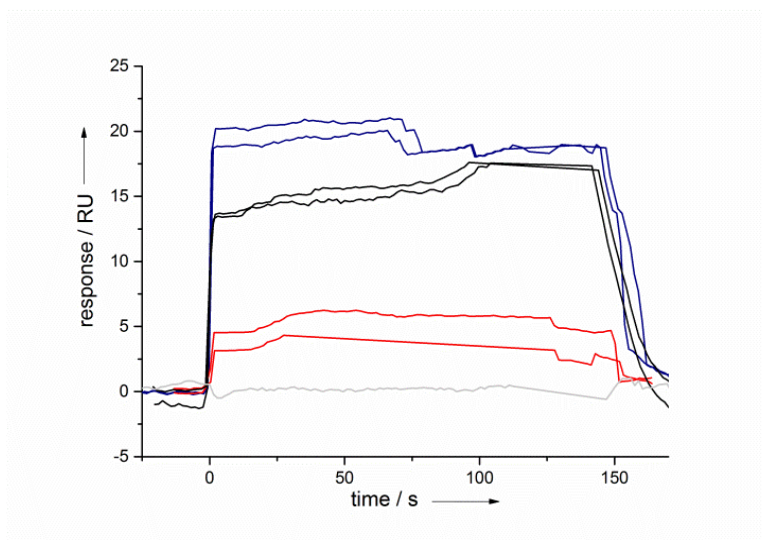
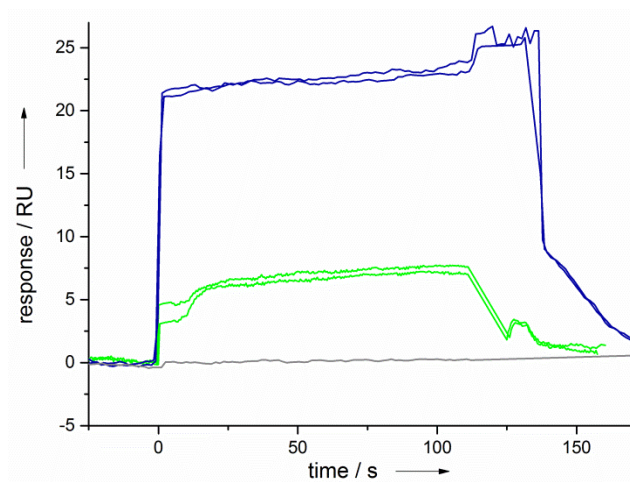


**Figure S3.** SPR-competition experiments with compounds **7** and competitor compounds **A** (black) and **B** (red) from the 2-nitrophenyl methanol class. Reference without competition is shown in blue. The reference signal is shown in grey.



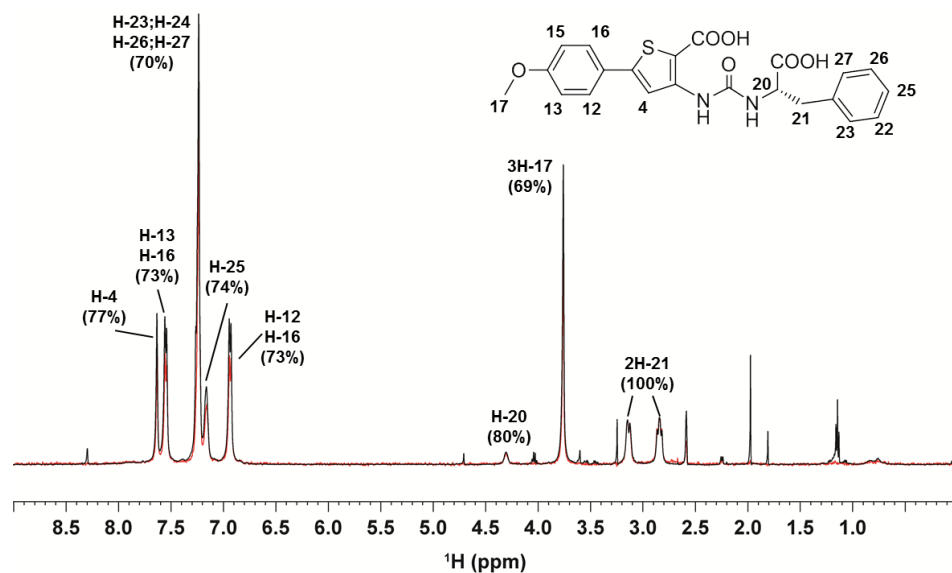
### 3.2 Experiment with R223A mutant and compound 2

**Figure S4.** SPR-experiment with compound 2 revealed different responses with PqsD wildtype (blue) and the R223A mutant (green)



#### 4. STD-NMR spectrum of 7

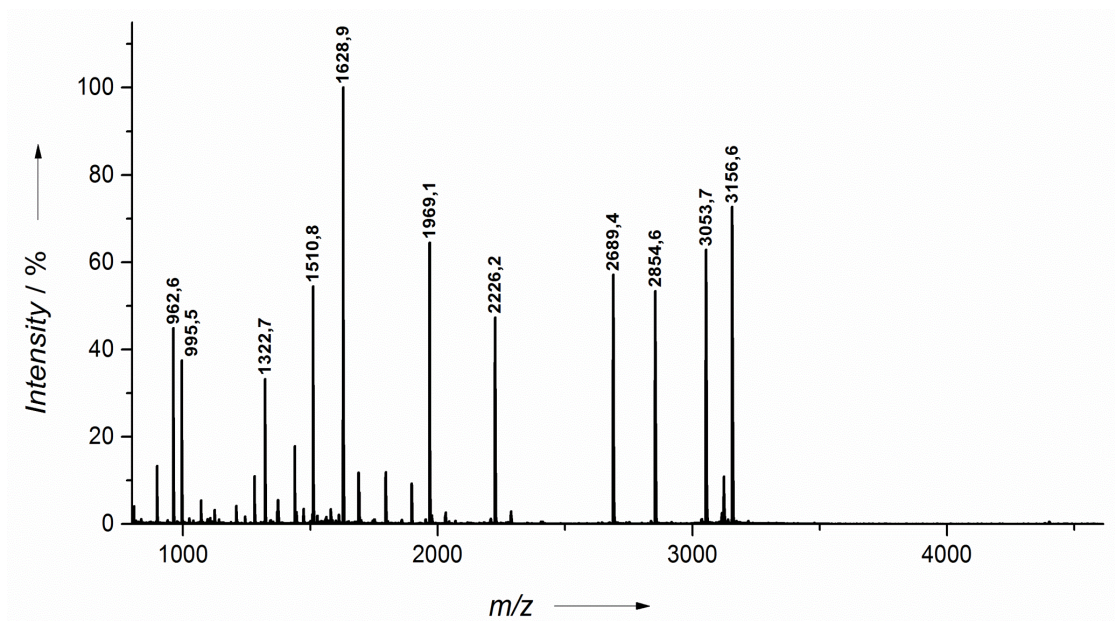
**Figure S5.** Reference (black) and STD NMR difference (red) spectra of compound **7** in complex with PqsD. Samples comprising 100:1 **7**/PqsD were prepared in 20 mM Na<sub>3</sub>PO<sub>4</sub>, 50 mM NaCl, and 5 mM MgCl<sub>2</sub>, pH 7.0, and spectra were recorded at 298 K. Overlaid spectra were normalized to the signals for 2H-21, which gave the strongest enhancement.



## 5. MALDI-ToF-MS spectra

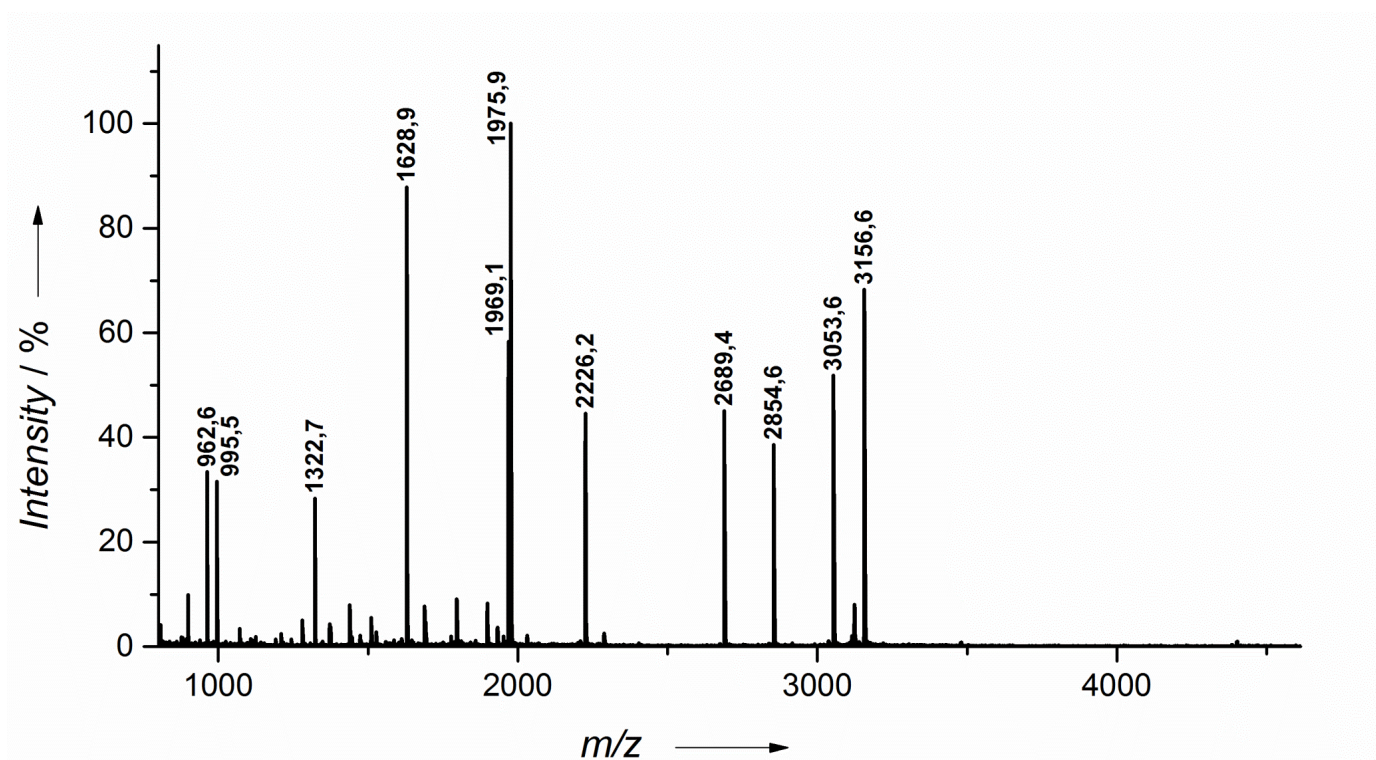
### 5.1 PqsD

**Figure S6.** MALDI-ToF-MS analysis of tryptic digested PqsD. For the sake of clarity, only signals >15% intensity are labeled.



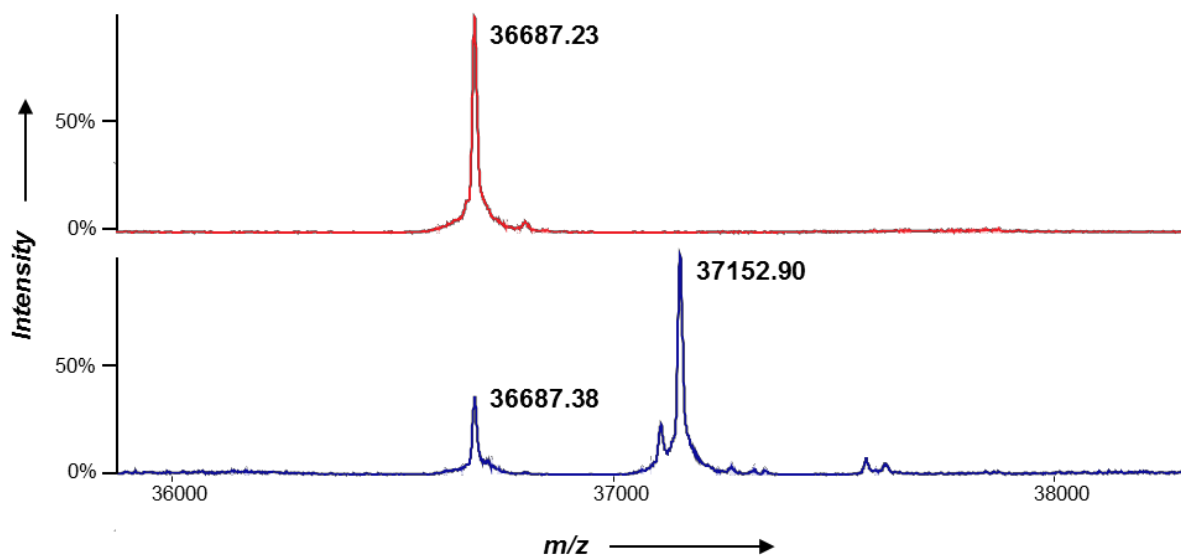
## 5.2 PqsD + 12

Figure S7. MALDI-ToF-MS analysis of tryptic digested PqsD after preincubation with **12**. For the sake of clarity, only signals >15% intensity are labeled.



## 6. LC-ESI-MS data

**Figure S8.** LC-ESI-MS data. Top panel (red): Reference sample containing only PqsD. Bottom panel (blue): PqsD after 30 minutes preincubation with compound **12**. Mass shift of 465 Da indicates covalent binding of **12**.



## 7. HPLC purities

**Table S2. Purities and retention times of compounds 1–12.**

Compou	Purity	Retention time [min] <sup>a</sup>
<b>1</b>	9	13.5
<b>2</b>	9	9.7
<b>3</b>	9	12.3
<b>4</b>	9	9.6
<b>5</b>	9	9.8
<b>6</b>	9	10.0
<b>7</b>	10	10.8
<b>8</b>	9	13.6
<b>9</b>	9	10.0
<b>1</b>	9	11.9
<b>1</b>	9	10.4
<b>1</b>	9	10.7

<sup>a</sup> In a gradient run the percentage of acetonitrile (containing 0.1% trifluoroacetic acid) was increased from an initial concentration of 0% at 0 min to 100% at 15 min and kept at 100% for 5 min.



**E Structure Optimization of 2-Benzamidobenzoic Acids as PqsD Inhibitors for Pseudomonas aeruginosa Infections and Elucidation of Binding Mode by SPR, STD NMR, and Molecular Docking**

Elisabeth Weidel, Johannes C. de Jong, Christian Brengel, Michael P. Storz, Matthias Negri, Alberto Plaza, Anke Steinbach, Rolf Müller, and Rolf W. Hartmann

J. Med Chem. 2013, 56, 6146-6155.

## Supporting Information

## Additional figures docking studies

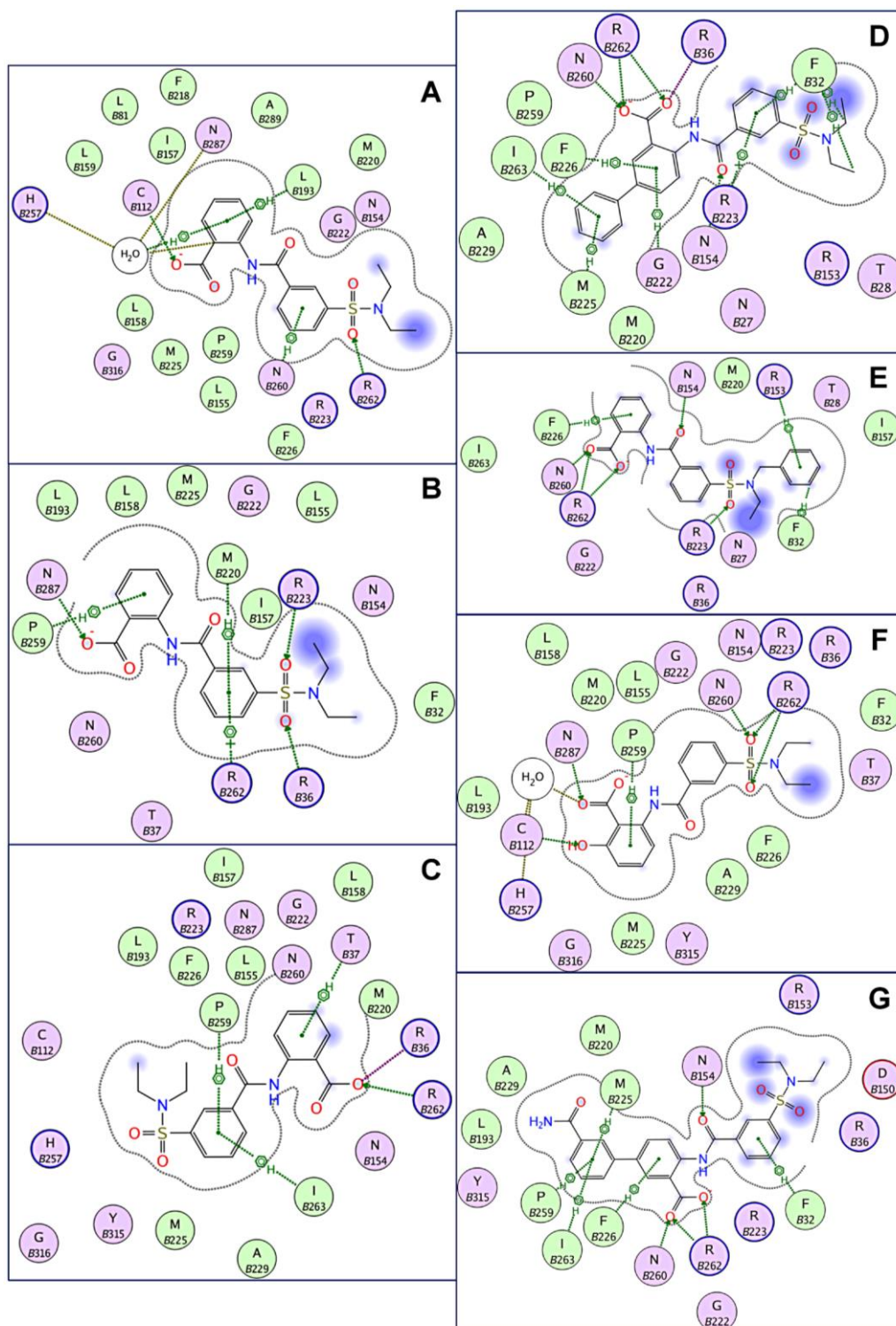


**Figure S1** Two dimensional representation of the interaction between compounds **2** (A-C), **48** (D), **64** (E), **52** (F) and **53** (G) and PqsD. Amino acids within 5.5 Å are shown and the key interactions are highlighted. Polar amino acids are colored in purple and hydrophobic amino acids in green circles (MOE).

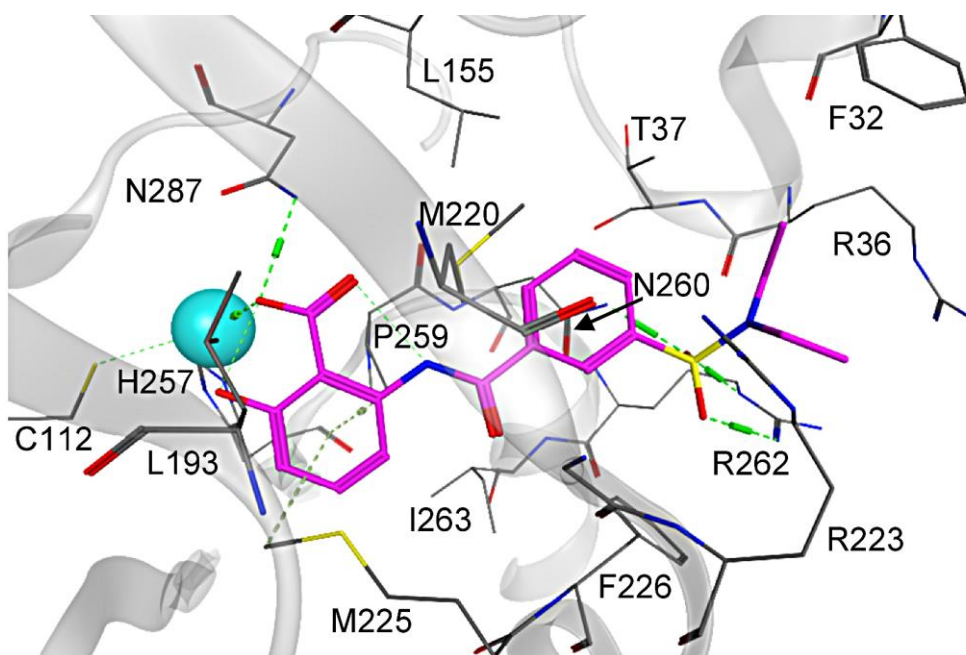


**Figure S2** Docking pose of compound **52**. In presence of a structural water molecule (cyan ball) a hydrogen bond network is formed between the hydroxyl group and the carboxylic moiety of **52** and the catalytic residues Cys112, His257, and Asn287 bridged by the water molecule.

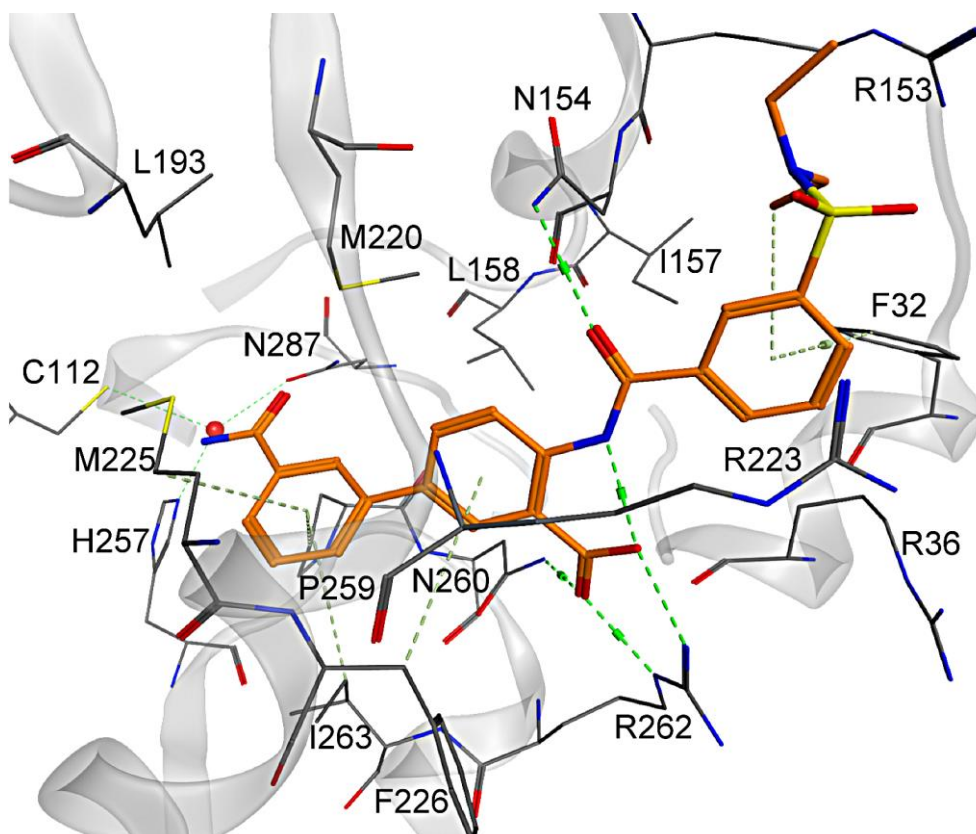


**Figure S3** Docking pose of compound **53** (orange sticks).



## Additional figures STD NMR study

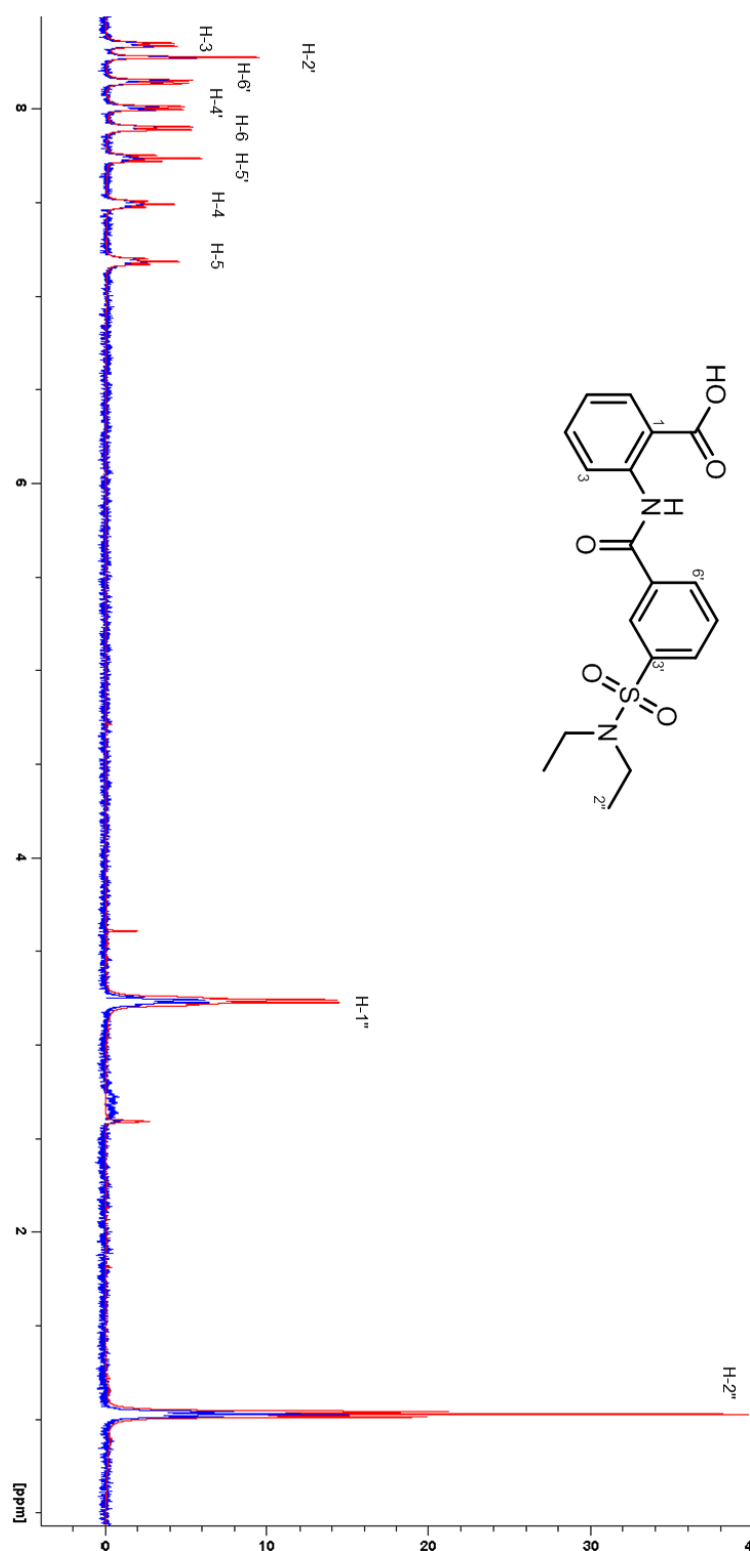


**Figure S4** Reference (red) and STD NMR difference (blue) spectra of **2** in complex with PqsD. Samples containing 80:1 **2**/PqsD were prepared in 20 mM sodium phosphate, 50 mM NaCl, 5 mM MgCl<sub>2</sub>, pH = 7.0, and spectra were recorded at 298 K. Overlaid spectra were normalized to the signal for H-6 ( $\delta$  7.90), which gave the strongest enhancement.

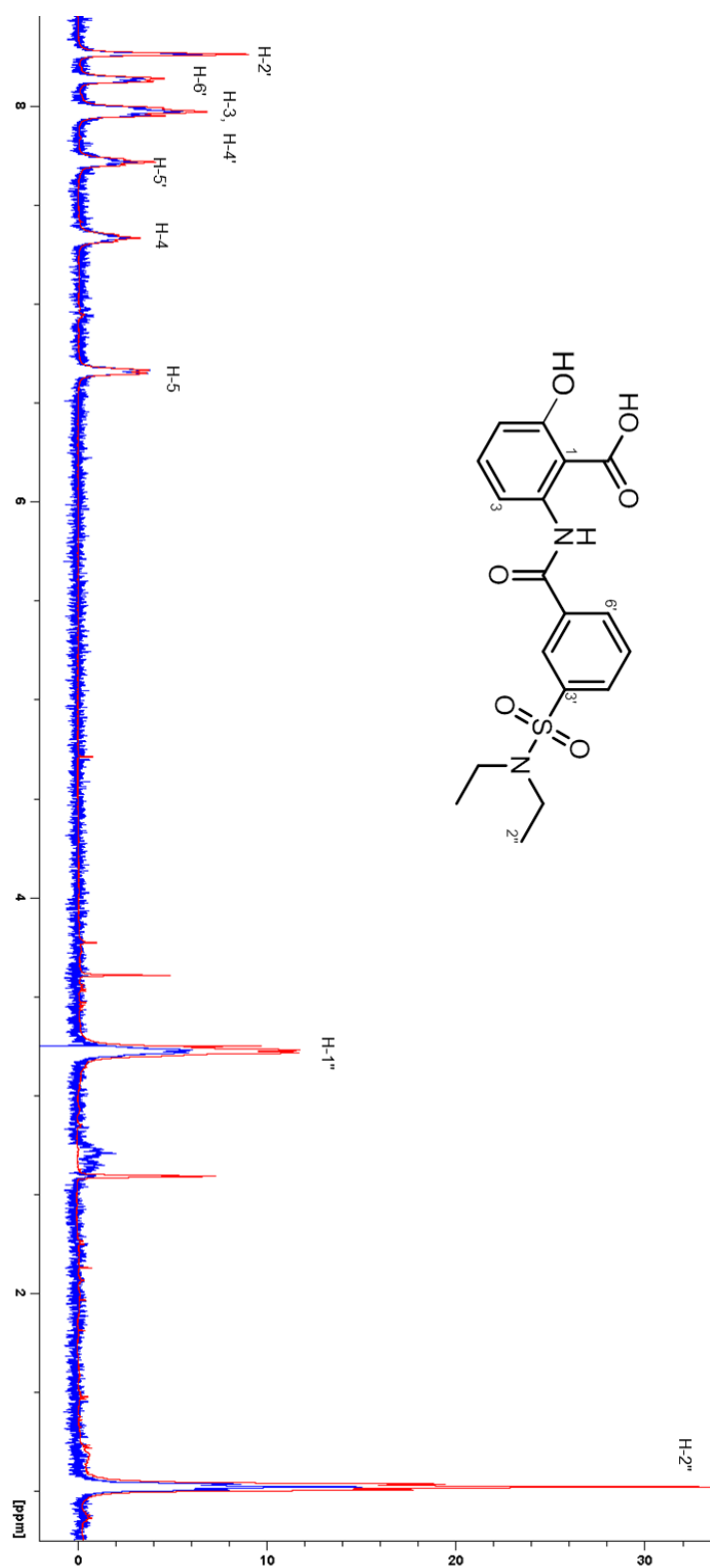


**Figure S5.** Reference (red) and STD NMR difference (blue) spectra of **52** in complex with PqsD. Samples containing 80:1 **52**/PqsD were prepared in 20 mM sodium phosphate, 50 mM NaCl, 5 mM MgCl<sub>2</sub>, pH = 7.0, and spectra were recorded at 298 K. Overlaid spectra were normalized to the signal for H-5 ( $\delta$  6.65), which gave the strongest enhancement.

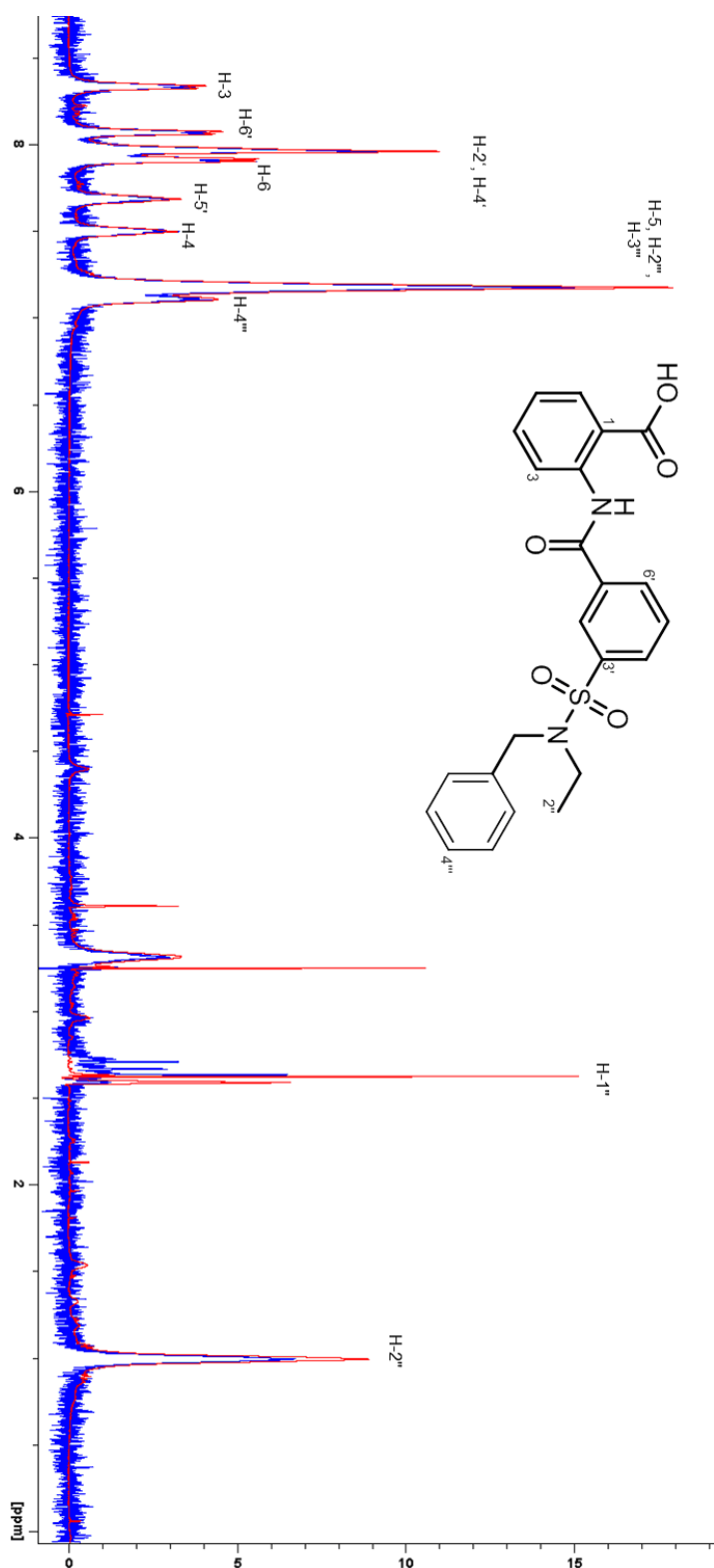


**Figure S6.** Reference (red) and STD NMR difference (blue) spectra of **64** in complex with PqsD. Samples containing 80:1 **64**/PqsD were prepared in 20 mM sodium phosphate, 50 mM NaCl, 5 mM MgCl<sub>2</sub>, pH = 7.0, and spectra were recorded at 298 K. Overlaid spectra were normalized to the signal for H-6 ( $\delta$  7.90), which gave the strongest enhancement.

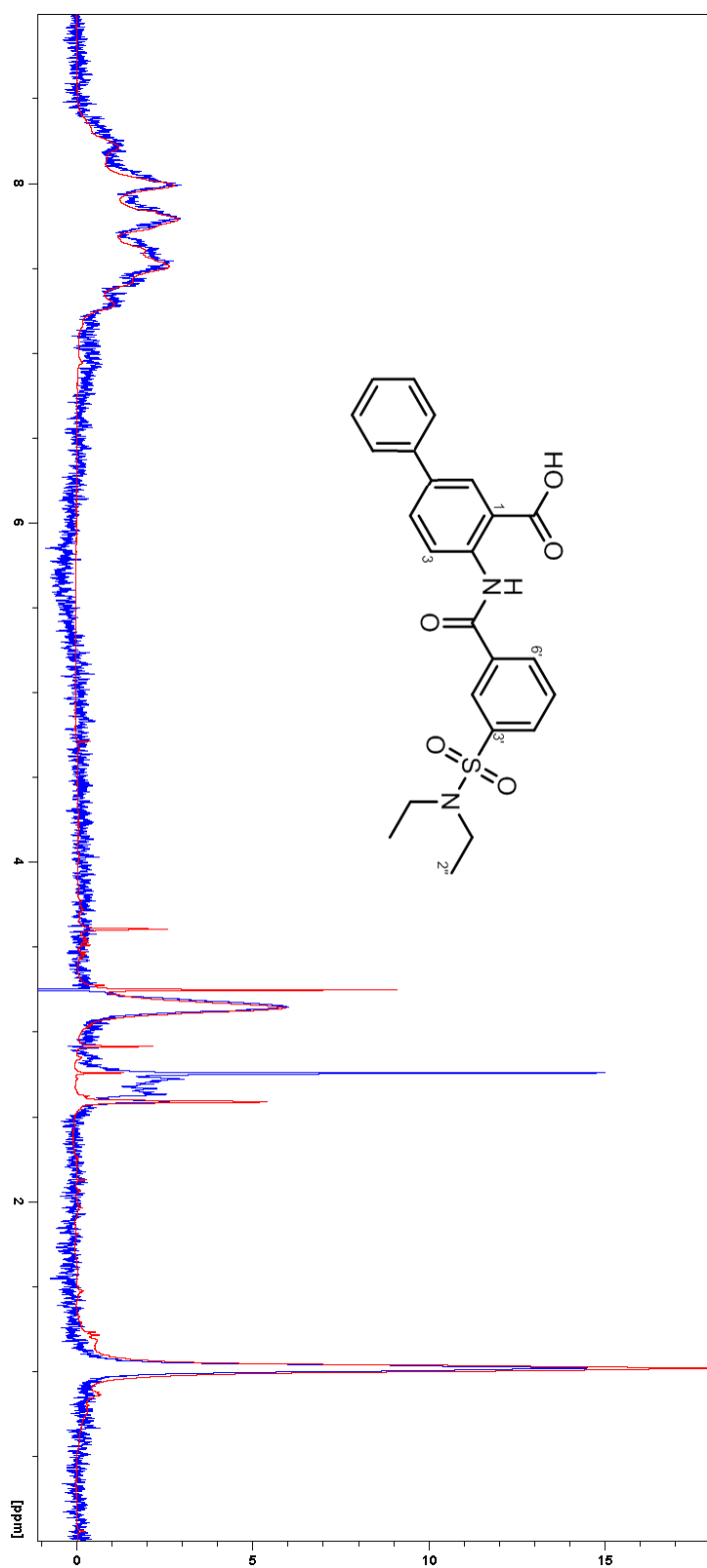


**Figure S7.** Reference (red) and STD NMR difference (blue) spectra of **48** in complex with PqsD. Samples containing 80:1 **48**/PqsD were prepared in 20 mM sodium phosphate, 50 mM NaCl, 5 mM MgCl<sub>2</sub>, pH = 7.0, and spectra were recorded at 298 K.



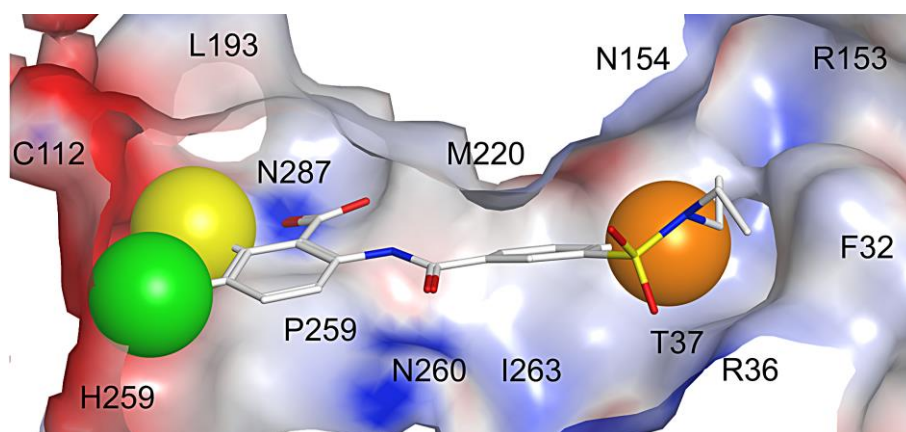


**Figure S8.** Docking pose of the 2-Benzamidobenzoic acid core structure (white sticks). Balls represent possible substituents that form specific interactions with amino acids of the active site.

## Chemistry

### *Syntheses of 3-(chlorosulfonyl)benzoic acids 18-20*

**4-Bromo-3-(chlorosulfonyl)benzoic acid (18)**<sup>S1</sup> A solution of 4-bromobenzoic acid (**15**, 5.03 g, 25.0 mmol) in chlorosulfonic acid (28 mL) was heated overnight at 100 °C. After cooling to room temperature the reaction mixture was added very slowly onto ice. The white solid was isolated by suction filtration, washed with water and dried under reduced pressure; 6.12 g, 82% yield. The material was used without further purification.

**3-(Chlorosulfonyl)-4-methylbenzoic acid (19)**<sup>S2</sup> A solution of 4-methylbenzoic acid (**16**, 3.00 g, 22.0 mmol) in chlorosulfonic acid (25 mL) was heated overnight at 100 °C. After cooling to room temperature the reaction mixture was added very slowly onto ice. The white solid was isolated by suction filtration, washed with water and dried under reduced pressure; 6.12 g, 82% yield. The material was used without further purification.

**3-(Chlorosulfonyl)-4-ethylbenzoic acid (20)**<sup>S1,S3</sup> A solution of 4-ethylbenzoic acid (**17**, 3.00 g, 20.0 mmol) in chlorosulfonic acid (25 mL) was heated overnight at 100 °C. After cooling to room temperature the reaction mixture was added very slowly onto ice. The white solid was isolated by suction filtration, washed with water and dried under reduced pressure; 4.57 g, 88% yield. The material was used without further purification.

### *Syntheses of 3-sulfamoylbenzoic acids 22-33*

**4-Bromo-3-(*N,N*-diethylsulfamoyl)benzoic acid (22)**<sup>S4</sup> The title compound was synthesized from 4-bromo-3-(chlorosulfonyl)benzoic acid (**18**) and diethylamine according to General Procedure A: 1.22 g, 91% yield. <sup>1</sup>H NMR (500 MHz, DMSO-*d*<sub>6</sub>): δ 1.06 (t, *J* = 7.1 Hz, 6H), 3.33 (q, *J* = 7.1 Hz, 4H), 7.97 (dd, *J* = 8.2 Hz, 1H), 8.00 (dd, *J* = 8.2, 1.9 Hz, 1H), 8.48 (d, *J* = 1.9 Hz, 1H).

**3-(*N,N*-Diethylsulfamoyl)-4-methylbenzoic acid (23)** The title compound was synthesized from 3-(chlorosulfonyl)-4-methylbenzoic acid (**19**) and diethylamine according to General Procedure A: 2.05 g, 76% yield. <sup>1</sup>H NMR (500 MHz, DMSO-*d*<sub>6</sub>): δ 1.04 (t, *J* = 7.1 Hz, 6H), 2.58 (s, 3H), 3.26 (q, *J* = 7.1 Hz, 4H), 7.57 (d, *J* = 7.9 Hz, 1H), 8.05 (dd, *J* = 7.9, 1.9 Hz, 1H), 8.33 (d, *J* = 1.9 Hz, 1H), 13.34 (bs, 1H); <sup>13</sup>C NMR (125 MHz, DMSO-*d*<sub>6</sub>): δ 13.59, 19.82, 40.65, 128.97, 129.36, 133.03, 133.31, 138.78, 141.95, 166.07; LC/MS: *m/z* = 271.83 [M + H]<sup>+</sup>, 312.87 [M + H + CH<sub>3</sub>CN]<sup>+</sup>, 542.54 [2M + H]<sup>+</sup>, *t*<sub>R</sub> = 9.35 min, 98.9% pure (UV).

**3-(*N,N*-Diethylsulfamoyl)-4-ethylbenzoic acid (24)** The title compound was synthesized from 3-(chlorosulfonyl)-4-ethylbenzoic acid (**20**) and diethylamine according to General Procedure A and purified by flash column chromatography (silica gel, ethyl acetate/*n*-hexane): 1.11 g, 39% yield. <sup>1</sup>H NMR (500 MHz, DMSO-*d*<sub>6</sub>): δ 1.20 (t, *J* = 7.1 Hz, 6H), 1.33 (t, *J* = 7.6 Hz, 3H), 3.12 (q, *J* = 7.5 Hz, 2H), 3.39 (q, *J* = 7.1 Hz, 4H), 7.50 (d, *J* = 7.9 Hz, 1H), 8.18 (dd, *J* = 7.9, 1.6 Hz, 1H), 8.50 (d, *J* = 1.6

Hz, 1H);  $^{13}\text{C}$  NMR (125 MHz,  $\text{DMSO-}d_6$ ):  $\delta$  14.00, 14.89, 26.07, 41.49, 127.03, 130.11, 131.30, 133.57, 139.46, 150.09, 170.61; LC/MS:  $m/z$  = 285.90  $[\text{M} + \text{H}]^+$ , 326.81  $[\text{M} + \text{H} + \text{CH}_3\text{CN}]^+$ , 570.56  $[2\text{M} + \text{H}]^+$ ,  $t_{\text{R}}$  = 10.11 min, 96.9% pure (UV).

**3-Sulfamoylbenzoic acid (25)** The title compound was synthesized from 3-(chlorosulfonyl)benzoic acid and ammonium hydroxide (28-30%) according to a published procedure<sup>S5</sup> and purified by crystallization from methanol/water: 1.25 g, 62% yield.  $^1\text{H}$  NMR (300 MHz,  $\text{DMSO-}d_6$ ):  $\delta$  7.48 (s, 2H), 7.68 (t,  $J$  = 7.3 Hz, 1H), 8.07 (d,  $J$  = 7.8 Hz, 1H), 8.14 (d,  $J$  = 7.6 Hz, 1H), 8.43 (s, 1H), 13.28 (bs, 1H).

**3-(*N,N*-Dimethylsulfamoyl)benzoic acid (26)**<sup>S6</sup> A solution of dimethylamine (40% in water, 45.3 mmol) was added to a stirred suspension of 3-(chlorosulfonyl)benzoic acid (**21**, 1.00 g, 4.53 mmol) in water (15 mL). After stirring overnight the solution was acidified with 1N HCl (aq.). The solid was isolated by suction filtration, washed thoroughly with water and dried under reduced pressure to yield the title compound: 637 mg, 61% yield.  $^1\text{H}$  NMR (500 MHz,  $\text{DMSO-}d_6$ ):  $\delta$  2.76 (s, 6H), 7.70 (dt,  $J$  = 7.9, 0.6 Hz, 1H), 8.04 (ddd,  $J$  = 7.9, 1.9, 1.3 Hz, 1H), 8.35 (dt,  $J$  = 7.9, 1.4 Hz, 1H), 8.51 (t,  $J$  = 1.6 Hz, 1H).

**3-(*N,N*-Diethylsulfamoyl)benzoic acid (27)**<sup>S7</sup> The title compound was synthesized from 3-(chlorosulfonyl)benzoic acid (**21**) and diethylamine according to General Procedure A: 2.19 g, 94% yield.  $^1\text{H}$  NMR (300 MHz,  $\text{CDCl}_3$ ):  $\delta$  1.15 (t,  $J$  = 7.1 Hz, 6H), 3.29 (q,  $J$  = 7.1 Hz, 4H), 7.64 (t,  $J$  = 7.7 Hz, 1H), 8.07 (d,  $J$  = 7.5 Hz, 1H), 8.29 (d,  $J$  = 7.5 Hz, 1H), 8.53 (s, 1H), 10.44 (bs, 1H).

**3-(*N,N*-Di-*n*-propylsulfamoyl)benzoic acid (28)** The title compound was synthesized from 3-(chlorosulfonyl)benzoic acid (**21**) and di-*n*-propylamine according to General Procedure A: 2.78 g, 97% yield.  $^1\text{H}$  NMR (300 MHz,  $\text{DMSO-}d_6$ ):  $\delta$  0.79 (t,  $J$  = 6.6 Hz, 1H), 1.46 (sextet,  $J$  = 7.0 Hz, 4H), 3.04 (t,  $J$  = 6.6 Hz, 4H), 7.74 (t,  $J$  = 7.7 Hz, 1H), 8.04 (d,  $J$  = 7.6 Hz, 1H), 8.19 (d,  $J$  = 7.6 Hz, 1H), 8.24 (s, 1H), 13.51 (bs, 1H).

**3-(Pyrrolidin-1-ylsulfonyl)benzoic acid (29)** A solution of 3-(chlorosulfonyl)benzoic acid (**21**, 1.16 g, 5.26 mmol) in dichloromethane (15 mL) was added to a stirred solution of pyrrolidine (3.74 g, 52.6 mmol) in dichloromethane (10 mL) over a period of 30 minutes. After stirring overnight at room temperature 1N HCl (aq.) was added and the aqueous phase was extracted twice with dichloromethane. The combined organic layers were dried over sodium sulfate, filtered and evaporated under reduced pressure to yield the title compound: 1.10 g, 82% yield.  $^1\text{H}$  NMR (500 MHz,  $\text{DMSO-}d_6$ ):  $\delta$  1.65 (m, 4H), 3.15 (m, 4H), 7.78 (dt,  $J$  = 7.7, 0.6 Hz, 1H), 8.05 (ddd,  $J$  = 7.7, 1.9, 1.3 Hz, 1H), 8.22-8.25 (m, 2H), 13.55 (bs, 1H);  $^{13}\text{C}$  NMR (125 MHz,  $\text{DMSO-}d_6$ ):  $\delta$  24.68, 47.84, 127.60, 130.15, 131.17, 131.88, 133.40, 136.75, 166.06; LC/MS:  $m/z$  = 296.92  $[\text{M} + \text{H} + \text{CH}_3\text{CN}]^+$ ,  $t_{\text{R}}$  = 7.98 min, >95% pure (UV).

**3-(Piperidin-1-ylsulfonyl)benzoic acid (30)**<sup>S8</sup> The title compound was synthesized from 3-(chlorosulfonyl)benzoic acid (**21**) and piperidine according to General Procedure A: 2.28 g, 85% yield.  $^1\text{H}$  NMR (500 MHz,  $\text{DMSO-}d_6$ ):  $\delta$  1.35 (m, 2H), 1.53 (m, 4H), 2.90 (m, 4H), 7.79 (t,  $J$  = 1.6 Hz, 1H),

7.97 (ddd,  $J = 7.6, 2.8, 1.6$  Hz, 1H), 8.18 (t,  $J = 1.6$  Hz, 1H), 8.23 (ddd,  $J = 7.6, 1.6, 0.9$  Hz, 1H), 13.54 (bs, 1H);  $^{13}\text{C}$  NMR (125 MHz, DMSO- $d_6$ ):  $\delta$  22.69, 24.63, 46.50, 127.68, 130.08, 131.39, 131.89, 133.46, 136.16; LC/MS:  $m/z = 270.09$   $[\text{M} + \text{H}]^+$ , 310.57  $[\text{M} + \text{H} + \text{CH}_3\text{CN}]^+$ , 538.43  $[2\text{M} + \text{H}]^+$ ,  $t_{\text{R}} = 9.10$  min, 97.3% pure (UV).

**3-(Azepan-1-ylsulfonyl)benzoic acid (31)** The title compound was synthesized from 3-(chlorosulfonyl)benzoic acid (**21**) and hexamethyleneimine according to General Procedure A: 2.55 g, 90% yield.  $^1\text{H}$  NMR (300 MHz, DMSO- $d_6$ ):  $\delta$  1.48 (m, 4H), 1.61 (m, 4H), 3.21 (m, 4H), 7.74 (t,  $J = 7.6$  Hz, 1H), 8.02 (d,  $J = 8.0$  Hz, 1H), 8.19 (d,  $J = 7.7$  Hz, 1H), 8.22 (s, 1H), 13.54 (bs, 1H).

**3-(Morpholin sulfonyl)benzoic acid (32)**<sup>S6</sup> The title compound was synthesized from 3-(chlorosulfonyl)benzoic acid (**7**) and morpholine according to General Procedure A: 2.15 g, 79% yield.  $^1\text{H}$  NMR (300 MHz, DMSO- $d_6$ ):  $\delta$  2.89 (m, 4H), 3.63 (m, 4H), 7.82 (dt,  $J = 7.9, 0.6$  Hz, 1H), 7.98 (ddd,  $J = 7.9, 1.9, 0.9$  Hz, 1H), 8.18 (dt,  $J = 1.6, 0.6$  Hz, 1H), 8.27 (ddd,  $J = 7.9, 1.6, 0.9$  Hz, 1H), 13.57 (bs, 1H); LC/MS:  $m/z = 312.91$   $[\text{M} + \text{H} + \text{CH}_3\text{CN}]^+$ , 542.44  $[2\text{M} + \text{H}]^+$ ,  $t_{\text{R}} = 7.22$  min, >99.9% pure (UV).

**3-(*N*-Benzyl-*N*-ethylsulfamoyl)benzoic acid (33)** The title compound was synthesized from 3-(chlorosulfonyl)benzoic acid (**21**) and *N*-ethylbenzylamine according to General Procedure A, followed by crystallization from toluene: 1.38 g, 43% yield.  $^1\text{H}$  NMR (500 MHz, DMSO- $d_6$ ):  $\delta$  0.84 (t,  $J = 7.1$  Hz, 3H), 3.15 (q,  $J = 7.1$  Hz, 2H), 4.36 (s, 2H), 7.26-7.36 (m, 5H), 7.77 (t,  $J = 7.7$  Hz, 1H), 8.11 (ddd,  $J = 7.9, 1.9, 1.3$  Hz, 1H), 8.23 (dt,  $J = 7.9, 1.3$  Hz, 1H), 8.30 (t,  $J = 1.7$  Hz, 1H), 13.54 (bs, 1H);  $^{13}\text{C}$  NMR (125 MHz, DMSO- $d_6$ ):  $\delta$  13.35, 42.57, 50.52, 127.15, 127.53, 127.94, 128.43, 130.23, 130.81, 131.97, 133.25, 136.80, 140.26; LC/MS:  $m/z = 319.71$   $[\text{M} + \text{H}]^+$ , 360.69  $[\text{M} + \text{H} + \text{CH}_3\text{CN}]^+$ , 638.46  $[2\text{M} + \text{H}]^+$ ,  $t_{\text{R}} = 10.68$  min, 96.7% pure (UV).

### *Syntheses of 3-sulfamoylbenzoyl chlorides 22a-33a*

**4-Bromo-3-(*N,N*-diethylsulfamoyl)benzoyl chloride (22a)** The title compound was synthesized from 4-bromo-3-(*N,N*-diethylsulfamoyl)benzoic acid (**22**, 1.20 g, 3.57 mmol) according to General Procedure B. The product was analyzed as the corresponding methyl ester; LC/MS:  $m/z = 349.50$  and 351.54  $[\text{M} + \text{H}]^+$ ,  $t_{\text{R}} = 11.68$  min.

**3-(*N,N*-Diethylsulfamoyl)-4-methylbenzoyl chloride (23a)** The title compound was synthesized from 3-(*N,N*-diethylsulfamoyl)-4-methylbenzoic acid (**23**, 2.04 g, 7.52 mmol) according to General Procedure B. The product was analyzed as the corresponding methyl ester; LC/MS:  $m/z = 285.85$   $[\text{M} + \text{H}]^+$ , 326.84  $[\text{M} + \text{H} + \text{CH}_3\text{CN}]^+$ , 570.49  $[2\text{M} + \text{H}]^+$ ,  $t_{\text{R}} = 11.28$  min.

**3-(*N,N*-Diethylsulfamoyl)-4-ethylbenzoyl chloride (24a)** The title compound was synthesized from 3-(*N,N*-diethylsulfamoyl)-4-ethylbenzoic acid (**24**, 1.11 g, 3.92 mmol) according to General Procedure B. The product was analyzed as the corresponding methyl ester; LC/MS:  $m/z = 300.02$   $[\text{M} + \text{H}]^+$ , 341.05  $[\text{M} + \text{H} + \text{CH}_3\text{CN}]^+$ ,  $t_{\text{R}} = 12.61$  min.

**3-Sulfamoylbenzoyl chloride (25a)**<sup>S9</sup> 3-Sulfamoylbenzoic acid (**25**, 1.25 g, 6.21 mmol) was dissolved in thionyl chloride (10 mL), followed by the addition of 2 drops of DMF. The solution was heated to reflux overnight. After cooling to room temperature *n*-hexane was added and the white solid was isolated by suction filtration, washed with *n*-hexane and dried under reduced pressure at 50 °C. <sup>1</sup>H NMR and LC-MS showed the title compound together with a small amount of 3-(*N*-((dimethylamino)methylene)sulfamoyl)benzoyl chloride. The product was used without further purification. <sup>1</sup>H NMR (300 MHz, DMSO-*d*<sub>6</sub>): δ 7.65 (t, *J* = 8.0 Hz, 1H), 7.95 (d, *J* = 7.6 Hz, 1H), 8.07 (d, *J* = 7.6 Hz, 1H), 8.24 (s, 1H), 10.02 (bs, 1H). The product was analyzed as the corresponding methyl ester; LC/MS: *m/z* = 256.91 [M + H + CH<sub>3</sub>CN]<sup>+</sup>, 430.75 [2M + H]<sup>+</sup>, *t*<sub>R</sub> = 6.59 min.

**3-(*N,N*-Dimethylsulfamoyl)benzoyl chloride (26a)** Thionyl chloride (915 mg, 7.69 mmol) was added slowly to a stirred suspension of 3-(*N,N*-dimethylsulfamoyl)benzoic acid (**26**, 630 mg, 2.75 mmol) in toluene (6 mL), followed by 1 drop of DMF. The reaction mixture was heated at 80 °C for 4 h. After stirring overnight at room temperature the solution was evaporated under reduced pressure. The residue was redissolved in dichloromethane (6 mL). Thionyl chloride (3.27 g, 27.5 mmol) and 1 drop of DMF were added. After stirring overnight at room temperature the solution was evaporated under reduced pressure to yield the title compound. The product was analyzed as the corresponding methyl ester; LC/MS: *m/z* = 243.94 [M + H]<sup>+</sup>, 284.98 [M + H + CH<sub>3</sub>CN]<sup>+</sup>, *t*<sub>R</sub> = 9.46 min.

**3-(*N,N*-Diethylsulfamoyl)benzoyl chloride (27a)** The title compound was synthesized from 3-(*N,N*-diethylsulfamoyl)benzoic acid (**27**, 2.19 g, 8.51 mmol) according to General Procedure B. The product was analyzed as the corresponding methyl ester; LC/MS: *m/z* = 272.04 [M + H]<sup>+</sup>, 313.04 [M + H + CH<sub>3</sub>CN]<sup>+</sup>, 542.98 [2M + H]<sup>+</sup>, *t*<sub>R</sub> = 11.48 min.

**3-(*N,N*-Di-*n*-propylsulfamoyl)benzoyl chloride (28a)** The title compound was synthesized from 3-(*N,N*-di-*n*-propylsulfamoyl)benzoic acid (**28**, 1.14 g, 4.00 mmol) according to General Procedure B. The product was analyzed as the corresponding methyl ester; LC/MS: *m/z* = 300.11 [M + H]<sup>+</sup>, 340.78 [M + H + CH<sub>3</sub>CN]<sup>+</sup>, 598.79 [2M + H]<sup>+</sup>, *t*<sub>R</sub> = 12.97 min.

**3-(Pyrrolidin-1-ylsulfonyl)benzoyl chloride (29a)** Thionyl chloride (1.43 g, 12.1 mmol) was added slowly to a stirred suspension of 3-(pyrrolidin-1-ylsulfonyl)benzoic acid (**29**, 1.10 g, 4.31 mmol) in toluene (9 mL), followed by 1 drop of DMF. The reaction mixture was heated at 80 °C for 4 h. After stirring overnight at room temperature the solution was evaporated under reduced pressure to yield the title compound. The product was analyzed as the corresponding methyl ester; LC/MS: *m/z* = 269.95 [M + H]<sup>+</sup>, 311.00 [M + H + CH<sub>3</sub>CN]<sup>+</sup>, 538.79 [2M + H]<sup>+</sup>, *t*<sub>R</sub> = 10.25 min.

**3-(Piperidin-1-ylsulfonyl)benzoyl chloride (30a)** Thionyl chloride (2.81 g, 23.6 mmol) was added slowly to a stirred suspension of 3-(piperidin-1-ylsulfonyl)benzoic acid (**30**, 2.15 g, 8.42 mmol) in toluene (17 mL), followed by 1 drop of DMF. The reaction mixture was heated at 80 °C for 4 h. After stirring overnight at room temperature the solution was evaporated under reduced pressure. The residue was redissolved in dichloromethane (20 mL). Thionyl chloride (10.0 g, 84.2 mmol) and 1 drop of DMF were added. After stirring overnight at room temperature the solution was evaporated under

reduced pressure to yield the title compound. The product was analyzed as the corresponding methyl ester; LC/MS:  $m/z = 283.81 [M + H]^+$ ,  $324.88 [M + H + CH_3CN]^+$ ,  $566.47 [2M + H]^+$ ,  $t_R = 11.01$  min.

**3-(Azepan-1-ylsulfonyl)benzoyl chloride (31a)** The title compound was synthesized from 3-(azepan-1-ylsulfonyl)benzoic acid (**31**, 1.13 g, 4.00 mmol) according to General Procedure B. The product was analyzed as the corresponding methyl ester; LC/MS:  $m/z = 297.86 [M + H]^+$ ,  $338.84 [M + H + CH_3CN]^+$ ,  $t_R = 12.28$  min.

**3-(Morpholinosulfonyl)benzoyl chloride (32a)**<sup>S10</sup> Thionyl chloride (2.80 g, 23.5 mmol) was added slowly to a stirred suspension of 3-(morpholinosulfonyl)benzoic acid (**32**, 2.28 g, 8.40 mmol) in toluene (17 mL), followed by 1 drop of DMF. The reaction mixture was heated at 80 °C for 4 h. After stirring overnight at room temperature the solution was evaporated under reduced pressure. The residue was redissolved in dichloromethane (20 mL). Thionyl chloride (9.99 g, 84.0 mmol) and 1 drop of DMF were added. After stirring overnight at room temperature the solution was evaporated under reduced pressure to yield the title compound. The product was analyzed as the corresponding methyl ester; LC/MS:  $m/z = 285.80 [M + H]^+$ ,  $326.79 [M + H + CH_3CN]^+$ ,  $570.31 [2M + H]^+$ ,  $t_R = 8.84$  min.

**3-(N-Benzyl-N-ethylsulfamoyl)benzoyl chloride (33a)** The title compound was synthesized from 3-(N-benzyl-N-ethylsulfamoyl)benzoic acid (**33**, 1.35 g, 4.23 mmol) according to General Procedure B. The product was analyzed as the corresponding methyl ester; LC/MS:  $m/z = 334.01 [M + H]^+$ ,  $t_R = 12.85$  min.

#### *Syntheses of methyl esters 2a, 4a, 9a-10a, 13a-14a, 35a-52a, 57a-64a*

**Methyl 2-(3-(N,N-diethylsulfamoyl)benzamido)benzoate (2a)** The title compound was synthesized from methyl anthranilate (236 mg, 1.56 mmol) and 3-(N,N-diethylsulfamoyl)benzoyl chloride (**27a**, 430 mg, 1.56 mmol) in pyridine (5 mL) according to General Procedure C1: 526 mg, 86% yield. <sup>1</sup>H NMR (500 MHz, CDCl<sub>3</sub>):  $\delta$  1.17 (t,  $J = 7.1$  Hz, 6H), 3.32 (q,  $J = 7.1$  Hz, 4H), 3.96 (s, 3H), 7.15 (ddd,  $J = 7.9, 7.3, 1.3$  Hz, 1H), 7.62 (ddd,  $J = 8.5, 7.3, 1.6$  Hz, 1H), 7.67 (t,  $J = 8.0$  Hz, 1H), 8.02 (ddd,  $J = 7.9, 1.9, 1.3$  Hz, 1H), 8.10 (dd,  $J = 7.9, 1.6$  Hz, 1H), 8.21 (ddd,  $J = 7.9, 1.9, 1.3$  Hz, 1H), 8.47 (t,  $J = 1.9$  Hz, 1H), 8.89 (dd,  $J = 8.5, 0.9$  Hz, 1H), 12.20 (bs, 1H); <sup>13</sup>C NMR (125 MHz, CDCl<sub>3</sub>):  $\delta$  14.23, 42.28, 52.51, 115.25, 120.36, 123.07, 125.91, 129.65, 130.08, 130.76, 131.01, 134.93, 136.08, 141.42, 141.49, 163.95, 169.10; LC/MS:  $m/z = 390.79 [M + H]^+$ ,  $431.79 [M + H + CH_3CN]^+$ ,  $780.76 [2M + H]^+$ ,  $t_R = 14.16$  min.

**Methyl 3-(3-(N,N-diethylsulfamoyl)benzamido)benzoate (4a)** The title compound was synthesized from methyl 3-aminobenzoate (151 mg, 1.00 mmol) and 3-(N,N-diethylsulfamoyl)benzoyl chloride (**27a**, 414 mg, 1.50 mmol) in acetonitrile (1 mL) according to General Procedure C2. After workup the product was filtered over a short pad of silica gel (ethyl acetate/*n*-hexane 1/1). The solvent was evaporated under reduced pressure and the residue was crystallized from MeOH: 113 mg, 29% yield. <sup>1</sup>H NMR (500 MHz, CDCl<sub>3</sub>):  $\delta$  1.09 (t,  $J = 7.1$  Hz, 6H), 3.23 (q,  $J = 7.1$  Hz, 4H), 3.88 (s, 3H), 7.44 (t,  $J = 8.0$  Hz, 1H), 7.60 (t,  $J = 7.9$  Hz, 1H), 7.82 (d,  $J = 7.6$  Hz, 1H), 7.92 (d,  $J = 7.9$  Hz, 1H), 8.00 (d,  $J$

= 7.6 Hz, 1H), 8.09 (d,  $J = 7.9$  Hz, 1H), 8.22 (s, 1H), 8.26 (s, 1H), 8.36 (bs, 1H);  $^{13}\text{C}$  NMR (125 MHz,  $\text{CDCl}_3$ ):  $\delta$  14.13, 42.18, 52.27, 121.45, 124.94, 125.27, 125.96, 129.24, 129.79, 129.94, 131.02, 131.35, 137.83, 141.18, 164.41, 166.60; LC/MS:  $m/z = 358.86$   $[\text{M} - \text{OMe}]^+$ , 390.81  $[\text{M} + \text{H} + \text{CH}_3\text{CN}]^+$ , 780.97  $[2\text{M} + \text{H}]^+$ ,  $t_{\text{R}} = 11.99$  min.

**Methyl 2-(4-(*N,N*-diethylsulfamoyl)benzamido)benzoate (9a)** The title compound was synthesized from methyl anthranilate (151 mg, 1.00 mmol) and 4-(*N,N*-diethylsulfamoyl)benzoyl chloride (414 mg, 1.50 mmol) in acetonitrile (4 mL) according to General Procedure C2. After stirring overnight and workup the product was heated with MeOH (2mL). After cooling to room temperature, the solids were isolated by filtration, washed with cold MeOH and dried under reduced pressure: 284 mg, 73% yield.  $^1\text{H}$  NMR (500 MHz,  $\text{CDCl}_3$ ):  $\delta$  1.13 (t,  $J = 7.1$  Hz, 6H), 3.26 (q,  $J = 7.1$  Hz, 4H), 3.96 (s, 3H), 7.15 (ddd,  $J = 8.2, 7.6, 1.3$  Hz, 1H), 7.61 (ddd,  $J = 8.8, 7.6, 1.6$  Hz, 1H), 7.94 (AB-system,  $J = 8.5$  Hz, 2H), 8.09 (dd,  $J = 8.2, 1.9$  Hz, 1H), 8.14 (AB-system,  $J = 8.5$  Hz, 2H), 8.88 (dd,  $J = 8.5, 0.9$  Hz, 1H), 12.16 (bs, 1H);  $^{13}\text{C}$  NMR (125 MHz,  $\text{CDCl}_3$ ):  $\delta$  14.43, 42.38, 52.87, 115.53, 120.71, 123.40, 127.68, 128.36, 131.29, 135.23, 138.51, 141.67, 143.78, 164.33, 169.45; LC/MS:  $m/z = 390.97$   $[\text{M} + \text{H}]^+$ ,  $t_{\text{R}} = 13.72$  min.

**Methyl 5-bromo-2-(4-(*N,N*-diethylsulfamoyl)benzamido)benzoate (10a)**<sup>S11</sup> The title compound was synthesized from methyl 2-amino-5-bromobenzoate (230 mg, 1.00 mmol) and 4-(*N,N*-diethylsulfamoyl)benzoyl chloride (414 mg, 1.50 mmol) in acetonitrile (3 mL) according to General Procedure C2. After stirring overnight and workup the product was heated with MeOH (2mL). After cooling to room temperature, the solids were isolated by filtration, washed with cold MeOH and dried under reduced pressure: 359 mg, 76% yield.  $^1\text{H}$  NMR (500 MHz,  $\text{CDCl}_3$ ):  $\delta$  1.13 (t,  $J = 7.1$  Hz, 6H), 3.26 (q,  $J = 7.1$  Hz, 4H), 3.97 (s, 3H), 7.70 (dd,  $J = 8.8, 2.5$  Hz, 1H), 7.94 (AB-system,  $J = 8.8$  Hz, 2H), 8.12 (AB-system,  $J = 8.5$  Hz, 2H), 8.21 (d,  $J = 2.5$  Hz, 1H), 8.82 (d,  $J = 8.8$  Hz, 1H), 12.07 (bs, 1H);  $^{13}\text{C}$  NMR (125 MHz,  $\text{CDCl}_3$ ):  $\delta$  14.16, 42.12, 52.93, 115.60, 116.80, 122.11, 127.48, 128.10, 133.60, 137.68, 137.84, 140.43, 143.77, 164.04, 168.06; LC/MS:  $m/z = 470.88$  and 471.86  $[\text{M} + \text{H}]^+$ ,  $t_{\text{R}} = 15.11$  min.

**Methyl 2-(3-(diethylcarbamoyl)benzamido)benzoate (13a)** The title compound was synthesized from methyl anthranilate (151 mg, 1.00 mmol) and 3-(diethylcarbamoyl)benzoyl chloride (360 mg, 1.50 mmol) in acetonitrile (3 mL) according to General Procedure C2. After stirring for 2 days and workup the product was crystallized from MeOH. After cooling to room temperature, the solids were isolated by filtration, washed with cold MeOH and dried under reduced pressure: 185 mg, 52% yield.  $^1\text{H}$  NMR (500 MHz,  $\text{CDCl}_3$ ):  $\delta$  1.14 (bs, 3H), 1.25 (bs, 3H), 3.27 (bs, 2H), 3.56 (bs, 2H), 3.94 (s, 3H), 7.12 (ddd,  $J = 7.9, 7.3, 1.3$  Hz, 1H), 7.54-7.61 (m, 3H), 8.03-8.08 (m, 3H), 8.89 (dd,  $J = 8.5, 0.9$  Hz, 1H), 12.07 (bs, 1H);  $^{13}\text{C}$  NMR (125 MHz,  $\text{CDCl}_3$ ):  $\delta$  12.85, 14.17, 39.33, 43.37, 52.49, 115.25, 120.49, 122.81, 125.63, 127.61, 129.13, 130.04, 130.95, 134.83, 135.02, 137.96, 141.64, 164.90, 169.01, 170.26; LC/MS:  $m/z = 355.40$   $[\text{M} + \text{H}]^+$ , 709.07  $[2\text{M} + \text{H}]^+$ ,  $t_{\text{R}} = 12.34$  min.

**Methyl 5-bromo-2-(3-(diethylcarbamoyl)benzamido)benzoate (14a)** The title compound was synthesized from methyl 2-amino-5-bromobenzoate (230 mg, 1.00 mmol) and 3-(diethylcarbamoyl)benzoyl chloride (360 mg, 1.50 mmol) in acetonitrile (3 mL) according to General Procedure C2. After stirring overnight and workup the product was heated with MeOH (2mL). After cooling to room temperature, the solids were isolated by filtration, washed with cold MeOH and dried under reduced pressure: 360 mg, 83% yield.  $^1\text{H}$  NMR (500 MHz,  $\text{CDCl}_3$ ):  $\delta$  1.13 (bs, 3H), 1.25 (bs, 3H), 3.27 (bs, 2H), 3.56 (bs, 2H), 3.95 (s, 3H), 7.55 (dt,  $J = 7.6, 0.6$  Hz, 1H), 7.58 (dt,  $J = 7.6, 1.6$  Hz, 1H), 7.68 (dd,  $J = 9.1, 2.5$  Hz, 1H), 8.00-8.03 (m, 2H), 8.19 (d,  $J = 2.5$  Hz, 1H), 8.82 (d,  $J = 9.1$  Hz, 1H), 11.99 (bs, 1H);  $^{13}\text{C}$  NMR (125 MHz,  $\text{CDCl}_3$ ):  $\delta$  13.14, 14.44, 39.61, 43.68, 53.07, 115.48, 117.03, 122.41, 125.89, 127.85, 129.43, 130.48, 133.76, 134.93, 137.80, 138.29, 140.93, 165.12, 168.13, 170.41; LC/MS:  $m/z = 432.90$  and  $434.39$  [ $\text{M} + \text{H}$ ] $^+$ ,  $t_{\text{R}} = 14.05$  min.

**Methyl 2-(3-(*N,N*-diethylsulfamoyl)-4-methylbenzamido)benzoate (35a)** The title compound was synthesized from methyl anthranilate (151 mg, 1.00 mmol) and 3-(*N,N*-diethylsulfamoyl)-4-methylbenzoyl chloride (**23a**, 290 mg, 1.00 mmol) in pyridine (4 mL) according to General Procedure C1: 220 mg, 54% yield.  $^1\text{H}$  NMR (500 MHz,  $\text{CDCl}_3$ ):  $\delta$  1.21 (t,  $J = 7.1$  Hz, 6H), 2.71 (s, 3H), 3.43 (q,  $J = 7.1$  Hz, 4H), 3.97 (s, 3H), 7.14 (ddd,  $J = 7.9, 7.3, 0.9$  Hz, 1H), 7.47 (d,  $J = 8.2$  Hz, 1H), 7.61 (m, 1H), 8.08 (dd,  $J = 7.9, 2.2$  Hz, 1H), 8.09 (dd,  $J = 7.9, 1.3$  Hz, 1H), 8.46 (d,  $J = 1.9$  Hz, 1H), 8.89 (dd,  $J = 8.5, 0.9$  Hz, 1H), 12.13 (bs, 1H);  $^{13}\text{C}$  NMR (125 MHz,  $\text{CDCl}_3$ ):  $\delta$  14.19, 20.51, 41.69, 52.52, 115.21, 120.40, 122.91, 127.36, 130.56, 130.99, 132.85, 133.34, 134.88, 139.87, 141.53, 141.82, 164.08, 169.07; LC/MS:  $m/z = 404.57$  [ $\text{M} + \text{H}$ ] $^+$ ,  $445.72$  [ $\text{M} + \text{H} + \text{CH}_3\text{CN}$ ] $^+$ ,  $808.44$  [ $2\text{M} + \text{H}$ ] $^+$ ,  $t_{\text{R}} = 13.75$  min.

**Methyl 2-(3-(*N,N*-diethylsulfamoyl)-4-ethylbenzamido)benzoate (36a)** The title compound was synthesized from methyl anthranilate (151 mg, 1.00 mmol) and 3-(*N,N*-diethylsulfamoyl)-4-ethylbenzoyl chloride (**24a**, 304 mg, 1.00 mmol) in pyridine (4 mL) according to General Procedure C1: 117 mg, 28% yield.  $^1\text{H}$  NMR (500 MHz,  $\text{CDCl}_3$ ):  $\delta$  1.21 (t,  $J = 7.1$  Hz, 6 Hz), 1.32 (t,  $J = 7.4$  Hz, 3H), 3.12 (q,  $J = 7.4$  Hz, 2H), 3.43 (q,  $J = 7.1$  Hz, 4H), 3.95 (s, 3H), 7.13 (ddd,  $J = 7.9, 7.3, 1.3$  Hz, 1H), 7.53 (d,  $J = 7.9$  Hz, 1H), 7.60 (ddd,  $J = 8.5, 7.3, 1.6$  Hz, 1H), 8.08 (dd,  $J = 8.5, 1.7$  Hz, 1H), 8.11 (dd,  $J = 7.9, 1.9$  Hz, 1H), 8.39 (d,  $J = 1.9$  Hz, 1H), 8.88 (dd,  $J = 8.5, 0.9$  Hz, 1H), 12.11 (bs, 1H);  $^{13}\text{C}$  NMR (125 MHz,  $\text{CDCl}_3$ ):  $\delta$  14.41, 15.01, 25.98, 42.03, 52.52, 115.21, 120.42, 122.92, 127.02, 130.58, 131.01, 131.59, 132.55, 134.90, 139.68, 141.56, 147.90, 164.13, 169.11; LC/MS:  $m/z = 418.70$  [ $\text{M} + \text{H}$ ] $^+$ ,  $459.72$  [ $\text{M} + \text{H} + \text{CH}_3\text{CN}$ ] $^+$ ,  $836.60$  [ $2\text{M} + \text{H}$ ] $^+$ ,  $t_{\text{R}} = 14.40$  min.

**Methyl 4-chloro-2-(3-(*N,N*-diethylsulfamoyl)benzamido)benzoate (37a)** The title compound was synthesized from methyl 2-amino-4-chlorobenzoate (289 mg, 1.56 mmol) and 3-(*N,N*-diethylsulfamoyl)benzoyl chloride (**27a**, 430 mg, 1.56 mmol) in pyridine (5 mL) according to General Procedure C1: 340 mg, 51% yield. The material was used as such for the next step (hydrolysis of methyl ester).



**Methyl 2-(3-(*N,N*-diethylsulfamoyl)benzamido)-4-fluorobenzoate (38a)** The title compound was synthesized from methyl 2-amino-4-fluorobenzoate (169 mg, 1.00 mmol) and 3-(*N,N*-diethylsulfamoyl)benzoyl chloride (**27a**, 303 mg, 1.10 mmol) in pyridine (4 mL) according to General Procedure C1. Purification by flash column chromatography (silica gel, EtOAc/*n*-hexane 20/80 followed by 30/70): 526 mg, 86% yield.  $^1\text{H}$  NMR (500 MHz,  $\text{CDCl}_3$ ):  $\delta$  1.15 (t,  $J = 7.1$  Hz, 6H), 3.30 (q,  $J = 7.1$  Hz, 4H), 3.94 (s, 3H), 6.82 (ddd,  $J = 10.1, 7.3, 2.5$  Hz, 1H), 7.66 (t,  $J = 8.0$  Hz, 1H), 8.01 (ddd,  $J = 7.9, 1.9, 1.3$  Hz, 1H), 8.10 (dd,  $J = 8.8, 6.3$  Hz, 1H), 8.18 (ddd,  $J = 7.9, 1.9, 1.3$  Hz, 1H), 8.44 (dt,  $J = 1.9, 0.6$  Hz, 1H), 8.69 (dd,  $J = 12.0, 2.8$  Hz, 1H), 12.32 (bs, 1H);  $^{13}\text{C}$  NMR (125 MHz,  $\text{CDCl}_3$ ):  $\delta$  14.24, 42.29, 52.60, 107.63 (d,  $J_{\text{CF}} = 28$  Hz), 110.42 (d,  $J_{\text{CF}} = 22$  Hz), 111.43 (d,  $J_{\text{CF}} = 3$  Hz), 129.75, 130.33, 130.75, 133.34 (d,  $J_{\text{CF}} = 11$  Hz), 135.62, 141.60, 143.63 (d,  $J_{\text{CF}} = 13$  Hz), 164.10, 166.40 (d,  $J_{\text{CF}} = 255$  Hz), 168.47; LC/MS:  $m/z = 408.78$  [ $\text{M} + \text{H}$ ] $^+$ , 449.77 [ $\text{M} + \text{H} + \text{CH}_3\text{CN}$ ] $^+$ , 816.64 [ $2\text{M} + \text{H}$ ] $^+$ ,  $t_{\text{R}} = 14.42$  min.

**Methyl 2-(3-(*N,N*-diethylsulfamoyl)benzamido)-4-nitrobenzoate (39a)** The title compound was synthesized from methyl 2-amino-4-nitrobenzoate (110 mg, 0.56 mmol) and 3-(*N,N*-diethylsulfamoyl)benzoyl chloride (**27a**, 232 mg, 0.84 mmol) in acetonitrile (2 mL) according to General Procedure C2. After stirring overnight at room temperature, workup was performed as described. The isolated product was heated with MeOH (6 mL), cooled to room temperature, filtered and the solids were dried under reduced pressure: 157 mg, 64% yield.  $^1\text{H}$  NMR (500 MHz,  $\text{CDCl}_3$ ):  $\delta$  1.15 (t,  $J = 7.1$  Hz, 6H), 3.30 (q,  $J = 7.1$  Hz, 4H), 4.02 (s, 3H), 7.68 (t,  $J = 7.9$  Hz, 1H), 7.93 (dd,  $J = 8.8, 2.2$  Hz, 1H), 8.03 (ddd,  $J = 7.9, 1.9, 1.3$  Hz, 1H), 8.25 (d,  $J = 8.5$  Hz, 1H), 8.44 (t,  $J = 1.6$  Hz, 1H), 9.76 (d,  $J = 2.5$  Hz, 1H), 12.22 (bs, 1H);  $^{13}\text{C}$  NMR (125 MHz,  $\text{CDCl}_3$ ):  $\delta$  14.22, 42.27, 53.34, 115.32, 117.12, 119.48, 125.92, 129.88, 130.61, 130.78, 132.19, 135.08, 141.76, 142.31, 151.38, 164.11, 167.73; LC/MS:  $m/z = 435.85$  [ $\text{M} + \text{H}$ ] $^+$ , 476.76 [ $\text{M} + \text{H} + \text{CH}_3\text{CN}$ ] $^+$ , 870.51 [ $2\text{M} + \text{H}$ ] $^+$ ,  $t_{\text{R}} = 13.80$  min.

**Methyl 2-(3-(*N,N*-diethylsulfamoyl)benzamido)-5-methylbenzoate (40a)** The title compound was synthesized from methyl 2-amino-5-methylbenzoate (165 mg, 1.00 mmol) and 3-(*N,N*-diethylsulfamoyl)benzoyl chloride (**27a**, 414 mg, 1.50 mmol) in acetonitrile (1 mL) according to General Procedure C2. After stirring overnight at room temperature, workup was performed as described. The isolated product was heated with MeOH (3 mL), cooled to room temperature, filtered and the solids were dried under reduced pressure: 360 mg, 89% yield.  $^1\text{H}$  NMR (500 MHz,  $\text{CDCl}_3$ ):  $\delta$  1.15 (t,  $J = 7.1$  Hz, 6H), 2.35 (s, 3H), 3.30 (q,  $J = 7.1$  Hz, 4H), 3.94 (s, 3H), 7.41 (dd,  $J = 8.5, 2.2$  Hz, 1H), 7.64 (t,  $J = 8.0$  Hz, 1H), 7.88 (m, 1H), 7.99 (ddd,  $J = 7.9, 1.9, 1.3$  Hz, 1H), 8.18 (ddd,  $J = 7.9, 1.9, 1.3$  Hz, 1H), 8.44 (dt,  $J = 1.9, 0.6$  Hz, 1H), 8.76 (d,  $J = 8.5$  Hz, 1H), 12.07 (bs, 1H);  $^{13}\text{C}$  NMR (125 MHz,  $\text{CDCl}_3$ ):  $\delta$  14.25, 20.74, 42.29, 52.45, 115.12, 120.33, 125.87, 129.62, 129.99, 130.72, 131.13, 132.71, 135.64, 136.20, 139.04, 141.43, 163.76, 169.15; LC/MS:  $m/z = 372.86$  [ $\text{M} - \text{OMe}$ ] $^+$ , 445.82 [ $\text{M} + \text{H} + \text{CH}_3\text{CN}$ ] $^+$ , 808.69 [ $2\text{M} + \text{H}$ ] $^+$ ,  $t_{\text{R}} = 14.60$  min.

**Methyl 2-(3-(*N,N*-diethylsulfamoyl)benzamido)-5-(trifluoromethyl)benzoate (41a)** The title compound was synthesized from methyl 2-amino-5-trifluoromethylbenzoate<sup>S12</sup> (219 mg, 1.00 mmol) and 3-(*N,N*-diethylsulfamoyl)benzoyl chloride (**27a**, 414 mg, 1.50 mmol) in acetonitrile (1 mL) according to General Procedure C2. After stirring for 2.5 h at room temperature, workup was performed as described. The isolated product was heated with MeOH (2 mL), cooled to room temperature, filtered and the solids were dried under reduced pressure: 296 mg, 65% yield. <sup>1</sup>H NMR (500 MHz, CDCl<sub>3</sub>): δ 1.17 (q, *J* = 7.1 Hz, 6H), 3.32 (q, *J* = 7.1 Hz, 4H), 4.02 (s, 3H), 7.79 (t, *J* = 7.9 Hz, 1H), 7.85 (dd, *J* = 8.8, 2.2 Hz, 1H), 8.04 (ddd, *J* = 7.9, 1.9, 1.3 Hz, 1H), 8.21 (ddd, *J* = 7.9, 1.9, 0.9 Hz, 1H), 8.37 (dd, *J* = 1.6, 0.6 Hz, 1H), 8.58 (t, *J* = 1.9 Hz, 1H), 9.06 (d, *J* = 8.8 Hz, 1H), 12.33 (bs, 1H); <sup>13</sup>C NMR (125 MHz, CDCl<sub>3</sub>): δ 14.22, 42.27, 52.98, 115.10, 120.60, 123.54 (q, *J*<sub>CF</sub> = 272 Hz), 125.00 (q, *J*<sub>CF</sub> = 33.9 Hz), 125.99, 128.35 (q, *J*<sub>CF</sub> = 3.4 Hz), 129.81, 130.48, 130.81, 131.49 (d, *J*<sub>CF</sub> = 3.7 Hz), 135.43, 141.70, 144.13, 164.20, 168.17; LC/MS: *m/z* = 458.75 [M + H]<sup>+</sup>, 499.70 [M + H + CH<sub>3</sub>CN]<sup>+</sup>, 916.64 [2M + H]<sup>+</sup>, *t*<sub>R</sub> = 14.93 min.

**Methyl 2-(3-(*N,N*-diethylsulfamoyl)benzamido)-5-fluorobenzoate (42a)** The title compound was synthesized from methyl 2-amino-5-fluorobenzoate (264 mg, 1.56 mmol) and 3-(*N,N*-diethylsulfamoyl)benzoyl chloride (**27a**, 430 mg, 1.56 mmol) in pyridine (5 mL) according to General Procedure C1. The material was used as such for the next step (hydrolysis of methyl ester).

**Methyl 5-bromo-2-(3-(*N,N*-diethylsulfamoyl)benzamido)benzoate (43a)** The title compound was synthesized from methyl 2-amino-5-bromobenzoate (362 mg, 1.57 mmol) and 3-(*N,N*-diethylsulfamoyl)benzoyl chloride (**27a**, 414 mg, 1.50 mmol) in toluene (10 mL) according to General Procedure C3. After reflux for 2 h the solvent was evaporated under reduced pressure. The isolated product was heated with MeOH (3 mL), cooled to room temperature, filtered and the solids were dried under reduced pressure: 545 mg, 77% yield. <sup>1</sup>H NMR (500 MHz, CDCl<sub>3</sub>): δ 1.15 (t, *J* = 7.1 Hz, 6H), 3.30 (q, *J* = 7.1 Hz, 4H), 3.96 (s, 3H), 7.65 (t, *J* = 8.2 Hz, 1H), 7.69 (dd, *J* = 8.8, 2.5 Hz, 1H), 8.00 (ddd, *J* = 7.9, 1.9, 0.9 Hz, 1H), 8.15 (ddd, *J* = 7.9, 1.9, 0.9 Hz, 1H), 8.20 (d, *J* = 2.5 Hz, 1H), 8.43 (t, *J* = 1.9 Hz, 1H), 8.80 (d, *J* = 8.8 Hz, 1H), 12.09 (bs, 1H); <sup>13</sup>C NMR (125 MHz, CDCl<sub>3</sub>): δ 14.23, 42.27, 52.86, 115.54, 116.77, 122.02, 125.90, 129.73, 130.27, 130.74, 133.58, 135.70, 137.65, 140.44, 141.59, 163.92, 167.98; LC/MS: *m/z* = 509.79 and 511.77 [M + H + CH<sub>3</sub>CN]<sup>+</sup>, 936.65, 938.73 and 940.72 [2M + H]<sup>+</sup>, *t*<sub>R</sub> = 15.26 min.

**Methyl 5-cyano-2-(3-(*N,N*-diethylsulfamoyl)benzamido)benzoate (44a)** The title compound was synthesized from methyl 2-amino-5-cyanobenzoate<sup>S13</sup> (176 mg, 1.00 mmol) and 3-(*N,N*-diethylsulfamoyl)benzoyl chloride (**27a**, 414 mg, 1.50 mmol) in acetonitrile (1 mL) according to General Procedure C2. After stirring for 3 h at room temperature, workup was performed as described. The isolated product was heated with MeOH (3 mL), cooled to room temperature, filtered and the solids were dried under reduced pressure: 294 mg, 71% yield. <sup>1</sup>H NMR (500 MHz, CDCl<sub>3</sub>): δ 1.15 (t, *J* = 7.1 Hz, 6H), 3.30 (q, *J* = 7.1 Hz, 4H), 4.00 (s, 3H), 7.68 (t, *J* = 7.9 Hz, 1H), 7.84 (dd, *J* = 8.8, 2.2 Hz, 1H), 8.03 (ddd, *J* = 7.9, 1.9, 1.3 Hz, 1H), 8.18 (ddd, *J* = 7.9, 1.6, 0.9 Hz, 1H), 8.40 (d, *J* = 2.2 Hz,

1H), 8.45 (t,  $J = 1.6$  Hz, 1H), 9.05 (d,  $J = 8.8$  Hz, 1H), 12.36 (bs, 1H);  $^{13}\text{C}$  NMR (125 MHz,  $\text{CDCl}_3$ ):  $\delta$  14.23, 42.26, 53.21, 106.54, 115.55, 117.83, 120.90, 126.02, 129.89, 130.67, 130.84, 135.13, 135.45, 137.78, 141.82, 144.82, 164.26, 167.63; LC/MS:  $m/z = 416.06$   $[\text{M} + \text{H}]^+$ , 456.85  $[\text{M} + \text{H} + \text{CH}_3\text{CN}]^+$ , 830.80  $[2\text{M} + \text{H}]^+$ ,  $t_{\text{R}} = 14.93$  min.

**Methyl 2-(3-(*N,N*-diethylsulfamoyl)benzamido)-5-nitrobenzoate (45a)** The title compound was synthesized from methyl 2-amino-5-nitrobenzoate (196 mg, 1.00 mmol) and 3-(*N,N*-diethylsulfamoyl)benzoyl chloride (**27a**, 276 mg, 1.00 mmol) in toluene (5 mL) according to General Procedure C3. After reflux for 1 h the solvent was evaporated under reduced pressure. The isolated product was stirred with MeOH (3 mL), filtered and the solids were dried under reduced pressure: 304 mg, 70% yield. The material was used as such for the next step (hydrolysis of methyl ester).

**Methyl 2-(4-bromo-3-(*N,N*-diethylsulfamoyl)benzamido)-5-fluorobenzoate (46a)** The title compound was synthesized from methyl 5-fluoro-2-aminobenzoate (169 mg, 1.00 mmol) and 4-bromo-3-(*N,N*-diethylsulfamoyl)benzoyl chloride (**22a**, 400 mg, 1.13 mmol) in pyridine (5 mL) according to General Procedure C1: 130 mg, 27% yield.  $^1\text{H}$  NMR (500 MHz,  $\text{DMSO}-d_6$ ):  $\delta$  1.08 (q,  $J = 7.1$  Hz, 6H), 3.38 (q,  $J = 7.1$  Hz, 4H), 7.58 (ddd,  $J = 9.1, 8.2, 3.2$  Hz, 1H), 7.70 (dd,  $J = 9.1, 3.2$  Hz, 1H), 8.03 (dd,  $J = 8.2, 2.2$  Hz, 1H), 8.11 (d,  $J = 8.2$  Hz, 1H), 8.25 (dd,  $J = 9.1, 5.4$  Hz, 1H), 8.50 (d,  $J = 2.2$  Hz, 1H), 11.28 (bs, 1H);  $^{13}\text{C}$  NMR (125 MHz,  $\text{DMSO}-d_6$ ):  $\delta$  13.78, 41.25, 52.77, 116.66 (d,  $J_{\text{CF}} = 24.7$  Hz), 120.75 (d,  $J_{\text{CF}} = 21.2$  Hz), 121.74 (d,  $J_{\text{CF}} = 7.3$  Hz), 123.56, 124.79 (d,  $J_{\text{CF}} = 8.2$  Hz), 129.84, 132.00, 133.80, 135.14 (d,  $J_{\text{CF}} = 2.7$  Hz), 136.46, 139.98, 157.83, 162.95, 166.39; LC/MS:  $m/z = 527.41$  and 529.40  $[\text{M} + \text{H} + \text{CH}_3\text{CN}]^+$ , 974.22  $[2\text{M} + \text{H}]^+$ ,  $t_{\text{R}} = 14.10$  min.

**Methyl 5-bromo-2-(4-bromo-3-(*N,N*-diethylsulfamoyl)benzamido)benzoate (47a)** The title compound was synthesized from methyl 5-bromo-2-aminobenzoate (230 mg, 1.00 mmol) and 4-bromo-3-(*N,N*-diethylsulfamoyl)benzoyl chloride (**22a**, 400 mg, 1.13 mmol) in pyridine (5 mL) according to General Procedure C1: 165 mg, 30% yield.  $^1\text{H}$  NMR (500 MHz,  $\text{DMSO}-d_6$ ):  $\delta$  1.08 (q,  $J = 7.1$  Hz, 6H), 3.38 (q,  $J = 7.1$  Hz, 4H), 3.85 (s, 3H), 7.88 (dd,  $J = 9.1, 2.5$  Hz, 1H), 8.02 (dd,  $J = 8.2, 2.2$  Hz, 1H), 8.06 (d,  $J = 2.5$  Hz, 1H), 8.12 (d,  $J = 8.2$  Hz, 1H), 8.29 (d,  $J = 8.8$  Hz, 1H), 8.50 (d,  $J = 2.2$  Hz, 1H), 11.42 (bs, 1H);  $^{13}\text{C}$  NMR (125 MHz,  $\text{DMSO}-d_6$ ):  $\delta$  13.80, 41.28, 52.85, 115.74, 121.14, 123.73, 124.00, 129.79, 131.97, 132.73, 133.68, 136.51, 136.53, 138.18, 140.03, 162.94, 166.39.

**Methyl 4-(3-(*N,N*-diethylsulfamoyl)benzamido)-[1,1'-biphenyl]-3-carboxylate (48a)** The title compound was synthesized from methyl 4-amino-[1,1'-biphenyl]-3-carboxylate<sup>S14</sup> (227 mg, 1.00 mmol) and 3-(*N,N*-diethylsulfamoyl)benzoyl chloride (**27a**, 276 mg, 1.00 mmol) in pyridine (4 mL) according to General Procedure C1. Purification by flash column chromatography (silica gel, EtOAc/*n*-hexane 90/10 followed by MeOH/DCM). The isolated product was stirred with MeOH (3 mL), filtered and the solids were dried under reduced pressure: 84 mg, 18% yield.  $^1\text{H}$  NMR (500 MHz,  $\text{CDCl}_3$ ):  $\delta$  1.16 (t,  $J = 7.1$  Hz, 6H), 3.32 (q,  $J = 7.1$  Hz, 4H), 3.99 (s, 3H), 7.36 (m, 1H), 7.45 (m, 2H), 7.60 (dd,  $J = 8.5, 1.3$  Hz, 2H), 7.67 (t,  $J = 7.7$  Hz, 1H), 7.85 (dd,  $J = 8.8, 2.5$  Hz, 1H), 8.02 (ddd,  $J = 7.9, 1.9, 0.9$  Hz, 1H), 8.21 (ddd,  $J = 7.9, 1.9, 1.3$  Hz, 1H), 8.33 (d,  $J = 2.2$  Hz, 1H), 8.48 (t,  $J = 1.6$  Hz,

1H), 12.20 (bs, 1H); <sup>13</sup>C NMR (125 MHz, CDCl<sub>3</sub>): δ 14.26, 42.30, 52.65, 115.62, 120.84, 125.93, 126.78, 127.61, 128.94, 129.37, 129.70, 130.15, 130.78, 133.35, 136.02, 136.03, 139.44, 140.52, 141.51, 163.94, 169.10; LC/MS: *m/z* = 507.54 [M + H + CH<sub>3</sub>CN]<sup>+</sup>, 932.67 [2M + H]<sup>+</sup>, *t<sub>R</sub>* = 15.18 min.

**Methyl 2-(3-(*N,N*-diethylsulfamoyl)benzamido)-6-methoxybenzoate (49a)** The title compound was synthesized from methyl 2-amino-6-methoxybenzoate hydrochloride (218 mg, 1.00 mmol) and 3-(*N,N*-diethylsulfamoyl)benzoyl chloride (**27a**, 303 mg, 1.10 mmol) in pyridine (8 mL) according to General Procedure C1. Purification by flash column chromatography (silica gel, EtOAc/*n*-hexane 30/70 followed by 40/60) yielded an oil. The crude material was used as such for the next step (hydrolysis of methyl ester). <sup>1</sup>H NMR (500 MHz, CDCl<sub>3</sub>): δ 1.14 (t, *J* = 7.1 Hz, 6H), 3.29 (q, *J* = 7.1 Hz, 1H), 3.86 (s, 3H), 3.94 (s, 3H), 6.75 (d, *J* = 8.5, 1H), 7.46 (t, *J* = 8.5 Hz, 1H), 7.63 (t, *J* = 7.9 Hz, 1H), 7.98 (ddd, *J* = 7.9, 1.9, 1.3 Hz, 1H), 8.10 (ddd, *J* = 7.9, 1.9, 1.3 Hz, 1H), 8.23 (d, *J* = 8.5 Hz, 1H), 8.36 (t, *J* = 1.7 Hz, 1H), 10.96 (bs, 1H); <sup>13</sup>C NMR (125 MHz, CDCl<sub>3</sub>): δ 14.22, 42.26, 52.63, 56.35, 107.70, 113.60, 120.04, 125.76, 129.67, 130.07, 130.70, 133.66, 135.96, 139.94, 141.46, 159.64, 163.70, 169.14; LC/MS: *m/z* = 429.50 [M – OCH<sub>3</sub> + CH<sub>3</sub>CN]<sup>+</sup>, 461.71 [M + H + CH<sub>3</sub>CN]<sup>+</sup>, 840.55 [2M + H]<sup>+</sup>, *t<sub>R</sub>* = 11.38 min. Purity: 91% by UV (254 nm).

**Methyl 2-chloro-6-(3-(*N,N*-diethylsulfamoyl)benzamido)benzoate (50a)** The title compound was synthesized from methyl 2-amino-6-chlorobenzoate (186 mg, 1.00 mmol) and 3-(*N,N*-diethylsulfamoyl)benzoyl chloride (**27a**, 414 mg, 1.50 mmol) in acetonitrile (2 mL) according to General Procedure C2. After stirring for 3 h at 0 °C, workup was performed as described, yielding an oil. Attempts to crystallize the product from MeOH failed to give a solid. Therefore the crude material was used as such for the next step (hydrolysis of methyl ester). LC/MS: *m/z* = 424.66 [M + H]<sup>+</sup>, 465.71 [M + H + CH<sub>3</sub>CN]<sup>+</sup>, 848.52 [2M + H]<sup>+</sup>, *t<sub>R</sub>* = 12.31 min. Purity: 85% by UV (254 nm).

**Methyl 2-(3-(*N,N*-diethylsulfamoyl)benzamido)-6-fluorobenzoate (51a)** The title compound was synthesized from methyl 2-amino-6-fluorobenzoate (169 mg, 1.00 mmol) and 3-(*N,N*-diethylsulfamoyl)benzoyl chloride (**27a**, 414 mg, 1.50 mmol) in acetonitrile (1 mL) according to General Procedure C2. After stirring overnight at room temperature, workup was performed as described. The isolated product was heated with MeOH (3 mL), cooled to room temperature, filtered and the solids were dried under reduced pressure: 340 mg, 83% yield. <sup>1</sup>H NMR (500 MHz, CDCl<sub>3</sub>): δ 1.15 (t, *J* = 7.1 Hz, 6H), 3.30 (q, *J* = 7.1 Hz, 4H), 3.98 (s, 3H), 6.89 (ddd, *J* = 11.0, 8.2, 0.9 Hz, 1H), 7.53 (dt, *J* = 8.5, 6.0 Hz, 1H), 7.65 (t, *J* = 7.9 Hz, 1H), 8.00 (ddd, *J* = 7.9, 1.9, 0.9 Hz, 1H), 8.15 (ddd, *J* = 7.9, 1.9, 1.3 Hz, 1H), 8.41 (t, *J* = 1.7 Hz, 1H), 8.62 (d, *J* = 8.5 Hz, 1H), 11.80 (bs, 1H); <sup>13</sup>C NMR (125 MHz, CDCl<sub>3</sub>): δ 14.06, 41.87, 112.37 (d, *J<sub>CF</sub>* = 23 Hz), 113.52 (d, *J<sub>CF</sub>* = 16 Hz), 119.22 (d, *J<sub>CF</sub>* = 4 Hz), 125.29, 129.82, 130.05, 131.32, 132.86 (d, *J<sub>CF</sub>* = 11 Hz), 135.05, 138.75 (d, *J<sub>CF</sub>* = 5 Hz), 160.46 (d, *J<sub>CF</sub>* = 252 Hz), 163.70, 165.88; LC/MS: *m/z* = 376.84 [M – OMe]<sup>+</sup>, 449.83 [M + H + CH<sub>3</sub>CN]<sup>+</sup>, 816.77 [2M + H]<sup>+</sup>, *t<sub>R</sub>* = 14.93 min.

**Methyl 2-(3-(*N,N*-diethylsulfamoyl)benzamido)-6-hydroxybenzoate (52a)** The title compound was synthesized from methyl 2-amino-6-hydroxybenzoate (94 mg, 0.56 mmol) and 3-(*N,N*-

diethylsulfamoyl)benzoyl chloride (**27a**, 171 mg, 0.62 mmol) in toluene (5 mL) according to General Procedure C3. After reflux for 1 h the solvent was evaporated under reduced pressure. The isolated product was stirred with MeOH (1 mL). The solids were filtered, washed with MeOH (1 mL) and dried under reduced pressure: 150 mg, 66% yield.  $^1\text{H NMR}$  (500 MHz,  $\text{CDCl}_3$ ):  $\delta$  1.13 (t,  $J = 7.1$  Hz, 6H), 3.27 (q,  $J = 7.1$  Hz, 4H), 4.15 (s, 3H), 6.76 (m, 1H), 7.45 (dt,  $J = 8.2, 3.2$ , 1H), 7.65 (dt,  $J = 7.9, 1.6$  Hz, 1H), 7.96 (m, 1H), 8.17 (m, 1H), 8.29 (m, 1H), 8.35 (m, 1H), 10.43 (bs, 1H), 11.13 (bs, 1H);  $^{13}\text{C NMR}$  (125 MHz,  $\text{CDCl}_3$ ):  $\delta$  14.16, 42.17, 53.47, 101.71, 111.84, 113.52, 124.81, 129.94, 131.47, 136.15, 140.28, 141.35, 162.08, 163.59, 169.57; LC/MS:  $m/z = 447.77$  [ $\text{M} + \text{H} + \text{CH}_3\text{CN}$ ] $^+$ , 813.01 [ $2\text{M} + \text{H}$ ] $^+$ ,  $t_{\text{R}} = 12.21$  min.

**Methyl 2-(3-sulfamoylbenzamido)benzoate (57a)** The title compound was synthesized from methyl anthranilate (302 mg, 2.00 mmol) and 3-sulfamoylbenzoyl chloride (**25a**, 659 mg, 3.00 mmol) in acetonitrile (2 mL) according to General Procedure C2. After stirring for 2 h at 0 °C, workup was performed as described. The isolated product was heated with MeOH (15 mL), cooled to room temperature, filtered and the solids were dried under reduced pressure: 350 mg, 52% yield. As the purity was below 95% the compound was heated for a second time with MeOH (5 mL): 220 mg, 33% yield.  $^1\text{H NMR}$  (500 MHz,  $\text{DMSO}-d_6$ ):  $\delta$  3.88 (s, 3H), 7.28 (m, 1H), 7.55 (bs, 2H), 7.70 (m, 1H), 7.83 (t,  $J = 7.7$  Hz, 1H), 8.00 (dd,  $J = 8.2, 1.6$  Hz, 1H), 8.08 (ddd,  $J = 7.9, 1.9, 1.3$  Hz, 1H), 8.16 (ddd,  $J = 7.9, 1.9, 0.9$  Hz, 1H), 8.42-8.44 (m, 2H), 11.55 (bs, 1H);  $^{13}\text{C NMR}$  (125 MHz,  $\text{DMSO}-d_6$ ):  $\delta$  52.54, 118.27, 121.47, 123.84, 124.78, 128.94, 129.70, 129.77, 130.60, 134.05, 134.97, 139.40, 144.88, 163.62, 167.72; LC/MS:  $m/z = 389.71$  [ $\text{M} + \text{H}$ ] $^+$ , 430.65 [ $\text{M} + \text{H} + \text{CH}_3\text{CN}$ ] $^+$ , 778.24 [ $2\text{M} + \text{H}$ ] $^+$ ,  $t_{\text{R}} = 9.81$  min.

**Methyl 2-(3-(*N,N*-dimethylsulfamoyl)benzamido)benzoate (58a)** The title compound was synthesized from methyl anthranilate (151 mg, 1.00 mmol) and 3-(*N,N*-dimethylsulfamoyl)benzoyl chloride (**26a**, 303 mg, 1.00 mmol) in pyridine (4 mL) according to General Procedure C1: 100 mg, 28% yield.  $^1\text{H NMR}$  (500 MHz,  $\text{CDCl}_3$ ):  $\delta$  2.77 (s, 6H), 3.95 (s, 3H), 7.15 (ddd,  $J = 7.9, 7.3, 1.3$  Hz, 1H), 7.61 (ddd,  $J = 8.8, 7.6, 1.9$  Hz, 1H), 7.70 (dt,  $J = 7.9, 0.6$  Hz, 1H), 7.96 (ddd,  $J = 7.9, 1.9, 1.3$  Hz, 1H), 8.09 (dd,  $J = 6.3, 1.6$  Hz, 1H), 8.24 (ddd,  $J = 7.9, 1.9, 1.3$  Hz, 1H), 8.43 (dt,  $J = 1.9, 0.6$  Hz, 1H), 8.88 (dd,  $J = 8.5, 0.9$  Hz, 1H), 12.21 (bs, 1H);  $^{13}\text{C NMR}$  (125 MHz,  $\text{CDCl}_3$ ):  $\delta$  38.20, 52.81, 120.63, 123.40, 126.86, 129.96, 131.00, 131.30, 131.47, 135.23, 136.46, 137.06, 141.65, 164.16, 169.39; LC/MS:  $m/z = 403.65$  [ $\text{M} + \text{H} + \text{CH}_3\text{CN}$ ] $^+$ , 724.38 [ $2\text{M} + \text{H}$ ] $^+$ ,  $t_{\text{R}} = 12.07$  min.

**Methyl 2-(3-(*N,N*-dipropylsulfamoyl)benzamido)benzoate (59a)** The title compound was synthesized from methyl anthranilate (151 mg, 1.00 mmol) and 3-(*N,N*-di-*n*-propylsulfamoyl)benzoyl chloride (**28a**, 303 mg, 1.00 mmol) in pyridine (4 mL) according to General Procedure C1. The product was crystallized from MeOH: 232 mg, 55% yield.  $^1\text{H NMR}$  (500 MHz,  $\text{CDCl}_3$ ):  $\delta$  0.87 (t,  $J = 7.4$  Hz, 6H), 1.57 (sextet,  $J = 7.5$  Hz, 4H), 3.14 (m, 4H), 3.94 (s, 3H), 7.14 (m, 1H), 7.60 (ddd,  $J = 8.8, 7.6, 1.6$  Hz, 1H), 7.65 (t,  $J = 8.0$  Hz, 1H), 7.99 (ddd,  $J = 7.9, 1.9, 0.9$  Hz, 1H), 8.08 (dd,  $J = 8.2, 1.6$  Hz, 1H), 8.20 (ddd,  $J = 7.9, 1.9, 0.9$  Hz, 1H), 8.45 (t,  $J = 1.6$  Hz, 1H), 8.88 (dd,  $J = 8.5, 1.3$  Hz, 1H),

12.18 (bs, 1H);  $^{13}\text{C}$  NMR (125 MHz,  $\text{CDCl}_3$ ):  $\delta$  11.17, 22.14, 50.22, 52.55, 115.26, 120.38, 123.07, 125.84, 129.62, 130.18, 130.82, 131.03, 134.93, 136.01, 141.27, 141.43, 163.97, 169.09; LC/MS:  $m/z$  = 418.76  $[\text{M} + \text{H}]^+$ , 459.78  $[\text{M} + \text{H} + \text{CH}_3\text{CN}]^+$ , 836.75  $[2\text{M} + \text{H}]^+$ ,  $t_{\text{R}}$  = 15.18 min.

**Methyl 2-(3-(pyrrolidin-1-ylsulfonyl)benzamido)benzoate (60a)** The title compound was synthesized from methyl anthranilate (217 mg, 1.44 mmol) and 3-(pyrrolidin-1-ylsulfonyl)benzoyl chloride (**29a**, 393 mg, 1.44 mmol) in pyridine (5 mL) according to General Procedure C1. The product was crystallized from MeOH: 108 mg, 27% yield.  $^1\text{H}$  NMR (500 MHz,  $\text{CDCl}_3$ ):  $\delta$  1.77 (m, 4H), 3.31 (m, 4H), 3.93 (s, 3H), 7.13 (m, 1H), 7.60 (ddd,  $J$  = 8.8, 7.3, 1.6 Hz, 1H), 7.68 (dt,  $J$  = 7.9, 0.6 Hz, 1H), 8.00 (ddd,  $J$  = 7.6, 1.6, 0.9 Hz, 1H), 8.07 (dd,  $J$  = 7.9, 1.6 Hz, 1H), 8.21 (ddd,  $J$  = 7.9, 1.9, 1.3 Hz, 1H), 8.46 (t,  $J$  = 1.9 Hz, 1H), 8.86 (dd,  $J$  = 8.5, 0.9 Hz, 1H), 12.18 (bs, 1H);  $^{13}\text{C}$  NMR (125 MHz,  $\text{CDCl}_3$ ):  $\delta$  25.28, 48.01, 52.52, 115.22, 120.31, 123.07, 126.29, 129.62, 130.51, 131.00, 134.91, 136.16, 138.20, 141.36, 163.96, 169.08; LC/MS:  $m/z$  = 588.59  $[\text{M} + \text{H}]^+$ , 429.71  $[\text{M} + \text{H} + \text{CH}_3\text{CN}]^+$ , 776.38  $[2\text{M} + \text{H}]^+$ ,  $t_{\text{R}}$  = 12.61 min.

**Methyl 2-(3-(piperidin-1-ylsulfonyl)benzamido)benzoate (61a)** The title compound was synthesized from methyl anthranilate (151 mg, 1.00 mmol) and 3-(piperidin-1-ylsulfonyl)benzoyl chloride (**30a**, 287 mg, 1.00 mmol) in pyridine (4 mL) according to General Procedure C1. The product was crystallized from MeOH: 100 mg, 26% yield.  $^1\text{H}$  NMR (500 MHz,  $\text{CDCl}_3$ ):  $\delta$  1.42 (m, 2H), 1.65 (quintet,  $J$  = 5.8 Hz, 4H), 3.06 (t,  $J$  = 5.5 Hz, 4H), 3.94 (s, 3H), 7.15 (m, 1H), 7.61 (ddd,  $J$  = 8.5, 7.3, 1.6 Hz, 1H), 7.68 (t,  $J$  = 8.0 Hz, 1H), 7.94 (ddd,  $J$  = 7.6, 1.6, 0.9 Hz, 1H), 8.09 (dd,  $J$  = 8.0, 1.7 Hz, 1H), 8.22 (dd,  $J$  = 7.9, 1.9, 1.3 Hz, 1H), 8.39 (dt,  $J$  = 1.9, 0.6 Hz, 1H), 8.88 (dd,  $J$  = 8.5, 0.9 Hz, 1H), 12.20 (bs, 1H);  $^{13}\text{C}$  NMR (125 MHz,  $\text{CDCl}_3$ ):  $\delta$  23.47, 25.18, 47.04, 52.54, 115.25, 120.36, 123.12, 126.53, 129.62, 130.69, 131.04, 131.12, 134.97, 136.11, 137.48, 141.42, 163.99, 169.12; LC/MS:  $m/z$  = 443.59  $[\text{M} + \text{H} + \text{CH}_3\text{CN}]^+$ , 804.43  $[2\text{M} + \text{H}]^+$ ,  $t_{\text{R}}$  = 13.56 min.

**Methyl 2-(3-(azepan-1-ylsulfonyl)benzamido)benzoate (62a)** The title compound was synthesized from methyl anthranilate (151 mg, 1.00 mmol) and 3-(azepan-1-ylsulfonyl)benzoyl chloride (**31a**, 302 mg, 1.00 mmol) in pyridine (4 mL) according to General Procedure C1. The product was crystallized from MeOH: 247 mg, 59% yield.  $^1\text{H}$  NMR (500 MHz,  $\text{CDCl}_3$ ):  $\delta$  1.59 (m, 4H), 1.73 (m, 4H), 3.34 (t,  $J$  = 6.0 Hz, 4H), 3.94 (s, 3H), 7.14 (m, 1H), 7.60 (ddd,  $J$  = 8.8, 7.6, 1.6 Hz, 1H), 7.65 (t,  $J$  = 7.7 Hz, 1H), 7.98 (ddd,  $J$  = 7.9, 1.9, 1.3 Hz, 1H), 8.08 (dd,  $J$  = 8.2, 1.6, 1H), 8.19 (ddd,  $J$  = 7.6, 1.6, 0.9 Hz, 1H), 8.43 (t,  $J$  = 1.7 Hz, 1H), 8.87 (dd,  $J$  = 8.5, 0.9 Hz, 1H), 12.18 (bs, 1H);  $^{13}\text{C}$  NMR (125 MHz,  $\text{CDCl}_3$ ):  $\delta$  26.88, 29.19, 48.41, 52.53, 115.22, 120.34, 123.07, 125.71, 129.64, 130.06, 130.75, 131.02, 134.94, 136.06, 140.62, 141.42, 164.00, 169.10; LC/MS:  $m/z$  = 416.73  $[\text{M} + \text{H}]^+$ , 457.75  $[\text{M} + \text{H} + \text{CH}_3\text{CN}]^+$ , 832.80  $[2\text{M} + \text{H}]^+$ ,  $t_{\text{R}}$  = 14.70 min.

**Methyl 2-(3-(morpholinosulfonyl)benzamido)benzoate (63a)** The title compound was synthesized from methyl anthranilate (151 mg, 1.00 mmol) and 3-(morpholinosulfonyl)benzoyl chloride (**32a**, 290 mg, 1.00 mmol) in pyridine (4 mL) according to General Procedure C1. The product was crystallized from MeOH: 146 mg, 36% yield.  $^1\text{H}$  NMR (500 MHz,  $\text{CDCl}_3$ ):  $\delta$  3.09 (m, 4H), 3.77 (m, 4H), 3.96 (s,

3H), 7.17 (m, 1H), 7.63 (m, 1H), 7.73 (t,  $J = 7.9$  Hz, 1H), 7.96 (ddd,  $J = 7.6, 1.6, 0.9$  Hz, 1H), 8.10 (dd,  $J = 7.9, 1.6$  Hz, 1H), 8.28 (ddd,  $J = 7.9, 1.9, 1.3$  Hz, 1H), 8.42 (t,  $J = 1.6$  Hz, 1H), 8.89 (dd,  $J = 8.5, 0.9$  Hz, 1H), 12.23 (bs, 1H);  $^{13}\text{C}$  NMR (125 MHz,  $\text{CDCl}_3$ ):  $\delta$  46.08, 52.54, 66.08, 115.22, 120.33, 123.18, 126.77, 129.83, 130.76, 131.05, 131.55, 134.99, 136.32, 141.35, 163.73, 169.17; LC/MS:  $m/z = 445.67$   $[\text{M} + \text{H} + \text{CH}_3\text{CN}]^+$ , 808.37  $[2\text{M} + \text{H}]^+$ ,  $t_{\text{R}} = 11.94$  min.

**Methyl 2-(3-(*N*-benzyl-*N*-ethylsulfamoyl)benzamido)benzoate (64a)** The title compound was synthesized from methyl anthranilate (151 mg, 1.00 mmol) and 3-(*N*-benzyl-*N*-ethylsulfamoyl)benzoyl chloride (**33a**, 290 mg, 1.00 mmol) in pyridine (4 mL) according to General Procedure C1. The product was crystallized from MeOH: 118 mg, 26% yield.  $^1\text{H}$  NMR (500 MHz,  $\text{CDCl}_3$ ):  $\delta$  0.94 (t,  $J = 7.3$  Hz, 3H), 3.27 (q,  $J = 7.1$  Hz, 2H), 3.91 (s, 3H), 4.44 (s, 2H), 7.15 (ddd,  $J = 7.9, 7.3, 0.9$  Hz, 1H), 7.25-7.33 (m, 5H), 7.62 (ddd,  $J = 8.5, 7.3, 1.3$  Hz, 1H), 7.68 (t,  $J = 7.7$  Hz, 1H), 8.03 (ddd,  $J = 7.9, 1.9, 0.9$  Hz, 1H), 8.09 (dd,  $J = 8.2, 1.6$  Hz, 1H), 8.23 (ddd,  $J = 7.9, 1.9, 1.3$  Hz, 1H), 8.50 (t,  $J = 1.6$  Hz, 1H), 8.89 (dd,  $J = 8.5, 0.9$  Hz, 1H), 12.22 (bs, 1H);  $^{13}\text{C}$  NMR (125 MHz,  $\text{CDCl}_3$ ):  $\delta$  13.42, 42.60, 51.31, 52.56, 115.25, 120.38, 123.12, 125.91, 127.81, 128.24, 128.59, 129.78, 130.17, 131.05, 134.99, 136.21, 136.28, 141.44, 163.92, 169.16; LC/MS:  $m/z = 452.67$   $[\text{M} + \text{H}]^+$ , 493.62  $[\text{M} + \text{H} + \text{CH}_3\text{CN}]^+$ , 904.55  $[2\text{M} + \text{H}]^+$ ,  $t_{\text{R}} = 14.35$  min.

#### **Syntheses of test compounds 2, 4, 6, 9-10, 13-14, 34-64**

**2-(3-(*N,N*-Diethylsulfamoyl)benzamido)benzoic acid (2)** The title compound was synthesized from methyl 2-(3-(*N,N*-diethylsulfamoyl)benzamido)benzoate (**2a**, 506 mg, 1.30 mmol) according to General Procedure D, using THF/MeOH 2/1 (9 mL) and 1N NaOH (aq., 2.6 mL). The solution was acidified with 1N HCl (aq., 2.6 mL). The organic solvent was evaporated under reduced pressure. The solid was isolated by suction filtration, washed with water, redissolved in MeOH and evaporated to dryness under reduced pressure: 394 mg, 81% yield; mp: 218.1-219.7 °C;  $^1\text{H}$  NMR (500 MHz,  $\text{DMSO}-d_6$ ):  $\delta$  1.06 (t,  $J = 7.1$  Hz, 6H), 3.22 (q,  $J = 7.1$  Hz, 4H), 7.24 (t,  $J = 7.6$  Hz, 1H), 7.68 (dt,  $J = 7.9, 1.6$  Hz, 1H), 7.83 (t,  $J = 7.8$  Hz, 1H), 8.06 (m, 2H), 8.22 (d,  $J = 7.9$  Hz, 1H), 8.33 (s, 1H), 8.66 (d,  $J = 8.3$  Hz, 1H), 12.3 (bs, 1H), 13.9 (bs, 1H);  $^{13}\text{C}$  NMR (125 MHz,  $\text{DMSO}-d_6$ ):  $\delta$  14.10, 41.95, 117.11, 120.13, 123.37, 124.93, 129.96, 130.42, 131.06, 131.24, 134.26, 135.46, 140.63, 140.68, 163.17, 170.04; LC/MS:  $m/z = 417.88$   $[\text{M} + \text{H} + \text{CH}_3\text{CN}]^+$ , 752.73  $[2\text{M} + \text{H}]^+$ ,  $t_{\text{R}} = 12.53$  min, 99.8% pure (UV).

**3-(3-(*N,N*-Diethylsulfamoyl)benzamido)benzoic acid (4)** The title compound was synthesized from methyl 3-(3-(*N,N*-diethylsulfamoyl)benzamido)benzoate (**4a**, 486 mg, 1.24 mmol) according to General Procedure D, using THF/MeOH 2/1 (6 mL) and 1N NaOH (aq., 2 mL). The solution was acidified with 1N HCl (aq., 4 mL). Water was added and the solid was isolated by suction filtration, washed with water and dried under reduced pressure: 379 mg, 81% yield; mp: 231.5-233.6 °C;  $^1\text{H}$  NMR (500 MHz,  $\text{DMSO}-d_6$ ):  $\delta$  1.06 (t,  $J = 7.1$  Hz, 6H), 3.23 (q,  $J = 7.1$  Hz, 4H), 7.85 (t,  $J = 7.7$  Hz, 1H), 8.08 (d,  $J = 8.5$  Hz, 1H), 8.11 (dd,  $J = 8.8, 2.2$  Hz, 1H), 8.22 (d,  $J = 7.9$  Hz, 1H), 8.33 (s, 1H),

8.41 (d,  $J = 1.9$  Hz, 1H), 8.82 (d,  $J = 8.8$  Hz, 1H), 12.53 (s, 1H);  $^{13}\text{C}$  NMR (125 MHz, DMSO- $d_6$ ):  $\delta$  14.11, 41.96, 105.46, 117.86, 120.52, 125.07, 130.39, 130.57, 131.26, 134.87, 135.36, 137.52, 140.75, 144.17, 163.69, 168.60; LC/MS:  $m/z = 376.75$   $[\text{M} + \text{H}]^+$ , 417.76  $[\text{M} + \text{H} + \text{CH}_3\text{CN}]^+$ , 752.70  $[2\text{M} + \text{H}]^+$ ,  $t_{\text{R}} = 10.16$  min, 95.7% pure (UV).

***N*-(2-Carbamoylphenyl)-3-(*N,N*-diethylsulfamoyl)benzamide (6).** A solution of 2-aminobenzamide (**5**, 136 mg, 1.00 mmol) and 3-(*N,N*-diethylsulfamoyl)benzoyl chloride (**27a**, 276 mg, 1.00 mmol) in toluene (5 mL) was heated at 88 °C for 30 minutes. After cooling to room temperature the solid was isolated by suction filtration. Purification by flash chromatography (ethyl acetate/*n*-hexane 60/40) yielded the title compound (78 mg, 21% yield); mp: 148.9-152.2 °C;  $^1\text{H}$  NMR (500 MHz, DMSO- $d_6$ ):  $\delta$  1.13 (t,  $J = 7.1$  Hz, 6H), 3.27 (q,  $J = 7.1$  Hz, 4H), 6.88 (bs, 1H), 7.17 (ddd,  $J = 7.9, 7.3, 1.3$  Hz, 1H), 7.53 (bs, 1H), 7.57 (ddd,  $J = 7.6, 7.3, 1.6$  Hz, 1H), 7.64 (t,  $J = 7.7$  Hz, 1H), 7.67 (dd,  $J = 8.2, 1.6$  Hz, 1H), 7.97 (ddd,  $J = 7.9, 1.9, 1.3$  Hz, 1H), 8.27 (ddd,  $J = 7.9, 1.9, 1.3$  Hz, 1H), 8.43 (t,  $J = 1.6$  Hz, 1H), 8.89 (dd,  $J = 8.5, 1.1$  Hz, 1H), 12.90 (bs, 1H);  $^{13}\text{C}$  NMR (125 MHz, DMSO- $d_6$ ):  $\delta$  14.18, 42.25, 118.14, 121.15, 123.27, 125.06, 127.65, 129.74, 129.88, 131.92, 133.69, 136.15, 140.67, 140.96, 163.58, 172.38; LC/MS:  $m/z = 375.92$   $[\text{M} + \text{H}]^+$ , 750.92  $[2\text{M} + \text{H}]^+$   $t_{\text{R}} = 10.87$  min, 98.2% pure (UV).

**2-(4-(*N,N*-Diethylsulfamoyl)benzamido)benzoic acid (9)** The title compound was synthesized from methyl 2-(4-(*N,N*-diethylsulfamoyl)benzamido)benzoate (**9a**, 274 mg, 0.70 mmol) according to General Procedure D, using THF/MeOH 2/1 (4 mL) and 1N NaOH (aq., 2 mL). The solution was acidified with 1N HCl (aq., 4 mL). Water was added and the solid was isolated by suction filtration, washed with water and dried under reduced pressure: 248 mg, 94% yield; mp: 219.4-220.8 °C;  $^1\text{H}$  NMR (500 MHz, DMSO- $d_6$ ):  $\delta$  1.06 (t,  $J = 7.1$  Hz, 6H), 3.22 (q,  $J = 7.1$  Hz, 4H), 7.25 (ddd,  $J = 7.9, 7.6, 1.3$  Hz, 1H), 7.68 (ddd,  $J = 7.9, 7.6, 1.6$  Hz, 1H), 8.01 (d,  $J = 8.8$  Hz, 2H), 8.06 (dd,  $J = 8.2, 1.6$  Hz, 1H), 8.13 (d,  $J = 8.8$  Hz, 1H), 8.64 (dd,  $J = 8.5, 0.9$  Hz, 1H), 12.21 (bs, 1H), 13.81 (bs, 1H);  $^{13}\text{C}$  NMR (125 MHz, DMSO- $d_6$ ):  $\delta$  4.13, 41.93, 117.17, 120.24, 123.43, 127.34, 128.11, 131.23, 134.26, 137.97, 140.55, 142.79, 163.46, 169.88; LC/MS:  $m/z = 376.59$   $[\text{M} + \text{H}]^+$ ,  $t_{\text{R}} = 11.80$  min, 99.3% pure (UV).

**5-Bromo-2-(4-(*N,N*-diethylsulfamoyl)benzamido)benzoic acid (10)<sup>S11</sup>** The title compound was synthesized from methyl 5-bromo-2-(4-(*N,N*-diethylsulfamoyl)benzamido)benzoate (**10a**, 350 mg, 0.75 mmol) according to General Procedure D, using THF/MeOH 2/1 (4 mL) and 1N NaOH (aq., 1.5 mL). The solution was acidified with 1N HCl (aq., 3 mL). Water was added and the solid was isolated by suction filtration, washed with water and dried under reduced pressure: 318 mg, 94% yield; mp: 232.8-235.6 °C;  $^1\text{H}$  NMR (500 MHz, DMSO- $d_6$ ):  $\delta$  1.06 (t,  $J = 7.1$  Hz, 6H), 3.21 (q,  $J = 7.1$  Hz, 4H), 7.87 (dd,  $J = 9.1, 2.5$  Hz, 1H), 8.01 (d,  $J = 8.8$  Hz, 2H), 8.12 (d,  $J = 8.5$  Hz, 2H), 8.12 (d,  $J = 2.5$  Hz, 1H), 8.57 (d,  $J = 8.8$  Hz, 1H), 12.11 (bs, 1H), 14.2 (bs, 1H);  $^{13}\text{C}$  NMR (125 MHz, DMSO- $d_6$ ):  $\delta$  14.12, 41.93, 114.92, 119.62, 122.47, 127.36, 128.17, 133.25, 136.67, 137.67, 139.65, 142.92, 163.55, 168.49; LC/MS:  $m/z = 454.76$  and 457.38  $[\text{M} + \text{H}]^+$ ,  $t_{\text{R}} = 13.20$  min, 98.6% pure (UV).



**2-(3-(Diethylcarbamoyl)benzamido)benzoic acid (13)** The title compound was synthesized from methyl 2-(3-(diethylcarbamoyl)benzamido)benzoate (**13a**, 175 mg, 0.49 mmol) according to General Procedure D, using THF/MeOH 2/1 (3 mL) and 1N NaOH (aq., 1 mL). The solution was acidified with 1N HCl (aq., 2 mL). Water was added and the solid was isolated by suction filtration, washed with water and dried under reduced pressure: 155 mg, 92% yield; mp: 162.6-164.0 °C; <sup>1</sup>H NMR (500 MHz, DMSO-*d*<sub>6</sub>): δ 1.07 (bs, 3H), 1.17 (bs, 3H), 3.20 (bs, 2H), 3.46 (bs, 2H), 7.23 (dt, *J* = 7.7, 1.3 Hz, 1H), 7.62 (dt, *J* = 7.6, 1.4 Hz, 1H), 7.66 (d, *J* = 7.6 Hz, 1H), 7.68 (m, 1H), 7.89 (t, *J* = 1.4 Hz, 1H), 8.02 (dt, *J* = 7.9, 1.4 Hz, 1H), 8.06 (dd, *J* = 7.9, 1.6 Hz, 1H), 8.68 (dd, *J* = 8.5, 1.0 Hz, 1H), 12.20 (s, 1H), 13.82 (bs, 1H); <sup>13</sup>C NMR (125 MHz, DMSO-*d*<sub>6</sub>): δ 12.78 (bs), 14.00 (bs), 42.89 (bs), 116.81, 120.05, 123.14, 124.61, 127.60, 129.26, 129.69, 131.24, 134.58, 137.90, 140.86, 163.98, 169.02, 170.03; LC/MS: *m/z* = 340.98 [M + H]<sup>+</sup>, 382.00 [M + H + CH<sub>3</sub>CN]<sup>+</sup>, *t<sub>R</sub>* = 10.49 min, 99.0% pure (UV). Mp: 162.6-164.0 °C.

**5-Bromo-2-(3-(diethylcarbamoyl)benzamido)benzoic acid (14)** The title compound was synthesized from methyl 5-bromo-2-(3-(diethylcarbamoyl)benzamido)benzoate (**14a**, 350 mg, 0.81 mmol) according to General Procedure D, using THF/MeOH 2/1 (4.5 mL) and 1N NaOH (aq., 1.6 mL). The solution was acidified with 1N HCl (aq., 3.2 mL). Water was added and the solid was isolated by suction filtration, washed with water and dried under reduced pressure: 298 mg, 88% yield; mp: 169.6-170.3 °C; <sup>1</sup>H NMR (500 MHz, DMSO-*d*<sub>6</sub>): δ 1.07 (bs, 3H), 1.17 (bs, 3H), 3.20 (bs, 2H), 3.46 (bs, 2H), 7.62 (dt, *J* = 7.6, 1.6 Hz, 1H), 7.66 (dt, *J* = 7.6, 0.6 Hz, 1H), 7.86 (dd, *J* = 8.8, 2.5 Hz, 1H), 7.88 (t, *J* = 1.6 Hz, 1H), 8.00 (dt, *J* = 7.9, 1.6 Hz, 1H), 8.11 (d, *J* = 2.5 Hz, 1H), 8.62 (d, *J* = 8.8 Hz, 1H), 12.09 (s, 1H), 14.19 (bs, 1H); <sup>13</sup>C NMR (125 MHz, DMSO-*d*<sub>6</sub>): δ 12.79 (bs), 14.01 (bs), 42.91 (bs), 114.58, 119.24, 122.29, 124.68, 127.63, 129.29, 129.83, 133.23, 134.31, 136.68, 137.91, 139.95, 164.05, 168.63, 168.98; LC/MS: *m/z* = 418.84 and 420.85 [M + H]<sup>+</sup>, 459.92 and 461.88 [M + H + CH<sub>3</sub>CN]<sup>+</sup>, *t<sub>R</sub>* = 12.04 min, 99.2% pure (UV).

**2-(4-Bromo-3-(*N,N*-diethylsulfamoyl)benzamido)benzoic acid (34)** The title compound was synthesized as described by Nie *et al.*; mp: 190.9-192.4 °C; <sup>1</sup>H NMR (500 MHz, DMSO-*d*<sub>6</sub>): δ 1.08 (t, *J* = 7.1 Hz, 6H), 3.38 (q, *J* = 7.1 Hz, 4H), 7.25 (ddd, *J* = 7.9, 7.6, 1.3 Hz, 1H), 7.68 (ddd, *J* = 8.2, 7.6, 1.9 Hz, 1H), 8.04 (dd, *J* = 8.2, 2.2 Hz, 1H), 8.06 (dd, *J* = 7.9, 1.6 Hz, 1H), 8.11 (d, *J* = 8.2 Hz, 1H), 8.64 (d, *J* = 2.1 Hz, 1H), 8.76 (dd, *J* = 8.5, 1.0 Hz, 1H); <sup>13</sup>C NMR (125 MHz, DMSO-*d*<sub>6</sub>): δ 13.78, 41.25, 117.20, 120.24, 123.50, 123.58, 129.48, 131.22, 131.96, 134.10, 134.28, 136.58, 140.09, 140.47, 162.60, 170.00; LC/MS: *m/z* = 453.17 and 455.18 [M + H]<sup>+</sup>, *t<sub>R</sub>* = 12.48 min, >99% pure (UV).

**2-(3-(*N,N*-Diethylsulfamoyl)-4-methylbenzamido)benzoic acid (35)** The title compound was synthesized from methyl 2-(3-(*N,N*-diethylsulfamoyl)-4-methylbenzamido)benzoate (**35a**, 220 mg, 0.54 mmol) according to General Procedure D, using THF/MeOH 2/1 (3 mL) and 1N NaOH (aq., 1 mL). The solution was acidified with 1N HCl (aq., 2 mL). The organic solvent was evaporated under reduced pressure. The solid was isolated by suction filtration, washed with water and dried under

reduced pressure: 197 mg, 93% yield; mp: 170.4-171.0 °C;  $^1\text{H}$  NMR (500 MHz, DMSO- $d_6$ ):  $\delta$  1.07 (t,  $J = 7.1$  Hz, 6H), 2.61 (s, 3H), 3.31 (q,  $J = 7.1$  Hz, 4H), 7.23 (m, 1H), 7.67 (m, 2H), 8.06 (dd,  $J = 8.0$ , 1.7 Hz, 1H), 8.08 (dd,  $J = 7.9$ , 2.2 Hz, 1H), 8.37 (d,  $J = 2.2$  Hz, 1H), 8.68 (dd,  $J = 8.5$ , 1.0 Hz, 1H), 12.28 (bs, 1H), 13.87 (bs, 1H);  $^{13}\text{C}$  NMR (125 MHz, DMSO- $d_6$ ):  $\delta$  13.79, 19.80, 40.90, 116.78, 120.01, 123.22, 127.10, 130.77, 131.25, 132.48, 133.60, 134.32, 139.17, 140.80, 141.18, 163.16, 170.08; LC/MS:  $m/z = 431.72$  [M + H + CH<sub>3</sub>CN]<sup>+</sup>, 781.12 [2M + H]<sup>+</sup>,  $t_R = 11.98$  min, 98.0% pure (UV).

**2-(3-(*N,N*-Diethylsulfamoyl)-4-ethylbenzamido)benzoic acid (36)** The title compound was synthesized from methyl 2-(3-(*N,N*-diethylsulfamoyl)-4-ethylbenzamido)benzoate (**36a**, 103 mg, 0.25 mmol) according to General Procedure D, using THF/MeOH 2/1 (1 mL) and 1N NaOH (aq., 0.3 mL). The solution was acidified with 1N HCl (aq., 2 mL). The organic solvent was evaporated under reduced pressure. The solid was isolated by suction filtration, washed with water and dried under reduced pressure: 79 mg, 80% yield; mp: 135.5-138.5 °C;  $^1\text{H}$  NMR (500 MHz, DMSO- $d_6$ ):  $\delta$  1.08 (t,  $J = 7.1$  Hz, 6H), 1.24 (t,  $J = 7.4$  Hz, 3H), 3.00 (q,  $J = 7.4$  Hz, 2H), 3.34 (q,  $J = 7.1$  Hz, 4H), 7.15 (dt,  $J = 7.6$ , 1.3 Hz, 1H), 7.54 (dt,  $J = 7.9$ , 1.7 Hz, 1H), 7.67 (d,  $J = 7.9$  Hz, 1H), 8.09 (dd,  $J = 7.9$ , 1.6 Hz, 1H), 8.16 (dd,  $J = 7.9$ , 2.0 Hz, 1H), 8.31 (d,  $J = 1.9$  Hz, 1H), 8.69 (dd,  $J = 8.4$ , 0.8 Hz, 1H), 13.85 (bs, 1H);  $^{13}\text{C}$  NMR (125 MHz, DMSO- $d_6$ ):  $\delta$  14.24, 15.13, 25.26, 41.56, 119.21, 122.57, 126.40, 130.74, 131.27, 131.97, 132.48, 132.70, 138.98, 140.84, 146.76, 162.84, 170.26; LC/MS:  $m/z = 445.70$  [M + H + CH<sub>3</sub>CN]<sup>+</sup>, 808.42 [2M + H]<sup>+</sup>,  $t_R = 12.86$  min, 96.5% pure (UV).

**2-(3-(*N,N*-Diethylsulfamoyl)benzamido)-4-fluorobenzoic acid (37)** The title compound was synthesized from methyl 2-(3-(*N,N*-diethylsulfamoyl)benzamido)-4-fluorobenzoate (**37a**, 141 mg, 0.35 mmol) according to General Procedure D, using THF/MeOH 2/1 (3 mL) and 1N NaOH (aq., 1 mL). The solution was acidified with 1N HCl (aq., 2 mL). Water was added and the solid was isolated by suction filtration, washed with water and dried under reduced pressure. As the hydrolysis was incomplete the procedure as described above was repeated: 108 mg, 79% yield; mp: 241.2-243.7 °C;  $^1\text{H}$  NMR (500 MHz, DMSO- $d_6$ ):  $\delta$  1.06 (t,  $J = 7.1$  Hz, 6H), 3.22 (q,  $J = 7.1$  Hz, 4H), 7.08 (ddd,  $J = 16.7$ , 8.8, 2.8 Hz, 1H), 7.84 (t,  $J = 7.9$  Hz, 1H), 8.07 (m, 1H), 8.14 (dd,  $J = 8.8$ , 6.6 Hz, 1H), 8.21 (m, 1H), 8.32 (t,  $J = 1.6$  Hz, 1H), 8.52 (dd,  $J = 12.0$ , 2.8 Hz, 1H), 12.54 (bs, 1H), 14.04 (bs, 1H);  $^{13}\text{C}$  NMR (125 MHz, DMSO- $d_6$ ):  $\delta$  14.10, 41.96, 106.54 (d,  $J_{\text{CF}} = 28$  Hz), 110.31 (d,  $J_{\text{CF}} = 22$  Hz), 113.19 (d,  $J_{\text{CF}} = 3$  Hz), 124.91, 130.24, 130.54, 131, 11, 134.01 (d,  $J_{\text{CF}} = 11$  Hz), 140.72, 142.88, (d,  $J_{\text{CF}} = 13$  Hz), 164.99 (d,  $J_{\text{CF}} = 250$  Hz), 169.44; LC/MS:  $m/z = 435.67$  [M + H + CH<sub>3</sub>CN]<sup>+</sup>, 788.65 [2M + H]<sup>+</sup>,  $t_R = 12.62$  min, 97.1% pure (UV).

**4-Chloro-2-(3-(*N,N*-diethylsulfamoyl)benzamido)benzoic acid (38)** The title compound was synthesized from methyl 4-chloro-2-(3-(*N,N*-diethylsulfamoyl)benzamido)benzoate (**38a**, 340 mg, 0.80 mmol) according to General Procedure D, using THF/MeOH 2/1 (9 mL) and 1N NaOH (aq., 3 mL). The solution was acidified with 1N HCl. The organic solvent was evaporated under reduced pressure. The solid was isolated by suction filtration, washed with water, dried under reduced pressure

and crystallized from MeOH: 102 mg, 31% yield; mp: 222.0-223.5 °C; <sup>1</sup>H NMR (500 MHz, DMSO-*d*<sub>6</sub>): δ 1.07 (t, *J* = 7.2 Hz, 6H), 3.22 (q, *J* = 7.1 Hz, 4H), 7.29 (dd, *J* = 8.5, 2.2 Hz, 1H), 7.84 (t, *J* = 7.7 Hz, 1H), 8.06 (m, 2H), 8.20 (d, *J* = 7.9 Hz, 1H), 8.31 (s, 1H), 8.76 (d, *J* = 2.2 Hz, 1H), 12.38 (s, 1H), 14.1 (bs, 1H); <sup>13</sup>C NMR (125 MHz, DMSO-*d*<sub>6</sub>): δ 14.09, 41.95, 115.66, 119.40, 123.22, 124.93, 130.21, 130.50, 131.12, 132.90, 135.00, 138.64, 140.72, 141.71, 163.44, 169.38; LC/MS: *m/z* = 451.79 [M + H + CH<sub>3</sub>CN]<sup>+</sup>, 820.69 and 822.76 [2M + H]<sup>+</sup>, *t*<sub>R</sub> = 12.72 min, >99.9% pure (UV).

**2-(3-(*N,N*-Diethylsulfamoyl)benzamido)-4-nitrobenzoic acid (39)** The title compound was synthesized from methyl 2-(3-(*N,N*-diethylsulfamoyl)benzamido)-4-nitrobenzoate (**39a**, 157 mg, 0.36 mmol) according to General Procedure D, using THF/MeOH 2/1 (3 mL) and 1N NaOH (aq., 1 mL). The solution was acidified with 1N HCl (aq., 2 mL). Water was added and the solid was isolated by suction filtration, washed with water and dried under reduced pressure: 119 mg, 78% yield; mp: 229-231.5 °C; <sup>1</sup>H NMR (500 MHz, DMSO-*d*<sub>6</sub>): δ 1.07 (t, *J* = 7.1 Hz, 6H), 3.23 (q, *J* = 7.1 Hz, 4H), 7.86 (t, *J* = 7.7 Hz, 1H), 8.03 (dd, *J* = 8.8, 2.5 Hz, 1H), 8.08 (m, 1H), 8.22 (m, 1H), 8.26 (d, *J* = 8.8 Hz, 1H), 8.34 (t, *J* = 1.6 Hz, 1H), 9.43 (d, *J* = 2.5 Hz, 1H), 12.33 (bs, 1H); <sup>13</sup>C NMR (125 MHz, DMSO-*d*<sub>6</sub>): δ 14.12, 41.98, 114.66, 117.64, 122.88, 125.03, 130.34, 130.54, 131.23, 132.65, 134.79, 140.72, 140.98, 150.11, 163.70, 168.56; LC/MS: *m/z* = 462.78 [M + H + CH<sub>3</sub>CN]<sup>+</sup>, 842.38 [2M + H]<sup>+</sup>, *t*<sub>R</sub> = 12.27 min, 99.0% pure (UV).

**2-(3-(*N,N*-Diethylsulfamoyl)benzamido)-5-methylbenzoic acid (40)** The title compound was synthesized from methyl 2-(3-(*N,N*-diethylsulfamoyl)benzamido)-5-methylbenzoate (**40a**, 360 mg, 0.89 mmol) according to General Procedure D, using THF/MeOH 2/1 (6 mL) and 1N NaOH (aq., 2 mL). The solution was acidified with 1N HCl (aq., 4 mL). Water (10 mL) was added and the solid was isolated by suction filtration, washed with water and dried under reduced pressure: 330 mg, 95% yield; mp: 226.8-228.6 °C; <sup>1</sup>H NMR (500 MHz, DMSO-*d*<sub>6</sub>): δ 1.06 (t, *J* = 7.1 Hz, 6H), 2.33 (s, 3H), 3.22 (q, *J* = 7.1 Hz, 4H), 7.49 (d, *J* = 8.2 Hz, 1H), 7.82 (t, *J* = 7.9 Hz, 1H), 7.87 (s, 1H), 8.04 (d, *J* = 7.6 Hz, 1H), 8.20 (d, *J* = 7.9 Hz, 1H), 8.31 (s, 1H), 8.54 (d, *J* = 8.5 Hz, 1H), 12.17 (s, 1H), 13.79 (bs, 1H); <sup>13</sup>C NMR (125 MHz, DMSO-*d*<sub>6</sub>): δ 14.10, 20.24, 41.94, 120.24, 124.87, 129.88, 130.40, 131.00, 131.27, 132.59, 134.78, 135.52, 138.22, 140.63, 162.95, 170.03; LC/MS: *m/z* = 390.75 [M + H]<sup>+</sup>, 431.90 [M + H + CH<sub>3</sub>CN]<sup>+</sup>, 780.63 [2M + H]<sup>+</sup>, *t*<sub>R</sub> = 12.64 min, 99.4% pure (UV).

**2-(3-(*N,N*-Diethylsulfamoyl)benzamido)-5-(trifluoromethyl)benzoic acid (41)** The title compound was synthesized from methyl 2-(3-(*N,N*-diethylsulfamoyl)benzamido)-5-(trifluoromethyl)benzoate (**41a**, 157 mg, 0.36 mmol) according to General Procedure D, using THF/MeOH 2/1 (6 mL) and 1N NaOH (aq., 2 mL). The solution was acidified with 1N HCl (aq., 4 mL). The solid was isolated by suction filtration, washed with water and dried under reduced pressure: 232 mg, 81% yield; mp: 192.5-193.8 °C; <sup>1</sup>H NMR (500 MHz, DMSO-*d*<sub>6</sub>): δ 1.06 (t, *J* = 7.1 Hz, 6H), 3.22 (q, *J* = 7.1 Hz, 4H), 7.84 (t, *J* = 7.7 Hz, 1H), 8.01 (dd, *J* = 8.8, 1.9 Hz, 1H), 8.07 (d, *J* = 7.9 Hz, 1H), 8.23 (m, 1H), 8.29 (d, *J* = 1.9 Hz, 1H), 8.34 (m, 1H), 8.86 (d, *J* = 8.8 Hz, 1H), 12.79 (br.s, 1H); <sup>13</sup>C NMR (125 MHz, DMSO-*d*<sub>6</sub>): δ 14.03, 41.91, 18.08, 120.42, 123.04 (q, *J*<sub>CF</sub> = 32 Hz), 123.73 (q, *J*<sub>CF</sub> = 272 Hz), 125.02, 127.81 (q, *J*<sub>CF</sub>

= 4 Hz), 130.18, 130.43, 131.09, 134.99, 140.66, 143.73, 163.51, 168.77; LC/MS:  $m/z = 444.59$  [M + H]<sup>+</sup>, 485.65 [M + H + CH<sub>3</sub>CN]<sup>+</sup>, 888.77 [2M + H]<sup>+</sup>,  $t_R = 13.28$  min, 96.1% pure (UV).

**2-(3-(*N,N*-Diethylsulfamoyl)benzamido)-5-fluorobenzoic acid (42)** The title compound was synthesized from methyl 2-(3-(*N,N*-diethylsulfamoyl)benzamido)-5-fluorobenzoate (**42a**, 337 mg, 0.83 mmol) according to General Procedure D, using THF/MeOH 2/1 (9 mL) and 1N NaOH (aq., 3 mL). The solution was acidified with 1N HCl. The organic solvent was evaporated under reduced pressure. The solid was isolated by suction filtration, washed with water, dried under reduced pressure and crystallized from MeOH: 86 mg, 26% yield; mp: 212.5-213.9 °C; <sup>1</sup>H NMR (500 MHz, DMSO-*d*<sub>6</sub>):  $\delta$  1.06 (t,  $J = 7.1$  Hz, 6H), 3.22 (q,  $J = 7.1$  Hz, 4H), 7.56 (dt,  $J = 8.5, 3.2$  Hz, 1H), 7.76 (dd,  $J = 9.1, 3.2$  Hz, 1H), 7.82 (t,  $J = 7.9$  Hz, 1H), 8.05 (d,  $J = 8.2$  Hz, 1H), 8.20 (d,  $J = 8.2$  Hz, 1H), 8.32 (s, 1H), 8.61 (dd,  $J = 9.1, 5.0$  Hz, 1H), 12.03 (bs, 1H); <sup>13</sup>C NMR (125 MHz, DMSO-*d*<sub>6</sub>):  $\delta$  14.1, 41.9, 117.0 (d,  $J_{CF} = 23.8$  Hz), 119.7 (d,  $J_{CF} = 6.4$  Hz), 121.0 (d,  $J_{CF} = 2.2$  Hz), 122.7 (d,  $J_{CF} = 8.2$  Hz), 125.0, 130.0, 130.4, 131.1, 135.3, 136.9, 140.7, 157.2 (d,  $J_{CF} = 242$  Hz), 163.1, 168.7; LC/MS:  $m/z = 435.83$  [M + H + CH<sub>3</sub>CN]<sup>+</sup>, 788.64 [2M + H]<sup>+</sup>,  $t_R = 11.68$  min, 100% pure (UV).

**5-Bromo-2-(3-(*N,N*-diethylsulfamoyl)benzamido)benzoic acid (43)** The title compound was synthesized from methyl 5-bromo-2-(3-(*N,N*-diethylsulfamoyl)benzamido)benzoate (**43a**, 368 mg, 0.78 mmol) according to General Procedure D, using THF/MeOH 2/1 (9 mL) and 1N NaOH (aq., 3 mL). The organic solvent was evaporated under reduced pressure. 1N HCl (aq., 4 mL) was added and the solid was isolated by suction filtration, washed with water, dried under reduced pressure and crystallized from MeOH: 70 mg, 20% yield; mp: 206.5-209.0 °C; <sup>1</sup>H NMR (500 MHz, DMSO-*d*<sub>6</sub>):  $\delta$  1.06 (t,  $J = 7.1$  Hz, 6H), 3.22 (q,  $J = 7.1$  Hz, 4H), 7.81 (m, 2H), 7.82 (m, 1H), 8.13 (d,  $J = 2.5$  Hz, 1H), 8.21 (m, 1H), 8.32 (t,  $J = 1.7$  Hz, 1H), 8.60 (d,  $J = 8.8$  Hz, 1H), 12.8 (bs, 1H); <sup>13</sup>C NMR (125 MHz, DMSO-*d*<sub>6</sub>):  $\delta$  14.11, 41.96, 114.70, 120.78, 122.09, 125.03, 130.00, 130.41, 131.04, 133.31, 135.36, 136.04, 139.76, 140.66, 163.18, 168.53; LC/MS:  $m/z = 495.76$  and 497.48 [M + H + CH<sub>3</sub>CN]<sup>+</sup>, 910.86 [2M + H]<sup>+</sup>,  $t_R = 12.69$  min, 100% pure (UV).

**5-Cyano-2-(3-(*N,N*-diethylsulfamoyl)benzamido)benzoic acid (44)** The title compound was synthesized from methyl 5-cyano-2-(3-(*N,N*-diethylsulfamoyl)benzamido)benzoate (**44a**, 237 mg, 0.59 mmol) according to General Procedure D, using THF/MeOH 2/1 (4 mL) and 1N NaOH (aq., 1 mL). The solution was acidified with 1N HCl (aq., 2 mL). Water (10 mL) was added and the solid was isolated by suction filtration, washed with water, dried under reduced pressure and crystallized from MeOH: 137 mg, 60% yield; mp: 195.3-196.6 °C; <sup>1</sup>H NMR (500 MHz, DMSO-*d*<sub>6</sub>):  $\delta$  1.06 (t,  $J = 7.1$  Hz, 6H), 3.22 (q,  $J = 7.1$  Hz, 4H), 7.85 (t,  $J = 7.7$  Hz, 1H), 8.08 (ddd,  $J = 7.9, 1.9, 1.3$  Hz, 1H), 8.12 (dd,  $J = 8.8, 2.2$  Hz, 1H), 8.22 (ddd,  $J = 7.9, 1.9, 1.3$  Hz, 1H), 8.33 (t,  $J = 1.6$  Hz, 1H), 8.41 (d,  $J = 2.5$  Hz, 1H), 8.82 (d,  $J = 9.1$  Hz, 1H), 12.54 (bs, 1H). <sup>13</sup>C NMR (125 MHz, DMSO-*d*<sub>6</sub>):  $\delta$  14.11, 41.96, 105.46, 117.90, 118.07, 120.54, 125.08, 130.40, 130.58, 131.28, 134.89, 135.37, 137.52, 140.75, 144.17, 163.71, 168.61. LC/MS:  $m/z = 401.63$  [M + H]<sup>+</sup>, 442.73 [M + H + CH<sub>3</sub>CN]<sup>+</sup>, 802.54 [2M + H]<sup>+</sup>,  $t_R = 11.77$  min, 96.2% pure (UV).

**2-(3-(*N,N*-Diethylsulfamoyl)benzamido)-5-nitrobenzoic acid (45)** The title compound was synthesized from methyl 2-(3-(*N,N*-diethylsulfamoyl)benzamido)-5-nitrobenzoate (**45a**, 304 mg, 0.70 mmol) according to General Procedure D, using THF/MeOH 2/1 (3 mL) and 1N NaOH (aq., 0.7 mL). The solution was acidified with 1N HCl (aq., 4 mL). Water was added and the solid was isolated by suction filtration, washed with water, dried under reduced pressure and crystallized from MeOH: 115 mg, 39% yield; mp: 216.6-218.8 °C; <sup>1</sup>H NMR (500 MHz, DMSO-*d*<sub>6</sub>): δ 1.07 (t, *J* = 7.1 Hz, 6H), 3.23 (q, *J* = 7.1 Hz, 4H), 7.86 (t, *J* = 7.8 Hz, 1H), 8.09 (dt, *J* = 8.3, 1.5 Hz, 1H), 8.24 (dt, *J* = 7.9, 1.6 Hz, 1H), 8.34 (t, *J* = 1.6 Hz, 1H), 8.53 (dd, *J* = 9.3, 2.9 Hz, 1H), 8.78 (d, *J* = 2.8 Hz, 1H), 8.90 (d, *J* = 9.3 Hz, 1H), 12.67 (s, 1H); <sup>13</sup>C NMR (125 MHz, DMSO-*d*<sub>6</sub>): δ 14.12, 41.98, 48.56, 117.44, 120.34, 125.11, 126.52, 129.12, 130.50, 130.61, 131.32, 134.76, 140.77, 141.70, 145.87, 163.77, 168.55; LC/MS: *m/z* = 421.89 [M + H]<sup>+</sup>, 462.94 [M + H + CH<sub>3</sub>CN]<sup>+</sup>, 842.83 [2M + H]<sup>+</sup>, *t*<sub>R</sub> = 12.31 min, 99.5% pure (UV).

**2-(4-Bromo-3-(*N,N*-diethylsulfamoyl)benzamido)-5-fluorobenzoic acid (46)** The title compound was synthesized from methyl 2-(4-bromo-3-(*N,N*-diethylsulfamoyl)benzamido)-5-fluorobenzoate (**46a**, 110 mg, 0.23 mmol) according to General Procedure D, using THF/MeOH 2/1 (3 mL) and 1N NaOH (aq., 1 mL). The solution was acidified with 1N HCl (aq., 2 mL). The organic solvent was evaporated under reduced pressure. The solid was isolated by suction filtration, washed with water and dried under reduced pressure: 88 mg, 82% yield; mp 226.7-228.7 °C; <sup>1</sup>H NMR (500 MHz, DMSO-*d*<sub>6</sub>): δ 1.07 (t, *J* = 7.1 Hz, 6H), 3.37 (q, *J* = 7.1 Hz, 4H), 7.56 (ddd, *J* = 9.1, 8.2, 3.2 Hz, 1H), 7.75 (dd, *J* = 9.5, 3.2 Hz, 1H), 8.03 (dd, *J* = 8.2, 2.2 Hz, 1H), 8.10 (d, *J* = 8.2 Hz, 1H), 8.52 (d, *J* = 2.2 Hz, 1H), 8.56 (dd, *J* = 9.1, 5.0 Hz, 1H), 12.02 (bs, 1H), 14.14 (bs, 1H); <sup>13</sup>C NMR (125 MHz, DMSO-*d*<sub>6</sub>): δ 13.77, 41.24, 117.04 (d, *J*<sub>CF</sub> = 23.8 Hz), 119.89 (d, *J*<sub>CF</sub> = 6.4 Hz), 120.95 (d, *J*<sub>CF</sub> = 22.0 Hz), 122.85 (d, *J*<sub>CF</sub> = 7.3 Hz), 123.58, 129.54, 131.99, 133.96, 136.54, 136.69, 140.06, 157.30 (d, *J*<sub>CF</sub> = 241.91 Hz), 162.59, 168.65; LC/MS: *m/z* = 472.45 and 474.47 [M + H]<sup>+</sup>, 513.44 and 515.35 [M + H + CH<sub>3</sub>CN]<sup>+</sup>, 946.30 and 948.34 [2M + H]<sup>+</sup>, *t*<sub>R</sub> = 12.40 min, 99.7% pure (UV).

**5-Bromo-2-(4-bromo-3-(*N,N*-diethylsulfamoyl)benzamido)benzoic acid (47)** The title compound was synthesized from methyl 5-bromo-2-(4-bromo-3-(*N,N*-diethylsulfamoyl)benzamido)benzoate (**47a**, 145 mg, 0.26 mmol) according to General Procedure D, using THF/MeOH 2/1 (3 mL) and 1N NaOH (aq., 1 mL). The solution was acidified with 1N HCl (aq., 2 mL). The organic solvent was evaporated under reduced pressure. The solid was isolated by suction filtration, washed with water and dried under reduced pressure: 110 mg, 78% yield; mp: 218.6-220.0 °C; <sup>1</sup>H NMR (500 MHz, DMSO-*d*<sub>6</sub>): δ 1.07 (t, *J* = 7.1 Hz, 6H), 3.37 (q, *J* = 7.1 Hz, 4H), 7.85 (dd, *J* = 9.1, 2.5 Hz, 1H), 8.02 (dd, *J* = 8.2, 2.5 Hz, 1H), 8.11 (d, *J* = 8.2 Hz, 1H), 8.11 (d, *J* = 2.5 Hz), 8.51 (d, *J* = 2.2 Hz, 1H), 8.55 (d, *J* = 8.8 Hz, 1H), 12.18 (bs, 1H); <sup>13</sup>C NMR (125 MHz, DMSO-*d*<sub>6</sub>): δ 13.78, 41.25, 114.99, 119.59, 122.44, 123.75, 129.52, 131.99, 133.23, 133.82, 136.60, 136.68, 139.57, 140.10, 162.67, 168.62; LC/MS: *m/z* = 532.38 and 534.07 [M + H]<sup>+</sup>, 575.22 and 577.26 [M + H + CH<sub>3</sub>CN]<sup>+</sup>, *t*<sub>R</sub> = 13.36 min, 98.7% pure (UV).

**4-(3-(*N,N*-Diethylsulfamoyl)benzamido)-[1,1'-biphenyl]-3-carboxylic acid (48)** The title compound was synthesized from methyl 4-(3-(*N,N*-diethylsulfamoyl)benzamido)-[1,1'-biphenyl]-3-carboxylate (**48a**, 84 mg, 0.18 mmol) according to General Procedure D, using THF/MeOH 2/1 (1.5 mL) and 1N NaOH (aq., 0.42 mL). The solution was acidified with 1N HCl (aq., 1 mL). The organic solvent was evaporated under reduced pressure. The solid was isolated by suction filtration, washed with water and dried under reduced pressure: 60 mg, 74% yield; mp: 217.6-219.2 °C; <sup>1</sup>H NMR (500 MHz, DMSO-*d*<sub>6</sub>): δ 1.07 (t, *J* = 7.1 Hz, 6H), 3.23 (q, *J* = 7.1 Hz, 4H), 7.39 (t, *J* = 7.4 Hz, 1H), 7.49 (t, *J* = 7.6 Hz, 2H), 7.70 (d, *J* = 7.3 Hz, 2H), 7.84 (t, *J* = 7.9 Hz, 1H), 8.01 (dd, *J* = 8.7, 2.5 Hz, 1H), 8.06 (m, 1H), 8.23 (m, 1H), 8.30 (d, *J* = 2.5 Hz, 1H), 8.35 (m, 1H), 8.76 (d, *J* = 8.8 Hz, 1H), 12.32 (s, 1H); <sup>13</sup>C NMR (125 MHz, DMSO-*d*<sub>6</sub>): δ 14.12, 41.97, 117.64, 120.77, 124.95, 126.36, 127.63, 128.91, 129.07, 130.02, 130.47, 131.08, 132.28, 134.96, 135.39, 138.60, 139.86, 140.67, 163.16, 169.95; LC/MS: *m/z* = 493.75 [M + H + CH<sub>3</sub>CN]<sup>+</sup>, 904.57 [2M + H]<sup>+</sup>, *t*<sub>R</sub> = 13.49 min, 99.8% pure (UV).

**2-(3-(*N,N*-Diethylsulfamoyl)benzamido)-6-methoxybenzoic acid (49)** The title compound was synthesized from methyl 2-(3-(*N,N*-diethylsulfamoyl)benzamido)-6-methoxybenzoate (**49a**) according to General Procedure D, using THF/MeOH 2/1 (3 mL) and 1N NaOH (aq., 1 mL). 1N HCl (aq., 2 mL) was added and the organic solvent was evaporated under reduced pressure. The precipitate was isolated by suction filtration and crystallized from MeOH (2 mL) containing a small amount of water (0.5 mL). The white solid was isolated by suction filtration, washed with cold MeOH/water 1/1 and dried under reduced pressure: 110 mg, 27% yield over 2 steps; mp: 133.8-136.4 °C; <sup>1</sup>H NMR (500 MHz, DMSO-*d*<sub>6</sub>): δ 1.06 (t, *J* = 7.1 Hz, 6H), 3.21 (q, *J* = 7.1 Hz, 4H), 3.83 (s, 3H), 7.01 (d, *J* = 8.2 Hz, 1H), 7.29 (d, *J* = 7.9 Hz, 1H), 7.46 (t, *J* = 8.2 Hz, 1H), 7.77 (t, *J* = 7.7 Hz, 1H), 8.01 (d, *J* = 7.9 Hz, 1H), 8.17 (d, *J* = 7.9 Hz, 1H), 8.29 (s, 1H), 10.58 (s, 1H), 12.99 (bs, 1H); <sup>13</sup>C NMR (125 MHz, DMSO-*d*<sub>6</sub>): δ 14.16, 41.95, 56.04, 109.14, 117.60, 118.58, 125.50, 129.63, 129.90, 130.95, 131.42, 135.29, 136.40, 140.30, 157.24, 163.92, 167.25; LC/MS: *m/z* = 406.64 [M + H]<sup>+</sup>, 429.69 [M - OH + CH<sub>3</sub>CN]<sup>+</sup>, 812.53 [2M + H]<sup>+</sup>, *t*<sub>R</sub> = 11.05 min, 96.1% pure (UV).

**2-Chloro-6-(3-(*N,N*-diethylsulfamoyl)benzamido)benzoic acid (50)** The title compound was synthesized from methyl 2-chloro-6-(3-(*N,N*-diethylsulfamoyl)benzamido)benzoate (**50a**) according to General Procedure D, using THF/MeOH 2/1 (6 mL) and 1N NaOH (aq., 2 mL). The organic solvent was evaporated under reduced pressure. 1N HCl (aq., 4 mL) was added. A thick gum was formed. The water was decanted and MeOH (2 mL) was added to the residue. The mixture was stirred at room temperature yielding a white solid, which was crystallized from EtOH: 31 mg, 8% yield over 2 steps; mp: 184.3-186.3 °C; <sup>1</sup>H NMR (500 MHz, DMSO-*d*<sub>6</sub>): δ 1.06 (t, *J* = 7.1 Hz, 6H), 3.21 (q, *J* = 7.1 Hz, 4H), 7.22 (dd, *J* = 8.0, 1.1 Hz, 1H), 7.33 (t, *J* = 8.2 Hz, 1H), 7.78 (t, *J* = 7.7 Hz, 1H), 8.01 (m, 1H), 8.06 (br.d, 1H), 8.18 (m, 1H), 8.30 (t, *J* = 1.6 Hz, 1H), 12.17 (bs, 1H); <sup>13</sup>C NMR (125 MHz, DMSO-*d*<sub>6</sub>): δ 14.13, 41.96, 120.62, 125.53, 125.75, 129.17, 129.68, 130.07, 130.87, 131.21, 135.42, 137.51, 140.52, 163.10, 166.80; LC/MS: *m/z* = 410.61 and 412.66 [M + H]<sup>+</sup>, 822.55 [2M + H]<sup>+</sup>, *t*<sub>R</sub> = 10.90 min, 96.1% pure (UV).

**2-(3-(*N,N*-Diethylsulfamoyl)benzamido)-6-fluorobenzoic acid (51)** The title compound was synthesized from methyl 2-(3-(*N,N*-diethylsulfamoyl)benzamido)-6-fluorobenzoate (**51a**, 170 mg, 0.42 mmol) according to General Procedure D, using THF/MeOH 2/1 (3 mL) and 1N NaOH (aq., 1 mL). The solution was acidified with 1N HCl (aq., 2 mL). Water was added and the solid was isolated by suction filtration, washed with water and dried under reduced pressure: 152 mg, 93% yield; mp: 213.1-215.5 °C; <sup>1</sup>H NMR (500 MHz, DMSO-*d*<sub>6</sub>): δ 1.07 (t, *J* = 7.1 Hz, 6H), 3.22 (q, *J* = 7.1 Hz, 4H), 7.15 (dd, *J* = 9.8, 8.8 Hz, 1H), 7.60 (dd, *J* = 8.2, 6.3 Hz, 1H), 7.80 (t, *J* = 7.9 Hz, 1H), 7.83 (d, *J* = 8.5 Hz, 1H), 8.04 (d, *J* = 7.9 Hz, 1H), 8.20 (d, *J* = 7.9 Hz, 1H), 8.31 (s, 1H), 11.23 (s, 1H), 13.70 (bs, 1H); <sup>13</sup>C NMR (125 MHz, DMSO-*d*<sub>6</sub>): δ 14.06, 41.87, 112.37 (d, *J*<sub>CF</sub> = 23 Hz), 113.52 (d, *J*<sub>CF</sub> = 16 Hz), 119.22 (d, *J*<sub>CF</sub> = 4 Hz), 125.29, 130.05, 131.32, 132.86 (*J*<sub>CF</sub> = 11 Hz), 135.05, 138.75 (d, *J*<sub>CF</sub> = 5 Hz), 160.46 (d, *J*<sub>CF</sub> = 252 Hz), 163.70, 165.88; LC/MS: *m/z* = 394.71 [M + H]<sup>+</sup>, 788.78 [2M + H]<sup>+</sup>, *t*<sub>R</sub> = 11.79 min, 99.6% pure (UV).

**2-(3-(*N,N*-Diethylsulfamoyl)benzamido)-6-hydroxybenzoic acid (52)** The title compound was synthesized from methyl 2-(3-(*N,N*-diethylsulfamoyl)benzamido)-6-hydroxybenzoate (**52a**, 120 mg, 0.42 mmol) according to General Procedure D, using THF/MeOH 2/1 (3 mL) and 1N NaOH (aq., 1 mL). The solution was acidified with 1N HCl (aq., 3 mL) and extracted with dichloromethane (three times). The combined organic extracts were dried over sodium sulfate, filtered and evaporated under reduced pressure, yielding a slightly yellow oil that solidified upon standing. The product was crystallized from MeOH: 75 mg, 65% yield; mp: 175.8-176.7 °C; <sup>1</sup>H NMR (500 MHz, DMSO-*d*<sub>6</sub>): δ 1.06 (t, *J* = 7.1 Hz, 6H), 3.22 (q, *J* = 7.1 Hz, 4H), 6.71 (dd, *J* = 8.2, 0.9 Hz, 1H), 7.39 (t, *J* = 8.2 Hz, 1H), 7.79 (t, *J* = 7.9 Hz, 1H), 7.82 (dd, *J* = 8.2, 1.3 Hz, 1H), 8.02 (ddd, *J* = 7.9, 1.9, 0.9 Hz, 1H), 8.19 (ddd, *J* = 7.9, 1.9, 1.3 Hz, 1H), 8.30, (t, *J* = 1.7 Hz, 1H), 10.87 (bs, 2H), 12.14 (s, 1H); <sup>13</sup>C NMR (125 MHz, DMSO-*d*<sub>6</sub>): δ 14.12, 41.93, 106.98, 112.13, 112.80, 125.20, 129.69, 130.16, 130.99, 133.38, 135.84, 139.84, 140.53, 160.93, 163.20, 171.45; LC/MS: *m/z* = 392.88 [M + H]<sup>+</sup>, 433.92 [M + H + CH<sub>3</sub>CN]<sup>+</sup>, 784.83 [2M + H]<sup>+</sup>, *t*<sub>R</sub> = 10.51 min, 97.5% pure (UV).

**3'-Carbamoyl-4-(3-(*N,N*-diethylsulfamoyl)benzamido)-[1,1'-biphenyl]-3-carboxylic acid (53)** A solution of methyl 5-bromo-2-(3-(*N,N*-diethylsulfamoyl)benzamido)benzoate (**45a**, 219 mg, 0.48 mmol), (3-carbamoylphenyl)boronic acid (119 mg, 0.72 mmol) and cesium carbonate (470 mg, 1.44 mmol) in a mixture of DME/water 1/1 (20 mL) was degassed. A catalytic amount of tetrakis(triphenylphosphine)palladium was added. The reaction flask was put into a pre-heated oil bath (120 °C) and heated for 3.5 h under a nitrogen atmosphere. After cooling to room temperature water was added and the solution was acidified with 1N HCl (aq.). The white solid was isolated by suction filtration, washed with water and briefly heated to reflux with a few mL's of methanol. The solids were isolated by suction filtration, washed with a small amount of methanol and dried under reduced pressure to yield the title compound (182 mg, 76% yield); mp: 259.3-259.8 °C (dec.); <sup>1</sup>H NMR (500 MHz, DMSO-*d*<sub>6</sub>): δ 1.07 (t, *J* = 7.1 Hz, 6H), 3.23 (q, *J* = 7.1 Hz, 4H), 7.46 (bs, 1H), 7.57 (t, *J* = 7.7 Hz, 1H), 7.83-7.90 (m, 3H), 8.06-8.09 (m, 2H), 8.17 (bs, 1H), 8.21 (t, *J* = 1.6 Hz, 1H), 8.24 (dt, *J* =

7.6, 1.3 Hz, 1H), 8.35 (t,  $J = 1.7$  Hz, 1H), 8.38 (d,  $J = 2.2$  Hz, 1H), 8.78 (d,  $J = 8.8$  Hz, 1H), 12.37 (bs, 1H), 14.06 (bs, 1H);  $^{13}\text{C}$  NMR (125 MHz, DMSO- $d_6$ ):  $\delta$  14.12, 41.97, 117.80, 120.80, 124.97, 125.31, 126.75, 129.07, 129.10, 130.04, 130.46, 131.09, 132.40, 134.35, 135.03, 135.38, 138.58, 140.07, 140.67, 163.19, 167.67, 169.95; LC/MS:  $m/z = 495.99$  [M + H] $^+$ , 436.84 [M + H + CH<sub>3</sub>CN] $^+$ , 990.95 [2M + H] $^+$ ,  $t_R = 11.23$  min, 95.7% pure (UV).

**4'-Carbamoyl-4-(3-(*N,N*-diethylsulfamoyl)benzamido)-[1,1'-biphenyl]-3-carboxylic acid (54)** A solution of methyl 5-bromo-2-(3-(*N,N*-diethylsulfamoyl)benzamido)benzoate (**43a**, 341 mg, 0.75 mmol), (4-carbamoylphenyl)boronic acid (186 mg, 1.13 mmol) and cesium carbonate (733 mg, 2.25 mmol) in a mixture of DME/water 1/1 (15 mL) was degassed. A catalytic amount of tetrakis(triphenylphosphine)palladium was added. The reaction flask was put into a pre-heated oil bath (100 °C) and heated for 3.5 h under a nitrogen atmosphere. After cooling to room temperature water (15 mL) was added and the solution was filtered over a thin layer of Celite. The filtrate was acidified with 1N HCl (aq.). The white solid was isolated by suction filtration, washed twice with water and heated to reflux with methanol (30 mL). After cooling to room temperature the solids were isolated by centrifugation and dried under reduced pressure to yield the title compound (224 mg, 60% yield); mp: 282-285 °C;  $^1\text{H}$  NMR (500 MHz, DMSO- $d_6$ ):  $\delta$  1.07 (t,  $J = 7.1$  Hz, 6H), 3.24 (q,  $J = 7.1$  Hz, 4H), 7.40 (bs, 1H), 7.81 (d,  $J = 8.5$  Hz, 2H), 7.85 (t,  $J = 7.9$  Hz, 1H), 7.99 (d,  $J = 8.5$  Hz, 2H), 8.04 (bs, 1H), 8.08 (m, 2H), 8.24 (ddd,  $J = 7.6, 1.9, 1.0$  Hz, 1H), 8.35 (t,  $J = 1.6$  Hz, 1H), 8.37 (d,  $J = 2.5$  Hz, 1H), 8.78 (d,  $J = 8.8$  Hz, 1H), 12.41 (bs, 1H);  $^{13}\text{C}$  NMR (125 MHz, DMSO- $d_6$ ):  $\delta$  14.61, 42.46, 118.24, 121.28, 125.46, 126.60, 128.79, 129.61, 130.56, 130.97, 131.59, 132.94, 133.70, 134.43, 135.84, 140.79, 141.18, 141.61, 163.70, 167.92, 170.38; LC/MS:  $m/z = 495.97$  [M + H] $^+$ , 536.89 [M + H + CH<sub>3</sub>CN] $^+$ , 991.01 [2M + H] $^+$ ,  $t_R = 11.12$  min, 97.8% pure (UV).

**4-(3-(*N,N*-diethylsulfamoyl)benzamido)-[1,1'-biphenyl]-3,3'-dicarboxylic acid (55)** A solution of methyl 5-bromo-2-(3-(*N,N*-diethylsulfamoyl)benzamido)benzoate (**43a**, 341 mg, 0.75 mmol), (3-carboxyphenyl)boronic acid (187 mg, 1.13 mmol) and cesium carbonate (733 mg, 2.25 mmol) in a mixture of DME/water 1/1 (15 mL) was degassed. A catalytic amount of tetrakis(triphenylphosphine)palladium was added. The reaction flask was put into a pre-heated oil bath (100 °C) and heated for 3.5 h under a nitrogen atmosphere. After cooling to room temperature water (15 mL) was added and the solution was filtered over a thin layer of Celite. The filtrate was acidified with 1N HCl (aq.). The white solid was isolated by suction filtration, washed twice with water and heated to reflux with methanol (30 mL). After cooling to room temperature the solids were isolated by centrifugation and dried under reduced pressure to yield the title compound (235 mg, 63% yield); mp: 265.8-267.3 °C;  $^1\text{H}$  NMR (500 MHz, DMSO- $d_6$ ):  $\delta = 1.07$  (t,  $J = 7.1$  Hz, 6H), 3.23 (q,  $J = 7.1$  Hz, 4H), 7.62 (t,  $J = 7.7$  Hz, 1H), 7.84 (t,  $J = 7.7$  Hz, 1H), 7.94-7.98 (m, 2H), 8.04-8.07 (m, 2H), 8.21 (t,  $J = 1.7$  Hz, 1H), 8.23 (m, 1H), 8.32 (d,  $J = 2.2$  Hz, 1H), 8.35 (t,  $J = 1.6$  Hz, 1H), 8.78 (d,  $J = 8.8$  Hz, 1H), 12.33 (s, 1H), 13.15 (bs, 1H), 14.04 (bs, 1H);  $^{13}\text{C}$  NMR (125 MHz, DMSO- $d_6$ ):  $\delta = 14.12, 41.97, 117.69, 120.87, 124.96, 126.87, 128.40, 128.99, 129.48, 130.04, 130.46, 130.76, 131.09, 131.59,$



132.39, 133.93, 135.35, 138.91, 140.23, 140.67, 163.19, 167.13, 169.85; LC/MS:  $m/z = 496.90 [M + H]^+$ , 537.77  $[M + H + CH_3CN]^+$ , 992.79  $[2M + H]^+$ ,  $t_R = 12.02$  min, 95.1% pure (UV).

**4-(3-(*N,N*-diethylsulfamoyl)benzamido)-[1,1'-biphenyl]-3,4'-dicarboxylic acid (56)** The title compound was synthesized from methyl 5-bromo-2-(3-(*N,N*-diethylsulfamoyl)benzamido)benzoate (**43a**, 341 mg, 0.75 mmol) and (4-carboxyphenyl)boronic acid (187 mg, 1.13 mmol) using the same procedure as described for compound **55**. The product was purified by heating with methanol, filtered and isolated as a white solid: 251 mg, 67%; mp: 282.4-283.3 °C;  $^1H$  NMR (500 MHz, DMSO- $d_6$ ):  $\delta$  = 1.07 (t,  $J = 7.1$  Hz, 6H), 3.23 (q,  $J = 7.1$  Hz, 4H), 7.83-7.87 (m, 3H), 8.03-8.09 (m, 4H), 8.23 (d,  $J = 7.9$  Hz, 1H), 8.34 (d,  $J = 1.7$  Hz, 1H), 8.39 (d,  $J = 2.2$  Hz, 1H), 8.79 (d,  $J = 8.5$  Hz, 1H), 12.37 (s, 1H), 13.02 (bs, 1H);  $^{13}C$  NMR (125 MHz, DMSO- $d_6$ ):  $\delta$  14.12, 41.97, 117.64, 120.76, 124.95, 126.42, 129.23, 129.70, 130.07, 130.46, 131.09, 132.52, 133.62, 135.30, 140.53, 140.67, 142.61, 163.20, 167.03, 169.85; LC/MS:  $m/z = 537.70 [M + H^+ CH_3CN]$ , 992.84  $[2M + H^+]$ ,  $t_R = 11.07$  min, 96.6% pure (UV).

**2-(3-Sulfamoylbenzamido)benzoic acid (57)** The title compound was synthesized from methyl 2-(3-sulfamoylbenzamido)benzoate (**57a**, 220 mg, 0.66 mmol) according to General Procedure D, using THF/MeOH 2/1 (3 mL) and 1N NaOH (aq., 1 mL). After stirring for 2 days at room temperature 1N HCl (aq., 4 mL) was added and stirring continued overnight. The solid was isolated by suction filtration, washed with water and dried under reduced pressure: 176 mg, 84% yield; mp: 224-234 °C;  $^1H$  NMR (500 MHz, DMSO- $d_6$ ):  $\delta$  7.24 (m, 1H), 7.36 (s, 2H), 7.69 (m, 1H), 7.82 (t,  $J = 7.9$  Hz, 1H), 8.07 (m, 2H), 8.16 (m, 1H), 8.44 (t,  $J = 1.7$  Hz, 1H), 8.67 (dd,  $J = 8.5, 1.0$  Hz, 1H), 12.28 (s, 1H);  $^{13}C$  NMR (125 MHz, DMSO- $d_6$ ):  $\delta$  117.01, 120.19, 123.37, 124.51, 129.06, 129.90, 129.93, 131.24, 134.31, 135.11, 140.65, 144.95, 163.44, 170.02; LC/MS:  $m/z = 361.78 [M + H + CH_3CN]^+$ , 640.62  $[2M + H]^+$ ,  $t_R = 8.75$  min, 95.3% pure (UV).

**2-(3-(*N,N*-Dimethylsulfamoyl)benzamido)benzoic acid (58)** The title compound was synthesized from methyl 2-(3-(*N,N*-dimethylsulfamoyl)benzamido)benzoate (**58a**, 100 mg, 0.28 mmol) according to General Procedure D, using THF/MeOH 2/1 (1.5 mL) and 1N NaOH (aq., 0.5 mL). The solution was acidified with 1N HCl (aq., 1 mL). Water was added and the solution was extracted with ethyl acetate (three times). The combined organic extracts were washed with 1N HCl (aq.), dried over sodium sulfate, filtered and evaporated under reduced pressure. The residue was stirred with a small amount of water. The solid was isolated by suction filtration, washed with water and dried under reduced pressure: 44 mg, 46% yield; mp: 226.6-229.5 °C;  $^1H$  NMR (500 MHz, DMSO- $d_6$ ):  $\delta$  2.68 (s, 6H), 7.25 (dt,  $J = 7.6, 1.3$  Hz, 1H), 7.69 (dt,  $J = 7.9, 1.6$  Hz, 1H), 7.89 (t,  $J = 8.0$  Hz, 1H), 8.01 (dd,  $J = 7.9, 1.4$  Hz, 1H), 8.06 (dd,  $J = 7.9, 1.6$  Hz, 1H), 8.26 (m, 2H), 8.67 (dd,  $J = 8.5, 0.9$  Hz, 1H), 12.31 (bs, 1H), 13.89 (bs, 1H);  $^{13}C$  NMR (125 MHz, DMSO- $d_6$ ):  $\delta$  37.55, 117.08, 120.13, 123.41, 125.64, 130.42, 130.77, 131.27, 131.58, 134.31, 135.51, 135.65, 140.62, 163.18, 170.06; LC/MS:  $m/z = 389.69 [M + H + CH_3CN]^+$ , 696.57  $[2M + H]^+$ ,  $t_R = 10.35$  min, 98.4% pure (UV).

**2-(3-(*N,N*-Dipropylsulfamoyl)benzamido)benzoic acid (59)** The title compound was synthesized from methyl 2-(3-(*N,N*-dipropylsulfamoyl)benzamido)benzoate (**59a**, 217 mg, 0.52 mmol) according to General Procedure D, using THF/MeOH 2/1 (3 mL) and 1N NaOH (aq., 1 mL). The solution was acidified with 1N HCl (aq., 2 mL). Water was added and the solid was isolated by suction filtration, washed with water and dried under reduced pressure: 195 mg, 93% yield; mp: 213.0-213.8 °C; <sup>1</sup>H NMR (500 MHz, DMSO-*d*<sub>6</sub>): δ 0.81 (t, *J* = 7.4 Hz, 6H), 1.49 (sextet, *J* = 7.4 Hz, 4H), 3.08 (t, *J* = 7.6 Hz, 4H), 7.24 (t, *J* = 7.6 Hz, 1H), 7.68 (dt, *J* = 7.7, 1.4 Hz, 1H), 7.84 (t, *J* = 7.9 Hz, 1H), 8.06 (, 2H), 8.22 (d, *J* = 7.9 Hz, 1H), 8.33 (s, 1H), 8.67 (d, *J* = 8.2 Hz, 1H), 12.30 (bs, 1H), 13.86 (bs, 1H); <sup>13</sup>C NMR (125 MHz, DMSO-*d*<sub>6</sub>): δ 10.94, 21.57, 49.61, 117.06, 120.15, 123.38, 125.02, 130.04, 130.40, 131.00, 131.24, 134.29, 135.40, 140.42, 140.63, 163.18, 170.03. LC/MS: *m/z* = 445.78 [M + H + CH<sub>3</sub>CN]<sup>+</sup>, 808.72 [2M + H]<sup>+</sup>, *t*<sub>R</sub> = 13.20 min, 98.8% pure (UV).

**2-(3-(Pyrrolidin-1-ylsulfonyl)benzamido)benzoic acid (60)**<sup>S15</sup> The title compound was synthesized from methyl 2-(3-(pyrrolidin-1-ylsulfonyl)benzamido)benzoate (**60a**, 82 mg, 0.21 mmol) according to General Procedure D, using THF/MeOH 2/1 (1.5 mL) and 1N NaOH (aq., 0.42 mL). The solution was acidified with 1N HCl (aq., 1 mL). The solid was isolated by suction filtration, washed with water and dried under reduced pressure: 33 mg, 42% yield; mp: 226.6-227.8 °C; <sup>1</sup>H NMR (500 MHz, DMSO-*d*<sub>6</sub>): δ 1.67 (m, 4H), 3.20 (m, 4H), 7.25 (m, 1H), 7.69 (m, 1H), 7.87 (t, *J* = 7.9 Hz, 1H), 8.06 (m, 1H), 8.08 (m, 1H), 8.26 (m, 1H), 8.33 (m, 1H), 8.67 (dd, *J* = 8.5, 0.9 Hz, 1H), 12.3 (bs, 1H); <sup>13</sup>C NMR (125 MHz, DMSO-*d*<sub>6</sub>): δ 29.96, 53.14, 122.40, 125.36, 128.64, 130.67, 135.67, 135.76, 136.50, 136.70, 139.52, 140.69, 142.35, 145.87, 168.46, 175.29; LC/MS: *m/z* = 415.67 [M + H + CH<sub>3</sub>CN]<sup>+</sup>, 748.42 [2M + H]<sup>+</sup>, *t*<sub>R</sub> = 10.85 min, >99% pure (UV).

**2-(3-(Piperidin-1-ylsulfonyl)benzamido)benzoic acid (61)**<sup>S15</sup> The title compound was synthesized from methyl 2-(3-(piperidin-1-ylsulfonyl)benzamido)benzoate (**61a**, 146 mg, 0.36 mmol) according to General Procedure D, using THF/MeOH 2/1 (1.5 mL) and 1N NaOH (aq., 0.40 mL). The solution was acidified with 1N HCl (aq., 1 mL). The solid was isolated by suction filtration, washed with water and dried under reduced pressure: 50 mg, 48% yield; mp: 224.4-227.0 °C; <sup>1</sup>H NMR (500 MHz, DMSO-*d*<sub>6</sub>): δ 1.34 (m, 2H), 1.55 (m, 4H), 2.95 (m, 4H), 7.25 (dt, *J* = 7.6, 1.3 Hz, 1H), 7.69 (dt, *J* = 7.9, 1.6 Hz, 1H), 7.88 (t, *J* = 8.0 Hz, 1H), 7.99 (dd, 7.9, 1.4 Hz, 1H), 8.07 (dd, *J* = 7.9, 1.6 Hz, 1H), 8.26 (m, 2H), 8.67 (dd, *J* = 8.5, 0.9 Hz, 1H), 12.32 (bs, 1H), 13.88 (bs, 1H); <sup>13</sup>C NMR (125 MHz, DMSO-*d*<sub>6</sub>): δ 22.72, 24.65, 46.58, 117.10, 120.12, 123.41, 125.61, 130.39, 130.66, 131.27, 131.47, 134.31, 135.45, 136.45, 140.61, 163.16, 170.04; LC/MS: *m/z* = 429.72 [M + H + CH<sub>3</sub>CN]<sup>+</sup>, 776.56 [2M + H]<sup>+</sup>, *t*<sub>R</sub> = 11.72 min, 99.3% pure (UV).

**2-(3-(Azepan-1-ylsulfonyl)benzamido)benzoic acid (62)** The title compound was synthesized from methyl 2-(3-(azepan-1-ylsulfonyl)benzamido)benzoate (**62a**, 230 mg, 0.55 mmol) according to General Procedure D, using THF/MeOH 2/1 (3 mL) and 1N NaOH (aq., 1 mL). The solution was acidified with 1N HCl (aq., 2 mL). Water was added and the solid was isolated by suction filtration, washed with water and dried under reduced pressure: 209 mg, 94% yield; mp: 210.7-211.8 °C; <sup>1</sup>H

NMR (500 MHz, DMSO- $d_6$ ):  $\delta$  1.50 (m, 4H), 1.64 (m, 4H), 3.26 (t,  $J = 5.8$  Hz, 4H), 7.24 (dt,  $J = 7.6$ , 1.3 Hz, 1H), 7.68 (m, 1H), 7.84 (t,  $J = 7.7$  Hz, 1H), 8.04 (m, 1H), 8.07 (dd,  $J = 7.9$  Hz, 1H), 1.6 Hz, 1H), 8.22 (m, 1H), 8.31 (t,  $J = 1.7$  Hz, 1H), 8.66 (dd,  $J = 8.5$ , 0.9 Hz, 1H), 12.30 (bs, 1H), 13.87 (bs, 1H);  $^{13}\text{C}$  NMR (125 MHz, DMSO- $d_6$ ):  $\delta$  26.28, 28.52, 47.79, 117.09, 120.14, 123.38, 124.83, 129.91, 130.42, 131.07, 131.25, 134.28, 135.44, 139.85, 140.63, 163.19, 170.04; LCMS:  $m/z = 443.79$  [ $\text{M} + \text{H} + \text{CH}_3\text{CN}$ ] $^+$ , 804.62 [ $2\text{M} + \text{H}$ ] $^+$ ,  $t_{\text{R}} = 12.66$  min, 97.8% pure (UV).

**2-(3-(Morpholinosulfonyl)benzamido)benzoic acid (63)**<sup>S15</sup> The title compound was synthesized from methyl 2-(3-(morpholinosulfonyl)benzamido)benzoate (**63a**, 146 mg, 0.36 mmol) according to General Procedure D, using THF/MeOH 2/1 (3 mL) and 1N NaOH (aq., 1 mL). The solution was acidified with 1N HCl (aq., 1 mL). Water was added and the solution was extracted with ethyl acetate (three times). The combined organic extracts were washed with 1N HCl (aq.), dried over sodium sulfate, filtered and evaporated under reduced pressure. The residue was stirred with a small amount of water. The solid was isolated by suction filtration, washed with water and dried under reduced pressure: 85 mg, 60% yield; mp: 245-248 °C;  $^1\text{H}$  NMR (500 MHz, DMSO- $d_6$ ):  $\delta$  2.94 (m, 4H), 3.65 (m, 4H), 7.25 (dt,  $J = 7.6$ , 1.3 Hz, 1H), 7.69 (dt,  $J = 7.9$ , 1.6 Hz, 1H), 7.90 (t,  $J = 7.7$  Hz, 1H), 8.00 (dd, 7.9, 1.4 Hz, 1H), 8.07 (dd,  $J = 7.9$ , 1.6 Hz, 1H), 8.27 (m, 2H), 8.66 (dd,  $J = 8.5$ , 0.9 Hz, 1H), 12.34 (bs, 1H), 13.89 (bs, 1H);  $^{13}\text{C}$  NMR (125 MHz, DMSO- $d_6$ ):  $\delta$  45.88, 65.23, 117.24, 120.13, 123.42, 125.92, 130.51, 130.84, 131.26, 131.81, 134.25, 135.35, 135.68, 140.59, 163.15, 170.00; LC/MS:  $m/z = 431.70$  [ $\text{M} + \text{H} + \text{CH}_3\text{CN}$ ] $^+$ , 780.44 [ $2\text{M} + \text{H}$ ] $^+$ ,  $t_{\text{R}} = 10.23$  min, >99.9% pure (UV).

**2-(3-(*N*-Benzyl-*N*-ethylsulfamoyl)benzamido)benzoic acid (64)** The title compound was synthesized from methyl 2-(3-(*N*-benzyl-*N*-ethylsulfamoyl)benzamido)benzoate (**64a**, 118 mg, 0.26 mmol) according to General Procedure D, using THF/MeOH 2/1 (3 mL) and 1N NaOH (aq., 1 mL). The solution was acidified with 1N HCl (aq., 1 mL). Water was added and the solution was extracted with ethyl acetate (three times). The combined organic extracts were washed with 1N HCl (aq.), dried over sodium sulfate, filtered and evaporated under reduced pressure. The residue was stirred with a small amount of water. The solid was isolated by suction filtration, washed with water and dried under reduced pressure: 70 mg, 61% yield; mp: 182.0-183.9 °C;  $^1\text{H}$  NMR (500 MHz, DMSO- $d_6$ ):  $\delta$  0.86 (t,  $J = 7.1$  Hz, 3H), 3.19 (q,  $J = 7.1$  Hz, 2H), 4.40 (s, 2H), 7.25 (dt,  $J = 7.6$ , 1.3 Hz, 1H), 7.29 (m, 1H), 7.34 (m, 4H), 7.69 (dt,  $J = 7.9$ , 1.6 Hz, 1H), 7.86 (t,  $J = 8.0$  Hz, 1H), 8.06 (dd,  $J = 7.9$ , 1.6 Hz, 1H), 8.13 (m, 1H), 8.25 (m, 1H), 8.38 (t,  $J = 1.7$  Hz, 1H), 8.67 (dd,  $J = 8.5$ , 0.9 Hz, 1H), 12.31 (bs, 1H), 13.87 (bs, 1H);  $^{13}\text{C}$  NMR (125 MHz, DMSO- $d_6$ ):  $\delta$  13.49, , 42.74, 50.68, 117.17, 120.19, 123.42, 124.99, 127.54, 128.00, 128.43, 130.12, 130.52, 131.26, 131.31, 134.29, 135.54, 136.89, 140.52, 140.61, 163.16, 170.03. LC/MS:  $m/z = 438.73$  [ $\text{M} + \text{H}$ ] $^+$ , 479.66 [ $\text{M} + \text{H} + \text{CH}_3\text{CN}$ ] $^+$ , 876.53 [ $2\text{M} + \text{H}$ ] $^+$ ,  $t_{\text{R}} = 12.71$  min, 99.7% pure (UV).

### Biological Methods

**Expression and purification of recombinant PqsD from *E. coli* for STD NMR analysis.** Following the expression procedure described above, the cell pellet was resuspended in 80 mL binding buffer (20 mM sodium phosphate, pH 7.0, 50 mM NaCl, 5 mM MgCl<sub>2</sub>, 20 mM imidazole) and lysed by sonication for a total process time of 4.0 min. Cell debris were removed by centrifugation (18500 rpm, 40 min, 4 °C) and the supernatant was filtered through a syringe filter (0.20 μm). The clarified supernatant was immediately applied to a Ni-NTA column, washed with binding buffer and eluted with 20 mM sodium phosphate, pH 7.0, 50 mM NaCl and 250 mM imidazole. The protein containing fractions were buffer-exchanged into storage buffer (20 mM sodium phosphate, pH 7.0, 50 mM NaCl, 5 mM MgCl<sub>2</sub>) using a PD10 column. Subsequently the His-tag was removed by thrombin cleavage using 1 unit thrombin per mg protein in presence of 2.5 mM CaCl<sub>2</sub> for 16 h at 16 °C. The protein was separated from any uncleaved or His-containing protein by running the mixture through another Ni-NTA column under the same conditions as the first time. The cleaved protein was buffer-exchanged into storage buffer using a PD10 column and further purified by a HiLoad 16/600 Superdex 200 column and storage buffer as eluent. The protein containing fractions were pooled, concentrated using a Vivaspin 20, 10K MWCO to a final concentration of 377 μM and stored in aliquots at -80 °C.

**Synthesis of ethyl 3-oxodecanoate**<sup>S17</sup> At 0 °C octanoyl chloride (24 mL, 141 mmol) was added slowly by means of a syringe to a stirred solution of Meldrum's acid (20.0 g, 139 mmol), 4-dimethylaminopyridine (4.0 g, 32.7 mmol) in a mixture of pyridine (150 mL) and dichloromethane (350 mL). The cooling bath was removed and the reaction was stirred for 5½ h at room temperature. Dichloromethane (50 mL) was added and the solution was extracted with 2N aqueous HCl (4 x 250 mL). The organic layer was dried over sodium sulfate and evaporated under reduced pressure. The residue was dissolved in ethanol (150 mL) and refluxed overnight. The solvent was evaporated under reduced pressure. The product was purified by column chromatography (SiO<sub>2</sub>, petroleum ether/ethyl acetate 20/1) to give the title compound as a yellow oil: 25 g, 83% yield. <sup>1</sup>H NMR (500 MHz, CDCl<sub>3</sub>): δ 0.84 (t, *J* = 7.0 Hz, 3H), 1.23-1.28 (m, 11H), 1.54 (quintet, *J* = 7.0 Hz, 2H), 2.49 (t, *J* = 7.0 Hz, 2H), 3.39 (s, 2H), 4.16 (m, 2H).

*Primer sequence of mutations*

Mutant	Primer	
	forward 5' → 3'	reverse 3' → 5'
<b>S317 F</b>	GCTGGTCCTGACCTACGGT <u>TTT</u> GGCGC GACCTGGGGCG	CGCCCCAGGTCGCGCCA <u>AAA</u> ACCGTAG GTCAGGACCAGC
<b>C112 A</b>	GCTGGATATCCGGGCACAG <u>GCG</u> GAGCG GGTTGCTGTACG	CGTACAGCAACCCGCT <u>CGC</u> CTGTGCC CGGATATCCAGC
<b>H25 7F</b>	CGACCATGTGATCTGCT <u>TTT</u> CAACCGA ACCTGC	GCAGGTTTCGGTTG <u>AAAG</u> CAGATCACA TGGTCG

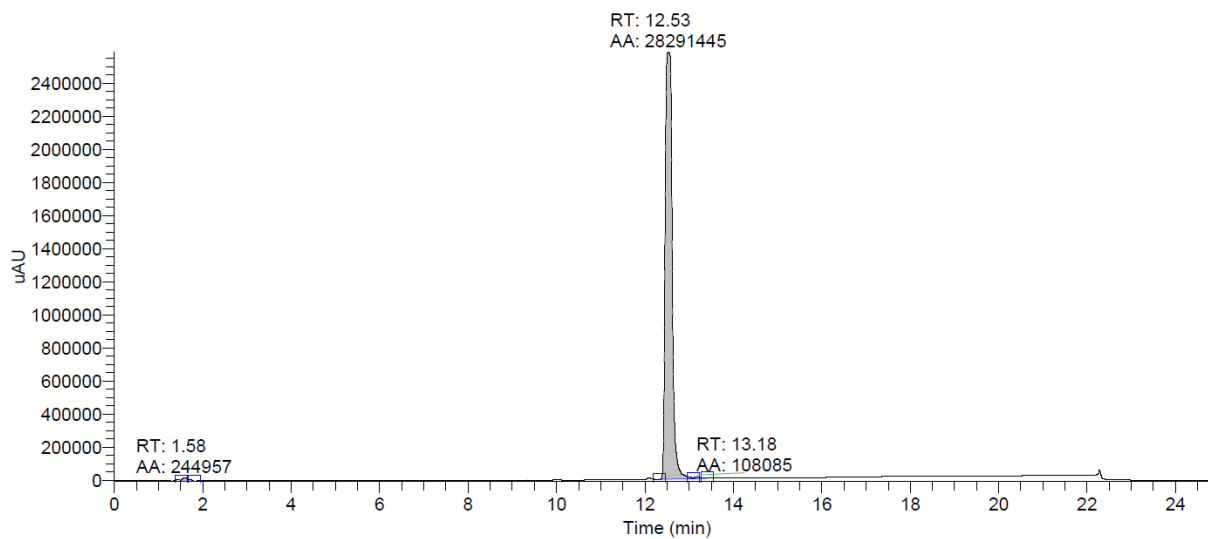
**References**

- (S1) Dolle, R. E.; Worm, K.; Zhou, Q. J. Sulfamoyl benzamide derivatives and methods of their use. U.S. Patent Application 2006/0079557 A1, Adolor Corporation, 2006.
- (S2) Kendall, J. D.; Giddens, A. C.; Yee Tsang, K.; Frédérick, R.; Marshall, E. S.; Singh, R.; Lill, C. L.; Lee, W.-J.; Kolekar, S.; Chao, M.; Malik, A.; Yu, S.; Chaussade, C.; Buchanan, C.; Rewcastle, G. W.; Baguley, B. C.; Flanagan, J. U.; Jamieson, S. M. F.; Denny, W. A.; Shepherd, P. R. Novel pyrazolo[1,5-a]pyridines as p110 $\alpha$ -selective PI3 kinase inhibitors: Exploring the benzenesulfonohydrazide SAR. *Bioorg. Med. Chem.* **2012**, *20*, 58–68.
- (S3) Ichinose, M.; Suematsu, H.; Yasutomi, Y.; Nishioka, Y.; Uchida, T.; Katsuki, T. Enantioselective intramolecular benzylic C-H bond amination: Efficient synthesis of optically active benzosultams. *Angew. Chem. Int. Ed.* **2011**, *50*, 9884–9887.
- (S4) Nie, Z.; Perretta, C.; Lu, J.; Su, Y.; Margosiak, S.; Gajiwala, K. S.; Cortez, J.; Nikulin, V.; Yager, K. M.; Appelt, K.; Chu, S. Structure-based design, synthesis, and study of potent inhibitors of  $\beta$ -ketoacyl-acyl carrier protein synthase III as potential antimicrobial agents. *J. Med. Chem.* **2005**, *48*, 1596–1609.
- (S5) Gaillard, P.; Quattropani, A.; Pomel, V.; Rueckle, T.; Klicic, J.; Church, D. Pyrazine derivatives and use as PI3K inhibitors. WO Patent Application 2007/023186 A1, Applied Research Systems ARS Holding N.V., 2007.
- (S6) Bernotas, R. C.; Singhaus, R.; Nagpal, S.; Thompson, C. Novel quinoline esters useful for treating skin disorders. WO Patent Application 2012/004748 A1, Wyeth LLC, 2012.
- (S7) Ji, J.; Lee, C.-H.; Sippy, K. B.; Li, T.; Gopalakrishnan, M. Novel 1,2,4 oxadiazole compounds and methods of use thereof. WO Patent Application 2009/148452, Abbott Laboratories, 2009.
- (S8) Armer, R. E.; Maillol, C. E. A.; Dorgan, C. R.; Wynne, G. M.; Vile, J. Compounds having CRTH2 antagonist activity. WO Patent Application 2009/093029, Oxagen Limited, 2009.
- (S9) Lang, H.-J.; Muschaweck, R. Thiazolidinderivate und Verfahren zu ihrer Herstellung. Ger. Offen. DE 2436263, February 12, 1976.
- (S10) Stiff, C. M.; Zhong, M.; Sarver, R. W.; Gao, H.; Andrea M. Ho, A. M.; Sweeney, M. T.; Zurenkod, G. E.; Romero, D. L. Correlation of carboxylic acid pK<sub>a</sub> to protein binding and antibacterial activity of a novel class of bacterial translation inhibitors. *Bioorg. Med. Chem. Lett.* **2007**, *17*, 5479–5482.
- (S11) Thorarensen, A.; Ruble, C. J.; Romero, D.L. Antibacterial agents. WO Patent Application 2004/018414 A2, Pharmacia & Upjohn Company, 2004.
- (S12) Castro Palomino Laria, J. L.; Terricabras Belart, E.; Erra Sola, M.; Navarro Romero, E.; Fonquerna Pou, S.; Cardus Figueras, A.; Lozoya Toribio, M. E. Azabiphenylaminobenzoic acid derivatives as DHODH inhibitors. WO Patent Application 2009/021696 A1, Laboratorios Almirall, S.A., 2009.

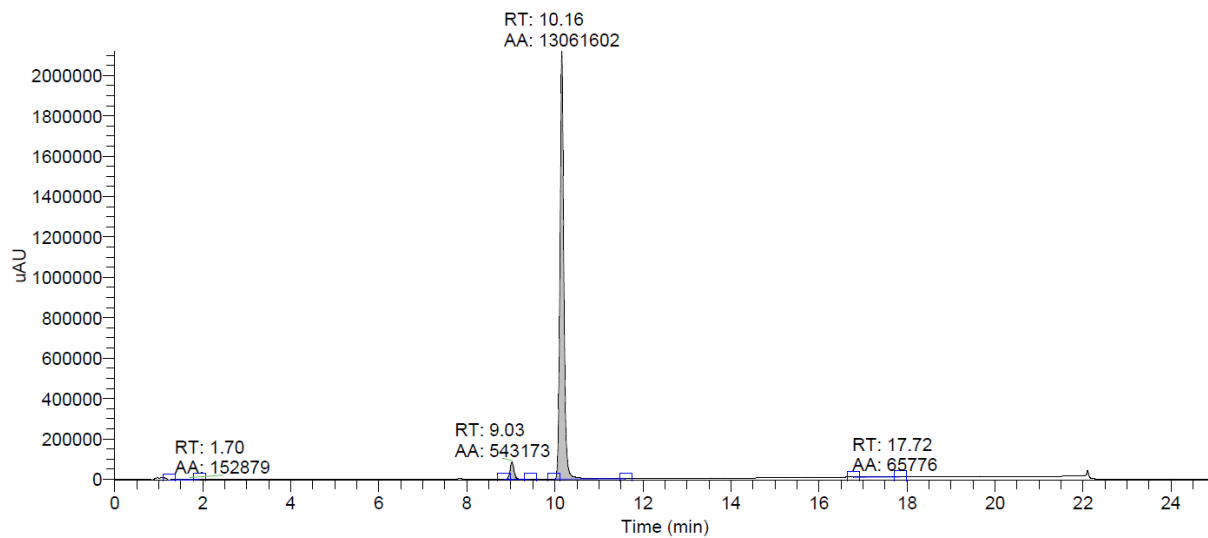
- (S13) Wall, M. J.; Player, M. R.; Patch, R. J.; Meegalla, S.; Liu, J.; Illig, C.R.; Chueng, W.; Chen, J.; Asgari, D. Quinolinone derivatives as inhibitors of C-FMS kinase. WO Patent Application 2005/009967 A2, Janssen Pharmaceutica, N.V., 2005.
- (S14) Andersen, H. S.; Olsen, O. H.; Iversen, L. F.; Sørensen, A. L. P.; Mortensen, S. B.; Christensen, M.S.; Branner, S.; Hansen, T.K.; Lau, J.F.; Jeppesen, L.; Moran, E.J.; Su, J.; Bakir, F.; Judge, L.; Shahbaz, M.; Collins, T.; Vo, T.; Newman, M. J.; Ripka, W. C.; Møller, N. P. H. Discovery and SAR of a Novel Selective and Orally Bioavailable Nonpeptide Classical Competitive Inhibitor Class of Protein-Tyrosine Phosphatase 1B *J. Med. Chem.* **2002**, *45*, 4443–4459.
- (S15) Ulven, T.; Frimurer, T.; Rist, Ø.; Kostenis, E.; Högberg, T. CRTH2 receptor ligands for therapeutic use. WO Patent Application 2005/115374 A1, 7TM Pharma A/S, 2005.
- (S16) Simon, E. J.; Shemin, D. The preparation of S-succinyl coenzyme. A. *J. Am. Chem. Soc.* **1953**, *75*, 2520.
- (S17) Kocieński, P. J.; Pelotier, B.; Pons, J.-M.; Prideaux, H. Asymmetric syntheses of panclicins A–E via [2+2] cycloaddition of alkyl(trimethylsilyl)ketenes to a  $\beta$ -silyloxyaldehyde. *J. Chem. Soc., Perkin Trans. 1* **1998**, 1373–1382.
- (S18) Cook, L.; Ternai, B.; Ghosh, P. Inhibition of human sputum elastase by substituted 2-pyrones. *J. Med. Chem.* **1987**, *30*, 1017–1023.

## LC/MS chromatograms (UV, 254 nm) of test compounds

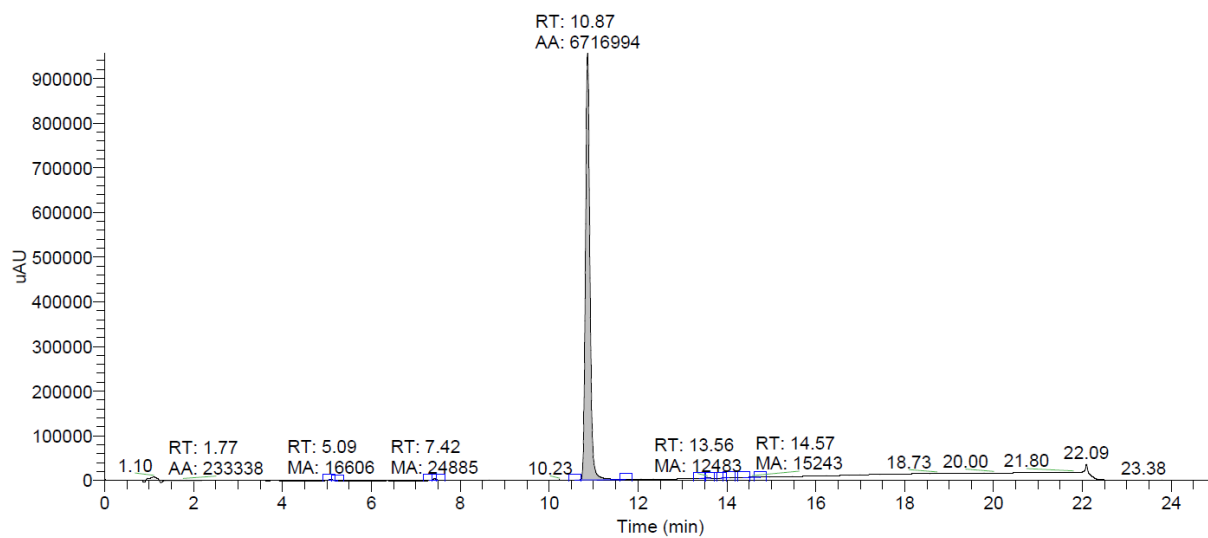
## Compound 2



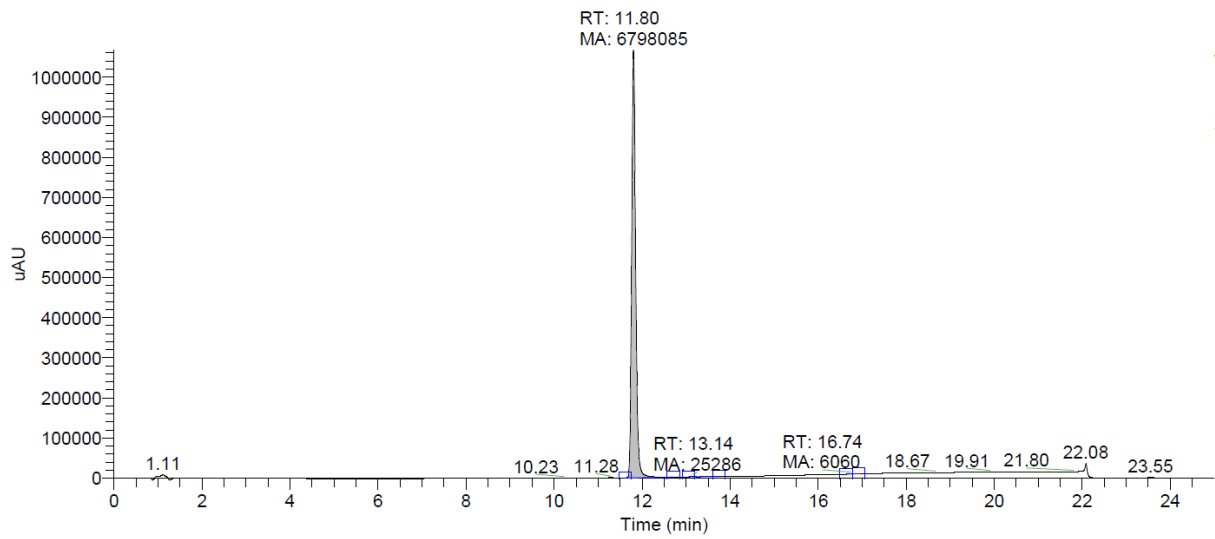
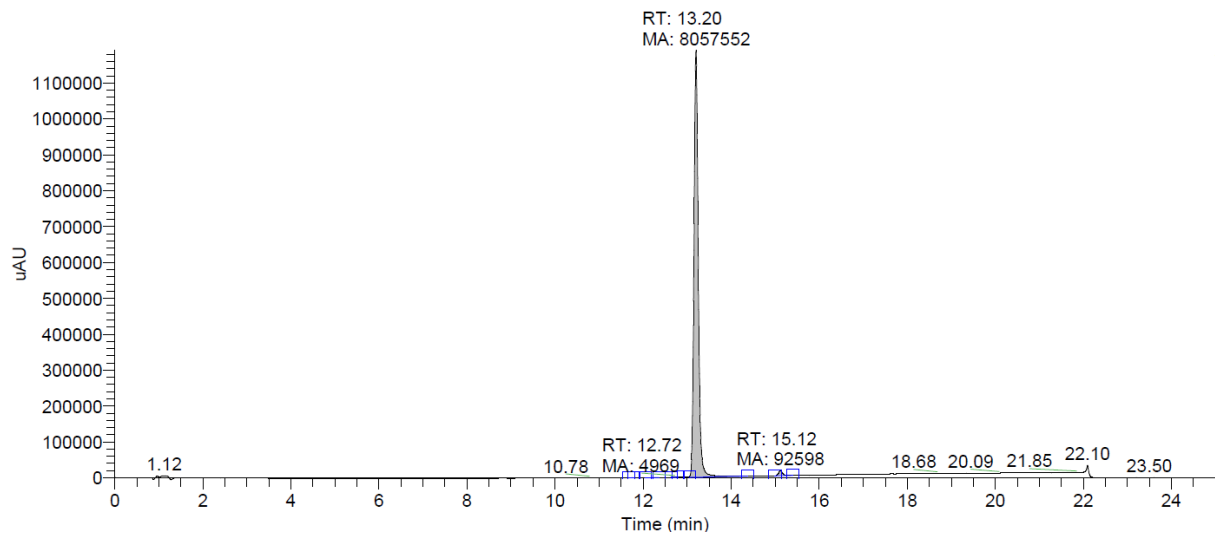
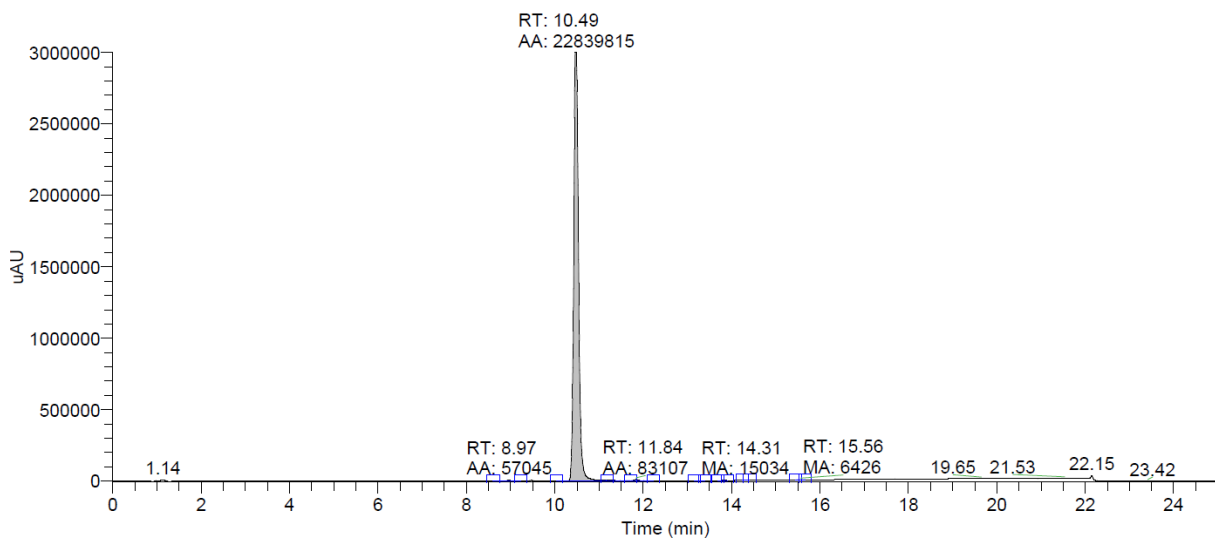
## Compound 4



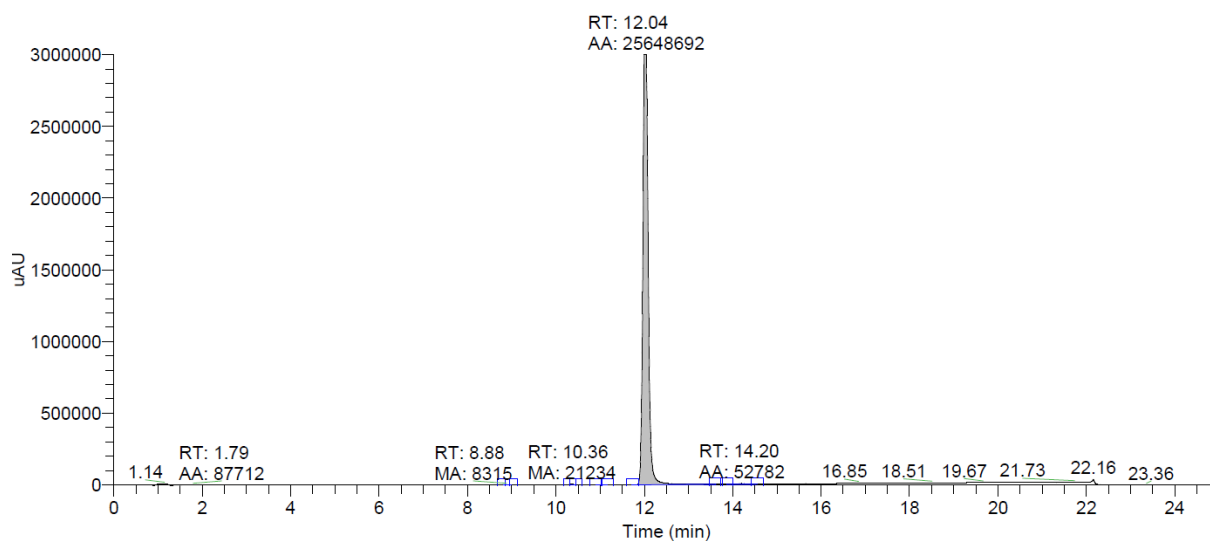
## Compound 6



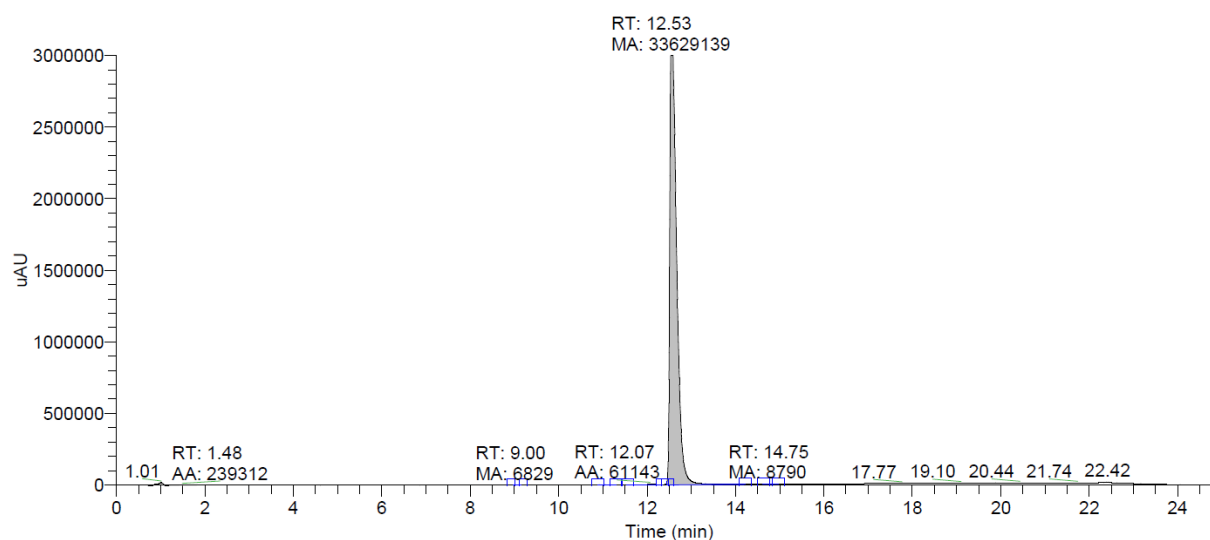


**Compound 9****Compound 10****Compound 13**

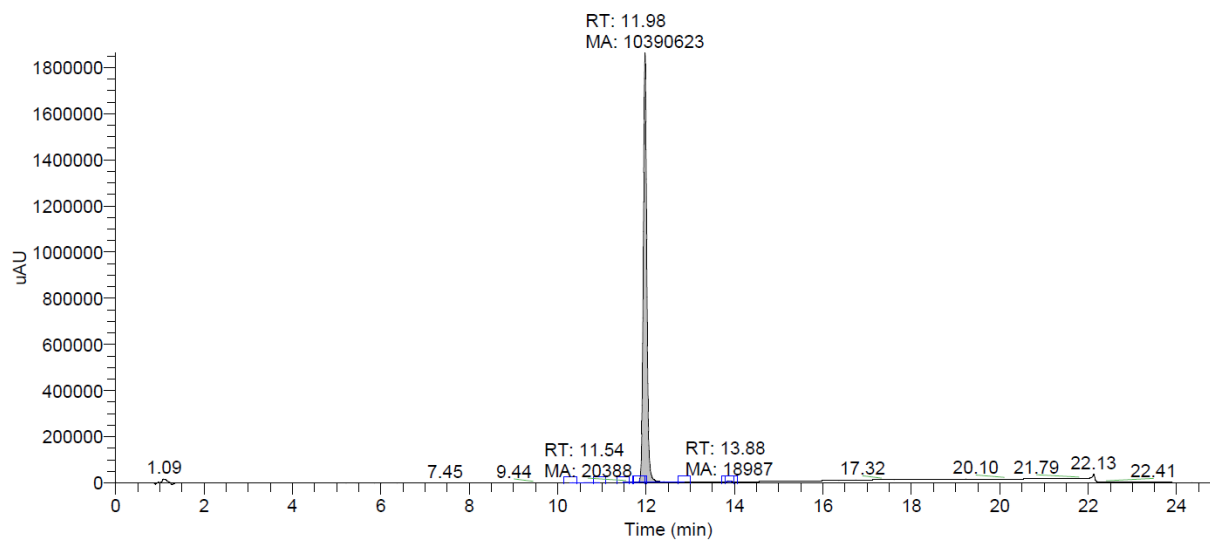
**Compound 14**

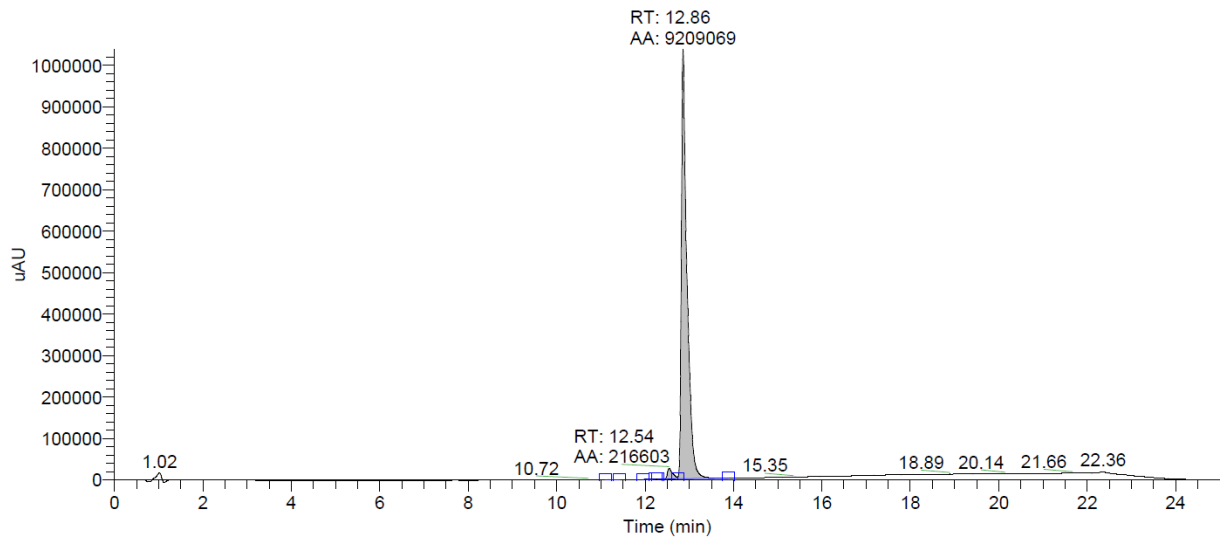
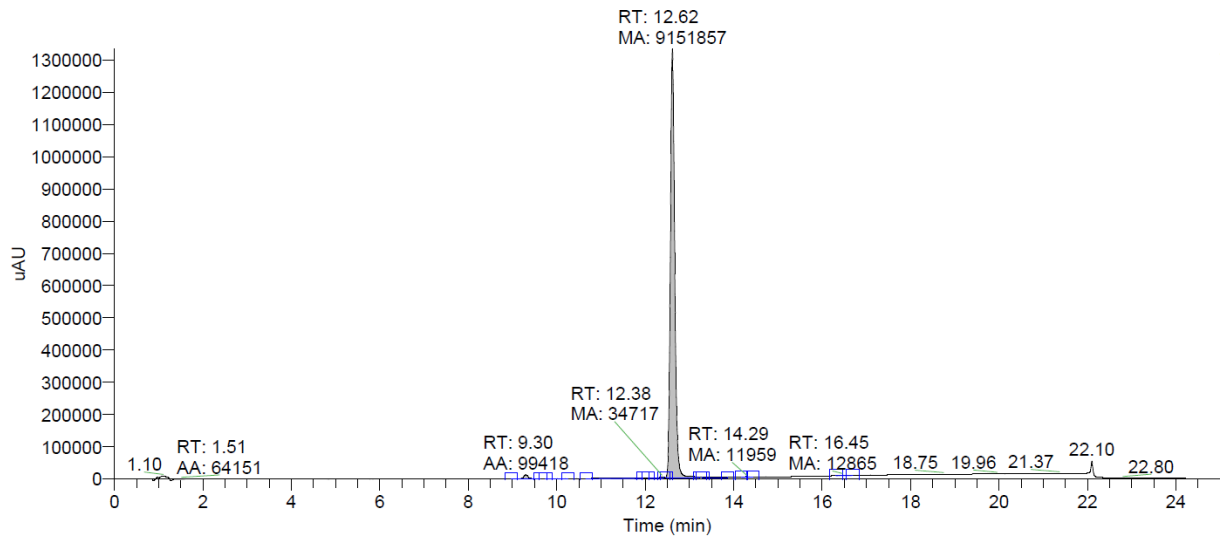
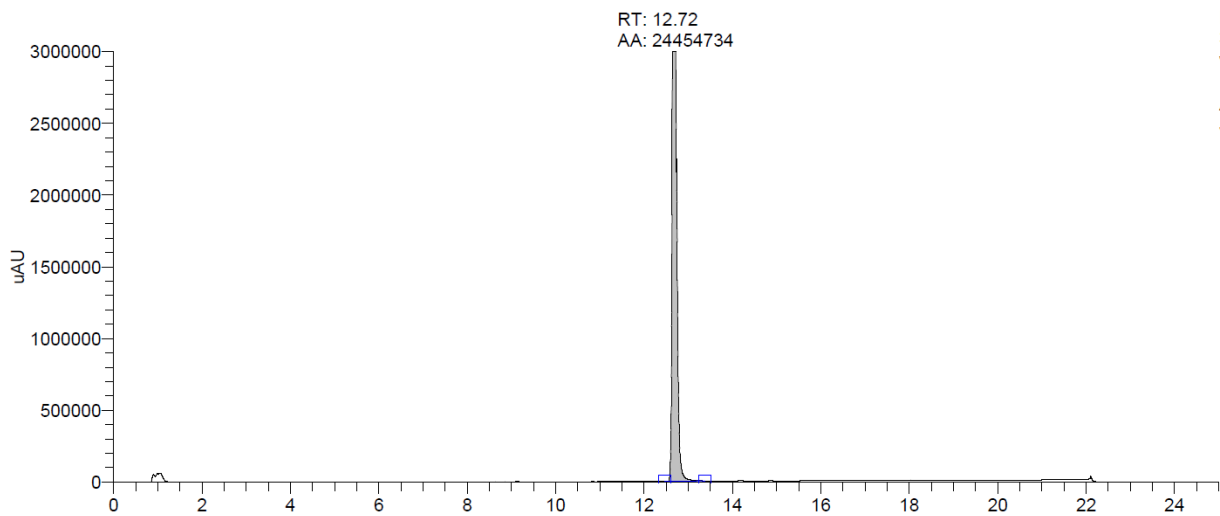


**Compound 34**

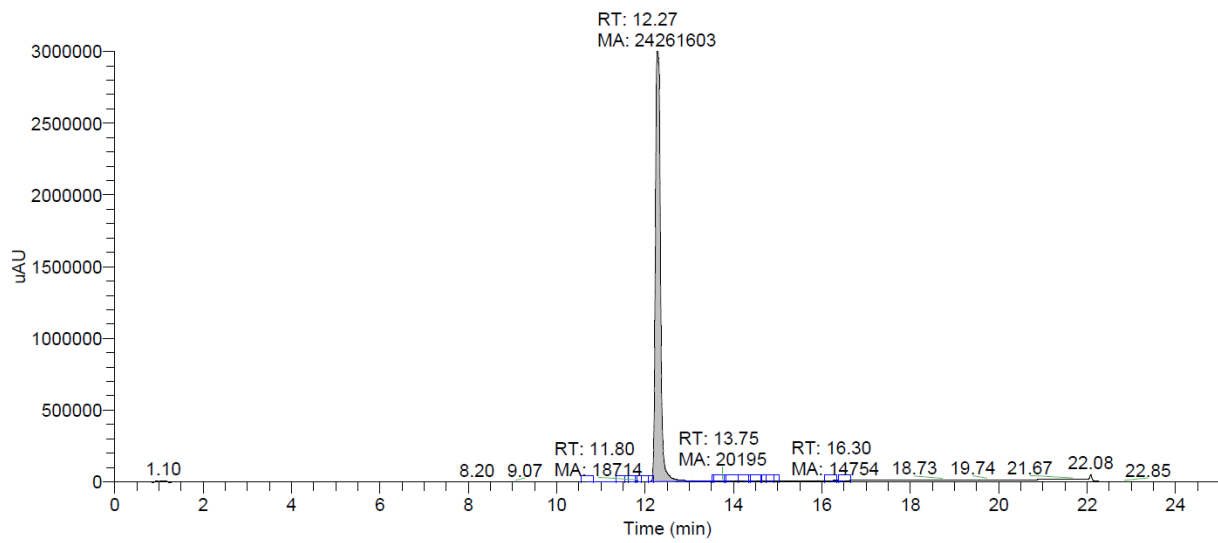


**Compound 35**

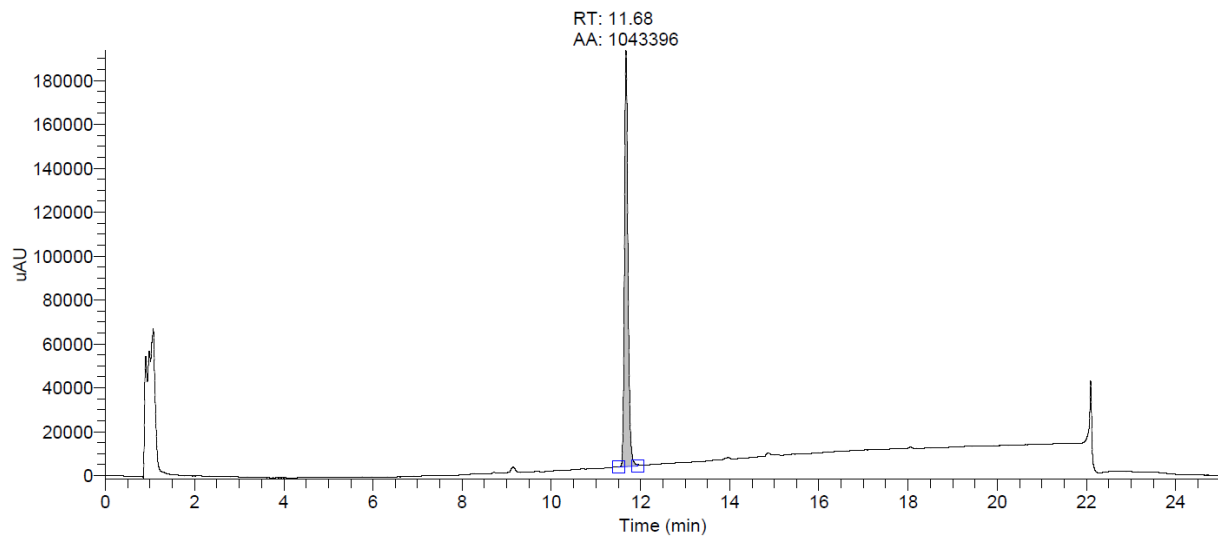


**Compound 36****Compound 37****Compound 38**

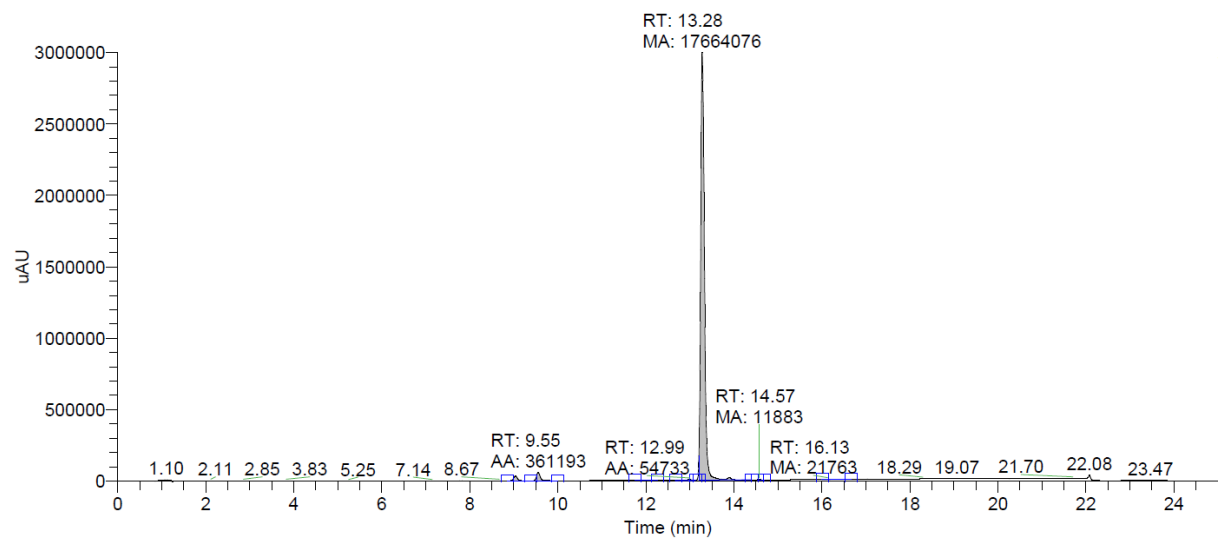
**Compound 39**

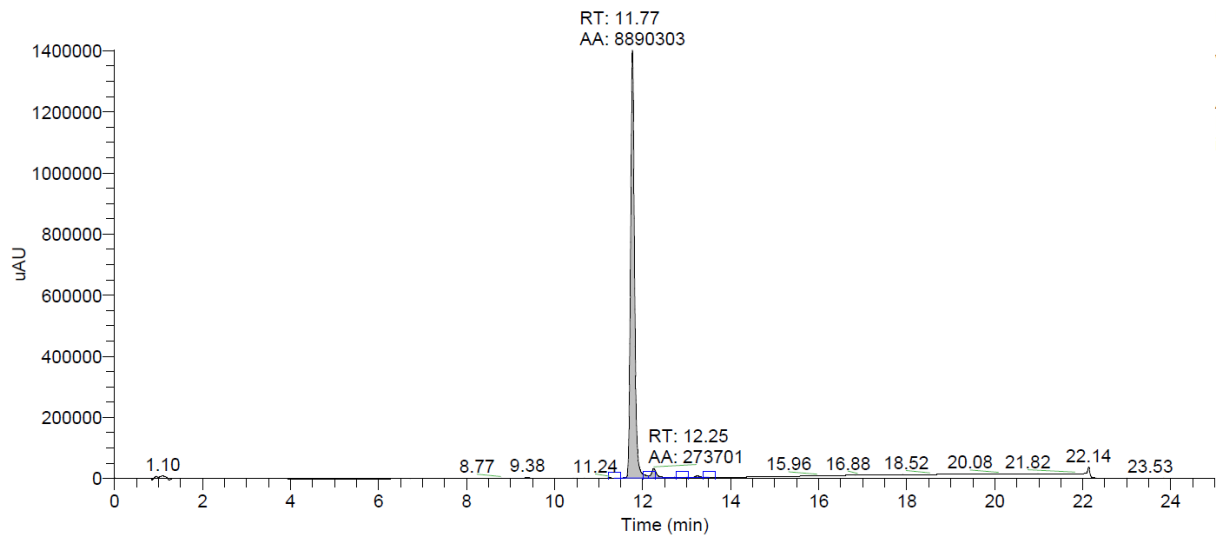
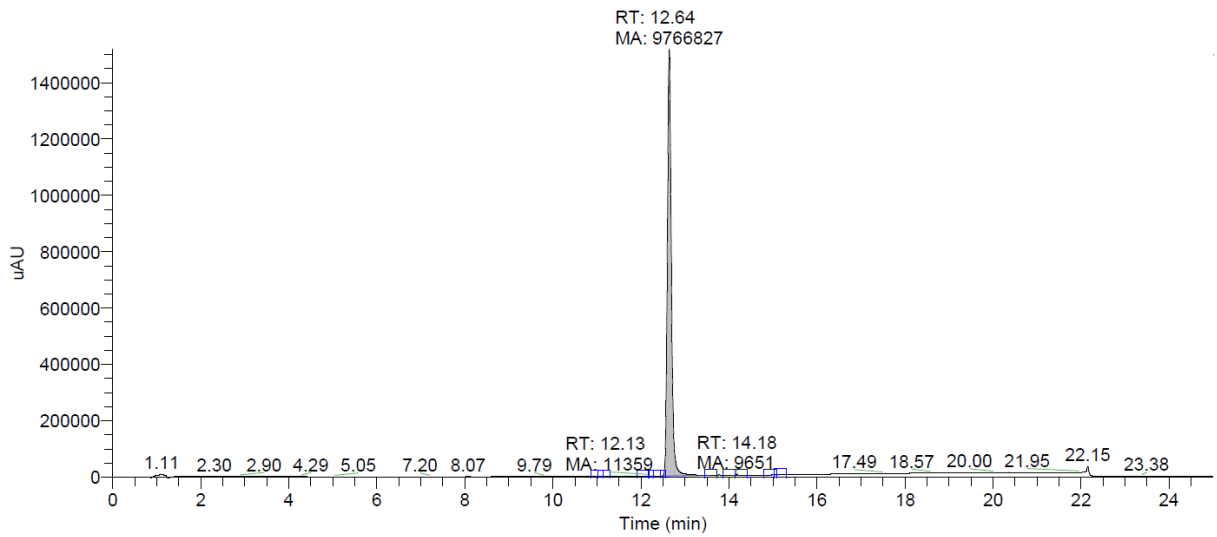
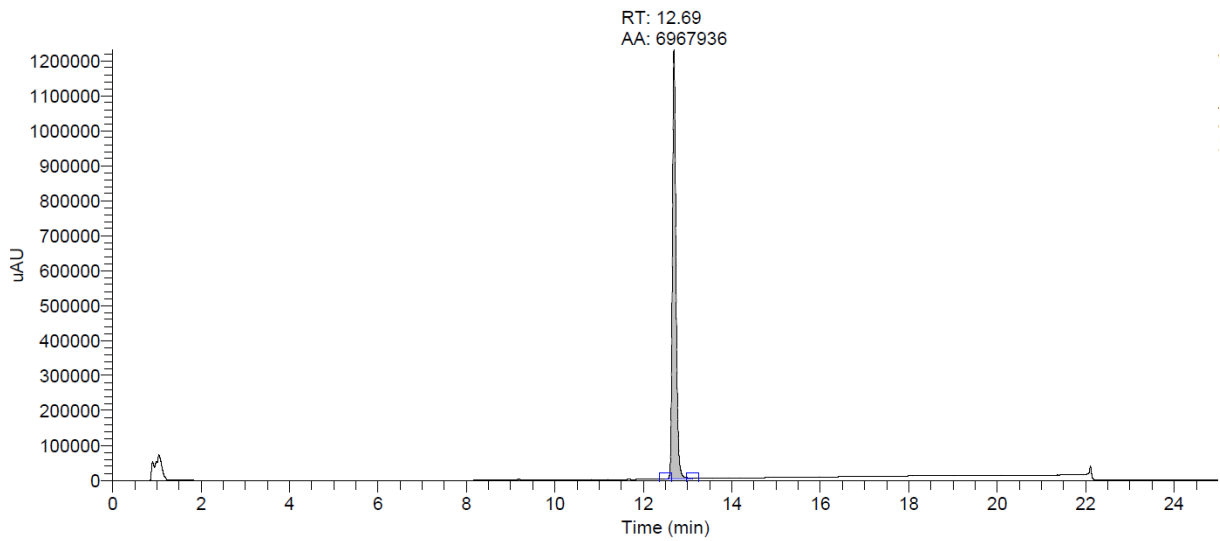


**Compound 40**

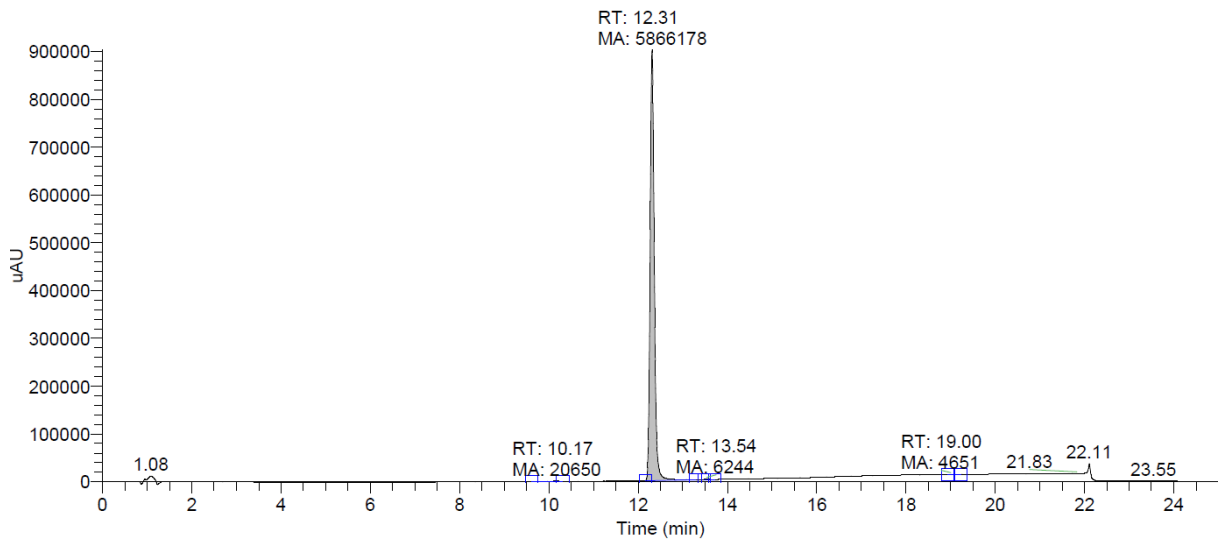


**Compound 41**

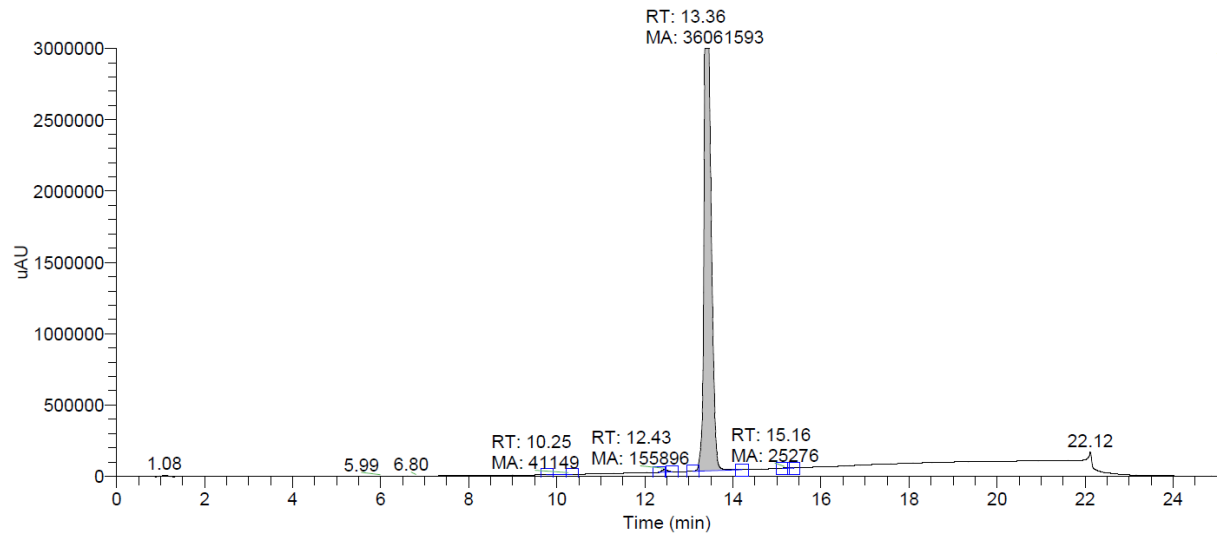


**Compound 42****Compound 43****Compound 44**

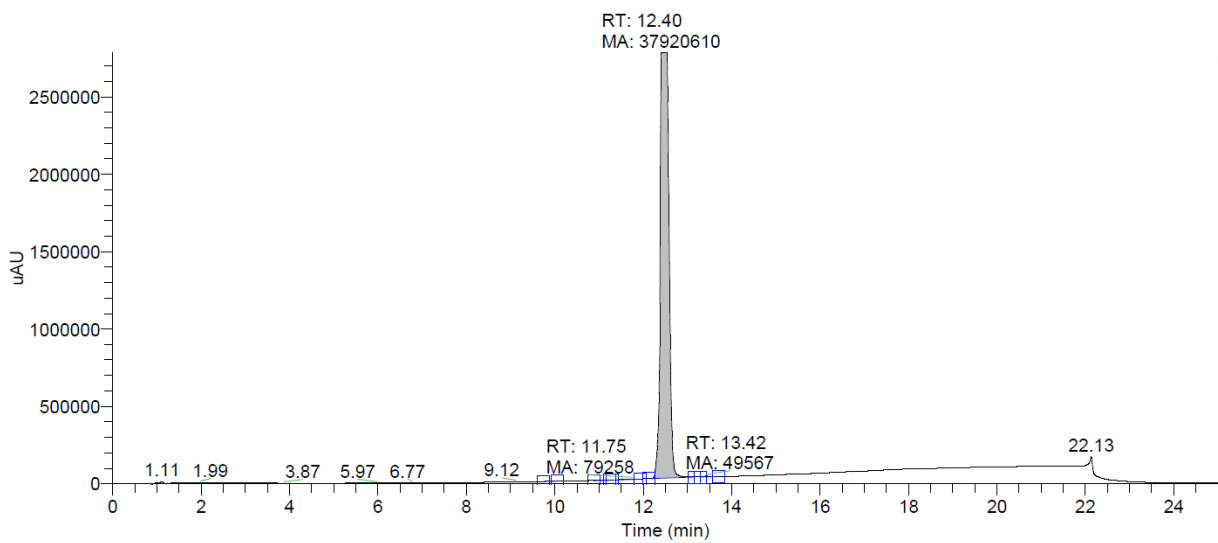
**Compound 45**

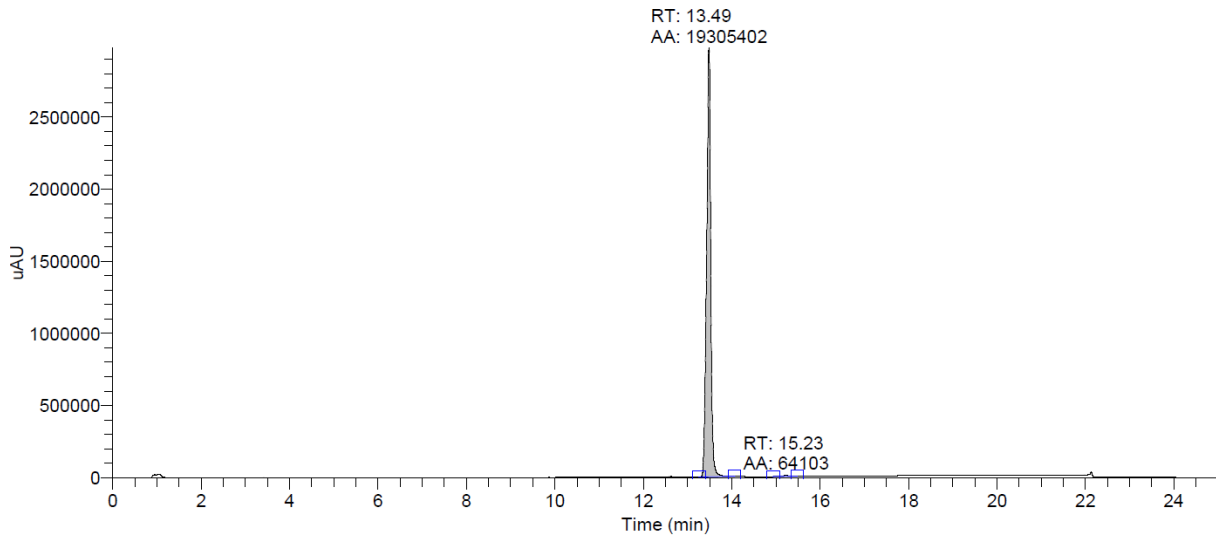
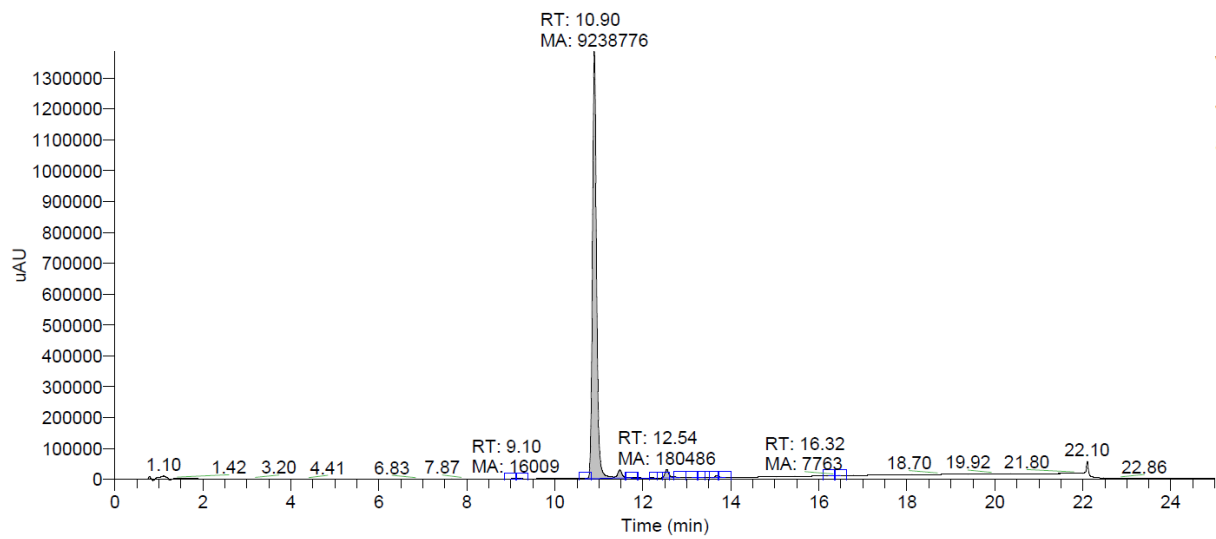
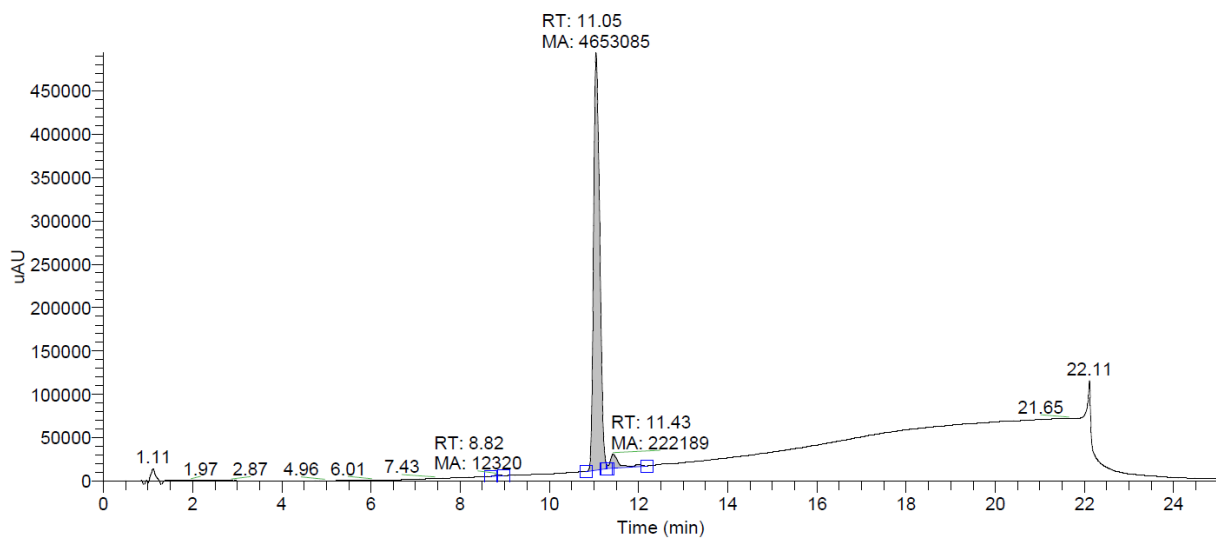


**Compound 46**

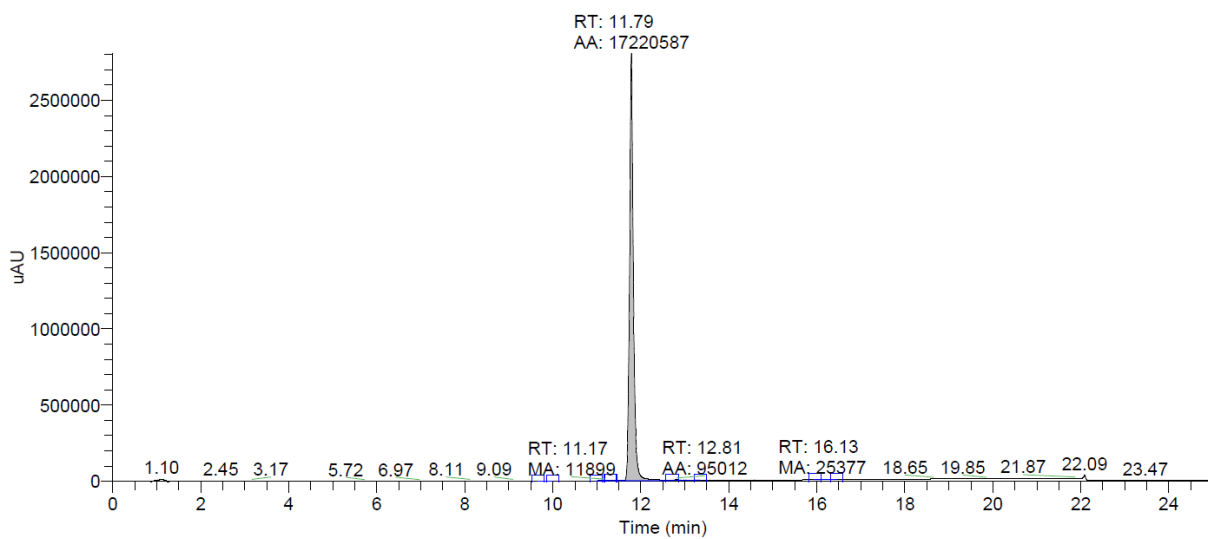


**Compound 47**

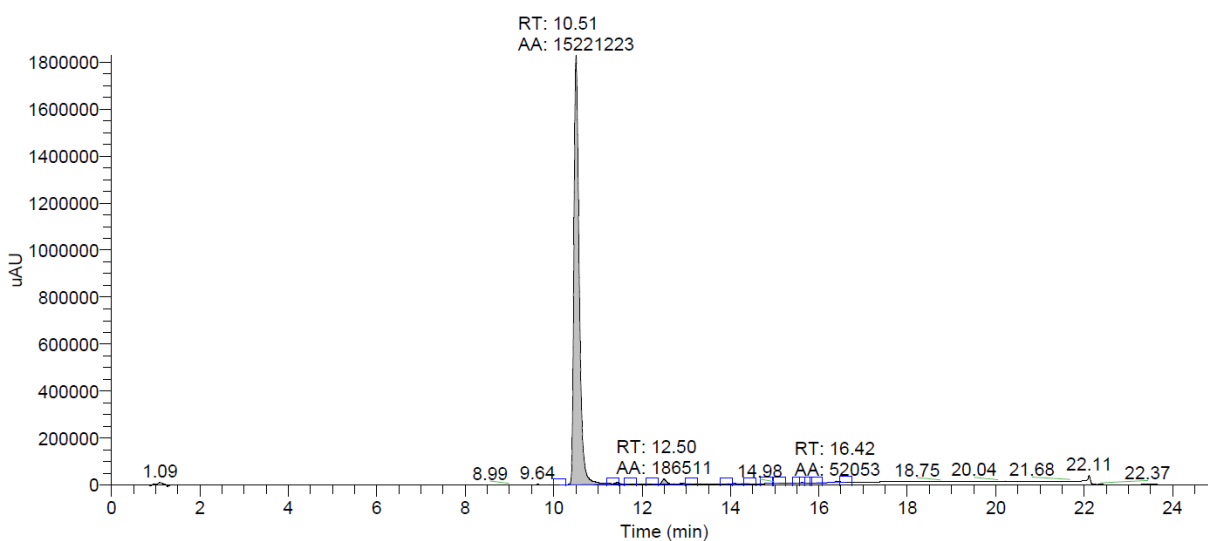


**Compound 48****Compound 49****Compound 50**

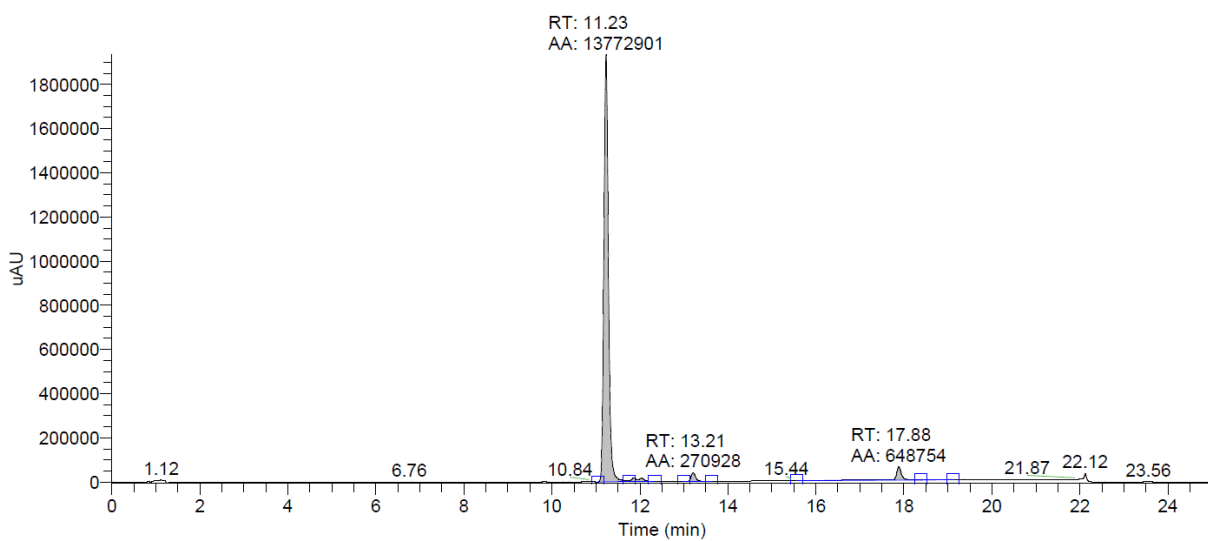
**Compound 51**



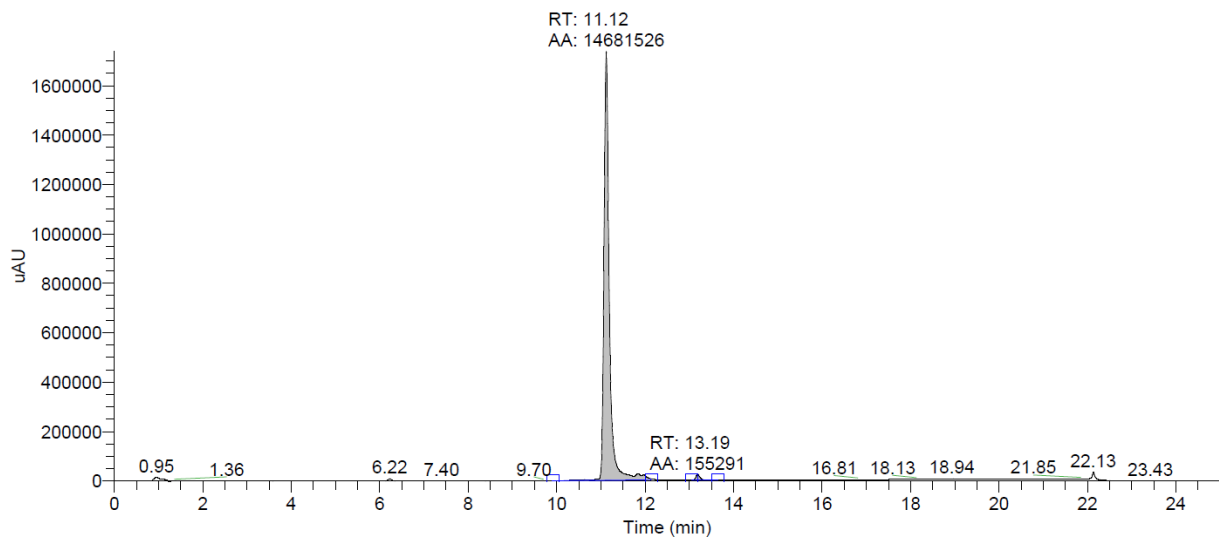
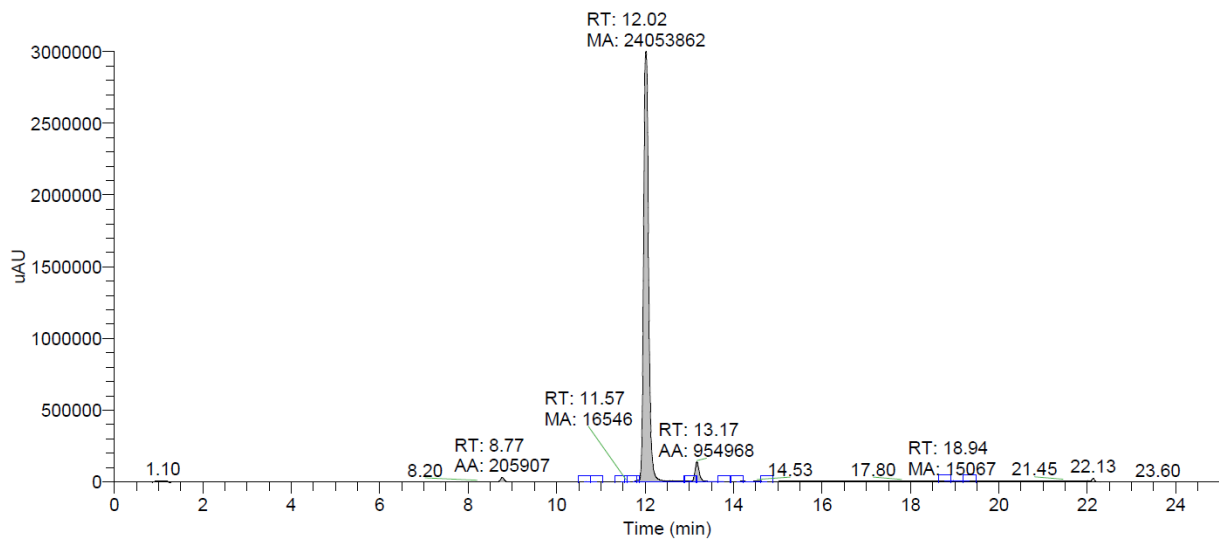
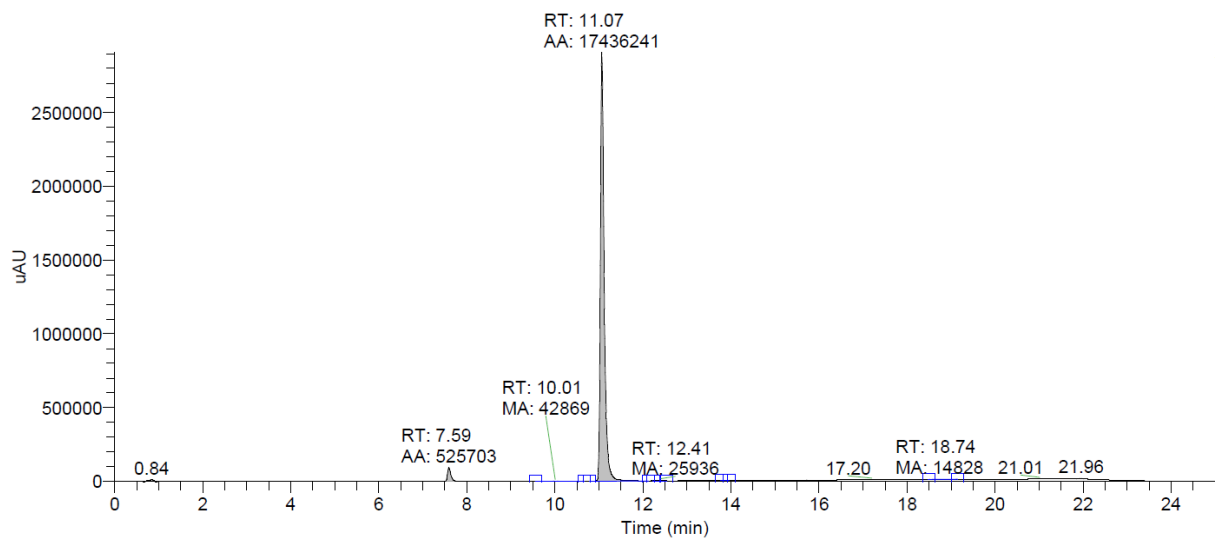
**Compound 52**



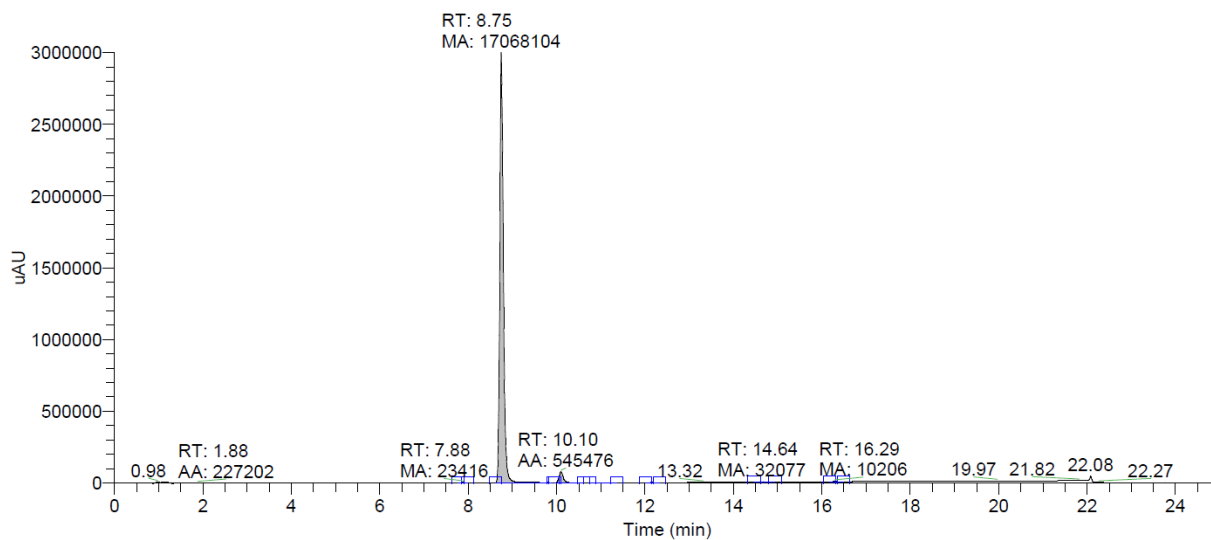
**Compound 53**



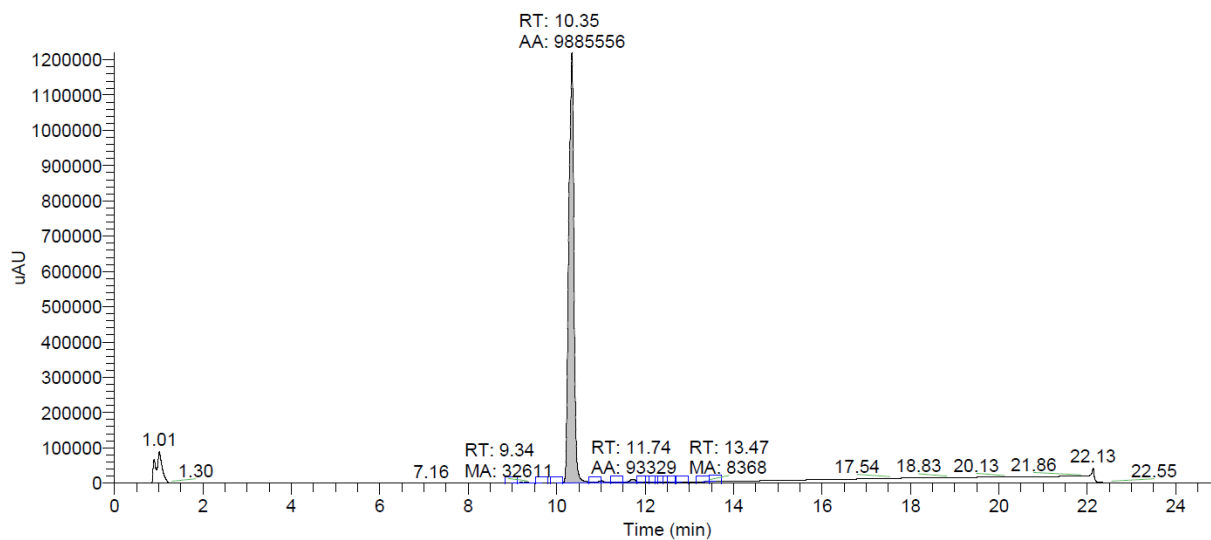


**Compound 54****Compound 55****Compound 56**

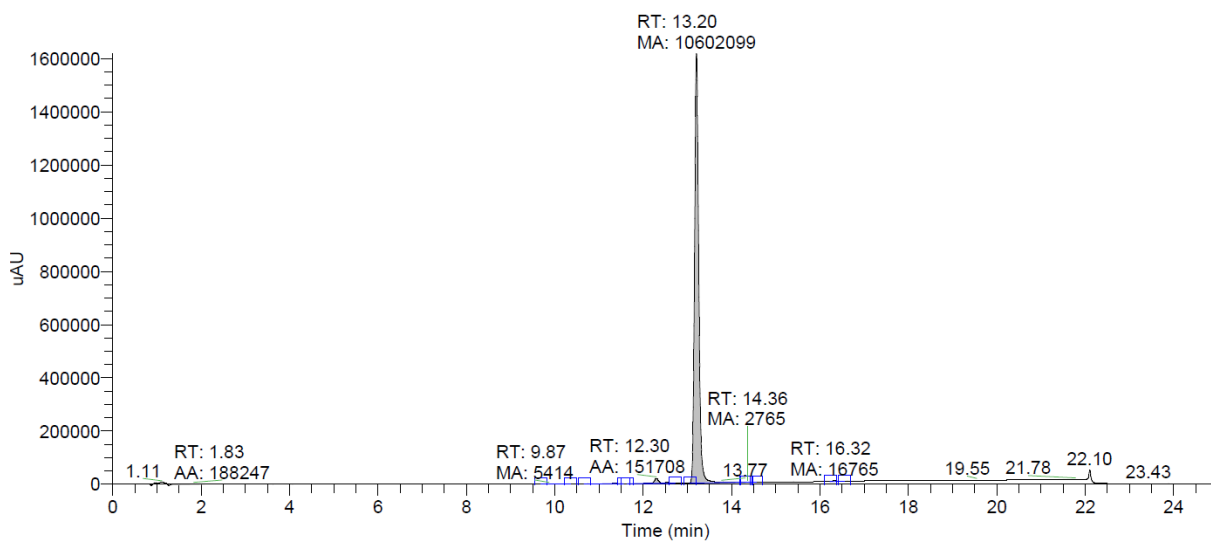
**Compound 57**

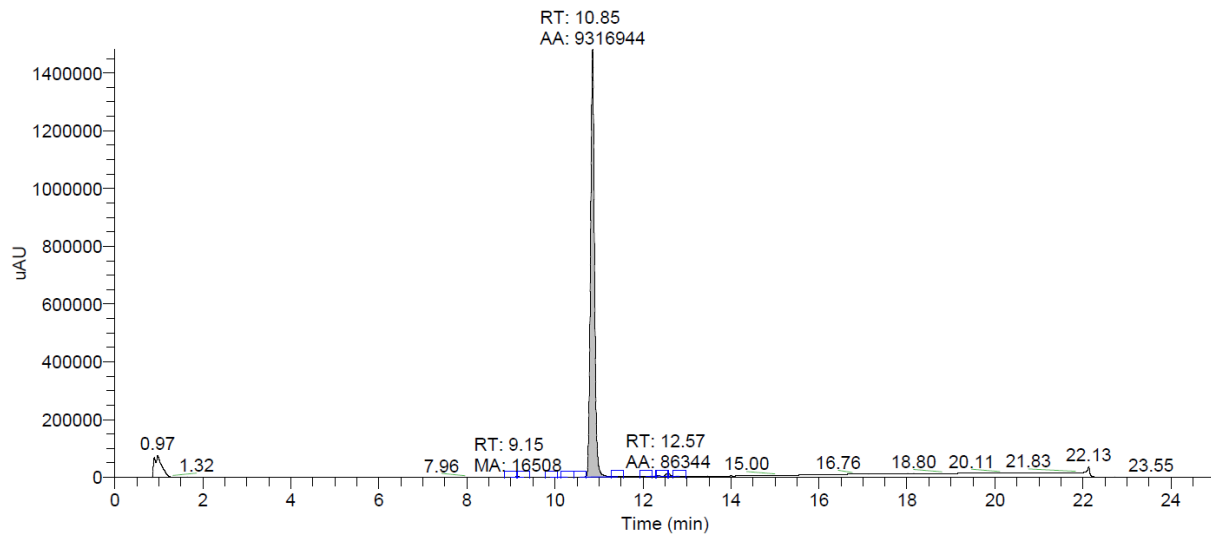
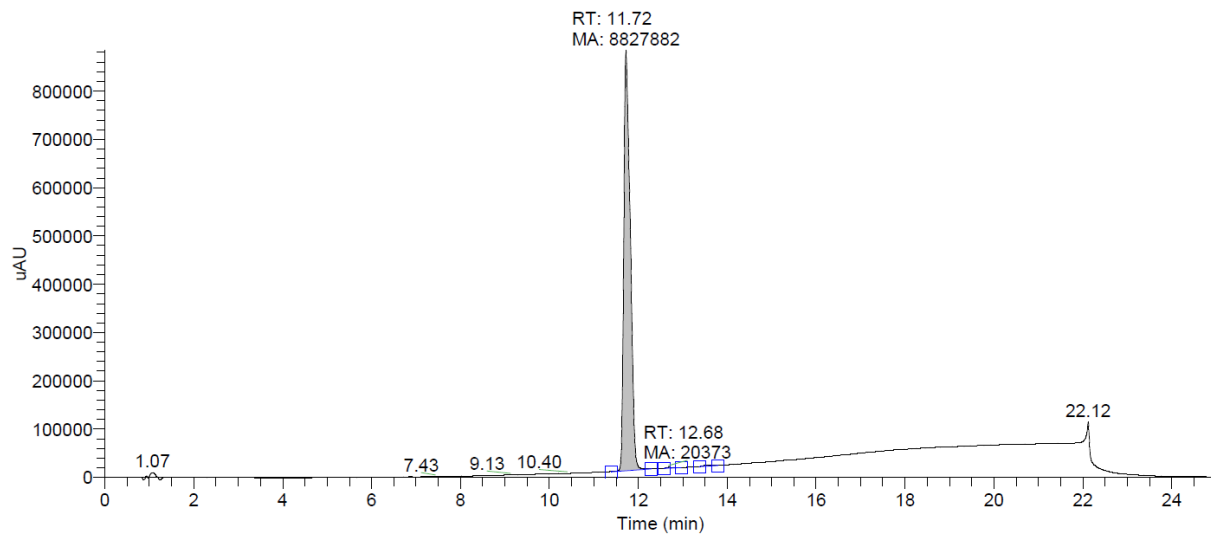
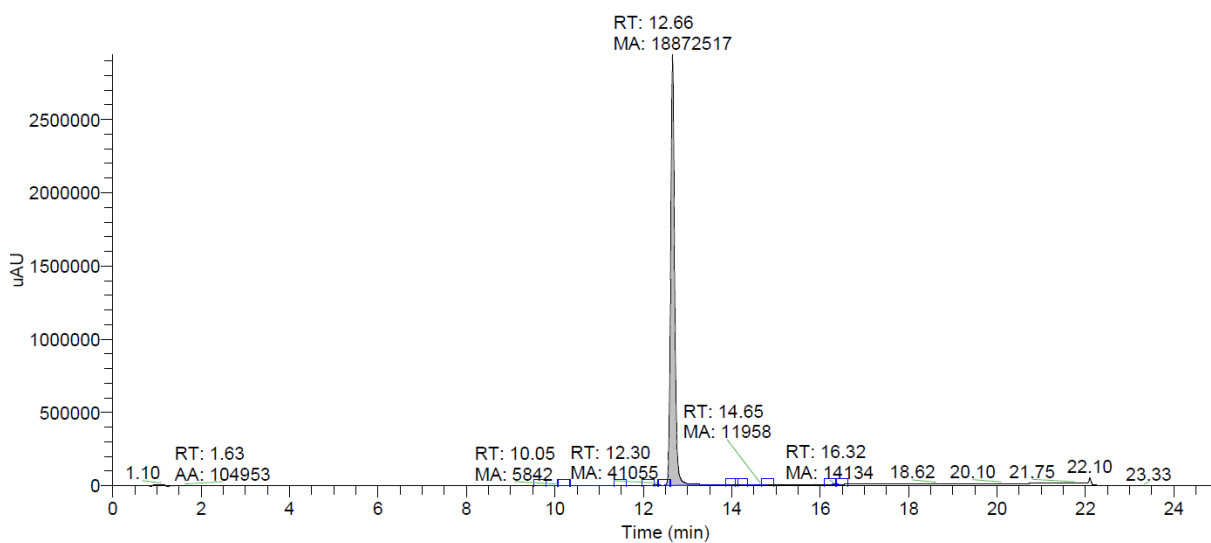


**Compound 58**

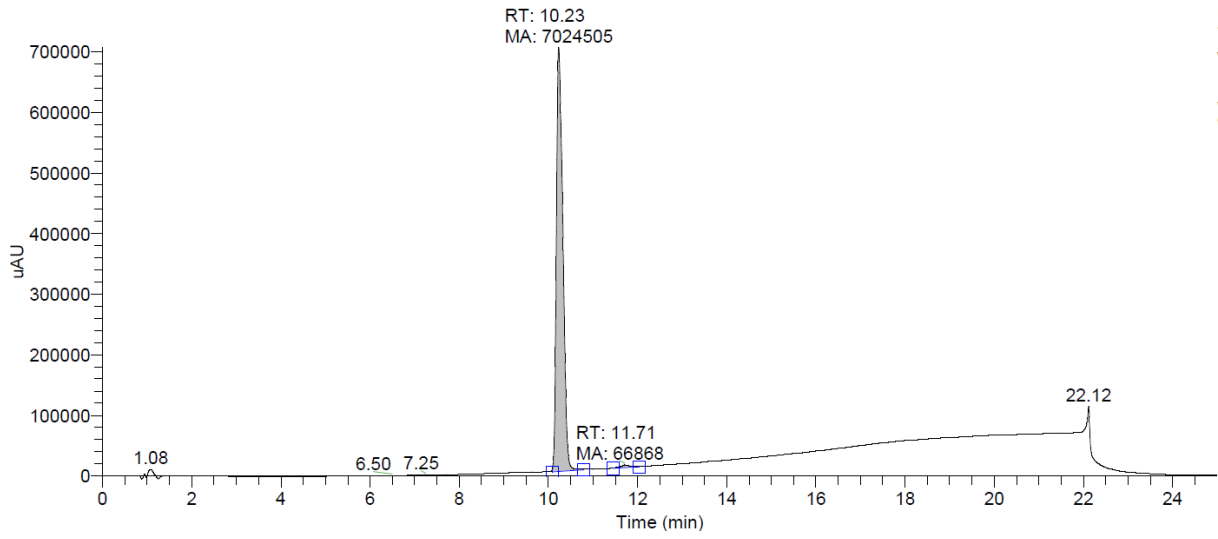


**Compound 59**

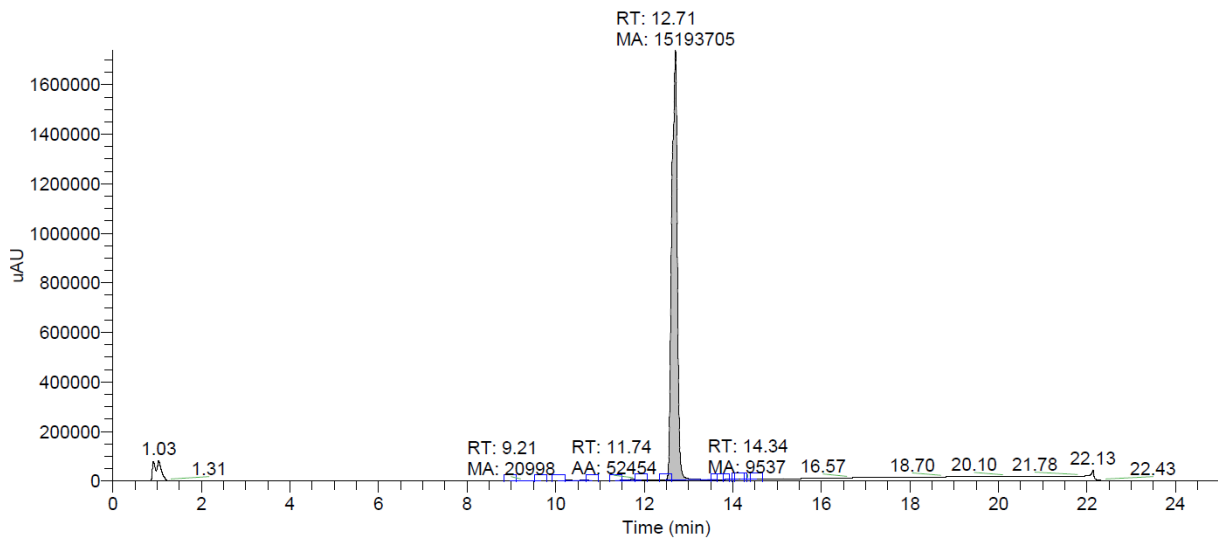


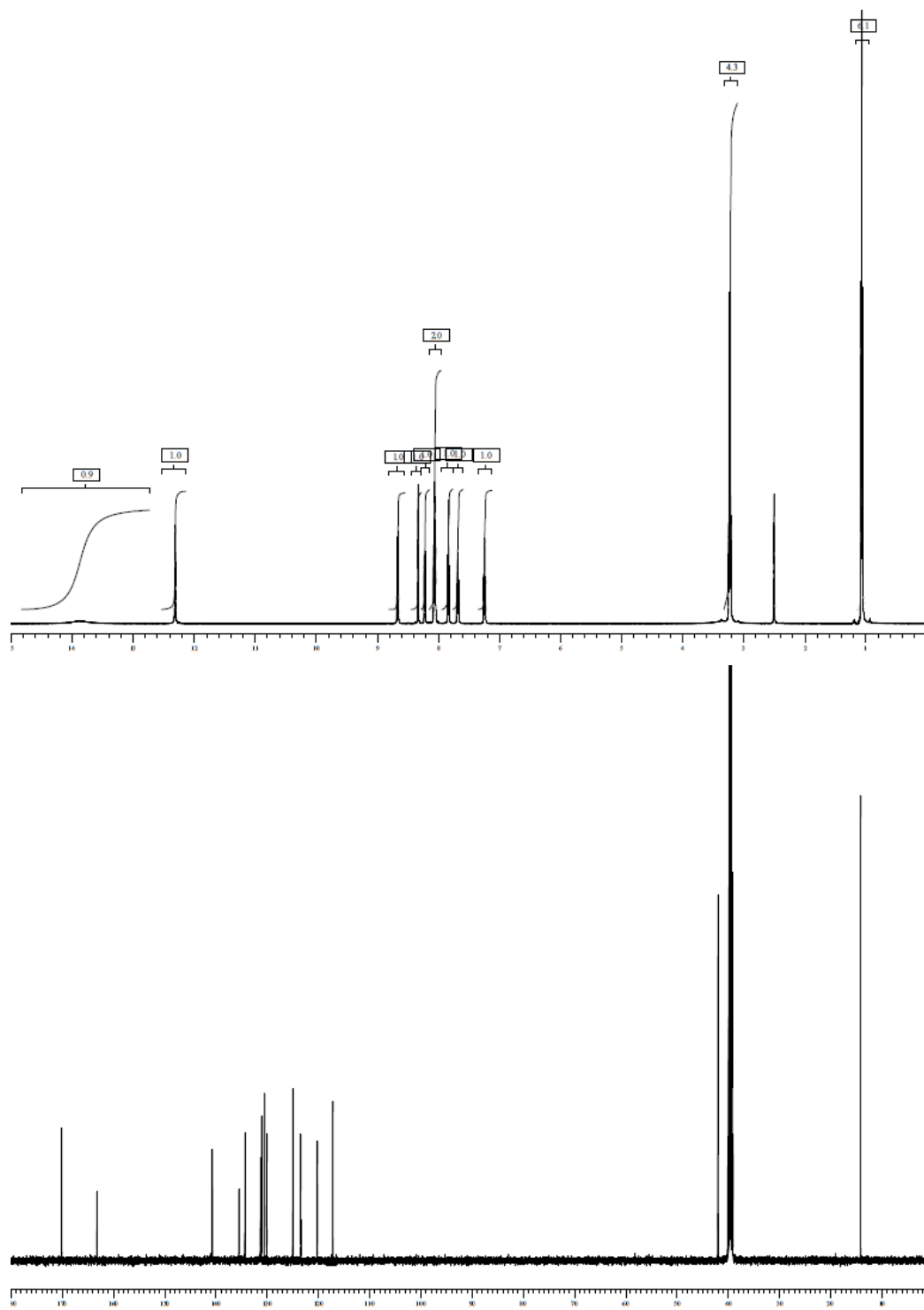
**Compound 60****Compound 61****Compound 62**

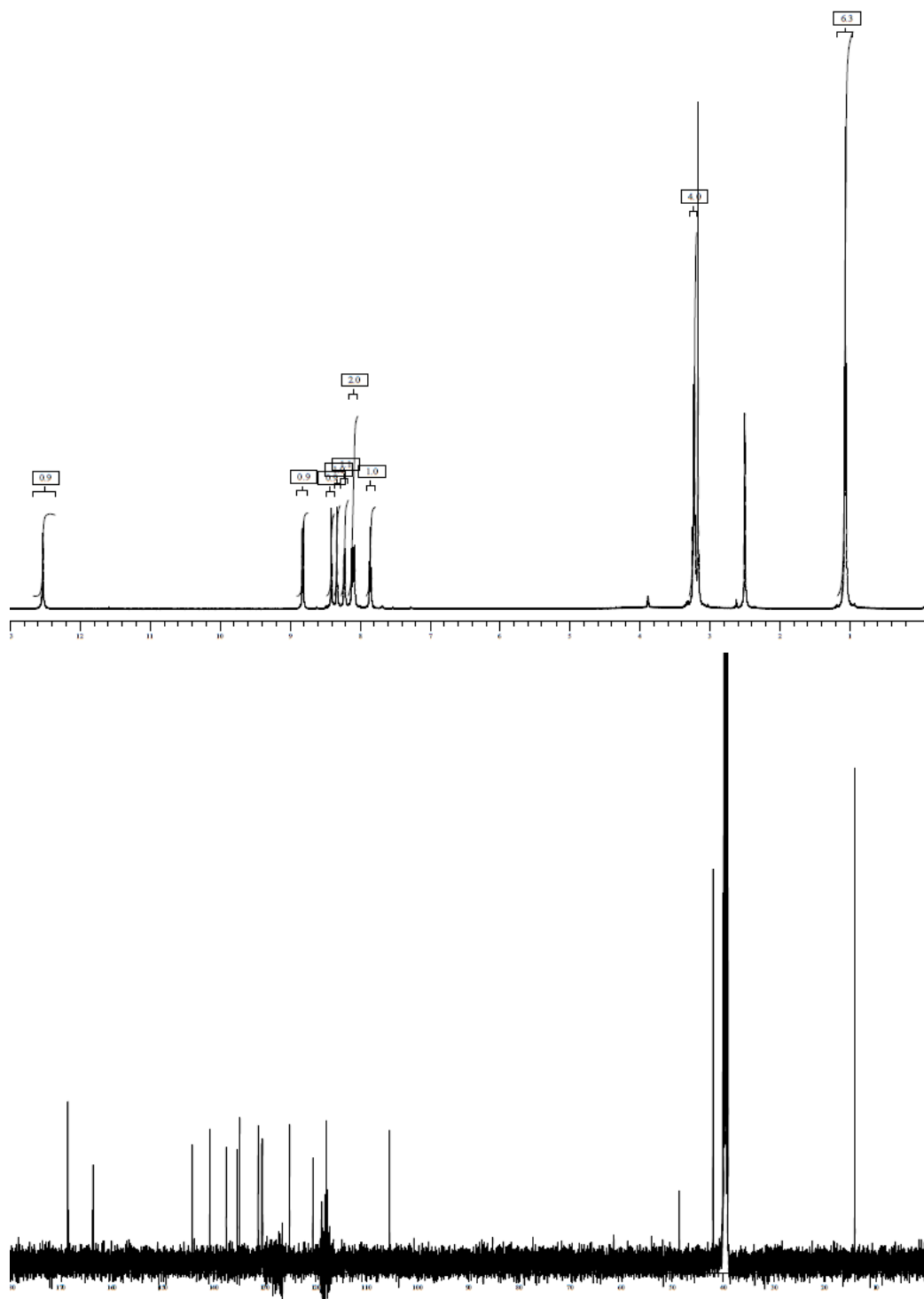
### Compound 63



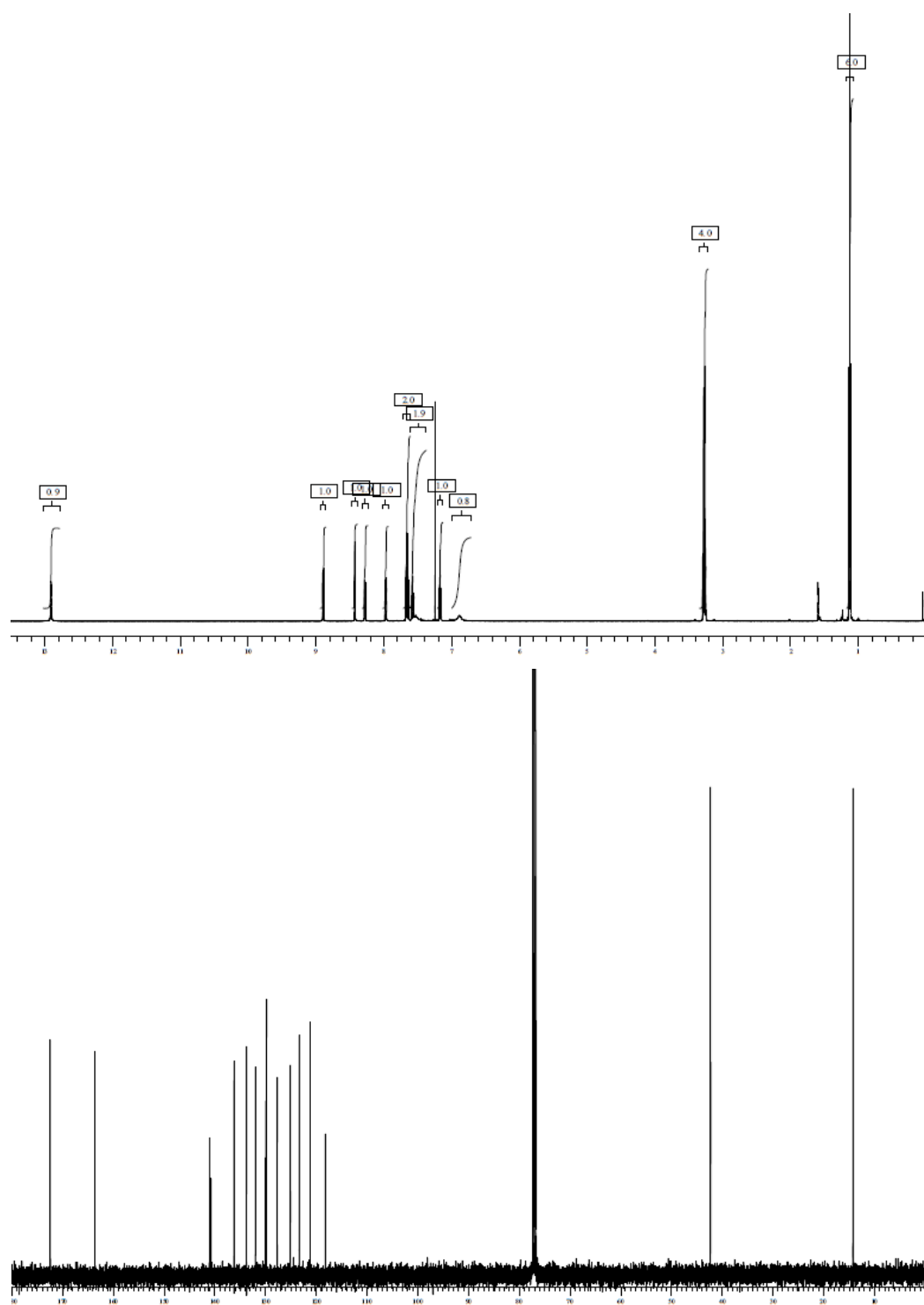
### Compound 64



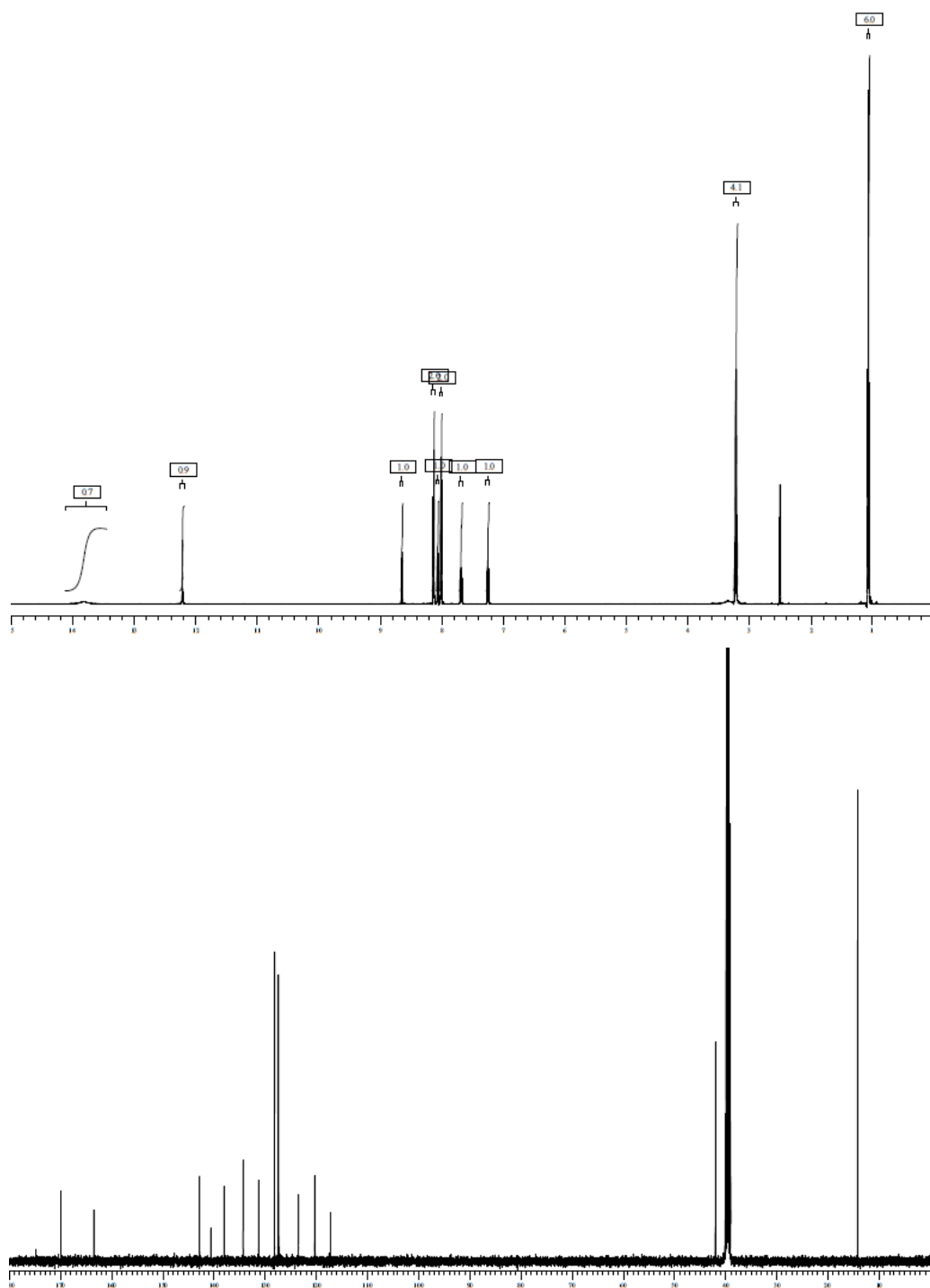
**<sup>1</sup>H and <sup>13</sup>C spectra of test compounds****Compound 2****Compound 4**



## Compound 6

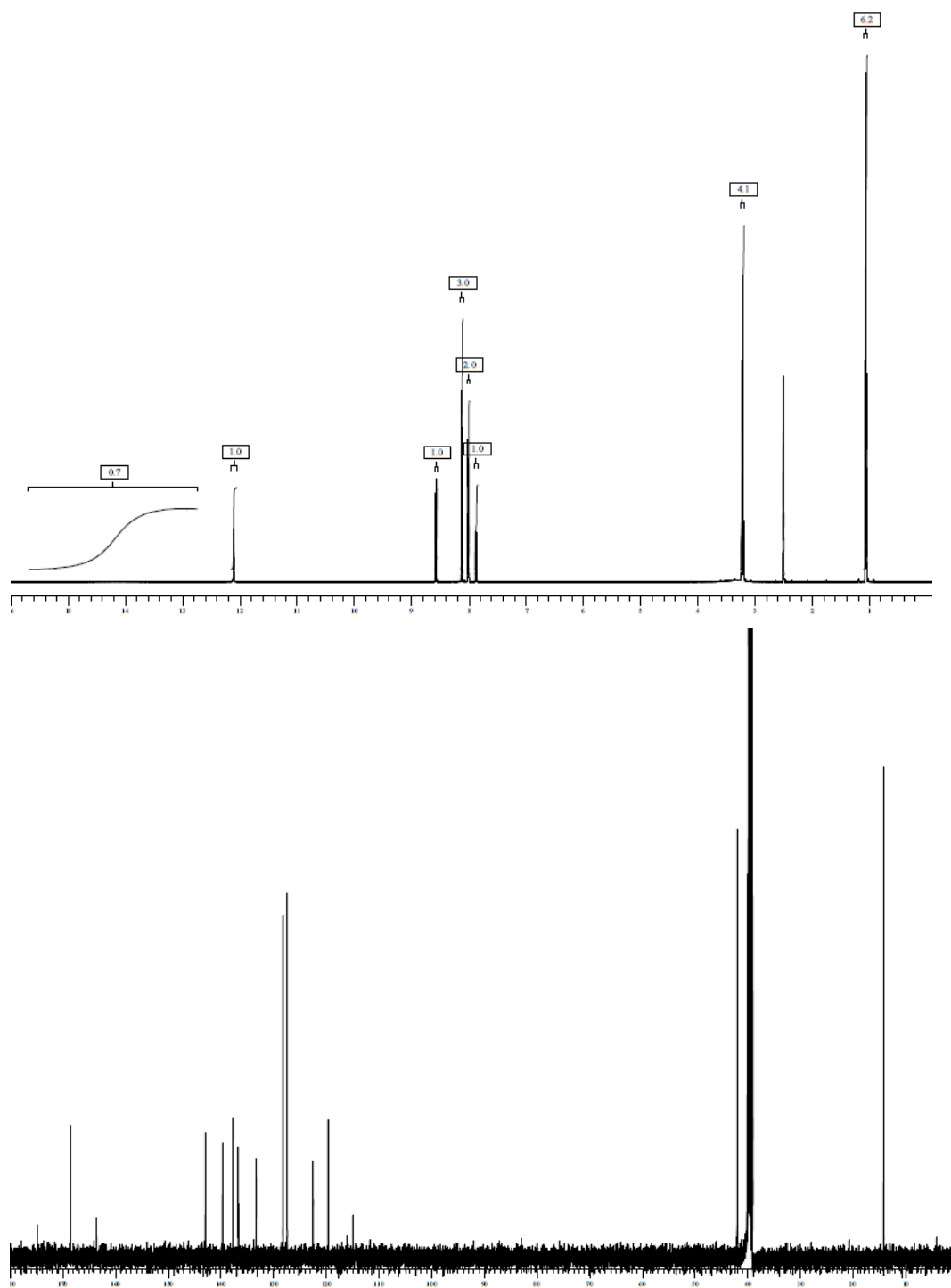


## Compound 9

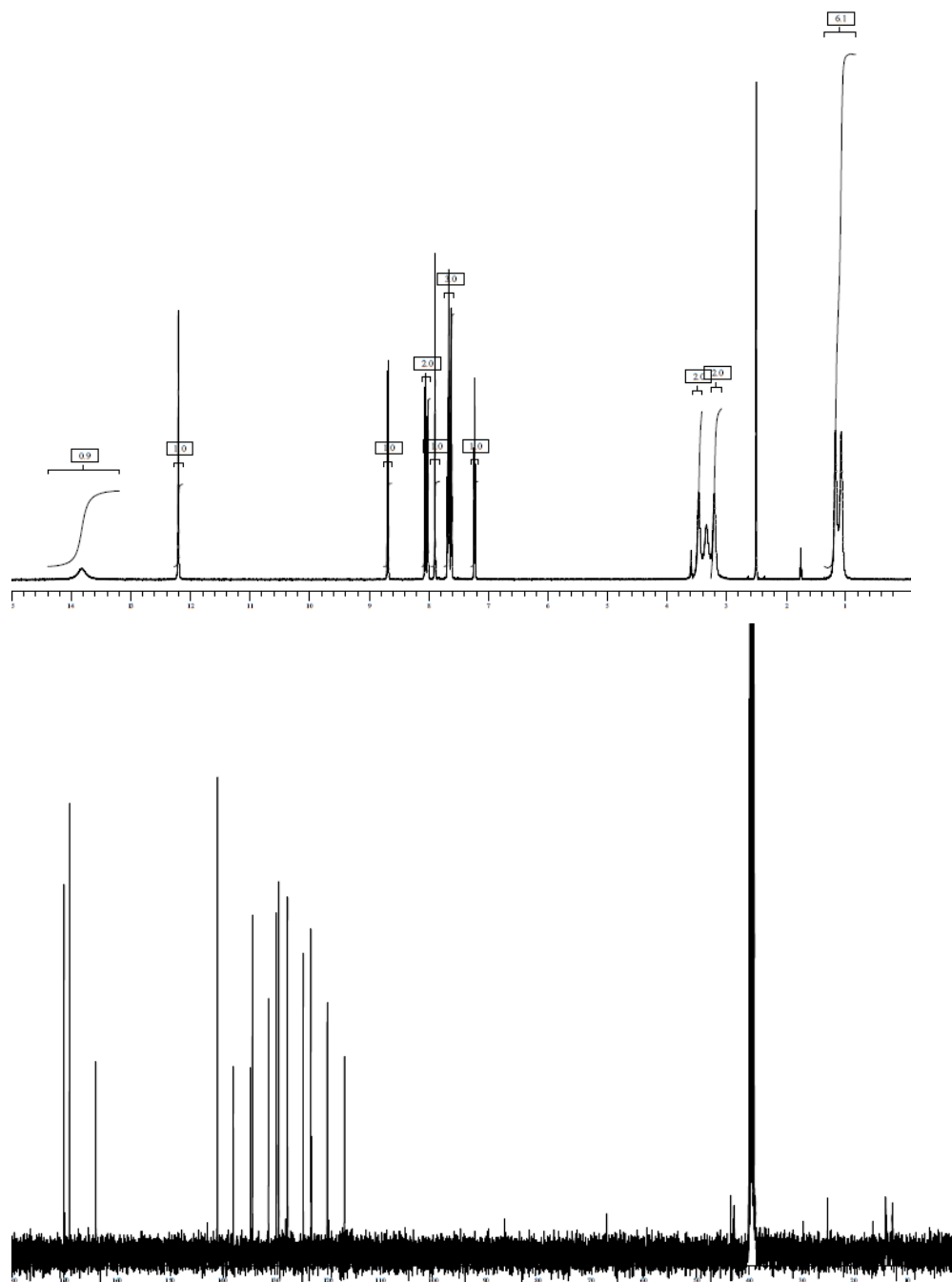




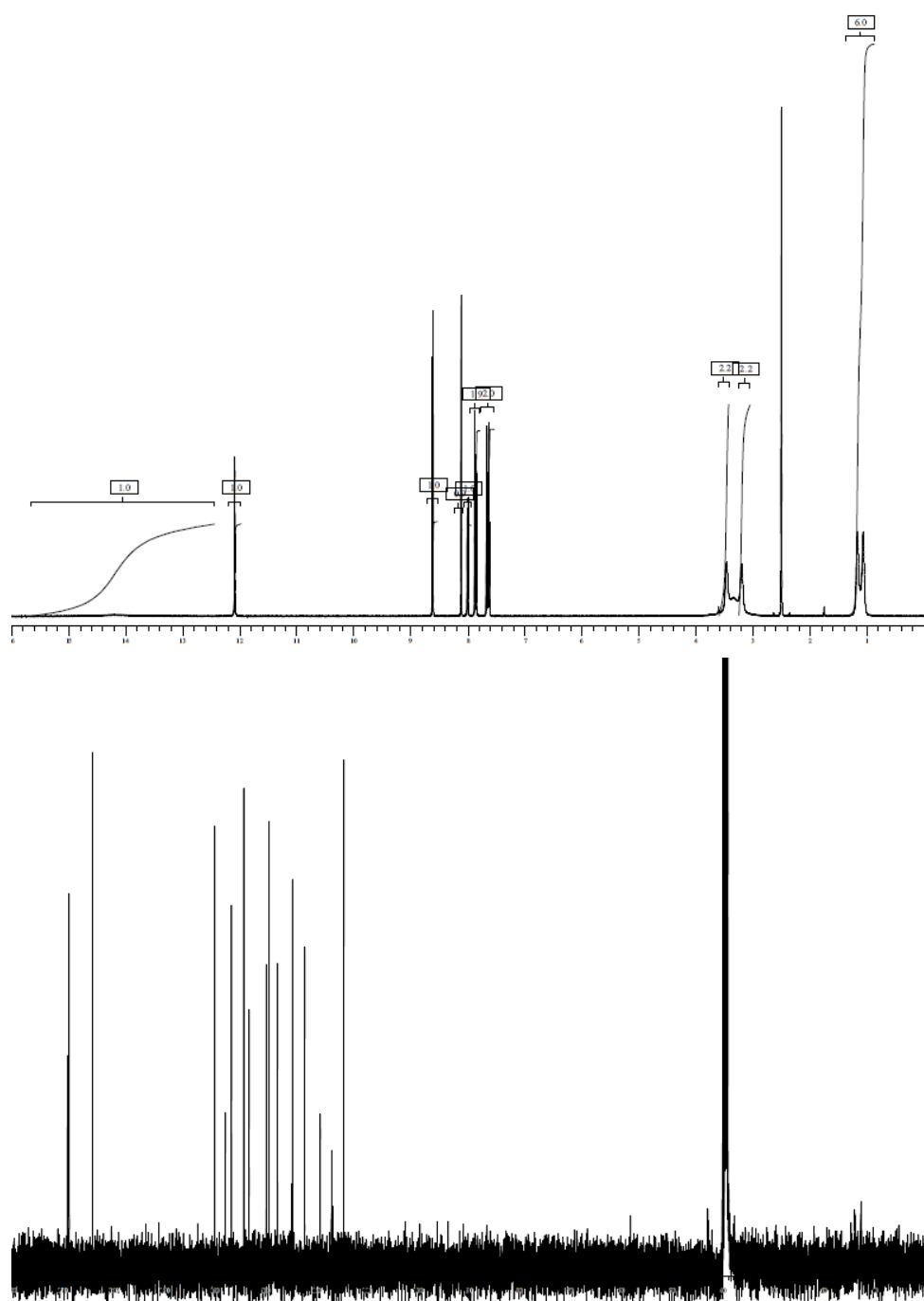
## Compound 10



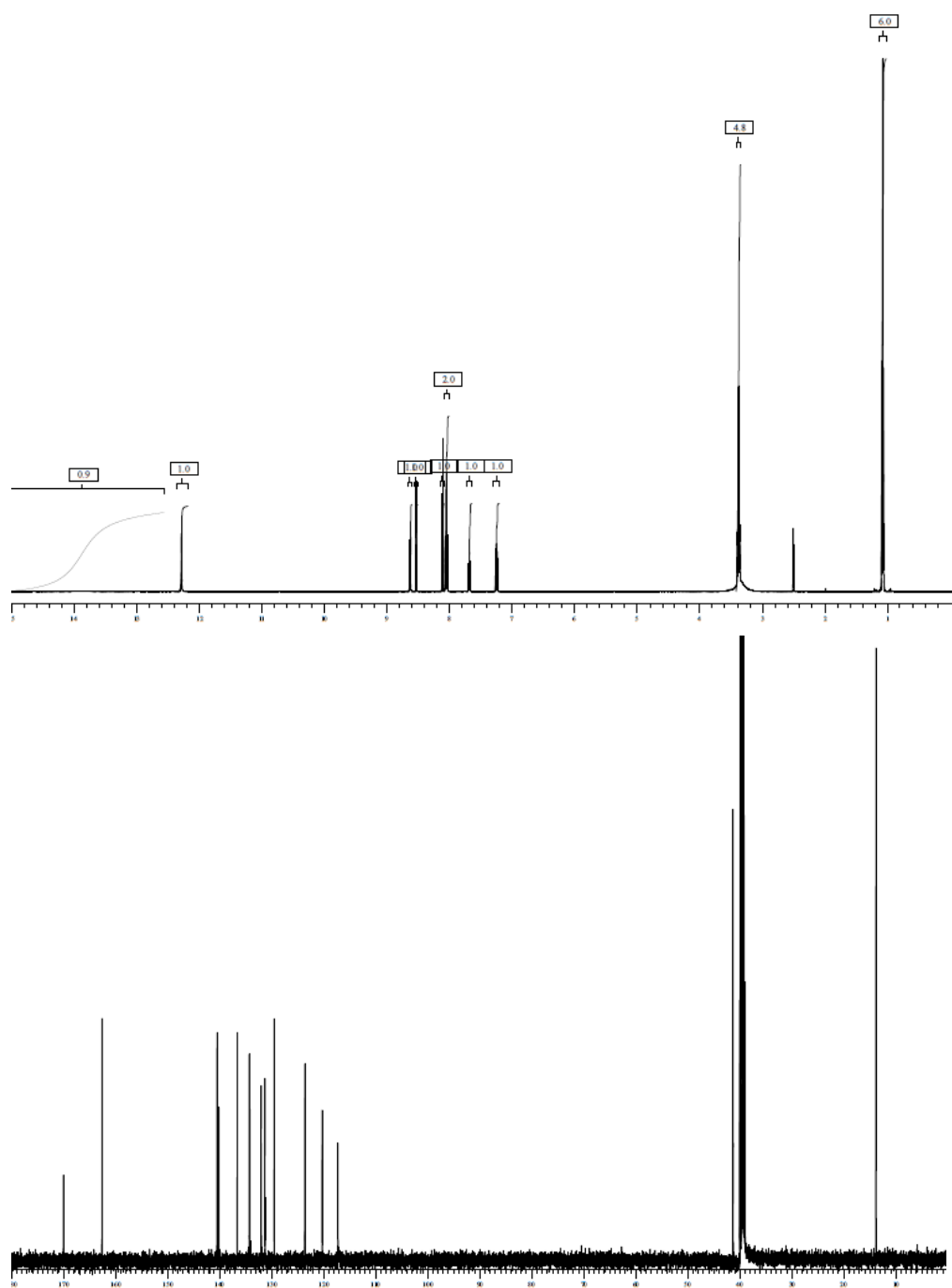
Compound 13



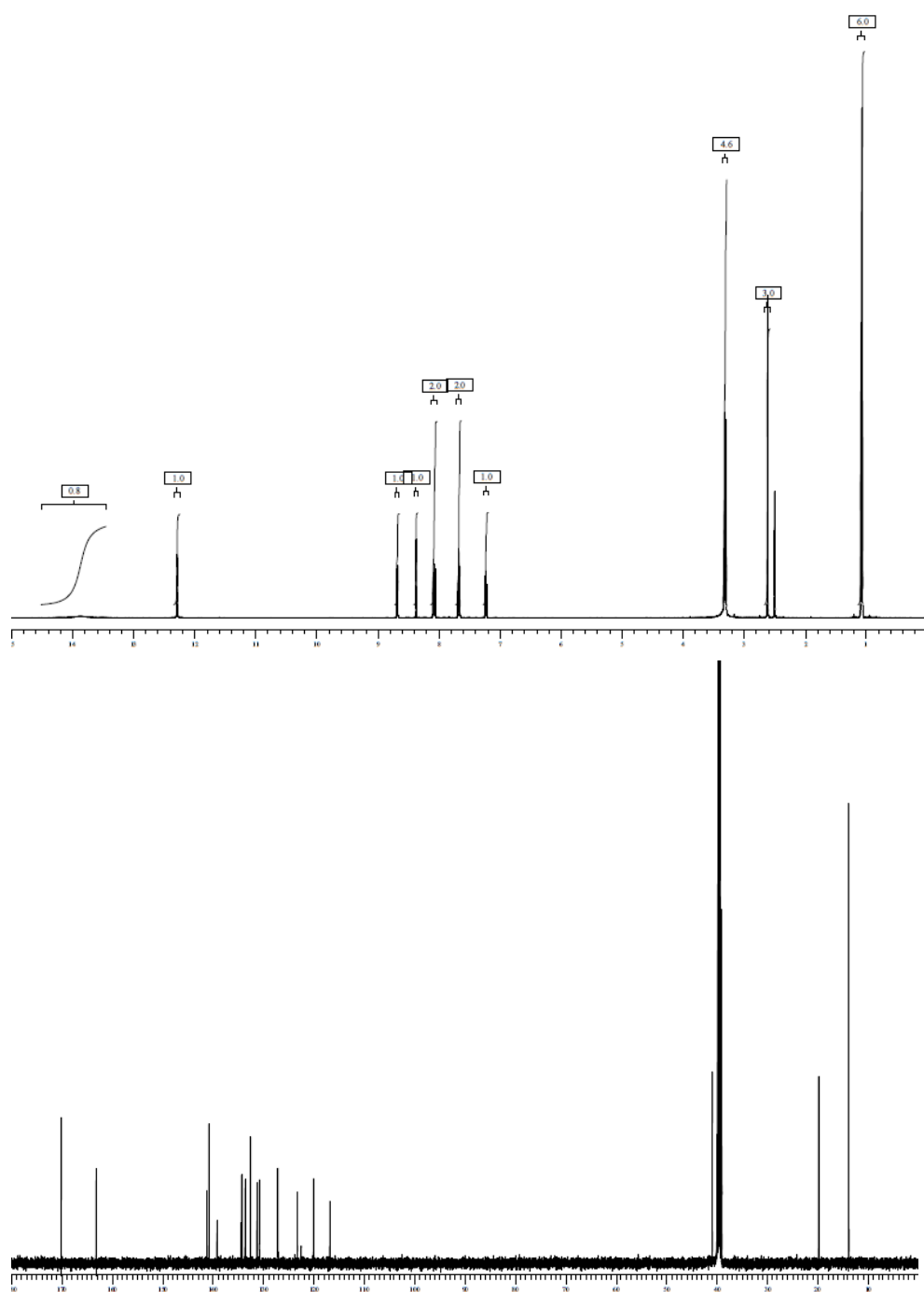
## Compound 14



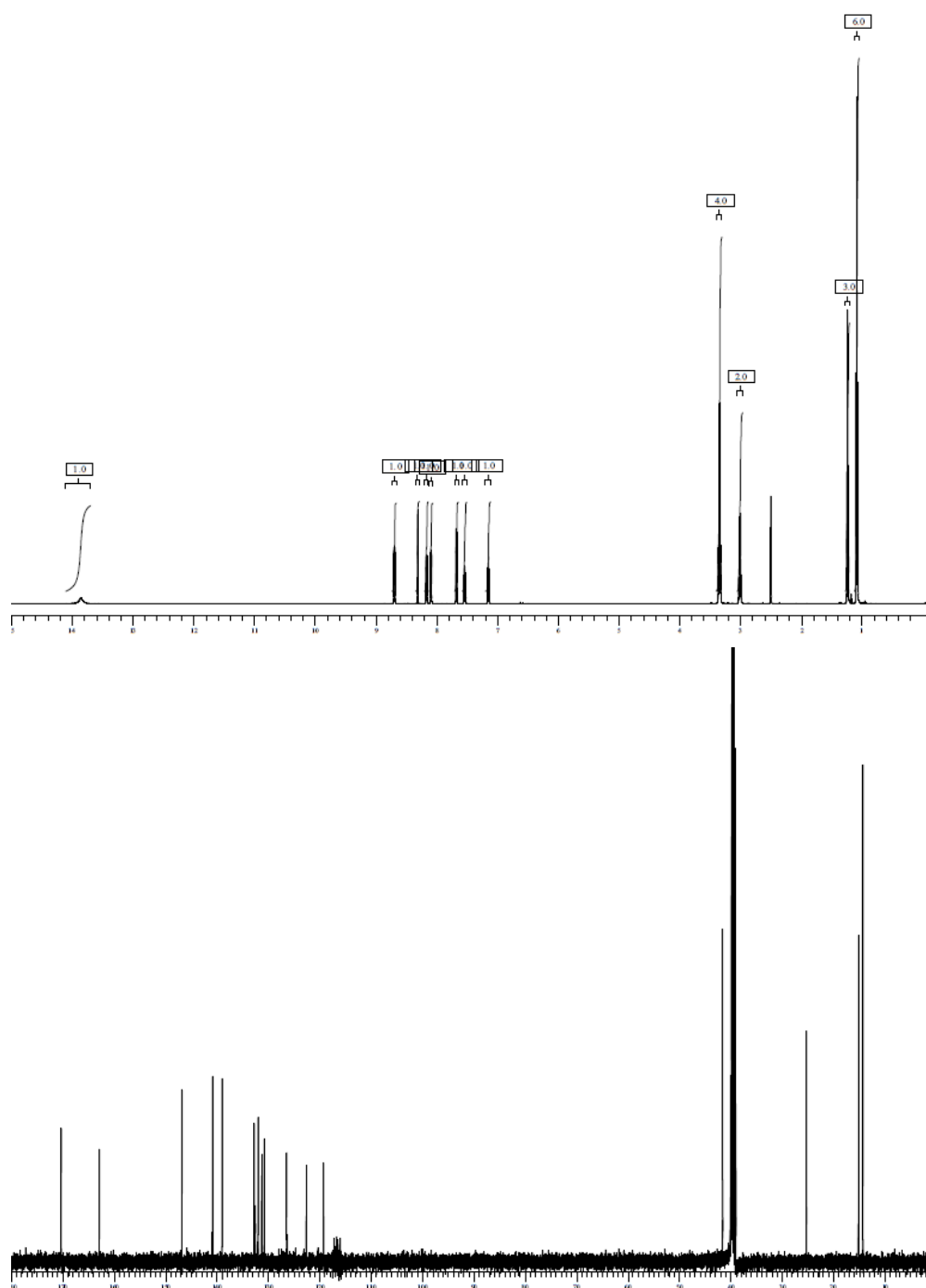
## Compound 34



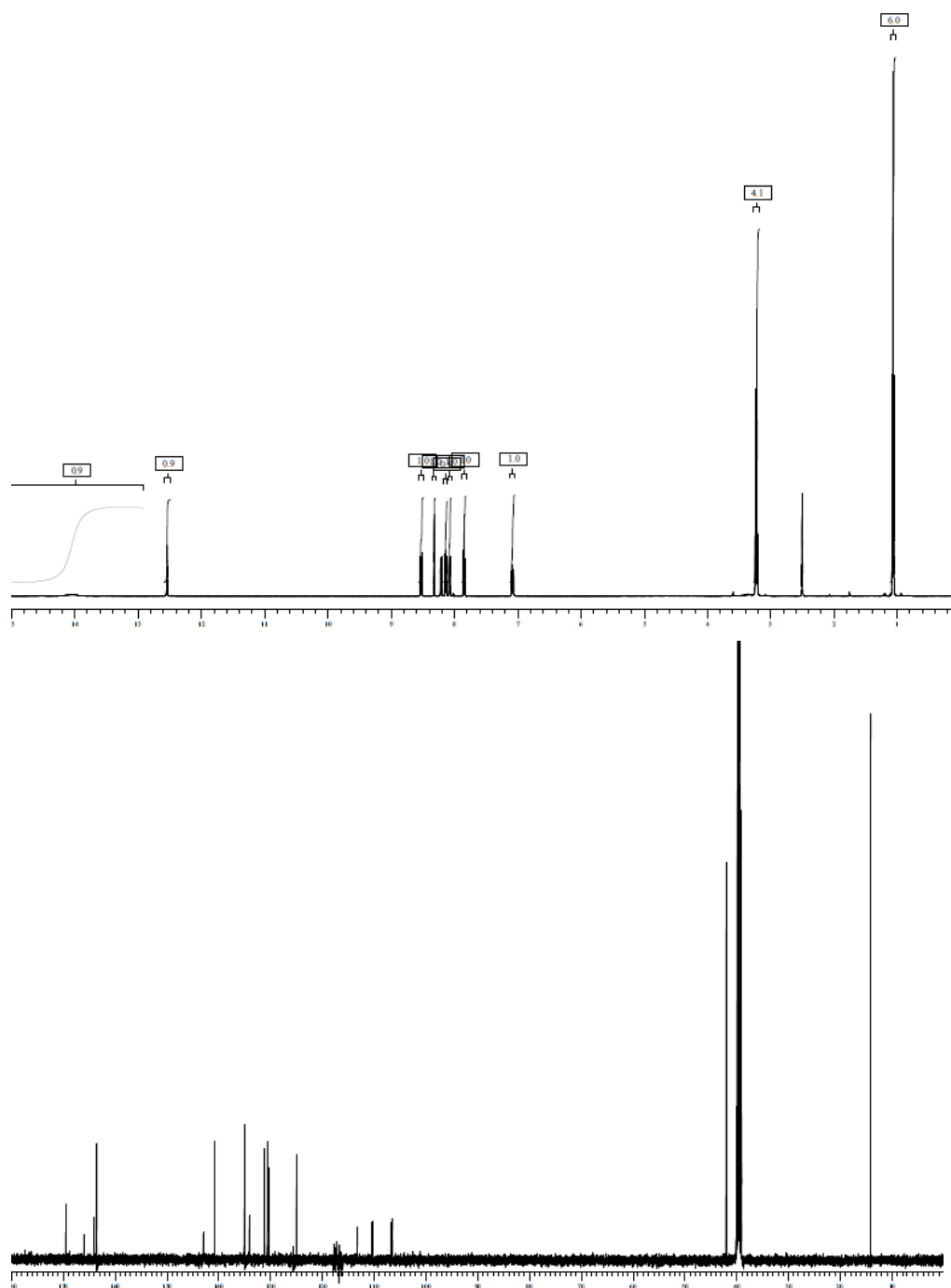
## Compound 35



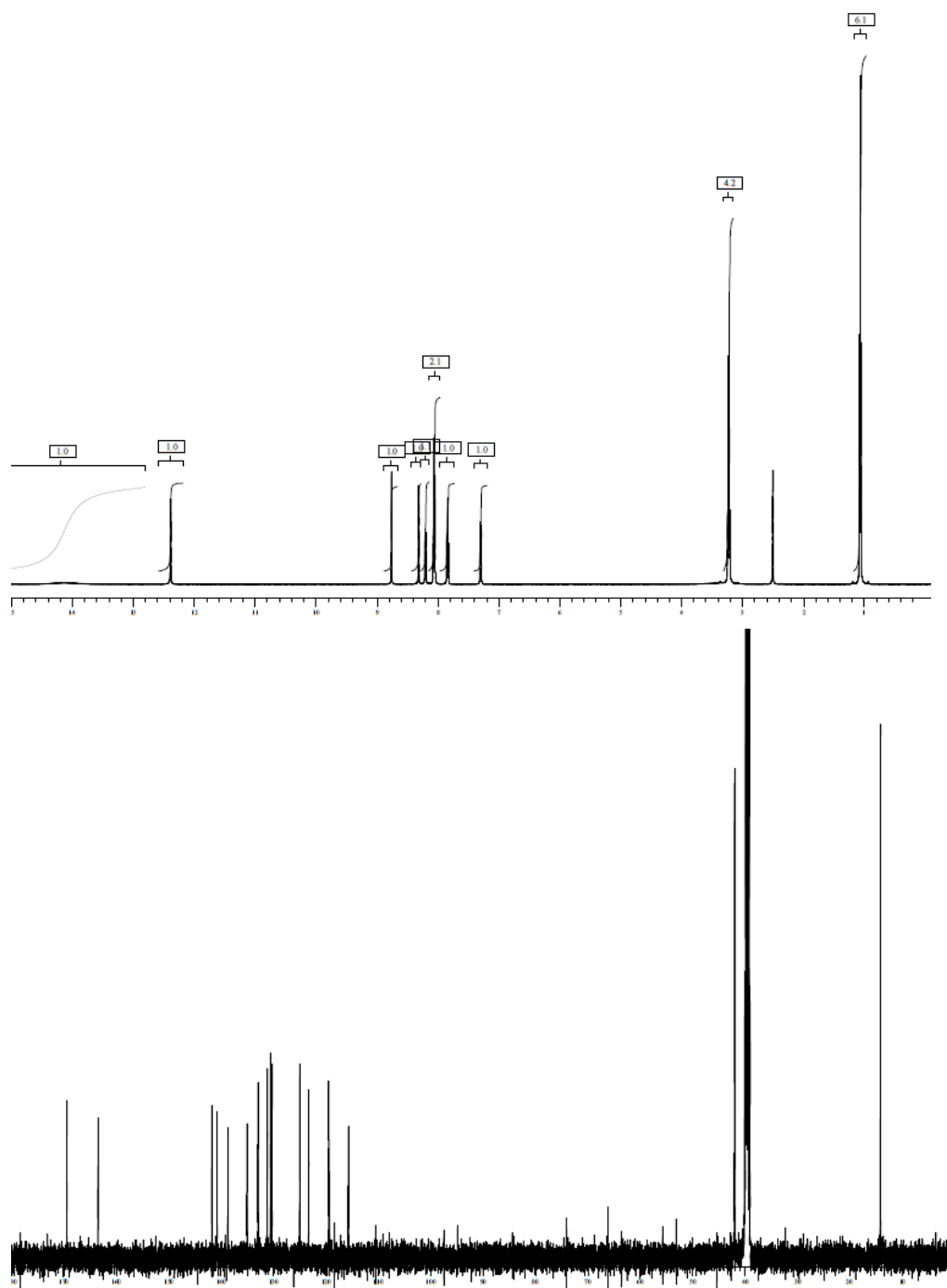
## Compound 36



## Compound 37

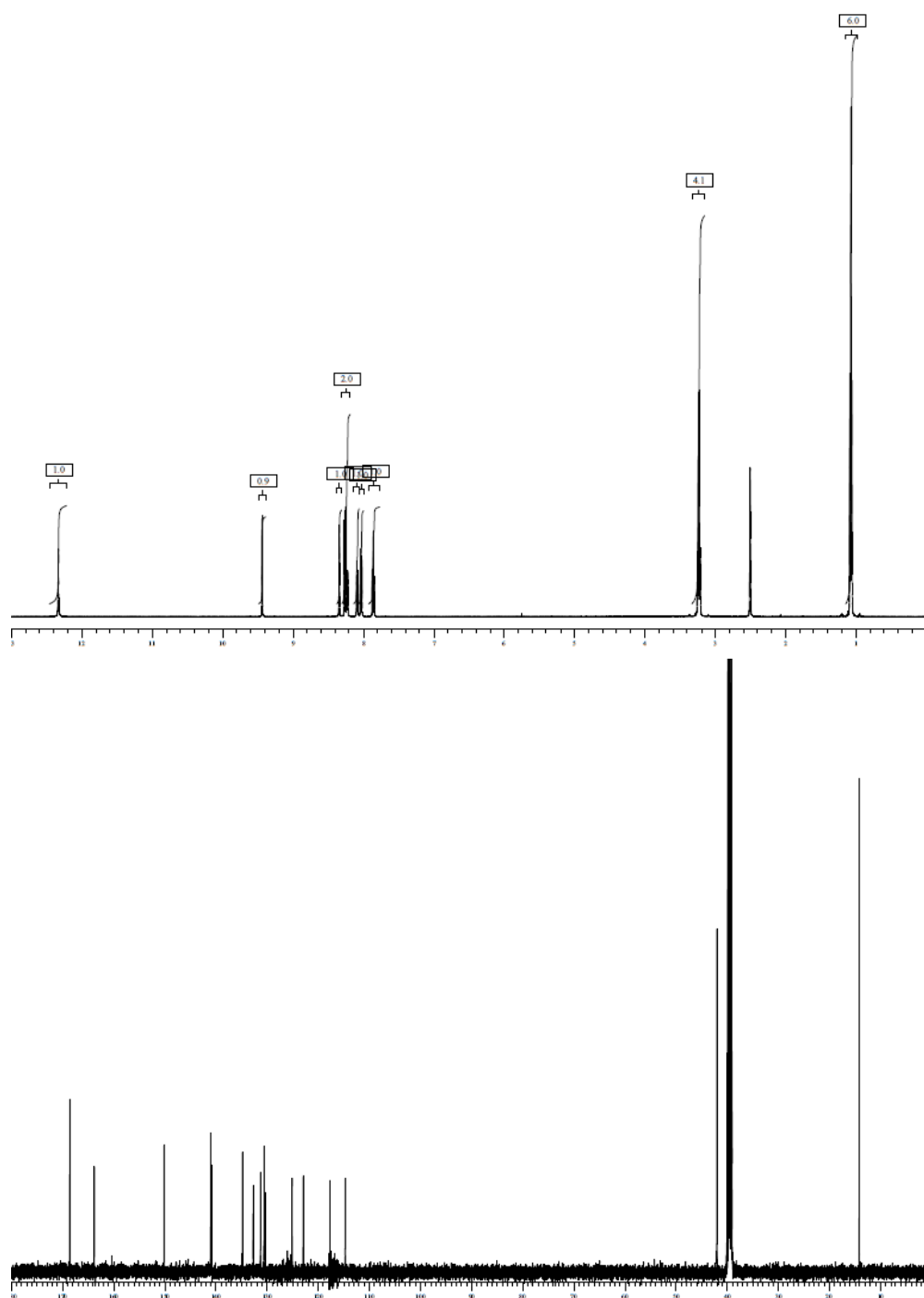


## Compound 38

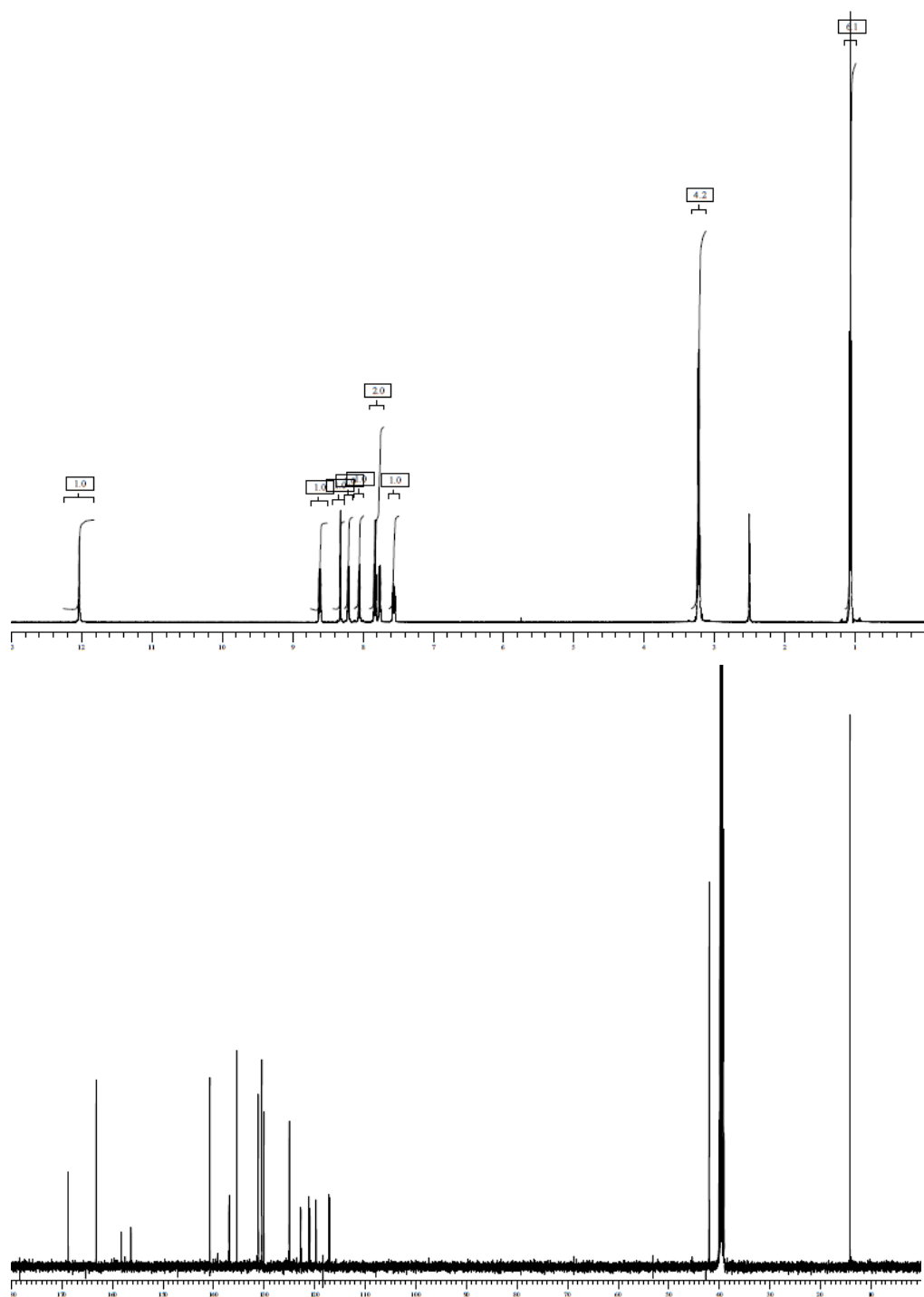




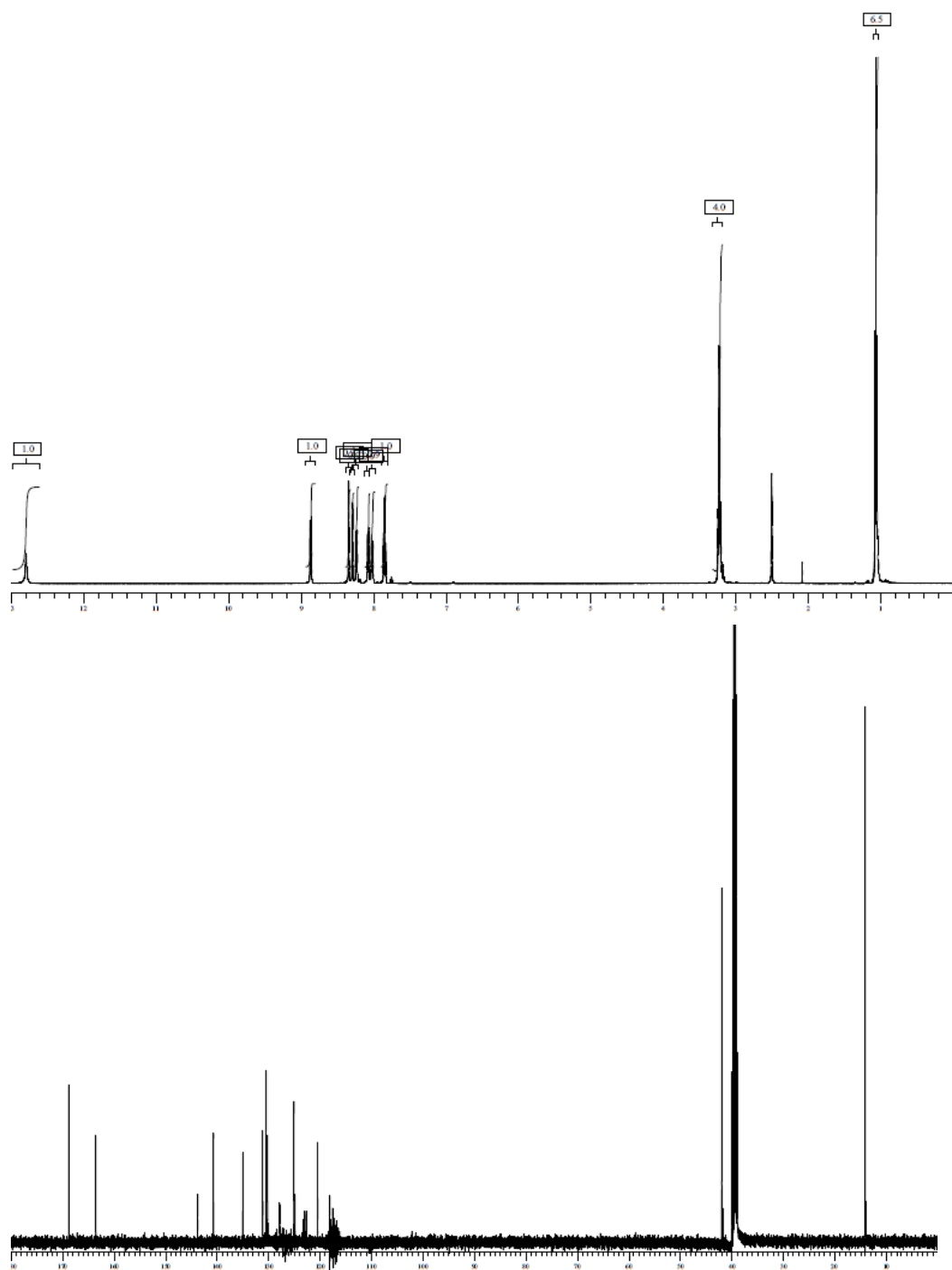
## Compound 39



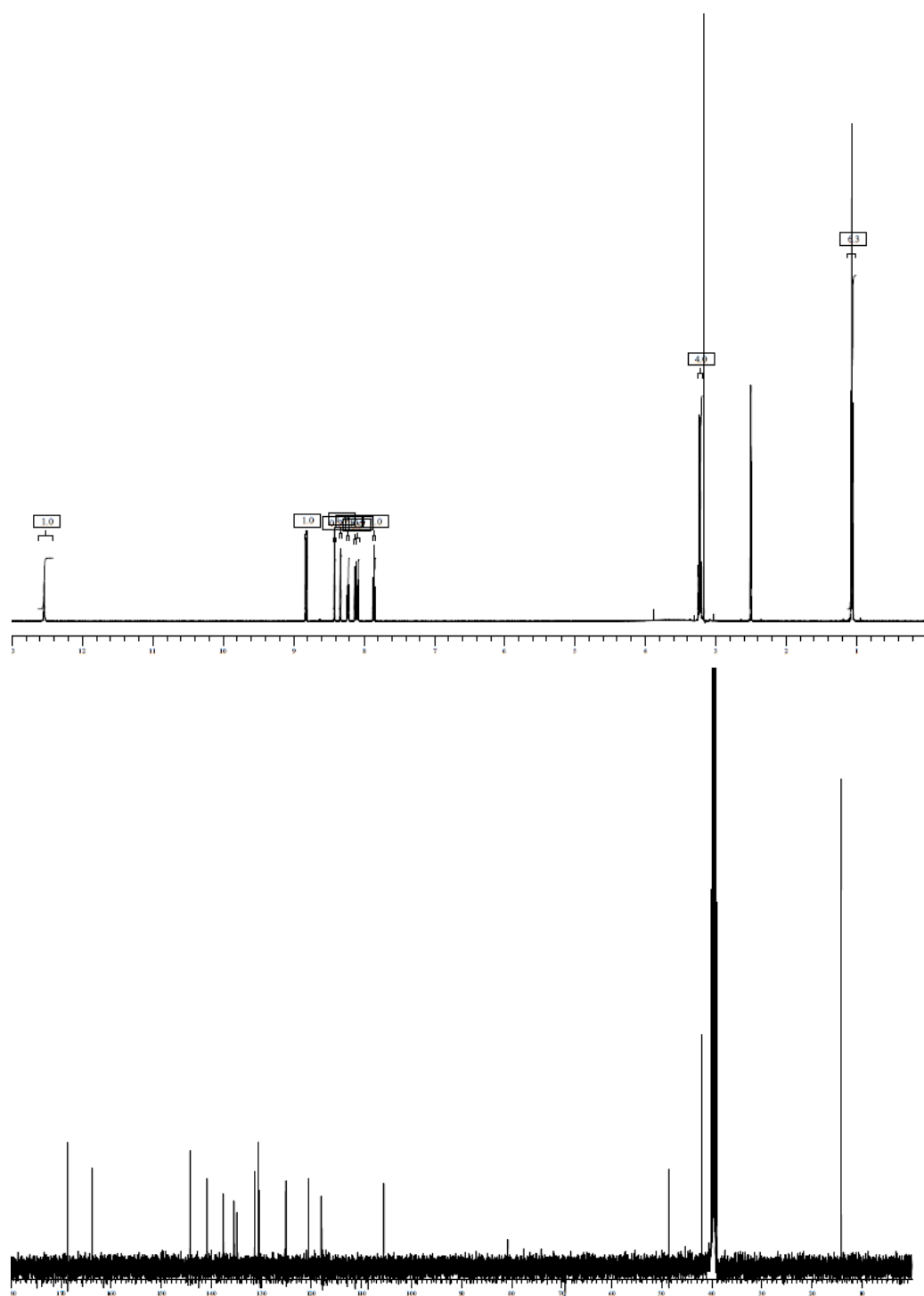
## Compound 40



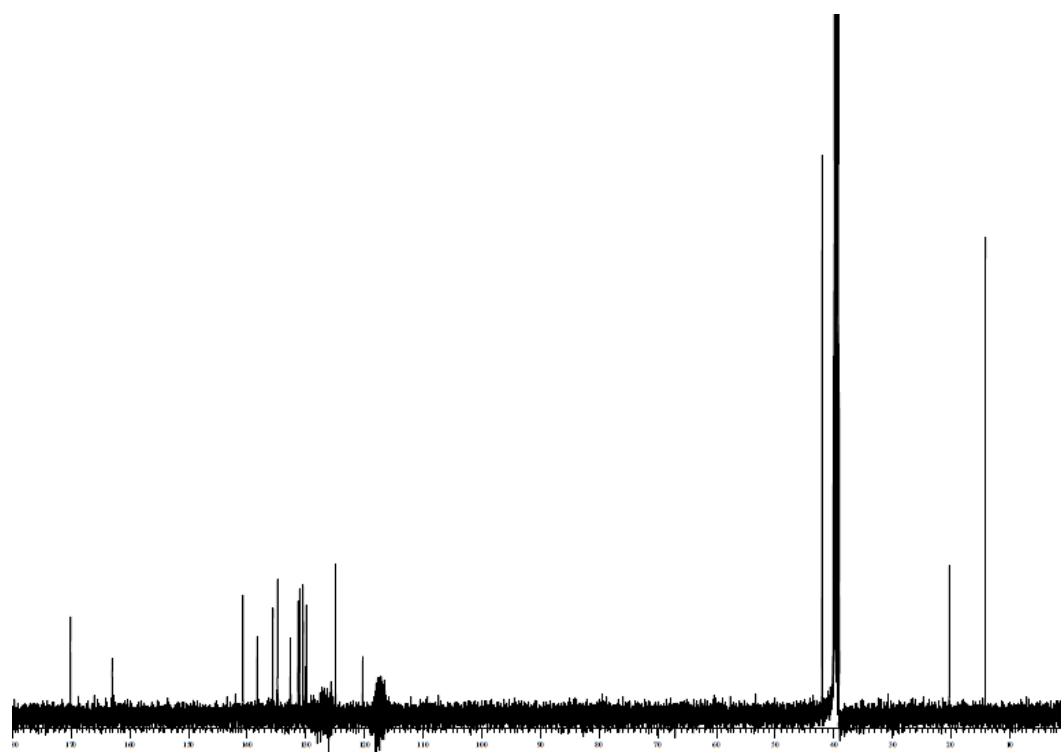
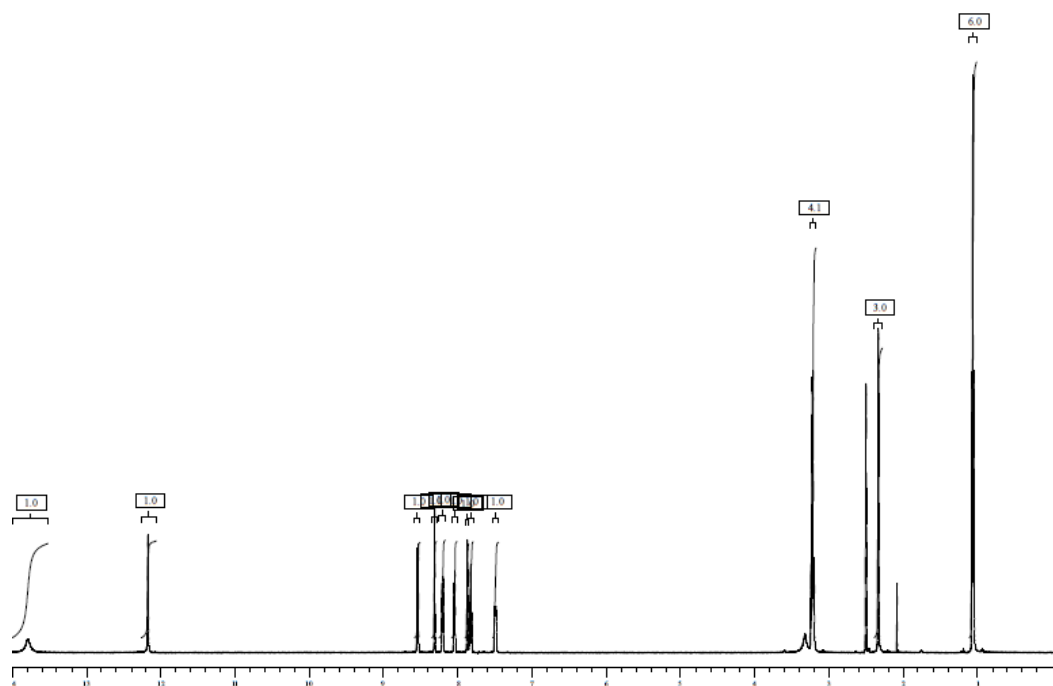
## Compound 41



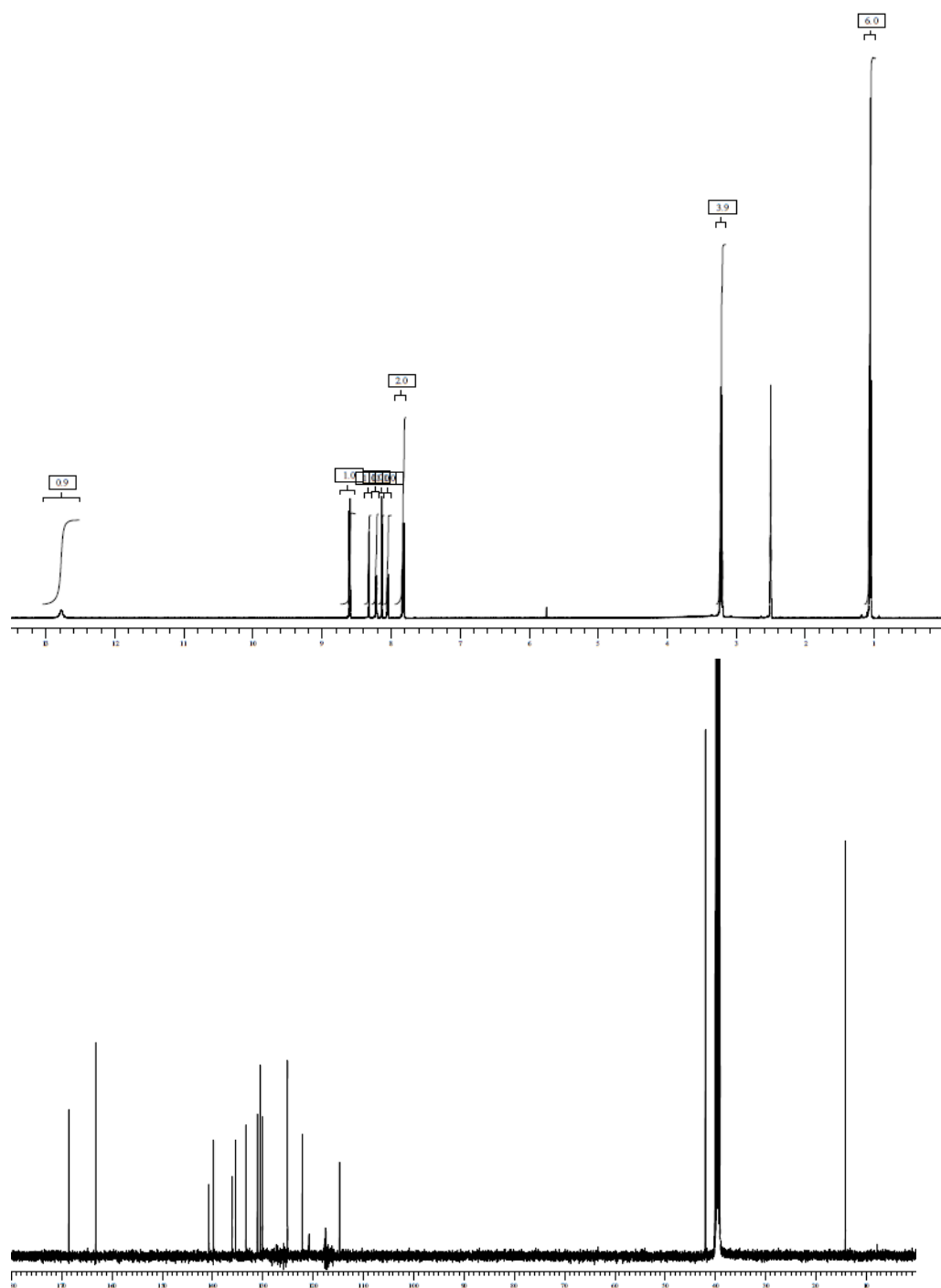
## Compound 42



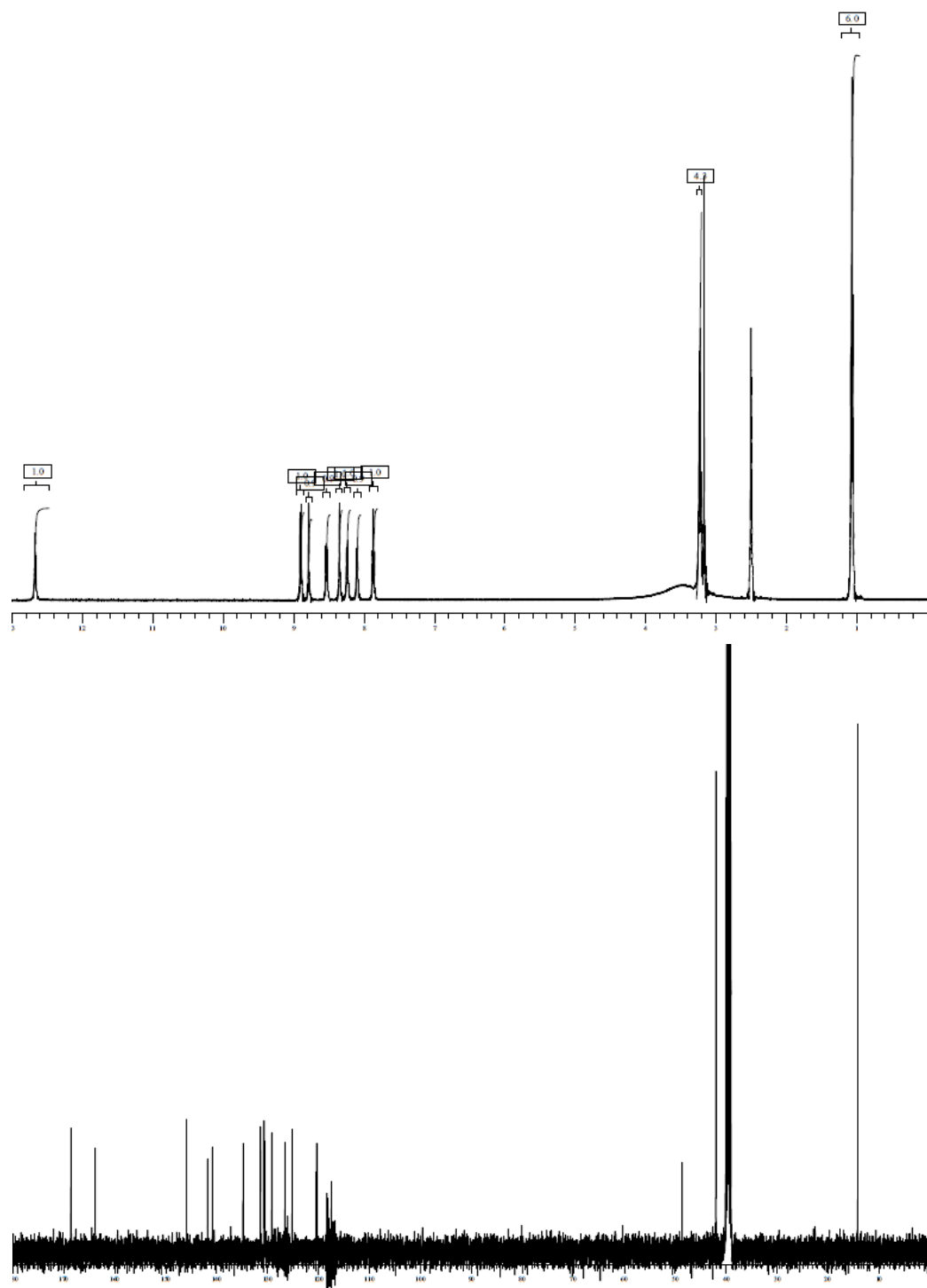
## Compound 43



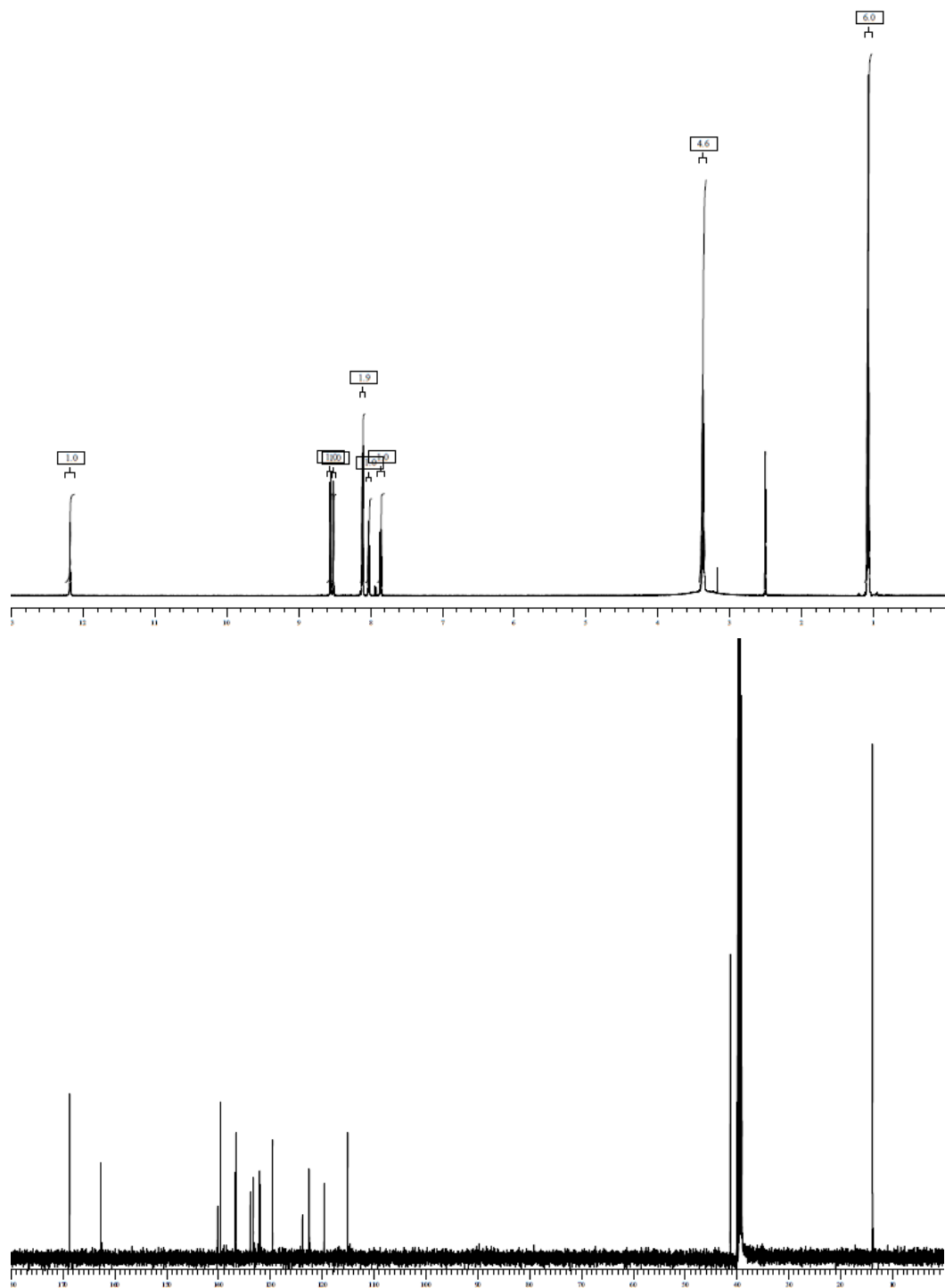
## Compound 44



## Compound 45

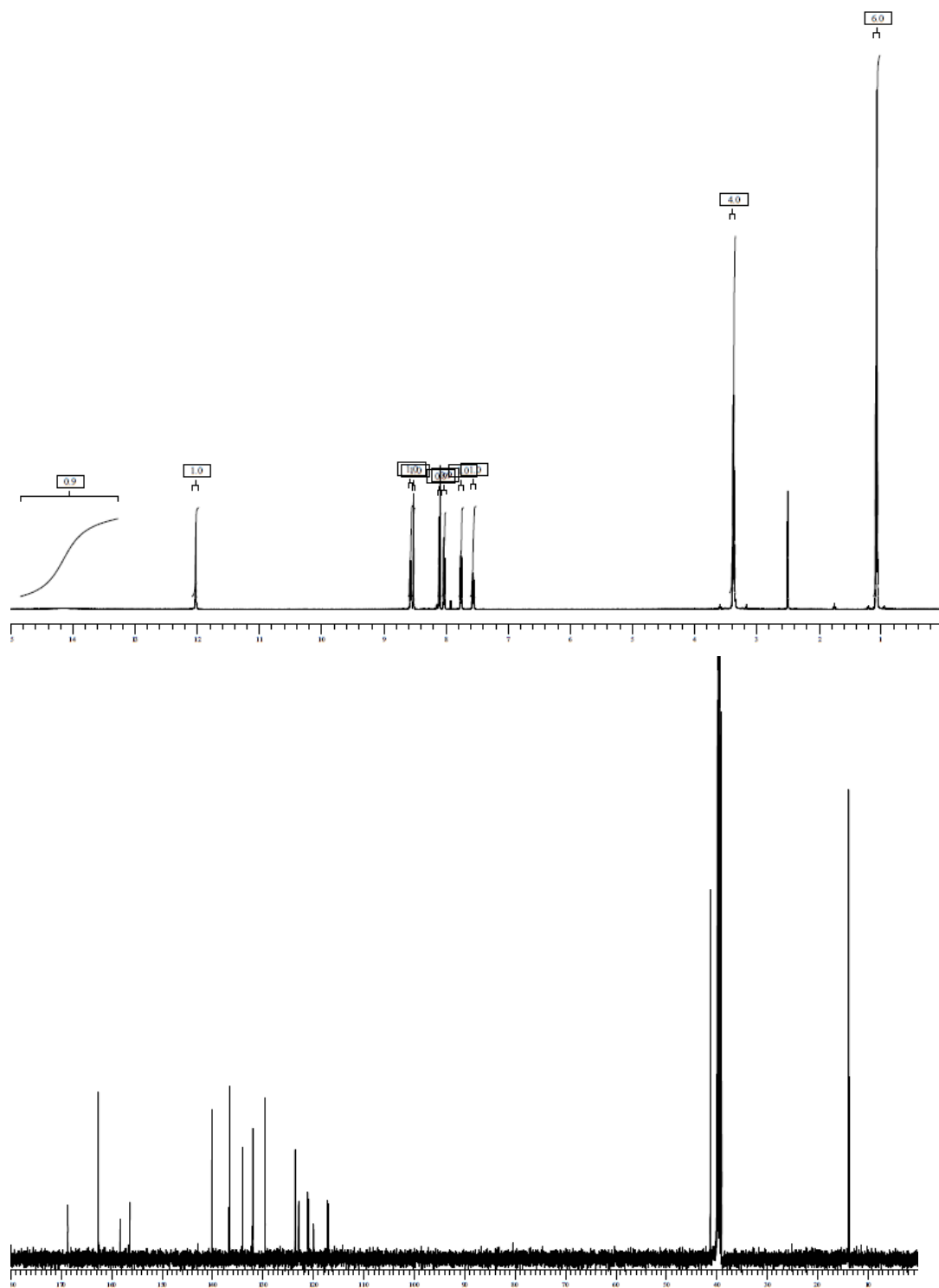


## Compound 46

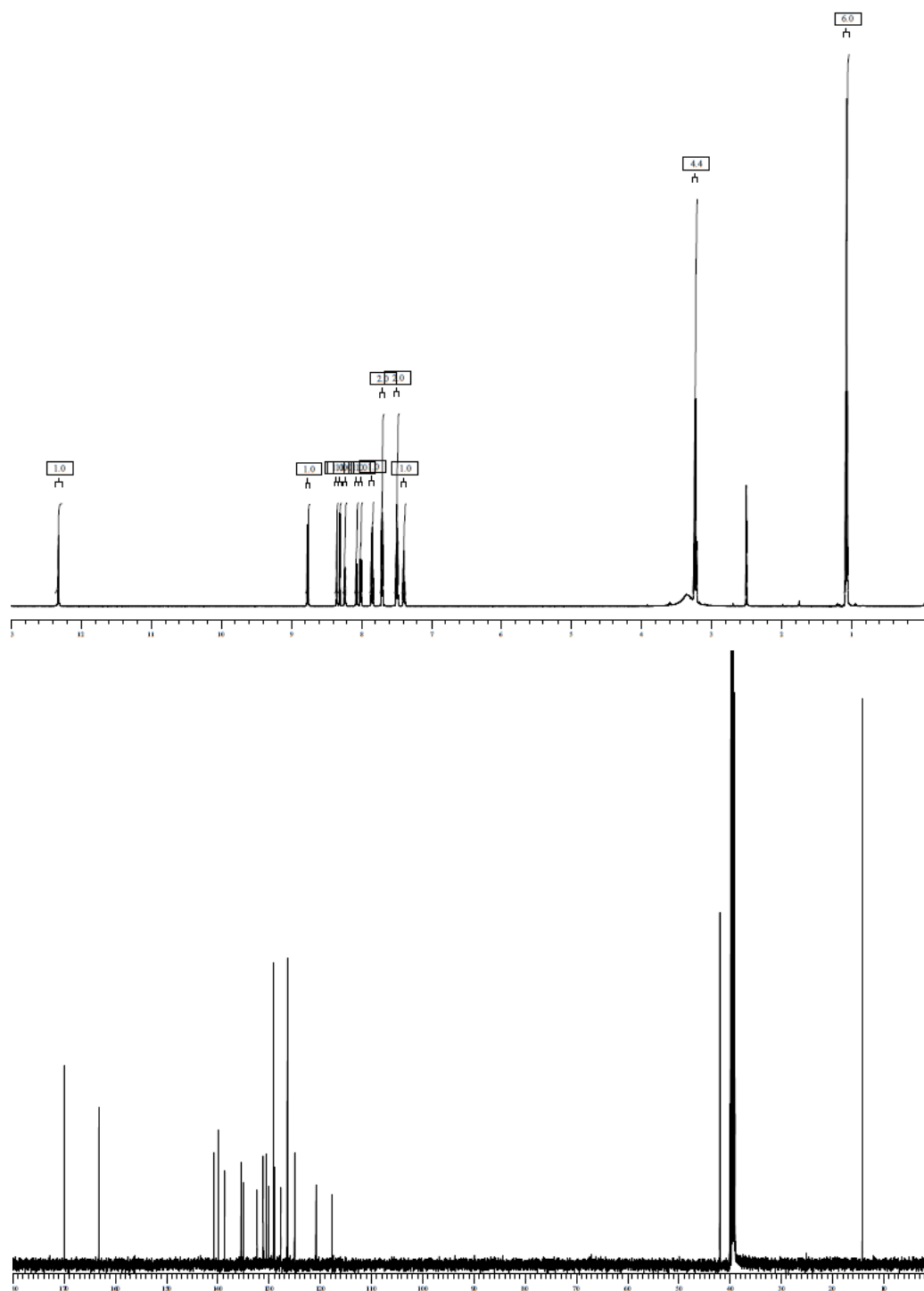




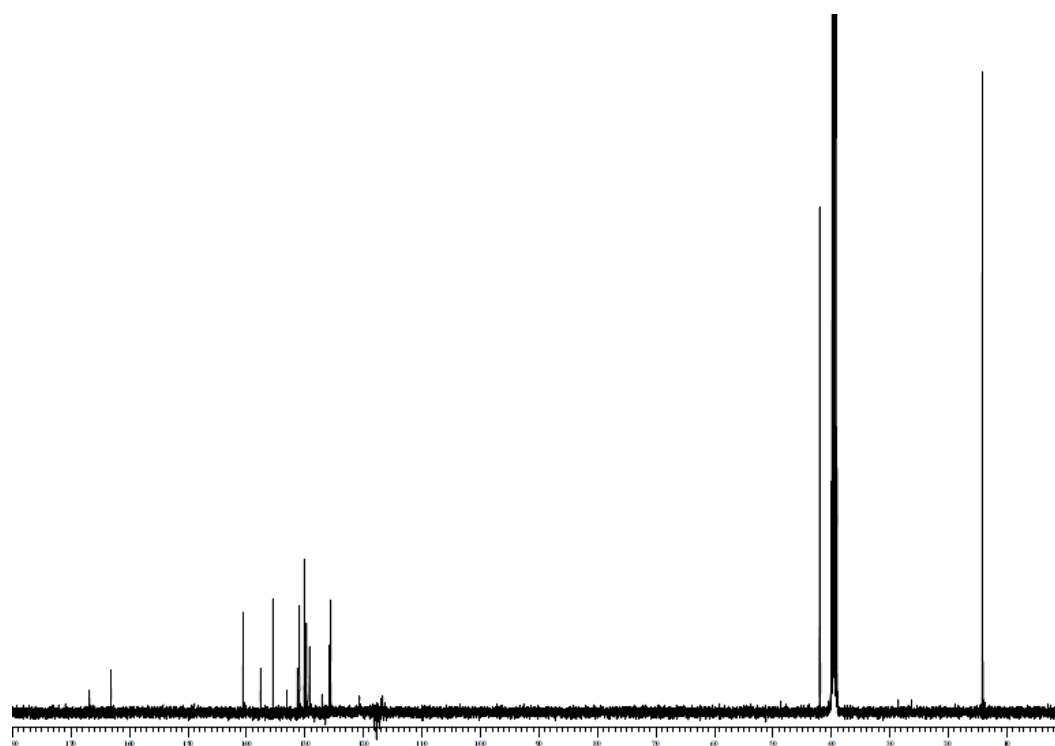
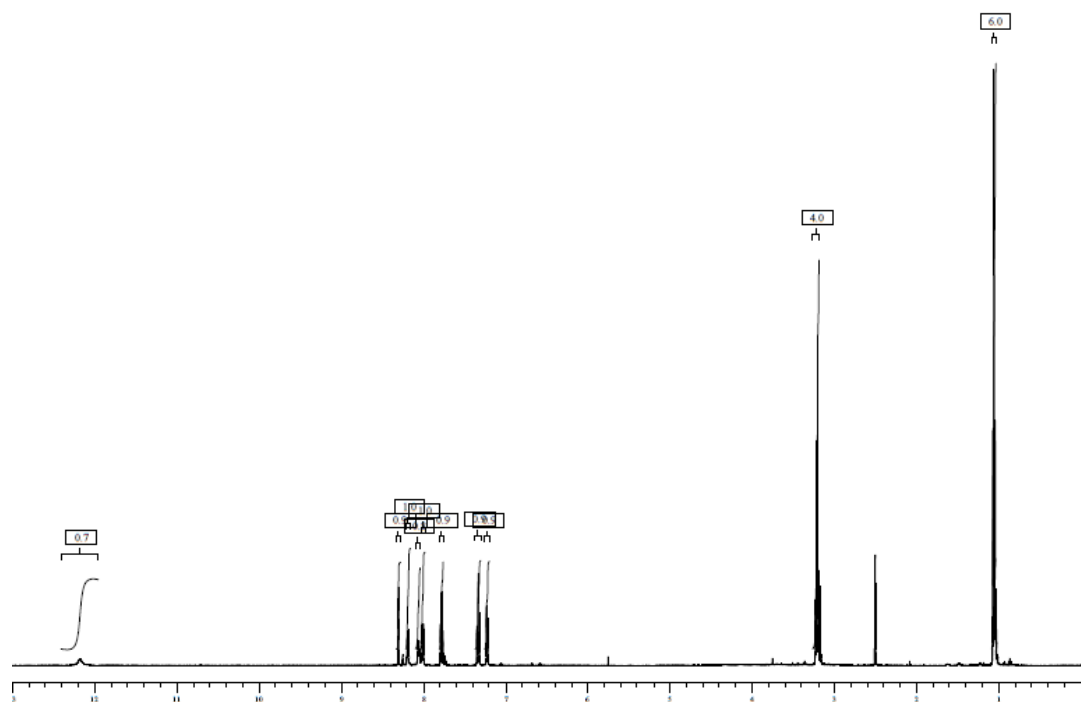
## Compound 47



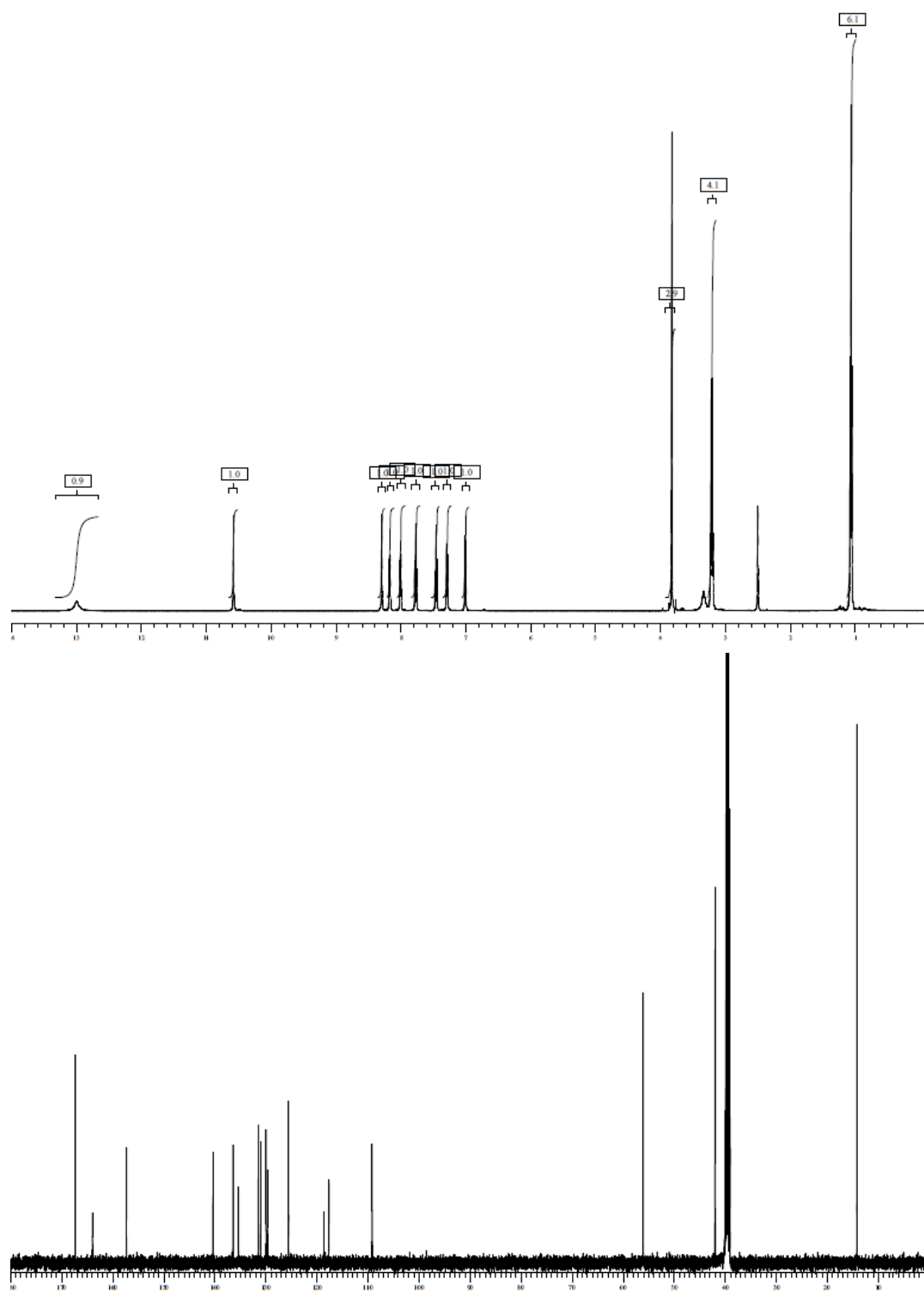
## Compound 48



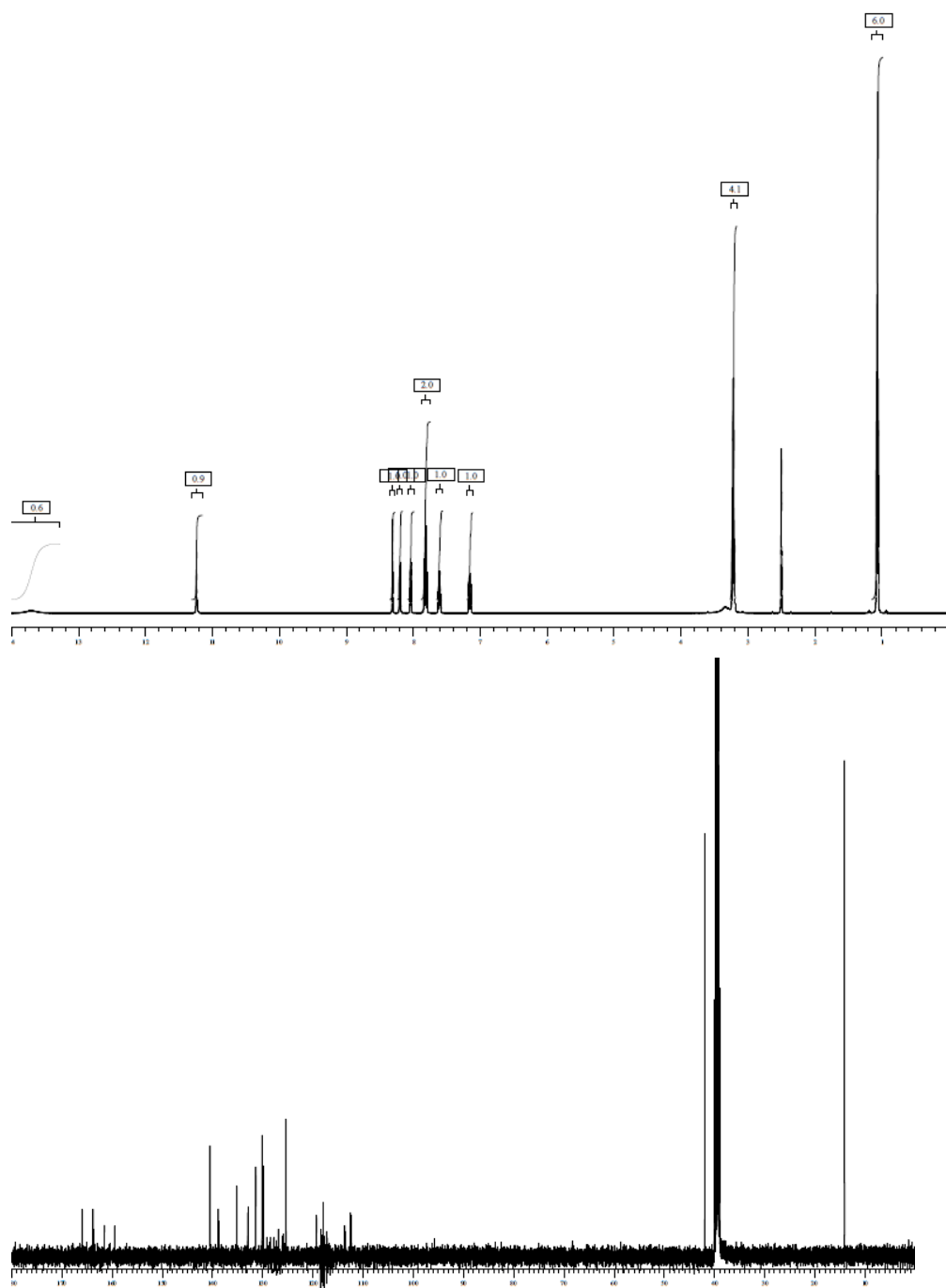
## Compound 49



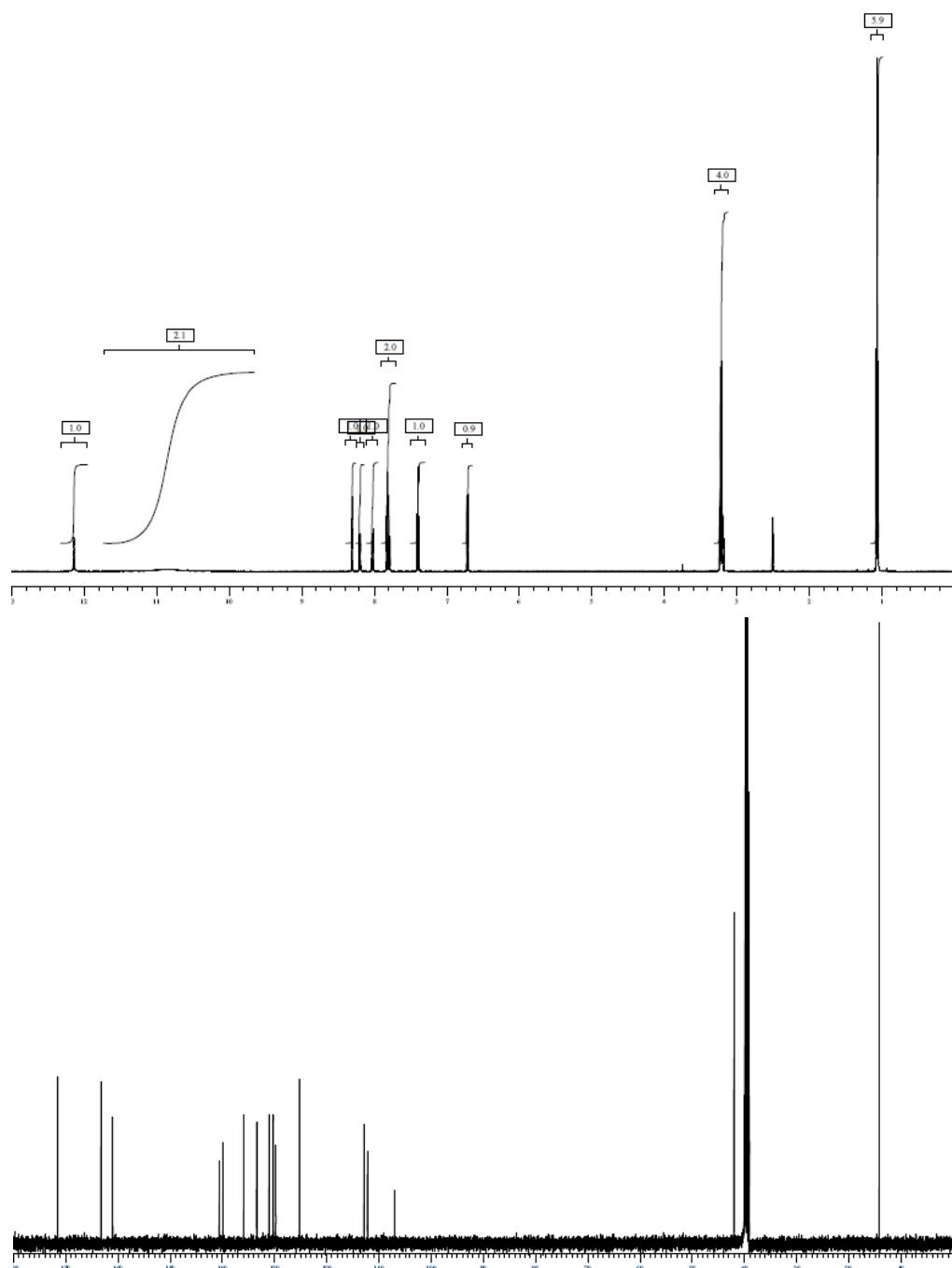
## Compound 50



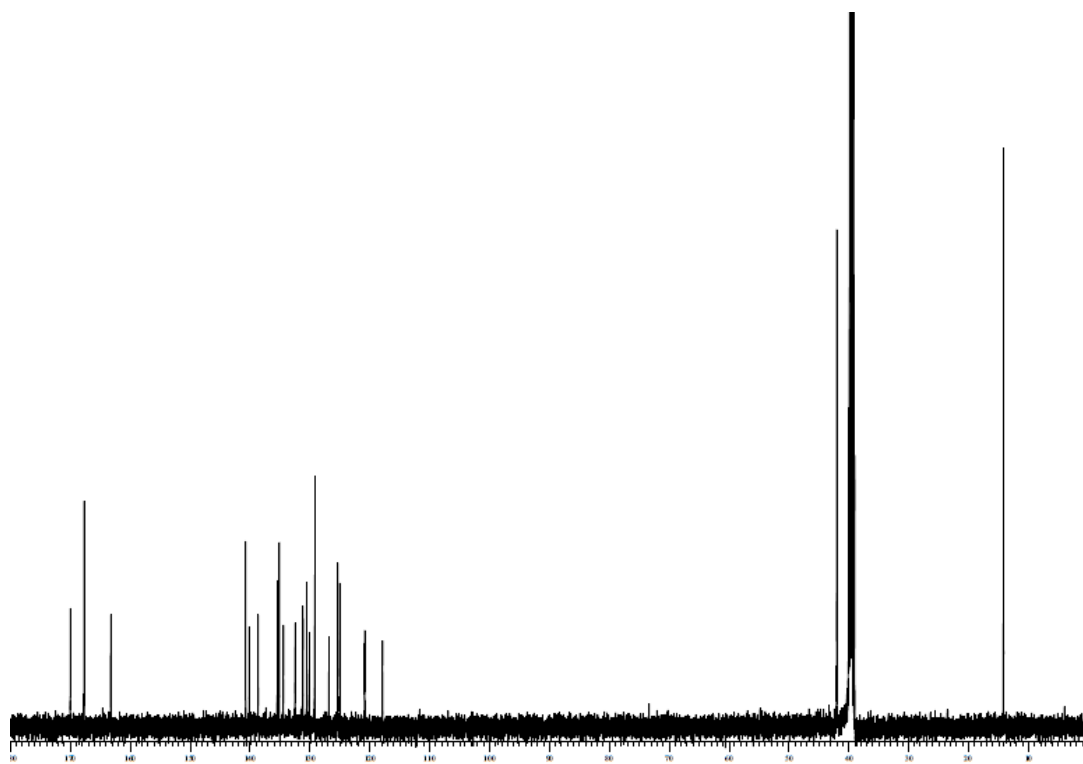
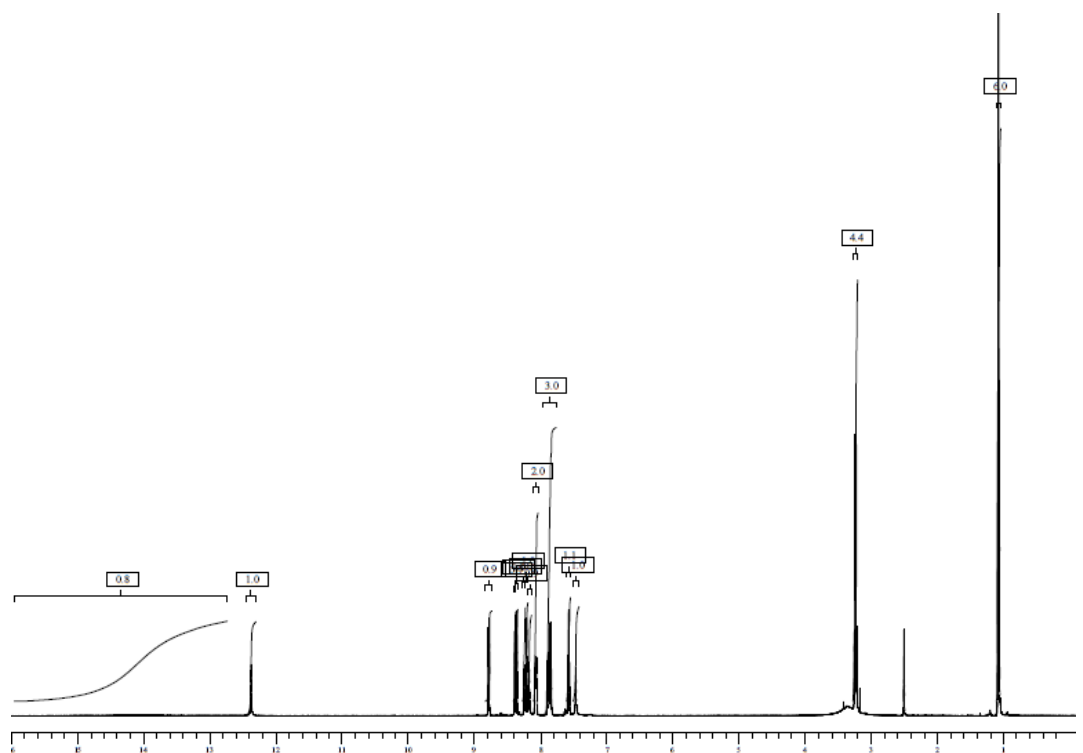
## Compound 51



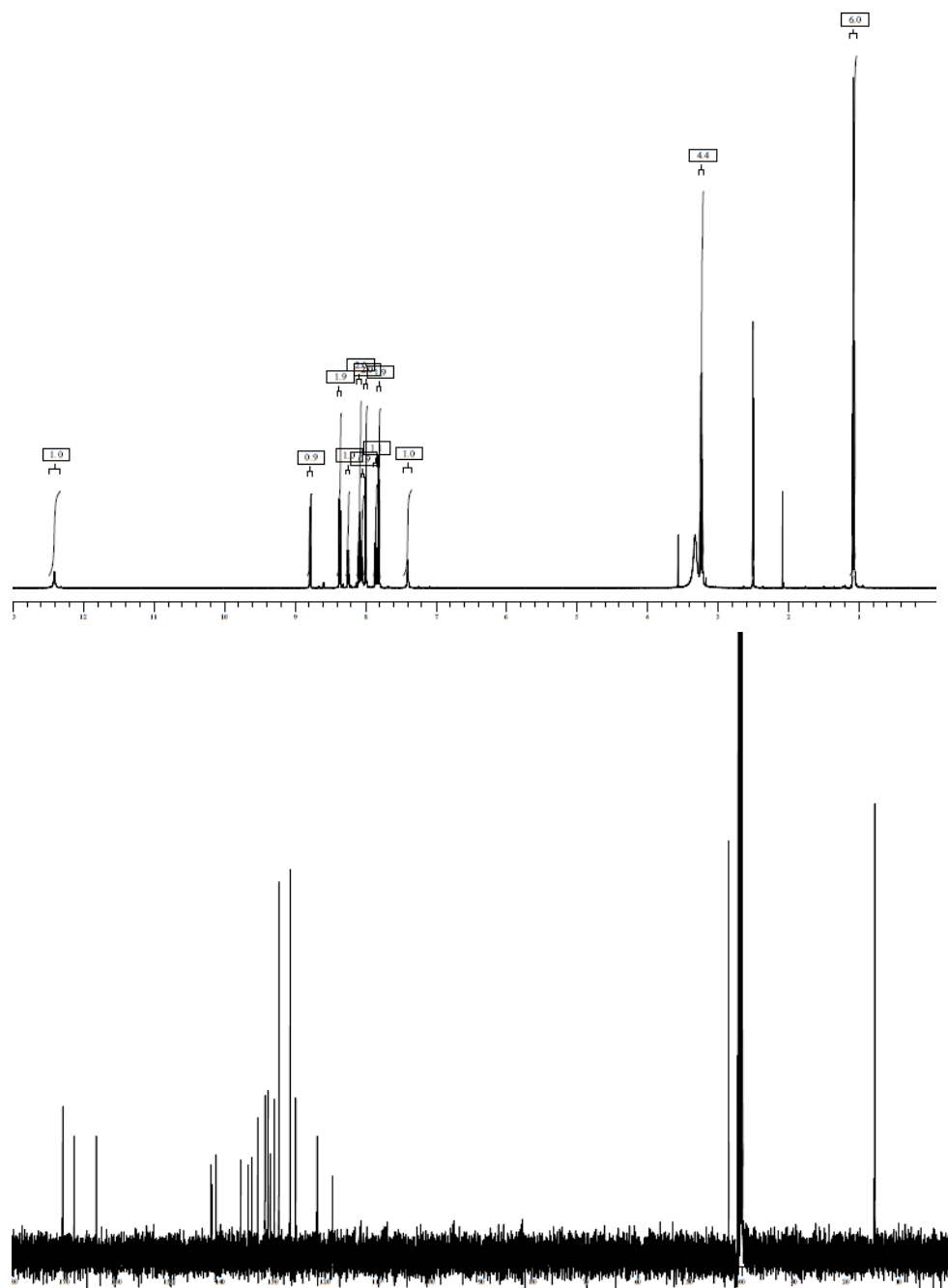
## Compound 52



## Compound 53

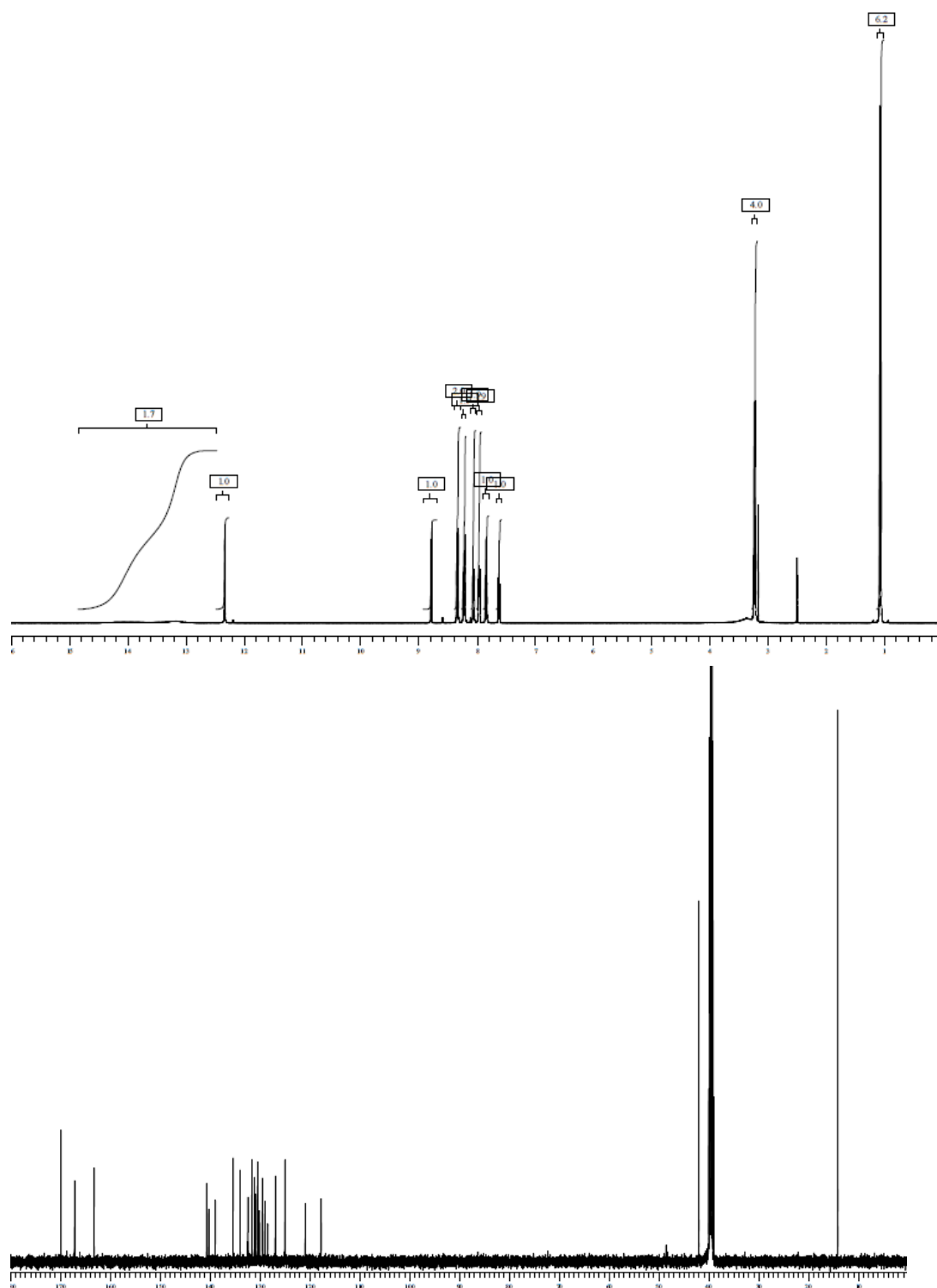


## Compound 54

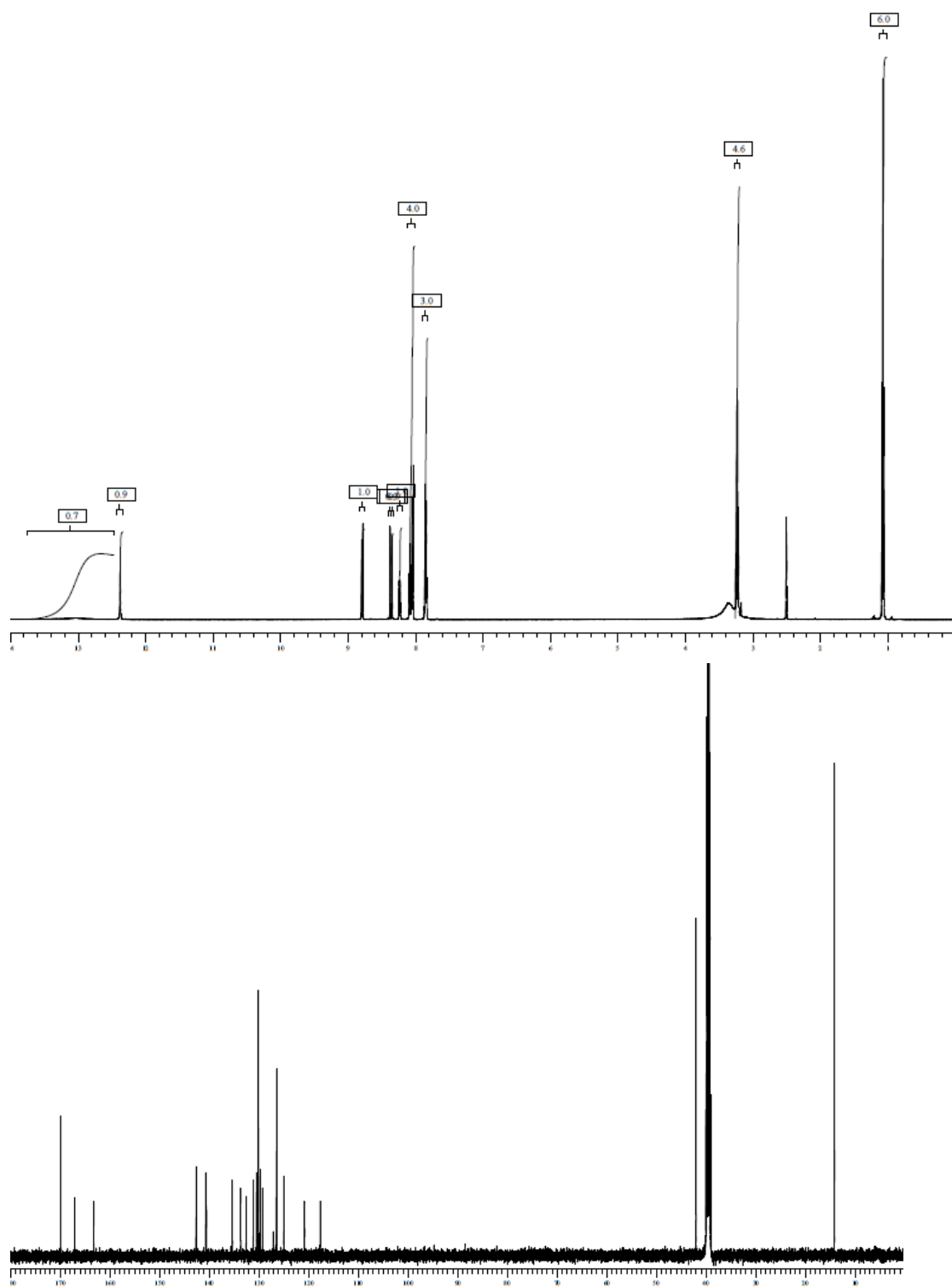




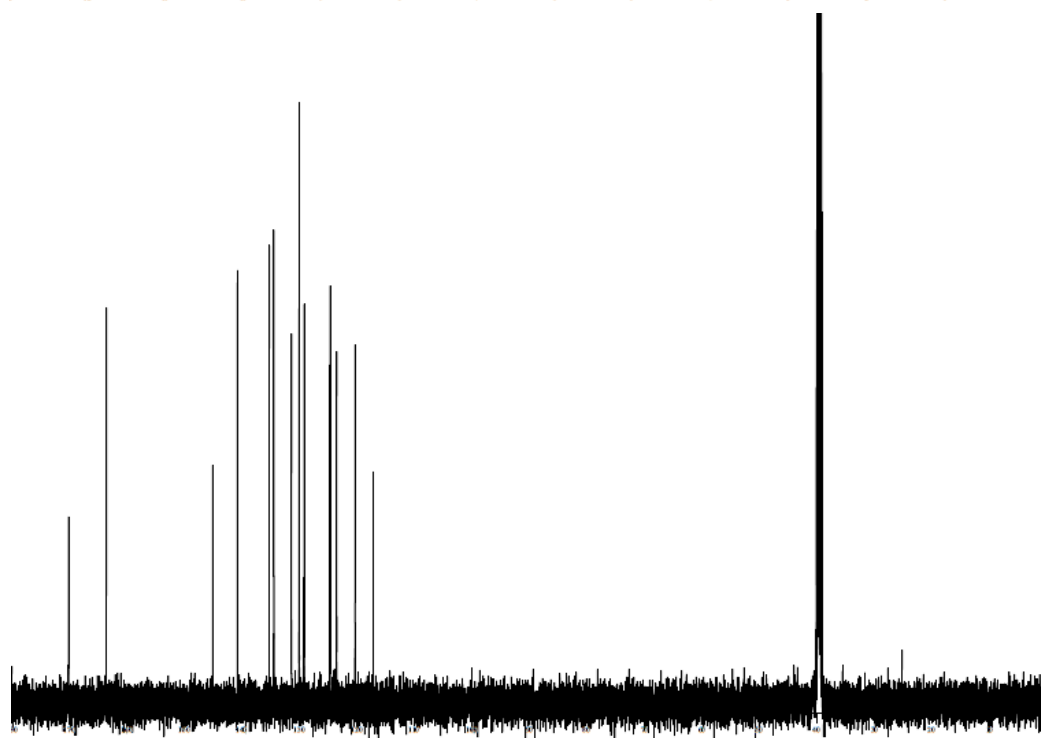
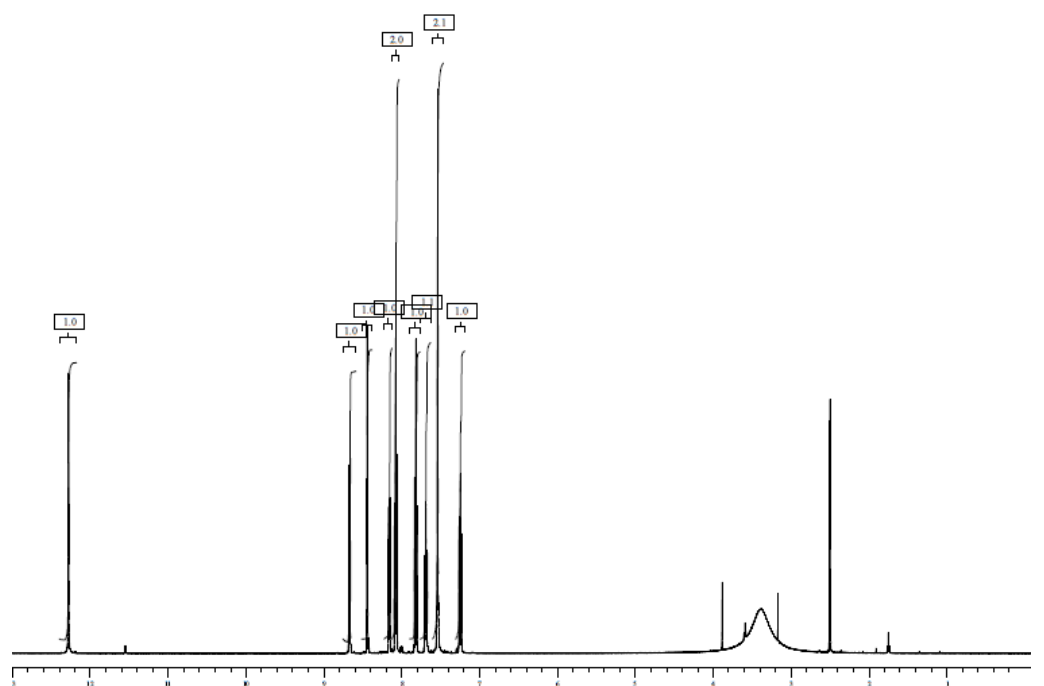
## Compound 55



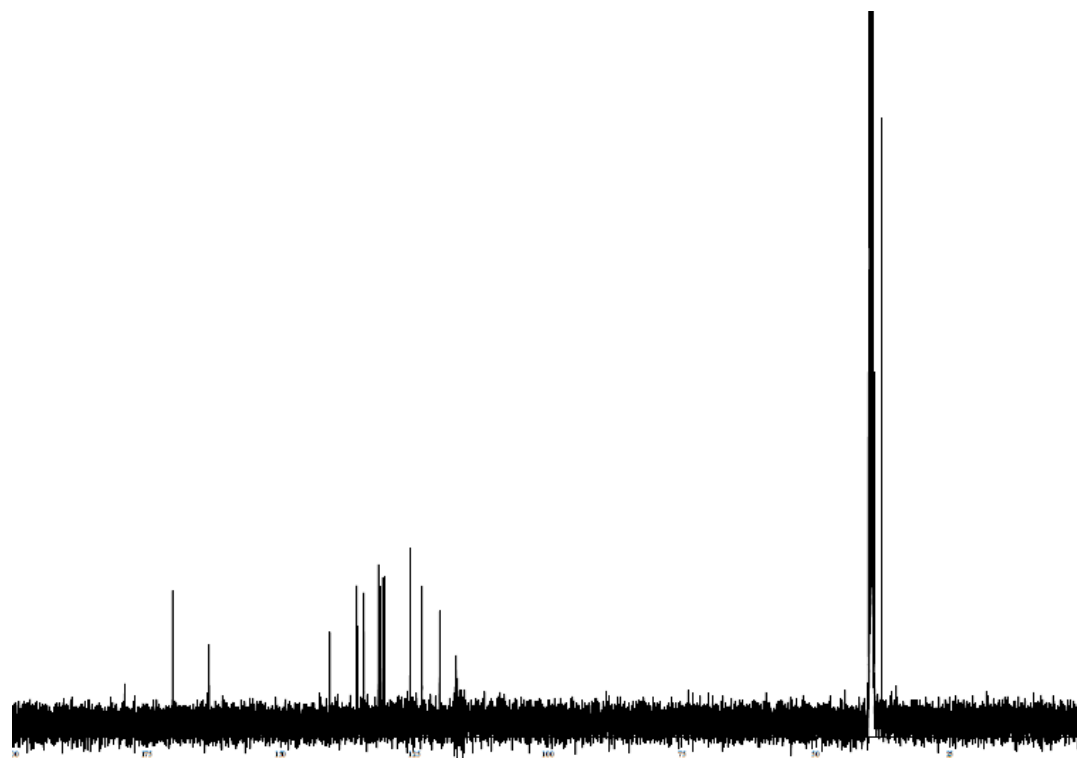
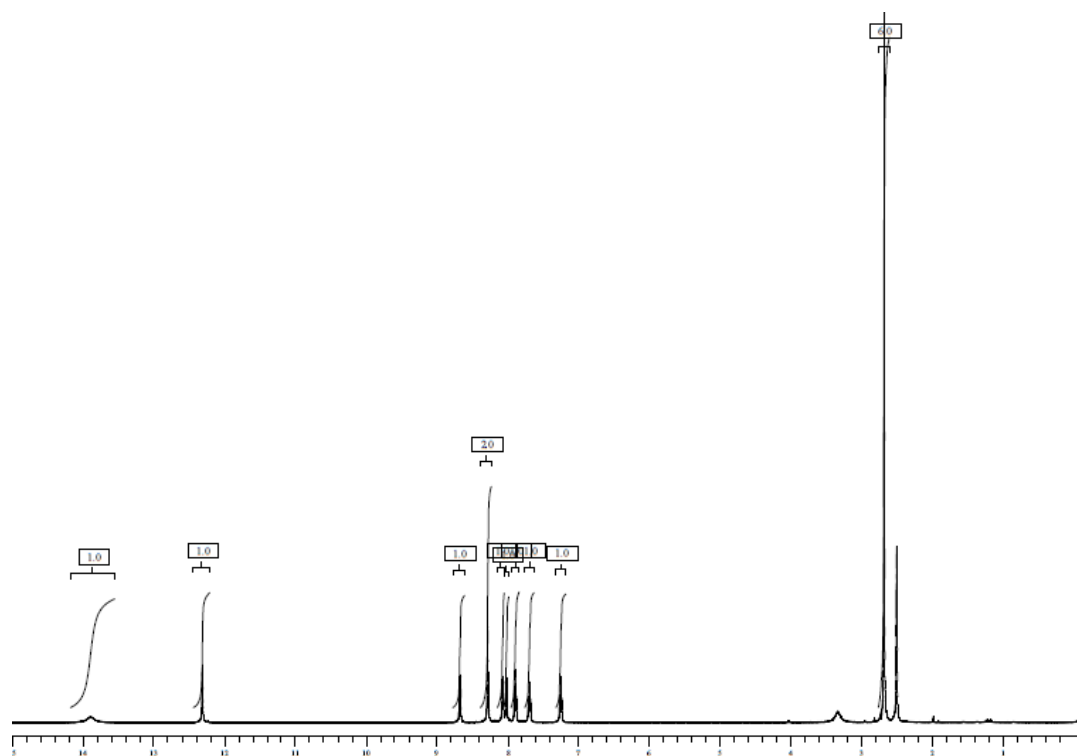
## Compound 56



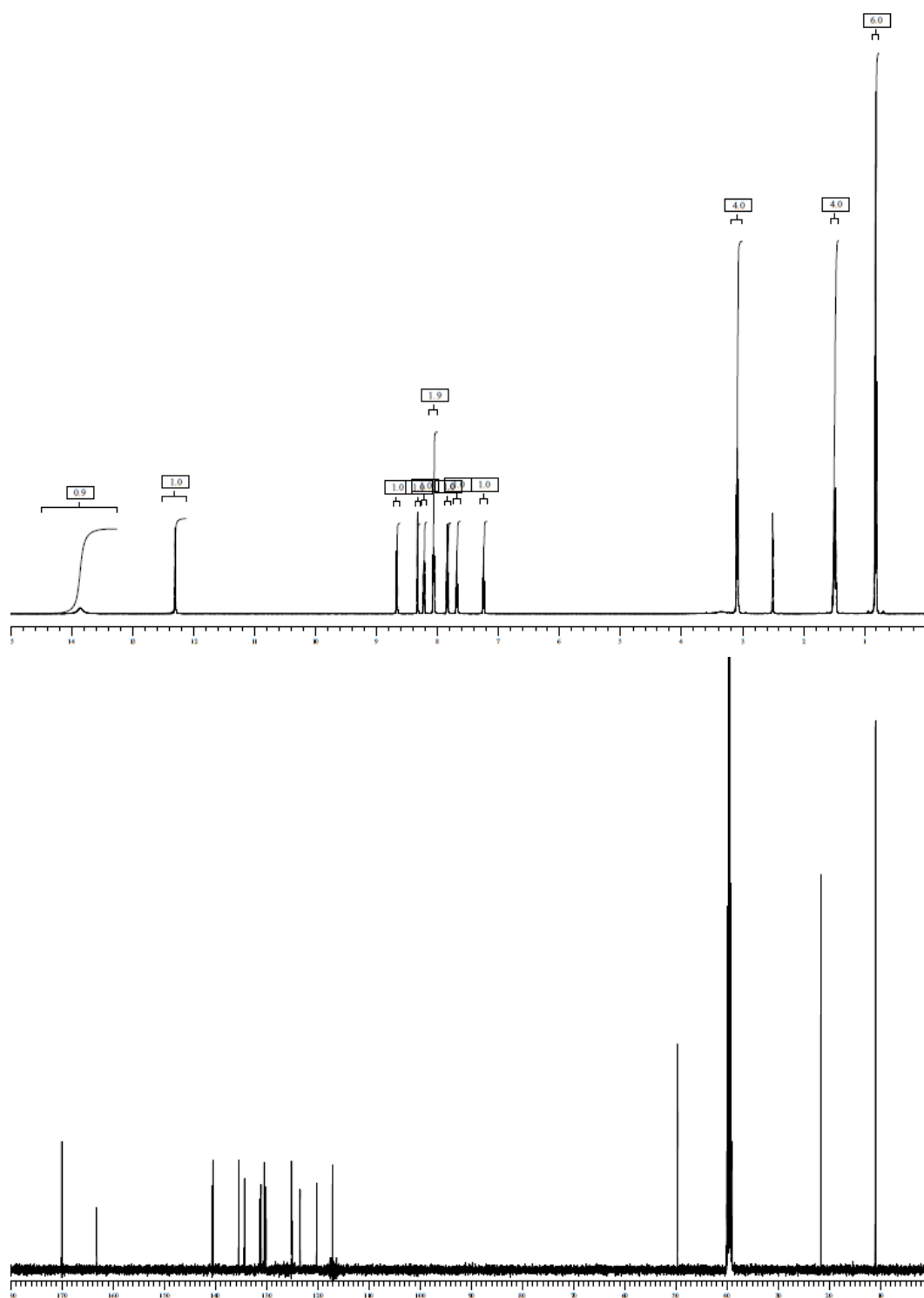
## Compound 57



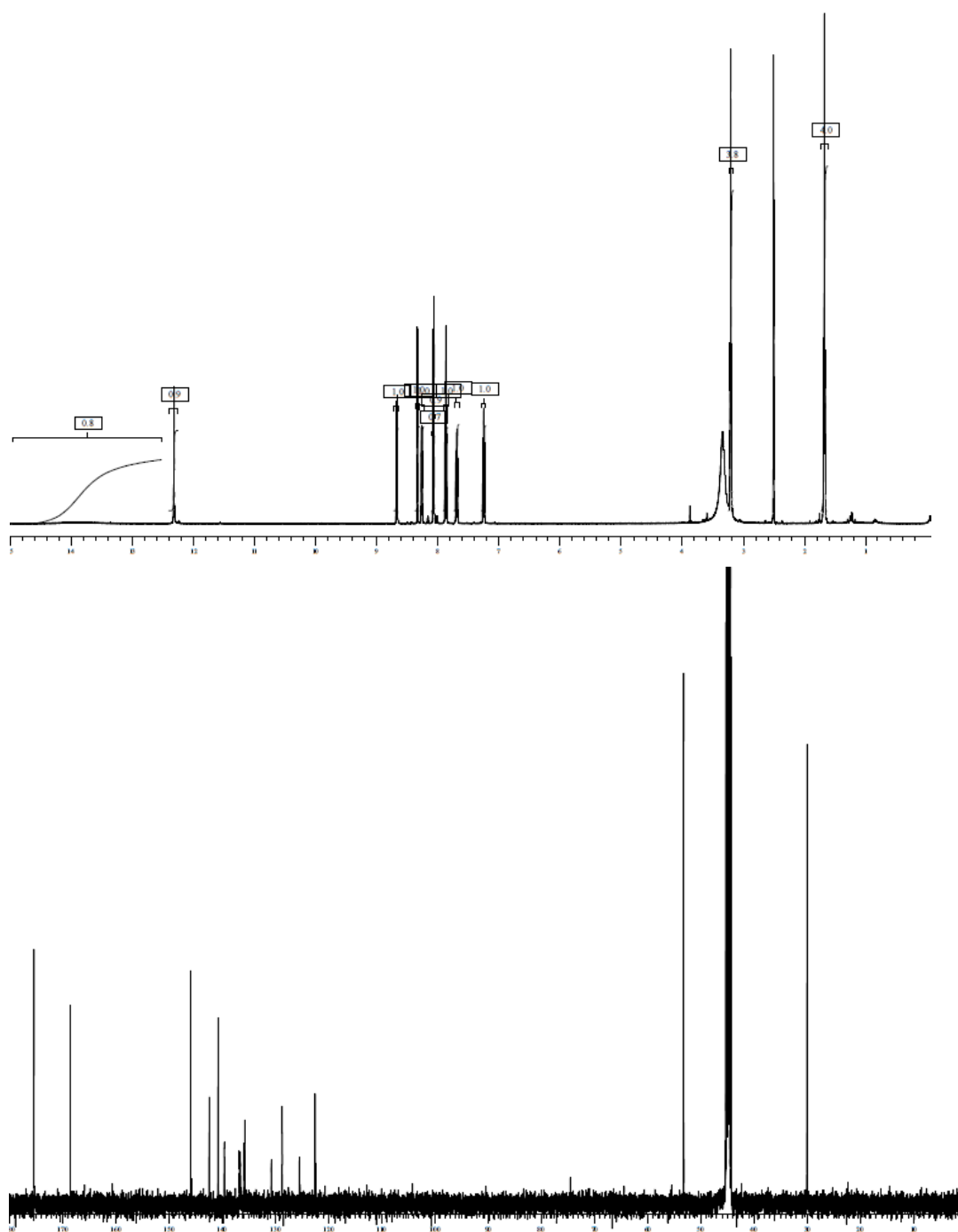
Compound 58



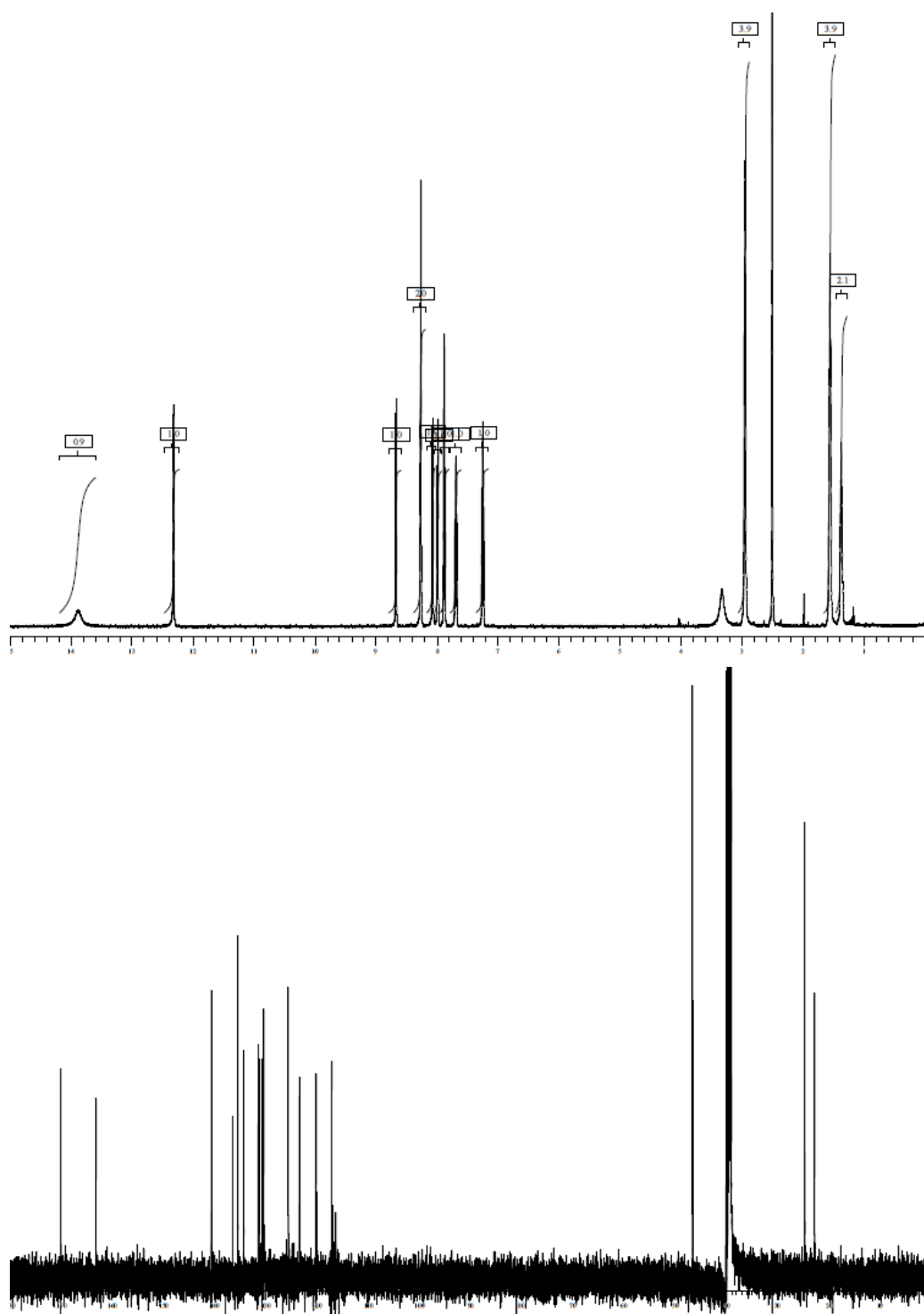
## Compound 59



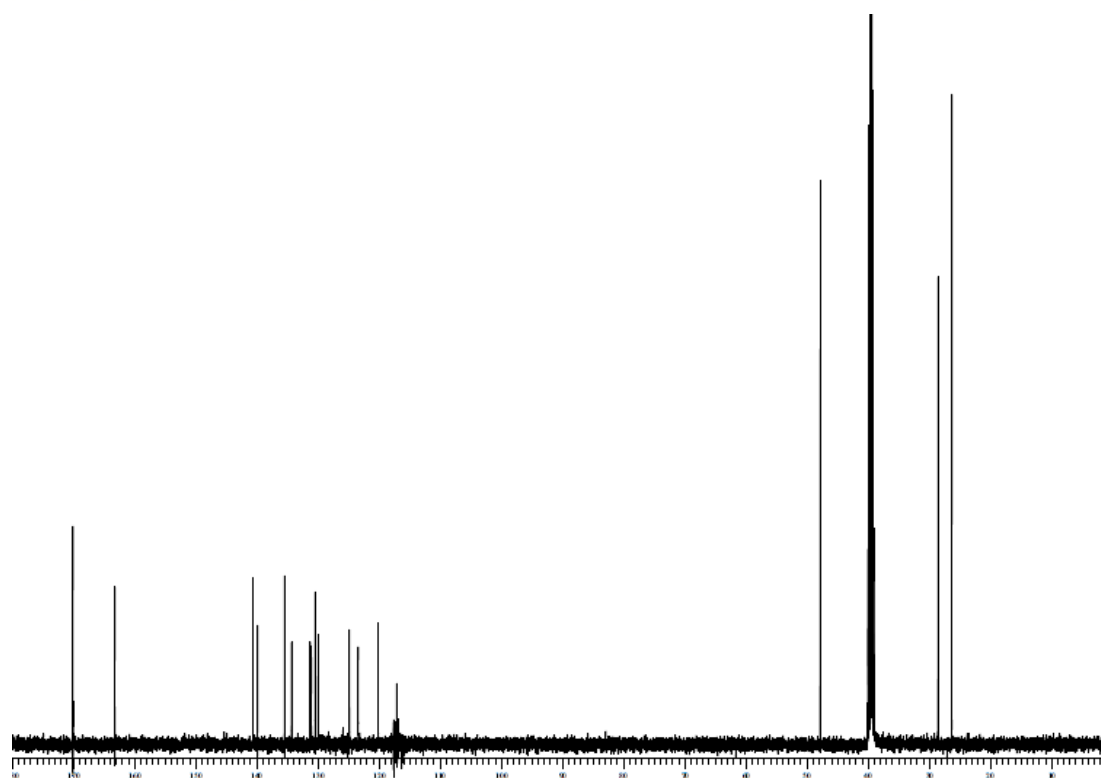
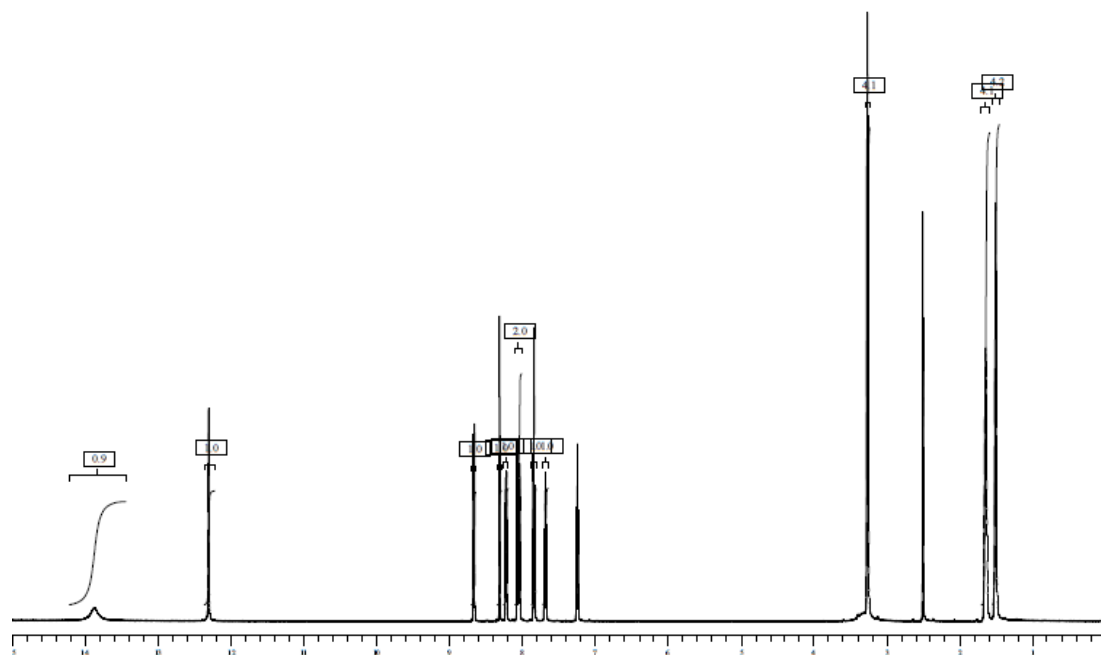
## Compound 60



## Compound 61

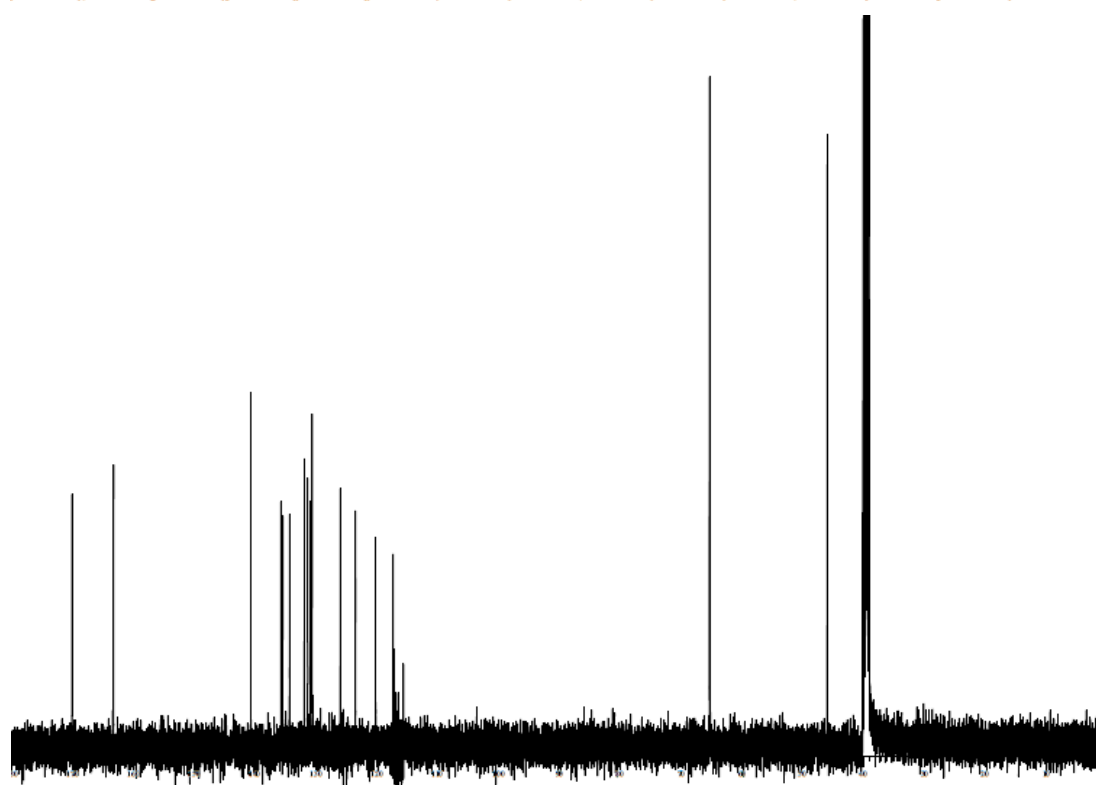
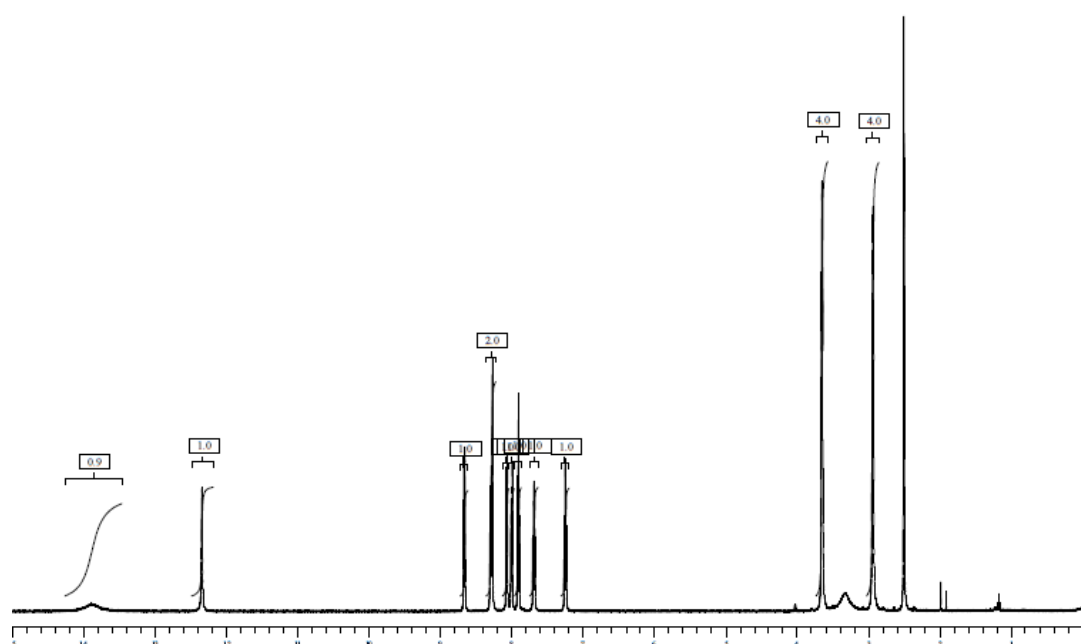


## Compound 62

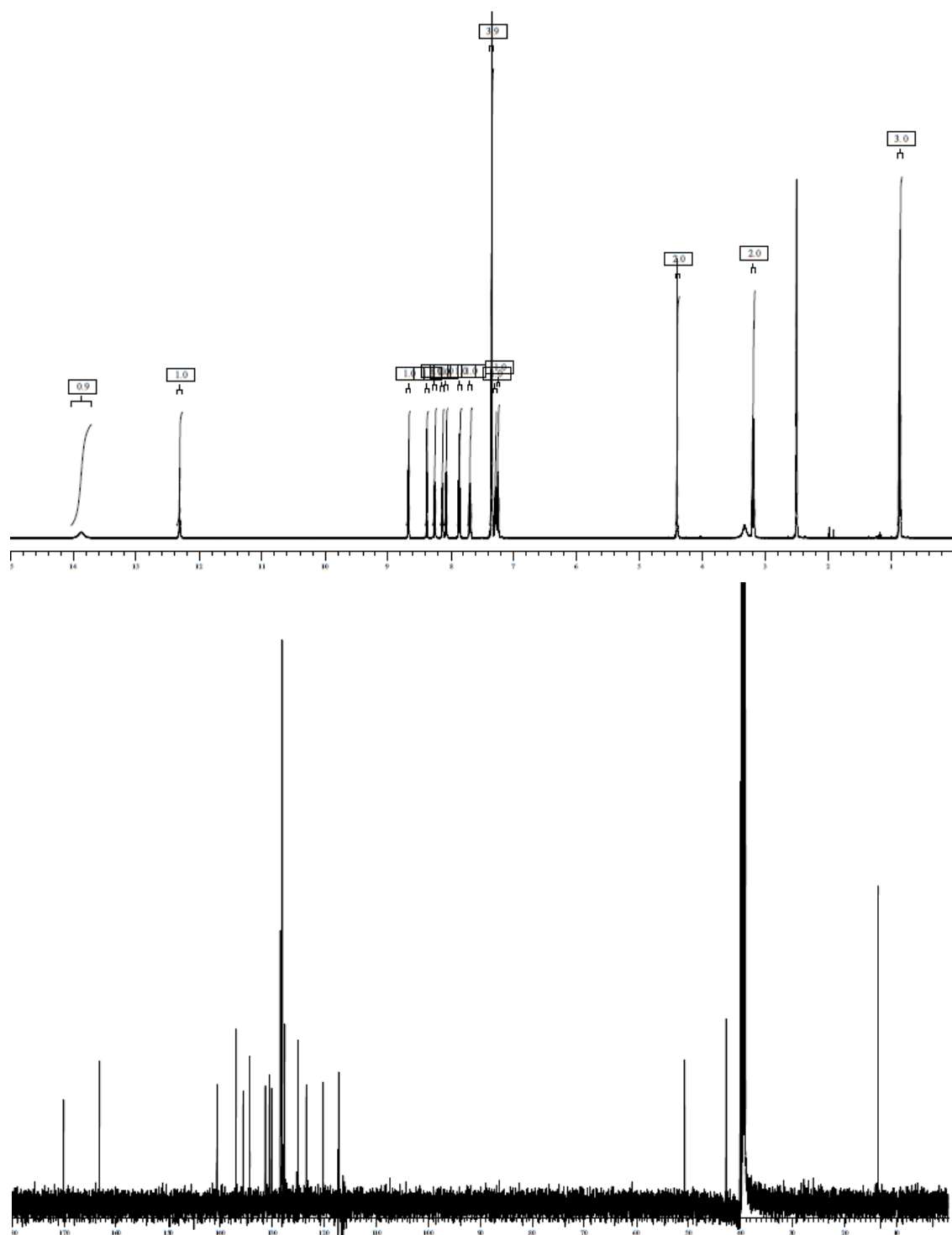




## Compound 63



## Compound 64



**F      Application of dual inhibition concept within looped autoregulatory system toward antivirulence agents against *Pseudomonas aeruginosa* infections**

Andreas Thomann, Antonio G. Gomes de Mello Martins, Christian Brengel, Martin Empting and Rolf W. Hartmann

ACS Chem. Biol. 2016, 11, 1279–1286

## Supporting Information

### Content

#### I. General experimental information - Chemistry

- a. Chemical synthesis of compounds **3–6**
- b. Crystallization of **6a** and X-ray crystallography
- c. <sup>13</sup>C-NMR and HSQC spectra of compounds **3–6**
- d. LC purity of compounds **3–6**

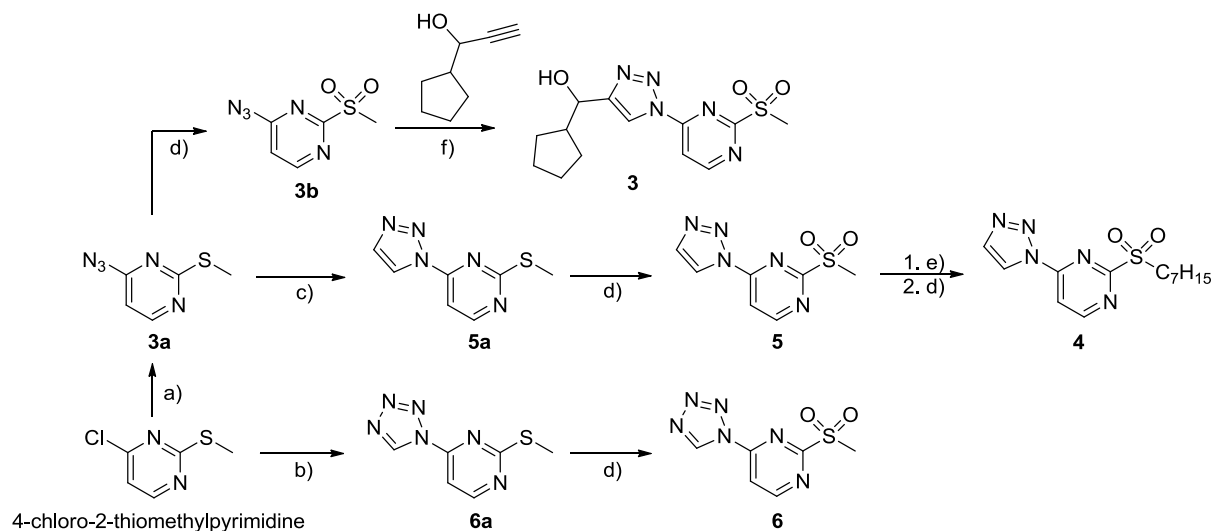
#### II. General experimental information - Biology

- a. Chemicals, bacterial strains, and media
- b. Pyocyanin assay
- c. Prolonged pyocyanin assay
- d. Growth curves of *P. aeruginosa* PA14
- e. Biofilm inhibition by compound **2**
- f. PqsD *in vitro* assay
- g. PqsR *in vitro* assay

#### III. References

## I. General experimental information - Chemistry

### a. Chemical Synthesis of compounds 3–6



**Scheme S1.** a) see reference 1b; b) See reference 1a; c) TMS-Acetylene, CuSO<sub>4</sub>, sodium ascorbate, *tert*BuOH:H<sub>2</sub>O, r.t.; d) Oxone, EtOAc:H<sub>2</sub>O, r.t.; e) heptane-1-thiol, DMF, K<sub>2</sub>CO<sub>3</sub>, 0°C; f) 1-cyclopentylprop-2-yn-1-ol, CuSO<sub>4</sub>, sodium ascorbate, *tert*BuOH:H<sub>2</sub>O, r.t.

Compounds **3a**, **3b** and **6a** were synthesized as reported before.<sup>1,2</sup>

**2-(methylthio)-4-(1H-1,2,3-triazol-1-yl)pyrimidine (5a):** To a solution of **3a** (1.0 eq) and TMS-acetylene (2.0 eq) in *tert*BuOH:water (1:1) was added CuSO<sub>4</sub>·5H<sub>2</sub>O (0.02 eq) and sodium ascorbate (0.1 eq). The mixture was stirred at room temperature for 16 h. Brine was added and the aqueous layer was extracted three times with ethyl acetate. The combined organic layers were concentrated in vacuum and purified by flash chromatography (petroleum ether/ethyl acetate 8:2) to yield **5a** as a white solid (58% yield). <sup>1</sup>H NMR (300 MHz, CDCl<sub>3</sub>) δ 2.64 (s, 3H), 7.84 (d, J = 5.5, 1H), 7.87 (s, 1H), 8.62 (s, 1H), 8.71 (d, J = 5.4 Hz, 1H). <sup>13</sup>C NMR (75 MHz, CDCl<sub>3</sub>) δ 14.3, 104.9, 121.1, 134.6, 154.9, 159.8, 173.7. MS (ESI) m/z: 194.1 [M+H]<sup>+</sup>.

**cyclopentyl(1-(2-(methylsulfonyl)pyrimidin-4-yl)-1H-1,2,3-triazol-4-yl)methanol (3):** To a solution of **3b** (1.0 eq) and 1-cyclopentylprop-2-yn-1-ol (1.0 eq) in *tert*BuOH:water (1:1) was added CuSO<sub>4</sub>·5H<sub>2</sub>O (0.02 eq) and sodium ascorbate (0.1 eq). The mixture was stirred at room temperature for 16 h. Brine was added and the aqueous layer was extracted three times with ethyl acetate. The combined organic layers were concentrated in vacuum and purified by flash chromatography (hexane/ethyl acetate 7:3) to yield **3** as a white solid (49% yield). <sup>1</sup>H NMR (300 MHz, DMSO-d<sub>6</sub>) δ 1.63 - 2.19 (m, 9 H), 3.51 (s, 3H), 5.29 (s, 1H), 8.42 (d, J = 5.6 Hz, 1H), 8.80 (s, 1H), 9.26 (d, J = 5.6

Hz, 1H).  $^{13}\text{C}$  NMR (75 MHz, DMSO- $d_6$ )  $\delta$  23.9 (2C), 24.1, 39.7, 41.1, 41.4, 77.2, 112.7, 118.8, 155.4, 156.5, 162.0, 165.4. MS (ESI)  $m/z$ : not found  $[\text{M}+\text{H}]^+$ . Purity 96%.

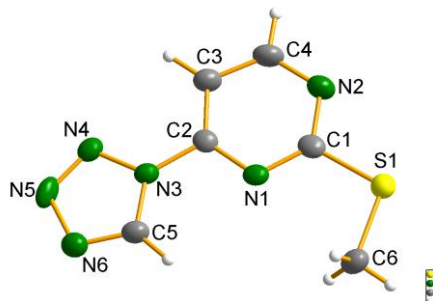
**2-(heptylsulfonyl)-4-(1H-1,2,3-triazol-1-yl)pyrimidine (4):** To a solution of **5** (1.0 eq) in anhydrous DMF was added  $\text{K}_2\text{CO}_3$  (3.0 eq) at  $0^\circ\text{C}$ . To the vigorously stirred suspension was added heptane-1-thiol (0.9 eq). The reaction was allowed to proceed for 20 min at  $0^\circ\text{C}$  and then quenched with an excess of water. Brine was added and the mixture was extracted three times with ethyl acetate. The combined organic layers were concentrated in vacuum and residual DMF was removed by azeotropic distillation using heptane. The crude product was purified by flash chromatography (petroleum ether/ethyl acetate 9:1) to yield 2-(heptylthio)-4-(1H-1,2,3-triazol-1-yl)pyrimidine as white solid (45% yield).  $^1\text{H}$  NMR (300 MHz,  $\text{CDCl}_3$ )  $\delta$  0.89 (t,  $J = 6.5$  Hz, 3H), 1.19 - 1.41 (m, 6H), 1.41 - 1.58 (m, 2H), 1.78 (quin,  $J = 7.4$  Hz, 2H), 3.20 (t,  $J = 7.4$  Hz, 2H), 7.80 (d,  $J = 5.4$  Hz, 1H), 7.85 (d,  $J = 1.1$  Hz, 1H), 8.57 (d,  $J = 1.0$  Hz, 1H), 8.68 (d,  $J = 5.4$  Hz, 1H).  $^{13}\text{C}$  NMR (75 MHz,  $\text{CDCl}_3$ )  $\delta$  14.0, 22.5, 28.8, 28.9, 29.0, 31.2, 31.7, 104.8, 121.0, 134.5, 154.9, 159.8, 173.5. MS (ESI)  $m/z$ : 278.1  $[\text{M}+\text{H}]^+$ . 2-(heptylthio)-4-(1H-1,2,3-triazol-1-yl)pyrimidine (1.0 eq) was dissolved in ethyl acetate and Oxone<sup>R</sup> (3.0 eq) dissolved in water was added. The biphasic system was vigorously stirred until TLC showed full conversion. Water was added and the aqueous layer was extracted three times with ethyl acetate. The combined organic layers were concentrated and the crude material was purified by flash chromatography (hexane/ethyl acetate 1:1) to yield **4** as a white solid (72% yield).  $^1\text{H}$  NMR (300 MHz,  $\text{CDCl}_3$ )  $\delta$  0.88 (t,  $J = 6.9$  Hz, 3H), 1.21 - 1.40 (m, 6H), 1.41 - 1.56 (m, 2H), 1.91 (quin,  $J = 7.8$  Hz, 2H), 3.58 (t,  $J = 7.7$  Hz, 2H), 7.92 (d,  $J = 1.3$  Hz, 1H), 8.41 (d,  $J = 5.5$  Hz, 1H), 8.75 (d,  $J = 1.4$  Hz, 1H), 9.09 (d,  $J = 5.5$  Hz, 1H).  $^{13}\text{C}$  NMR (75 MHz,  $\text{CDCl}_3$ )  $\delta$  14.0, 22.0, 22.5, 28.4, 28.6, 31.4, 51.3, 112.6, 121.9, 135.2, 156.4, 160.9, 166.0. MS (ESI)  $m/z$ : 351.1  $[\text{M}+\text{ACN}+\text{H}]^+$ . Purity 97%.

**2-(methylsulfonyl)-4-(1H-1,2,3-triazol-1-yl)pyrimidine (5):** **5a** (1.0 eq) was dissolved in ethyl acetate and Oxone<sup>R</sup> (3.0 eq) dissolved in water was added. The biphasic system was vigorously stirred for 1 h. Water was added and the aqueous layer was extracted three times with ethyl acetate. The combined organic layers were concentrated and the crude material was purified by flash chromatography (hexane/ethyl acetate 8:2) to yield **5** as a white solid (19% yield).  $^1\text{H}$  NMR (300 MHz,  $\text{CDCl}_3$ )  $\delta$  3.43 (d,  $J = 0.9$  Hz, 3H), 7.92 (s, 1H), 8.42 (dd,  $J = 5.5, 0.9$  Hz, 1H), 8.74 (s, 1H), 9.08 (dd,  $J = 5.5, 0.9$  Hz, 1H).  $^{13}\text{C}$  NMR (75 MHz,  $\text{CDCl}_3$ )  $\delta$  39.2, 112.7, 121.9, 135.2, 156.4, 160.8, 166.2. MS (ESI)  $m/z$ : 226.1  $[\text{M}+\text{H}]^+$ . Purity >99%.

**2-(methylsulfonyl)-4-(1H-tetrazol-1-yl)pyrimidine (6):** **6a** (1.0 eq) was dissolved in ethyl acetate and Oxone<sup>R</sup> (3.0 eq) dissolved in water was added. The biphasic system was vigorously stirred until TLC showed full conversion. Water was added and the aqueous layer was extracted three times with ethyl acetate. The combined organic layers were concentrated and filtered over a pad of silica to yield

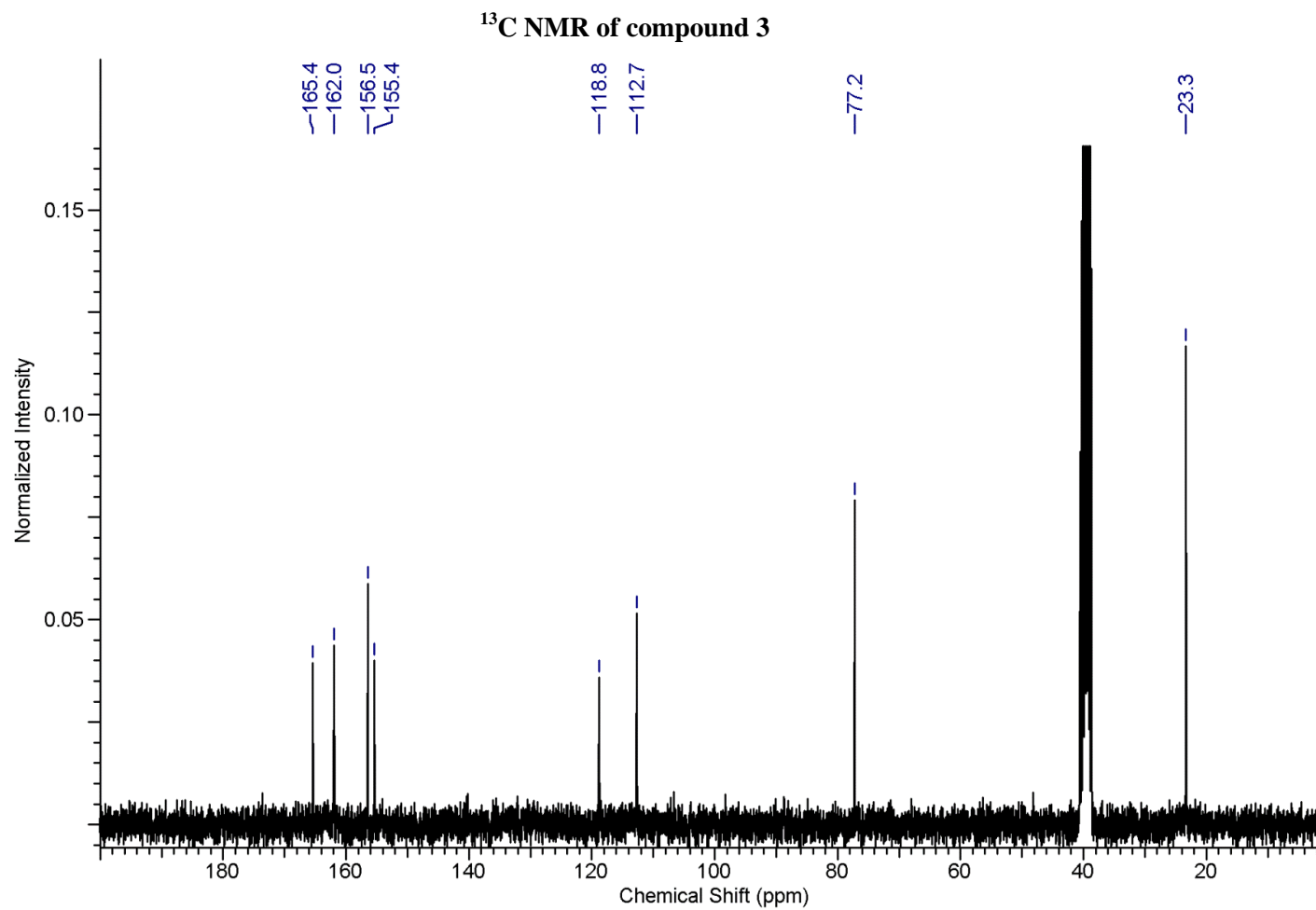
**6** as a white solid (99% yield).  $^1\text{H}$  NMR (300 MHz,  $\text{CDCl}_3$ )  $\delta$  3.46 (s, 3 H), 8.33 (d,  $J=5.4$  Hz, 1 H), 9.20 (d,  $J=5.4$  Hz, 1 H), 9.74 (s, 1 H).  $^{13}\text{C}$  NMR (126 MHz,  $\text{CDCl}_3$ )  $\delta$  39.2, 113.3, 140.6, 154.4, 161.9, 166.5. MS (ESI)  $m/z$ : 227.0  $[\text{M}+\text{H}]^+$ , 199.1  $[\text{M}-\text{N}_2+\text{H}]^+$ . Purity 98%.

b. Crystallization of **6a** for X-ray crystallography



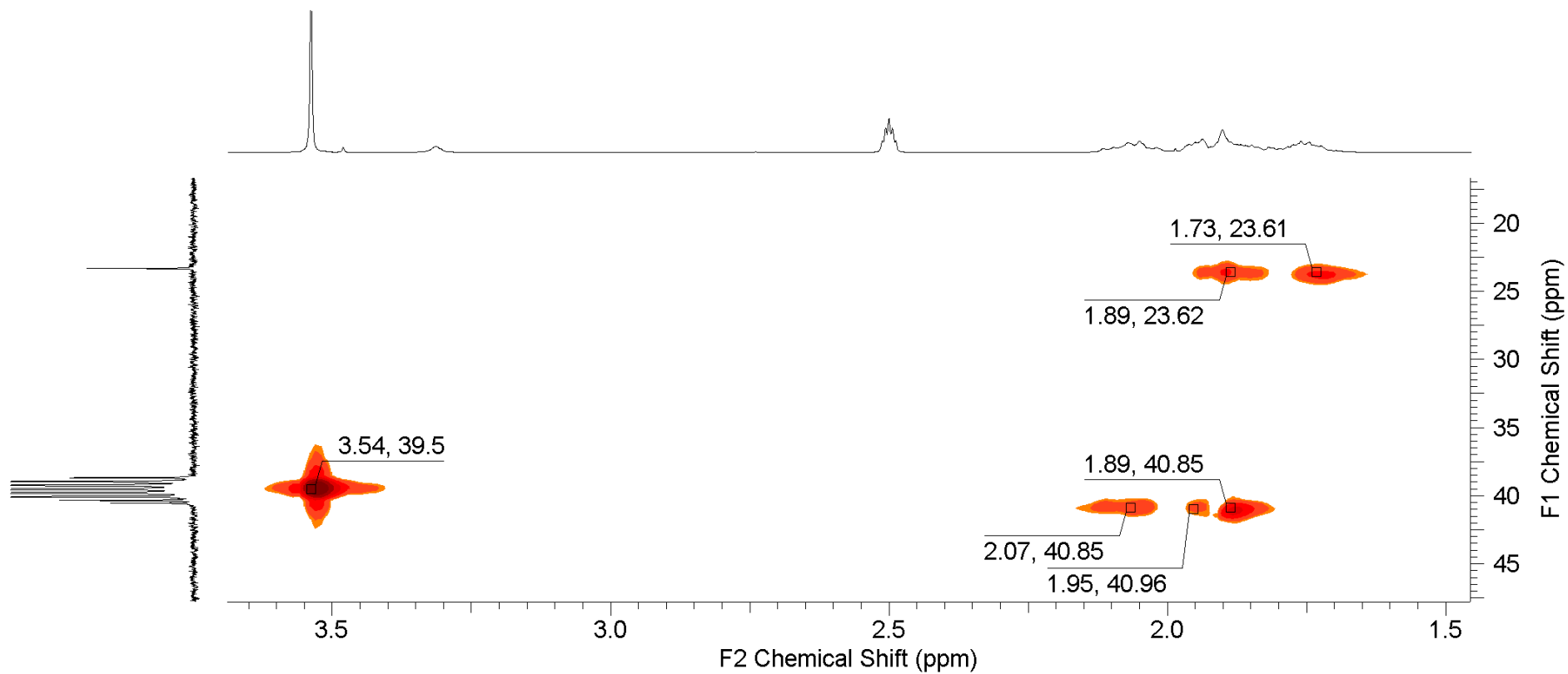
**Figure S1.** X-ray crystal structure of compound **6a** (green = nitrogen, grey = carbon, yellow = sulfur, white = hydrogen).

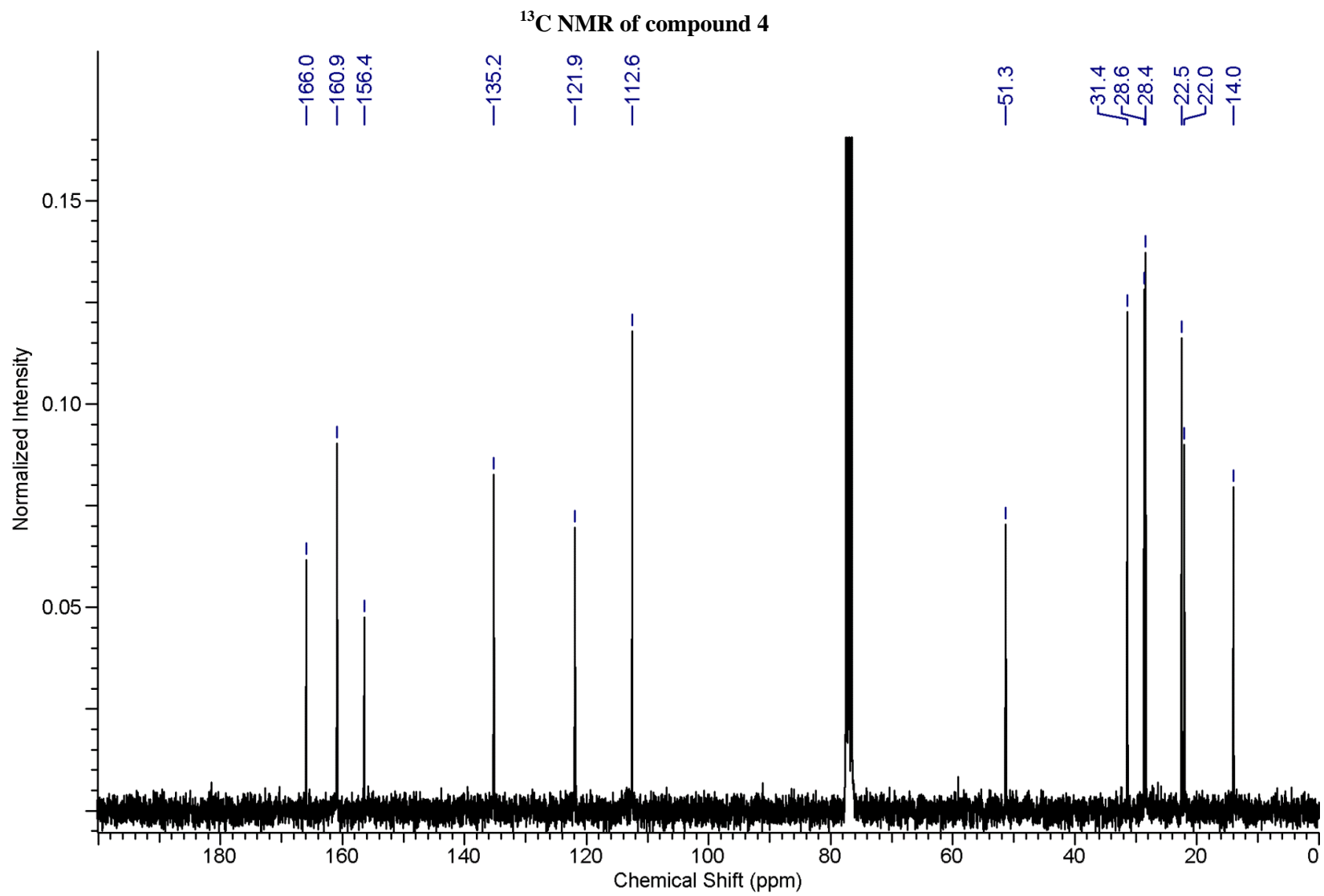
**6a** was dissolved in hot chloroform and left standing open to atmosphere to allow evaporation. Colorless needles formed after 3 weeks. CCDC 1432241 contains the supplementary crystallographic data for this paper. These data can be obtained free of charge from The Cambridge Crystallographic Data Centre via [www.ccdc.cam.ac.uk/getstructures](http://www.ccdc.cam.ac.uk/getstructures).

c.  $^{13}\text{C}$ -NMR spectra

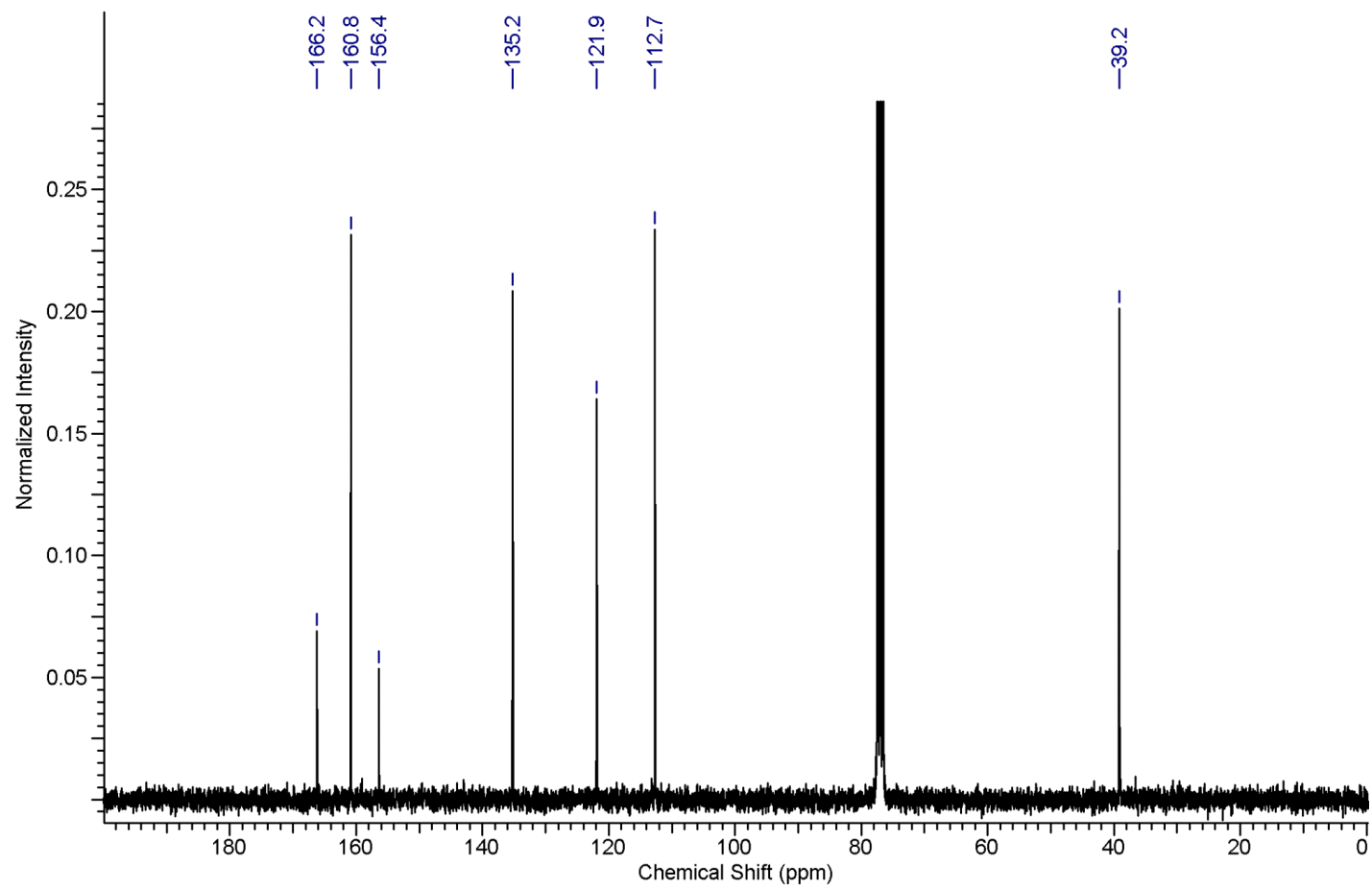
## HSQC NMR of compound 3



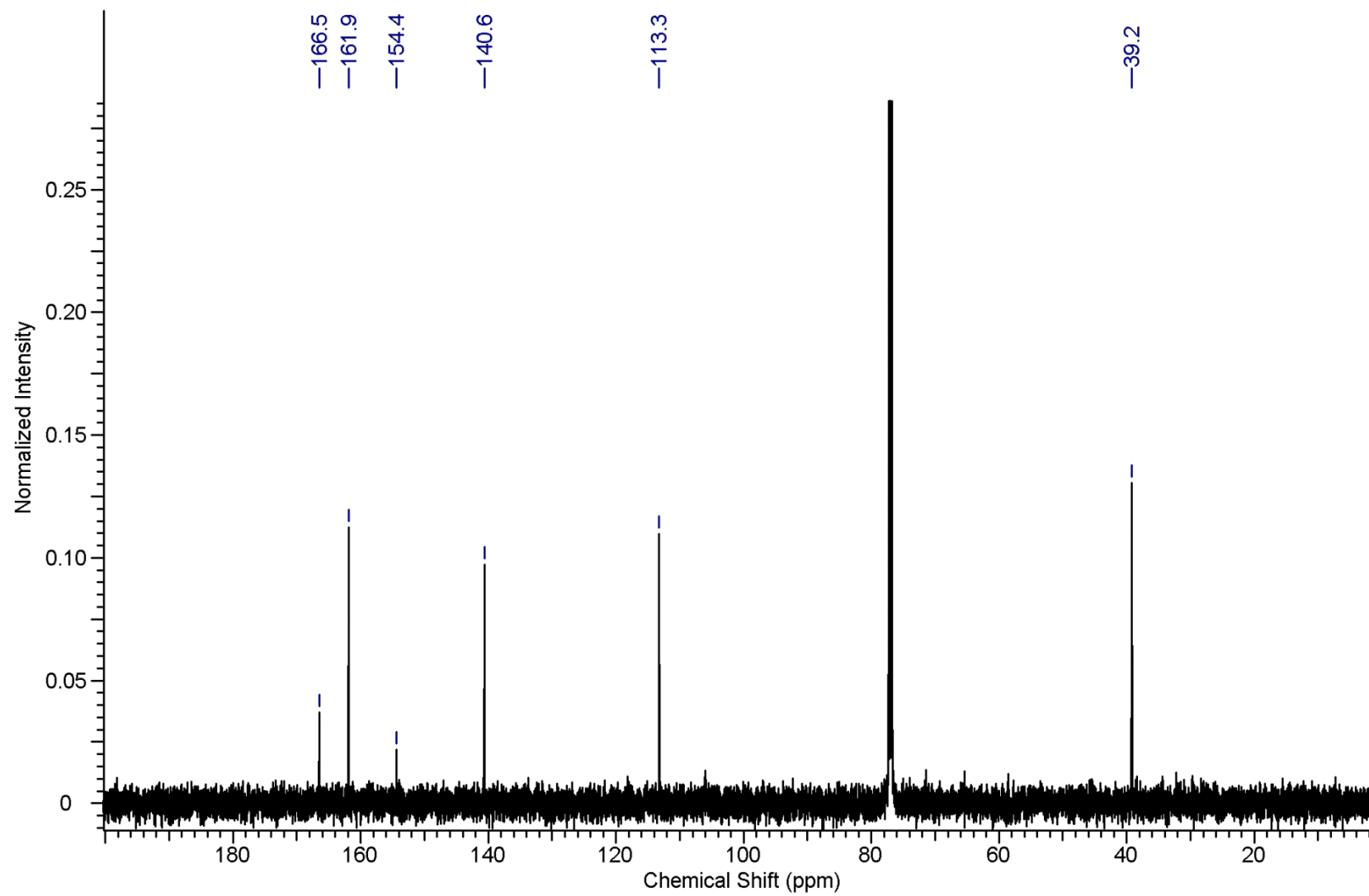




**<sup>13</sup>C NMR of compound 5**

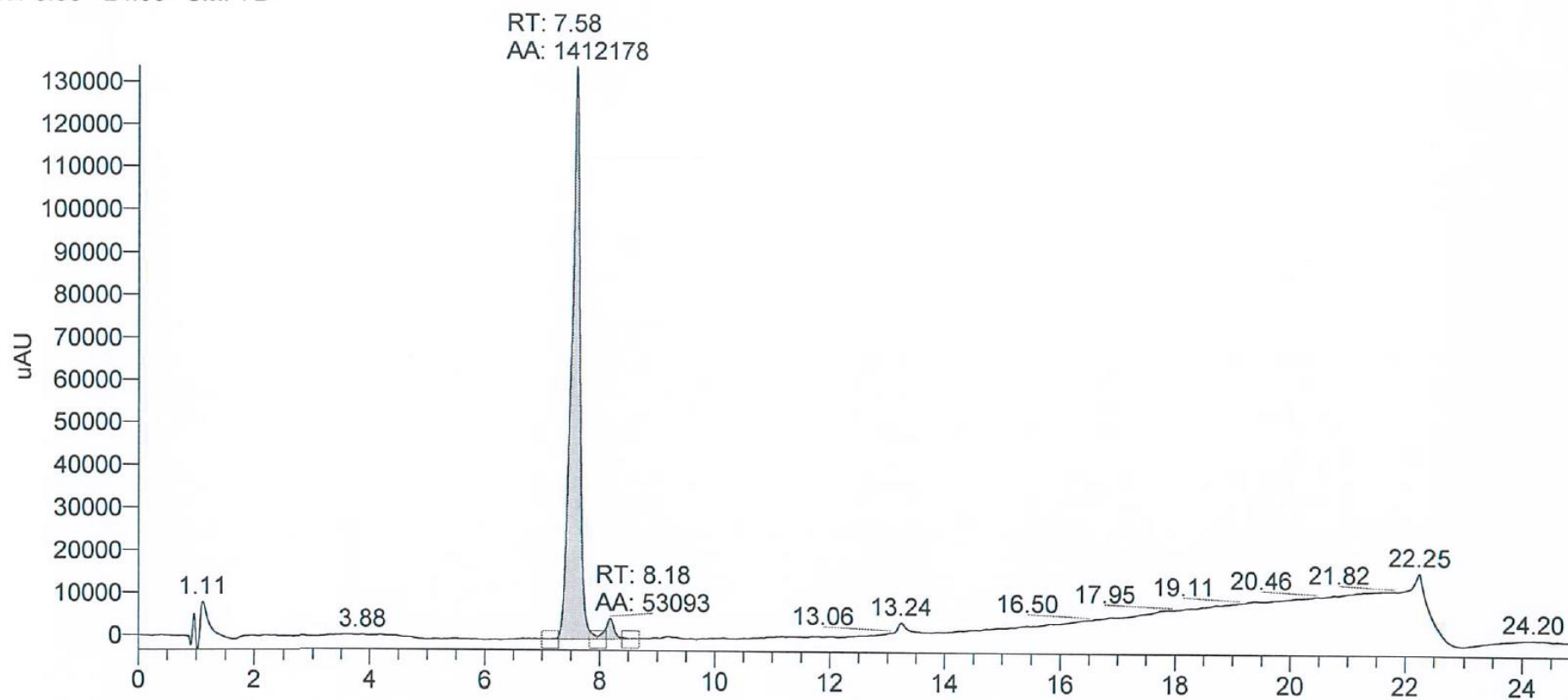


<sup>13</sup>C NMR compound 6

d. LC purity of compounds **3–6**

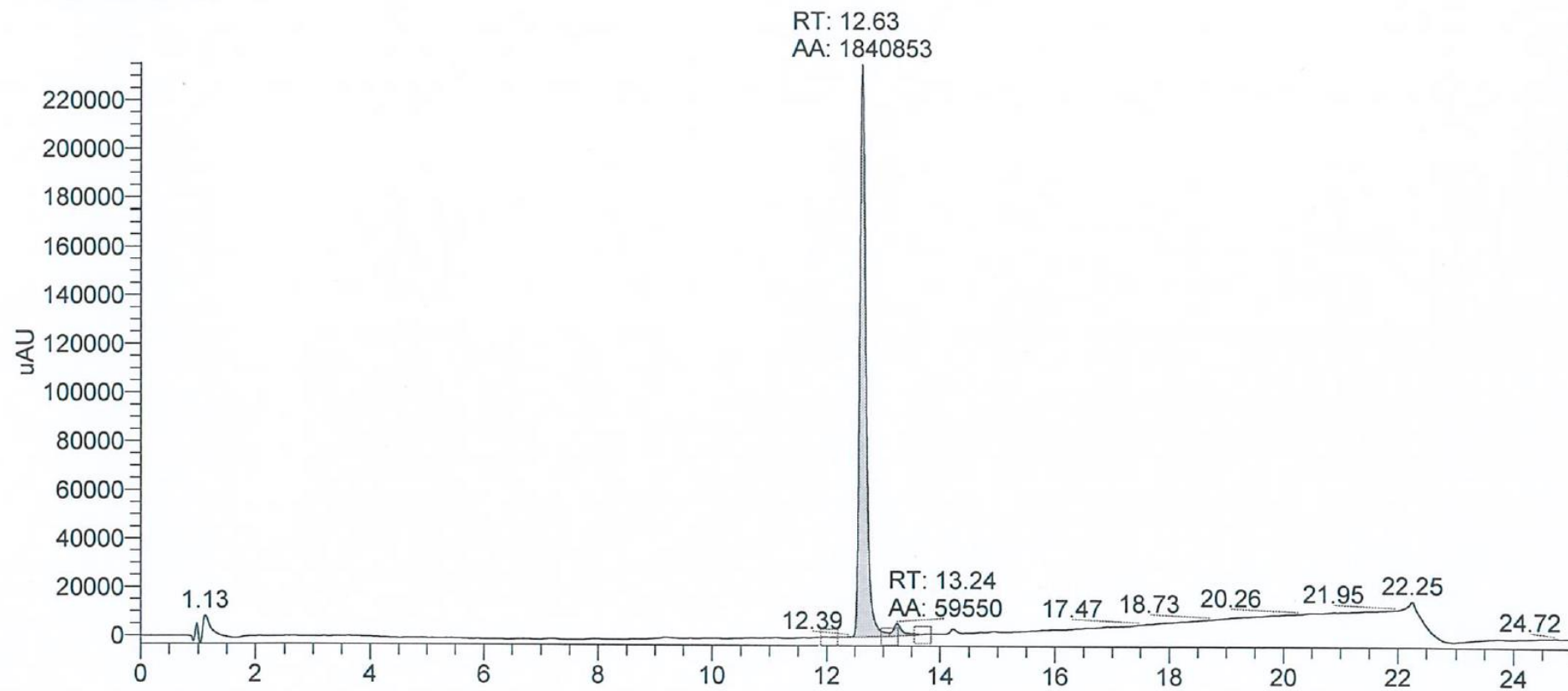
## Compound 3

RT: 0.00 - 24.99 SM: 7B



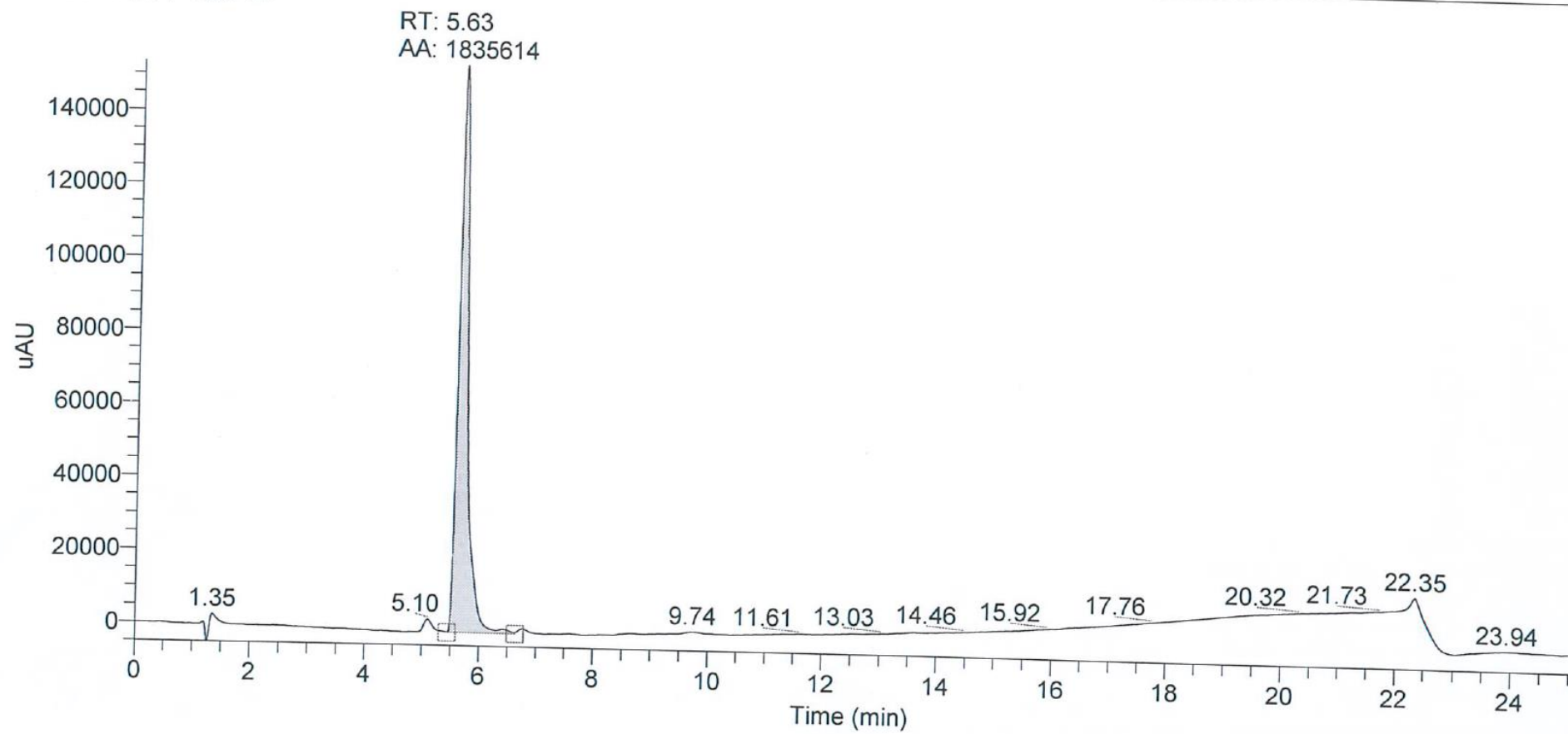
## Compound 4

RT: 0.00 - 25.00 SM: 7B

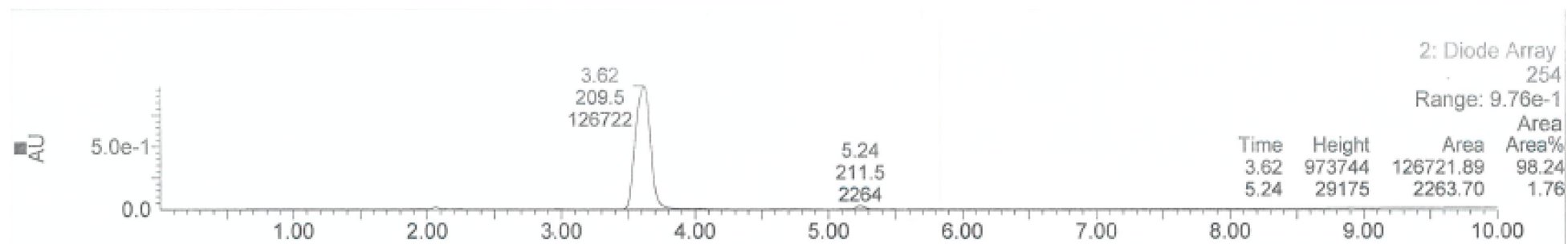


## Compound 5

RT: 0.00 - 25.01 SM: 7B



## Compound 6





## II. General experimental information – Biology

### a. Chemicals, bacterial strains, and media

Yeast extract was obtained from Fluka, peptone and casein from Merck, Bacto™ Tryptone from BD Biosciences, and Gibco® PBS from Life Technologies. Salts and organic solvents of analytical grade were obtained from VWR.

*P. aeruginosa* PA14 strain, and isogenic *pqsR* knockout mutant were stored in glycerol stocks at  $-80$  °C.

Minimal medium PPGAS<sup>3</sup> and Luria Bertani (LB) were used.

### b. Pyocyanin assay

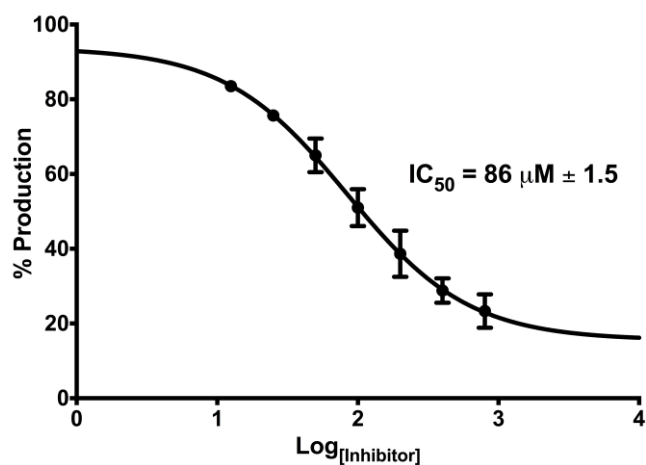
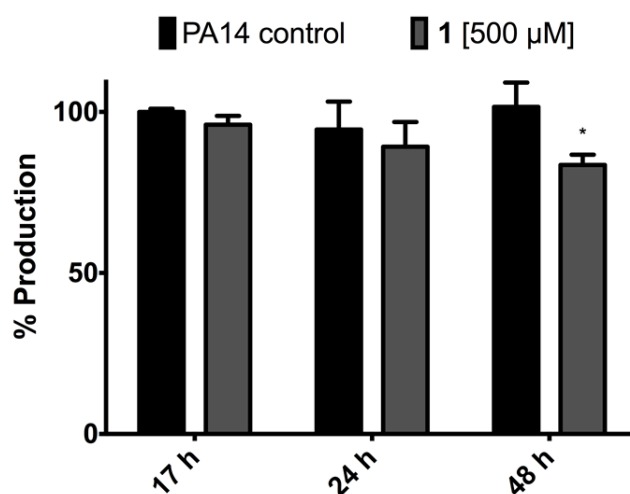


Figure S2. IC<sub>50</sub> curve of the improved inhibitory effect of 6 on pyocyanin production, an indicative of PqsR antagonism. Error bars represent standard error of three independent experiments ( $n = 3$ ).

## c. Prolonged Pyocyanin Assay.

Effect of long-term PqsD inhibition on pyocyanin formation was assessed as previously described (pyocyanin assay) with slight modifications. Initially, treated (compound **1**) and untreated cultures were incubated for 24 h under aerobic conditions. pyocyanin levels and bacterial density were determined from extracted culture aliquots. Obtained OD<sub>600</sub> values were used to re-calculate the necessary dilution factors of each replicate for a final density of 0.02, transferred into a new plate with fresh PPGAS medium and dimethyl sulfoxide (DMSO) or compound **1** for additional 24 h, accordingly. Pyocyanin formation and cell growth were again assessed as previously described, making up for a total of 48 h of incubation with treated samples under constant, long-term PqsD inhibition.



**Figure S3.** Long-term effect of PqsD inhibitor **1** on pyocyanin production in PA14 wild type. Treatment with 500 μM of **1** led to a reduction of pyocyanin levels to 83.5% ± 3.2 after 48 h of incubation. The differences in values (compared to control) determined for 17 h and 24 h were not significant. All values are relative to a DMSO control without addition of inhibitors. Error bars represent the standard deviation of three independent experiments (n = 3). \* = p < 0.05.

d. Growth curves of *P. aeruginosa* PA14

Cultures of PA14 were diluted in PPGAS medium, adjusted to an initial OD<sub>600</sub> of 0.02, and 1.5 mL added in triplicates into 24-well plates (Greiner Bio-One). Cultivation conditions as described above (SI, section IIa). Stock solutions of compound **6** in DMSO were diluted 1:100 to a final DMSO concentration of 1% (v/v), DMSO alone was used as control. Bacterial growth was measured over 48 h as a function of OD<sub>600</sub> using FLUOstar Omega (BMG LabTech).

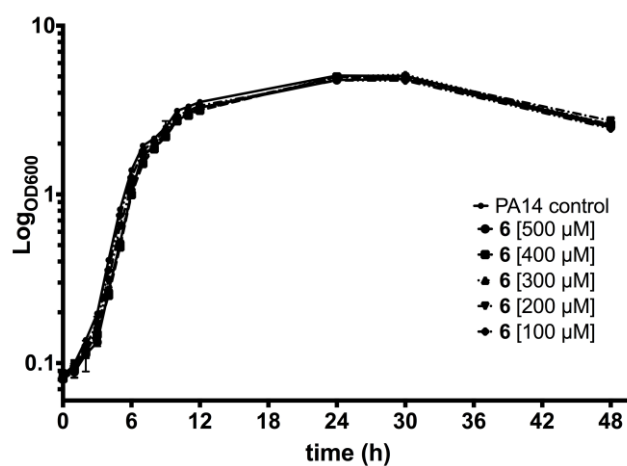


**Figure S4.** Growth curves of PA14 in PPGAS minimal medium in the absence (control) and presence of varying concentrations (100 μM to 500 μM) of compound **6**.

## e. Antibiofilm effects of compound 2

Effects of compound 2 on Biofilm

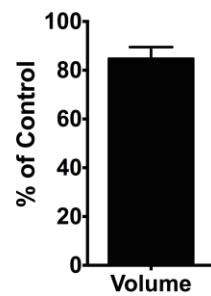


**Figure S5.** Effects of compound 2 (15  $\mu$ M; solubility maximum) on volume of *P. aeruginosa* strain PA14 biofilm. Experiment was performed as described in the experimental section of the main text. Error bars represent standard error of at least two independent experiments.

f. PqsD *in vitro* assay

The assay was performed as reported before.<sup>4</sup>

g. PqsR *in vitro* assay

The assay was performed in *E. coli* DH5 $\alpha$  as reported before.<sup>5</sup>

### III. References

- (1) Thomann, A., Börger, C., Empting, M., and Hartmann, R. (2014) Microwave-Assisted Synthesis of 4-Substituted 2-Methylthiopyrimidines. *Synlett* 25, 935–938.
- (2) Thomann, A., Zapp, J., Hutter, M., Empting, M., and Hartmann, R. W. (2015) Steering the azido-tetrazole equilibrium of 4-azidopyrimidines via substituent variation - implications for drug design and azide-alkyne cycloadditions. *Org. Biomol. Chem.* 13, 10620–10630.
- (3) Zhang, Y., and Miller, R. M. (1992) Enhanced octadecane dispersion and biodegradation by a *Pseudomonas rhamnolipid* surfactant (biosurfactant). *Appl. Environ. Microbiol.* 58, 3276–3282.
- (4) Storz, M. P., Maurer, C. K., Zimmer, C., Wagner, N., Brengel, C., de Jong, Johannes C, Lucas, S., Müsken, M., Häussler, S., Steinbach, A., and Hartmann, R. W. (2012) Validation of PqsD as an anti-biofilm target in *Pseudomonas aeruginosa* by development of small-molecule inhibitors. *J. Am. Chem. Soc.* 134, 16143–16146.
- (5) Lu, C., Maurer, C. K., Kirsch, B., Steinbach, A., and Hartmann, R. W. (2014) Overcoming the unexpected functional inversion of a PqsR antagonist in *Pseudomonas aeruginosa*: an in vivo potent antivirulence agent targeting pqs quorum sensing: An In Vivo Potent Antivirulence Agent Targeting pqs Quorum Sensing. *Angew. Chem. Int. Ed. Engl.* 53, 1109–1111

## 7.2 Curriculum Vitae

### Christian Brengel

(Approb. Apotheker)

Geburtsdatum: 08.01.1986  
Adresse: Im Gassengarten 4  
66440 Wolfersheim  
Telefon: +49 175 9056760  
Email: brengel.chris@gmx.net

#### Ausbildung

---

- |                          |   |
|--------------------------|---|
| <b>01/2012 - heute</b>   | <b>Promotionsstudium</b> am Helmholtz-Institut für Pharmazeutische Forschung Saarland (HIPS) in Kooperation mit der Universität des Saarlandes <ul style="list-style-type: none"><li>▪ Betreuung durch Prof. Dr. Rolf Hartmann, Abteilung: „Drug Design and Optimization (DDOP)“.</li><li>▪ Thema der Arbeit: Verwendung biophysikalischer und biochemischer Methoden zur Identifizierung und Charakterisierung von Hemmstoffen neuer Zielstrukturen im Bereich Antiinfektiva<ul style="list-style-type: none"><li>▪ Methoden: Klonierung, Mutagenese, Proteinexpression, -aufreinigung und -charakterisierung, PCR, SDS-PAGE, AAS, SEC, IEC, FPLC-UV/Vis, SPR, DSF, ITC, GC-MS/MS, HPLC-MS/MS, TLC, UHPLC-UV/Vis, enzymatische und zellbasierte Assays (eukaryotische und prokaryotische Zellen)</li></ul></li></ul> |
| <b>12/2011</b>           | <b>Approbation als Apotheker</b>  |
| <b>11/2011</b>           | <b>Pharmazeutische Prüfung (Note:1,8)</b>   |
| <b>11/2010 – 11/2011</b> | <b>Praktisches Jahr</b><br>im Rahmen der Approbationsordnung Pharmazie  |
| <b>10/2006 – 09/2010</b> | <b>Pharmaziestudium</b>   |

Universität des Saarlandes

**05/2005 – 01/2006**

**Zivildienst**

Ev.KH Zweibrücken

**2002 – 2005**

**Abitur**

Hofenfels-Gymnasium in Zweibrücken

**Mittlere Reife**

**1996 – 2002**

Geschwister – Scholl – Realschule in Blieskastel

**Lehrtätigkeiten**

---

**02/2011 – 12/2013**

**Wissenschaftlicher Mitarbeiter** an der Universität des Saarlandes

- Betreuung des Praktikums „Medizinische Chemie und Molecular Modelling“ für Pharmazeuten, Chemiker und Bioinformatiker
- Betreuung des Studentenseminars „Medizinische Chemie“
- Betreuung einer Masterarbeit und verschiedenster Praktika innerhalb unseres Forschungsinstitutes

**Berufserfahrung & Praktika**

---

**05/2011 – 10/2011**

**Brunnen-Apotheke, Homburg**

Ausbildung im Rahmen des praktischen Jahres

**11/2010 – 04/2011**

**Bayer Health Care, Leverkusen**

Pharmaziepraktikum im Bereich Qualitätskontrolle

Thema: Entwicklung einer neuen UHPLC Methode zur Verbesserung der Qualitätskontrolle eines Produkts aus dem Health Care Portfolio

**04/2010 – 05/2010**

**Universität des Saarlandes, Institut für exp. und klin. Toxikologie**

Wahlpflichtpraktikum unter Anleitung von Prof. Dr. Dr. h.c. Maurer

- Thema: A validated GC-MS procedure for fast, simple and cost-effective quantification of glycols and GHB in human plasma and their identification in urine and plasma developed for emergency toxicology

**01/03/2009 – 17/04/2009**

**Freiwilliges Praktikum, Fresenius Medical Care**

Labor: Inprozesskontrolle, Ansatz (Methodenoptimierung und -validierung)

**08/2007 – 09/2007**

**Barbara-Apotheke, St.Ingbert**

ganztägige Famulatur im Rahmen der Studienordnung Pharmazie

**02/2007 – 03/2007**

**Löwen-Apotheke, Blieskastel**

ganztägige Famulatur im Rahmen der Studienordnung Pharmazie

**Weitere Qualifikationen**

---

- Sprachen: Deutsch (Muttersprachler), Englisch (fließend in Wort und Schrift)
- Sehr guter Umgang mit gängiger Büro- und Laborsoftware (MS-Word, Excel, PowerPoint, ChemDraw, Microcal Origin, MOE, BioEdit, GraphPad Prism, SigmaPlot)



## Veröffentlichungen

---

### **Publikationen:**

**A Biochemical and Biophysical Analysis of a Chiral PqsD Inhibitor Revealing Tight-Binding Behavior and Enantiomers with Contrary Thermodynamic Signatures**

Michael P. Storz,<sup>+</sup> Christian Brengel,<sup>+</sup> Elisabeth Weidel, Michael Hoffmann, Klaus Hollemeyer, Anke Steinbach, Rolf Müller, Martin Empting, and Rolf W. Hartmann

*ACS Chem. Biol.* 2013, 8, 2794-2801.

**B Combining in Silico and Biophysical Methods for the Development of Pseudomonas aeruginosa Quorum Sensing Inhibitors: An Alternative Approach for Structure-Based Drug Design**

J. Henning Sahner,<sup>+</sup> Christian Brengel,<sup>+</sup> Michael P. Storz, Matthias Groh, Alberto Plaza, Rolf Müller, and Rolf W. Hartmann

*J. Med. Chem.* 2013, 56, 8656-8664.

**C Structure Optimization of 2-Benzamidobenzoic Acids as PqsD Inhibitors for Pseudomonas aeruginosa Infections and Elucidation of Binding Mode by SPR, STD NMR, and Molecular Docking**

Elisabeth Weidel, Johannes C. de Jong, Christian Brengel, Michael P. Storz, Matthias Negri, Alberto Plaza, Anke Steinbach, Rolf Müller, and Rolf W. Hartmann

*J. Med Chem.* 2013, 56, 6146-6155.

**D Mechanistic details for anthraniloyl transfer in PqsD: the initial step in HHQ biosynthesis**

Michael C. Hutter, Christian Brengel, Matthias Negri, Claudia Henn, Christina Zimmer, Rolf W. Hartmann, Anke Steinbach, Rolf Müller, Martin Empting

*J. Mol. Model.* 2014, 2:2255.

**E Molecular basis of HHQ biosynthesis: molecular dynamic simulation, enzyme kinetic and surface plasmon resonance studies**

Anke Steinbach Christine K. Maurer, Elisabeth Weidel, Christian Brengel, Rolf W. Hartmann, Matthias Negri

*BMC Biophys.* 2013, 6:10.

**F Validation of PqsD as an Anti-biofilm Target in *Pseudomonas aeruginosa* by Development of Small-Molecule Inhibitors**

Michael P. Storz, Christine K. Maurer, Christina Zimmer, Nathalie Wagner, Christian Brengel, Johannes C. de Jong, Simon Lucas, Mathias Müsken, Susanne Häussler, Anke Steinbach, and Rolf W. Hartmann

*J. Am. Chem. Soc.* 2012, 134, 16143-16146

**G Application of dual inhibition within looped autoregulatory systems towards anti-virulence agents against *Pseudomonas aeruginosa* infections**

Andreas Thomann, Antonio G. Gomes de Mello Martins, Christian Brengel, Martin Empting and Rolf W. Hartmann

*ACS Chem. Biol.* 2016, 11, 1279–1286

**Conference Contributions:****A Biological evaluation of an *in vivo*-potent dual target PQS-Quorum Sensing inhibitor that hinders biofilm formation**

Andreas Thomann, Antonio de Mello Martins, Christian Brengel, Elisabeth Weidel, Alberto Plaza, Carsten Börger, Martin Empting and Rolf W. Hartmann

250<sup>th</sup> ACS American Chemical Society National Meeting, August 2015, Boston, USA.

**B Biophysical Screening of a Focused Library for the Discovery of Novel Antimycobacterials targeting CYP121**

Christian Brengel, Andreas Thomann, Alexander Schiffrin, Rita Bernhardt, Sang Hyun Cho, Scott G. Franzblau and Rolf W. Hartmann

5<sup>th</sup> HIPS Symposium on Pharmaceutical Research, July 2015, Saarbrücken, Germany

**C Biochemical and Biophysical Analysis of PqsD Inhibitors Revealing Contrary Thermodynamic Profile of Enantiomers with Tight-binding Mechanism**

Christian Brengel, Michael P. Storz, Elisabeth Weidel, Michael Hoffmann, Martin Empting, Anke Steinbach, Rolf Müller, Rolf W. Hartmann

*Frontiers in Medicinal Chemistry*, March 2015, Marburg, Germany

**D      Anti-infectives with novel mode of action: Development of PqsD inhibitors to interrupt *P. aeruginosa* cell-to-cell communication**

Christian Brengel, Michael Storz, Elisabeth Weidel, Christine Maurer, Mathias Müsken, Susanne Häussler, Anke Steinbach and Rolf W. Hartmann

*4<sup>th</sup> HIPS Symposium on Pharmaceutical Research*, June 2014, Saarbrücken, Germany